UNIVERSIDADE BEIRA INTERIOR

Human vitreous proteome in vitreoretinal diseases

Fátima Raquel Milhano dos Santos

Tese para obtenção do Grau de Doutor em
Bioquímica
(3º ciclo de estudos)

Orientador: Professor Doutor Luís António Paulino Passarinha
Coorientadora: Professora Doutora Cândida Ascensão Teixeira Tomaz
Coorientador: Doutor Alberto Paradela Elizalde

Covilhã, dezembro de 2020

As provas de doutoramento (3º ciclo de estudos) no ramo de **Bioquímica** requeridas por **Fátima Raquel Milhano dos Santos** foram realizadas no dia 22 de dezembro de 2020 na sala de atos da Reitoria da Universidade da Beira Interior, de modo presencial e por videoconferência.

A tese intitulada "Human vitreous proteome in vitreoretinal diseases" foi aprovada após deliberação do júri, constituído por:

Presidente do júri: Professor Doutor Paulo Jorge da Silva Almeida
Professor Catedrático da Universidade da Beira Interior

Arguente principal: Doutor Marco André Miranda Galésio
Especialista de caracterização química R&D Analítica na Farmacêutica Hovione

Arguente principal: Professor Doutor João Pereira Figueira
Professor Auxiliar na Universidade de Coimbra

Arguente: Professor Doutor António José Geraldes de Mendonça
Professor Auxiliar na Universidade da Beira Interior

Arguente: Professora Doutora Maria Eugénia Gallardo Alba
Professora Auxiliar na Universidade da Beira Interior

Arguente: Doutor Eduardo Oliveira Calçada
Consultor científico da Bayer Portugal Ld.

Coorientador: Doutor Alberto Paradela Elizalde
Cientista Sénior no Centro Nacional de Biotecnologia (CNB-CSIC)

À melhor parte de mim

Ao Diogo, à minha mãe e às minhas irmãs

Acknowledgments

No culminar deste processo, quero expressar a minha gratidão por todos aqueles que de alguma forma me apoiaram ou contribuiriam para a concretização deste projeto. Este foi um projeto desafiante e com muitos percalços, mas tive o privilégio de estar rodeada das pessoas certas que me deram motivação para nunca desistir das minhas aspirações.

At the culmination of this process, I want to express my gratitude to all those who have somehow supported or contributed to the realization of this project. This was a challenging project with many mishaps, but I was privileged to be surrounded by the right people who gave me the motivation to never give up on my aspirations.

Agradeço aos meus orientadores por me desafiarem e incentivarem a desenvolver este projeto. Ao Professor Doutor Luís Passarinha agradeço por me ter impulsionado a enveredar pela área da proteómica, pela confiança que depositou em mim para o desenvolvimento deste e de outros projetos e por me ter integrado numa excelente equipa, com quem aprendi muito nestes últimos anos. À Professora Cândida, que me acompanhou em todo o meu percurso académico, agradeço todo o apoio e carinho que me deu nos últimos anos. As suas críticas construtivas e rigor científico contribuíram, sem dúvida, para melhorar a qualidade deste trabalho. A Alberto Paradela, quien compartió conmigo sus valiosos conocimientos del *multiple reaction monitoring*, siempre de una manera muy sencilla y divertida. Gracias por haberme acompañado en esta última fase del trabajo, aprendí muchísimo.

Agradezco a Sergio Ciordia, quien para mí también fue un director de esta tesis. Gracias por todo lo que me has enseñado y por la motivación que hizo que tuviese siempre ganas de hacerlo mejor. Ha sido un placer trabajar contigo.

Ao Doutor João Paulo Castro Sousa que foi o impulsionador deste projeto. Admiro-o por ter tido a coragem de pensar *out of the box* e compreender que a cooperação entre investigação clínica e investigação básica era essencial para compreender o papel do "nosso" vítreo na patogénese das doenças vitreorretinianas.

Agradezco a Fernando Corrales y a su fantástico equipo por darme la bienvenida al laboratorio de proteómica del CNB-CSIC. Aprendí mucho con vosotros durante mi estancia y espero seguir aprendiendo en el futuro.

Un agradecimiento especial a Adán Alpízar (que literalmente salvó mi tesis), a mi gemela Lorena, al joven bioquímico Pablo y a Marta García Flores.

Gostaria também de agradecer à professora Carla Cruz e à professora Eugénia Gallardo não apenas pelo suporte científico, mas também pela disponibilidade e pelas palavras de apoio que me deram confiança para continuar.

Agradeço aos investigadores do CICS-UBI Catarina Ferreira, Telma Quintela, Catarina Duarte, Raquel Ferreira, Marta Pereira, Julieta Oliveira, Henrique Cardoso, Professora Elisa Cairrão, Professora Graça Baltazar, e Professora Sílvia Socorro por me providenciarem algumas amostras de anticorpos para testar na validação de biomarcadores por western-blot.

O CICS-UBI foi o local onde dei os meus primeiros passos e cresci como investigadora. Por isso, não podia deixar de demonstrar o meu apreço por todos os membros do CICS-UBI e do meu grupo de investigação que me ajudaram ao longo deste percurso. Foram tantas as pessoas que cruzaram o meu caminho nestes últimos anos, mas quero agradecer especialmente ao Augusto Pedro, Margarida Gonçalves, Diana Duarte, Ângelo Luís, Leonor Gaspar, Sílvia Rocha e Joana Mesquita pela partilha salutar de conhecimentos, pela entreajuda e companheirismo.

Às minhas companheiras de "luta" Daniela Talhada, Tânia Albuquerque, Joana Feiteiro, Melissa Mariana e Sandra Rocha. Os nossos encontros diários nos sofás e nossas conversas/desabafos foram realmente dos melhores momentos que passei no CICS-UBI. Obrigada pela vossa amizade e apoio, sem vocês tinha sido bem mais difícil.

Quero também agradecer às minha colegas do MED que me acompanharam nestes últimos meses, especialmente à Hélia, Lénia e Carla, que me deram muito apoio nesta última fase. Trabalhar com vocês e no MED melhorou a minha confiança no meu trabalho e nas minhas capacidades.

Aos meus amigos que são a família que escolhi, sejam os que sempre me acompanharam, os que conheci durante este processo e os que redescobri recentemente. Vocês sabem o quanto significam para mim! Quero agradecer especialmente às minhas queridas amigas do "quarteto" (Inês e Angie), ao Bruno, à minha amiga de infância Sónia, e à Filomena Silva. Obrigada por ouvirem os meus desabafos!

À minha família, que sempre me acompanhou, aos meus cunhados, à minha sogra e aos meus lindos sobrinhos (Malú, Gustavo e Luís Afonso). Obrigada por tudo!

E o meu agradecimento mais especial é dirigido às pessoas mais importantes da minha vida, a quem dedico inteiramente esta tese. Mesmo sem muitas vezes compreenderem as dificuldades subjacentes, deram sempre o vosso melhor para me apoiar durante este percurso. Obrigada por tudo. Não teria chegado aqui sem o vosso amor, paciência e compreensão.

Ao Diogo, por todo o amor e apoio incondicionais nestes últimos anos (e especialmente nos últimos meses). Obrigada por me ouvires, por seres o meu aconchego naqueles dias de fragilidade, e por me fazeres sorrir todos os dias. Sei que este último ano não foi fácil para nenhum de nós e tenho noção que fui pessimista, derrotista, e extremamente chata (diria mesmo insuportável), mas tu nunca me deixaste cair. És o amor da minha vida, nunca teria conseguido sem ti. Amo-te mais que tudo.

À minha mãe galinha, uma verdadeira mulher coragem, que fez muitos sacrifícios para nos dar a melhor educação. Contigo aprendi a lutar sempre pelos meus ideais, mesmo que por vezes esse seja o caminho mais difícil, e a nunca desistir dos meus sonhos. És simplesmente a pessoa mais incrível e resiliente que conheci em toda a minha vida. Amo-te muito. Obrigada por nunca desistires.

Às minhas lindas irmãs e companheiras de uma vida, Xana e Inês. Crescer e aprender com vocês fez de mim uma pessoa melhor. Partilhamos uma ligação tão especial e única que nada nem ninguém pode destruir. A minha vida sem vocês não faria sentido, tenho muito orgulho em vocês. *I love you from here to the moon and back* …

Ao meu pai, um dos grandes exemplos da minha vida. Espero que saibas que ainda ponho um pouco de ti em tudo o que faço e que os teus valores me guiam em todos os momentos da minha vida. Estás e sempre estarás no meu coração.

Funding

This project was financed by the Portuguese Foundation for Science and Technology (FCT) through a doctoral fellowship (SFRH/BD/112526/2015), by Health Sciences Research Center (CICS-UBI) through National Funds by FCT (UID/Multi/00709/2013) and (UID/Multi/00709/2019), and by FEDER funds through the POCI—COMPETE 2020—Operational Programme Competitiveness and Internationalisation in Axis I—Strengthening research, technological development and innovation Project (POCI-01-0145-FEDER-007491). This project was also supported by CNB-CSIC proteomics lab, member of Proteored PRB2-ISCIII supported by grant PT13/0001, of the PE I+D+i 2013–2016, funded by ISCIII and FEDER, Applied Molecular Biosciences Unit-UCIBIO financed by national funds from FCT/MCTES (UID/Multi/04378/2019), and by Novartis Farma-Produtos Farmacêuticos, SA.

Preface

When we started to plotting the first details of this project in 2012, I was not aware of the professional challenge, but also personal, that I was about to face. This thesis emerges from this new project that aimed to reveal the pathogenic mechanisms underlying several vitreoretinal diseases through the analysis of the vitreous proteome. For me, what was initially a professional challenge rapidly became truly a passion, which helped me carry this work through to the end, despite all the obstacles. Although vitreous has been unappreciated for a long time by scientific and medical communities, with this work I was able to understand that this fascinating structure is more complex and biologically active than initially thought. Therefore, I hope that this work opens up new perspectives on the importance of vitreous and its central role in the development of vitreoretinal diseases.

"Vitreous is more than a vestigial space filler within the eye."

Charles Luc Schepens, 1989

Resumo alargado

O vítreo, também denominado por corpo vítreo ou humor vítreo, é um fluido transparente que preenche a cavidade posterior do olho entre a retina neurossensorial e o cristalino. Durante muitos anos, o papel do vítreo na saúde e na doença foi negligenciado, pensando-se que a sua função era meramente estrutural. No entanto, tem-se registado um crescente interesse pela análise do proteoma vítreo nos últimos anos. Estes estudos comprovaram que o vítreo é altamente complexo e biologicamente mais ativo do que se pensava inicialmente. De facto, alterações a nível do proteoma do vítreo refletem o estado fisiológico e patológico do olho e, portanto, esta é a matriz ideal para o estudo das doenças vitreorretinianas. Embora a procura de biomarcadores no vítreo, mais sensíveis e específicos para cada patologia ocular, não tenha sido bem-sucedida até o momento, a análise do proteoma vítreo mostrou-se promissora na elucidação de alguns dos mecanismos patológicos subjacentes a estas patologias. Neste projeto, diversas técnicas proteómicas baseadas na separação de proteínas em gel de poliacrilamida (*gel-based proteomics*) ou no fracionamento de péptidos por cromatografia líquida (*gel-free proteomics*) foram desenvolvidas e aplicadas para a análise do proteoma do vítreo no descolamento da retina (RD), na retinopatia diabética (DR) e na degeneração macular relacionada com a idade (AMD).

Desde os primeiros estudos em proteómica, a eletroforese bidimensional do gel (2DE) foi o método preferencial para a separação e a identificação de proteínas do vítreo. A 2DE é uma ferramenta valiosa para a separação com elevada resolução e análise de rotina de proteoformas, principalmente se for combinada com técnicas de deteção mais sensíveis, com um processamento de imagem mais refinado e com uma preparação adequada das amostras. Portanto, na primeira parte deste trabalho, aplicou-se uma rede neural artificial (ANN) para a otimização da extração de proteínas do vítreo e da sua análise por 2DE, através da combinação de vários agentes solubilizantes (CHAPS, Genapol, DTT, tampão IPG) e parâmetros físicos (temperatura e voltagem total). Pela aplicação de um modelo matemático criado por ANN, a extração de proteínas e o número de spots detetados após a sua análise por 2DE melhoram significativamente. A resposta otimizada (580 spots detetados) representa um incremento melhoria de 2,4 vezes comparando com as condições padrão utilizadas no desenho experimental inicial. Os resultados alcançados indicam claramente que é crucial combinar as concentrações adequadas de agentes solubilizantes para melhorar a extração, solubilização e a deteção das proteínas do vítreo, assim como para obter géis bem resolvidos. Para além disso, os nossos

resultados também indicam que os parâmetros físicos têm uma influência significativa na focagem isoelétrica e, por esta razão, devem ser ajustados e monitorizados neste tipo de análise. Quando se trabalha com fluidos biológicos também é importante reduzir a sua complexidade antes da análise por 2DE, de modo a facilitar a deteção de proteínas pouco abundantes e a aumentar a cobertura do proteoma. Após a remoção da albumina e da imunoglobulina G, o número de proteínas detetadas no gel aumentou 1,3 vezes quando comparado com o ponto ótimo do modelo proposto por ANN, com uma média de 761 spots detetados no vítreo em doenças vitreorretinianas, como, por exemplo, o descolamento regmatogénico da retina (RRD) ou a retinopatia diabética proliferativa (PDR).

Na segunda tarefa deste projeto de doutoramento, testou-se a performance das técnicas de marcação isobárica, na análise de amostras de vítreo de RRD. O RRD é uma das causas de cegueira e é caracterizado por uma separação física entre a retina neurossensorial e o epitélio pigmentar da retina (RPE). O vítreo tem um papel central no aparecimento do RRD, que pode ser provocado pela liquefação do vítreo. Esta reduz a adesão vitreorretiniana, conduzindo assim à acumulação de líquido do vítreo no espaço subretinal, e, consequentemente, à separação física entre a retina e o RPE. Assim, a proteómica quantitativa pode contribuir para a compreensão das alterações que ocorrem no olho, providenciando uma informação complementar sobre os mecanismos moleculares subjacentes à patogénese do RRD. No presente estudo, o proteoma do vítreo recolhido de doentes com RRD foi analisado e comparado com amostras de vítreo de membranas epimaculares (MEM) usando reagentes iTRAQ (*Isobaric tags for relative and absolute quantitation*) em combinação com análise por Cromatografia Líquida Bidimensional acoplada à Espectrometria de Massa em Tandem (2D-LC-MS/MS). A análise destas amostras por LC-MS/MS resultou na identificação de 6078 péptidos relativos a 1030 proteínas, 2613 dos quais correspondem a péptidos únicos. Das proteínas identificadas, um total de 150 estava diferencialmente expressa no vítreo de doentes com RRD, incluindo 96 proteínas sobreexpressas e 54 subexpressas. Entre as sobreexpressas encontraram-se várias enzimas glicolíticas (frutose-bifosfato aldolase A, gama-enolase e fosfoglicerato cinase 1), transportadores de glicose (GLUT-1), e inibidores de proteases (inibidor da metaloproteinase 1, inibidor do ativador de plasminogénio 1) que são regulados pelo fator induzido por hipóxia (HIF-1), o que sugere que a via de sinalização HIF-1 pode ser activada em resposta à RRD. Além disso, a acumulação no vítreo de proteínas intracelulares dos fotorreceptores, incluindo fosducina, rodopsina e S-arrestina, ou da vimentina revela que a RRD leva a uma degeneração significativa das células fotorreceptoras. No entanto, a sobreexpressão de

proteínas envolvidas no metabolismo do carbono ou chaperones moleculares, entre outras, indica que diversos mecanismos são ativados em resposta ao RRD de forma a promover a sobrevivência das células retinianas através de respostas celulares complexas, como por exemplo, a ativação da via de sinalização HIF-1.

Na terceira tarefa, aplicou-se um método quantitativo label-free (LFQ) para analisar o proteoma do vítreo na PDR e na forma seca da AMD (dry AMD). DR e AMD são as principais causas de deficiência visual e cegueira em indivíduos com idade igual ou superior a 50 anos, em países industrializados ou de rendimento médio. Embora as terapias direcionadas à inibição do fator de crescimento vascular (VEGF) tenham melhorado o tratamento da forma neovascular da AMD (nAMD) e da PDR, neste momento não existem opções terapêuticas para a AMD seca. Portanto, a proteómica quantitativa pode contribuir para o conhecimento dos mecanismos biológicos subjacentes a estas patologias e a encontrar novos potenciais biomarcadores e/ou alvos terapêuticos. Com esta finalidade, o proteoma do vítreo recolhido de doentes com PDR (n=4) foi comparado com o de doentes com AMD seca (n=4) e com membranas epiretinianas (ERM) (n=4) utilizando um método LFQ, que combina o fracionamento "curto" por eletroforese desnaturante em gel de poliacrilamida e análise por LC-MS/MS. Foram identificadas 680 proteínas, das quais 586 foram identificadas com recurso ao software MASCOT e 580 com o software MaxQuant. Posteriormente, foram realizados testes *post hoc*, métodos hierárquicos para análise de agrupamento de dados e testes t múltiplos para diferenciar os três grupos de doenças em termos de expressão proteica com base na sua intensidade. Os testes *post hoc* revelaram que 96 proteínas são capazes de diferenciar entre os diferentes grupos, enquanto 118 proteínas (17 para sobreexpressas e 101 subexpressas) foram identificados como diferencialmente expressas na PDR em comparação com doentes com ERM e 95 proteínas (10 sobreexpressas e 85 subexpressas) em comparação com os doentes com AMD seca. A análise de enriquecimento funcional indica que estas proteínas subexpressas estão correlacionadas com vias/processos biológicos, como reorganização da matriz extracelular (ECM), desgranulação das plaquetas, digestão intracelular nos lisossomas, adesão celular e desenvolvimento do sistema nervoso central. Por sua vez, os resultados indicam que o vítreo de doentes com PDR é enriquecido em mediadores dos sistemas de complemento e coagulação e da fase aguda da inflamação, reforçando o papel destas vias na sua patogénese.

Por último, alguns potenciais biomarcadores foram selecionados de acordo com os resultados obtidos na quantificação do proteoma do vítreo por iTRAQ e LFQ e validados pela monitorização de múltiplas reações (MRM) num maior número de amostras de

vítreo. Assim, desenvolveu-se um método de MRM scheduled para a análise de 35 proteínas, em amostras de vítreo recolhidas de doentes com ERM (n=21), DR/PDR (n=20), AMD (n=11) e RRD (com e sem vitreorretinopatia proliferativa) (n=13). Desta forma, 26 proteínas demostraram potencial para discriminar entre os diferentes grupos de doenças de acordo com os resultados obtidos no MRM e as respectivas curvas ROC (receiver operating characteristic curve). Componentes das cascatas do complemento e coagulação (C6, C8B, protrombina), proteínas de fase aguda (alfa-1-antiquimotripsina), moléculas de adesão (proteína galectina-3), componentes da ECM (opticina) e biomarcadores de neurodegeneração (beta-amilóide, proteína tipo-precursora amilóide 2) destacam-se como os biomarcadores mais eficientes para discriminar entre os diferentes grupos de doenças.

Em conclusão, foram desenvolvidas e implementadas diversas estratégias para a preparação e análise do proteoma do vítreo em diferentes doenças vitreorretinianas, baseadas na separação por 2DE ou por LC. Em relação ao método baseado na separação em gel, um modelo matemático criado por ANN permitiu o desenvolvimento de um protocolo altamente eficiente para a análise de elevada resolução do proteoma do vítreo por 2DE, o que pode ser vantajoso para a detecção de proteoformas específicas, incluindo diferentes isoformas e proteínas com modificações pós-traducionais. Por outro lado, métodos de alta produtividade, como iTRAQ e LFQ, proporcionaram uma análise mais aprofundada do proteoma do vítreo. Nestas técnicas, foram identificadas 1030 proteínas pela técnica de iTRAQ e 680 por LFQ, sendo que algumas não tinham sido identificadas anteriormente. Ainda mais relevante é o fato de que a análise do proteoma do vítreo, com base nestas técnicas, forneceu novos perspetivas sobre a patogénese do RRD, PDR e AMD. Além disso, estes estudos forneceram informações fundamentais sobre potenciais biomarcadores, o que permitiu a validação de 26 proteínas por MRM. No entanto, deve ter-se em consideração que os biomarcadores encontrados no vítreo não podem ser utilizados para um diagnóstico médico regular, devido ao modo de recolha invasivo deste tipo de amostras. Porém, estes podem ser candidatos a novos alvos farmacêuticos e, quando as amostras são obtidas como parte da rotina clínica, podem ser usados para o prognóstico da evolução da doença e/ou para prever a resposta adequada ao tratamento.

Palavras-chave

Biomarcadores; Degeneração macular relacionada com a idade; Descolamento regmatogénico da retina; Eletroforese bidimensional; iTRAQ; Proteómica do vítreo; Proteómica quantitativa Label-free; Retinopatia diabética.

Abstract

Vitreous, also termed vitreous body or vitreous humor, is a transparent fluid that fills the posterior cavity of the eye, surrounded by the neurosensorial retina, and lens. For a long time, the vitreous was not appreciated for its role in health and disease, and its function was thought to be merely structural. Nevertheless, the analysis of vitreous proteome has gained a growing interest in recent years. These studies proved that vitreous is highly complex and biologically more active than initially thought. As a matter of fact, changes in vitreous proteome reflect the physiological and pathological state of the eye, and, therefore, it is the ideal matrix for studying vitreoretinal diseases. Although the search for sensitive and specific vitreous biomarkers in ocular disease has not been successful so far, the analysis of vitreous proteome has been seen to be promising in elucidating some of the pathological mechanisms underlying vitreoretinal diseases. In this project, several gel-based and gel-free techniques were developed and applied for the analysis of vitreous proteome in retinal detachment (RD), diabetic retinopathy (DR), and age-related macular degeneration (AMD).

Since the early proteomic studies, two-dimensional gel electrophoresis (2DE) has been the preferential method for the separation and identification of vitreous proteins. If combined with more sensitive detection techniques, refined gel image processing, and proper sample preparation, 2DE is still a valuable tool for high-resolution separation and routine analysis of proteoforms. Despite technological advances, 2DE of biological fluids, such as vitreous, remains a major challenge. Therefore, in the first part of this work, an artificial neural network was applied to optimize the recovery of vitreous proteins and their detection by 2DE analysis through the combination of several solubilizing agents (CHAPS, Genapol, DTT, IPG buffer) and physical parameters (temperature and total voltage). Using a mathematical model created by ANN, both the protein recovery and the number of spots detected in 2DE gels were significantly improved. The optimized response (580 spots) represents a 2.4-fold improvement over the standard conditions applied for vitreous analysis by 2DE. Our results clearly indicate that it is crucial to combine appropriate amounts of solubilizing agents to improve the extraction, solubilization, and detection of vitreous proteins, and to obtain well-resolved gels. Beyond that, our results also indicate that physical parameters have a significant influence on isoelectric focusing and, thereby, should be adjusted and monitored. When working with biological fluids, it is also important to reduce their complexity before 2DE analysis to facilitate the detection of low-abundant proteins, and to increase the

proteome coverage. After the removal of albumin and IgG, the number of proteins detected in the gel increased 1.3-fold over the optimal output refined by the ANN model, with an average of 761 spots detected in vitreous from different vitreoretinopathies, including rhegmatogenous retinal detachment (RRD) and the proliferative diabetic retinopathy (PDR).

In the second task of this Ph.D. project, the performance of gel-free proteomic techniques combined with stable-isotope labeling was tested for the analysis of vitreous samples in RRD. RRD is a potentially blinding condition characterized by a physical separation between the neurosensory retina and retinal pigment epithelium. Vitreous has a central role in the onset of RRD, which may be triggered by vitreous liquefaction. It reduces the vitreoretinal adhesion, leading to the accumulation of vitreous fluid in subretinal space, and, subsequently, to the physical separation between the neuronal retina and the retinal pigment epithelium. Quantitative proteomics can help to understand the changes that occur in the eye, providing additional information about the molecular mechanisms underlying RRD pathogenesis. In this study, the proteome of vitreous collected from patients with RRD was analyzed and compared to epimacular membranes (MEM) using iTRAQ reagents (Isobaric tags for relative and absolute quantitation) combined with analysis by two-dimensional liquid chromatography coupled to tandem mass spectrometry (2D-LC-MS/MS). Using this strategy, we identified 6078 peptides corresponding to 1030 proteins, with 2613 out of these corresponded to unique peptides. Overall, 150 proteins were found differentially expressed in the RRD vitreous, including 96 overexpressed and 54 underexpressed. Among overexpressed proteins, several glycolytic enzymes (fructose-bisphosphate aldolase A, gamma-enolase, and phosphoglycerate kinase 1), glucose transporters (GLUT-1), and protease inhibitors (metalloproteinase inhibitor 1, plasminogen activator inhibitor 1) are regulated by hypoxia-inducible factor-1 (HIF-1), which suggests that HIF-1 signaling pathway can be triggered in response to RRD. Also, the accumulation of photoreceptor proteins, including phosducin, rhodopsin, and s-arrestin, and vimentin in vitreous may indicate that photoreceptor degeneration occurs in RRD. Nevertheless, the overexpression of proteins of carbon metabolism or molecular chaperones or, among others, suggests that different mechanisms are activated after RRD to promote the survival of retinal cells through complex cellular responses, e.g. the activation of the HIF-1 signaling pathway.

In the third task, a label-free quantitative (LFQ) method was applied to analyze the vitreous proteome in PDR and dry AMD. DR and AMD are leading causes of visual impairment and blindness in people aged 50 years or older in middle-income and industrialized countries. Although Anti-VEGF therapies have improved the management

of neovascular AMD (nAMD) and PDR, no treatment options exist for dry AMD. Therefore, quantitative proteomics can help to recognize the biological mechanisms underlying these pathologies and to find new potential biomarkers and/or pharmaceutical targets. For this purpose, the proteome of vitreous collected from patients with PDR (n=4) were compared to dry AMD (n=4) and epiretinal membranes (ERM) (n=4) using an LFQ method that combines a fractionation by short SDS–polyacrylamide gel electrophoresis and analysis by LC-MS/MS. A total of 680 proteins were identified, of which 586 were identified using the software search engine MASCOT and 580 using MaxQuant. Subsequently, post hoc tests, hierarchical clustering, and multiple t-tests were performed for differentiating the three disease groups in terms of protein expression based on their intensity. Post hoc tests revealed that 96 proteins are capable of differentiating among the different groups, whereas 118 proteins (17 up- and 101 down-regulated) were found differentially regulated in PDR compared to ERM and 95 proteins (10 up- and 85 down-regulated) in PDR compared to dry AMD. Functional enrichment analysis indicates that these underexpressed proteins are correlated to pathways/ biological processes, such as extracellular matrix (ECM) disassembly and organization, platelet degranulation, lysosomal degradation, cell adhesion, and central nervous system development. In turn, mediators of complement and coagulation cascades and acute-phase inflammatory responses were found enriched in PDR vitreous, reinforcing the role of these pathways in its pathogenesis of PDR.

For last, some potential biomarkers were selected according to iTRAQ and LFQ experiments and validated by multiple reaction monitoring (MRM) in a larger set of vitreous samples. Therefore, we develop a scheduled MRM method for the analysis of 35 proteins in vitreous samples collected from patients with ERM (n=21), DR/PDR (n=20), AMD (n=11), and RRD (with and without proliferative vitreoretinopathy) (n=13). Of these, 26 proteins have been shown the potential to differentiate between different disease groups according to MRM results and respective receiver operating characteristic curves. Complement and coagulation components (C6, C8B, prothrombin), acute-phase proteins (alpha-1-antichymotrypsin), adhesion molecules (galectin-3-binding protein), ECM components (opticin), and neurodegeneration biomarkers (beta-amyloid, amyloid-like protein 2) stand out as the more efficient biomarkers to discriminate among the different disease groups.

In conclusion, several gel-based and gel-free strategies were developed and implemented for the preparation and analysis of the proteome of vitreous in different vitreoretinal diseases. Concerning the gel-based method, a mathematical model created by ANN provided an effective 2DE protocol for high-resolution analysis of vitreous proteome,

which can be advantageous for analysis of specific proteoforms, including different isoforms and post-translational modified proteins. On the other hand, high-throughput methods, such as iTRAQ and LFQ, provided a more in-depth analysis of vitreous proteome. In these techniques, we identified 1030 proteins by iTRAQ and 680 by LFQ, some of them have not been previously identified. Even more relevant is the fact that vitreous analysis using these techniques provided new insights on the pathogenesis of RRD, PDR, and AMD. Beyond that, they provided fundamental information regarding potential biomarkers, which enabled the successful validation of 26 proteins by MRM. Nevertheless, it must be taken into consideration that vitreous biomarkers cannot be used for regular diagnosis due to invasive sampling. However, they can be candidates for new pharmaceutical targets and, when the samples are obtained as part of the clinical routine, be used for the prognosis of the patient's disease evolution and/or to predict the proper response to treatment.

Keywords

Age-related macular degeneration; Biomarkers, Diabetic Retinopathy; iTRAQ Label-free quantitative proteomics; Rhegmatogenous retinal detachment; Two-dimensional gel electrophoresis; Vitreous proteomics.

Thesis Overview

This thesis is structured into five main chapters.

Chapter 1 consists of an introduction to the theme, and it is divided into three sections.

The Introduction (section 1) presents the anatomy and physiology of vitreous, followed by a state of the art of the ocular diseases and a description of the importance of characterizing vitreous proteome to improve its management. Therefore, it provides an overview of the studies conducted for the characterization of the vitreous proteome in health and the disease, and the techniques applied.

Section 2 of Chapter 1 contains the first paper developed in the scope of this thesis, which reviews the first proteomics strategies used for the characterization of the vitreous proteome.

- **Paper I** – Trends in proteomic analysis of human vitreous humor samples.

Lastly, **Section 3** of Chapter 1 contains a review paper that summarizes the potential biomarkers of proliferative diabetic retinopathy (PDR), proliferative vitreoretinopathy (PVR), and neovascular age-related macular degeneration (nAMD) found in vitreous. This review provides some insights into the role of these biomarkers in eye physiology and the onset of proliferative pathologies.

- **Paper II** – Vitreous humor proteome: unraveling the molecular mechanisms underlying proliferative vitreoretinal diseases.

Chapter 2 presents the global aims of this thesis, as well as the intermediate aims established for the implementation and development of this project.

Chapter 3 includes the original research papers developed during this Ph.D. project, and are organized as follows:

- **Paper III** – Refinement of two-dimensional electrophoresis for vitreous proteome profiling using an artificial neural network.

- **Paper IV** – iTRAQ Quantitative Proteomic Analysis of Vitreous from Patients with Retinal Detachment.

- **Paper V** – Differentiating the Vitreous Proteome in Age-Related Macular Degeneration, Diabetic Retinopathy from other Vitreoretinal Diseases by Label-Free Relative Quantification and Multiple Reaction Monitoring.

Chapter 4 contains a general discussion of the results obtained to integrate and complement the information presented in the original research papers.

Chapter 5 presents the main conclusions achieved in this thesis, mostly concerning the most appropriate strategy for vitreous proteome analysis, and which potential biomarkers of vitreoretinal diseases were discovered and validated. In the culmination of this thesis, some perspectives of new investigation lines that can be conceived are presented in light of the results obtained throughout these years of experimental work.

Table of Contents

List of Figures

List of Tables

List of Abbreviations

2DE	Two-Dimensional Electrophoresis
AMD	Age-related Macular Degeneration
ANN	Artificial Neural Network
CE	Capillary Electrophoresis
CE-MS	Capillary Electrophoresis coupled to Mass Spectrometry
CLU	Clusterin
DDA	Data-Dependent Acquisition
DIA	Data-Independent Acquisition
DR	Diabetic Retinopathy
ECM	Extracellular matrix
ERM	Epiretinal Membranes
ESI	Electrospray Ionization
GAGs	Glycosaminoglycans
GeLC-MS	Gel-enhanced Liquid Chromatography coupled to Mass Spectrometry
HA	Hyaluronan
ICAT	Isotope-Coded Affinity Tags
ICPL	Isotope-Coded Protein Labeling
IEX	Ion-exchange chromatography
IT	Ion Trap
iTRAQ	Isobaric Tag for Relative and Absolute Quantitation
LC	Liquid Chromatography
LC-MS	Liquid Chromatography coupled to Mass Spectrometry
LC-MS/MS	Liquid Chromatography coupled to tandem Mass Spectrometry
m/z	Mass to Charge Ratio
MALDI	Matrix-assisted laser desorption/ionization
MALDI-TOF/TOF	Matrix-Assisted Laser Desorption/Ionization with tandem Time Of Flight
MEM	Macular Epiretinal Membranes
MH	Macular Hole
MRM	Multiple Reaction Monitoring
MS	Mass Spectrometry
MS/MS	Tandem mass spectrometry
MS1	Precursor-ion spectra

MS2	Fragmentation spectra
MSVI	Moderate or Severe Visual Impairment
MudPit	Multidimensional chromatography protein identification technology
MW	Molecular Weight
nAMD	Neovascular Age-related Macular Degeneration
OPTC	Opticin
PDR	Proliferative Diabetic Retinopathy
PEDF	Pigment Epithelium-Derived Factor
pI	Isoelectric Point
PTMs	Post-Translational Modifications
PVD	Posterior Vitreous Detachment
PVR	Proliferative Vitreoretinopathy
Q	Quadrupole
RD	Retinal Detachment
RRD	Rhegmatogenous Retinal Detachment
RVO	Retinal Vein Occlusion
SC	Spectral Counting
SCX	strong cation-exchange
SDS-PAGE	Sodium Dodecyl Sulfate-Polyacrylamide Gel Electrophoresis
SILAC	Amino Acids in Cell Culture
SRM	Selected Reaction Monitoring
TMT	Tandem Mass Tags
TOF	Time-of-flight
TTR	Transthyretin
VI	Visual impairment
WG	Week of Gestation
AUC	Area under the curve
RHO	Rhodopsin

List of Scientific Publications

Papers related to this doctoral thesis

I. **Trends in proteomic analysis of human vitreous humor samples.**
Ana S. Rocha*, Fátima M. Santos*, João P. Monteiro, João P. Castro-de-Sousa, João A. Queiroz, Cândida T. Tomaz, Luís A. Passarinha;
Electrophoresis, 35(17): 2495–2508, September 2014.

II. **Vitreous humor proteome: unraveling the molecular mechanisms underlying proliferative vitreoretinal diseases.**
Fátima M. Santos, João P. Castro-de-Sousa, Sergio Ciordia, Alberto Paradela, Cândida T. Tomaz, Luís A. Passarinha;
Submitted for publication (2020).

III. **Refinement of two-dimensional electrophoresis for vitreous proteome profiling using an artificial neural network.**
Fátima M. Santos, Tânia Albuquerque, Leonor M. Gaspar, João M. L. Dias, João P. Castro e Sousa, Alberto Paradela, Cândida T. Tomaz, Luís A. Passarinha;
Analytical and Bioanalytical Chemistry, 411(20): 5115-5126, May 2015.

IV. **iTRAQ Quantitative Proteomic Analysis of Vitreous from Patients with Retinal Detachment.**
Fátima M. Santos, Leonor M.Gaspar, Sergio Ciordia, Ana S. Rocha 1,2, João Paulo Castro e Sousa, Alberto Paradela, Luís A. Passarinha, Cândida Teixeira Tomaz;
International Journal of Molecular Sciences, 19(4): 1–22, April 2018.

V. **Differentiating the Vitreous Proteome in Age-Related Macular Degeneration and Diabetic Retinopathy by Label-Free Relative Quantification and Multiple Reaction Monitoring.**
Fátima M. Santos, Sergio Ciordia, Alberto Paradela, João P. Castro-de-Sousa, Carla Cruz, Marta Garcia-Flores, Cândida T. Tomaz, Luís A. Passarinha;
Manuscript in preparation.

*These authors have contributed equally to this work

Papers unrelated to this doctoral thesis

I. **An Improved HPLC Method for Quantification of Metanephrine with Coulometric Detection.**
Augusto Q. Pedro*, RF Soares*, D Oppolzer, Fátima M. Santos, Ana M. Gonçalves, Maria J. Bonifácio, JA Queiroz, E Gallardo, Luís A. Passarinha;
Journal of Chromatography & Separation Techniques. 5(2): 1-7, May 2014.

II. **Trends in Protein-Based Biosensor Assemblies for Drug Screening and Pharmaceutical Kinetic Studies.**
Ana M. Gonçalves*, Augusto Q. Pedro*, Fátima M. Santos*, Luís M. Martins, Cláudio J. Maia, João A. Queiroz, Luís A. Passarinha;
Molecules, 19(8): 12461-12485, August 2014.

III. **Vitreous humor in the pathologic scope: Insights from proteomic approaches.**
João P. Monteiro, Fátima M. Santos, Ana S. Rocha, João P. Castro-de-Sousa, João A. Queiroz, Luís A. Passarinha, Cândida T. Tomaz;
Proteomics - Clinical Applications, 9(1-2): 187-202, December 2014.

IV. **Biosynthesis and purification of histidine-tagged human soluble catechol-O-methyltransferase.**
Augusto Q. Pedro, Filipa F. Correia, Fátima M. Santos, Guilherme Espírito-Santo, Ana M. Gonçalves, Maria J. Bonifácio, João A. Queiroz, Luís A. Passarinha;
Journal of Chemical Technology and Biotechnology, 91(12): 3035-3044, March 2016.

V. **VEGF-B Levels in the Vitreous of Diabetic and Non-Diabetic Patients with Ocular Diseases and Its Correlation with Structural Parameters.**
Joana Mesquita, João P. Castro-de-Sousa, Sara Vaz-Pereira, Arminda Neves, Paulo Tavares-Ratado, Fátima M. Santos, Luís A. Passarinha, Cândida T. Tomaz;
Medical Sciences, 5(3): 1-11, August 2017.

VI. **Proteome analysis of vitreous humor in retinal detachment using two different flow-charts for protein fractionation.**
Leonor M. Gaspar*, Fátima M. Santos*, Tânia Albuquerque, João P. Castro-de-Sousa, Luís A. Passarinha, Cândida T. Tomaz;
Journal Chromatography B, 1061-1062: 334-341, September 2017.

List of Scientific Communications

Oral communications related to the doctoral thesis

I. **Preliminary Studies on Human Vitreous Proteomics.**
João P. Castro-e-Sousa, Ana S. Rocha, Fátima M. Santos, Luís A. Passarinha, Cândida T. Tomaz; *SIRCOVA Intenational Meeting*, Valencia, Espanha, 06/2013.

II. **Ocular Proteomics: characterization of human vitreous humor in retinal diseases**
Fátima M. Santos; *III Jornadas de Bioengenharia*, Universidade da Beira Interior, Covilhã, Portugal, May 2014.

III. **Preliminary results on quantitative proteome analysis of vitreous humor samples using ITRAQ.**
Fátima M. Santos, Ana S Rocha, Sergio Ciordia, João P. Castro-de-Sousa, JA Queiroz, Alberto Paradela, Cândida T. Tomaz, Luís A. Passarinha; *II jornadas de Toxicologia*, Universidade da Beira Interior, Covilhã, Portugal, November 2014.

IV. **iTRAQ quantitative proteomics in analysis of vitreous humor from patients with Retinal Detachment.**
Leonor M. Gaspar, Fátima M. Santos, Sergio Ciordia, Ana S. Rocha, João P. Castro-de-Sousa, Alberto Paradela, Luís A. Passarinha, Cândida T. Tomaz; *XI Annual CICS-UBI Symposium*, Universidade da Beira Interior, Covilhã, Portugal, July 2016.

V. **Improvement of bidimensional electrophoretic experimental conditions for vitreous humor protein analysis using an artificial neural network.**
Fátima M. Santos, Leonor M. Gaspar, Tânia Albuquerque, João P. Castro-de-Sousa, Alberto Paradela, Cândida T. Tomaz, Luís A. Passarinha*; II Congress in Health Sciences Research: Towards Innovation and Entrepreneurship (UBI-HSR): Trends in Biotecnhnology for Biomedical Applications*, Universidade da Beira Interior, Covilhã, Portugal, May 2017.

VI. **Enhancement of bidimensional electrophoretic operation conditions by an artificial neural network for vitreous humor protein analysis.**
Fátima M. Santos, Leonor M. Gaspar, Tânia Albuquerque, João M.L. Dias, João P. Castro-de-Sousa, Alberto Paradela, Cândida T. Tomaz, Luís A. Passarinha; *V International Conference on Analytical Proteomics (ICAP)*, Costa da Caparica, Portugal, July 2017.

VII. **Quantitative analysis of vitreous from patients with retinal detachment using iTRAQ-based proteomics.**
Fátima M. Santos, Leonor M. Gaspar, Sergio Ciordia, Ana S. Rocha, João Paulo Castro e Sousa, Alberto Paradela, Luís A. Passarinha, Cândida Teixeira Tomaz; *XIII Annual CICS-UBI Symposium*, Covilhã, Portugal, July 2018.

VIII. **Development of an artificial neural network for vitreous protein profiling by bidimensional electrophoresis.**
Fátima M. Santos, Leonor M. Gaspar, Tânia Albuquerque, João M.L. Dias, João P. Castro-de-Sousa, Alberto Paradela, Cândida T. Tomaz, Luís A. Passarinha; *38th International Symposium on the Purification of Proteins, Peptides and Polynucleotides (ISPPP)*, Berlin, Germany, November 2018.

Poster communications related to the doctoral thesis

I. **iTRAQ quantitative proteomics in analysis of vitreous humor from patients with retinal detachment.**
Fátima M. Santos, Leonor M. Gaspar, Ana S. Rocha, Sergio Ciordia, João P. Castro-de-Sousa, Alberto Paradela, Luís A. Passarinha, Cândida T. Tomaz; *IV International Conference on Analytical Proteomics (ICAP)*, Costa da Caparica, Portugal, September 2015.

II. **Análise proteómica de amostras de humor vítreo no Descolamento de retina.**
Fátima M. Santos, Leonor M. Gaspar, Tânia Albuquerque, João P. Castro-de-Sousa, Luís A. Passarinha, Cândida T. Tomaz; *V Ciclo de Conferências da Faculdade de Ciências*, Universidade da Beira Interior, Covilhã, Portugal, January 2017.

III. **ITRAQ quantitative analysis of vitreous in Proliferative Diabetic Retinopathy.**

Fátima M. Santos, Leonor M. Gaspar, Sergio Ciordia, João P. Castro-de-Sousa, Alberto Paradela, Luís A. Passarinha, Cândida T. Tomaz; *Dia da Ciência*, Centro de congressos de Lisboa, Lisbon, Portugal, July 2017.

IV. **Enhancement of bidimensional electrophoretic operation conditions by an artificial neural network for vitreous humor protein analysis.**

Fátima M. Santos, Leonor M. Gaspar, Tânia Albuquerque, João M.L. Dias, João P. Castro-de-Sousa, Alberto Paradela, Cândida T. Tomaz, Luís A. Passarinha; *V International Conference on Analytical Proteomics (ICAP)*, Costa da Caparica, Portugal, July 2017.

V. **Proteome of vitreous humor in retinal detachment.**

Fátima M. Santos, Leonor M. Gaspar, Sergio Ciordia, João P. Castro-de-Sousa, Alberto Paradela, Luís A. Passarinha, Cândida T. Tomaz; *XII Annual CICS-UBI Symposium*, Universidade da Beira Interior, Covilhã, Portugal, July 2017.

VI. **Characterization of proteome of vitreous humor in retinal detachment using different experimental setups.**

Fátima M. Santos, Leonor M. Gaspar, Sergio Ciordia, João P. Castro-de-Sousa, Alberto Paradela, Luís A. Passarinha, Cândida T. Tomaz; *16th Human Proteome Organisation World Congress (HUPO)*, Dublin, Ireland, September 2017.

VII. **Improvement of bidimensional electrophoretic conditions for vitreous protein analysis using an artificial neural network.**

Fátima M. Santos, Leonor M. Gaspar, Tânia Albuquerque, João M.L. Dias, João P. Castro-de-Sousa, Alberto Paradela, Cândida T. Tomaz, Luís A. Passarinha; *12th European Symposium on Biochemical Engineering Sciences (ESBES)*, Lisbon, Portugal, September 2018.

VIII. **Vitreous proteome profiling in age-related macular degeneration and diabetic retinopathy.**

Fátima M. Santos, Sergio Ciordia, Alberto Paradela, João P. Castro-de-Sousa, Marta Garcia-Flores, Carla Cruz, Cândida T. Tomaz, Luís A. Passarinha; *XIV Annual CICS-UBI Symposium*, Universidade da Beira Interior, Covilhã, Portugal, July 2019.

IX. **Label-Free Relative Quantification for Vitreous Proteome Profiling In Age-Related Macular Degeneration And Diabetic Retinopathy.**
Fátima M. Santos, Sergio Ciordia, Alberto Paradela, João P. Castro-de-Sousa, Marta Garcia-Flores, Carla Cruz, Cândida T. Tomaz, Luís A. Passarinha; *III International Congress in Health Sciences Research towards innovation and entrepreneurship: Trends in Aging and Cancer*, Universidade da Beira Interior, Covilhã, Portugal, November 2019.

Oral communications unrelated to the doctoral thesis

I. **Recovery of biological active catechol-O-methyltransferase isoforms from Q-Sepharose.**
Filipa F. Correia, Fátima M. Santos, Augusto Q. Pedro, Maria J. Bonifácio, João A. Queiroz, Luís A. Passarinha; *8º Encontro Nacional de Cromatografia*, Universidade da Beira Interior, Covilhã, Portugal, 12/2013.

II. **Advances in the biosynthesis, purification, and characterization of biotechnological products.**
Fátima M. Santos; II Ciclo *de conferências de Biomédicas*, Universidade da Beira Interior, Covilhã, Portugal, November 2016.

III. **Biosynthesis and Purification of recombinant STEAP1 from Komagataella pastoris X33 methanol-induced cultures.**
Diana R. Duarte, Ana M. Gonçalves, Fátima M. Santos, Augusto Q. Pedro, Cláudio J. Maia, Luís A. Passarinha; *XIII Annual CICS-UBI Symposium*, Covilhã, Portugal, July 2018.

IV. **Performance of octyl- and butyl-sepharose on isolation of six transmembrane epithelial antigen of the prostate 1.**
Diogo P. Monteiro, Diana R. Duarte, Fátima M. Santos, Cláudio J. Maia, Luís A. Passarinha; *XIII Annual CICS-UBI Symposium*, Covilhã, Portugal, July 2018.

V. **Performance of traditional hydrophobic ligands on isolation of Six Transmembrane Epithelial Antigen of the Prostate.**
Luís A. Passarinha, Diogo P. Monteiro, Diana R. Duarte, Fátima M. Santos, Cláudio J. Maia; *12th European Symposium on Biochemical Engineering Sciences (ESBES)*, Lisbon, Portugal, September 2018.

Poster communications unrelated to the doctoral thesis

I. **Quantification and comparison of VEGF-B in the vitreous of patients with diabetic ocular disease and a control group of patients with non-diabetic ocular disease.**
Joana Mesquita, João P. Castro-e-Sousa, Ana S. Rocha, Fátima M. Santos, João P. Monteiro, Luís A. Passarinha, Cândida T. Tomaz; *Association for Research in Vision and Ophthalmology congress (ARVO)* 2014, Orlando, Florida, May 2014.

II. **Preliminary results on quantitative proteomic analysis of vitreous humor samples using iTRAQ in retinal inflammatory diseases.**
Ana S. Rocha, Fátima M. Santos, Sergio Ciordia, João P. Castro de Sousa, João A. Queiroz, Alberto Paradela, Luís A. Passarinha, Cândida T. Tomaz; *Semana da Ciência* 2014, Universidade da Beira Interior, Covilhã, Portugal, September 2014.

III. **Comparison of serum and intravitreous PIGF in diabetic retinopathy patients and non-diabetic patients.**
Joana Mesquita, João P. Castro-Sousa, Paulo Tavares-Ratado, Sara Vaz-Pereira, Arminda Neves, Ana S. Rocha, Fátima M. Santos, Luís A. Passarinha, Cândida T. Tomaz; *Association for Research in Vision and Ophthalmology congress (ARVO)* 2015, Denver, Colorado, May 2015.

IV. **Proteomic analysis of the human vitreous humor in retinal detachment.**
Leonor M. Gaspar, Fátima M. Santos, João P. Castro e Sousa, Luís A. Passarinha, Cândida T. Tomaz; *International Conference on Analytical Proteomics (ICAP)* 2015, Costa da Caparica, Portugal, September 2015.

V. **Improvement of two-dimensional gel electrophoresis data for proteomic profiling of Escherichia coli cells**
Andreia G. Amaral, Fátima M. Santos, Leonor M. Gaspar, Mafalda Espírito Santo, João A. Queiroz, Luís A. Passarinha; *XI Annual CICS-UBI Symposium*, Universidade da Beira Interior, Covilhã, Portugal, July 2016.

VI. **Proteomic and metabolomic characterization of pcDNA-FLAG-p53 biosynthesis in Escherichia coli using agro-food nutritive extracts.**
Andreia G. Amaral, Fátima M. Santos, Leonor M. Gaspar, José A. Teixeira, João A. Queiroz, Luís A. Passarinha; *II Congress in Health Sciences Research: Towards Innovation and Entrepreneurship (UBI-HSR): Trends in Biotecnhnology for Biomedical Applications*, Universidade da Beira Interior, Covilhã, Portugal, May 2017.

VII. **Proteomic and metabolomic classification of pcDNA-FLAG-p53 biosynthesis in Escherichia coli using agro-food nutritive extracts.**
Andreia G. Amaral, Fátima M. Santos, Leonor M. Gaspar, José A. Teixeira, João A. Queiroz, Luís A. Passarinha; *V International Conference on Analytical Proteomics (ICAP)*, Costa da Caparica, Portugal, July 2017.

VIII. **A new multiple reaction monitoring method for the assessment of catechol-O-methyltransferase Val/Met108.**
Ana M. Gonçalves, Fátima M. Santos, Joana Diogo, Eugénia Gallardo, Cláudio J. Maia, Luís A. Passarinha; *10º Encontro Nacional de Cromatografia*, Bragança, Portugal, December 2017.

IX. **Design of a chromatographic strategy for STEAP1 isolation using octyl-sepharose.**
Diogo P. Monteiro, Diana R. Duarte, Fátima M. Santos, Cláudio J. Maia, Luís A. Passarinha; *10º Encontro Nacional de Cromatografia*, Bragança, Portugal, December 2017.

X. **Evaluation of glycerol feeding profiles onto glycosylation patterns of recombinant STEAP1 biosynthesized in Pichia pastoris X33.**
Diana R. Duarte, Ana M. Gonçalves, Fátima M. Santos, Augusto Q. Pedro, Cláudio J. Maia, Luís A. Passarinha; *From protein structure to biological function through interactomics: an integrated view*, Biocant, Cantanhede, Portugal, February 2018.

XI. **Proteome profiling of human LNCaP prostate cancer cells upon STEAP1-knockdown.**
Sandra M. Rocha, Fátima M. Santos, Luís A. Passarinha, Sílvia Socorro, Cláudio J. Maia; *XIV Annual CICS-UBI Symposium*, Universidade da Beira Interior, Covilhã, Portugal, July 2019.

XII. **Proteomic analysis of human prostate cancer LNCaP cells upon STEAP1 knockdown.**

Sandra M. Rocha, Fátima M. Santos, Luís A. Passarinha, Sílvia Socorro, Cláudio J. Maia*; III International Congress in Health Sciences Research towards innovation and entrepreneurship: Trends in Aging and Cancer*, Universidade da Beira Interior, Covilhã, Portugal, November 2019.

XIII. **Use of Near-Infrared Spectroscopy (FT-NIR) to assess seed viability and varietal discrimination – Pisum sativum as a case study.**

Lénia Rodrigues, Hélia Cardoso, Fátima Santos, Amaia Nogales, Steven Groot, Lee Hansen, Julio Nogales-Bueno, Ana Elisa Rato; *LIVESEED Annual Project Meeting*, online, May 2020.

XIV. **Calorespirometry – a phenotyping tool to assess pea germination efficiency under different temperatures.**

Lénia Rodrigues, Amaia Nogales, Lee Hansen, Fátima Santos, Steven Groot, Ana Elisa Rato, Hélia Cardoso; *LIVESEED Annual Project Meeting*, online, May 2020.

Chapter 1

Section 1 - Introduction

1. Vitreous humor

The eye is a remarkable and complex organ, capable of transducing photons into neural signals with high efficiency [1]. The eye is capable of constantly adjusting the light reaching the retina to focus on near and far objects and it is responsible for about 38 to 40% of the total sensory input to the brain [2]. The human eye is a globe-shaped structure that is allocated into the eye socket and protected by eyelids, fat, and the walls of the skeletal orbit. As seen in Figure 1, it is composed of three concentric layers; (A) outer layer, (B) middle layer, and (C) inner layer [3].

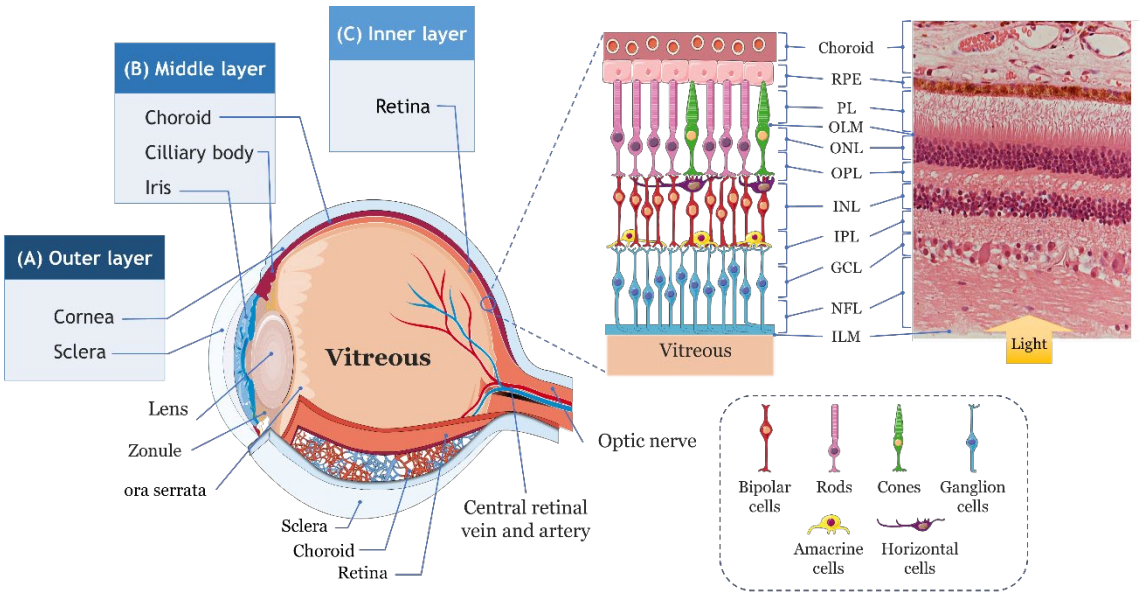

Figure 1– Schematic illustration of the structure and anatomy of the eye, representing the three layers: (A) outer, (B) middle, and (C) inner. The choroid and retinal layers are represented in detail in the schematic illustration and histological image. Light rays penetrate the eye and are converged at the cornea and the lens into the retina. These rays pass through the outer limiting membrane (OLM), nerve fiber layer (NFL), ganglion cell layer (GLC), the synaptic connection (IPL, inner plexiform layer) between these and bipolar cells in the inner nuclear layer (INL), and finally by the synaptic connection bipolar cells and photoreceptors (OPL, Outer Plexiform Layer). The rays that diverged back to the retinal pigment epithelium (RPE), which is the outermost retinal layer firmly attached to the choroid layer, are reflected back to rods and cones (PL, photoreceptor layer; ONL, Outer Nuclear Layer; OLM, Outer limiting membrane). Adapted from [3–5].

The outer layer is the protective layer of the eye and consists of the cornea and the sclera. The sclera is a dense and white connective tissue coat, composed of almost entirely of collagen, that protects the eye from internal and external forces and maintains its shape [3, 5]. The cornea is a transparent structure that covers the anterior chamber, protects the eye against infection and structural damage, and refracts and transmits two-third of the focusing of light to the retina [3, 6]. The other one-third of the light is focused by the

lens, a biconvex, avascular, and almost completely transparent structure located behind the iris [5, 6]. The middle or vascular layer is formed by the uvea composed of iris, choroid, and ciliary body. The iris controls the amount of light reaching the retina by adjusting the size of the pupil, while the ciliary body controls the power and shape of the lens allowing the focus to be adjusted for different visual distances (visual accommodation) [3]. The choroid is a vascular posterior segment of the uveal tract, localized between the Bruch's membrane and the sclera, which provides oxygen and nutrients to the outer retinal layers [3, 5]. The inner layer consists of the retina, a thin and complex nerve tissue whose function is to capture and process light [3]. The neural retina consists of photoreceptors, bipolar, horizontal, amacrine, and ganglion cells, which capture and process light signals, the retinal pigment epithelium that nourishes retinal layers. The retina is also composed of Müller glia that acts as the organizational backbone of the neural retina and microglia, resident immune cells that are constantly surveying the surrounding neural tissue. The cells of the neural retina are arranged in several parallel layers, as shown in Figure 1 [3–5]. Two types of photoreceptors are responsible for phototransduction: cones and rods, which are approximately 20 times more abundant. Cones, which are responsible for color vision, contain pigments with absorption peaks in the blue, green, or yellow parts of the spectrum, while rods have pigments with an absorption peak in the blue-green. The density of rods and cones varies between different regions of the retina, but the density of cones is higher in the macula, reaching maximum levels in the fovea, the thinnest zone of the retina that contains only cone photoreceptors, allowing a sharp central vision [3].

The eye is also composed of two fluids, the aqueous humor, and vitreous humor. The aqueous humor is produced by the ciliary body, and it flows into and fills a small region anterior to the lens but behind the iris, known as the posterior chamber [3]. Aqueous humor stabilizes and ensures the accurate positioning of the optical elements of the eye, supplies nutrients, and removes waste products from the avascular lens and the central cornea [1, 5]. Vitreous, also termed vitreous body or vitreous humor, is a transparent fluid that fills the posterior cavity of the eye. In the adult human eye, vitreous have approximately 16.5 mm of axial length and has a volume of about 4.5 ml, occupying more than two-thirds of the intraocular volume, and it is surrounded by the neurosensorial retina, pars plana, and lens [7–10]. Vitreous is highly hydrated, avascular, and virtually acellular, consisting of a network of collagen fibrils surrounded by glycosaminoglycans (GAGs), inorganic salts, sugars, lipids, and soluble proteins [9, 11]. The nature of vitreous humor is not consensual; some authors refer that vitreous is an extracellular matrix (ECM), others consider that it is a specialized, but simple, type of connective tissue [9]. The two concepts are not yet reconciled but vitreous share similar characteristics to

connective tissue [12, 13]. Compared with other connective tissues, the vitreous contains fewer cells, which are confined to the vitreous cortex.

1.1 Embryology of vitreous

The formation of vascularized primary vitreous is evidenced at 3-4 weeks of gestation (WG). Space resultant from the separation of neural ectoderm from the surface ectoderm is filled with a fibrillar material, believed to be of collagenous nature. At this phase, vitreous is considered an extension of the hyaloid vascular system and is composed of ectodermal and mesodermal-derived cells (Figure 2) [14–17]. The primary vitreous develops along with the hyaloid vasculature and fibrillar components are produced by neuroectodermal and surface ectodermal cells, which will originate the neurosensory retina and lens, respectively [14, 15, 17].

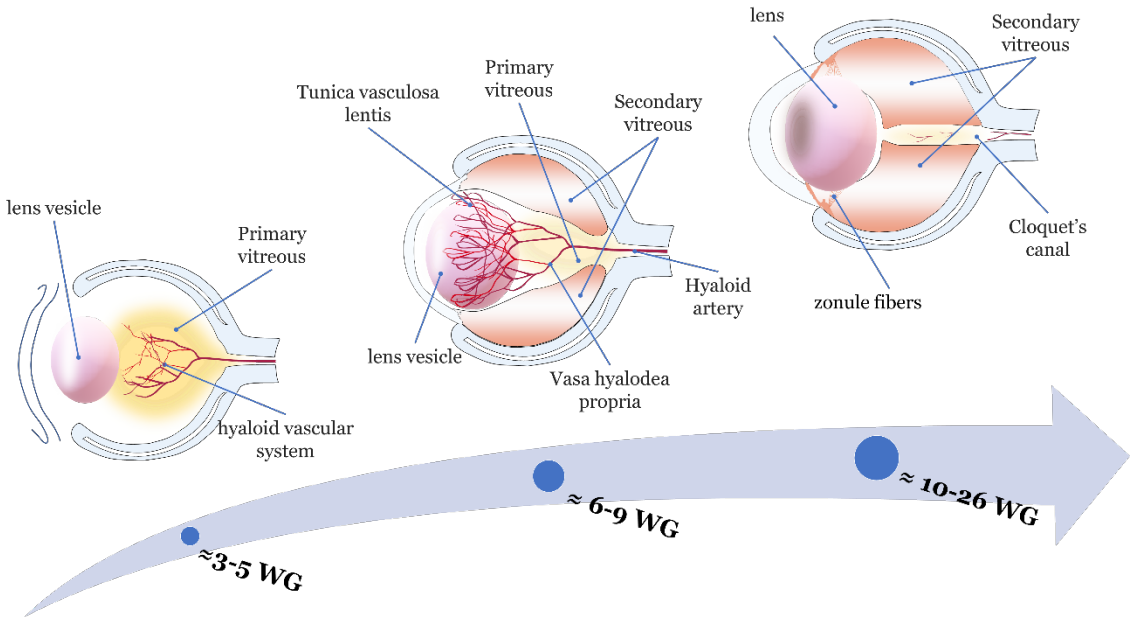

Figure 2 – Stages of vitreous humor development. The primary vitreous is formed after the 3rd-4th week of gestation (WG). By the 7 WG, the secondary vitreous is already developed, surrounding the primary vitreous in the embryonic eye. In the final phase, hyaloid vasculature and primary vitreous begins to atrophy progressively, evidencing the formation of the Cloquet's canal.

The secondary vitreous is an acellular and avascular material derived from neural crest cells and is formed between 6 and 13 WG. As the secondary vitreous increases in volume, the primary vitreous is pushed into a more central position in the embryonic eye (Figure 2). Around the 9 WG, primary vitreous ceased its grown, and the hyaloid system reaches its maximum development. As seen in Figure 2, hyaloid vasculature and primary vitreous begins to atrophy progressively, approximately 13–26 WG, evidencing the formation of the Cloquet's canal [16, 18]. In the final period of vitreous development, the blood flow in the hyaloid artery ceases, followed by regression of hyaloid vasculature and primary

vitreous, which is completed at around 35-36 WG [14, 17, 18]. The secondary vitreous acquires similar characteristics of the fully developed vitreous. The human vitreous is highly active during the embryological period, resulting in an avascular and transparent matrix at birth [16]. For a short postnatal period, liquid vitreous is produced to fill the eyeball as it develops, doubling its volume from development until adulthood.

1.2 Vitreous structure and biochemistry

Vitreous is essentially composed of water (98-99%), and its gel structure is maintained by a tridimensional network composed mainly of unbranching collagen fibrils and hyaluronic acid [19, 20]. The macromolecular composition and the viscosity of vitreous samples depend on the anatomical region, the age of the patient, the state of the lens, and the presence of a pathological state [7, 21, 22]. Changes in the supramolecular organization and the physiology of the vitreous are closely associated with changes in the concentration, distribution, and interaction of collagen and GAGs [23]. As seen in Figure 3, the vitreous is non-uniform and is mainly composed of three different anatomical regions: (A) the vitreous base, (B) the core or central vitreous, and (C) the vitreous cortex [7, 11, 24, 25]. Some authors also consider the intermediate vitreous, localized between the cortex and core vitreous [16], ciliary zonules (embryologically classified as the tertiary vitreous) [7], and anterior hyaloid [25, 26], a thin layer that extends from the pars plana to the posterior lens [27].

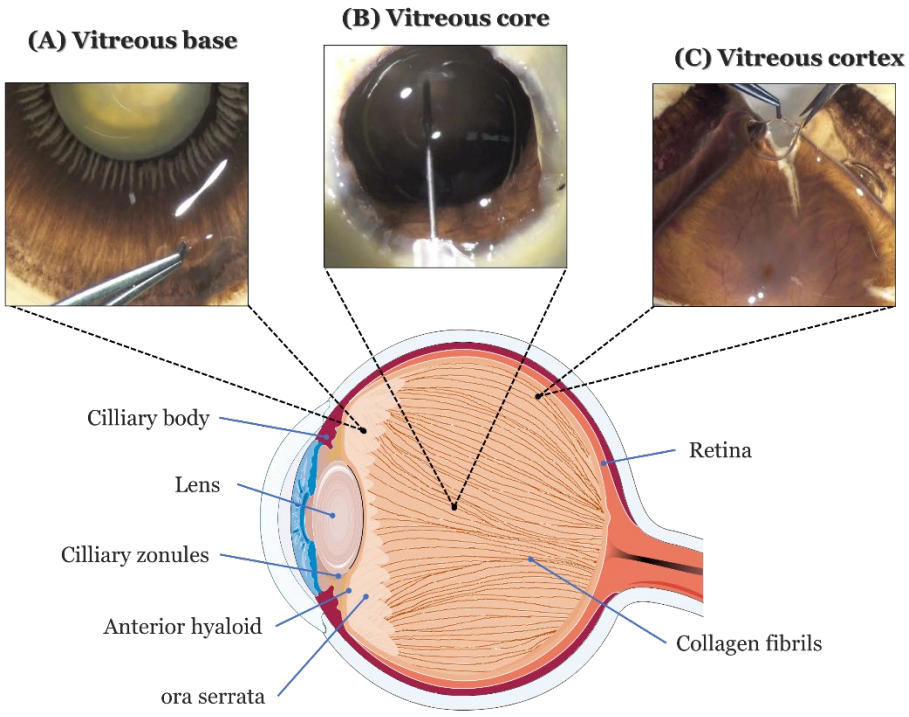

Figure 3 – Vitreous anatomical regions and the distribution of collagen fibrils. Adapted from [7, 25].

The vitreous core is the bulk of vitreous and is the substructure that is collected by pars plana vitrectomy [7, 11, 25]. The vitreous core contains lower concentrations of collagen fibrils that are aligned in an anterior-posterior direction, inserting into the vitreous base anteriorly and the vitreous cortex posteriorly (Figure 3) [7, 11, 28]. These fibers are continuous, being that peripheral fibers are circumferential with the vitreous cortex, while central fibers undulate parallel to Cloquet's canal [10]. The anterior vitreous cortex extends from the anterior vitreous base to the posterior surface of the lens, while the posterior vitreous cortex is adherent to the inner surface of the retina [10, 11, 28]. The vitreous cortex is absent on the optic disk and is thinner on the macula [7, 11, 28]. The vitreous base is a three-dimensional annular zone composed of dense bundles of collagen fibrils that adhere firmly to the retina and the non-pigmented ciliary epithelium [7, 16, 28]. The higher collagen concentration and the orientation perpendicular to the retina result in strong vitreoretinal adhesion at the vitreous base [11, 29].

The overall protein concentration in human vitreous ranges between 0.5 mg/mL to 1.2 mg/mL, [23, 30, 31], with albumin representing about 80% of the soluble content [22, 32]. Soluble proteins as albumin, transferrin, immunoglobulin G, and alpha 1-antitrypsin were reported as highly abundant in the human vitreous [33]. Collagens are insoluble and fibrous proteins that provide mechanical strength to vitreous but can be involved in other processes, such as regulation of cell adhesion, chemotaxis and migration, and tissue development [7, 23]. Collagen is present within the vitreous at low concentrations (approximately 300 μg/ml) but this concentration is higher at the vitreous base and lower at the vitreous core [11, 20]. In vitreous, most of the collagen is arranged in thin, uniform, and heterotypic fibrils containing collagen types II, IX and, V/XI [11, 34]. Collagen type II and type IX accounts for 60–75% and 25% of all the collagen in the vitreous, respectively [11]. The collagen structure of vitreous is surrounded by GAGs, linear polymers composed of repeating disaccharide units. All GAGs in vitreous are proteoglycans, except hyaluronan (HA), which is not attached to a protein core [11, 35]. The HA is abundant in vitreous and fills the spaces between the collagen fibrils. The HA inflates and stabilizes the collagen network through interacting with collagen, providing hydration and spacing to the vitreous matrix, decreasing light scattering, and enhancing vitreous transparency [20, 23]. The viscosity, high solubility, and hydrophilicity of HA render to vitreous its viscous and viscoelastic properties [35]. Like collagen, HA is not uniformly distributed within vitreous, with concentrations ranging between 65 and 400 μg/ml, and with higher concentrations being found in posterior cortical vitreous [11, 16, 20]. Besides HA, other GAGs, such as chondroitin sulfate proteoglycans (e.g. versican and type IX collagen) and heparan sulfate

proteoglycans (e.g. agrin), non-collagenous structural components (e.g. fibrillins and fibulins), and glycoproteins, such as opticin (OPTC) are present in vitreous [7, 11, 16, 23]. Although the specific function of these structural components is not fully elucidated, it is known that they play a significant role in maintaining the vitreous matrix structure and vitreoretinal interface [16].

For many decades, the source of vitreous proteins was the subject of some speculation, but recently it was shown that they can be synthesized by distinct types of cells depending on the developmental stage [36]. The concentration of vitreous proteins has a peak in the embryonic phase but its synthesis declines during late embryonic and early postnatal stages [36–38]. The majority of vitreous components has origin in the ciliary body, with a small contribution of the inner retina, optic disc, and lens [16, 37, 38]. Hyalocytes, ciliary body, and retina, specifically the human retinal Müller cells, seem to be responsible for the postnatal synthesis of vitreous collagen [16, 39]. Although most of the components of vitreous have an embryonic origin, many proteins may be synthesized elsewhere before being accumulated into vitreous from the vasculature and other adjacent tissues [37, 38, 40]. A considerable proportion of vitreous proteins is derived from plasma, but vitreous proteome is substantially different from the plasma proteome [31]. Besides plasmatic and structural proteins, vitreous is composed of inflammatory mediators, angiogenic and anti-angiogenic factors, glycolysis and gluconeogenesis proteins, anti-oxidant proteins, among others, which means that vitreous function is more than merely structural [25, 41–43].

1.3 Function

Despite its pivotal localization in the eye, vitreous was never regarded as possessing critical active functions [44]. Although some of the vitreous physiological functions remain unclear, vitreous contributes to the total transparency of the ocular pathways, regulates eye growth and shape during development, serves as a barrier to biomolecules and cells, and allows the repository and diffusion of the substances involved in the eye metabolism [9, 11, 45, 46]. More recently, vitreous has been associated with the regulation and distribution of oxygen within the eye in an ascorbate-dependent manner [47]. Shui and colleagues show that the high concentration of ascorbate available in vitreous metabolizes molecular oxygen, decreasing lens exposure to oxygen, and protecting it from oxidative damage [48]. In this environment, vitreous oxygenates highly vascularized tissues, such as the retina or ciliary body, while protecting neighboring tissues sensitive to oxidative stress, including the lens and trabecular meshwork [20]. It was also suggested that the vitreous humor plays a minor role in the

regulation of intraocular pressure [9]. Other studies indicate that vitreous has an anti-angiogenic nature and is capable of inhibiting neovascularization in physiological conditions [49–52]. In the mammalian eye, vessels are normally excluded from the cornea and vitreous, which have shown to have anti-angiogenic properties [53]. Pigment epithelium-derived factor (PEDF) [53–55], OPTC [56], thombospondins [56, 57] are some of the anti-angiogenic proteins found in vitreous. Even its physiological roles are incompletely understood, it is consensual that vitreous is essential for ocular health. Aging-related changes, such as vitreous liquefaction and posterior vitreous detachment (PVD), may be underlying in the onset and progression of several vitreoretinal diseases, including retinal detachment (RD), cystoid macular edema, macular hole (MH) formation, age-related Macular Degeneration (AMD), and proliferative diabetic retinopathy (PDR) [11, 16, 20, 47, 58]. Therefore, it not surprising that the peak incidence of retinal conditions matches the peak age of incidence of PVD [47].

2. Ocular diseases and the Precision Health Era

2.1 Visual impairment and blindness in the world population

Visual impairment (VI) and blindness cause a significant social-economic burden in modern society. Besides the economic costs, ocular diseases largely affect the quality of life of the patients by interfering with their daily activities, reduce economic and educational opportunities, and increasing the risk of death [59, 60]. In 2015, it was estimated that about 36 million people were blind, 217 million had moderate or severe visual impairment (MSVI), and 188.5 million had mild vision impairment [60, 61]. Globally, the prevalence of VI was higher in people older than 50 years and women and more pronounced in some developing regions from western sub-Saharan Africa, eastern sub-Saharan Africa, and South Asia [60, 62]. Notwithstanding, the global prevalence of blindness and MSVI were reduced in people with more than 50 years, while the greatest changes were visible in African and southern Asian regions [63]. Whereas the incidence and prevalence of VI and blindness are decreasing, the number of people affected is increasing [60, 61, 63]. The reduction in age-specific prevalence, socioeconomic development, targeted public health programs, and improved access to eye health services explain the decline of the prevalence, while the aging and growth of the world population lead to an increase in the number of people affected by VI [60, 62]. In 2015, uncorrected refractive error and cataract were the main causes of MSVI and blindness among the global and the European populations (Figure 4) [61, 64]. Over the last two decades, the prevalence of uncorrected refractive error remained unchanged, while cataract prevalence was significantly reduced [63]. While VI caused by uncorrected

presbyopia is more concerning in rural areas of low-resource countries [65], pathologies such as AMD, glaucoma, and diabetic retinopathy (DR) have emerged as priority eye diseases in middle-income and industrialized countries. The prevalence of MSVI due to these pathologies in developed countries is increasing, although there was a small decrease in blindness [61, 63].

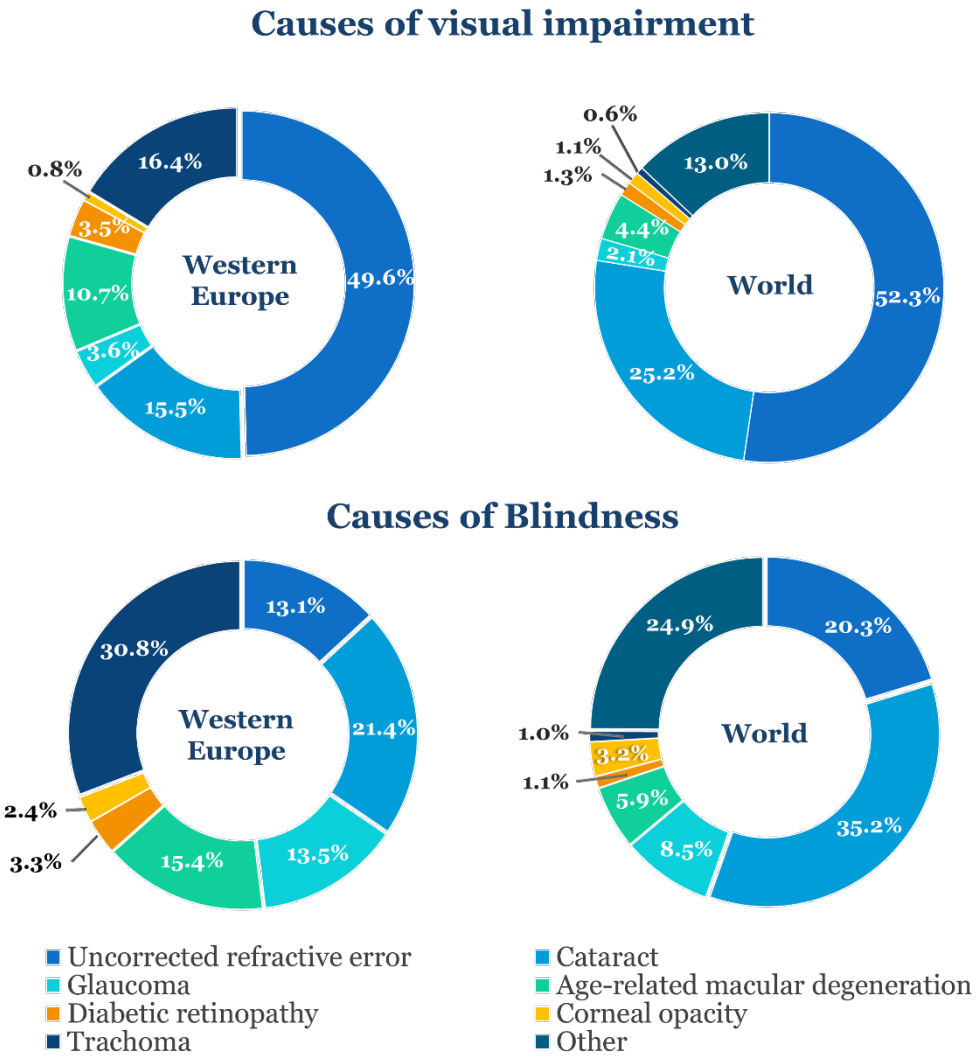

Figure 4 - Causes of visual impairment and blindness among adults aged 50 years and older in the world and the European population in 2015. Adapted from [61].

The World Health Organization estimates that 80% of VI is either preventable or curable with proper management and treatment [42]. Pathologies such as cataracts cannot be prevented, but the surgery is cost-effective, resulting in almost immediate visual rehabilitation. However, the proportion of preventable or treatable blindness is projected to decrease to 80.8% in 2020 [61], as a result of the increase of the number of people with potentially blinding conditions, such as glaucoma, AMD, and DR [42]. Despite the

multiple treatment options, including anti-angiogenic drugs, topical medications, surgery, and laser photocoagulation, some of these patients still progress to VI and blindness [66]. Therefore, it is necessary to globally strengthen the health care system, especially in low-income countries. It is necessary to promote universal and equitable access to eye care services, manage the risk factors (e.g. hyperglycemia and hypertension) for the development of eye diseases, and help to rehabilitate patients when these conditions cannot be treated [63, 67, 68]. Furthermore, the reinforcement of the investment in the research could improve the collection and analysis of epidemiologic data and its integration in health information systems and develop innovative solutions to assist in the diagnosis, treatment, and prevention of chronic eye diseases [62, 68].

2.2 Proteomics in ophthalmic research

Multi-omics approaches are revolutionizing the field of healthcare by shifting the paradigm of integrating multiple biomarkers for disease diagnosis and progression, for discovering new therapeutic targets, and for assessing the efficacy and safety of current and new treatments [69–72]. The Human Genome Project has opened new doors for exploring the vastness and complexity of biological systems [73–76]. For most of the complete genome, it was discovered that the function of the proteins remains largely unknown [74]. Therefore, proteomics was established as a post-genomics field, focusing on the understanding of biological systems through the study of proteins [77–79]. In 1994, Marc R. Wilkins defined the concept of proteome for the first time, as the set of proteins expressed by a genome, cell, or tissue at a given time and under specific physiological or pathological conditions [73]. The proteome is highly complex and dynamic as it continuously adjusts in response to external or internal stimuli, resulting in a balance between synthesis and degradation, protein modifications (e.g. cleavages, post-translational modifications [PTMs]), interaction with other biomolecules, among other biological processes [80, 81]. Although the human genome consists of approximately 20 to 300 protein-coding genes, it is estimated that more than 100 proteoforms can be produced from a single gene, encompassing all the genetic variants, including polymorphisms, alternative splicing, and PTMs [75, 78, 82–84]. The study of the human proteome is also hampered by its wide dynamic range of protein concentration, ranging from 7 orders of magnitude in cells to 12 orders in more complex proteomes, such as human plasma [75, 78, 83, 85]. Nevertheless, the development of new technologies for peptide/protein separation and labeling methods for relative and absolute quantification and improvements in mass spectrometers and bioinformatics platforms helped to overcome some of these difficulties, contributing to the rapid growth of proteomics in many biological fields [72, 75, 86].

Likewise, ocular proteomics has emerged as an opportunity for discovering new biomarkers, which could help to unveil the pathophysiology of many ocular diseases and anticipate their progressive states [66, 87]. The Human Eye Proteome Project (Eyeome), created in 2013 under the leadership of Professor Richard Semba, recently reported the identification of 9782 non-redundant proteins in various eye tissues and biofluids, as shown in Figure 5 [42]. Even using more restricted criteria for the selection of the studies, this represents an increase of more than 2-fold compared to the number of identified proteins in 2013 [42, 66]. Indeed, the proteome of the iris, ciliary body, optic nerve, and sclera was largely uncharacterized before 2013 [42]. Among the characterized ocular matrices, there has been a growing interest in the vitreous proteome in recent years. It is reinforced by the fact that the number of proteins identified in vitreous increased from 545 to 6538 in only 5 years (Figure 5) [42, 66]. Therefore, although vitreous has been unappreciated for a long time concerning its role in health and disease [8, 45], proteomics studies proved that vitreous is complex and more biologically active than initially thought [25, 42].

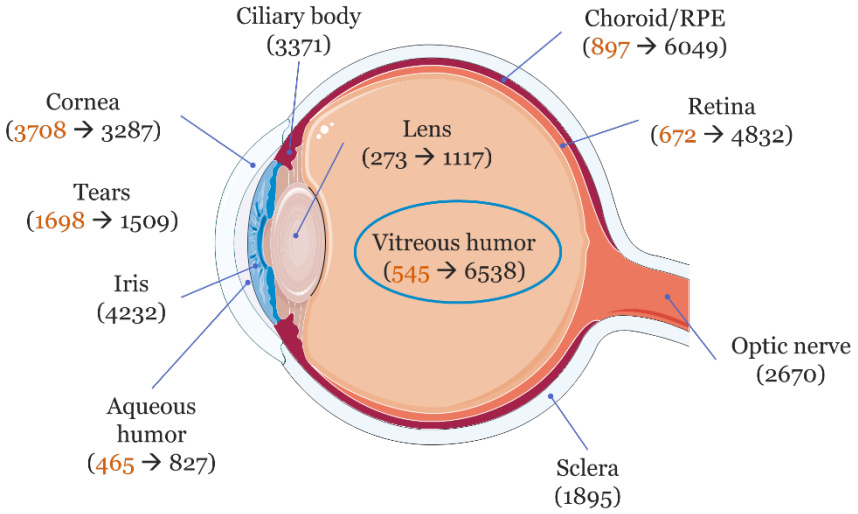

Figure 5 – Schematic diagram of the human eye representing the number of non-redundant proteins identified in eye tissues and biofluids, as reviewed in 2018 [42] and 2013 [66] (colored at orange). The decreasing of the number of identified proteins in some tissues is related to more restricted criteria used for the selection of identified proteins.

Several reasons demonstrate that vitreous is very attractive to biological and analytical perspectives. From an analytical point of view, vitreous is more easily obtained compared to other ocular matrices, such as retina [88]. Vitreous can be removed without marked detriment to the eye by pars plana vitrectomy or vitreous biopsies as part of the clinical routine [22]. Pars plana vitrectomy is commonly performed for several ocular conditions, including RD, proliferative vitreoretinopathy, ocular trauma, MH, vitreous hemorrhage, and epiretinal membranes (ERM), among others [89, 90]. Of course, the collection of

vitreous is restricted to patients suffering from these conditions, and therefore, obtaining samples from healthy eyes to serve as controls in proteomics studies is not possible for ethical reasons [22, 41, 66]. As a result, vitreous collected from healthy human eyes from biobanks [91–93] or patients with ERM or MH [31, 66, 93] have been used as control samples. Although are likely that vitreous changes occur at these conditions [88, 91, 93], the eye is less affected by severe pathological changes, such as neovascularization, inflammation, and/or ischemia [94]. From a biological perspective, vitreous has a pivotal localization in the eye, close to the inner retina, lens, and ciliary body. Therefore, some vitreous proteins have origin in these ocular tissues, but a considerable fraction seems to be synthesized elsewhere before being trafficked to the vitreous [22, 92, 95, 96]. Consequently, the proteome and biochemical properties of vitreous seems to be affected by the physiological and pathological conditions of the eye [22, 41]. Considering that vitreous changes reflect the state of the retina, it has been suggested the vitreous collection could be used as an indirect method for molecular biopsy of the retina [25, 97, 98]. Furthermore, abnormal mechanical traction of the vitreous on the neurosensory retina may be the underlying several vitreoretinal diseases, including RD, ERM, MH, AMD, proliferative vitreoretinopathy (PVR), and PDR [21, 95, 99]. Therefore, the study of vitreous proteome has been a means of indirectly exploring the biological events taking place in the eye in many vitreoretinal diseases [41, 95, 96]. Proteomics studies have the potential to provide specific biomarkers, molecules capable of correlating with the onset and progression of vitreoretinal diseases, and with the response to therapy [41, 88]. Although many advances have been made towards this goal, the demand for suitable vitreous biomarkers in ocular disease has not been completely successful so far [22].

3. Proteomics of human vitreous humor

Recent advances in proteomics technology improve the identification and quantitation of proteins in samples with reduced availability of protein volume and quantity [75, 100], a common challenge in the analysis of ocular fluids, such as vitreous [101, 102]. Generally, the experimental workflow applied for vitreous proteomics consists of (i) sample collection and preparation, (ii) sample fractionation (protein or peptide level), (iii) peptide/protein analysis by MS or other techniques, and (iv) bioinformatics and statistical analysis [72, 75, 85, 103, 104]. Figure 6 reviews the pipeline of proteomics strategies applied to vitreous, while its advantages and drawbacks are summarized in Table 1 of Paper I.

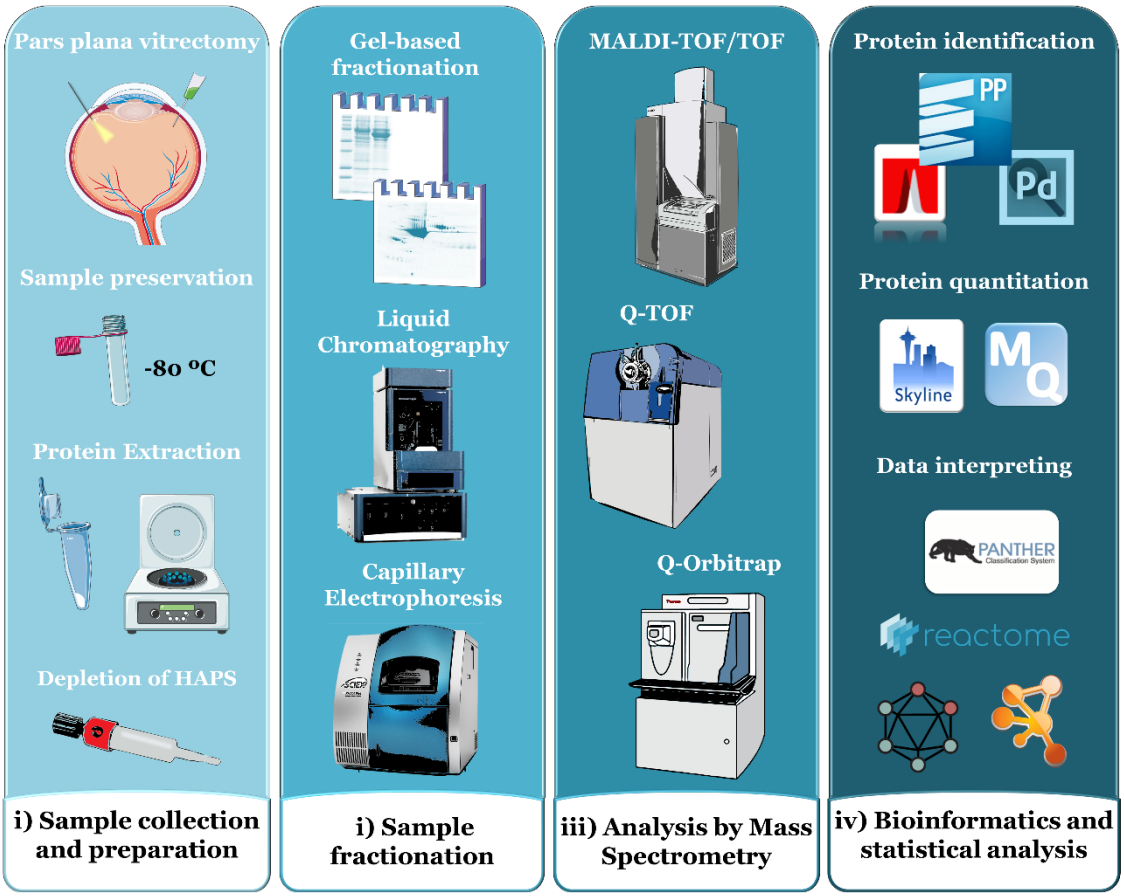

Figure 6 – General proteomic workflow applied for vitreous proteome analysis. The proteomics strategies represented in the figure are overview in section 3. HAPs – High-abundant proteins, MALDI-TOF/TOF – Matrix-Assisted Laser Desorption/Ionization with tandem Time Of Flight, Q – Quadrupole, Q-TOF – Quadrupole - Time Of Flight mass spectrometry.

In recent years, many researchers have contributed to the characterization of the human vitreous proteome using different experimental set-ups [21, 25, 31, 40, 92, 97, 105–108]. The main focus of vitreous humor proteomics has been the measurement of protein expression, which allows finding quantitative differences in protein profiles between distinct vitreoretinal diseases. Vitreous proteome was characterized in pathologies, including DR [91, 109–121], diabetic macular edema [122–124], AMD [125–127], glaucoma [128], RD [129], PVR [130–133], among others [134–142]. Paper II summarizes some of the results obtained in these studies but it is mainly focused on the vitreous proteome in PDR, PVR, and neovascular AMD (nAMD), the main pathologies studied in this thesis. This review highlights potential disease biomarkers and provides some insights into the role of vitreous proteins in eye physiology and on the pathogenesis of these pathologies.

Mass Spectrometry (MS) has been the technique of choice for the identification and quantitation of proteins on a large scale, as a result of the development of soft ionization methods [143–145]. The sample is introduced in MS instruments via ion source and, the

produced ions are separated according to their mass to charge ratio (m/z) in the mass analyzer under vacuum, and measured by the detector [143, 146, 147]. In tandem mass spectrometry (MS/MS or MS2), the peptide ion to be analyzed is first selectively isolated and fragmented to obtain an MS^2 spectrum [72, 143]. Matrix-assisted laser desorption/ionization (MALDI) and electrospray ionization (ESI) are the ionization techniques most used for proteins or peptides [75, 144, 146]. In MALDI, the analyte is mixed with an organic matrix (usually alpha-cyano-hydroxycinnamic acid (CHCA) is used for peptides) to form crystals, which are pulsed with a laser (typically a nitrogen laser at 337 nm) to produce single charged peptide ions (1+). In an ESI source, analytes flow through a needle subjected to high voltages (1-6 kV) and temperatures (40–100°C), which leads to a formation of highly charged drops that dissociate into multi charged peptide ions (2^+, 3^+, and 4^+) due to electrostatic repulsion [72, 144, 147]. While ESI is coupled directly to liquid-based separation tools, such as liquid chromatography (LC) or capillary electrophoresis (CE), MALDI is usually combined with a gel-based separation [75, 146]. Although proteomics was initially driven by the development of these soft techniques, it is now possible to identify thousands of proteins in complex biological samples based on improvements made to the mass analyzer, increasing the resolution, mass accuracy, sensitivity, and scan rate of mass spectrometers [75, 146, 148]. Mass analyzers include Time-of-flight (TOF) [1], Quadrupole (Q)[2], Ion Trap (IT)[3], and orbitrap[4] [72, 146, 147].

Nowadays, a wide range of instrument configurations is available, which can be combined to take advantage of its strengths and to fit different purposes (Figure 7) [81, 104, 146]. MALDI is usually coupled to TOF (MALDI-TOF) or tandem TOF (MALDI-TOF/TOF) for the identification of simpler protein mixtures [146]. ESI has been coupled to IT, quadrupoles, and, lately, to Q-TOF or Q-orbitrap and it is widely applied for discovery proteomics or shotgun proteomics employing data-dependent acquisition (DDA) [81, 146]. In DDA, MS equipment scans all the parent ions that co-elute at a specific retention time (RT) in the chromatographic separation (precursor-ion spectra, MS^1) and selects the most abundant ions for fragmentation. The instrument alternates

[1] TOF consists of a flight tube, where ions are accelerated in a strong electrical field with equal energies but reach different velocities, which are inversely proportional to their m/z.
[2] Quadrupole consist of four cylindrical rods, where ions are separated based on the stability of their trajectories in the oscillating electric fields that are applied to the rods.
[3] In Ion-Trap analyzers, the ions at specific m/z are captured ("trapped") in an oscillating electrical field for a certain amount of time, and then subject MS and MS/MS analysis.
[4] In Orbitrap, ions are "trapped" under high vacuum in a high magnetic field, and the m/z is inversely proportional to the frequency of the oscillation.

between a full-scan acquisition and the acquisition of fragment-ion spectra, in which precursors are sequentially isolated and fragmented (at the MS^2 level) [75, 81, 149].

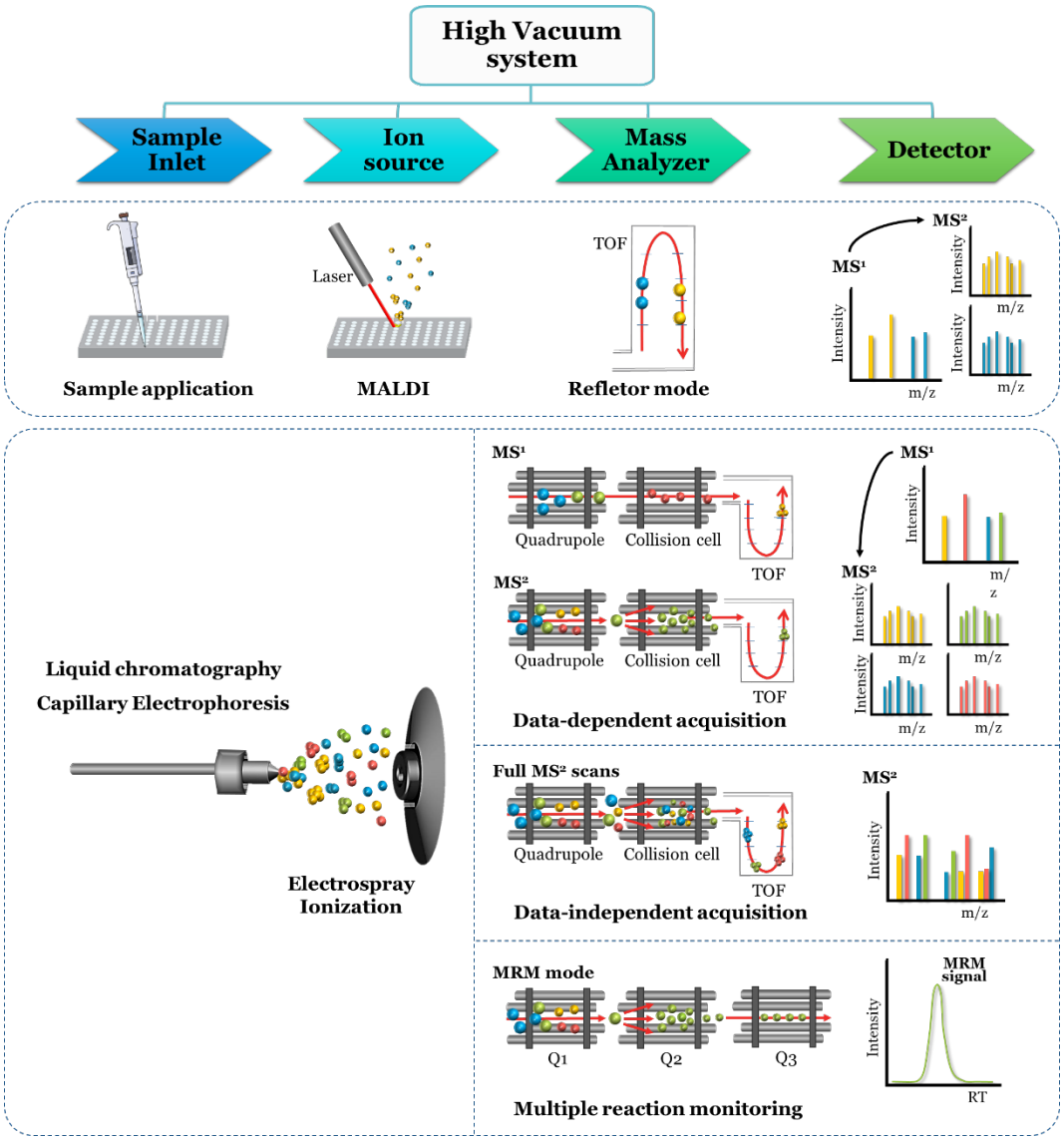

Figure 7 – Representative scheme of the main components of a mass spectrometer and instrument configurations commonly used in each acquisition method. m/z – mass/charge, MALDI – Matrix-Assisted Laser Desorption/Ionization; Q – Quadrupole, RT – retention time, TOF – Time Of Flight.

Triple quadrupole instruments are widely used for targeted proteomics using selected reaction monitoring (SRM) or multiple reaction monitoring (MRM). In this approach, proteotypic peptides of a target protein are selectively and recursively isolated (Q1) and fragmented (Q2) over their RT, whereas the specific fragments are selected in Q3 and detected. MRM offers improved specificity, reproducibility, and accuracy to peptide/protein quantification by allowing multiple and highly specific transitions to be selected per peptide [81, 100, 150]. Alternatively, high-resolution instruments, such as quadrupole orbitraps, are used for parallel reaction monitoring, a targeted proteomics

analysis where all fragment ions of a target peptide are simultaneously monitored [81, 151]. More recently, data-independent acquisition (DIA) was introduced as an alternative to DDA. In DIA methods (e.g. SWATH), entire ranges of precursors are fragmented at the same time, without a pre-selection of the precursor ions, thus leading to an unbiased fragmentation of the entire set of peptide precursors of a specific sample [81, 149]. This method eliminates some of the constraints of DDA, such as missing of low abundant proteins (undersampling), but protein identification is very challenging. The link between the intact peptide and its peptide fragmentation information is retrieved based on previously acquired DDA-based single-peptide fragmentation spectra or by searching on the database generated by 'pseudo' fragment-ion spectra obtained directly from the DIA data [81, 149].

At last, peptide identification is achieved after the MS analysis by comparing the MS (MS^1) spectra derived from peptide fragmentation (MS^2) with theoretical tandem mass spectra generated from in silico digestion of a protein database [75, 143]. Algorithms, such as Andromeda, SEQUEST, Mascot, or ProteinProphet, have been developed to search raw MS data against protein databases. National Center for Biotechnology Information (NCBI), European Bioinformatics Institute (EMBL-EBI), and Swiss Institute of Bioinformatics (SIB) are some of the entities that provide freely available databases like SWISS-PROT [72, 86, 148]. Considering the massive amounts of data that are generated by MS analysis, multiple bioinformatics tools have been developed for protein identification and quantitation (e.g. MaxQuant, Skyline) and for interpreting (e.g. Panther, Reactome, String) and depositing (e.g. PRIDE, Human Protein Atlas project) the data from proteomic assays [72, 81, 86].

3.1 Vitreous sample preparation

Regardless of the approach, adequate sample preservation and preparation are crucial to successful proteomics analysis, especially if the goal is the quantitative analysis of relevant proteins. Good practices in sample preparation maximize protein detection and improve the quantitative data through the enrichment of target proteome, removal of the interferents, and diminishing of sample complexity [104, 152–154]. After vitreous collection, it is highly recommended to store the samples in liquid nitrogen or dry ice or, if not possible, its immediate placement on ice until storage at –80ºC [22]. Also, some authors recommend adding protease inhibitors to vitreous to ensure protein protection against proteolytic degradation [91, 102, 119, 124, 128, 132, 155].

One of the major problems in the preparation and extraction of proteins from vitreous is its viscous nature attributed to its abundance of proteoglycan, collagen, glycoproteins,

and HA [120]. As a consequence, vitreous handling can be extremely complex, which prevents accurate pipetting of samples [22]. Thus, the separation of soluble proteins from structural components can reduce the viscous nature of vitreous and facilitate the manipulation of samples for further analysis. Although many strategies have been proposed, a cycle of centrifugation at 14000-21000 x g at 4ºC for 5-15 min was commonly applied to separate the soluble from the structural and cellular components [97, 106, 110, 119, 129–133, 139, 142, 156–158]. Other strategies such acetone precipitation [107, 118, 119], trichloroacetic acid/acetone precipitation [31, 113, 115, 117, 131, 132], methanol/chloroform precipitation [91, 128, 129, 133], sonication [91, 119, 125, 126, 128, 132, 135, 136], heating at 95ºC [25, 99, 125, 126, 135], dialysis [158, 159] and filtration [117–119, 122, 160] were applied for reduce vitreous viscosity and/or to extract vitreous proteins. The advantages and drawbacks of each methodology used for the preparation of vitreous samples are summarized in Table 1.

Table 1 – Methodologies applied for the preparation of human vitreous samples.

Methodology	Advantages	Disadvantages	References
Acetone Precipitation	▪ Eliminate acetone soluble interferences. ▪ Enables easier protein resuspension than TCA precipitation. ▪ Sample concentration.	▪ Organic solvents lead to incomplete precipitation. ▪ Lower protein recovery compared to other methods.	[152, 161]
Trichloroacetic Acid/Acetone Precipitation	▪ More effective than any of the reagents used alone. ▪ Useful for the precipitation of basic proteins. ▪ Eliminate interfering compounds (salts, polyphenols, lipids, and nucleic acids). ▪ Minimizes proteolysis. ▪ Sample concentration.	▪ Proteins may be difficult to resolubilize. ▪ Prolonged exposure to low pH may result in protein degradation or modification. ▪ Protein loss due to incomplete precipitation or solubilization.	[117, 153, 161, 162]
Methanol/ Chloroform Precipitation	▪ Useful for the precipitation of membrane protein and very diluted samples. ▪ Eliminate MS interfering compounds (salts, detergents, and lipids). ▪ Sample concentration.	▪ Protein loss due to incomplete precipitation.	[154, 163]

Table 1 – Methodologies Applied For The Preparation Of Human Vitreous Samples (Continued).

Methodology	Advantages	Disadvantages	References
Centrifugation	▪ Ultracentrifugation may be useful for the removal of larger polysaccharides and nucleic acids. ▪ Protein enrichment.	▪ Doesn't remove interferences.	[22, 152, 153]
Filtration	▪ A useful method for salt removal and sample concentration (e.g. after depletion). ▪ Filter-aided sample preparation combines sample preparation, digestion, and peptide extraction for LC-MS analysis.	▪ Risk of protein loss by adsorption in the filter. ▪ Filter often blocked. ▪ Filtration devices are expensive.	[154, 164]
Dialysis	▪ A useful method for salt removal.	▪ Time-consuming, which may lead to protein loss or/and degradation. ▪ Requires large volumes of buffers.	[152, 153]
Sonication	▪ Help to improve protein solubilization. ▪ Reduce sample losses since it avoids vigorous agitation and protein adsorption in the tubes. ▪ Reduces the viscosity of vitreous humor through the breakup of hyaluronic polymers.	▪ Care must be taken to minimize heating to prevent protein degradation. ▪ Doesn't remove interferences.	[125, 152, 154, 161]
Boiling	▪ Reduce the viscosity of vitreous humor. ▪ Boiling the sample in an SDS buffer improves protein solubilization and inactivates proteases.	▪ Doesn't remove interferences.	[22, 152, 162]

The high complexity and wide dynamic range of human vitreous is another challenge in proteomics analysis. Albumin and immunoglobulin account for over 80% of the whole protein content of vitreous, which jeopardizes the detection of low abundant proteins [22, 109, 115, 165, 166]. The complexity of biological fluids as vitreous exceeds the high resolving power of the widely used fractionation techniques. Therefore, vitreous complexity should be drastically reduced before proteomics analysis to unmask low-

abundant proteins [101, 152, 165, 167, 168]. Affinity chromatography has been the method of choice to circumscribe the problem of abundant proteins in vitreous. Several commercial depletion columns and kits have been applied for the depletion of highly abundant proteins, as seen in Table 2 [97, 102, 105, 106, 117, 118, 122, 127, 129, 134, 140, 155].

Table 2 - Affinity columns and kits used for the depletion of high abundant proteins in vitreous.

Depleted Proteins	Commercial Columns/Kits
HSA	▪ ProteoExtract® Albumin Removal Kit (Calbiochem) [155].
IGG	▪ Protein A Sepharose™ 4 Fast Flow (Amersham Pharmacia Biotech) [114].
HSA, IGG	▪ HiTrap™ Albumin & IgG Depletion (GE Healthcare) [118, 122, 129]; ▪ ProteoPrep® Immunoaffinity depletion kit (Sigma-Aldrich) [102]; ▪ Aurum Serum Protein Mini Kit (Bio-Rad) [106]; ▪ ProteoExtract albumin/IgG removal kit (Calbiochem) [117]; ▪ Albumin and IgG Depletion SpinTrap (GE Healthcare) [140].
Haptoglobin, HSA, IGA, IGG, Transferrin, α1-antitrypsin	▪ Multiple Affinity Removal System 6 (Agilent Technologies) [134].
Fibrinogen, Haptoglobin, HSA, IGA, IGG, Transferrin, α1-Antitrypsin	▪ Multiple Affinity Removal Spin Cartridge Human 7 (Agilent Technologies) [127].
APO A-I, APO A-II, Fibrinogen, Haptoglobin, HSA, IGA, IGG, IGM, Transferrin, α1-acid glycoprotein, α1-antitrypsin, α2- Macroglobulin	▪ ProteomeLab® IgY-12 (Beckman Coulter) [117].
APO A-I, APO A-II, Fibrinogen, Haptoglobin, HSA, IGA, IGG, IGM, Transferrin, TTR, α1-acid glycoprotein, α1-antitrypsin, α2- Macroglobulin	▪ Multiple Affinity Removal System 14 (Agilent Technologies) [97, 105, 169]**.**

Apo A-I - Apolipoprotein A-I, Apo A-II - Apolipoprotein A-II, C3 – complement C3, HSA – Human serum albumin, IgA – Immunoglobulin A, IgG – Immunoglobulin G, IgM – Immunoglobulin M, TTR – Transthyretin.

The majority of these systems are based on high-specificity antibodies that bind high-abundant proteins, such as albumin, or on immobilized protein A or protein G, which allow the IgG removal [170]. The depletion of these proteins allows the identification of less abundant proteins [105, 117, 118], and a significant reduction of plasma components [106, 118, 122, 127]. Zhao and co-workers [105] identified 360 additional proteins after the depletion of 14 abundant plasma proteins, but 89 proteins were lost in the depletion procedure. Kim and colleagues [117] identified few proteins using two-dimensional electrophoresis (2DE) coupled to MS after the depletion of 12 high abundant proteins. So, they opted for a mild depletion method that removes only albumin and IgG [117]. After this step, 363 proteins were identified in PDR by combining LC-MALDI-TOF/TOF and LC coupled to tandem mass spectrometry (LC-MS/MS), while only 147 proteins were identified in non-depleted samples [117]. Nevertheless, proteins of interest can also be depleted using this procedure [117, 126, 134, 135]. For this reason, many authors opted not to deplete the abundant proteins [110, 126, 135], even though it may prevent the detection of less abundant proteins.

Enrichment of specific protein fractions or subcellular compartments is another strategy that is widely used in discovery proteomics experiments [104, 171, 172]. Tamburro and co-workers used a titanium dioxide column to enrich the phosphoproteome of vitreous, identifying 85 unique phosphopeptides from 44 proteins [108]. Vitreous phosphoproteome was also studied by microarray analysis of tyrosine phosphorylation levels [173] and Western blot [174]. Other components that have gained interest in the last years are the extracellular vesicles, in particular, the exosomes. Exosomes are extracellular vesicles of endosomal origin released by most eukaryotic cells, including retinal cells, which contain molecular constituents (e.g. proteins and RNA) [175, 176]. Zhao and co-workers [105] enriched exosomes from postmortem vitreous samples using ExoQuick (System Biosciences) and analyzed proteins frequently identified in exosomes by Western blot. Although their origin has not been elucidated, the authors proved that exosomes are constitutive components of the vitreous and, therefore, they may be relevant players in eye communication in physiological and pathological conditions. Furthermore, the study of exosomes in pathological conditions may contribute to our knowledge about the mechanisms underlying several vitreoretinal diseases, as well as contribute to the detection of novel therapeutic targets [105].

3.2 Gel-based Proteomics

Gel-based proteomics is a technology that includes sodium dodecyl sulfate-polyacrylamide gel electrophoresis (SDS-PAGE) and 2DE and has been employed in the proteomics field for over three decades [75]. These techniques contributed significantly

for in-depth proteome analyses of vitreous [92, 97, 105, 107, 109, 114–117, 120, 124, 129, 131, 139–141, 159]. This section summarizes the most recent applications of these technologies to vitreous proteome analysis, but a more detailed description is given in section 4 ("Gel-based" proteomics) of Paper I.

3.1.1. One-dimensional electrophoresis

One-dimensional electrophoresis or SDS-PAGE is a classic separation technique introduced in 1949 and, lately, improved by Laemmli [177, 178]. In SDS-PAGE, proteins charged negatively are separated by their molecular weight (MW) in polyacrylamide gel under an electric field [104, 152]. Due to its many advantages, SDS-PAGE is nowadays widely used as a pre-fractionation method in bottom-up proteomics experiments [75, 152, 154, 179]. SDS-PAGE is a simple procedure that reduces the sample complexity and allows protein conservation into acrylamide gels until MS analysis. It is very tolerant to chemicals and interferents and easily removes low MW compounds, such as detergents and buffer components, that interfere with MS analysis [75, 104, 154]. Another main advantage of this technique is the use of the harsh ionic detergent SDS in sample preparation, which improves the solubility of difficult proteins and allows their identification [179]. The combination of SDS-PAGE and LC-MS has been standardized as gel-enhanced LC-MS (GeLC-MS)[5] [75, 179, 180].

In recent years, SDS-PAGE has been applied for vitreous fractionation in proteomic studies, whether combined with LC-MS [40, 97, 105, 136] or MALDI/TOF/TOF [129, 141]. Gao and colleagues [120] combined SDS-PAGE and LC-MS/MS to analyze the proteome of vitreous collected from PDR, diabetic and non-diabetic individuals. They identified 252 proteins, including 30 associated with the kallikrein-kinin, coagulation, and complement systems [120]. Using a GeLC-MS strategy, Zhao and colleagues [105] identified a total of 1121 nonredundant proteins using either a QExactive or Orbitrap Velos instrument. With the same strategy, Yee and co-workers [40] compared fetal and young adult vitreous using an LTQ linear ion trap MS and found that 37 proteins significantly changed from 14 to 20 WG, including the anti-angiogenic protein PEDF. Zhang used this strategy [136] for studying the pathophysiology of MH, discovering 5912 non-redundant proteins. Murthy and co-workers [97] identified 1205 proteins in vitreous by combining multiple fractionation techniques, including strong cation exchange chromatography, SDS-PAGE, and OFFGEL[6] fractionation, followed by LC-

[5] GeLC-MS is a technique in which polyacrylamide gel is cut in slices after the separation by SDS-PAGE, followed by in-gel trypsin digestion, peptide extraction and analysis by LC-MS.
[6] OFFGEL electrophoresis separates proteins or peptides according to their isoelectric point, whereby the separated components are recovered in liquid phase.

MS/MS analysis. Kasudhan and co-workers [141] identified 25 differently expressed proteins between infectious and non-infections uveitis in vitreous fractionated by SDS-PAGE, while 22 proteins were identified by 2DE and MALDI-TOF. Our research group compared two different strategies for the analysis of vitreous collected from patients with RRD, a strategy combining ion-exchange chromatography (IEX), SDS-PAGE, and MALDI-TOF/TOF analysis and other using only IEX and MALDI-TOF/TOF analysis. A total of 127 proteins were identified, but the majority (117 proteins) were identified using a combined fractionation strategy (IEX and SDS-PAGE). This strategy largely improved the number of identified proteins, proving that further fractionation by SDS-PAGE offers advantages in the improvement of the coverage of the vitreous proteome [129].

3.1.2. Two-dimensional electrophoresis

In the early proteomic studies, 2DE combined with MS has been the preferential method for the separation and identification of vitreous proteins [107, 109, 114–117, 124, 139–141, 181]. 2DE combines isoelectric focusing with SDS-PAGE, allowing a high-resolution separation of complex protein mixtures according to their isoelectric point (pI) and MW [162, 182–186]. In 2DE methodology, complex protein samples are solubilized and separated under denaturing and reducing conditions, visualized by protein staining methods, and the target spots are identified by MS [162, 187]. Although traditional 2DE has been widely used for the analysis of vitreous protein profiles, the results are not very encouraging when the goal is to detect minimal quantitative differences between protein expression patterns in multiple 2DE gels. Therefore, with the technical improvements in MS equipment and the development of labeling methods, gel-free techniques have led to a reduction in 2D gel-based separations [75, 167]. Gel-free techniques have overcome some of the limitations of 2DE [75, 146, 167], including the low reproducibility and throughput, narrow dynamic range, and the inability to analyze the entire proteome, especially acid/basic and very hydrophobic proteins and low abundance proteins [167, 168, 187, 188].

Nevertheless, 2DE remains a valuable tool for the separation and analysis of proteoforms, including isoforms and PTMs variants, due to its high-resolution, affordable price, and ease of obtaining information at a protein level [162, 167, 168, 187–189]. If combined with more sensitive detection techniques, refined gel image processing, and proper sample preparation, 2DE is a valuable tool for routine and high-resolution analysis of proteoforms [190, 191]. Few proteomics studies have recently applied 2DE for the comparative analysis of vitreous in eye diseases [140, 141]. Using 2DE and MALDI-TOF, Sugioka and co-workers [140] identified 13 and 6 proteins in the

vitreous from patients with retinopathy of prematurity and cataracts, respectively. Transthyretin (TTR) and PEDF and were found underexpressed in retinopathy of prematurity when compared to vitreous from cataracts, which was confirmed by Western blot [140]. Kasudhan and colleagues analyzed vitreous collected from patients with infectious and non-infections uveitis by 2DE, identifying 22 proteins, of which serpin B3 and carbonic anhydrase are associated with autoimmunity and acute anterior uveitis [141].

3.3 Gel-free Proteomics

In the last years, improvements in proteomics technologies have been able to address some of the limitations of gel-based methodologies [77, 170, 192, 193]. Gel-free fractionation methods have improved sensitivity, reproducibility, resolution, throughput, speed, and dynamic range of proteomics analysis [75, 77, 179, 194]. Therefore, gel-free techniques as LC-MS and CE coupled to mass spectrometry (CE-MS) have emerged as a promising alternative for the characterization of the vitreous proteome [25, 110, 125, 126, 135].

3.1.3. Liquid chromatography coupled to mass spectrometry

Nowadays, LC-MS became a valuable powerful technical platform in biomarker research, allowing both the identification and quantitation of a large number of proteins in highly complex samples [80]. Compared to 2DE where separation is performed at the protein level, in LC-MS, tryptic peptides are separated by reverse-phase LC, directly ionized via electrospray ionization and analyzed by MS [77, 80, 104], or off-line eluted peptides are spotted on a plate and analyzed by MALDI-TOF/TOF [143, 195]. As the complexity of samples still far exceeds the capacity of a single LC method, several multidimensional techniques, including multidimensional chromatography protein identification technology (MudPit)[7], were introduced [77, 78, 80, 82]. Multidimensional LC-MS requires less sample handling and reduces the ion-suppression effects in MS caused by overlapping signals, leading to a decrease of sample complexity and improving the proteome coverage [77, 82, 179]. In addition to multidimensional separation, the application of a nano-flow in peptide separation results in a significant improvement in MS sensitivity [82, 100]. Nevertheless, LC-MS analysis presents some limitations, including its inability to cover the entire proteome, insufficient peak resolution and

[7] In MudPit, tryptic peptides are separated and analyzed by two-dimensional LC coupled to tandem MS. The peptides are first separated by strong cation-exchange (SCX), followed by reversed-phase chromatography that is directly coupled to MS.

robustness of nanoscale one-dimensional separation, the loss of information at protein level (e.g. pI, MW), and high costs of equipment [77, 196].

Most LC-MS applications for vitreous analysis are relatively recent. Balaiya and co-workers [111] analyzed aqueous humor and vitreous collected from patients PDR by LC-MS/MS. Of the proteins identified in vitreous, 16 proteins were uniquely detected in PDR vitreous, including proteins associated with coagulation, complement, and kallikrein-kinin systems [111]. Skeie and co-workers [25] applied MudPIT to characterize the proteome of vitreous dissected from distinct anatomical regions of healthy post-mortem eyes. They identified 2079 proteins in the anterior hyaloid, 2440 in the vitreous cortex, 2117 in the vitreous base, and 1612 in the vitreous core and discovered that many proteins are unique for each substructure [25]. In another study, they compared the proteomic profile of vitreous collected by needle biopsies and vitrectomy, suggesting that both techniques are suitable for proteomics and biomarker discovery analysis of vitreoretinal diseases [106]. Nevertheless, a significant part of the studies takes advantage of both gel-based and gel-free approaches, including GeLC-MS [31, 40, 97, 105, 120, 131, 136] and 2DE combined with LC-MS [114, 117].

3.1.4. Capillary electrophoresis coupled to mass spectrometry

CE-MS was introduced in 1984 and separates molecules in narrow capillaries (20-200 μm i.d.) using an electroosmotic flow determined by the electric field strength [197, 198]. Originally, CE was applied for the pre-fractionation of peptides or proteins before their analysis by MS, but the development of ESI and MALDI interfaces expanded its applicability for shotgun proteomics [75, 85, 199]. CE-MS offers a suitable alternative to conventional LC, mainly in the analysis of polar and chargeable compounds [199, 200]. CE is more robust, sensitive, and inexpensive than LC, tolerates a wide range of interferents, provides a faster and high-resolution separation and easy miniaturization, and requires low sample volumes [200–203]. Furthermore, ionization parameters are not affected since isocratic conditions and constant low flow rates are applied for peptide/protein separation, improving ionization efficiency [201–203].

Nevertheless, CE-MS is still less used in proteomics analysis than LC-MS [85, 197]. As a counterpart of miniaturization and the reduced detection path length, less than 1 μl of low concentration samples (1-3 fold lower than LC) can be loaded to maximize the separation performance, which requires the coupling of CE to high sensitive detectors, such as MS [197, 199, 202, 203]. This leads to other major problems, including the acquisition speed of the MS, and the CE-MS interface. Fast and sensitive MS instruments are required for the detection of the narrow peaks eluted from CE, as enough points must

be acquired across the peak, mainly for quantitative purposes. More recent MS configurations can overcome these issues because they allow faster acquisition speeds [197, 201]. More difficult to overcome is the problem of the interface between CE and MS equipment since it is necessary to complete the electrical circuit in the capillary to maintain the stability of the electric field through the separation, without interfering with ESI. Several approaches towards a solution to this problem have been made, but most of them proved to be quite feeble, leading to a loss of sensitivity, fast corrosion of coating, and problems in ESI (e.g. unstable spray) [197, 199, 201, 202]. Even compared to ESI-MS, the coupling of CE to MALDI-TOF presents major disadvantages, including loss of resolution, higher variability of signals due to matrix effects and, the signal suppression caused by high-intensity peaks, which results in fewer polypeptides detectable in high-complex samples [201, 203].

Recently, CE-MS was applied to vitreous samples [125, 126, 135]. For the analysis of vitreous proteome, samples were digested with trypsin, loaded on an untreated silica capillary, and analyzed using a P/ACE MDQ CE System (Beckman Coulter) coupled online to a micro-TOF MS (Bruker Daltonic), as previously reported by Theodorescu and co-workers [204]. CE-MS was used for detection and semi-quantification of peptides, while LC-MS/MS was used for the determination of peptide sequencing [125, 126, 135]. Combining these two techniques, 97 unique proteins were identified, of which 19 were found overexpressed in AMD compared to idiopathic floaters [125]. In another study, Nobl and colleagues [135] used the same strategy to analyze a large set of vitreous samples, 108 collected from patients with nAMD and 24 from controls with idiopathic floaters. They identified 101 proteins and proposed 4 proteins as potential biomarkers of nAMD, including clusterin (CLU), OPTC, PEDF, and prostaglandin-H2 D-isomerase [126]. Reich and colleagues identified 94 proteins in vitreous collected from patients with retinal vein occlusion (RVO) and with idiopathic floaters by combining CE-MS and LC-MS. From these, 16 proteins were found differentially expressed in RVO compared with idiopathic floaters, of which CLU, complement C3, Ig lambda-like polypeptide 5, and vitronectin were found significantly overexpressed, and OPTC underexpressed [135].

3.4 Quantitative proteomics

Quantitative proteomics provides a more in-depth understanding of the dynamics of biological systems, facilitating the identification of diagnostic or prognostic disease markers, and contributing to the discovery of new therapeutic targets [145, 205]. Gel-based quantitation was the first approach to be applied, mainly by 2DE, in which the quantitation is performed by comparing the intensity in specific spots from different

samples [85, 145]. However, the quantification of proteins by gel-based approaches is impaired by its low sensibility due to incomplete labeling, ambiguity since each spot can correspond to more than one protein, and the requirement of many replicates [85, 206]. Many high-throughput quantitation technologies have been developed for relative and absolute quantitation, which can be divided into two categories: the stable isotope labeling-based quantitation, and label-free quantitation, as seen in Figure 8 [85, 145, 193, 206, 207].

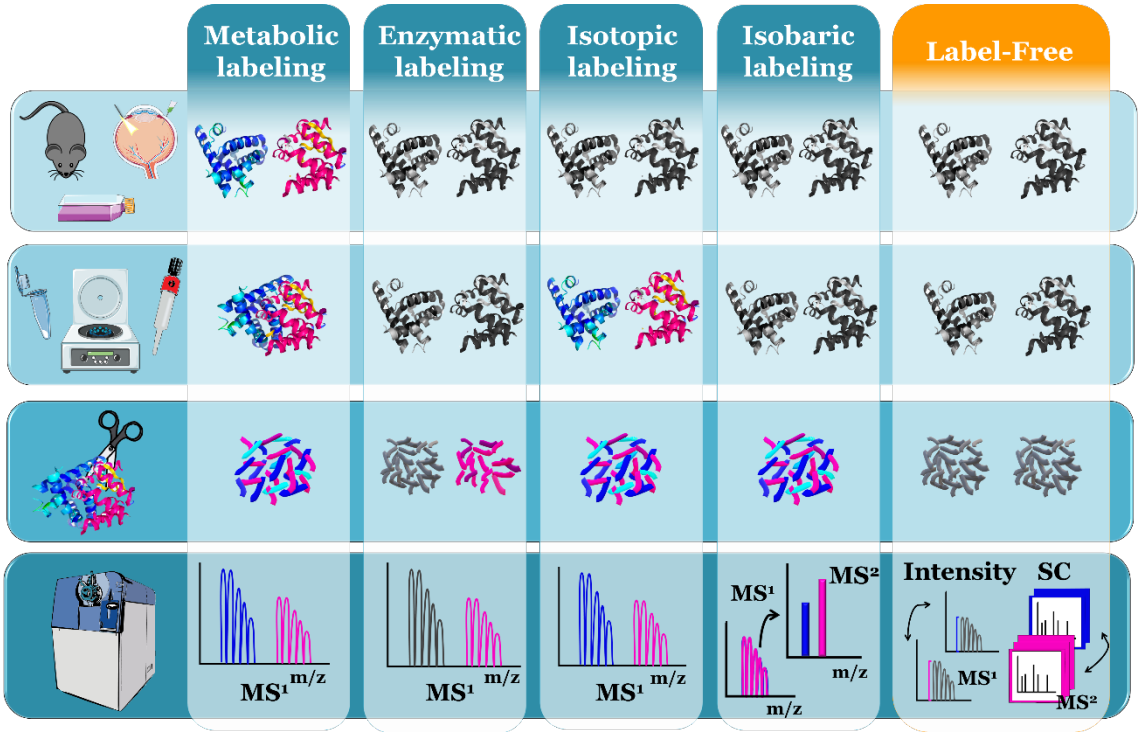

Figure 8 – Quantitative proteomics strategies for relative and absolute quantitation, which can be divided into the stable isotope labeling-based quantitation methods (at blue), and label-free quantitation (at orange). Labeled proteins/peptides are colored at blue and pink, while non-labeled species are colored at gray, as well as the color of the MS signal corresponds to the color of labeled and non-labeled peptides.

In recent years, these gel-free quantitation technologies gained applicability in the characterization of the vitreous proteome in several vitreoretinal diseases. With the latest advances in label-free proteomics, most of the vitreous quantitative studies applied this technique [25, 110, 112, 120, 121, 127, 132, 133, 137, 142, 208], while few authors have applied stable isotope labeling methods for this purpose [102, 134, 155, 209]. Nevertheless, the absolute quantification based on LC-MS remains an untargeted goal, and most studies use techniques, such as ELISA [157, 210–223] or multiplex assays [94, 224–231]. Compared to relative quantitation, absolute quantification provides a far more accurate description of molecular events occurring in the biological systems [75, 143], but the time-consuming and costly synthetic stable isotope-labeled peptides to be used as internal standard makes it prohibitive [85, 143, 232]. For this reason, Kim and

colleagues developed an MRM method for relative quantitation of 12 potential biomarkers in vitreous and plasma collected from patients with DR, PDR, and MH [232].

3.1.5. Stable-isotope labeling methods

Stable-isotope labeling methods include isotope labeling by Amino Acids in Cell Culture (SILAC) [233], Isotope-Coded Affinity Tags (ICAT) [234], Isotope-Coded Protein Labeling (ICPL) [235], proteolytic O^{18} labeling [236], AQUA [237], Tandem Mass Tags (TMT) [238], and Isobaric Tag for Relative and Absolute Quantitation (iTRAQ) [239]. In metabolic labeling (e.g. SILAC), isotopes are metabolically introduced in vivo protein synthesis by feeding cells or an entire organism with a medium enriched with stable isotopes (amino acids), whereas in enzymatic labeling (proteolytic O^{18} labeling) they are incorporated during the digestion with trypsin. Isotopic (ICAT, ICPL) or isobaric tags (TMT, iTRAQ) are chemically introduced into the proteins/peptides using a covalent coupling reagent [80, 145, 206]. These methods take advantage of stable isotopic peptides and their native counterparts exhibiting the same chemical properties and, consequently, the same behavior during chromatographic separation and ESI, which increases quantification accuracy [85, 207, 240]. However, compared to label-free quantitation, these approaches involve a time-consuming and complex sample preparation, require larger amounts of samples and high-cost reagents, and, even using multiplex assays, only a limited number of samples can be analyzed [192]. SILAC technique cannot be directly applied to the investigation of biological fluids, such as vitreous, but it can be used for the search of specific biomarkers in vitro cell cultures (e.g. RPE cells) to be further validated in vitreous samples [193, 205]. To the best of our knowledge, SILAC and ICAT were been applied for other ocular matrices but not for vitreous [93, 101]. The application of stable isotope labeling methods for vitreous relative quantitation is been restricted to iTRAQ [102, 134, 155, 241], and TMT [128, 242]., frequently to compare the vitreous proteome with other ocular matrices.

TMT and iTRAQ are chemically incorporated into the N-terminal and lysine residues of peptides obtained from different biological samples, allowing the identification and relative quantitation of proteins in multiplex assays [75, 240, 243]. Each tag consists of a peptide reactive group, a reporter ion, and a balance group, which maintains the total mass of isobaric reagents constant [75, 240]. Upon peptide fragmentation, low MW reporter ions, which can be observed in MS^2 spectra, are released from isobaric tags (Figure 8). Therefore, proteins are simultaneously identified using the fragmentation spectra and quantified by comparing the intensities of the reporter ions corresponding to the respective samples under investigation [244–246]. Isobaric tags present many

advantages compared to isotopic tagging. Lower sample concentration is required due to multiplex analysis, the quantitation is more accurate due to reduction of the noise level (assessed at MS^2 level), and, as the labeled peptides are eluted as a single precursor, the number of peaks is reduced in MS^1 spectrum and chromatogram [245–249]. Besides the high cost of isobaric tags, another significant limiting factor is the fact that precursor ions near the specified m/z window are co-fragmented with the target precursor, contributing to the intensity of reporter ions. Consequently, this has a negative influence on the quantification accuracy and causes a systematic underestimation of protein/peptide abundance ratios [244, 246, 250]. Moreover, TMT and iTRAQ labeling approaches are limited to MS apparatus capable of efficiently detecting the reporter ions, which are found in the low m/z range in the MS^2 spectrum [240]. Although iTRAQ has been most frequently used [251], TMT increases multiplexation up to 10 and 16 simultaneous experiments, compared to 8-plex of iTRAQ [248, 249]. Several technically orientated articles have evaluated the potentialities of multiplex quantification [246, 250–253] but, as reproducibility is dependent on many factors, including the complexity of the sample, workflow, and MS configuration, the conclusions were not definitive [252].

In a pilot application of iTRAQ, Len and colleagues [155] compared vitreous and retina samples collected from macular Telangiectasia type 2 eyes to diabetic donors using iTRAQ and 2D-LC-MS/MS. They identify 168 proteins in the vitreous and 594 in the retina, of which 63 were significantly differentially expressed in vitreous [155]. Pollreisz and co-workers [102] labeled vitreous and aqueous humor collected from eyes with idiopathic ERM with iTRAQ 4-plex, and analyzed them by 2D-LC-MS/MS, finding only 12 proteins differentially expressed between these ocular compartments of a total of 323 proteins. In a study performed by Naru and co-workers [134], depleted vitreous samples were labeled with iTRAQ, and analyzed by 2D-LC-MS/MS to compare the proteome in retinoblastoma with healthy donated eyes, with 431 non-redundant proteins identified (362 upregulated and 69 downregulated). More recently, Wu and co-workers [241] identified 750 proteins by combining iTRAQ, SCX fractionation, and RP-LC-MS/MS, of which 103 were found differentially expressed in RD with choroidal detachment compared to RD. Mirzaei and co-workers [128] recently applied a 10-plex TMT experiment for the analysis of vitreous and retina collected from post-mortem eyes of patients with glaucoma and healthy controls. They identified 4765 proteins (252 up- and 133 down-regulated proteins) in retinal tissue, and 4987 proteins in vitreous (554 up- and 599 down-regulated proteins), of which 122 were found linked with the pathophysiology of Alzheimer's disease [128]. Although the application of TMT to vitreous analysis is more scarce compared to iTRAQ, its high multiplexing capacity offers

many advantages in this type of study, in which it is intended to analyze a large number of samples and/or to compare different types of ocular matrices.

3.1.6. Label-free quantitative proteomics

Label-free quantitation has been developed as a simpler, cost-effective, and less time-consuming alternative to other quantitative approaches, as it requires no expensive labeling steps and lower quantities of sample, and allows the analysis of a larger number of samples [85, 192, 193, 254, 255]. Free-label has only become widespread in recent years since it requires more sophisticated analytical and bioinformatic platforms, such as high-resolution LC and MS equipment, reproducible LC systems, and improved algorithms for data processing [80, 256–258]. Since label-free experiments do not allow sample multiplexing, samples are analyzed independently by LC-MS/MS and comparative measurements are made between individual runs [255, 258]. Therefore, the label-free approach is more sensitive to technical deviations between runs, and, as a result, experimental conditions should be meticulously controlled to ensure reliable quantitative comparisons between samples [193, 258]. Label-free quantitation relies on two different strategies; spectral counting (SC) and quantitation based ion peak intensity measurement [86, 193, 206, 257–260]. Both methods have a good quantitative performance [80, 261, 262], but intensity-based measures are more accurate [258, 263], and reproducibility is better [261], while SC is more sensitive [263].

In SC, the quantitation is based on the sum of the total number of MS^2 spectra (spectral counts) acquired for a specific peptide in an LC-MS/MS run. Spectral counts can be linearly correlated with the abundance of a specific protein in the analyzed sample, and its relative abundance is measured by comparing the spectral counts for all its peptides across different samples [193, 257, 258, 264]. This approach is based on the observation that more abundant proteins produce more MS^2 spectra than less abundant proteins, and abundant peptides are fragmented more often than are low abundance peptides [193]. The SC methodology is easy to implement and can be performed on low-resolution mass spectrometers [258, 259, 262]. Even though, faster instruments deliver more and higher quality spectrums for counting data, providing more reliable quantifications [257]. However, SC is less reliable for low MW and less abundant proteins and less sensitive to small expression changes in response (2-3 orders of magnitude), favoring the quantitation of high-abundant proteins [193, 262]. To overcome some of its limitations [258, 260–262], SC has been modified into forms, such as exponentially modified protein abundance index (emPAI) [265], the normalized spectral abundance factor (NSAF) [266], absolute protein expression (APEX) [267], and normalized spectral index

(SIN) [268]. To the best of our knowledge, the simplest form of SC was the first and only strategy to be applied for vitreous quantitation [25, 120, 132, 136]. In the studies mentioned previously, Gao [120] and Skeie [25] used spectral counting to assess protein abundance in vitreous samples from diabetic and non-diabetic patients, and distinct anatomical regions, respectively. By applying label-free spectral counting, Yu and his research group [132] found 23 differentially expressed proteins comparing moderate and severe PVR vitreous with healthy post-mortem eyes, including 12 upregulated (plasma proteins, complement components, and serine proteinase inhibitors), and 11 downregulated proteins (cytoskeletal and metabolism proteins). Zhang and its research group [136] found 32 overexpressed and 39 underexpressed proteins in MH vitreous compared with controls. The results revealed an increased expression of complement proteins α-2-macroglobulin, fibrinogen, and ECM proteins, and a decreased expression of proteins involved in protein folding and actin filament binding [136].

In the second strategy, the quantitation is performed by the integration of chromatographic peaks of a peptide in the MS spectrum at a specific RT, and relative abundance is measured by comparing them between LC-MS runs of different samples [80, 85, 192, 193, 260]. In this approach, the measurement of chromatographic peaks can be computed by the area under the curve (AUC) or maximum height/intensity from the raw data (the peak apex), which are linearly proportional to the concentration of the measured peptide [80, 85, 258, 260, 269]. Although it has some advantages over SC, intensity-based quantitation is more sensitive to experimental drifts in m/z and RT. Therefore, it is more demanding and requires a higher number of replicates, better LC-MS platforms, and an accurate normalization to ensure the correct correlation between LC-MS runs [80, 193, 262]. As the intensity signal obtained from the extracted ion chromatogram (XIC) for each peptide must be correlated between multiple LC-MS runs according to specific m/z and RT, bioinformatics tools are required for extensive processing of raw LC/MS data [80, 254, 257, 260]. Data processing involves several steps, including peak detection, feature detection, map alignment, and normalization [80, 258, 259, 269]. For correct quantitative analysis peak detection and chromatographic alignment are crucial, particularly in complex samples, where detection of the target peak may be impaired by overlapping spectral peaks or an increase in background noise [257]. Normalization is performed to account for biases in the measured intensities due to systematic errors in the experimental procedure, including errors in the sample preparation, drifts in the LC-MS system, among others [80, 258].

For this purpose, a large collection of software tools has been developed for label-free proteomics, of which platforms as Progenesis (Nonlinear Dynamics) and MaxQuant

remain the most popular [258, 259, 262, 269]. DeCyderTM (GE Healthcare) was used in the preliminary applications of intensity-based label-free proteomics for vitreous quantitative analysis [121, 137]. Wang and co-workers [121] identified 96 differentially expressed proteins (37 up- and 59 downregulated proteins) in PDR vitreous, while Yu and colleagues [137] identified 226 (104 up- and 122 downregulated proteins) in the vitreous from patients with ERM, both in comparison with healthy donors. Progenesis was used for label-free quantification of vitreous samples collected from patients with DR [110, 112], AMD [127], MH [142], and ERM [142]. Li and co-workers [112] compared the vitreous of type 2 PDR patients and MH using an LC-MS-based label-free quantitative method and found differential levels of apolipoproteins, components of the kallikrein-kinin, and complement systems in the vitreous of patients with PDR [112]. Using a label-free relative quantification, Schori and his group [127] compared the intravitreal levels of 677 proteins in dry AMD, nAMD, and PDR to ERM, showing a characteristic enrichment of proteins related to oxidative stress in dry AMD, focal adhesion in nAMD, and complement and coagulation cascade in PDR patients. Öhman and co-workers [142] found 211 and 297 differentially expressed proteins in the proteome of ERM and MH, respectively, compared to diabetic macular edema, of which a large number of neuronal proteins were present at higher levels in the ERM and MH vitreous. In a study by the same research group [110], 1351 proteins were quantified in 138 vitreous samples from patients with DR or PDR, including patients treated with the anti-VEGF agent bevacizumab. Of the 230 proteins overexpressed in PDR vitreous compared to non-proliferative DR, many were involved in the inflammatory process, including complement and coagulation cascade proteins, protease inhibitors, apolipoproteins, immunoglobulins, or in cell adhesion [110]. These results were obtained using both intensity-based quantitation and SC. Indeed, information about the number of spectra obtained for each protein can be useful when few peptides are available for intensity-based quantitation.

Section 2 – Paper I

Trends in proteomic analysis of human vitreous humor samples

Ana S. Rocha∗, Fátima M. Santos∗, João P. Monteiro, João P. Castro-de-Sousa, João A. Queiroz, Cândida T. Tomaz, Luís A. Passarinha

Electrophoresis, 35 (17): 2495–2508, September 2014.
(DOI: 10.1002/elps.201400049)

This paper reviews the separation and analysis techniques that were applied for the characterization of vitreous proteome earlier in this doctoral thesis. Firstly, it provides an overview of the vitreous and the importance of characterizing its proteomics for the study of ocular diseases. After mentioning the role of separation techniques in vitreous proteomics research, sample preparation strategies and depletion of high-abundant protein are presented as elegant solutions to overcome the complexity and a wide dynamic range of vitreous samples. Hereafter, a comparison between gel-based and gel-free techniques is performed by exploring its methodological demands and its advantages. It also refers to the importance of combining different strategies to improve the coverage of qualitative and quantitative information of vitreous proteome. Furthermore, this review shows the relevance of vitreous proteomic analysis as a tool for the study of the mechanisms underlying some ocular diseases and for the development of new therapeutic approaches.

∗These authors have contributed equally to this work

Electrophoresis 2014, *00*, 1–14

Ana S. Rocha[1,2]*
Fátima M. Santos[1,2]*
João P. Monteiro[1]
João P. Castro-de-Sousa[3,4]
João A. Queiroz[1,2]
Cândida T. Tomaz[1,2]
Luís A. Passarinha[1,3]

[1]CICS-UBI - Health Sciences Research Centre, University of Beira Interior, Covilhã, Portugal
[2]Chemistry Department, Faculty of Sciences, University of Beira Interior, Covilhã, Portugal
[3]Medical Sciences Department, Faculty of Health sciences, University of Beira Interior, Covilhã, Portugal
[4]Ophthalmology Service, Leiria-Pombal Hospital Center, Pombal, Portugal

Received January 30, 2014
Revised May 2, 2014
Accepted May 2, 2014

Review

Trends in proteomic analysis of human vitreous humor samples

Proteomic analysis of human vitreous humor (VH) may elucidate the pathogenesis of retinal ocular diseases and may provide information for the development of potential therapeutic targets due to its pivotal location near lens and retina. The discovery of whole VH proteome involves a complex analysis of thousands of proteins simultaneously. Therefore, in proteomic studies the protein fractionation is important for reducing sample complexity, facilitating the access to the low-abundant proteins, and recognizing them as biotargets for clinical research. Although several separation methods have been used, gel-based proteomics are the most popular and versatile ones applied for global protein separation. However, chromatographic methods and its combination with other separation techniques are now beginning to be used as promising set-ups for VH protein identification. This review attempts to offer an overview of the techniques currently used with VH, exploring its methodological demands, exposing its advantages, and helping the reader to plan future experiences. Moreover, this review shows the relevance of VH proteomic analysis as a tool for the study of the mechanisms underlying some ocular diseases and for the development of new therapeutic approaches.

Keywords:
Gel-based Proteomics / Gel-free Proteomics / Ocular Proteomics / Pre-Fractionation / Vitreous Humor
DOI 10.1002/elps.201400049

1 Introduction

Proteomics, a highly sophisticated research tool, is the study of the protein profile or proteome of an organism, cell, tissue, or biological fluid in a particular state, such as, homeostasis, disease, or response to a specific treatment. Over the last few years proteomic studies have become increasingly common and have provided important information in the fields of ophthalmology and ocular science [1]. The main focus in proteomic analysis of the vitreous humor (VH) is to identify and to compare protein profiles to elucidate the pathogenesis of various diseases for further development of new biomarkers or potential therapeutic targets. VH has been unappreciated with respect to its role in health and disease, as compared with lens or retina and since it is limited to surgical access its substructures have been difficult to study at molecular level [2, 3]. However, the use of VH in proteomic studies is attractive because of less complex protein content, which presumably allows easier identification of subtle changes in the expression of lower abundance proteins [4].

Over the last few years a great deal of interest has gravitated around the development of new biomarkers for early disease detection and drug development. The research in different ocular matrices besides VH, namely, cornea, tears, crystalline lens, retinal pigment epithelium, sclera, conjunctiva, aqueous humor, uvea, and neurosensory retina, have already been reported [5, 6]. Since the VH is in contact with the retina over a large area, the physiological and pathological conditions of the retina affect VH protein components. Thus, this matrix can provide a mean of indirectly exploring the events taking place in the retina during several disease states. Quantitative and qualitative protein analysis of the VH could give additional information about the disease mechanisms and improve our understanding of the pathogenesis of several eye diseases [7]. Abnormal interactions between VH substructures and the retina underlie several vitreoretinal diseases, such as retinal tear and detachment, macular pucker, macular hole (MH), age-related macular degeneration, vitreomacular traction, proliferative vitreoretinopathy (PVR), and proliferative diabetic retinopathy (PDR) [3].

Correspondence: Dr. Luís António Paulino Passarinha, Faculty of Health Sciences, Health Sciences Research Centre (CICS-UBI), University of Beira Interior, Av. Infante D. Henrique, 6200–506 Covilhã, Portugal
E-mail: lpassarinha@fcsaude.ubi.pt
Fax: +351-275-329-099

Abbreviations: **DME**, diabetic macular edema/oedema; **DR**, diabetic retinopathy; **FA**, formic acid; **iTRAQ**, isobaric tagging for relative and absolute quantitation; **ISTD**, internal standard; **MH**, macular hole; **MW**, molecular weight; **PDR**, proliferative diabetic retinopathy; **PVR**, proliferative vitreoretinopathy; **RRD**, rhegmatogenous retinal detachment; **TCA**, trichloroacetic acid; **VH**, vitreous humor

*These authors have contributed equally to this work.

1.1 Vitreous Humor

The VH gel is a transparent extracellular matrix that fills the cavity behind the lens of the eye and is surrounded by and attached to the retina [8]. It contains proteins accumulated by local secretion, filtration from the blood, or diffusion from the surrounding tissues and vasculature [7, 9]. The VH consists mainly of water (about 98%) and other components such as collagens (type II, V, VI, IX, and X), glycosaminoglycans, and inorganic salts and lipids [8, 10]. The macromolecular composition and the viscosity of VH samples differ according to the anatomical region where the sample is taken, the age of patient, the state of the lens, and the presence of any vitreous pathology [3, 8, 9]. The VH is the largest structure of the eye, making up to about 80% of its volume, with albumin and Ig representing about 80% of its whole soluble protein concentration [9, 11]. Its physiological functions remain unclear. Still, there is evidence that it regulates eye growth and shape during development, serves as a barrier to the cellular invasion/migration and the diffusion of large macromolecules, which may help to maintain transparency within its cavity [12, 13]. Recently, it has been associated with oxygen regulation and distribution within the eye.

One aspect of VH aging is progressive liquefaction, which results from the vanishing of collagen fibrils. So far, the mechanism underlying this process is poorly understood and little studied [2, 14]. Deemter et al. have recently investigated the possibility of trypsins involvement in VH type II collagen degradation [15].

In 25–30% of the population the residual gel structure eventually collapses away from the posterior retina in a process called posterior vitreous detachment. This process plays a pivotal role in a number of common aged-related blinding conditions including rhegmatogenous retinal detachment (RRD), PDR, and MH formation [8]. Interestingly, all of these retinal conditions have a peak age of incidence after 50 years, matching the peak age of incidence of posterior VH separation. Thus, these common retinal disorders are all likely to have liquefaction of the VH gel as the underlying cause [14].

2 Role of separation techniques in ophthalmologic proteomics research

Application of proteomics to ophthalmic research can provide insights into the expression of proteins in a biochemical pathway, changes in the way proteins function due to PTMs, pathogenesis of disease and protein changes in response to pharmaceutical intervention [4]. Although it has been greatly underappreciated in the field of ophthalmology, there is a great deal of current interest in its application to the study of individual retinal diseases, and research in these areas is continually expanding [16]. Recent developments in proteomic technologies allow the comparison of expression levels of proteins from two or more samples, such as disease state versus normal [4, 5]. To date, some comprehensive proteomic studies in relation to VH have been conducted employing different separation techniques, namely, 1DE, 2DE, affinity chromatography, DIGE, and LC [17–34] The VH has not been thoroughly studied, which may be, at least in part, due to the difficulty in acquiring ocular tissue to act as a comparative control, since healthy eyes are a difficult option, for several ethical reasons.

There lies a common challenge in the analysis of ocular fluids, since sample volume and protein concentration are very low, therefore, very sensitive methods are needed [6]. One of the major challenges to identify proteins in complex proteomes, such as some ocular human fluids, is the presence of proteins in wide dynamic concentration ranges from very high levels for albumin and IgG to low levels for specific hormone or regulatory proteins, which may represent potential biological markers or may be a likely biotarget for drug intervention [35]. Due to its less complex protein content, VH has become an interesting matrix for proteomic studies [4].

The complexity of the entire sample should be drastically reduced, and several methods of sample fractionation and techniques of proteins enrichment of our interest through concentration methods could be used to achieve this goal [36]. The strategy will depend on the sample nature being analyzed and on the research focus: a single specific protein, a group of proteins, or all the proteins in the VH. Therefore, according to the goal, a technique, a combination of techniques, or a selective separation must be defined [37].

3 Prefractionation methods

The sample can be fractionated using a variety of approaches including precipitation [27,29], centrifugation [27,29], LC, and gel electrophoresis based methods [24, 30], filtration [22], and velocity or equilibrium sedimentation [6, 36]. Despite the attractiveness of fractionation to improve sensitivity, this strategy can be undesirable for the analysis of samples with limited availability due to losses at each fractionation stage [38]. This statement is really important in the proteomics fields, because usually low-abundant proteins carry valuable biochemical diagnostic information and are responsible for several processes ongoing in the target cells [36].

The most common protein fractionation techniques can be divided into two main categories: gel-based and gel-free. Gel-based techniques include all types of 1DE and 2DE: SDS-PAGE, nondenaturing PAGE, and IEF using IPG gel strips [38]. Gel-free fractionation, commonly used in proteomics, applies distinct liquid-phase chromatographic methods such as RP, SEC, IEC, affinity chromatography [21,22,34], and IEF [30]. Gel-free fractionation methods have improved sample recovery, reproducibility, throughput, compatibility with automation, and easiness of coupling with MS [38, 39]. Yet, most of the more recent technological advances for proteomics have not been used extensively in the field of ocular research, but present multiple potential applications in future studies. Some isobaric-labeling and isotope-labeled derivatizing agents and systems have now been developed for quantification of relative abundance of proteins without the need for

gel-based methods, namely, multidimensional protein identification technology, ICAT, stable isotopic labeling with amino acids in cell culture (SILAC), and isobaric tagging for relative and absolute assessment (iTRAQ) [1, 6, 40].

Normally, one important difficulty encountered in proteomic analysis of VH is the fact that proteins presented in major quantity interferes with the detection of less abundant ones, with lower molecular weights (MWs), so precluding their identification [29]. It has been reported that albumin and Ig account for more than 80% of whole-VH protein, and the large spots of these proteins overlap other small spots, corresponding to less-abundant proteins [28]. The separation of the most abundant proteins prior to techniques such as 2DE could be particularly relevant in improving its efficacy and might be a requirement for the detection of more important VH proteins [29].

In most proteomic studies that have been performed for VH until now, 2DE has been the method of choice for its protein separation [18, 21, 22, 24–29, 31–33]. Recently, most developed efforts have been focused on alternative approaches, and 1DE has been coupled to subsequent analysis in LC prior to MS [20, 22, 23, 30, 34].

3.1 Depletion of highly abundant proteins

In previous studies of VH, affinity chromatography has been the method of choice to deplete highly abundant proteins and enhance detection of low-abundant ones [21, 22, 32, 41]. Canãs et al. presented most of the commercially available kits for albumin and IgG depletion [42]. For VH, this has been achieved using Protein A Sepharose 4 Fast Flow (Amersham Pharmacia Biotech) [26], ProteoPrep immunoaffinity albumin, and IgG depletion kit (Sigma-Aldrich, St. Louis, MO, USA) [41], and the ProteoExtract Albumin/IgG Removal Kit (Calbiochem, San Diego, CA, USA) [22].

Kim et al. obtained VH protein profiles for PDR patients by 2DE and MALDI-TOF/TOF in both MS and MS/MS modes [29]. Like in other VH studies [43], the vascular endothelial growth factor was not detected. In this study, another limitation has been found and depicted, the inability to detect lower MW proteins than the three abundant proteins that were identified, namely, albumin, transferrin, and α1-antitrypsin. Therefore, they concluded that the elimination of the most abundant proteins, and the subsequent analysis of all remaining proteins, would be a requirement for the detection of more, and perhaps more relevant, VH proteins. As a next step, they undertook to detect proteins present at lower levels in PDR patients and nondiabetic controls, by the removal of high-abundance proteins. They have used several proteomic methods to identify components of the VH proteome, namely the immunoaffinity subtraction followed by a 2DE and MALDI-TOF [22]. The immunoaffinity subtraction technique has been an alternative approach that allows bounding and retrieval of the 12 most abundant plasma proteins (HSA, IgG, fibrinogen, transferrin, IgA, IgM, apolipoprotein A-I, apolipoprotein A-II, haptoglobin, α1-antitrypsin, α1-acid glycoprotein, and α2- macroglobulin) from biological fluids using a commercially available system Beckman Coulter ProteomeLab IgY-12 column [22]. Like in other studies, they found that other potential proteins of interest can also be depleted using this procedure [44]. So, in the case of the nano-LC-MALDI-TOF/TOF set-up, they decided to apply a relatively mild depletion method, like the Calbiochem kit, to remove only the two most abundant proteins, i.e., albumin and IgG [22].

In VH proteomic analysis, the implementation of an efficient fractionation strategy is essential, and, depending on the goal, more than one strategy could be used to characterize the proteome [22, 26, 41]. Although fractionation may lead to losses of other important proteins with lower affinity that may also be removed, it seems to be the only possible approach to detect a higher number of low-abundance proteins. Kim et al. found enormous differences in the total number of proteins achieved in 2DE gels: 69 spots without depletion and 232 spots after depletion, corresponding to 28 and 49 identified proteins, respectively. Also, this article gives us a great example of how proteomics is strictly dependent on the technology employed: 49 proteins have been identified using 2DE and 531 proteins using LC-MS/MS on the same set of VH from PDR eyes [22].

4 "Gel-based" proteomics

4.1 One-dimensional gel electrophoresis

After protein separation on SDS gels, the entire gel lane is excised and divided into slices prior to the proteolytic digestion. Hereafter, peptide fractions are subjected to a second separation in LC prior to MS analysis. The main advantage is the harsh ionic detergent use of the SDS that ensures protein solubility during the size-separation step aiming to reduce sample complexity prior to LC, and therefore, increasing the chance of identifying low-abundant proteins [9, 36, 39].

In the last few years, 1DE has been applied as a prefractionation approach in some proteomic studies of VH in various retinal diseases, whether applied before to MS analysis or coupled to LC prior to MS [17, 20, 23, 30, 34]. Wu et al. [17] have identified the major soluble proteins in human VH of patients with diabetic retinopathy (DR) using a simple 1DE strategy combined with MALDI-TOF, and confirmed by Western blot. They found two additional bands of β and α-chain hemoglobin on 1DE gel in diabetic samples when compared to controls that correspond clinically to the VH hemorrhage present in the PDR samples.

4.2 Two-dimensional electrophoresis

Since the early proteomic studies, 2DE combined with MS has been the preferential method for separation and identification of proteins in many biological fields [45–49] including human ocular proteomics [1, 9, 18, 24, 26, 28, 29, 31, 50–52].

Indeed, the unique characteristics of 2DE and some technical improvements have maintained this "classical" approach as a core technology of proteome research [35, 42, 46, 47, 53]. 2DE is able to simultaneously resolve and visualize hundreds or thousands of protein spots on a single gel [45, 47, 48, 53–56]. The separation of intact proteins allows the determination of specific attributes such as p*I*, MW, and relative protein abundance [47, 48]. Also, 2DE can provide information on detection of different isoforms, variants, and PTMs [45, 47, 48, 54, 56]. In fact, multiple spots were frequently identified as the same protein in many VH studies [18, 22, 26, 28, 29].

In last few years, some 2DE limitations were evidenced mainly due to its widespread application and emergence of numerous proteomics projects [46, 47]. The main challenge of traditional 2DE analysis is its low reproducibility [45–48, 56, 57], but many VH studies showed that it is quite efficient in obtaining reproducible results [22, 24, 26, 28, 29, 31]. Generally, two or three experiments were carried out for each VH sample in order to obtain consistently spots detection [22, 24, 29].

Another important drawback is its inability to analyze the entire proteome [47]. In complex samples, proteins present distinct expression levels and solubilities and so the detection of some target proteins can be restricted under standard conditions. The groups of proteins that are generally poorly accessible include very hydrophobic and membrane proteins, highly acidic or basic proteins, very small or large proteins, and low-abundance proteins [46–48, 53, 56, 57]. Thus, VH proteins identified could only represent a subproteome fraction and, therefore, the application of complementary methods, may be required [1].

Sample preservation and preparation is crucial for a successful protein separation by 2DE, largely affecting the reliability of the results and the number of relevant proteins identified [6, 9, 35, 36, 42, 54, 58]. The first step in VH sample preparation is its storage by deep freezing immediately upon collection [6, 9, 18, 22, 24, 26, 31]. The use of specific protease inhibitors is relevant to ensure proteins protection against proteolytic degradation [24, 36, 42, 45].

VH samples handling can be extremely complex due to its viscous nature that prevents accurate pipetting and sample loading in IPG gels and can lead to clogging of pores of gel [9, 36, 42, 45]. So, several treatments including boiling [9], high-speed centrifugation [27, 31], centrifugal devices [22, 28], dialysis [28, 31], dilution [9, 26], and hyaluronidase treatment [9] have been used to reduce VH viscosity and/or to separate the liquid constituent from its structural one. Also, salt concentrations higher than 40–50 mM, commonly present in biological fluids, interfere with the efficacy of electrophoretic separation [36, 42]. Hence, methods as dialysis [28, 31] and TCA (trichloroacetic acid) or/and acetone precipitation [18, 28, 29] have been applied to salt removal. TCA/acetone precipitation is very efficient in removal of salts, lipids, nucleic acids, and other contaminants that may interfere with 2DE procedure and contribute for minimize protein degradation once it leads to proteases inactivation [36, 42, 45, 53]. However, Kim et al. reported VH protein losses after a TCA/acetone precipitation from 560 to 500 μg [22]. Nevertheless, it was reported that there is no spots losses after TCA precipitation compared with starting material but instead intensity losses in the albumin and IgG spots [59]. Dialysis is also effective but is time-consuming, requires large volumes of solutions and may lead to proteins losses and degradation [36, 42]. Other alternative methodologies include ultrafiltration, gel filtration, SPE, or the use of commercially available clean-up kits [36, 42, 45]. Ultrafiltration has been widely applied, allowing a total protein recovery. However, it can be problematic due to VH viscous nature of VH samples that may result in filter blocking [59].

After the cleaning step, native proteins must be denatured, disaggregated, and reduced in order to avoid further modifications or losses and insure its complete solubilization [6, 36, 42, 56]. The solubilization of all proteins remains a great challenge due to high degree of heterogeneity and difficulty of breaking macromolecular and structural interactions [36, 42]. VH samples have been solubilized using a composed by urea (8–9.5 M), CHAPS (2–4%), DTT (10–65 mM), and carrier ampholytes (0.2–5%) [18, 22, 24, 26, 28, 29, 31, 45, 60]. Some authors included in the buffer 2 M thiourea combined with 7 M urea for improve challenging proteins solubility [22, 26, 31, 60]. Generally, the same pH gradient is applied for both IPG gels and carrier ampholytes, but curiously some authors described the application of pH 3–10 carrier ampholytes in protein solubilization for 4–7 pH strip gels [22, 24, 26, 60].

The VH preparation buffer is often applied for gel rehydration, [22, 24, 26, 28, 61]. The preferential pH gradients for IEF gels have been were pH 3–10 and 4–7, although different IPGs lengths (7, 13, 18, and 24 cm) were used [22, 24, 26, 28, 29, 31, 60]. Sample in-gel rehydration is the most frequently loading method, but the applied VH quantities were lower than the generally applied for other matrices [22, 24, 26]. Alternatively, samples dissolved in lysis buffer are applied into disposable cups onto the surface of the IPG strip after its rehydration without sample. The amount of sample loaded depends on pH gradient, IEF gel length, and protein extract complexity [45, 53]. Neal et al. loaded larger sample amounts (50–350 μg) onto 18 cm strips than onto 7 cm strips, where 5–40 μg were loaded [31].

VH studies applied relatively low voltages/h in IEF and the values are included in the range of 8.7–36 kVh [18, 22, 24, 28, 29, 31]. Generally, applied voltages must be very low because initial high conductivity caused by salts [46, 61]. but, as samples are usually desalted before IEF, initial voltages higher than 100 V have been applied [18, 22, 24, 26, 28, 60]. Finally, high voltages were applied reaching up to 8000/1000 V [53]. The strips are then equilibrated using DTT to reduce disulfide bonds and iodoacetamide to alkylate reduced thiol groups and subjected to an SDS-PAGE run [18, 24, 26, 28, 29, 31].

Despite its stated disadvantages, silver staining was the most used staining method [22, 26, 28, 29, 31, 60]. Some authors have also opted for Coomassie staining [18, 28, 31], but in most of these studies it was eventually replaced by silver staining [28, 31]. So far, perhaps due to its high cost, fluorescent staining hasn't been extensively. Using this technique,

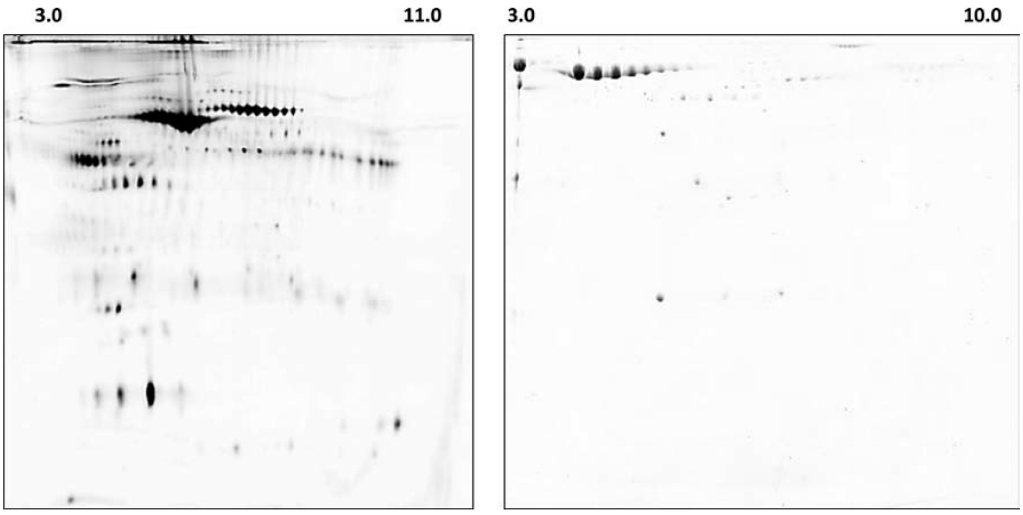

Figure 1. VH analysis by 2DE from patients with rhegmatogenous retinal detachment (RRD) using (A) fluorescent staining and (B) Coomassie blue as detection methodologies. (A) In the first 2DE gel a sample (100 μg of protein) was prestained by DIGE Cy5Dye labeling and IEF was performed on an IPG strip pH 3–11NL, 18 cm. (B) In the second 2DE gel a sample (500 μg of protein) was loaded on an IPG strip pH 3–10, 24 cm.

Ouchi et al. performed a quantitative comparison of VH 2DE profiles from patients with and without diabetic macular edema (DME), detecting more than 200 spots [24]. Preliminary results obtained by our group clearly demonstrate the advantages of the application of fluorescent staining for VH 2DE analysis. Comparing the gels obtained by our research group (Fig. 1), the fluorescent staining enables the detection of a larger number of spots compared to Coomassie staining, even when lower protein quantities are applied.

High sensitivity methods detect proteins down to femtomol levels and so spots may contain very low protein levels [47]. Then, the available amounts for posterior MS analysis is very low and additionally some proteins loss may occur during proteins digestion [47]. Although hundreds of spots were typically identified, only a small percentage were evaluated by MS and an even smaller number of proteins was identified due to ambiguous protein identification [18, 22, 24, 26, 28, 29]. Techniques such as silver and fluorescence stains are able to detect in nanogram range but there is no method able to cover the enormous dynamic range present in biological fluids [48]. Indeed, key proteins involved in ocular diseases mechanisms are present in VH samples at a picogram level [29]. Then, biochemical or immunological techniques such as ELISA [19, 62–69] RIA [62, 70, 71], protein microarray analysis [69, 72–74], or Western blotting [15, 63, 65, 66, 68, 75, 76] are often used for detection and quantification of target VH proteins [1, 6, 9, 60, 77]. These methodologies can be useful as complementary techniques or as confirmatory tests since they detect proteins to the subfemto molar level [6]. However, these measurements are only advantegeous for proteins targeted in advance and can be challenging due to poor availability of VH samples and specific antibodies for such a wide range of proteins [26].

In-gel digestion is complex and time-consuming [78, 79], but an adequate optimization can improve its efficiency [80]. Overall, optimization includes the adjustment of parameters as enzyme/protein ratio, temperature, pH, and time of digestion and the improvement of peptides extraction to minimize sample losses [78, 81, 82]. Before in-gel digestion, VH protein spots have been destained [18, 22, 26, 29, 31, 60], reduced, and alkylated [24, 28]. Usually, gel pieces are dried first and only then rehydrated with trypsin buffer [18, 22, 24, 26, 28, 60] to improve the diffusion of trypsin the protein substrate in gel matrix [79, 80, 83]. VH proteins have been digested overnight at 37°C using trypsin concentrations ranging from 0.01 to 0.025 μg/μL [18, 22, 24, 26, 28, 31, 60]. In order to minimize the autolysis of trypsin, some authors performed the rehydration with trypsin buffer in ice before digestion [22] or use a modified form of trypsin [18, 22, 24, 28, 29, 79, 83]. Finally, peptides have been extracted using organic solvents such as ACN [28] combined with acid TFA [2, 18, 24, 26, 60], or formic acid (FA) [31]. The extracted VH peptides were then mixed with a saturated α-cyano-4-hydroxy-cinnamic acid solution for MALDI experiments [18, 22, 28, 31, 60] or loaded into a chromatographic column for ESI-MS/MS experiments [26, 60]. Nevertheless, minimal processing of extracted peptides and vacuum drying removal are recommended to avoid losses by adsorption on surfaces of pipette tips and digestion tubes [80, 82].

4.3 2D Fluorescence DIGE

Due to the lack of reproducibility of tradicional 2DE, it is difficult to distinguish the technical variability and the biological induced changes when comparing different protein spot

patterns [84–86]. The 2DE variant, 2D DIGE, allows more than one sample to be separated in a single gel [84,85,87–90]. Although it is a relatively expensive method, it allows the detection of qualitative and quantitative changes in protein expression in a more sensitive, rapid, reproducible, and accurate way [84,85,91].

Only few studies have been published regarding VH analysis by DIGE, but García-Ramírez et al. developed some interesting work in this field [21,33,92,93]. DIGE was applied for identifying new potential candidates in several ocular pathologies including PDR, non-PDR, and DME using as control group patients with MH [21, 33, 92, 93]. For the first time, 11 differentially expressed proteins were identified by DIGE when comparing PDR and MH patients (Fig. 2). Six spots positions are marked, corresponding to three overexpressed proteins (zinc-α2-glycoprotein, apoH, and complement factor B) and three underexpressed proteins (pigment epithelial derived factor, interstitial retinol-binding protein, and inter-α-trypsin inhibitor heavy chain) in PDR patients. [21]. In another VH study, Hernández et al. were able to identify 25 proteins differentially expressed from 1300 detected protein spots [33]. Wang et al. also detected about 1200 protein spots, discovering 70 protein spots significantly altered in PDR compared with normal controls, 19 of which correspoding to altered proteins [25]. Western blot is normally used to confirm DIGE results [21,25,92,93].

DIGE methodology is quite similar to the one applied for tradicional 2DE. As previously stated, VH samples are prepared using methods such as ultrafiltration [21,93] high speed centrifugation [25,93], organic precipitation [21,25,93], sonication [25], and/or abundant proteins depletion [21,93]. The main technical difference is that pools of protein samples are differentially labeled using fluorescent cyanine dyes (CyDyes®) and mixed before its application in IEF gel [84, 85, 87, 89, 91]. Prelabeling consists in the sample incubation with respective CyDyes® and the addition of lysine to stop labeling reaction. Also, lower amounts of proteins are applied than in traditional 2DE, generally 50 μg per gel [21,25]. After 2DE run, differentially labeled protein samples can then be visualized separately applying distinct detection channels on a fluorescence gel scanner, since dyes differ in their excitation and emission wavelengths [84,85,89]. Then, the images are normalized and compared to identify differences in protein patterns such as spot density or mass shift [63,64,81,84].

Some details must be taken into account when DIGE analysis is performed. First, an internal standard (ISTD) has been included in VH DIGE analysis [21,25,92,93] to minimize experimental variation and normalize measurements [84,85, 87,88]. ISTD generally consists of pooled mixture in equal amounts from all samples in the experiment [84,85,89]. Cy3 and Cy5 are applied for disease/control samples labeling, while Cy2 is used as ISTD [84,87].

In most studies, minimal labeling have been applied [21,25,33,92,93]. Indeed, it is recommended for DIGE analysis that the dye/protein ratios must be kept low (3% or less). This ratio has been optimized to improve less abundant proteins labeling, keeping highly abundant proteins in the linear dynamic range for quantitative image analysis [84,89,91,94]. Higher dye/protein ratios may change proteins properties including charge and MW and reduce sample solubility due the high hydrophobicity of the fluorochromes. These changes may also lead to protein precipitation during electrophoresis and/or to the appearance of multiple spots per protein. [56,88,89,94].

Another fact that must be considered is the large dependence of minimal staining on protein lysine contents. Therefore, proteins with higher percentages of lysine residues are more efficiently labeled, while proteins with poor lysine contents may remain unlabeled [84]. These problems can be solved by application of ISTDs, since target protein spot intensity can be related to the correspondent standard spots [6]. In order to avoid some labeling issues, half of the samples from each disease/control group could be alternately labeled with Cy3 and Cy5 [21,93].

5 Proteomics application of HPLC

Although 2DE stands as the most applied separation technique for proteomic analyses, it presents the previously described drawbacks. Therefore, "nongel" techniques have emerged as a complementary proteomic technology to overcome some of its limitations [36, 39, 42, 95, 96]. LC coupled to MS/MS is a reproducible and resolving separation method that enables prompt detection and quantitative measurements [1, 97, 98]. Nowadays, LC can easily be interfaced to an ESI-MS/MS instrument by an online connection than allows the adjustment of sensitivity. Also, LC can be followed by MALDI-TOF/TOF analysis, where peptides are previously spotted on a MALDI plate [99]. Bottom-up aproach is frequently applied in VH studies [27,41,100,101], where the entire proteome is digested into peptides and then chromatographically fractionated and identified by MS/MS [27,100,101].

Improvements on LC-MS analysis have greatly increased the dynamic range and the sensitivity of complex protein mixtures [9]. Therefore, LC coupled with MS enables a high-throughput proteins analysis with enhanced specificity, speed, sensitivity, and good resolution of proteins or peptides. LC is preferable to 2DE for challenging proteins screening due to its capability to detect low-copy proteins among high-abundance species [100]. Indeed, it is possible to enrich the low ones and deplete a specific classes using affinity chromatography [35, 95, 102]. Also, LC presents a broad selection of stationary and mobile phases and a large number of separation modes [98]. However, LC-MS analysis presents some limitations in terms of time consumption and robustness [98,100,103]. Aditionally, informations such as MW and p*I* are temporarily lost after proteins digestion, contrasting with 2DE, being revovered during database search of proteins [45]

Sample handling and preparation prior to LC run are minimal [98] because it is tolerant to moderate contaminant levels [36]. VH samples have been prepared using

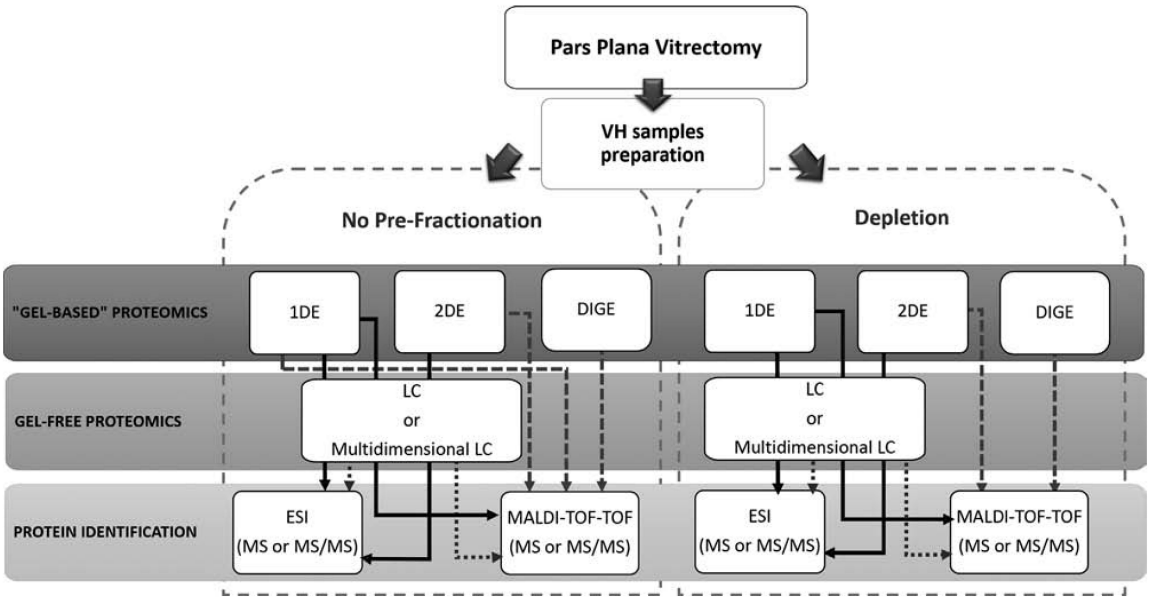

Figure 2. The scheme summarizes the experimental methodologies applied to VH samples. In general, VH proteomics analysis may or may not be preceded by prefractionation methods such as immune-affinity subtraction and highly abundant proteins depletion. Then, VH samples were separated using "gel-based" proteomics methods represented here by dark gray blocks and arrows, gel-free proteomics represented here by light gray blocks and arrows, or a combination of these methodologies represented by black arrows. After its separation, VH proteins can be identified using as ionization technique ESI or MALDI, followed by MS or MS/MS detection.

methods as high-speed centrifugation [100], acetone/TCA precipitation [27], or sample desalting devices (ZipTips pipette Tips) [101]. VH samples have been desalted and concentrated prior to LC separation using trap columns [27, 100, 101]. For LC separation, the addition of protease inhibitors are advised [36]. Yu et al. included 100 mg/mL PMSF into solubilization buffer [27].

In bottom-up aproach, proteins are then digested in peptides using in-solution digestion, which is more efficient, faster, and simple than in-gel digestion [78, 104]. Here, proteins are trapped in a gel matrix, reducing enzyme accessibility to the substrate. When proteins are free in solution, enhanced peptide yields and peptide sequence coverage are obtained, even using lower trypsin/proteins ratios [42, 104]. Prior to in-solution digestion, VH samples have been denatured, reduced, and alkylated using urea, DTT, and iodoacetamide [27, 30, 100, 101]. The total protein denaturation facilitates the access of proteolytic enzyme to cleavage sites, improving digestion efficiency [78]. Then, VH samples have been digested at 37°C overnight or for 6 h using trypsin/protein ratios of 1/50 and 1/100 [27, 30, 100, 101].

Single- or multidimensional LC-MS analysis can be performed for separation and identification of peptide/protein mixtures [36]. One-dimensional LC separation is an economic and effective [89, 91], widely applied approach for VH studies [22, 23, 26, 28, 30, 100, 105]. However, few of these studies have been performed using exclusively chromatographic methods [7, 27, 41, 100, 101]. In these studies, RP-LC was the most applied method for VH peptides separation, where were applied increasing ACN gradients and FA/acetic acid, as mobile phases' supplements VH peptides were also separated by IEC using linear sodium chloride gradients [28]. The nonexclusively chromatographic methods have been more frequent and included purification and enrichment of specific target proteins [71, 101] or gel-based strategies, followed by LC [22–24, 26, 30, 34, 71].

Regarding proteome complexity, most 1D-LC methods can be limited due its insufficient peak resolution capacity [106]. Therefore, multidimensional separations are often required to increase resolution and proteome coverage [39, 98, 106]. Due to its high resolving power, reduces the ion-suppression effects in MS caused by overlapping signals [98, 103]. Affinity and RP chromatography [101] or ionic and RP chromatography [27] have already been combined to separate VH samples. In most LC-based proteomics analysis, the last dimension is performed by RP chromatography due to its compatibility with MS [39, 42, 98, 103, 107].

Applying LC, some interesting discoveries have already been made. Yu et al. have analyzed VH protein profiles from PVR patients and biobank eyes as control samples, identifying 129, 97 and 137 proteins in VH of normal control, moderate and severe PVR, respectively [27]. Wang et al. have also identified 96 significant differentially expressed proteins in PDR using RP-HPLC coupled to ESI-MS/MS [100]. Nakanishi et al. have also identified five VH-specific proteins using IEC and ESI-MS/MS analysis, four of them were not

identified by 2DE [28]. Tamburro et al. identified 85 unique phosphopeptides by affinity chromatography followed by LC-MS/MS [101]. Compared to 2DE, a larger number of proteins were identified combining LC with other methods. Kim et al. identified 531 proteins by nano-LC-MALDI-TOF/TOF and nano-LC-ESI-MS/MS, but only 49 proteins using 2DE [22].

Additionally, some VH quantitative proteomic studies have been performed using LC coupled to MS/MS [41,100,105]. Wang [100], Kim [105], and respective coworkers applied free-label quantification to VH from DR patients using LC-ESI-MS/MS. Alternatively, Pollreisz et al. applied LC-MS as both separation and quantitative method using iTRAQ methodology in VH and aqueous humor samples from eyes with idiopathic epiretinal membranes, identifying 12 differentially expressed of a total of 323 proteins [41]. Despite this methodology being rarely applied to VH studies, it has gain increased interest in proteomics research [108] and may offer a promising alternative for VH quantitative studies.

6 Experimental set-up design for VH proteomic analysis

The individual techniques normally applied to simplify the VH samples complexity have been described as their advantages and drawbacks (Table 1). However, due to proteome

Table 1. Summary of the advantages and drawbacks of the separation methodologies usually applied for VH samples

Methodology	Advantages	Disadvantages	Reference
Depletion	• Removes highly abundant proteins, enhancing the detection of low abundance ones.	• Loss of potential target proteins • High costs of specific affinity columns	[21, 22, 32, 41, 44, 97]
1DE	• Traditional well-established method; • SDS detergent ensures proteins solubility during procedure; • Removes low molecular organic and inorganic impurities.	• Incompatible for highly complex biological samples; • Low dynamic range; • Poor resolving power; • Separation based only on proteins size; • Inability to separate proteins with extreme p*I*; • Very time consuming and hands-on complexity.	[9, 36, 39, 97]
2DE	• High resolution power; • Determination of p*I*, MW, relative abundance; • Detects isoforms, variants and PTM proteins; • Separated proteins can be preserved on a dried gel for extended periods of time.	• Low reproducibility, sensitivity and dynamic range; • Poor quantitation capacity; • Inability to analyze the entire proteome; • Very time consuming and laborious; • Complex sample handling; • Difficult to automate.	[37, 39, 45–48, 55–59, 97]
DIGE	• Ability to separate more than one sample on a single gel; • Improved sensitivity and resolution power; • Accurate and reproducible quantitative analysis; • Higher linearity and less time consuming than traditional 2DE; • Capability to apply an internal standard to minimize experimental variations and normalize measurements;	• High costs of reagents and equipment; • Some problems associated with labeling method;	[45, 55, 56, 84–90]
LC-MS	• High reproducibility and dynamic range; • Prompt detection and quantitative measurements; • Good resolution; • Versatility (broad selection of stationary, mobile phases and separation modes); • Enhanced specificity, speed and sensitivity; • Directly compatible with MS; • Can be applied as enrichment and pre-concentration methods; • Less sample handling; • Inexpensive reagents.	• Time consuming due to the required method development for each specific matrix. • Informations such as MW and p*I* are temporarily lost after proteins digestion; • High costs of equipment;	[1, 45, 97–100, 103, 106]

complexity, no individual technology can give complete coverage of its whole, being extremely difficult to separate and identify thousands of proteins with large dynamic range. For a particular proteome, comprehensive coverage can only be achieved using subproteome strategies along with complementary proteomic technologies [1].

The approaches applied over the last few years to characterize the VH proteome in several pathologies, most of them conducted for PDR, are synthesized in Table 2 and Fig. 2. In recent years, most developmental efforts have been focused on alternative approaches for VH studies, taking advantage of both gel-based and gel-free separation, [22–24, 26, 30, 34, 71].

Currently, in-gel LC-MS/MS method, a combination of 1DE separation with LC-MS/MS is frequently applied in studies for VH [36, 39]. Koyama et al. [23] have applied 1DE to patients with DR with subsequent analysis by capillary-column RP-HPLC coupled with ESI-MS/MS in order to improve the recovery of proteins in VH. Eighty-four different proteins were identified; some of those were not detected by 2DE.

Afterwards, Gao et al. [20] have identified 252 proteins of VH from individuals with diabetes using preparative 1DE and nano-LC-MS/MS. In recent studies, the approach 1DE coupled with RP-LC-MS/MS has proven to be a valuable resource to aid the characterization of the proteome and in order to understand the molecular mechanisms of RRD with PVR [34].

By applying different proteomic strategies including 2DE-MALDI-TOF, nano-LC-MALDI-TOF/TOF, and nano-LC-ESI-MS/MS. Kim et al. have identified a total of 531 individual proteins, 415 proteins in patients with PDR, and 346 in nondiabetic control group. This study is a perfect example of how the employment of an unique technique that can be limited since only 49 from the 531 identified proteins were discovered using 2DE [22].

Ouchi et al. detected more than 200 spots, identifying 14 proteins from 23 spots in the DME VH, and 15 proteins from 22 spots in non-DME samples using 2DE combined with LC-MS/MS [24]. Using the same strategy, Yamane et al. detected more than 400 spots in MH 2DE gels and 600 proteins in PDR 2DE gels, indentifying, respectively, 18 and 38 proteins [26].

Aretz et al. have recently applied different protein prefractionation strategies including liquid-phase IEF, 1DE, and its combination. They compared the number of identified proteins detected by the respective method in VH of three patients undergoing vitrectomy from "surrogate normal patients" with epiretinal gliosis [30]. They demonstrated that liquid-phase IEF followed by 1DE increased the number of identified proteins by a factor of five compared to the analysis of unseparated VH crude. The resulting peptides were analyzed on an UPLC system coupled online to a LTQ Orbitrap XL mass spectrometer. The result of protein prefractionation by 1DE (standard procedure) followed by LC-ESI-MS/MS achieved 434 unique proteins detected. Additional prefractionation strategy was used by combining the same sample to liquid-phase IEF prior to 1DE. The total number of identified proteins increased to 916, although, 66 proteins detectable by the standard procedure were lost. By applying only the liquid IEF the total number of identified proteins was 284, in which 17 additional proteins were not detected in the standard procedure. Likewise, direct analysis of the VH proteome without any prefractionation revealed only 186 proteins, but two new proteins were detected. Briefly, with this strategy, they have identified 1111 unique proteins. Although they applied a highly sensitive state-of-the-art methodology to map the VH proteome, only further prefractionation of the samples enabled detection of very low abundance proteins. Thus, by applying liquid-phase IEF in combination with 1DE, they have facilitated a striking increase in the dynamic range of detection, and have increased the number of detected proteins from 434 to 916. On the other hand, during prefractionation some proteins will be lost, thus, a combination of different strategies will be necessary to cover the complete VH proteome. These authors also compared the complete list of the 1111 proteins detected in the VH samples and found that only about 27% are also listed as plasma proteins. They concluded that human VH appears to be a discrete and unique body fluid with only partial overlap to the plasma proteome [30].

7 Conclusions and future perspectives

In the last few years, biomarkers discovery in human VH have remained a challenging task due to samples' complexity and a wide dynamic range in protein abundance. Prefractionation and separation procedures are a valuable tool in targeting proteins, limiting the problematic dynamic range of protein expression, unmasking low-level components, and thus reaching for the "hidden" protein fraction.

Currently, there is no single method capable of providing qualitative and quantitative information of all VH proteome. In many studies, 2DE coupled to MALDI-TOF/TOF still constitutes the basis for protein identification but LC coupled to MS/MS has arisen like an interesting alternative. The combination of several approaches is a valuable option to proteomic studies, providing complementary information for an overall richer analysis. So, gel-based approaches have been complemented with other gel-free methods, such as LC-MS in some VH proteomic studies. This methodology may contribute to a better reproducibility and dynamic range.

Although many progresses have been made in terms of separation and identification methodologies, few VH studies have applied quantitative approaches. Besides comparing disease and normal proteome profiles and founding proteins that could be potentially used as biological markers, the aim is to recognize and to understand global processes underlying ocular diseases. Quantitative proteomics studies may provide additional information in that way. Namely, high-throughput quantitation technologies include free-label methodologies or labeling techniques such as ICAT, SILAC, or iTRAQ. Indeed, gel-free high-throughput quantitation technologies could gain applicability in VH studies in the near future. Ophthalmic proteomics research will offer many opportunities of improving the diagnosis of eye diseases and contributing to the

Table 2. Summary of the VH proteomic studies from several retinal diseases/controls and respective applied methodologies

Pathologies	Methodology	Control	Results	Reference
Diabetic retinopathy	2DE and MALDI-TOF 2DE and ESI-MS/MS IEC and ESI-MS/MS	Macular hole	51 proteins identified in VH samples, which 30 have not been reported in 2D plasma profiles. Also, five VH-specific proteins were found using IEC	[28]
Diabetic retinopathy	1DE and ESI-QIT-MS/MS	—	84 proteins were identified including four angiogenic factors and three anti-angiogenic factors	[23]
Proliferative diabetic retinopathy (VH and serum)	2DE and ESI-Q-TOF/TOF 2DE and MALDI-TOF	Macular Hole (VH and serum)	The 18 proteins identified in Macular Hole were also identified in Proliferative Diabetic Retinopathy from a total of 38 proteins	[26]
Diabetic retinopathy	1DE and MALDI-TOF Western blot	Normal human eyes (eye bank)	8 bands on SDS-PAGE in normal eyes and 2 additional bands (hemoglobin) in eyes with Diabetic Retinopathy	[17]
Pseudophakic and Phakic human donor eyes	2DE and MALDI-TOF	—	Significant alterations in abundance and/or modification of several proteins such as transthyretin, alpha antitrypsin, and retinoic acid binding protein were observed	[31]
Pre- Proliferative diabetic retinopathy associated with Diabetic Macula Edema	2DE and LC-ESI-Q-TOF/TOF	Pre- Proliferative Diabetic Retinopathy without Diabetic Macula Edema	A total of 14 and 15 proteins were identified, respectively, in Diabetic Macula Edema group and nondiabetic macula edema group. Eight spots were upexpressed in Diabetic Macula Edema samples and one spot was detected only in nondiabetic macula edema samples	[24]
Proliferative diabetic retinopathy	2DE and MALDI-TOF/TOF	Macular Hole	From the 8 proteins differently expressed, five proteins were upregulated and 3 downregulated in Proliferative Diabetic Retinopathy.	[29]
Type 1 diabetes with proliferative diabetic retinopathy	Affinity chromatography for Albumin and IgG depletion DIGE and MALDI-TOF Western blot	Macular Hole	8 proteins (zinc- α2-glycoprotein, apolipoprotein A1, apoH, fibrinogen A, and complement factors) were highly produced and three proteins (pigment epithelial derived factor, interstitial retinol-binding protein, and inter-α-trypsin inhibitor heavy chain) were underproduced in Proliferative Diabetic Retinopathy	[21]
Proliferative diabetic retinopathy	IS, 2DE and MALDI-TOF 1DE, nano-LC and MALDI-TOF/TOF 1DE, nano-LC-ESI-MS/MS	Macular Hole	531 proteins were identified (415 proteins in Proliferative Diabetic Retinopathy and 346 in nondiabetic VH), where the majority were identified using nano-LC-ESI-MS/MS	[22]
Diabetic retinopathy (VH and serum)	2DE and LC-ESI-QIT-TOF/TOF 2DE and MALDI-TOF	Macular Hole (VH and serum)	18 unique proteins were identified in MH samples, while 38 unique proteins were identified in Diabetic Retinopathy samples. Enolase and catalase were identified in Diabetic Retinopathy but not in MH vitreous or Diabetic Retinopathy serum samples.	[60]
Proliferative diabetic retinopathy (diabetic diseases with no diabetic retinopathy)	1DE and nano-LC-MS/MS	Nondiabetic diseases	252 proteins were identified (30 proteins associated with the kallikrein-kinin, coagulation, and complement systems)	[20]
Proliferative diabetic retinopathy	Affinity chromatography for Albumin and IgG depletion DIGE and MALDI-TOF Western blot	Macular Hole (nondiabetic)	Levels of apo A-I and apo H are elevated in VH samples of patients with Proliferative Diabetic Retinopathy when compared with nondiabetic patients	[93]
Nonproliferative diabetic retinopathy	2DE and MALDI-TOF	Macular Hole, Epiretinal Membranes, and from healthy postmortem donors	Levels of inflammation-associated proteins significantly higher in four types of vitreoretinal diseases studied than in control samples	[18]
Proliferative diabetic retinopathy	2DE and MALDI-QIT-TOF/TOF			
Proliferative vitreoretinopathy				
Rhegmatogenous retinal detachment				

Table 2. Continued

Pathologies	Methodology	Control	Results	Reference
Proliferative vitreoretinopathy with rhegmatogenous retinal detachment (VH and serum)	2D-nano-LC-ESI-MS/MS	Normal human eyes (eye bank)	129, 97, and 137 proteins were identified respectively in vitreous of normal control, moderate and severe Proliferative Vitreoretinopathy	[27]
Proliferative diabetic retinopathy non proliferative diabetic retinopathy	Affinity chromatography for Albumin and IgG depletion DIGE and MALDI-TOF Western Blot	Macular Hole (nondiabetic)	Interphotoreceptor retinoid-binding protein (IRBP) is underexpressed in Proliferative Diabetic Retinopathy	[92]
Diabetic macula edema without proliferative diabetic retinopathy	Affinity chromatography for Albumin and IgG depletion	Macular Hole (nondiabetic)	81 spots were differentially expressed between groups and 25 intravitreal proteins were identified (4 proteins associated with Diabetic Macula Edema)	[33]
Proliferative diabetic retinopathy and without diabetic macula edema	DIGE and MALDI-TOF-TOF			
Diabetic diseases (HV, retinal detachment and ischemic cardiopathy)	Affinity chromatography for phosphopeptide enrichmentLC-ESI-MS/MS	Nondiabetic diseases (HV, Retinal Detachment)	85 unique phosphopeptides and 44 phosphorylation sites were identified	[101]
Proliferative diabetic retinopathy	DIGE and MALDI-TOF-TOF Western blot	Normal human eyes (eye bank)	19 proteins differentially produced in Proliferative Diabetic Retinopathy patients compared with normal subjects	[25]
Rhegmatogenous retinal detachment with proliferative vitreoretinopathy	1DE and nano-LC-ESI-MS/MS	Normal human eyes (eye bank)	516 proteins identified in Rhegmatogenous Retinal Detachment patients with Proliferative Vitreoretinopathy and 364 identified in normal samples (48 overlapping proteins)	[34]
Epiretinal gliosis	1DE and LC-ESI-MS/MS IEF, 1DE and LC-ESI-MS/MS IEF and LC-ESI-MS/MS	—	1111 proteins were identified in total	[30]
Proliferative diabetic retinopathy	LC-ESI-MS/MS	Normal human eyes (eye bank)	96 significant differentially expressed proteins were identified; including 37 and 59 proteins up- and downregulated in Proliferative Diabetic Retinopathy vitreous	[100]
Idiopathic epiretinal membranes	2DE and LC-ESI-Q-TOF/TOF	Idiopathic Macular Hole	High-abundance protein spots were identified as α1-antitrypsin, apolipoprotein A-1, transthyretin and serum albumin and its fragments in disease group. None of the identified spots changed more than 1.5-fold between disease/control groups.	[109]
Diabetic macula edema without proliferative diabetic retinopathy proliferative diabetic retinopathy without diabetic macula edema	Affinity chromatography for Albumin and IgG depletion DIGE and MALDI-TOF ELISA	Macular Hole (nondiabetic)	Four proteins differently expressed associated with Diabetic Macula Edema in comparison with Proliferative Diabetic Retinopathy patients and nondiabetic controls	[32]

VH: Vitreous Humor.
MH: Macular Hole.
ESI-QIT-MS/MS – electrospray ionization-quadrupole ion trap-tandem mass spectrometry.
ESI-Q-TOF/TOF – electrospray ionization-quadrupole-time-of-flight tandem mass spectrometry.
ESI-QIT-TOF/TOF: electrospray ionization-quadrupole ion trap-time-of-flight tandem mass spectrometry.
MALDI-QIT-TOF/TOF- matrix-assisted laser desorption/ionization-quadrupole ion trap-time of flight tandem mass spectrometry.
IS: immunoaffinity subtraction.

development of new potential therapies based on VH biomarkers discovery.

This project was supported by University of Beira Interior – Health Sciences Research Centre (CICS). Rocha A.S. acknowledges PhD fellowship of Sciences Faculty financed by ICI and Santander Totta. F. M. Santos acknowledges a fellowship (CENTRO-07-ST24-FEDER-002014) financed by the program 2007–2013 QREN. J. P. Monteiro acknowledges a fellowship (CENTRO-07-ST24-FEDER-002015). The authors also acknowledge the program COMPETE, the FCT project (Pest-C/SAU/UI0709/2011) and to Bruno Bacher from GE Healthcare for the DIGE gel image.

The authors have declared no conflict of interest.

8 References

[1] Cryan, L., O'Brien, C., *Proteomics Clin. Appl.* 2008, *2*, 762–775.

[2] Kodama, M., Matsuura, T., Hara, Y., *J. Biomed. Sci. Eng.* 2013, *6*, 739–745.

[3] Skeie, J. M., Mahajan, V. B., *J. Vis. Exp.* 2011, *47*, 5–8.

[4] Jay, N. L., Gillies, M., *Clin. Experiment. Ophthalmol.* 2012, *40*, 755–763.

[5] Lam, T. C., Chun, R. K. M., Li, K.-K., To, C.-H., *Clin. Exp. Optom.* 2008, *91*, 23–33.

[6] Mandal, N., Heegaard, S., Prause, J. U., Honoré, B., Vorum, H., *Biol. Proced. Online* 2009, *12*, 56–88.

[7] Sjöstrand, J., Karlsson, J. O., Andersson, K., *Acta Ophthalmol.* 1992, *70*, 814–819.

[8] Bishop, P. N., *Prog. Retin. Eye Res.* 2000, *19*, 323–344.

[9] Angi, M., Kalirai, H., Coupland, S. E., Damato, B. E., Semeraro, F., Romano, M. R., *Mediators Inflamm.* 2012, *2012*, 1–7.

[10] Theocharis, A. D., Papageorgakopoulou, N., Feretis, E., Theocharis, D. A., *Biochimie* 2002, *84*, 1237–1243.

[11] Grus, F. H., Joachim, S. C., Pfeiffer, N., *Proteomics Clin. Appl.* 2007, *1*, 876–888.

[12] Le Goff, M. M., Bishop, P. N., *Eye* 2008, *22*, 1214–1222.

[13] Sebag, J., *Br. J. Ophthalmol.* 2009, *93*, 989–991.

[14] Holekamp, N. M., *Am. J. Ophthalmol.* 2010, *149*, 32–36.

[15] Van Deemter, M., Kuijer, R., Harm Pas, H., Van der Worp, R. J., Hooymans, J. M. M., Los, L. I., *Mol. Vis.* 2013, *19*, 1591–1599.

[16] Chambers, G., Lawrie, L., Cash, P., Murray, G. I., *J. Pathol.* 2000, *192*, 280–288.

[17] Wu, C. W., Sauter, J. L., Johnson, P. K., Chen, C.-D., Olsen, T. W., *Am. J. Ophthalmol.* 2004, *137*, 655–661.

[18] Shitama, T., Hayashi, H., Noge, S., Uchio, E., Oshima, K., Haniu, H., Takemori, N., Komori, N., Matsumoto, H., *Proteomics Clin. Appl.* 2008, *2*, 1265–1280.

[19] Yoshimura, T., Sonoda, K., Sugahara, M., Mochizuki, Y., Enaida, H., Oshima, Y., Ueno, A., Hata, Y., Yoshida, H., Ishibashi, T., *PLoS One* 2009, *4*, 1–9.

[20] Gao, B.-B., Chen, X., Timothy, N., Aiello, L. P., Feener, E. P., *J. Proteome Res.* 2008, *7*, 2516–2525.

[21] García-Ramírez, M., Canals, F., Hernández, C., Colomé, N., Ferrer, C., Carrasco, E., García-Arumí, J., Simó, R., *Diabetologia* 2007, *50*, 1294–1303.

[22] Kim, T., Kim, S. J., Kim, K., Kang, U.-B., Lee, C., Park, K. S., Yu, H. G., Kim, Y., *Proteomics* 2007, *7*, 4203–4215.

[23] Koyama, R., Nakanishi, T., Ikeda, T., Shimizu, A., *J. Chromatogr. B* 2003, *792*, 5–21.

[24] Ouchi, M., West, K., Crabb, J. W., Kinoshita, S., Kamei, M., *Exp. Eye Res.* 2005, *81*, 176–182.

[25] Wang, H., Feng, L., Hu, J. W., Xie, C. L., Wang, F., *Proteome Sci.* 2012, *10*, 1–11.

[26] Yamane, K., Minamoto, A., Yamashita, H., Takamura, H., Miyamoto-Myoken, Y., Yoshizato, K., Nabetani, T., Tsugita, A., Mishima, H. K., *Mol. Cell. Proteomics* 2003, *2*, 1177–1187.

[27] Yu, J., Liu, F., Cui, S.-J., Liu, Y., Song, Z.-Y., Cao, H., Chen, F.-E., Wang, W.-J., Sun, T., Wang, F., *Proteomics* 2008, *8*, 3667–3678.

[28] Nakanishi, T., Koyama, R., Ikeda, T., Shimizu, A., *J. Chromatogr. B. Analyt. Technol. Biomed. Life Sci.* 2002, *776*, 89–100.

[29] Kim, S. J., Kim, S., Park, J., Lee, H. K., Park, K. S., Yu, H. G., Kim, Y., *Curr. Eye Res.* 2006, *31*, 231–240.

[30] Aretz, S., Krohne, T. U., Kammerer, K., Warnken, U., Hotz-Wagenblatt, A., Bergmann, M., Stanzel, B. V., Kempf, T., Holz, F. G., Schnölzer, M., Kopitz, J., *Proteome Sci.* 2013, *11*, 1–10.

[31] Neal, R. E., Bettelheim, F., Lin, C., Winn, K. C., Garland, D. L., Zigler, J. S., *Exp. Eye Res.* 2005, *80*, 337–347.

[32] Hernández, C., García-Ramírez, M., Colomé, N., Corraliza, L., García-Pascual, L., Casado, J., Canals, F., Simó, R., *Diabetes Metab. Res. Rev.* 2013, *29*, 499–506.

[33] Hernández, C., García-Ramírez, M., Colomé, N., Villarroel, M., Corraliza, L., García-Pacual, L., Casado, J., Canals, F., Simó, R., *Diabetes Care* 2010, *33*, 92.

[34] Yu, J., Peng, R., Chen, H., Cui, C., Ba, J., *Invest. Ophthalmol. Vis. Sci.* 2012, *53*, 8146–8153.

[35] Ahmed, N., Rice, G. E., *J. Chromatogr. B. Analyt. Technol. Biomed. Life Sci.* 2005, *815*, 39–50.

[36] Bodzon-Kulakowska, A., Bierczynska-Krzysik, A., Dylag, T., Drabik, A., Suder, P., Noga, M., Jarzebinska, J., Silberring, J., *J. Chromatogr. B. Analyt. Technol. Biomed. Life Sci.* 2007, *849*, 1–31.

[37] Issaq, H. J., *Electrophoresis* 2001, *22*, 3629–3638.

[38] Jafari, M., Primo, V., Smejkal, G. B., Moskovets, E. V., Kuo, W. P., Ivanov, A. R., *Electrophoresis* 2012, *33*, 2516–2526.

[39] Abdallah, C., Dumas-Gaudot, E., Renaut, J., Sergeant, K., *Int. J. Plant Genomics* 2012, *2012*, 1–17.

[40] Chandramouli, K., Qian, P.-Y., *Hum. Genomics Proteomics* 2009, *2009*, 1–22.

[41] Pollreisz, A., Funk, M., Breitwieser, F. P., Parapatics, K., Sacu, S., Georgopoulos, M., Dunavoelgyi, R., Zlabinger, G. J., Colinge, J., Bennett, K. L., Schmidt-Erfurth, U., *Exp. Eye Res.* 2013, *108*, 48–58.

[42] Cañas, B., Piñeiro, C., Calvo, E., López-Ferrer, D., Gallardo, J. M., *J. Chromatogr. A* 2007, *1153*, 235–258.

[43] Duh, E. J., Yang, H. S., Haller, J., De Juan, E., Humayun, M. S., Gehlbach, P., Melia, M, Pieramici, D., Harlan, J. B., Campochiaro, P., Zack, D. J., *Am. J. Ophthalmol.* 2004, *137*, 668–674.

[44] Liu, T., Qian, W., Mottaz, H. M., Gritsenko, M. A., Norbeck, A. D., Moore, R. J., Purvine, S. O., Camp, D. G., Smith, R. D., *Mol. Cell. Proteomics* 2006, *5*, 2167–2174.

[45] Görg, A., Weiss, W., Dunn, M. J., *Proteomics* 2004, *4*, 3665–3685.

[46] Görg, A., Drews, O., Lück, C., Weiland, F., Weiss, W., *Electrophoresis* 2009, *30*, 122–132.

[47] Beranova-Giorgianni, S., *Trends Analyt. Chem.* 2003, *22*, 273–281.

[48] Rabilloud, T., Chevallet, M., Luche, S., Lelong, C., *J. Proteomics* 2010, *73*, 2064–2077.

[49] Ong, S. E., Pandey, A., *Biomol. Eng.* 2001, *18*, 195–205.

[50] Semba, R. D., Enghild, J. J., Venkatraman, V., Dyrlund, T. F., Van Eyk, J. E., *Proteomics* 2013, *13*, 2500–2511.

[51] Laicine, E. M., Haddad, A., *Exp. Eye Res.* 1994, *59*, 441–445.

[52] Shimizu, A., Nakanishi, T., Koyama, R., Ikeda, T., *Rinsho Byori* 2002, *50*, 169–172.

[53] Boguth, G., Harder, A., *Electrophoresis* 2000, *21*, 1037–1053.

[54] Carrette, O., Burkhard, P. R., Sanchez, J., Hochstrasser, D. F., *Nat. Protoc.* 2006, *1*, 812–823.

[55] Penque, D., *Proteomics Clin. Appl.* 2009, *3*, 155–172.

[56] Chevalier, F., *Proteome Sci.* 2010, *8*, 1–10.

[57] Lilley, K. S., Razzaq, A., Dupree, P., *Curr. Opin. Chem. Biol.* 2002, *6*, 46–50.

[58] Fichmann, J., Westermeier, R., in: Link, A. J. (Ed.), *2-D proteome analysis protocols*, Humana Press, New Jersey 1999, pp. 1–7.

[59] Jiang, L., He, L., Fountoulakis, M., *J. Chromatogr. A* 2004, *1023*, 317–320.

[60] Thongboonkerd, V., in: Thongboonkerd, V. (Ed.), *Proteomics of Human Body Fluids*, Humana Press, New Jersey 2007, pp. 495–507.

[61] Garfin, D. E., *Trends Analyt. Chem.* 2003, *22*, 263–272

[62] Funatsu, H., Yamashita, H., Nakanishi, Y., Hori, S., *Br. J. Ophthalmol.* 2002, *86*, 311–315.

[63] Mohan, N., Monickaraj, F., Balasubramanyam, M., Rema, M., Mohan, V., *J. Diabetes Complications* 2012, *26*, 435–441.

[64] Patel, J. I., Tombran-Tink, J., Hykin, P. G., Gregor, Z. J., Cree, I. A., *Exp. Eye Res.* 2006, *82*, 798–806.

[65] Shao, J., Xin, Y., Yao, Y., *Clin. Chim. Acta* 2011, *412*, 2117–2121.

[66] Yan, Q., Clark, J. I., Sage, E. H., *Exp. Eye Res.* 2000, *71*, 81–90.

[67] Clausen, R., Weller, M., Wiedemann, P., Heimann, K., Hilgers, R. D., Zilles, K., *Graefes Arch. Clin. Exp. Ophthalmol.* 1991, *229*, 186–190.

[68] Zhang, S. X., Wang, J. J., Gao, G., Parke, K., Ma, J., *J. Mol. Endocrinol.* 2006, *37*, 1–12.

[69] Arimura, N., Otsuka, H., Yamakiri, K., Sonoda, Y., Nakao, S., Noda, Y., Hashiguchi, T., Maruyama, I., Sakamoto, T., *Ophthalmology* 2009, *116*, 921–926.

[70] García-Arumí, J., Fonollosa, A., Macià, C., Hernandez, C., Martinez-Castillo, V., Boixadera, A., Zapata, M. A., Simo, R., *Eye* 2009, *23*, 1066–1071.

[71] Hernández, C., Carrasco, E., Casamitjana, R., Deulofeu, R., García-Arumí, J., Simó, R., *Diabetes Care* 2005, *28*, 1941–1947.

[72] Davuluri, G., Espina, V., Petricoin, E. F., Ross, M., Deng, J., Liotta, L. A., Glaser, B. M., *Arch. Ophthalmol.* 2009, *127*, 613–621.

[73] Reverter, J. L., Nadal, J., Fernández-Novell, J. M., Ballester, J., Ramió-Lluch, L., Rivera, M. M., Elizalde, J., Abengoechea, S., Guinovart, J. J., Rodríguez-Gil, J. E., *Invest. Ophthalmol. Vis. Sci.* 2009, *50*, 1378–1382.

[74] Funk, M., Karl, D., Georgopoulos, M., Benesch, T., Sacu, S., Polak, K., Zlabinger, G. J., Schmidt-Erfurth, U., *Ophthalmology* 2009, *116*, 2393–2399.

[75] Friedman, J. S., Faucher, M., Hiscott, P., Biron, V. L., Malenfant, M., Turcotte, P., Raymond, V., Walter, M. A., *Hum. Mol. Genet.* 2002, *11*, 1333–1342.

[76] Zhu, Q., Ziemssen, F., Henke-Fahle, S., Tatar, O., Szurman, P., Aisenbrey, S., Schneiderhan-Marra, N., Xu, X., Grisanti, S., *Ophthalmology* 2008, *115*, 1750–1755.

[77] Walia, S., Clermont, A. C., Gao, B.-B., Aiello, L. P., Feener, E. P., *Semin. Ophthalmol.* 2010, *25*, 289–294.

[78] Hustoft, H., Malerod, H., Wilson, S., Reubsaet, L., Lundanes, E., Greibrokk, T., in: Leung, H.-C. (Ed.) *Integrative Proteomics*, InTech, Rijeka 2012, pp. 73–92.

[79] Westermeier, R., Naven, T., *Proteomics Practice*, Wiley-VCH, Weinheim 2002.

[80] Granvogl, B., Plöscher, M., Eichacker, L. A., *Anal. Bioanal. Chem.* 2007, *389*, 991–1002.

[81] Shevchenko, A., Shevchenko, A., *Anal. Biochem.* 2001, *296*, 279–283.

[82] Speicher, K. D., Kolbas, O., Harper, S., Speicher, D. W., *J. Biomol. Tech.* 2000, *11*, 74–86.

[83] Michalski, W. P., Shiell, B. J., *Anal. Chim. Acta* 1999, *383*, 27–46.

[84] Marouga, R., David, S., Hawkins, E., *Anal. Bioanal. Chem.* 2005, *382*, 669–678.

[85] Van den Bergh, G., Arckens, L., *Expert Rev. Proteomics* 2005, *2*, 243–252.

[86] Issaq, H., Veenstra, T., *Biotechniques* 2008, *44*, 697–700.

[87] Patton, W. F., *J. Chromatogr. B. Analyt. Technol. Biomed. Life Sci.* 2002, *771*, 3–31.

[88] Riederer, B. M., *J. Proteomics* 2008, *71*, 231–244.

[89] Miller, I., Crawford, J., Gianazza, E., *Proteomics* 2006, *6*, 5385–5408.

[90] Unlü, M., Morgan, M. E., Minden, J. S., *Electrophoresis* 1997, *18*, 2071–2077.

[91] Tannu, N. S., Hemby, S. E., *Nat. Protoc.* 2006, *1*, 1732–1742.

[92] Garcia-Ramírez, M., Hernández, C., Villarroel, M., Canals, F., Alonso, M. A., Fortuny, R., Masmiquel, L., Navarro, A., García-Arumí, J., Simó, R., *Diabetologia* 2009, *52*, 2633–2641.

[93] Simó, R., Higuera, M., García-Ramírez, M., Canals, F., García-Arumí, J., Hernández, C., *Arch. Ophthalmol.* 2008, *126*, 1076–1081.

[94] Van den Bergh, G., Arckens, L., *Curr. Opin. Biotechnol.* 2004, *15*, 38–43.

[95] Azarkan, M., Huet, J., Baeyens-Volant, D., Looze, Y., Vandenbussche, G., *J. Chromatogr. B. Analyt. Technol. Biomed. Life Sci.* 2007, *849*, 81–90.

[96] Butt, A., Davison, M. D., Smith, G. J., Young, J. A., Gaskell, S. J., Oliver, S. G., Beynon, R. J., *Proteomics* 2001, *1*, 42–53.

[97] Finoulst, I., Pinkse, M., Van Dongen, W., Verhaert, P., *J. Biomed. Biotechnol.* 2011, *2011*, 1–14.

[98] Shi, Y., Xiang, R., Horváth, C., Wilkins, J. A., *J. Chromatogr. A* 2004, *1053*, 27–36.

[99] Mitulovic, G., Mechtler, K., *Brief. Funct. Genomic. Proteomic.* 2006, *5*, 249–260.

[100] Wang, H., Feng, L., Hu, J., Xie, C., Wang, F., *Exp. Eye Res.* 2013, *108*, 110–119.

[101] Tamburro, D., Facchiano, F., Petricoin, E. F., Liotta, L. A., Zhou, W., *Proteomics Clin. Appl.* 2010, *4*, 839–846.

[102] Lee, W.-C., Lee, K. H., *Anal. Biochem.* 2004, *324*, 1–10.

[103] Ma, Y., Yang, C., Tao, Y., Zhou, H., Wang, Y., *FEBS J.* 2013, *280*, 5668–5681.

[104] Gundry, R. L., White, M. Y., Murray, C. I., Kane, L. A., Fu, Q., Stanley, B. A., Van Eyk, J. E., *Curr. Protoc. Mol. Biol.* 2009, *10*, 2–29.

[105] Kim, K., Kim, S. J., Yu, H. G., Yu, J., Park, K. S., Jang, I.-J., Kim, Y., *J. Proteome Res.* 2010, *9*, 689–699.

[106] Gedela, S., Medicherla, N., *Chromatographia* 2007, *65*, 511–518.

[107] Chiu, C.-W., Chang, C.-L., Chen, S.-F., *J. Sep. Sci.* 2012, *35*, 3293–3301.

[108] Luo, R., Zhao, H., *Stat. Interface* 2012, *5*, 99–107.

[109] Mandal, N., Kofod, M., Vorum, H., Villumsen, J., Eriksen, J., Heegaard, S., Prause, J. U., Ahuja, S., Honoré, B., La Cour, M., *Acta Ophthalmol.* 2013, *9*, 333–334.

Section 3 – Paper II

Vitreous humor proteome: unraveling the molecular mechanisms underlying proliferative vitreoretinal diseases

Fátima M. Santos, João Paulo Castro de Sousa, Alberto Paradela, Sergio Ciordia, Cândida T. Tomaz, Luís A. Passarinha

Submitted for publication (2020)

This paper summarizes the potential biomarkers of PDR, nAMD, and PVR found in the study of the vitreous proteome. This review offers a state of art of ocular diseases, including data about their prevalence in the world population, and a perspective on how multi-OMICS approaches can improve its management. After that, it explains the relevance of vitreous and why this is a suitable matrix to find new pharmaceutical targets and to elucidate some of the pathological mechanisms underlying proliferative retinal diseases. A summary of the clinical features and candidate biomarkers found in the studies of the vitreous proteome is posteriorly made for PDR, nAMD, and PVR. Moreover, it provides some insights into the role of these biomarkers in eye physiology and pathophysiology. Here, the vitreous is seen as the scene of a complex interplay between inflammation, angiogenesis, fibrosis, oxidative stress, neurodegeneration, and remodeling of the extracellular matrix.

The supplementary material of this article is available in the Appendix.

Review

Vitreous humor proteome: unraveling the molecular mechanisms underlying proliferative vitreoretinal diseases

Fátima M. Santos[1,2,3], João Paulo Castro de Sousa[1,4], Alberto Paradela[5], Sergio Ciordia[5], Cândida T. Tomaz[1,2], Luís A. Passarinha[1,3,6]*

[1] CICS-UBI – Centro de Investigação em Ciências da Saúde, Universidade da Beira Interior, 6201001 Covilhã, Portugal.

[2] Chemistry Department, Faculty of Sciences, University of Beira Interior, 6201-001 Covilhã, Portugal

[3] UCIBIO – Applied Molecular Biosciences Unit, Departamento de Química, Faculdade de Ciências e Tecnologia, Universidade NOVA de Lisboa, 2829-516 Caparica, Portugal

[4] Department of Ophthalmology, Centro Hospitalar de Leiria, 2410-197 Leiria, Portugal.

[5] Unidad de Proteómica, Centro Nacional de Biotecnología, CSIC, Calle Darwin 3, Campus de Cantoblanco, 28049 Madrid, Spain.

[6] Laboratory of Pharmacology and Toxicology—UBIMedical, University of Beira Interior, 6200-284 Covilhã, Portugal.

Abstract

Proliferative diabetic retinopathy (PDR), proliferative vitreoretinopathy (PVR), and wet age-related macular degeneration (AMD) are leading causes of visual impairment and blindness in middle-income and industrialized countries. As proliferative diseases are multifactorial, multi-omics approaches are required for a better understanding of pathophysiologic processes underlying the shift between the non-proliferative and proliferative etiology. For a long time, vitreous has been unappreciated concerning its role in health and disease, but recently it has been gaining a growing interest. Proteomics studies proved that vitreous is more complex and biologically active than initially thought, and its changes reflect the physiological and pathological state of the eye. The vitreous is the scene of a complex interplay between inflammation, angiogenesis, fibrosis, oxidative stress, neurodegeneration, and remodeling of the extracellular matrix. Therefore, vitreous proteome reflects the pathological events that occur in proliferative diseases, but the vitreous itself may also play a pathological role in the eye. Although the demand for suitable vitreous biomarkers in ocular disease has not been successful so far, the study of the vitreous proteome is promising to elucidate some of the pathological mechanisms underlying proliferative retinal diseases and to find potential pharmaceutical targets.

Keywords: Age-Related Macular Degeneration, Proliferative Diabetic Retinopathy, Proliferative Vitreoretinopathy, Vitreous Proteomics.

***Corresponding Author**: UCIBIO, Departmento de Química, Faculdade de Ciências e Tecnologia, Universidade Nova de Lisboa, 2829-516 Caparica, Portugal; Tel.: +351 275 329 069; Fax: +351 275 329 099; Email address: lpassarinha@fcsaude.ubi.pt,lapp@ubi.pt.

Table of Contents

1. Background - Translational research in proliferative vitreoretinal diseases

Visual impairment and blindness severely impact the quality of life of the affected individuals and are a significant burden for healthcare systems (Bourne et al., 2017; Köberlein et al., 2013; Sabanayagam and Cheng, 2017). Despite improvements achieved in the prevention and control of ocular diseases in the past 30 years, the number of people with moderate or severe visual impairment will increase due to the exacerbated growth and aging of the world population and increasing prevalence of diabetes mellitus (Ackland et al., 2018; Guariguata et al., 2014; Wong et al., 2014). Diabetic retinopathy (DR), proliferative vitreoretinopathy (PVR), and age-related macular degeneration (AMD) are leading causes of visual impairment and blindness in middle-

Abbreviations: 2DE, Two-dimensional electrophoresis; AAT, Alpha-1-antitrypsin; AGEs, Advanced glycation end products; AMD, Age-related macular degeneration; APO4,Apolipoprotein A4; APP, Amyloid-beta A4 protein; BDNF, Brain-derived neurotrophic factor; BRB, Blood-retinal barrier; CCL3, Macrophage inflammatory protein; CCN2, Connective tissue growth factor; CE-MS, Capillary electrophoresis coupled to mass spectrometry; CFH, Complement factor H; CLU, Clusterin; CNTF, Ciliary neurotrophic factor; CNV, Choroidal neovascularization; CSF3, Granulocyte colony-stimulating factor; CSFs, Colony-stimulating factors; CXCL8, Interleukin-8; DME, Diabetic macular edema; DR, Diabetic retinopathy; ECM, Extracellular matrix; EMT, Epithelial-mesenchymal transition; ENO2, Gamma-enolase; ERM, Epiretinal membranes; FGF, Fibroblast growth factor; GDNF, Glial cell-derived neurotrophic factor; HIF-1, Hypoxia-inducible factor; iBRB, Inner blood-retinal barrier; oBRB, Outer blood-retinal barrier; IGFBPs, Insulin-like growth factor-binding proteins; IGFs, Insulin-like growth factors; INF-γ, Interferon-gamma; LC-MS, Liquid chromatography coupled to mass spectrometry; MCP-1, Monocyte chemoattractant protein-1; MMP9, Matrix metalloproteinase 9; MMP2, 72 kda type IV collagenase; MMPs, Metalloproteinases; nAMD, "Wet" or Neovascular age-related macular degeneration; NGF, Nerve growth factor; NT3, Neurotrophin-3; NT4, Neurotrophin-4; NV, Neovascularization; OPTC, Opticin; PDGF, Platelet-derived growth factor; PDR, Proliferative diabetic retinopathy; PEDF, Pigment epithelium-derived factor; PGF, Placenta growth factor; PVD, Posterior vitreous detachment; PVR, Proliferative vitreoretinopathy; ROS, Reactive oxygen species; RPE, Retinal pigment epithelium; RRD, Rhegmatogenous retinal detachment; SOD3, Extracellular superoxide dismutase; SOD1, Superoxide dismutase; SRF, Subretinal fluid; TGF-β, Transforming growth factor; TIMP1, Metallopeptidase inhibitor 1; TNF-α, Tumor necrosis factor; TTR, Transthyretin; VEGF, Vascular endothelial growth factor; VEGFR-1, Vascular endothelial growth factor receptor 1.

income and industrialized countries (Kuiper et al., 2006; Yoshida et al., 2017). Despite the multiple options available, there is still progression to visual impairment and blindness in proliferative etiology (Semba et al., 2013), which reinforces the necessity of globally strengthen the eye health care system, and find better strategies for the prevention and treatment of these diseases (Ramke and Gilbert, 2017). Considering these diseases result from a complex interaction between numerous pathophysiological processes, multi-omics approaches are necessary for a deeper understanding of the changes underlying the transition from a non-proliferative to proliferative etiology. Multi-omics approaches allow the integration of multiple biomarkers for diagnosis and prognosis, for discovering new therapeutic targets, and for assessing the efficacy and safety of treatment (Pulley et al., 2020; Subramanyam and Goyal, 2016; van Karnebeek et al., 2018). In this sense, ocular proteomics has emerged as an opportunity for discovering new biomarkers, which could help to unveil the pathophysiology of many ocular diseases, anticipate its progressive states and predict the response to therapy (Jay and Gillies, 2012; Monteiro et al., 2015; Semba et al., 2013; Velez et al., 2018).

2. Vitreous humor proteomics

Vitreous, also termed vitreous body or vitreous humor, is a transparent fluid that fills the posterior cavity of the eye, surrounded by the retina, pars plana, and lens (Chirila and Hong, 2016; Kodama et al., 2013; Sebag, 2010). It is a highly hydrated, avascular, and virtually acellular connective tissue, consisting of a network of collagen fibrils surrounded by glycosaminoglycans, inorganic salts, sugars, lipids, and soluble proteins (Chirila and Hong, 2016; Le Goff and Bishop, 2008). For many years, it was thought that vitreous function was merely structural, allowing to support and protect the surrounding ocular tissues from physical impacts and vibration (Alovisi et al., 2017; Chirila and Hong, 2016; De Smet et al., 2013). Although many of the vitreous physiological functions remain unclear, vitreous contributes to the total transparency of the ocular pathways, regulates eye growth and shape during development, serves as a barrier to biomolecules and cells, allows the repository and diffusion of the substances involved in the eye metabolism, and regulates oxygen within the eye (Alovisi et al., 2017; Chirila and Hong, 2016; Holekamp, 2010; Le Goff and Bishop, 2008; Sebag, 2009). Despite the fact that vitreous has been unappreciated concerning its role in health and disease for a long time (Kodama et al., 2013; Sebag, 2009), vitreous proved to be extremely attractive from biological and analytical perspectives. The proteome and biochemical properties of vitreous reflect the physiological and pathological conditions of the eye due to its close contact with the inner retina, lens, and ciliary body (Angi et al., 2012; Mahajan and Skeie, 2014; Monteiro et al., 2015). Also, vitreous can be obtained without marked detriment to the eye as part of the clinical routine, and so it could be used as an indirect molecular biopsy of the retina (Monteiro et al., 2015; Skeie et al., 2015; Velez et al., 2018). Furthermore, aging-related changes of vitreous, such as vitreous liquefaction and posterior vitreous detachment (PVD), are presumed to be underlying several retinal diseases (De Smet et al., 2013; Holekamp, 2010; Le Goff and Bishop, 2008; Ponsioen et al., 2010). The growing interest in vitreous in health and disease is demonstrated by the fact that the number of proteins identified increased from 545 to more than 6538 in only 5 years (Ahmad et al., 2018; Semba et al., 2013).

The outcome from vitreous proteome studies is promising to elucidate some of the pathological mechanisms underlying proliferative retinal diseases. This review summarizes the changes in vitreous proteome reported in patients with PDR, neovascular AMD (nAMD), and PVR, and how these could be correlated with pathological events, such as angiogenesis, inflammation, fibrosis, oxidative stress, neurodegeneration, and vitreous remodeling.

3. Characterization of the vitreous proteome in vitreoretinal diseases

3.1. Diabetic retinopathy

DR is one of the major complications in patients with diabetes (Nentwich, 2015; Saaddine et al., 2008; Wang and Lo, 2018), accounting for 1.1% of blindness among adults aged 50 years and older in 2015 (Flaxman et al., 2017). The most recent world report on vision from World Health Organization (WHO) foresees that about 146 million (34.6%) of 422 million adults with diabetes had some form of DR (World Health Organization, 2019). The public health burden with DR will be intensified as a result of the dramatic increase in the prevalence of diabetes in middle- and low-income countries (Duh et al., 2017; Guariguata et al., 2014; Santos et al., 2017). The duration and type of diabetes, poor glycemic control, hypertension, and high levels of glycated hemoglobin A1c and triglycerides are the main risk factors for DR (Ding and Wong, 2012; Ting et al., 2016; Yau et al., 2012). The pathophysiology of DR and current treatment were recently reviewed by several authors (Duh et al., 2017; Kusuhara et al., 2018; Wang and Lo, 2018) and are summarized in figure 1. In an early stage, microvascular changes occur in response to hyperglycemia, but increasing pieces of evidence suggest that neuroglial degeneration may precede microvascular changes (Duh et al., 2017; Kusuhara et al., 2018; Lechner et al., 2017; Wang and Lo, 2018; Wong et al., 2016). As the severity of DR progresses, capillary nonperfusion and occlusion lead to retinal ischemia, which gradually drives pathological intra-retinal and intravitreal neovascularization (NV) (Duh et al., 2017; Lechner et al., 2017; Wong et al., 2016). The continuous formation of leaky and brittle vessels causes vitreous hemorrhage and retinal detachment (RD), but other events, such as Müller cell gliosis, neural apoptosis, inflammation, and fibrosis, are exacerbated with the progression to PDR (Lechner et al., 2017; Wong et al., 2016). Furthermore, changes in the regulation of the tight junctions of the endothelial cells result in increased vascular permeability and breakdown of the inner blood-retinal barrier (iBRB), which contributes to diabetic macular edema (DME) (Daruich et al., 2018; Eshaq et al., 2017; Klaassen et al., 2013; Lee et al., 2015). Furthermore, the production of advanced glycation end products (AGEs), due to hyperglycemia, triggers abnormal crosslinks between collagen fibrils, causing biochemical and structural alterations in the vitreous, and destabilization of gel structure (Gale et al., 2014; Kandarakis et al., 2014; Stitt, 2001). The involvement of structural and molecular changes in vitreous and at the vitreoretinal surface in progression for PDR leads to the concept of proliferative diabetic vitreoretinopathy (Kroll et al., 2014, 2007; Nawaz et al., 2019). The standard treatment for more advanced phases of DR and DME is a combination of laser photocoagulation (Fong et al., 2007; Romero-Aroca et al., 2014), intravitreal injections of corticosteroids (Boyer et al., 2014; Busch et al., 2018; Iglicki et al., 2019) or anti-vascular endothelial growth factor (VEGF) agents (Bressler

et al., 2017; Cai and Bressler, 2015; Gonzalez et al., 2016; Gross et al., 2015), and vitreoretinal surgery (Sharma et al., 2016). However, these treatments are invasive, expensive, display a significant number of secondary effects and a considerable percentage of patients is non-responsive to the treatment. Therefore, an in-depth understanding of the pathological and protective mechanisms in DR can help to explore cost-effective therapeutic alternatives (Duh et al., 2017; Hernández et al., 2017; Stitt et al., 2016).

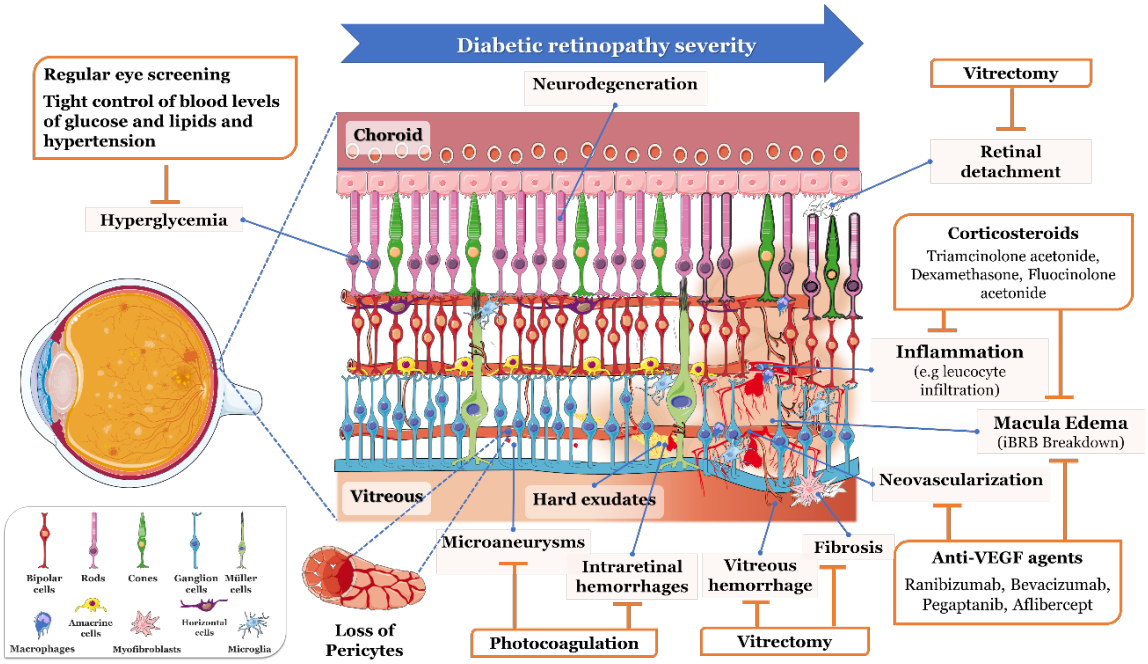

Fig. 1 - Vitreous and retinal anatomy in pathophysiological events in diabetic retinopathy and proliferative diabetic retinopathy and current treatments for each clinical feature. iBRB – inner blood-retinal barrier.

The characterization of the proteome of vitreous humor has contributed extensively to the recognition of pathways involved in DR and to identify biomarkers for its treatment (Csősz et al., 2017; Nawaz et al., 2019; Simó-Servat et al., 2012; Walia et al., 2010). A complete list of the proteins found differentially expressed in DR and PDR patients using proteomic and multiplex approaches is shown in Supplementary Table 1.1. In the first proteomic approaches by two-dimensional electrophoresis (2DE) coupled with mass spectrometry, increased levels of plasma proteins, such as immunoglobulins, complement and coagulation proteins, and acute-phase proteins were consistently reported (García-Ramírez et al., 2007; Kim et al., 2006; Minamoto et al., 2007; Nakanishi et al., 2002; Shitama et al., 2008; Simó et al., 2008). In turn, the levels of pigment epithelium-derived factor (PEDF), and glycolytic/ gluconeogenesis enzymes (e.g. gamma-enolase [ENO2], malate dehydrogenase) and apolipoprotein A4 (APO4) were inconsistent among studies (García-Ramírez et al., 2007; Kim et al., 2006; Minamoto et al., 2007; Shitama et al., 2008; Simó et al., 2008; H. Wang et al., 2012; Yamane et al., 2003), whereas clusterin (CLU), inter-alpha-trypsin inhibitor heavy chain H2, retinol-binding proteins, and crystallins were reported as underexpressed in PDR (García-Ramírez et al., 2007; Simó et al., 2008; H. Wang et al., 2012). Although these studies provided some potential biomarkers of DR progression, the complexity and wide dynamic range of human vitreous represent a challenge for

quantitative analysis by 2DE (Angi et al., 2012; Mandal et al., 2010; Rocha et al., 2014; Santos et al., 2019). To overcome some of these limitations, gel-free techniques, such as liquid chromatography coupled to mass spectrometry (LC-MS) and capillary electrophoresis coupled to mass spectrometry (CE-MS), have emerged as an alternative for vitreous characterization. In these studies, acute-phase proteins, serine protease inhibitors, apolipoproteins, inter-alpha-trypsin inhibitor heavy chains, kallikrein-kinin system activators, and complement and coagulation factors were once again implicated in PDR pathogenesis (Balaiya et al., 2017; Gao et al., 2008, 2007; Gardner and Sundstrom, 2017; Kim et al., 2010, 2007; Li et al., 2018; Loukovaara et al., 2015; Schori et al., 2018; Wang et al., 2013). The role of the complement system in PDR was recently investigated (Shahulhameed et al., 2020). They suggested that the alternative pathway of complement is activated in PDR since increased levels of both C3 and its activated fragment and complement factor H (CFH) were found in vitreous and serum samples of patients with PDR. However, many other proteins, that had not yet been reported, have been found differentially expressed in these gel-free proteomics approaches. In addition to its contribution to the understanding of the role of carbonic anhydrase in the activation of the kallikrein-kinin system, Gao and co-workers reported lower levels of extracellular superoxide dismutase (SOD3), neuroserpin, cell adhesion molecules (e.g. calsyntenin-1), and amyloid-forming proteins (e.g. amyloid-beta A4 protein [APP]) in PDR compared with diabetic patients without DR (Gao et al., 2008, 2007). Wang and co-workers (2013) identified 96 differentially expressed proteins in PDR vitreous compared to healthy donor samples, many of them related to glycolytic process, visual perception, phagosome pathways, and hypoxia-inducible factor (HIF-1) pathways (Wang et al., 2013). In (Balaiya et al., 2017) study, anti-angiogenic proteins, immune modulators, acute-phase proteins, proteases, and extracellular matrix (ECM) components (e.g. collagens, opticin [OPTC]) were only detected in patients with epiretinal membranes (ERM) or macular hole, whereas proteins that participate in complement, coagulation, and kinin-kallikrein system were uniquely identified PDR. In another study, the authors proposed a new personalized medicine method for the prevention and treatment of early DR based on proteomics approaches. NRF2-mediated oxidative stress response and cell proliferation signaling are some of the pathways that were found activated in PDR vitreous, while HIPPO signaling pathway and central nervous system development were found inhibited (Gardner and Sundstrom, 2017). In a more recent study, Schori and colleagues (2018) found 142 proteins significantly differently expressed (84 up- and 58 downregulated) in PDR vitreous compared to ERM. Proteins involved in the regulation of angiogenesis (e.g. VEGF), cell adhesion, and ECM organization, including metalloproteinases (MMPs) and inhibitors, and proteoglycans, were found upregulated in PDR. In turn, the downregulated molecules were associated with lysosomal activity/ autophagy and biological processes in the nervous system, including developmental processes, ECM organization, and cell adhesion. Interestingly, the reduction in the levels of some of these proteins, including APP, neuroserpin, acid ceramidase, and ceroid-lipofuscinosis neuronal protein 5, has been related to neurodegeneration (Schori et al., 2018). Based on intensity-measurements and spectral counting, 138 vitreous samples collected from patients with DR or PDR, including patients treated with bevacizumab, were analyzed by label-free quantitative proteomics. Of the 1351 quantified

proteins, higher levels of inflammatory mediators, cell adhesion molecules, oxidative stress markers, and ECM proteoglycans were found in the vitreous of patients with PDR. The authors also reported the downregulation of 72 proteins after the administration of bevacizumab, including apolipoproteins, crystallins, immunoglobulins, insulin-like growth factor-binding proteins (IGFBPs), and proteins involved in cell adhesion and apoptosis (Loukovaara et al., 2015). Zou and co-workers (2018) studied the changes induced by ranibizumab in the vitreous proteome of patients with PDR and found that platelet degranulation and integrin cell surface interaction are pathways severely affected by this treatment. Many complement and coagulation proteins, crystallins, immunoglobulins were not detected in the vitreous after treatment. By contrast, TIMP2 was found upregulated in response, while several proteins related to HIF-1 signaling pathway (e.g. metalloproteinase inhibitor 1 [TIMP1] and glycolytic proteins), carbon metabolism, and oxidative stress were significantly reduced (Zou et al., 2018).

Alternatively to proteomic assays, many authors have applied multiplex assays for the quantification of the vitreous proteome for the detection of key proteins (e.g. VEGF) whose intravitreal concentration varies in the range of picograms (Klaassen et al., 2017; Koskela et al., 2013; Maier et al., 2008; Srividya et al., 2018; Suzuki et al., 2011; Tsai et al., 2018). VEGF has been established as one of the key molecules in the pathology of DR, and its levels in vitreous and plasma have been correlated with the progression of PDR (Wang et al., 2014) and clinical features such as macular volume and central retinal thickness (Mesquita et al., 2018a, 2017). Several studies find a positive correlation between VEGF intravitreal levels in PDR and levels of vascular cell adhesion protein 1 (Hernández et al., 2001), alpha-crystallin B chain (Chen et al., 2017), MMPs (Abu El-Asrar et al., 2013; Ishizaki et al., 2006), oxidative stress markers (Brzović-Šarić et al., 2015; Izuta et al., 2010, 2009), and proteins related to the renin-angiotensin system (Funatsu et al., 2002; Ishizaki et al., 2006). Besides VEGF, other regulators of angiogenesis were found upregulated in the vitreous, including angiopoietin-2 (Huber and Wachtlin, 2012; Klaassen et al., 2017), IGFBPs (Klaassen et al., 2017; Simó et al., 2002), placenta growth factor (PGF) (Al Kahtani et al., 2017; Klaassen et al., 2017; Kovacs et al., 2015; Tsai et al., 2018), platelet-derived growth factor (PDGF) (Klaassen et al., 2017; Kovacs et al., 2015; Srividya et al., 2018; Suzuki et al., 2011), PEDF (Duh et al., 2004), hepatocyte growth factor (Klaassen et al., 2017; Kovacs et al., 2015; Patel et al., 2006), and soluble VEGF receptor 1 (VEGFR-1) (Huber and Wachtlin, 2012). Other studies tried to recognize the role of chronic neuroinflammation in DR through the quantitation of inflammatory mediators, adhesion molecules, and neurotrophic factors (Boss et al., 2017; Klaassen et al., 2017). These studies found higher levels of these factors in DR, including neurotrophins (NT3, NT4), nerve growth factor (NGF), brain-derived, glial-derived, and ciliary neurotrophic factors (BDNF, GDNF, and CNTF), interleukins (IL-1β, CXCL8), tumor necrosis factor (TNF-α), intercellular adhesion molecule 1 (ICAM1) (Boss et al., 2017; Klaassen et al., 2017). Many other studies reported the up-regulation of cytokines in DR vitreous, including interferon-gamma (INF-γ) (Srividya et al., 2018; Tsai et al., 2018), TNF-α (Kovacs et al., 2015; Srividya et al., 2018), colony-stimulating factor (CSF3) (Srividya et al., 2018), interleukins (e.g. IL1β, IL-6) (Koskela et al., 2013; Kovacs et al., 2015; Srividya et al., 2018; Suzuki et al., 2011; Tsai et al., 2018), chemokines (e.g CXCL8, CXCL10, CCL2) (Koskela et al., 2013; Maier et al., 2008;

Srividya et al., 2018; Suzuki et al., 2011), and adhesion molecules (e.g ICAM1, VCAM1) (Hernández et al., 2001; Koskela et al., 2013). Conversely, other studies reported the downregulation of neurotrophins/anti-angiogenic molecules (e.g. PEDF, VEGFR-1, NGF) in diabetic vitreous (Huber and Wachtlin, 2012; Mysona et al., 2015; Patel et al., 2006), whereas higher levels of TNF-α, CXCL8, NT-3, NGF, GDNF, and CNTF were detected in early DR than in active PDR (Boss et al., 2017). By measuring the levels of inflammatory mediators at distinct stages of DR, Kovacs and co-workers (2015) found a significant increase of IL-6 levels in an early phase of DR, while CXCL8 levels were found to progressively increase with the progression of the disease (Kovacs et al., 2015). Koskela and colleagues (2013) found higher levels of IL-6 and CXCL8, but not of adhesion molecules, in vitreous compared to the plasma of patients with PDR, which suggests an active local production of these interleukins at the retinal level (Koskela et al., 2013). Reverter and co-workers (2009) observed a significant decrease in phosphorylation levels of colony-stimulating factors (CSFs), interleukins, and chemokines by comparing the vitreous of diabetic patients to control subjects. Although the exact mechanisms that contribute to decreased phosphorylation are not known, changes in the functionality of inflammatory proteins may contribute to the DR pathogenesis (Reverter et al., 2009).

3.2. Age-related macular degeneration

AMD is a multifactor ocular disease characterized by a degeneration of photoreceptors and retinal pigment epithelium (RPE) in the macula, which affects the central vision and high-resolution visual acuity (Ardeljan and Chan, 2013; Ehrlich et al., 2008; Jager et al., 2008; Lim et al., 2012). AMD represents the most common cause of blindness among the elderly in developed countries (Rudnicka et al., 2012; Wong et al., 2014). According to WHO, 195.6 million people aged 30 to 97 years have AMD, of which about 10.4 million have moderate to severe vision impairment or blindness (World Health Organization, 2019). With the aging of the world population, it was predicted that the number of people affected by AMD will increase to 243.4 million in 2030, and, to 288 million in 2040 (Wong et al., 2014; World Health Organization, 2019). Risk factors such as age, smoking, high body mass index, and genetic factors were strongly associated with the development of AMD (Age-Related Eye Disease Study Research Group, 2005a; Lambert et al., 2016; Rudnicka et al., 2012). The first signs of AMD are the accumulation of soft drusen, microglia, and choroidal macrophages, the thickening of Bruch's membrane, and changes in pigmentation of the RPE (Figure 2) (Ambati et al., 2013; Ardeljan and Chan, 2013; Jager et al., 2008).

From this early stage, AMD can progress to two distinct forms, a "dry" form, also referred to as geographic atrophy (GA) or non-exudative form, or a "wet" or nAMD (Coleman et al., 2008; Ehrlich et al., 2008; Yonekawa et al., 2015). GA is characterized by extensive atrophy and changes in the pigmentation of RPE, degeneration of overlying photoceptor cells, and loss or closure of the choriocapillaris (Ambati et al., 2013; Coleman et al., 2008; Klein et al., 2008; Yonekawa et al., 2015). GA is mainly developed in the area of regression of soft drusen (Klein et al., 2008), but may also occur independently of the presence of drusen in other regions that showed prior

changes in pigmentation, suggesting an RPE dysfunction (Yonekawa et al., 2015). Approximately 10-15% of all AMD patients end up developing nAMD, which is characterized by choroidal NV (CNV) that extends through Bruch's membrane and RPE into the subretinal or sub-RPE space (Coleman et al., 2008; Gehrs et al., 2006; Jager et al., 2008). As a result, a lipid-rich fluid is accumulated under RPE and neuroretina leading to retinal and vitreous hemorrhages, swelling of the neuro-retinal tissue, and eventually to the development of subretinal fibrous tissue, which can be accompanied by RPE tears, RD, serous exudation, and gliosis (Age-Related Eye Disease Study Research Group, 2005b; Coleman et al., 2008; Gehrs et al., 2006). Currently, therapies for "dry" AMD are still an unmet requirement and its management relies only on the prevention of risk factors or the increase of the consumption of carotenoids, vitamins, zinc and omega-3 acids and practice of physical exercise (Age-Related Eye Disease Study Research Group, 2001; Richer et al., 2016; SanGiovanni, 2008; Seddon, 2006). The most significant advances in management have been made for targeting the "wet" AMD, but many clinical trials are in progression both for dry AMD and nAMD (Forest et al., 2015; Hernández-Zimbrón et al., 2018; Supuran, 2019). Thermal laser photocoagulation (Macular Photocoagulation Study Group, 1994, 1993) and photodynamic therapy (Kertes, 2004; Wormald et al., 2005) were the early treatment for nAMD, but anti-VEGF drugs (Gragoudas et al., 2004; Heier et al., 2012; Mekjavic et al., 2011; Rosenfeld et al., 2006) and anti-angiogenic steroids (Ciulla et al., 2007; Slakter et al., 2006) proved to be more effective in the reduction of CNV.

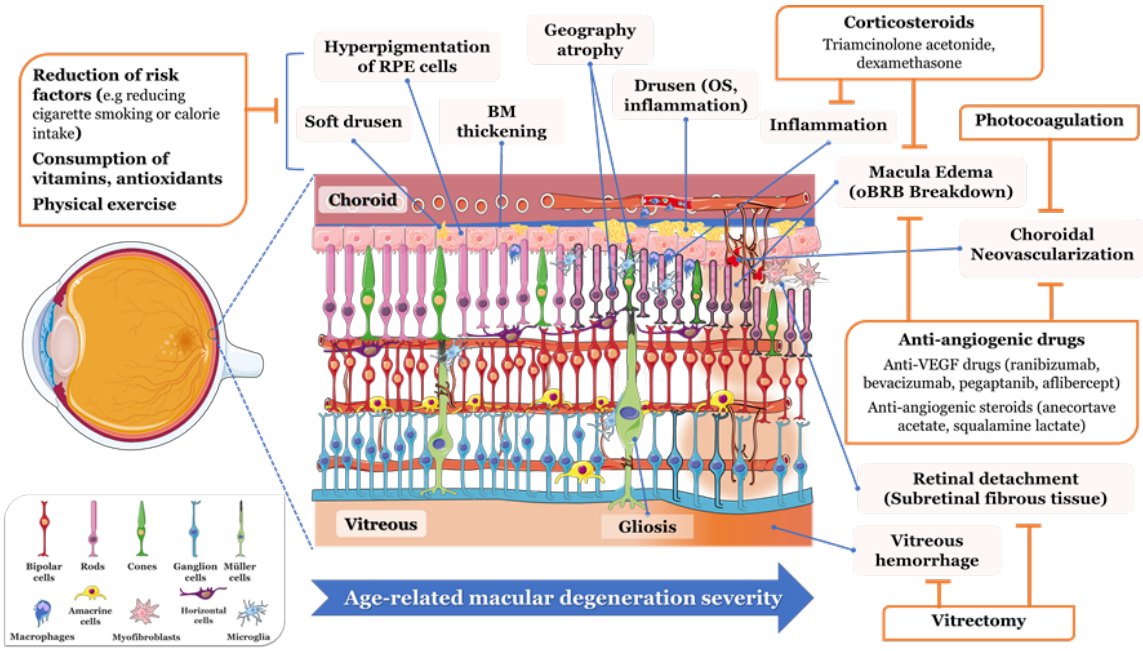

Fig. 2 - Vitreous and retinal anatomy in pathophysiological events in the dry age-related macular degeneration (geography atrophy) and age-related macular degeneration and current treatments for each clinical feature. BM – Bruch's membrane, oBRB – outer blood-retinal barrier, OS – Oxidative stress, RPE– retinal pigment epithelium.

Although complement factors mediated inflammation, angiogenesis, and oxidative stress have been pointed as key pathways (Fritsche et al., 2014; Hernández-Zimbrón et al., 2018), a better understanding of AMD pathophysiologic processes may be crucial for the implementation of more

effective treatments (Lim et al., 2012; Yonekawa et al., 2015). Few studies have been focused on the characterization of vitreous proteomics in AMD, nevertheless, these provided some potential disease biomarkers (Supplementary Table 1.2) (Koss et al., 2014; Nobl et al., 2016; Schori et al., 2018). Koss and co-workers (2014) identified 19 candidate proteins by CE-MS in vitreous of nAMD patients compared to patients with idiopathic floaters. Changes in vitreous proteome reflected the up-regulation of biological processes, such as transport (e.g albumin, transthyretin [TTR], serotransferrin), immune responses (e.g. platelet degranulation, serine protease inhibitor activity), complement cascades, and protection against oxidative stress (e.g. glutathione peroxidase 3) in nAMD (Koss et al., 2014). Nobl and colleagues (2016) identified four biomarkers (OPTC, CLU, PEDF, prostaglandin-H2 D-isomerase) combining the analysis of vitreous samples, collected from 108 patients with nAMD with different degrees of CNV and 24 controls with idiopathic floaters, by CE-MS and LC-MS and the validation by ELISA (Nobl et al., 2016). In another study, 34 and 33 were found differentially expressed proteins in dry AMD and nAMD, respectively, compared to ERM controls, using a label-free LC-MS/MS quantitative method. Cholinesterase was found to be specifically upregulated in dry AMD, while ribonuclease pancreatic (RNAS1) and serine carboxypeptidase were found upregulated in both forms of AMD. Cell adhesion molecules, coagulation factors, lysosomal proteins, and inflammatory mediators were found downregulated in dry AMD. The upregulation of the lysosomal proteins cathepsin Z and prosaposin, and inflammatory mediators (e.g. chitinase-3-like protein 1) suggests that some of these pathways may be activated later in nAMD. Other proteins associated with the glycolytic process (e.g phosphoglycerate mutase 2), oxidative stress (e.g. superoxide dismutase [SOD1]), glutathione reductase), and APP fibril formation (beta-2-microglobulin) were also found upregulated in nAMD. In turn, VEGF and respective receptors were analyzed by ELISA, but surprisingly, these levels were lower in dry AMD and nAMD than in ERM controls, except for VEGFR-1 levels that increased in nAMD (Schori et al., 2018).

Given the role of inflammation and NV in nAMD, it is thought that imbalance levels of inflammatory, angiogenic, and anti-angiogenic factors may be involved in its onset and progression. The role of VEGF in CNV, a hallmark of nAMD, has been strongly supported by its expression in choroidal neovascular membranes and by the clinical efficacy of anti-VEGF treatment (Amadio et al., 2016; Funk et al., 2009). Nevertheless, VEGF was not consistently found upregulated in vitreous of nAMD patients and, in some cases, it was even undetectable in vitreous samples from patients with CNV (Duh et al., 2004). Our research group found lower levels of both VEGF-A and VEGF-B in nAMD compared to patients with retinal vein occlusion and PDR, but it was suggested that this result could be related to reminiscent NV or due to the effect of anti-VEGF treatment (Mesquita et al., 2018a). Huber and colleagues (2012) found increased intravitreal levels of VEGFR-1 and decreased levels of PEDF in nAMD vitreous, but the concentration of angiogenic proteins, such as VEGF and angiopoietin-2, were not different from the controls (Huber and Wachtlin, 2012). The detection of lower levels of PEDF in patients with CNV is consistent with other studies (Duh et al., 2004; Holekamp et al., 2002), which may indicate that the conducive environment for CNV during AMD can be created by the diminished anti-

angiogenic activity of vitreous rather than the increasing of angiogenic molecules. By quantify inflammatory and angiogenic proteins using a cytometric bead assay, Koss and co-workers (2011) found higher levels of monocyte chemoattractant protein-1 (MCP-1) but lower levels of IL-6 and VEGF in nAMD than in DME (Koss et al., 2011). Higher levels of the inactive (pro-IL-1β) and active forms of IL-β (Zhao et al., 2015) and transforming growth factor (TGF-β) (Bai et al., 2014) were also detected in the vitreous of patients with nAMD relatively to controls. Particularly in the (Bai et al., 2014) study, they found evidence that semaphorin 3A inhibits the CNV mediated by TGF-β1, as well as the VEGF and TGF-β responses. Increased levels of matrix metalloproteinase 9 (MMP9), interleukins (CXCL8, IL-12), PDGF receptor, and BCL-2 associated death promoter, among other molecules, are associated with AMD patients with subretinal fluid (SRF) accumulation. Indeed, a positive correlation was found between the intravitreal levels of MMP9 and the accumulation of SRF in nAMD (Ecker et al., 2012). To determine the role of the complement activation in the progression of AMD, C3, and factors B and D were quantified in vitreous at distinct severity levels. Although levels of these factors did not increase gradually in vitreous with AMD progression, the activation alternative pathway complement is suggested by the detection of higher levels of fragments of factor B in more advanced AMD (Loyet et al., 2012).

3.3. Proliferative Vitreoretinopathy

PVR is a major complication of rhegmatogenous RD (RRD) characterized by the growth and contraction of cellular membranes on both surfaces of the detached retina and within the vitreous cavity (Idrees et al., 2019; Pastor et al., 2016). In the developed countries, PVR occurs in 3.9% to 13.7% of all RRD cases and represents the most common cause of failure in surgery (Constable and Nagpal, 2013; Pastor et al., 2016). Although it may occur in untreated eyes with RD, PVR incidence increases after surgical interventions (Constable and Nagpal, 2013). Higher duration and extension of RD, larger number and size of retinal tears, and the presence of choroidal detachment, vitreous hemorrhage, prolonged intraocular inflammation, low intraocular pressure, and aphakia are predisposing factors to the development of PVR (Garweg et al., 2013; Kon et al., 2005; Rodríguez De La Rúa et al., 2005). The pathogenesis of PVR is summarized in figure 3. PVR develops into three main wound-healing phases; inflammation, proliferation, and scar modulation (Kwon et al., 2010; Wiedemann et al., 2013). Blood-retinal barrier (BRB) breakdown leads to the influx of growth factors and inflammatory mediators, which increases the chemotactic and mitogenic activity in vitreous and foments inflammatory recruitment, and cellular proliferation (Constable and Nagpal, 2013; Idrees et al., 2019; Kwon et al., 2010). The physical separation of the neurosensory retina and the underlying RPE creates an ischemic environment that leads to the death of the photoreceptors and neurons (Idrees et al., 2019; Pastor et al., 2016). The loss of signaling as a result of the death of neuronal and photoreceptor cells, the loss of cell-cell contact, and the presence of growth and inflammatory factors into the vitreous and retina incite structural and cellular changes in surrounding RPE and glial cells by mechanisms that are not fully recognized (Fisher and Lewis, 2003; Sethi et al., 2005; Tamiya et al., 2010). One of these mechanisms is the epithelial-mesenchymal transition (EMT) of the RPE cells, in which cells lose their epithelial characteristics, gain the capacity of migrating, proliferating, and producing ECM

components (Pastor et al., 2016; Tamiya et al., 2010). In this early phase of PVR, vitreous haze, protein flare, and the presence of pigment clumps are manifested in the eye due to the multiplication of RPE in vitreous (Guidry, 2010). RPE, glial cells, among other cells, migrate and proliferate uncontrollably into the vitreous cavity, adhering to the surface of the detached retina, and producing ECM components (Garweg et al., 2013; Wiedemann et al., 2013). ECM remodeling results in the formation and contraction of fibroproliferative membranes, of which tractional forces pull the retina into fixed folds (Garweg et al., 2013; Wiedemann et al., 2013). If not addressed promptly, these forces progressively create retinal wrinkles, folds, tears, and tractional retinal detachment, which hinders the surgical reattachment (Constable and Nagpal, 2013; Kwon et al., 2010; Wiedemann et al., 2013). Scleral buckling, pars plana vitrectomy, and pneumatic retinopexy are generally used for the management of early or moderate PVR (grade A-B) (Giuliari and Sadaka, 2012), whereas other surgical procedures, described in Figure 3, are recommended at more advanced states (Pastor et al., 2016). Although numerous drugs have been proposed to prevent PVR, including anti-inflammatory (Ahmadieh et al., 2008; Jonas et al., 2001; Reibaldi et al., 2013), anti-neoplastic/anti-proliferative (Chang et al., 2008; Nourinia et al., 2019; Schaub et al., 2018), anti-VEGF (Ghasemi Falavarjani et al., 2014; Pennock et al., 2013), and antioxidant agents (Lei et al., 2010), none of them have been incorporated routinely into clinical treatments (Pastor et al., 2016).

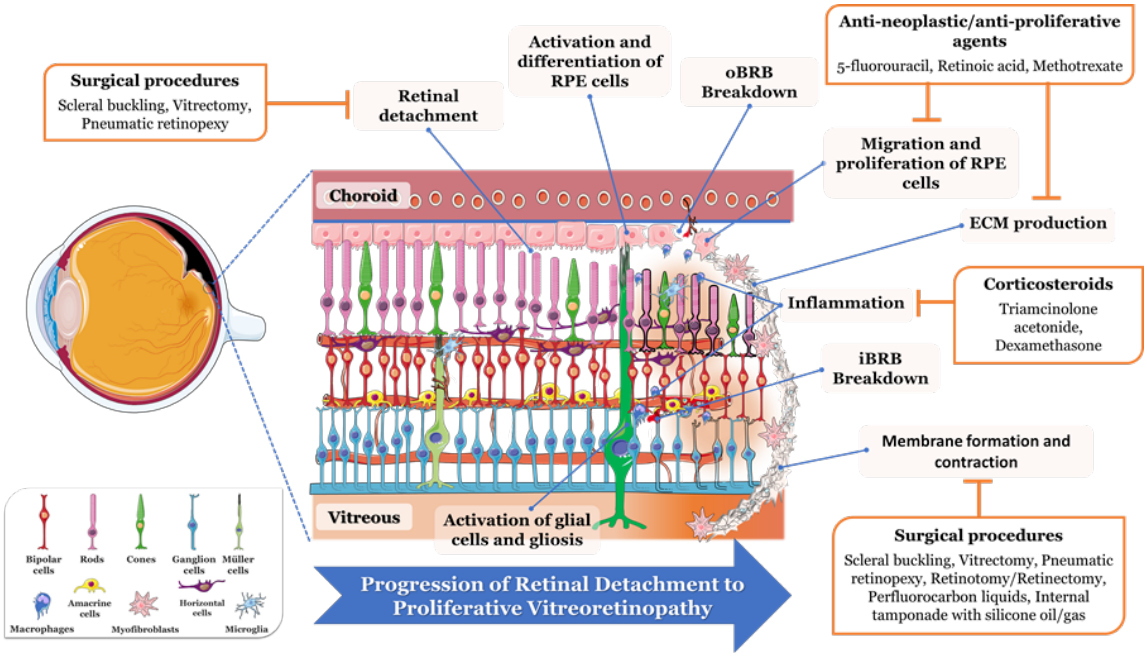

Fig. 3 - Vitreous and retinal anatomy in pathophysiological events related to the progression from retinal detachment to proliferative vitreoretinopathy and current treatments for each clinical feature. RPE–retinal pigment epithelium, iBRB – inner blood-retinal barrier, oBRB – outer blood-retinal barrier, ECM – extracellular matrix.

In recent years, different studies of vitreous proteome promised to clarify some of the mechanisms adjacent to the pathogenesis of PVR. One of the first proteomic approaches conducted in PVR studied the vitreous proteome in several vitreoretinal diseases. They found the highest levels of alpha-1-antitrypsin (AAT) and APO4 in PVR, while higher levels of PEDF were reported in RRD

compared to PVR. Significantly higher levels of cathepsin D, TTR, and CLU were also found in RRD and PVR compared to DR and PDR samples (Shitama et al., 2008). Higher levels of TTR and C4B in PVR vitreous were also reported in another study based on the analysis by 2DE and ELISA (Chen et al., 2011). By applying distinct proteomics approaches, kininogen 1 and insulin-like growth factor-binding protein 6 (IGFBP-6) were suggested as new biomarkers of PVR, and p53 and transcription factor E2F1 as potential therapeutic targets (Yu et al., 2014, 2012, 2008). Both studies showed an increase of alpha-2-HS-glycoprotein, alpha-1B-glycoprotein, serpin family members, and complement factors in PVR samples, suggesting that these plasmatic proteins accumulate in vitreous as the PVR progresses (Yu et al., 2012, 2008). Although the increase of these components in vitreous is a non-specific sign of PVR, it can provide information on the integrity of BRB, the state of inflammation, and the severity of wound healing (Kon et al., 2005; Monteiro et al., 2015). Nevertheless, the results of these studies suggest that complement and coagulation cascade may have an important role in PVR pathogenesis (Yu et al., 2012, 2008). Furthermore, tubulin, actin family members, and OPTC were found downregulated or undetectable in PVR, which suggests that both cytoskeleton and ECM are remodeled during PVR (Yu et al., 2012, 2008). Glycolysis/gluconeogenesis proteins, some associated with the HIF-1 signaling pathway (pyruvate kinase 3, glyceraldehyde-3-phosphate dehydrogenase, ENO1 and 2), were found downregulated in moderate and severe PVR and some of them were only detected in controls (Yu et al., 2008). Interestingly, some results of our research group showed that glycolytic enzymes are upregulated in RRD vitreous, suggesting that in an early phase, there is an effort to obtain more energy through glycolysis to compensate for the metabolic "stress" state of the retina (Santos et al., 2018).

Some comprehensive multiplex and ELISA assays have been applied to analyze the vitreous collected from patients with PVR. Among the factors found differently expressed in PVR are IFN-γ (Banerjee et al., 2007; Roybal et al., 2018), interleukins (e.g. IL-6, IL-8) (Banerjee et al., 2007; Canataroglu et al., 2005; Roybal et al., 2018; Symeonidis et al., 2011a; Wladis et al., 2013), chemokines (e.g. CCL3, CXCL10) (Roybal et al., 2018; Wladis et al., 2013), CSFs (Banerjee et al., 2007; Wladis et al., 2013), growth factors (e.g. VEGF, PDGF, TGF-β) (Banerjee et al., 2007; Citirik et al., 2011; Roybal et al., 2018; Sydorova and Lee, 2005), and MMPs (Symeonidis et al., 2011a) (supplementary table 1.3). In the light of these experiments, it was possible to link these factors with PVR events, such as exacerbated wound healing, loss of adhesion and proliferation of RPE and glial cells, ECM secretion, and even to potential survival mechanisms (Morescalchi et al., 2013; Moysidis et al., 2012). Banerjee and co-workers (2007) found a complex pattern of inflammatory mediators in PVR vitreous compared to the other vitreoretinal disorders, such as PDR, ERM, uveitis, or chronic choroidal neovascular membrane, among others. The detection of IL-6, IL-10, TNF-α, IFN-γ, CSF3, and chemokines in PVR vitreous supports the crucial role of inflammation in PVR. Curiously, VEGF was found at higher levels in PVR than in PDR, whereas fibroblast growth factor (FGF) was only detected in PVR (Banerjee et al., 2007). The increase of VEGF levels in the vitreous and SRF from patients with PVR was confirmed by other authors (Citirik et al., 2011; Ricker et al., 2012; Roybal et al., 2018; Sydorova and Lee, 2005), which can indicate a role in the pathogenesis of PVR. In another study, among the 48 cytokines and

chemokines measured in vitreous, the levels of CSF3, interleukins (e.g. IL-5, IL -6), and inflammatory chemokines (CXCL10, CCL3) were increased more expressively in PVR compared with ERM controls than in primary RD, suggesting that the levels of these factors increase with the progression of the disease (Wladis et al., 2013). In a more recent study, Roybal and co-workers (2018) performed a screening of 200 cytokines in the vitreous samples collected from patients at distinct stages of PVR. Of the 29 cytokines found upregulated in PVR, the 20 emphasizing advanced PVR were selected for further validation. The levels of cell adhesion molecules (ICAM-1, platelet endothelial cell adhesion molecule [PECAM-1]), growth factors (VEGF, PGF), chemotactic factors (CXCL10, CCL15) increased gradually from the early stages to the more severe stages of PVR. The upregulation of markers of T-cell recruitment, profibrotic cytokines (e.g. PDGF), and cytokines downstream of mTOR activation (e.g. IL-6) was more expressive in the early stages of PVR. In turn, the levels of fibroblast markers (e.g. CXCL12), macrophage inflammatory proteins (e.g. CCL3), and stromal cell-derived factor 1 were more predominant in PVR-C (Roybal et al., 2018).

4. Molecular mechanisms underlying proliferative vitreoretinal diseases

The proteins associated with DR/PDR, AMD, and PVR in proteomics and multiplex studies are summarized in supplementary table 2. The proteins found differentially expressed in more than one of these pathologies were analyzed by STRING v11 (Szklarczyk et al., 2019) based on their protein interactions, gene ontology, and KEGG pathways (Figure 4 and supplementary table 2). These proteins were found to be involved in pathological events, such as angiogenesis, inflammation, fibrosis, oxidative stress, neurodegeneration, and vitreous remodeling, as discussed below.

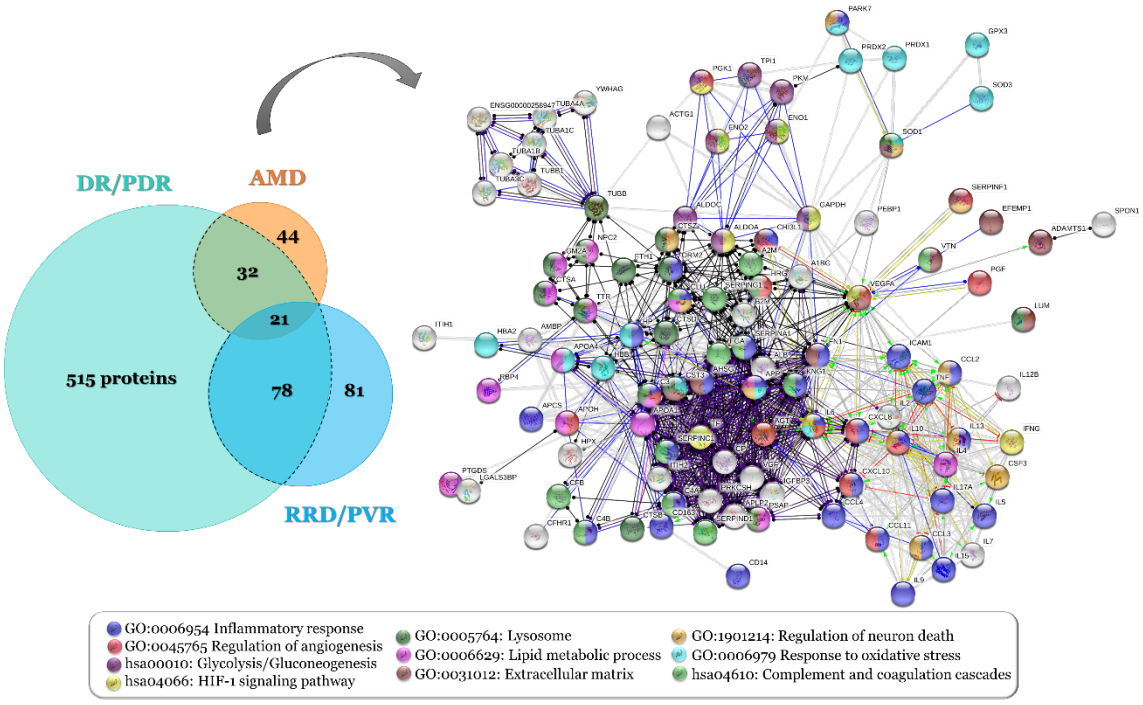

Fig. 4 - Venn graph and protein-protein interaction network (STRING v11.) representative of the proteins found differentially expressed in diabetic retinopathy and proliferative diabetic retinopathy (DR/PDR), age-

related macular degeneration (AMD), and rhegmatogenous retinal detachment and proliferative vitreoretinopathy (RRD/PVR) in proteomics and multiplex studies.

4.1. Mechanisms of angiogenesis

Angiogenesis is the result of a complex balance between growth factors, vascular endothelial cells, ECM molecules, and chemokines, being that loss in favor of angiogenesis is the basis of many proliferative pathologies (Casey and Li, 1997; Qazi et al., 2009). While the proliferation in PVR is non-angiogenic, CNV or retinal NV are central hallmarks of nAMD and PDR, respectively (Amadio et al., 2016; Jeganathan et al., 2008; Sapieha et al., 2010). VEGF and PGF are key players in vascular development and stimulation of the angiogenic environment in PDR and nAMD, as reviewed recently by our research group (Mesquita et al., 2018b). Upon its stimulation under hypoxia conditions via HIF-1, VEGF orchestrates the formation of new vessels, regulates vascular permeability, and promotes cell migration, proliferation, and survival through the expression of other growth factors, nitric oxide, adhesion molecules, and MMPs, (Mesquita et al., 2018b). HIF-1 induces the expression of several growth factors, cytokines, chemokines, and glycolytic proteins that promote adaptive cellular responses to hypoxia, including the anaerobic metabolism, inflammation, vascular permeability, and angiogenesis (Campochiaro, 2008; Semenza, 2001; Vadlapatla et al., 2013). In addition to VEGF, many pro-angiogenic mediators induced by HIF-1 were found upregulated in vitreous of patients with PDR and nAMD, including IGFBPs (Klaassen et al., 2017; Loukovaara et al., 2015; Schori et al., 2018), PDGF (Klaassen et al., 2017; Kovacs et al., 2015; Srividya et al., 2018; Suzuki et al., 2011), angiopoietin (Huber and Wachtlin, 2012; Klaassen et al., 2017), and TIMP1 (Schori et al., 2018). These mediators may have a direct effect on angiogenesis and stimulate the proliferation or differentiation of endothelial cells or indirect action by mobilizing the cells to expressed growth factors (Wiedemann, 1992). Furthermore, pro-inflammatory cytokines also promote intraocular angiogenesis and fibrocellular proliferation, directly or through the production of more growth factors. In turn, these growth factors could endorse the inflammation through the production of inflammatory mediators (e.g. INF-γ) or adhesion molecules (e.g. ICAM-2), which proves that angiogenesis and inflammation are interconnected processes (Capitão and Soares, 2016; Nawaz et al., 2019).

At physiologic conditions, the human vitreous is capable of inhibiting the NV due to the presence of angiogenic proteins, such as OPTC (Bishop, 2015), PEDF (Mori et al., 2001; Park et al., 2011), and thrombospondins (Bishop, 2015; Lawler and Lawler, 2012). However, the levels of these proteins were found to be differentially expressed in nAMD and PDR (supplementary Table 1), as reported in sections 3.1 and 3.2. While the PEDF levels are not consistent across studies, OPTC was reported as downregulated and thrombospondin-1 as upregulated. Nevertheless, antiangiogenic and neurotrophic activities of PEDF are not only controlled by its levels of expression but also by the levels of phosphorylation (Maik-Rachline et al., 2005; Maik-Rachline and Seger, 2006), which explains some of the discrepancies. Other molecules, such as TGF-β, have been shown to have both pro- and anti-angiogenic effects. TGF-β can act as an anti-

angiogenic factor, protecting RPE cells and retinal vasculature, but it also induces the expression of VEGF-A and promotes CNV and EMT (Tosi et al., 2018b, 2018a; Wang et al., 2018).

4.2. Mechanisms of inflammation

Nowadays, inflammation is known to play a central role in the development of proliferative pathologies, such as PDR (Adamis, 2002; Joussen et al., 2004; Kern, 2007; Tang and Kern, 2011), AMD (Ambati et al., 2013; Whitcup et al., 2013) and PVR (Chaudhary et al., 2020; Moysidis et al., 2012). Although the exact mechanism has not been fully elucidated, pro-inflammatory cytokines, growth factors, ECM components, proteolytic enzymes, among other mediators, provide crosstalk between inflammation and other processes, including angiogenesis (Capitão and Soares, 2016; Tsutsumi et al., 2003; Wang et al., 2017), fibrosis (Morescalchi et al., 2013; Sonoda et al., 2009), oxidative stress (X. Shaw et al., 2016), and retinal degeneration (Fernando et al., 2016; Rashid et al., 2019). The presence of these mediators in the vitreous can provides information on the integrity of BRB and the state of inflammation (Kon et al., 2005; Monteiro et al., 2015). The breakdown of the BRB and the massive influx of plasma proteins into the retina and vitreous cavity is a suitable predictor of the progression to a proliferative etiology (Campochiaro et al., 1986; Cunha-Vaz, 2009). Increased intravitreal chemotactic and mitogenic activity stimulates the migration of macrophages and the proliferation of RPE and/or glial cells (Campochiaro et al., 1986, 1984; Gilbert et al., 1988). Nevertheless, growing evidence indicates that changes in the immunosuppressive ocular microenvironment may predate the changes in vascular permeability and BRB dysfunction (Taylor, 2009). Hyperglycemia-induced pathways (Hernández et al., 2017; Kandarakis et al., 2014; Xu et al., 2018), hypoxic-ischemic conditions (Kaur et al., 2008), activation of retinal glial cells, macrophages, and retinal neurons (Gardner et al., 2002; Gerhardinger et al., 2005; Rangasamy et al., 2014; Rübsam et al., 2018) promote a pro-inflammatory environment that may disrupt the delicate balance of BRB. VEGF (Harhaj et al., 2006; Miyamoto et al., 2000), TGF-β (Lu et al., 1999), TNF-α (Aveleira et al., 2010), IL-1β (Bamforth et al., 1997), IGFBPs (Haurigot et al., 2009), CCL2 (Rangasamy et al., 2014), ICAM-1 (Funatsu et al., 2005; Lu et al., 1999), MMPs (Giebel et al., 2005; Navaratna et al., 2007) and the kallikrein-kinin system (Gao et al., 2007; Kita et al., 2015) induce the BRB breakdown through increased vascular and endothelial cells permeability, changes in tight junction proteins and cadherins, leukocyte recruitment, activation of PKC, among other mechanisms. While most of these studies are associated with dysfunction of iBRB in hypoxic-ischemic and diabetic conditions, the outer BRB (oBRB) disruption in nAMD is more related to oxidative stress (Kaur et al., 2008).

The inflammation in PVR/PDR is associated with the hypoxic retinal environment resulting from BRB disruption or changes in vascular permeability (Adamis, 2002; Chaudhary et al., 2020; Kern, 2007; Moysidis et al., 2012), whereas chronic inflammation in AMD may be a consequence of dysfunction of lipid homeostasis and, in particular, drusen formation, that occurs in this pathology (X. Shaw et al., 2016). Several studies suggest that IL-1β liberation is mediated through the activation NLRP3 inflammasome complex in response to the accumulation of drusen

components (e.g. APP) and consequent necrosis of adjacent RPE cells (Halle et al., 2008; Iyer et al., 2009; Liu et al., 2013). IL-1β was reported as the initiator of ocular inflammation (Da Cunha et al., 2018) and, in combination with TNF-α, amplifies the inflammatory cascade through the modulation of VEGF and other cytokines, CSFs, MMPs, and adhesion molecules (Da Cunha et al., 2018; Liu et al., 2015). Active IL-1β, TNF-α, and the induced proinflammatory mediators, such as IL-6 or IL-17, trigger the recruitment of inflammatory cells, dysfunction and proliferation of RPE, microglia and Müller cells, complement activation, and the production of ECM components, which result in degeneration of retinal neurons, RPE, and vascular endothelial cells (Da Cunha et al., 2018; Kutty et al., 2016; Liu et al., 2015; Vinores et al., 2007; Wooff et al., 2019). In turn, IL-6 regulates the synthesis of acute-phase proteins, beyond its role in the hematopoiesis, proliferation of fibroblast and glial cells, and the synthesis of pro-inflammatory mediators and collagen (El-Ghrably et al., 2001; Karkhur et al., 2019; Liu et al., 2015). Acute-phase proteins are expressed by Müller cells in response to an inflammatory stimulus to restore homeostasis, but they can exert a protective effect or exacerbate tissue damage (Gerhardinger et al., 2005). While AAT may have a protective effect (Ortiz et al., 2014), the presence of c-reactive protein, AAT, serum amyloid in drusen has been associated with the activation of complement factors, macrophages, and platelets, and neurodegeneration (Copland et al., 2018; Karkhur et al., 2019; Lambert et al., 2016).

Lastly, adhesion molecules such as ICAM-1 and VCAM-1 contributes for inflammation by mediating the adhesion of leukocytes to activated endothelial cells, in the case, (Blum et al., 2018; Miyamoto et al., 2000), whereas other mediates leukocyte transmigration (e.g. PECAM1) (Sorokin, 2010). High levels of adhesion molecules are constitutively expressed by human retinal endothelial cells and further increased in pathological conditions, which can predispose the retina to inflammation but also lead to the death of endothelial cells and pericytes if leukocyte activation is sustained (Bharadwaj et al., 2013; Lu et al., 1999). Vascular dysfunction favors a retinal ischemic environment, which eventually induces the expression of VEGF and triggers the NV (Joussen et al., 2004; Miyamoto et al., 2000). Increased levels of ICAM-1 in vitreous, vascular endothelium, and ERM have also been correlated with the risk of developing PVR (Barile et al., 1999; Limb and Chignell, 1999). These correlations suggest that adhesion molecules could be common mediators between inflammatory, fibrosis, and angiogenesis.

4.3. Activation of complement and coagulation cascades and fibrosis

Low levels of activation of complement and coagulation cascades are a characteristic feature of the immune-privileged status that contributes to retinal homeostasis and integrity, but its chronic activation has been implicated in a variety of pathophysiological processes on the eye (Clark and Bishop, 2018; Mukai et al., 2018; Sweigard et al., 2015). Genetic variants in complement genes such as C3, CFH, and CFB are considered a risk factor for AMD (Loyet et al., 2012; Toomey et al., 2018). CFH polymorphisms promote the sub-RPE accumulation of drusen and the extensive activation of the alternative pathway (Toomey et al., 2018). The activation of complement components like C3a and C5a and its deposition in drusen, RPE, and choriocapillaris layers

stimulate inflammatory responses, the recruitment of mononuclear phagocytes, and inhibits NV, while membrane attack complex has reported mediating the destruction of choroidal endothelium and the loss of pericytes (Mullins et al., 2014; Shahulhameed et al., 2020; Skei et al., 2010; Toomey et al., 2018; Whitmore et al., 2015). Although many genetic studies have strongly supported its association with AMD (Toomey et al., 2018), few have quantified complement factors in nAMD vitreous (Schori et al., 2018). Changes in complement pathways also have a genetic component in PDR (Yang et al., 2016), but unlike nAMD, many studies have reported the upregulation of these components in PDR vitreous, as reported above (see section 3.1). Although their exact role in the pathogenesis of DR is yet unclear (Shahulhameed et al., 2020), activation of complement and coagulation cascades could be related to the increased leukostasis and vascular permeability, BRB breakdown, and microglial activation (Abdulaal et al., 2016; Gao et al., 2008, 2007; Loukovaara et al., 2015; Wang et al., 2013). Likewise, the activation of complement pathways was reported in RD/PVR (Chen et al., 2011; Wu et al., 2016; Yu et al., 2012, 2008), as well as its involvement in pathological processes, such as increased vascular permeability, endothelial cell proliferation, and migration, RPE atrophy, reactive gliosis, loss of photoreceptor outer segments (Sweigard et al., 2015; Yu et al., 2012). Sweigard and co-workers (2015) demonstrated that the activation of alternative complement pathway promotes early photoreceptor cell death during RD but, by contrast, deficient levels of complement components were related to impaired signaling function in retinal layers, which demonstrates its relevance of this system to retinal homeostasis (Sweigard et al., 2015).

The role of the coagulation system in the development of PVR is well-established and is evidenced by intraocular fibrin deposition (Bastiaans et al., 2014). The exposition of RPE cells to serum components, such as thrombin, fibrin, plasmin, or fibronectin upon BRB breakdown, accelerates its EMT (Friedlander, 2007; Morescalchi et al., 2013). Increased levels of kininogen 1, Factor Xa, and thrombin activity were detected in vitreous, which can contribute to PVR pathogenesis through the increase of levels of PDGF, TGF, and pro-inflammatory cytokines (Bastiaans et al., 2014, 2013; Yu et al., 2014, 2012). It was suggested that these effects are exerted in RPE cells via NF-κB, which initiates the transcriptional activation of mediators implicated in proinflammatory signaling, angiogenesis, and fibrosis (Bastiaans et al., 2014, 2013; Yu et al., 2014). In addition to coagulation components, intraocular levels of IL-6 (Fielding et al., 2014; Pennock et al., 2011; Sato et al., 2018), osteopontin (Abu El-Asrar et al., 2012), connective tissue growth factor (CCN2) (Kuiper et al., 2006; Van Geest et al., 2013), insulin-like growth factors (IGFs) (Mukherjee and Guidry, 2007; Pennock et al., 2011), and other growth factors (e.g. TGF-β, PDGF) (Cui et al., 2009; Klaassen et al., 2017; Pennock et al., 2011; Zhang and Liu, 2012), were correlated to fibrosis in proliferative diseases. The role of inflammatory and fibrogenic factors in fibrosis and other pathological mechanisms of PVR was recently reviewed (Chaudhary et al., 2020). TGF-β is a key molecule in the activation of the EMT and fibrotic process and, besides stimulate the synthesis and degradation of ECM proteins, it is capable of inducing itself and other pro-fibrotic factors, interleukins, and MMPs (Chaudhary et al., 2020; Kimura et al., 2015; Kita et al., 2008; Saika, 2006). PDGF is a potent chemoattractant and mitogen for fibroblasts, glial cells, and RPE cells,

and promotes EMT, cellular contraction, and collagen synthesis (Cassidy et al., 1998; Robbins et al., 1994). The co-expression of PDGF and its receptor (PDGFR) in ERM suggests that RPE cells gain the capacity of an autocrine loop stimulation upon the loss of cell-cell contact after retinal damage (Campochiaro et al., 1994; Cui et al., 2009), which was also verified for IGFs (Campochiaro, 1997; Mukherjee and Guidry, 2007). Nevertheless, non-PDGFs growth factors are capable of activating the PDGFR, suggesting that these factors may be the main responsible for PVR, whereas PDGFs could act as a protective agent (Lei et al., 2009; Pennock et al., 2013, 2011). Some findings indicate that the role of VEGF in fibrosis is intermediated by its binding to PDGFR (Pennock et al., 2014, 2013), which is reinforced by its upregulation in vitreous, SRF, and ERM in vitreoretinal diseases associated with fibrosis (Citirik et al., 2011; Joshi et al., 2013; Ricker et al., 2012; Sydorova and Lee, 2005). The contribution of VEGF to the mechanisms that lead to an angio-fibrotic switch in angiogenic diseases, such as PDR or nAMD, is still unclear (Kuiper et al., 2008; Van Geest et al., 2012). A balance between the levels of VEGF and CCN2 has been associated with the switch from angiogenesis to fibrosis (Klaassen et al., 2015; Kuiper et al., 2008; Van Geest et al., 2013, 2012). The ratio between CCN2 and VEGF levels was found to be the strongest predictor of fibrosis (Kuiper et al., 2008; Van Geest et al., 2012), which means that angio-fibrotic switch may be accomplished by a reduction of intravitreal VEGF levels and a progressive increase in the levels of the CCN2 (Kuiper et al., 2008). This fact could explain the increased intraocular fibrosis observed after treatment with anti-VEGF drugs (Kuiper et al., 2008; Van Geest et al., 2012; Wei et al., 2017). So, it would be beneficial to control the levels of fibrosis after the administration of anti-VEGF drugs or combined it with anti-fibrotic therapy (Wei et al., 2017).

4.4. Oxidative stress

The human eye is constantly exposed to reactive oxygen species (ROS) in response to exogenous stimuli (e.g. UV and visible light, alcohol, and tobacco consumption) or as part of the eye's physiological functions (e.g. mitochondrial respiratory chain) (Kruk et al., 2015; Saccà et al., 2013). The high demand for energy and oxygen, the presence of high levels of polyunsaturated fatty acids, and constant light exposure make the retina particularly susceptible to oxidative stress and lipid peroxidation (Berra et al., 2002; Pinazo-Durán et al., 2014). Impaired redox balance in vitreous has been implicated in several ophthalmologic disorders, including DR (Brzović-Šarić et al., 2015; Cicik et al., 2003; Izuta et al., 2010; Mancino et al., 2011; Nebbioso et al., 2012), AMD (Berra et al., 2002; Holekamp et al., 2002), and PVR (Cicik et al., 2003). The high antioxidant potential of the vitreous provides a protective mechanism of the retina and surrounding tissues, but it is reduced with aging, which may lead to oxidative damages (Ankamah et al., 2019; Berra et al., 2002; Jarrett and Boulton, 2012). The activation of these protective mechanisms is suggested by the increase of intravitreal levels of antioxidant enzymes such as glutathione peroxidase, catalase, and peroxiredoxins (Supplementary Table 1), as recently reviewed (Ankamah et al., 2019). On the other hand, intravitreal levels of SOD1 was found to be inversely proportional to SOD3 levels in PDR (Gao et al., 2008; Zou et al., 2018), and PVR (Yu et al., 2008), which indicates that these proteins play different roles despite having the same catalytic activity. Other proteins

with antioxidant properties, namely PEDF, PARK7, reactive species modulator 1, serum albumin, transferrin, crystallins, and apolipoproteins, were found differentially expressed in vitreous (Supplementary Table 1).

Hyperglycemia is one of the complications that incites oxidative stress in the ocular tissues, which culminates in changes in vitreous structure, Bruch's' membrane thickening, and loss of retinal and capillary cells (Kowluru et al., 2015; Madsen-Bouterse and Kowluru, 2008). Multiple mechanisms in diabetes are responsible for mitochondrial dysfunction and subsequent ROS production, including the activation of PCK, hexosamine, and polyol pathways, auto-oxidation of glucose, accumulation of AGEs, among others, as recently reviewed (Calderon et al., 2017; Kowluru et al., 2015; Santiago et al., 2018). Likewise, polymorphisms in antioxidant enzyme genes, cigarette smoke, exposure to sunlight, among other environmental factors that are likely to contribute to oxidative stress, are risk factors for AMD (Datta et al., 2017; Jarrett and Boulton, 2012; X. Shaw et al., 2016). A combination of light exposition, dysfunction in lipid homeostasis, and oxidative stress leads to lipid peroxidation, which is one of the pathological events in AMD (X. Shaw et al., 2016). It has been suggested that these mediators could cause GA by promoting inflammatory responses and oxidative damages to cellular proteins, lipids, and DNA (particularly within mitochondria) (Maugeri et al., 2018; X. Shaw et al., 2016). Lipid peroxidation and the consequent accumulation of lipofuscin contribute to lysosomal dysfunction in RPE cells (Kaemmerer et al., 2007; Krohne et al., 2010). Phagocytosis and lysosomal-mediated removal of waste products in RPE are essential to maintain neural retina homeostasis and functional integrity (Kwon et al., 2017; Sinha et al., 2016). Impaired autophagy and exosome-mediated release of intracellular proteins contribute to the accumulation of more intracellular lipofuscin and drusen in Bruch's membrane (Hyttinen et al., 2017; Wang et al., 2009), which creates a physical barrier to the influx of oxygen and nutrients to the photoreceptors and the waste removal between RPE and choroid (Marmorstein et al., 2002). Metabolic dysregulation and hypoxia stimulate the production of growth factors and cytokines that compromises the integrity of oBRB (Frey and Antonetti, 2011; Kaur et al., 2008), while lipofuscin accumulation mediates light-induced damages in RPE cells and adjacent photoreceptors (Beatty et al., 2000; Krohne et al., 2010). Furthermore, the accumulation of free radicals, oxidative stress byproducts, and drusen can generate chronic inflammation through the production of pro-inflammatory interleukins and adhesion molecules (see sections 4.2 and 4.3) (Altmann and Schmidt, 2018; Datta et al., 2017; Rivera et al., 2017). It has been suggested that the expression of MCP-1, VCAM-1 or other NF-κB–modulated genes under oxidative stress conditions fosters a pro-angiogenic environment in the retina and choroid through the induction of inflammatory responses and increase in the expression of HIF-1α responsive genes (see section 4.1) (Dong et al., 2011, 2009; Suzuki et al., 2012). It was also reported that oxidative stress plays a role in EMT, which contributes to the pathogenesis of PVR and AMD (Datta et al., 2017; Ko et al., 2017). A synergistic effect between TGF, macrophage migration inhibitory factor, and hydrogen peroxide induces EMT through the upregulation of α-smooth muscle actin, vimentin, and fibronectin and downregulation of cadherins (Ko et al., 2017; Yang et al., 2020). Interestingly, some pathological events may be

mediated by exosomes since its secretion by RPE cells is increased in oxidative stress, aging, and in the presence of drusen (Atienzar-Aroca et al., 2016; Tong et al., 2016; Wang et al., 2009). Under stress conditions, RPE cells increase autophagic activity and the secretion of exosomes, probably for increasing the breakdown of undigested proteins and removal of damaged and toxic materials (Kang et al., 2014). Although these mechanisms are thought to contribute initially to retinal protection and survival, dysfunction of lysosomal degradation contributes to drusen formation, whereas exosomes may transmit proteins and miRNAs that promote NV and EMT in neighboring cells (Atienzar-Aroca et al., 2016; Kang et al., 2014; Tong et al., 2016; Wang et al., 2009).

4.5. Mechanisms of neurodegeneration and neuroprotection

The complex architecture and functionality of the retina and its high energy and oxygen requirements make it very susceptible to many forms of stress (Athanasiou et al., 2013; K.-G. Schmidt et al., 2008). As neurodegeneration depends on a balance between the levels of neurotoxic and neuroprotective factors, it has been suggested that neurotrophic factors, anti-oxidants, and anti-apoptotic therapy are capable of mitigating the effects of secondary degenerative events and slow down the loss of neurons in the retina (Barkana and Belkin, 2004; Osborne et al., 2001; Paulus and Campbell, 2015). Therefore, neuroprotection is gaining interest as an adjunct therapy for preserving the photoreceptors and ganglion cells after retinal damage in DR (Barber and Baccouche, 2017; Simó et al., 2018; Zafar et al., 2019), AMD (Chinskey et al., 2013; Medeiros and Curcio, 2001; Nian and C.Y. Lo, 2019), and RD/PVR (Lo et al., 2011; Murakami et al., 2013; Pastor et al., 2016). So, it is relevant to understand the endogenous protective mechanisms triggered in the eye, with RPE and Müller cells being the main ones responsible for the secretion of neurotrophic factors (Cuenca et al., 2014; Fortuny and Flannery, 2018). In response to acute stress signals, microglia produce neurotrophic mediators, such as GDNF and NT3, that act directly in neurons, while BDNF and CNTF induce Müller cells secretion of secondary mediators (e.g. FGF, GDNF) that mediate the survival of photoreceptors and inhibits microglial (Boss et al., 2017; Madeira et al., 2015; Rashid et al., 2019). RPE cells also contribute to activate cellular survival signaling by secreting a wide range of neurotrophic factors, including PEGF, FGF, IGFs, NGF, BDNF, among other factors, such as cytokines, chemokines, angiogenic and anti-angiogenic (Chaum, 2003; Ponnalagu et al., 2017; Strauss, 2005). Neurotrophic factors are also expressed in the retina in response to mechanical injury (e.g. RD), suggesting an important role in photoreceptor rescue. Several of these factors showed to be useful for limiting the death of photoreceptors in experimental models of RD (Kubay et al., 2005; Lo et al., 2011). However, the chronic activation of some of these mechanisms can instigate severe alterations in retinal integrity, and exacerbate neuronal death (Altmann and Schmidt, 2018; Rashid et al., 2019, 2018). Complement factors (Rutar et al., 2014; Shahulhameed et al., 2020), IL-6 (Erta et al., 2012; Spooren et al., 2011), TGF-β1 (Dobolyi et al., 2012; Tosi et al., 2018b), and VEGF (Calvo et al., 2018; Ricker et al., 2012; Witmer et al., 2003) act as neurotrophic factors and have an important role in neuronal, glial and vascular homeostasis. Nevertheless, their role in pathological events, such as microglial activation and recruitment, neuroinflammation, angiogenesis, and fibrosis, may eventually incite neurodegeneration (Calvo et al., 2018; Dobolyi et al., 2012; Erta et al., 2012;

Ricker et al., 2012; Rutar et al., 2014; Shahulhameed et al., 2020; Spooren et al., 2011; Tosi et al., 2018b; Witmer et al., 2003).

Glial and RPE dysfunction and the activation of Müller cells and the loss of neurotrophic support are critical for the survival of photoreceptors, and retinal ganglion cells (Chaum, 2003; Cuenca et al., 2014; Fortuny and Flannery, 2018). Activated Müller cells suffer morphological, biochemical, and physiological changes as a result of the dramatic increase in the expression of glial fibrillary acidic protein and vimentin (Jünemann et al., 2015; Lewis and Fisher, 2003). Photoreceptor degeneration is greatly reduced in the absence of glial fibrillary acidic protein, vimentin, and other intermediate filaments, which suggests that reactive gliosis contributes to retinal damage (Nakazawa et al., 2007; Verardo et al., 2008). Activated microglia also express retinal damage biomarkers such as ENO2 (Haque et al., 2018), and contribute to phagocytize toxic proteins such as APP (Cuenca et al., 2014; Gold and El Khoury, 2015). ENO2 has a dual role and can act as a neurotoxic or neuroprotector factor (e.g. against amyloid-β peptide toxicity), but upon neuron injury, it is expressed especially in M1 type microglia, which may promote neurodegeneration (Haque et al., 2018; Vizin and Kos, 2015). APP is a key component of drusen and its accumulation in the eye has been associated with neurodegeneration in AMD and glaucoma (Gupta et al., 2016; Luibl et al., 2006; Ratnayaka et al., 2015). The increased phagocytic capacity of microglia and the expression of APP degrading enzymes is suggested to contributing to Aβ clearance, but eventually, it promotes the neuroinflammation by the induction of pro-inflammatory cytokines and NLRP3 inflammasome (Cuenca et al., 2014; Gold and El Khoury, 2015). Likewise, it has been suggested that APP toxicity in neurons is mediated by its intralysosomal accumulation through macroautophagy, and consequent lysosomal membrane permeabilization (Zheng et al., 2009). On the other hand, the presence of αβ-crystallins in the drusen may reduce the aggregation of toxic proteins and augment autophagy-mediated clearance (Kannan et al., 2012). Animal models with mutations and knockout for crystallin genes exhibit inefficient lysosomal clearance that is evidenced by the accumulation of lipofuscin-like material, and high susceptibility of RPE to oxidative stress and apoptosis, which are pathological signs similar to some of those seen in AMD patients (Sinha et al., 2016; Zhou et al., 2014). Moreover, several studies in animal models indicated that the overexpression of heat shock proteins supports the survival of injured RPE, retinal ganglion cells, and photoreceptors (Böhm et al., 2012; Kayama et al., 2011; Zhou et al., 2014). AKT/mTOR pathway in RPE has also been correlated with impairment of autophagic flux and increased oxidative stress, glycolysis, and glycogen storage (Golestaneh et al., 2017; Yu et al., 2018; Zhang et al., 2020). mTOR is activated in response to RPE stress, which impairs autophagy and induces the dedifferentiation, hypertrophy, and metabolic reprogramming in RPE cells to promote its survival. However, a return to baseline levels of mTOR activity is necessary to diminish the RPE glycolytic metabolism, and increase the supply of glucose to photoreceptors, which means that chronic mTOR activation may lead to glucose deprivation and degeneration of photoreceptors (Yu et al., 2018; Zhao et al., 2011). In turn, degenerative photoreceptors display low levels of mTOR and high levels of HIF-1 and also the activation of chaperone-mediated autophagy, suggesting that nutrient deprivation and prolonged starvation may be underlying neurodegeneration.

4.6. Vitreous aging and ECM remodeling

With aging, human vitreous suffers a progressive e remodeling characterized by the loss of type IX collagen and short-range interactions with other ECM components (e.g. hyaluronan), as well as the new synthesis of collagen and aggregation of collagen fibrils, which eventually leads to vitreous liquefaction and PVR (De Smet et al., 2013; Gale et al., 2014; Gariano and Gardner, 2005). Although ECM changes occur as a normal part of aging, they are exacerbated by pathological events, such as hyperglycemia, ocular inflammation, and oxidative stress (Ankamah et al., 2019; De Smet et al., 2013; Gale et al., 2014; Ponsioen et al., 2010). Therefore, vitreous liquefaction and PVD have been associated with various retinal pathologies (De Smet et al., 2013; Holekamp, 2010; Ponsioen et al., 2010; J. C. Schmidt et al., 2008). ECM dynamics are tightly regulated by a balance between proteinases and their neutralizing substances (Bonnans et al., 2014; Lu et al., 2011; Ponsioen et al., 2010), which suggests that the deregulation of these mechanisms may be underlying the degenerative changes in vitreous and, consequently, vitreoretinal diseases (Vaughan-Thomas et al., 2000).

MMPs are the main proteases involved in the degradation of collagen and other ECM components (Kowluru et al., 2012; Lu et al., 2011), although other proteases are capable of degrading the ECM, including a disintegrin and metalloproteinase with thrombospondin motifs (ADAMTS), cathepsins, and plasminogen (Bonnans et al., 2014; Lu et al., 2011). Under physiological conditions, MMPs are synthesized and secreted into the vitreous in an inactive form (Ponsioen et al., 2010), but their expression and activity increase in tissue repair, inflammation, oxidative stress, or under remodeling processes (Kowluru et al., 2012). Levels of MMPs have been correlated with pathological features, such as SRF accumulation in nAMD (Ecker et al., 2012), the duration and extent of RD (Symeonidis et al., 2007), the grade of postoperative PVR (Symeonidis et al., 2011b) and PVD (Jin et al., 2001), and NV in DR (Van Geest et al., 2013). ECM dynamics seem to modulate a series of pathological features of these vitreoretinal diseases, like vascular permeability, NV (Bishop, 2015; Kowluru et al., 2012; Sottile, 2004), inflammation (Singh and Tyagi, 2017; Sorokin, 2010), and fibrosis (Chaudhary et al., 2020; Wynn, 2007). The degradation of ECM components by MMPs modulates these processes by providing a scaffolding via ECM–integrin-binding that facilitates the cell adhesion and migration of immune cells and vascular endothelial cells (Bishop, 2015; Lu et al., 2011; Sorokin, 2010; S. Wang et al., 2012). Proteolysis via MMPs also changes the bioavailability of factors sequestered in ECM, including growth factors, chemoattractants, and other signaling molecules (e.g. matricellular proteins, bioactive ECM fragments) (Bishop, 2015; Bonnans et al., 2014; Lu et al., 2011). Besides that, MMPs process other bioactive molecules, including growth factors and other cytokines, and cell surface molecules, which may promote their inactivation or potentiate its effects (Korpos et al., 2009; Lu et al., 2011; Singh and Tyagi, 2017; Sorokin, 2010).

On the other hand, high TIMP1 levels were found in RRD/PVR (Symeonidis et al., 2011a, 2011b, 2007), PDR (Schori et al., 2018; Van Geest et al., 2013) and, even if not significantly, in nAMD (Schori et al., 2018), whereas TIMP2 levels showed only a slight increase in PDR (Loukovaara et al., 2015). The upregulation of TIMP1 by pro-fibrotic factors (e.g. factor Xa, TGF-β) was associated

with fibrosis once its combining effect potentiates ECM production by fibroblasts or myofibroblasts and prevents the destruction of the newly synthesized matrix (Bastiaans et al., 2013; Symeonidis et al., 2011b). Nevertheless, it has been suggested that MMPs/TIMPs levels suffer concomitant changes during RRD/PVR, and that secretion of MMPs by RPE cells may assist in its migration into vitreous (Chaudhary et al., 2020; Symeonidis et al., 2011b). In accordance, ERM removed from patients with PVR and PDR are especially rich in structural (e.g. collagens) and adhesive ECM components (e.g. fibronectin) and matricellular proteins (e.g. tenascin, thrombospondin 1), but also contain MMPs/TIMPs (Hiscott et al., 1999; Ioachim et al., 2005; Klaassen et al., 2017; Salzmann et al., 2000). Decreased MMP2 and MMP9 activity levels were also associated with Bruch's membrane thickening and accumulation of lipid-rich debris in AMD (Hussain et al., 2011). Conversely, higher levels of MMPs were associated with the progression of CNV, which was confirmed using a knockout mouse for MMP2 and MMP9 (Lambert et al., 2003). TIMP1 levels were also correlated with the degree of NV. Nevertheless, its correlation with activated TGF-β2 levels was independent of the degree of DR, which suggests that TIMP-1 may have a more relevant role in the angiogenic phase rather than in the fibrotic phase of PDR (Van Geest et al., 2013). Furthermore, TIMP-1 could result from the breakdown of BRB, by contrast with TIMP-2 that is specifically secreted by intraocular tissues (Matsuo, 1998), which also explains its correlation with the degree of NV in PDR. More recently, it was verified that TIMP-1 is not detected after the treatment with ranibizumab, whereas TIMP2 and other protease inhibitors (e.g. SERPINA5) were found upregulated (Zou et al., 2018). TIMP2 seems to be more efficient at inhibiting angiogenesis than TIMP-1, and it may mediate the effects of treatment with ranibizumab (Zou et al., 2018). This can be related to the fact that TIMP-2 inhibits growth and angiogenesis, not only by inhibiting MMPs but also via α3β1 integrin-mediated binding of TIMP2's N-terminal domain to endothelial cells (Rodrigues et al., 2013). Although the role of ECM remodeling in proliferative diseases is not fully understood, it may be a unifying mechanism between vitreous degeneration and pathological events such as fibrosis, inflammation, and NV. Therefore, the structural integrity of the vitreous structure can be one of the decisive factors for the progression to a proliferating etiology, and ECM may be a potential therapeutic target.

5. Conclusions and future perspectives

During the progression of proliferative diseases, the vitreous acts as a repository of the mediators involved in inflammation, angiogenesis, fibrosis, oxidative stress, neurodegeneration, and remodeling of the ECM. Therefore, the study of vitreous proteome has been promising to elucidate some of the pathological mechanisms underlying these diseases and to discover potential pharmaceutical targets. The characterization of the proteome of vitreous humor has contributed extensively to the recognition of pathways involved in DR and PDR, and to identify candidate biomarkers for its treatment. However, the lack of validation in a larger number of samples may explain the absence of suitable vitreous biomarkers so far. The proteomics studies regarding nAMD and PVR are scarcer, although these already provide some evidence about the pathogenesis of these proliferative diseases. However, the understanding of proliferative pathologies is hampered by the presence of proteoforms (e.g. isoforms, post-translational modified) with

distinct or dual functions in vitreous. In this context, the information from proteomics studies should be supplemented with functional proteomics studies, and other -omics analysis (e.g. genomics and metabolomics), and in vitro and animal models studies. In particular, genomics analysis could be mainly relevant in nAMD, since this disorder has a significant genetic component. Furthermore, there is also a gap in our knowledge regarding the events underlying the onset of these pathologies, which has been subjected to intense discussion. In turn, it seems that chronic neuroinflammation and neurodegeneration, and changes in the vitreous structure are decisive factors for the progression to a proliferating etiology. The cooperation between clinicians and basic researchers is essential to correlate specific proteins and signaling pathways with the progression of these diseases and to find reliable biomarkers that could be incorporated into clinical routine. Nevertheless, vitreous is mainly collected in the more advanced stages of the pathologies (e.g. ERM and vitreous hemorrhage), which difficult the obtention of vitreous samples from the earliest stages of the disease and, of course, from healthy eyes. Lastly, it must be taken into account that the vitreous cannot be used for diagnosis due to its invasive sampling, but when obtained as part of clinical routine may serve to the prognosis of the patient's evolution and response to new and emergent treatments.

Acknowledgments

Santos FM acknowledges a doctoral fellowship [SFRH/BD/112526/2015] from FCT. This project was supported by the University of Beira Interior—Health Sciences Research Centre (CICS) supported by FEDER funds through National Funds by FCT (UID/Multi/00709/2013) and (UID/Multi/00709/2019), and by FEDER funds through the POCI—COMPETE 2020—Operational Programme Competitiveness and Internationalisation in Axis I—Strengthening research, technological development and innovation Project (POCI-01-0145-FEDER-007491). This work was also supported by the Applied Molecular Biosciences Unit- UCIBIO which is financed by national funds from FCT/MCTES (UID/Multi/04378/2019). CNB-CSIC proteomics lab is a member of Proteored, PRB2-ISCIII and is supported by grant PT13/0001, of the PE I +D+i 2013–2016, funded by ISCIII and FEDER.

Conflicts of Interest: The authors declare no conflict of interest

Credit authorship contribution statement

Fátima M. Santos: Conceptualization, Formal analysis, Writing - original draft, Writing - review & editing. **João Paulo Castro e Sousa**: Conceptualization; Writing - Review & Editing. **Alberto Paradela**: Supervision, Writing - Review & Editing. Sergio Ciordia: Conceptualization; Writing - Review & Editing. **Cândida T. Tomaz**: Supervision, Conceptualization, Writing - review & editing. **Luís A. Passarinha**: Supervision, Conceptualization Writing - review & editing.

References

Abdulaal, M., Haddad, N.M.N., Sun, J.K., Silva, P.S., 2016. The role of plasma kallikrein-kinin pathway in the development of diabetic retinopathy: Pathophysiology and therapeutic approaches. Semin. Ophthalmol. 31, 19–24.

Abu El-Asrar, A.M., Imtiaz Nawaz, M., Kangave, D., Siddiquei, M.M., Geboes, K., 2012. Osteopontin and other regulators of angiogenesis and fibrogenesis in the vitreous from patients with proliferative vitreoretinal disorders. Mediators Inflamm. 2012.

Abu El-Asrar, A.M., Mohammad, G., Nawaz, M.I., Siddiquei, M.M., Van Den Eynde, K., Mousa, A., De Hertogh, G., Opdenakker, G., 2013. Relationship between vitreous levels of matrix metalloproteinases and vascular endothelial growth factor in proliferative diabetic retinopathy. PLoS One 8, 1–11.

Ackland, P., Resnikoff, S., Bourne, R., 2018. World blindness and visual impairment: Despite many successes, the problem is growing. Community Eye Heal. J. 30, 71–73.

Adamis, A.P., 2002. Is diabetic retinopathy an inflammatory disease? Br. J. Ophthalmol. 86, 363–5.

Age-Related Eye Disease Study Research Group, 2005a. Risk Factors for the Incidence of Advanced Age-Related Macular Degeneration in the Age-Related Eye Disease Study (AREDS). Ophthalmology 112, 533-539.e1.

Age-Related Eye Disease Study Research Group, 2005b. The Age-Related Eye Disease Study Severity Scale for Age-Related Macular Degeneration. Arch. Ophthalmol. 123, 1484.

Age-Related Eye Disease Study Research Group, 2001. A Randomized, Placebo-Controlled, Clinical Trial of High-Dose Supplementation With Vitamins C and E, Beta Carotene, and Zinc for Age-Related Macular Degeneration and Vision Loss. Arch. Ophthalmol. 119, 1417.

Ahmad, M.T., Zhang, P., Dufresne, C., Ferrucci, L., Semba, R.D., 2018. The Human Eye Proteome Project: Updates on an Emerging Proteome. Proteomics 18, 1–31.

Ahmadieh, H., Feghhi, M., Tabatabaei, H., Shoeibi, N., Ramezani, A., Mohebbi, M.R., 2008. Triamcinolone Acetonide in Silicone-Filled Eyes as Adjunctive Treatment for Proliferative Vitreoretinopathy. A Randomized Clinical Trial. Ophthalmology 115, 1938–1943.

Al Kahtani, E., Xu, Z., Al Rashaed, S., Wu, L., Mahale, A., Tian, J., Abboud, E.B., Ghazi, N.G., Kozak, I., Gupta, V., Arevalo, J.F., Duh, E.J., 2017. Vitreous levels of placental growth factor correlate with activity of proliferative diabetic retinopathy and are not influenced by bevacizumab treatment. Eye 31, 529–536.

Alovisi, C., Panico, C., De Sanctis, U., Eandi, C.M., 2017. Vitreous Substitutes: Old and New Materials in Vitreoretinal Surgery.

Altmann, C., Schmidt, M.H.H., 2018. The role of microglia in diabetic retinopathy: Inflammation, microvasculature defects and neurodegeneration. Int. J. Mol. Sci. 19.

Amadio, M., Govoni, S., Pascale, A., 2016. Targeting VEGF in eye neovascularization: What's new?: A comprehensive review on current therapies and oligonucleotide-based interventions under development. Pharmacol. Res. 103, 253–269.

Ambati, J., Atkinson, J.P., Gelfand, B.D., 2013. Immunology of age-related macular degeneration. Nat. Rev. Immunol. 13, 438–451.

Angi, M., Kalirai, H., Coupland, S.E., Damato, B.E., Semeraro, F., Romano, M.R., 2012. Proteomic analyses of the vitreous humour. Mediators Inflamm. 2012.

Ankamah, E., Sebag, J., Ng, E., Nolan, J.M., 2019. Vitreous Antioxidants, Degeneration, and Vitreo-Retinopathy: Exploring the Links. Antioxidants 9, 7.

Ardeljan, D., Chan, C.C., 2013. Aging is not a disease: Distinguishing age-related macular degeneration from aging. Prog. Retin. Eye Res. 37, 68–89.

Athanasiou, D., Aguilà, M., Bevilacqua, D., Novoselov, S.S., Parfitt, D.A., Cheetham, M.E., 2013. The cell stress machinery and retinal degeneration. FEBS Lett. 587, 2008–2017.

Atienzar-Aroca, S., Flores-Bellver, M., Serrano-Heras, G., Martinez-Gil, N., Barcia, J.M., Aparicio, S., Perez-Cremades, D., Garcia-Verdugo, J.M., Diaz-Llopis, M., Romero, F.J., Sancho-Pelluz, J., 2016. Oxidative stress in retinal pigment epithelium cells increases exosome secretion and promotes angiogenesis in endothelial cells. J. Cell. Mol. Med. 20, 1457–1466.

Aveleira, C.A., Lin, C.M., Abcouwer, S.F., Ambrósio, A.F., Antonetti, D.A., 2010. TNF-α signals through PKCζ/NF-κB to alter the tight junction complex and increase retinal endothelial cell permeability. Diabetes 59, 2872–2882.

Bai, Y., Liang, S., Yu, W., Zhao, Min, Huang, L., Zhao, Mingwei, Li, X., 2014. Semaphorin 3A blocks the formation of pathologic choroidal neovascularization induced by transforming growth factor beta. Mol. Vis. 20, 1258–1270.

Balaiya, S., Zhou, Z., Chalam, K. V., 2017. Characterization of vitreous and aqueous proteome in humans with proliferative diabetic retinopathy and its clinical correlation. Proteomics Insights 8, 1–10.

Bamforth, S.D., Lightman, S.L., Greenwood, J., 1997. Interleukin-1β-induced disruption of the retinal vascular barrier of the central nervous system is mediated through leukocyte recruitment and histamine. Am. J. Pathol. 150, 329–340.

Banerjee, S., Savant, V., Scott, R.A.H., Curnow, S.J., Wallace, G.R., Murray, P.L., 2007. Multiplex bead analysis of vitreous humor of patients with vitreoretinal disorders. Investig. Ophthalmol. Vis. Sci. 48, 2203–2207.

Barber, A.J., Baccouche, B., 2017. Neurodegeneration in diabetic retinopathy: Potential for novel therapies. Vision Res. 139, 82–92.

Barile, G.R., Chang, S.S., Park, L.S., Reppucci, V.S., Schiff, W.M., Schmidt, A.M., 1999. Soluble cellular adhesion molecules in proliferative vitreoretinopathy and proliferative diabetic retinopathy. Curr Eye Res 19, 219–227.

Barkana, Y., Belkin, M., 2004. Neuroprotection in ophthalmology: A review. Brain Res. Bull. 62, 447–453.

Bastiaans, J., van Meurs, J.C., Mulder, V.C., Nagtzaam, N.M.A., Smits-te Nijenhuis, M., Dufour-van den Goorbergh, D.C.M., van Hagen, P.M., Hooijkaas, H., Dik, W.A., 2014. The role of thrombin in proliferative vitreoretinopathy. Investig. Ophthalmol. Vis. Sci. 55, 4659–4666.

Bastiaans, J., Van Meurs, J.C., Van Holten-Neelen, C., Nijenhuis, M.S. Te, Kolijn-Couwenberg, M.J., Van Hagen, P.M., Kuijpers, R.W.A.M., Hooijkaas, H., Dik, W.A., 2013. Factor Xa and thrombin stimulate proinflammatory and profibrotic mediator production by retinal pigment epithelial cells: A role in vitreoretinal disorders? Graefe's Arch. Clin. Exp. Ophthalmol. 251, 1723–1733.

Beatty, S., Koh, H.H., Phil, M., Henson, D., Boulton, M., 2000. The role of oxidative stress in the pathogenesis of age-related macular degeneration. Surv. Ophthalmol. 45, 115–134.

Berra, A., Ferreira, S., Stanga, P., Llesuy, S., 2002. Age-related antioxidant capacity of the vitreous and its possible relationship with simultaneous changes in photoreceptors, retinal pigment epithelium and Bruchs' membrane in human donors' eyes. Arch. Gerontol. Geriatr. 34, 371–377.

Bharadwaj, A.S., Appukuttan, B., Wilmarth, P.A., Pan, Y., Stempel, A.J., Chipps, T.J., Benedetti, E.E., Zamora, D.O., Choi, D., David, L.L., Smith, J.R., 2013. Role of the retinal vascular endothelial cell in ocular disease. Prog. Retin. Eye Res. 32, 102–180.

Bishop, P.N., 2015. The role of extracellular matrix in retinal vascular development and preretinal neovascularization. Exp. Eye Res. 133, 30–36.

Blum, A., Pastukh, N., Socea, D., Jabaly, H., 2018. Levels of adhesion molecules in peripheral blood correlat with stages of diabetic retinopathy and may serve as bio markers for microvascular complications. Cytokine 106, 76–79.

Böhm, M.R.R., Pfrommer, S., Chiwitt, C., Brückner, M., Melkonyan, H., Thanos, S., 2012. Crystallin-β-b2-overexpressing NPCs support the survival of injured retinal ganglion cells and photoreceptors in rats. Investig. Ophthalmol. Vis. Sci. 53, 8265–8279.

Bonnans, C., Chou, J., Werb, Z., 2014. Remodelling the extracellular matrix in development and disease. Nat. Rev. Mol. Cell Biol. 15, 786–801.

Boss, J.D., Singh, P.K., Pandya, H.K., Tosi, J., Kim, C., Tewari, A., Juzych, M.S., Abrams, G.W., Kumar, A., 2017. Assessment of Neurotrophins and Inflammatory Mediators in Vitreous of Patients With Diabetic Retinopathy. Investig. Opthalmology Vis. Sci. 58, 5594.

Bourne, R.R.A., Flaxman, S.R., Braithwaite, T., *et. al*, 2017. Magnitude, temporal trends, and projections of the global prevalence of blindness and distance and near vision impairment: a systematic review and meta-analysis. Lancet Glob. Heal. 5, e888–e897.

Boyer, D.S., Yoon, Y.H., Belfort, R., Bandello, F., Maturi, R.K., Augustin, A.J., Li, X.-Y., Cui, H., Hashad, Y., Whitcup, S.M., 2014. Three-Year, Randomized, Sham-Controlled Trial of Dexamethasone Intravitreal Implant in Patients with Diabetic Macular Edema. Ophthalmology 121, 1904–1914.

Bressler, S.B., Liu, D., Glassman, A.R., Blodi, B.A., Castellarin, A.A., Jampol, L.M., Kaufman, P.L., Melia, M., Singh, H., Wells, J.A., 2017. Change in diabetic retinopathy through 2 years secondary analysis of a randomized clinical trial comparing aflibercept, bevacizumab, and ranibizumab. JAMA Ophthalmol. 135, 558–568.

Brzović-Šarić, V., Landeka, I., Šarić, B., Barberić, M., Andrijašević, L., Cerovski, B., Oršolić, N., Đikić, D., 2015. Levels of selected oxidative stress markers in the vitreous and serum of diabetic retinopathy patients. Mol. Vis. 21, 649–64.

Busch, C., Zur, D., Fraser-Bell, S., Laíns, I., Santos, A.R., Lupidi, M., Cagini, C., Gabrielle, P.H., Couturier, A., Mané-Tauty, V., Giancipoli, E., Ricci, G.D.A., Cebeci, Z., Rodríguez-Valdés, P.J., Chaikitmongkol, V., Amphornphruet, A., Hindi, I., Agrawal, K., Chhablani, J., Loewenstein, A., Iglicki, M., Rehak, M., 2018. Shall we stay, or shall we switch? Continued anti-VEGF therapy versus early switch to dexamethasone implant in refractory diabetic macular edema. Acta Diabetol. 55, 789–796.

Cai, S., Bressler, N.M., 2015. Aflibercept, Bevacizumab, or Ranibizumab for Diabetic Macular Edema. N. Engl. J. Med. 372, 1193–1203.

Calderon, G.D., Juarez, O.H., Hernandez, G.E., Punzo, S.M., De La Cruz, Z.D., 2017. Oxidative stress and diabetic retinopathy: Development and treatment. Eye 31, 1122–1130.

Calvo, P., Pastor, A., De La Cruz, R., 2018. Vascular endothelial growth factor: An essential neurotrophic factor for motoneurons? Neural Regen. Res. 13, 1181–1182.

Campochiaro, P.A., 2008. Ocular neovascularization. Angiogenes. An Integr. Approach From Sci. to Med. 517–531.

Campochiaro, P.A., 1997. Pathogenic Mechanisms in Proliferative Vitreoretinopathy. Arch. Ophthalmol. 115, 237.

Campochiaro, P.A., Bryan, J.A., Conway, B.P., Jaccoma, E.H., 1986. Intravitreal Chemotactic and Mitogenic Activity: Implication of Blood-Retinal Barrier Breakdown. Arch. Ophthalmol. 104, 1685–1687.

Campochiaro, P.A., Hackett, S.F., Vinores, S.A., Freund, J., Csaky, C., LaRochelle, W., Henderer, J., Johnson, M., Rodriguez, I.R., Friedman, Z., Derevjanik, N., Dooner, J., 1994. Platelet-derived growth factor is an autocrine growth stimulator in retinal pigmented epithelial cells. J. Cell Sci. 107, 2459–2469.

Campochiaro, P.A., Jerdan, J.A., Glaser, B.M., 1984. Serum Contains Chemoattractants For Human Retinal Pigment Epithelial Cells. Arch. Ophthalmol. 102, 1830–1833.

Canataroglu, H., Varinli, I., Ozcan, A.A., Canataroglu, A., Doran, F., Varinli, S., 2005. Interleukin (IL)-6, interleukin (IL)-8 levels and cellular composition of the vitreous humor in proliferative diabetic retinopathy, proliferative vitreoretinopathy, and traumatic proliferative vitreoretinopathy. Ocul. Immunol. Inflamm. 13, 375–381.

Capitão, M., Soares, R., 2016. Angiogenesis and Inflammation Crosstalk in Diabetic Retinopathy. J. Cell. Biochem. 2443–2453.

Casey, R., Li, W.W., 1997. Factors controlling ocular angiogenesis. Am. J. Ophthalmol. 124, 521–529.

Cassidy, L., Barry, P., Shaw, C., Duffy, J., Kennedy, S., 1998. Platelet derived growth factor and fibroblast growth factor basic levels in the vitreous of patients with vitreoretinal disorders. Br. J. Ophthalmol. 82, 181–185.

Chang, Y.C., Hu, D.N., Wu, W.C., 2008. Effect of Oral 13-Cis-Retinoic Acid Treatment on Postoperative Clinical Outcome of Eyes With Proliferative Vitreoretinopathy. Am. J. Ophthalmol. 146, 440–447.

Chaudhary, R., Scott, R.A.H., Wallace, G., Berry, M., Logan, A., Blanch, R.J., 2020. Inflammatory and fibrogenic factors in proliferative vitreoretinopathy development. Transl. Vis. Sci. Technol. 9, 1–17.

Chaum, E., 2003. Retinal neuroprotection by growth factors: A mechanistic perspective. J. Cell. Biochem. 88, 57–75.

Chen, G., Li, T., Zheng, Q., Hou, J., Tang, S., Li, W., 2011. [Differential expression and significance of complement C4b and transthyretin in proliferative vitreoretinopathy]. Zhonghua. Yan Ke Za Zhi. 47, 726–31.

Chen, W., Lu, Q., Lu, L., Guan, H., 2017. Increased levels of alphaB-crystallin in vitreous fluid of patients with proliferative diabetic retinopathy and correlation with vascular endothelial growth factor. Clin. Exp. Ophthalmol. 45, 379–384.

Chinskey, N.D., Besirli, C.G., Zacks, D.N., 2013. Retinal neuroprotection in dry age-related macular degeneration. Drug Discov. Today Ther. Strateg. 10, e21–e24.

Chirila, T. V., Hong, Y., 2016. Chapter C2 The Vitreous Humor, in: Handbook of Biomaterial Properties. Springer New York, New York, NY, pp. 125–134.

Cicik, E., Tekin, H., Akar, S., Ekmekçi, Ö.B., Donma, O., Koldaş, L., Özkana, Ş., 2003. Interleukin-8, nitric oxide and glutathione status in proliferative vitreoretinopathy and proliferative diabetic retinopathy. Ophthalmic Res. 35, 251–255.

Citirik, M., Kabatas, E.U., Batman, C., Akin, K.O., Kabatas, N., 2011. Vitreous vascular endothelial growth factor concentrations in proliferative diabetic retinopathy versus proliferative vitreoretinopathy. Ophthalmic Res. 47, 7–12.

Ciulla, T., Oliver, A., Gast, M.J., 2007. Squalamine lactate for the treatment of age-related macular degeneration. Expert Rev. Ophthalmol. 2, 165–175.

Clark, S.J., Bishop, P.N., 2018. The eye as a complement dysregulation hotspot. Semin. Immunopathol. 40, 65–74.

Coleman, H.R., Chan, C.-C., Ferris, F.L., Chew, E.Y., 2008. Age-related macular degeneration. Lancet 372, 1835–1845.

Constable, I.J., Nagpal, M., 2013. Proliferative Vitreoretinopathy, in: Retina. Elsevier, pp. 1806–1825.

Copland, D.A., Theodoropoulou, S., Liu, J., Dick, A.D., 2018. A perspective of AMD through the eyes of immunology. Investig. Ophthalmol. Vis. Sci. 59, AMD83–AMD92.

Csősz, É., Deák, E., Kalló, G., Csutak, A., Tőzsér, J., 2017. Diabetic retinopathy: Proteomic approaches to help the differential diagnosis and to understand the underlying molecular mechanisms. J. Proteomics 150, 351–358.

Cuenca, N., Fernández-Sánchez, L., Campello, L., Maneu, V., De la Villa, P., Lax, P., Pinilla, I., 2014. Cellular responses following retinal injuries and therapeutic approaches for neurodegenerative diseases. Prog. Retin. Eye Res. 43, 17–75.

Cui, J., Lei, H., Samad, A., Basavanthappa, S., Maberley, D., Matsubara, J., Kazlauskas, A., 2009. PDGF receptors are activated in human epiretinal membranes. Exp. Eye Res. 88, 438–444.

Cunha-Vaz, J., 2009. The Blood–Retinal Barrier in Retinal Disease. Eur. Ophthalmic Rev. 03, 105.

Da Cunha, A.P., Zhang, Q., Prentiss, M., Wu, X.Q., Kainz, V., Xu, Y.Y., Vrouvlianis, J., Li, H., Rangaswamy, N., Leehy, B., McGee, T.L., Bell, C.L., Bigelow, C.E., Kansara, V., Medley, Q., Huang, Q., Wu, H.Y., 2018. The Hierarchy of Proinflammatory Cytokines in Ocular Inflammation. Curr. Eye Res. 43, 553–565.

Daruich, A., Matet, A., Moulin, A., Kowalczuk, L., Nicolas, M., Sellam, A., Rothschild, P.R., Omri, S., Gélizé, E., Jonet, L., Delaunay, K., De Kozak, Y., Berdugo, M., Zhao, M., Crisanti, P., Behar-Cohen, F., 2018. Mechanisms of macular edema: Beyond the surface. Prog. Retin. Eye Res. 63, 20–68.

Datta, S., Cano, M., Ebrahimi, K., Wang, L., Handa, J.T., 2017. The impact of oxidative stress and inflammation on RPE degeneration in non-neovascular AMD. Prog. Retin. Eye Res. 60, 201–218.

De Smet, M.D., Gad Elkareem, A.M., Zwinderman, A.H., 2013. The vitreous, the retinal interface in ocular health and disease. Ophthalmologica 230, 165–178.

Ding, J., Wong, T.Y., 2012. Current epidemiology of diabetic retinopathy and diabetic macular edema. Curr. Diab. Rep. 12, 346–354.

Dobolyi, A., Vincze, C., Pál, G., Lovas, G., 2012. The neuroprotective functions of transforming growth factor beta proteins. Int. J. Mol. Sci. 13, 8219–8258.

Dong, A., Shen, J., Zeng, M., Campochiaro, P.A., 2011. Vascular cell-adhesion molecule-1 plays a central role in the proangiogenic effects of oxidative stress. Proc. Natl. Acad. Sci. 108, 14614–14619.

Dong, A., Xie, B., Shen, J., Yoshida, T., Yokoi, K., Hackett, S.F., Campochiaro, P.A., 2009. Oxidative stress promotes ocular neovascularization. J. Cell. Physiol. 219, 544–552.

Duh, E.J., Sun, J.K., Stitt, A.W., 2017. Diabetic retinopathy: current understanding, mechanisms, and treatment strategies. JCI insight 2, 1–13.

Duh, E.J., Yang, H.S., Haller, J.A., De Juan, E., Humayun, M.S., Gehlbach, P., Melia, M., Pieramici, D., Harlan, J.B., Campochiaro, P.A., Zack, D.J., 2004. Vitreous levels of pigment epithelium-derived factor and vascular endothelial growth factor: Implications for ocular angiogenesis. Am. J. Ophthalmol. 137, 668–674.

Ecker, S.M., Pfahler, S.M., Hines, J.C., Lovelace, A.S., Glaser, B.M., 2012. Sequential in-office vitreous aspirates demonstrate vitreous matrix metalloproteinase 9 levels correlate with the amount of subretinal fluid in eyes with wet age-related macular degeneration. Mol. Vis. 18, 1658–67.

Ehrlich, R., Harris, A., Kheradiya, N.S., Winston, D.M., Ciulla, T.A., Wirostko, B., 2008. Age-related macular degeneration and the aging eye. Clin. Interv. Aging 3, 473–82.

El-Ghrably, I.A., Dua, H.S., Orr, G.M., Fischer, D., Tighe, P.J., 2001. Intravitreal invading cells contribute to vitreal cytokine milieu in proliferative vitreoretinopathy. Br. J. Ophthalmol. 85, 461–470.

Erta, M., Quintana, A., Hidalgo, J., 2012. Interleukin-6, a major cytokine in the central nervous system. Int. J. Biol. Sci. 8, 1254–1266.

Eshaq, R.S., Aldalati, A.M.Z., Alexander, J.S., Harris, N.R., 2017. Diabetic retinopathy: Breaking the barrier. Pathophysiology 24, 229–241.

Fernando, N., Natoli, R., Valter, K., Provis, J., Rutar, M., 2016. The broad-spectrum chemokine inhibitor NR58-3.14.3 modulates macrophage-mediated inflammation in the diseased retina. J. Neuroinflammation 13, 1–14.

Fielding, C.A., Jones, G.W., McLoughlin, R.M., McLeod, L., Hammond, V.J., Uceda, J., Williams, A.S., Lambie, M., Foster, T.L., Liao, C. Te, Rice, C.M., Greenhill, C.J., Colmont, C.S., Hams, E., Coles, B., Kift-Morgan, A., Newton, Z., Craig, K.J., Williams, J.D., Williams, G.T., Davies, S.J., Humphreys, I.R., O'Donnell, V.B., Taylor, P.R., Jenkins, B.J., Topley, N., Jones, S.A., 2014. Interleukin-6 signaling drives fibrosis in unresolved inflammation. Immunity 40, 40–50.

Fisher, S.K., Lewis, G.P., 2003. Müller cell and neuronal remodeling in retinal detachment and reattachment and their potential consequences for visual recovery: A review and reconsideration of recent data. Vision Res. 43, 887–897.

Flaxman, S.R., Bourne, R.R.A., Resnikoff, S., *et. al.*, 2017. Global causes of blindness and distance vision impairment 1990–2020: a systematic review and meta-analysis. Lancet Glob. Heal. 5, e1221–e1234.

Fong, D.S., Girach, A., Boney, A., 2007. Visual side effects of successful scatter laser photocoagulation surgery for proliferative diabetic retinopathy: A literature review. Retina 27, 816–824.

Forest, D.L., Johnson, L. V., Clegg, D.O., 2015. Cellular models and therapies for age-related macular degeneration. Dis. Model. Mech. 8, 421–427. Fortuny, C., Flannery, J.G., 2018. Mutation-Independent Gene Therapies for Rod-Cone Dystrophies. pp. 75–81.

Frey, T., Antonetti, D.A., 2011. Alterations to the blood-retinal barrier in diabetes: Cytokines and reactive oxygen species. Antioxidants Redox Signal. 15, 1271–1284.

Friedlander, M., 2007. Fibrosis and diseases of the eye. J. Clin. Invest. 117, 576–586.

Fritsche, L.G., Fariss, R.N., Stambolian, D., Abecasis, G.R., Curcio, C.A., Swaroop, A., 2014. Age-Related Macular Degeneration: Genetics and Biology Coming Together. Annu. Rev. Genomics Hum. Genet. 15, 151–171.

Funatsu, H., Yamashita, H., Nakanishi, Y., Hori, S., 2002. Angiotensin II and vascular endothelial growth factor in the vitreous fluid of patients with proliferative diabetic retinopathy. Br. J. Ophthalmol. 86, 311–315.

Funatsu, H., Yamashita, H., Sakata, K., Noma, H., Mimura, T., Suzuki, M., Eguchi, S., Hori, S., 2005. Vitreous levels of vascular endothelial growth factor and intercellular adhesion molecule 1 are related to diabetic macular edema. Ophthalmology 112, 806–816.

Funk, M., Karl, D., Georgopoulos, M., Benesch, T., Sacu, S., Polak, K., Zlabinger, G.J., Schmidt-Erfurth, U., 2009. Neovascular Age-related Macular Degeneration: Intraocular Cytokines and Growth Factors and the Influence of Therapy with Ranibizumab. Ophthalmology 116, 2393–2399.

Gale, J., Aiello, L.P., Sebag, J., 2014. I.E. Diabetic Vitreopathy, in: Vitreous. Springer New York, New York, NY, pp. 57–79.

Gao, B.-B., Chen, X., Timothy, N., Aiello, L.P., Feener, E.P., 2008. Characterization of the Vitreous Proteome in Diabetes without Diabetic Retinopathy and Diabetes with Proliferative Diabetic Retinopathy. J. Proteome Res. 7, 2516–2525.

Gao, B.B., Clermont, A., Rook, S., Fonda, S.J., Srinivasan, V.J., Wojtkowski, M., Fujimoto, J.G., Avery, R.L., Arrigg, P.G., Bursell, S.E., Aiello, L.P., Feener, E.P., 2007. Extracellular carbonic anhydrase mediates hemorrhagic retinal and cerebral vascular permeability through prekallikrein activation. Nat. Med. 13, 181–188.

García-Ramírez, M., Canals, F., Hernández, C., Colomé, N., Ferrer, C., Carrasco, E., García-Arumí, J., Simó, R., 2007. Proteomic analysis of human vitreous fluid by fluorescence-based difference gel electrophoresis (DIGE): A new strategy for identifying potential candidates in the pathogenesis of proliferative diabetic retinopathy. Diabetologia 50, 1294–1303.

Gardner, T.W., Antonetti, D.A., Barber, A.J., LaNoue, K.F., Levison, S.W., 2002. Diabetic retinopathy: More than meets the eye. Surv. Ophthalmol. 47, 253–262.

Gardner, T.W., Sundstrom, J.M., 2017. A proposal for early and personalized treatment of diabetic retinopathy based on clinical pathophysiology and molecular phenotyping. Vision Res. 139, 153–160.

Gariano, R.F., Gardner, T.W., 2005. Retinal angiogenesis in development and disease. Nature 438, 960–966.

Garweg, J.G., Tappeiner, C., Halberstadt, M., 2013. Pathophysiology of Proliferative Vitreoretinopathy in Retinal Detachment. Surv. Ophthalmol. 58, 321–329.

Gehrs, K.M., Anderson, D.H., Johnson, L. V., Hageman, G.S., 2006. Age-related macular degeneration - Emerging pathogenetic and therapeutic concepts. Ann. Med. 38, 450–471.

Gerhardinger, C., Costa, M.B., Coulombe, M.C., Toth, I., Hoehn, T., Grosu, P., 2005. Expression of acute-phase response proteins in retinal Müller cells in diabetes. Investig. Ophthalmol. Vis. Sci. 46, 349–357.

Ghasemi Falavarjani, K., Hashemi, M., Modarres, M., Hadavand Khani, A., 2014. Intrasilicone oil injection of bevacizumab at the end of retinal reattachment surgery for severe proliferative vitreoretinopathy. Eye 28, 576–580.

Giebel, S.J., Menicucci, G., McGuire, P.G., Das, A., 2005. Matrix metalloproteinases in early diabetic retinopathy and their role in alternation of the blood-retinal barrier. Lab. Investig. 85, 597–607.

Gilbert, C., Gilbert, C., Unger, W., Grierson, I., Mc Leod, D., 1988. Inflammation and the formation of epiretinal membranes. Eye 2, S140–S156.

Giuliari, G.P., Sadaka, 2012. Proliferative vitreoretinopathy: current and emerging treatments. Clin. Ophthalmol. 32, 1325.

Gold, M., El Khoury, J., 2015. β-amyloid, microglia, and the inflammasome in Alzheimer's disease. Semin. Immunopathol. 37, 607–611.

Golestaneh, N., Chu, Y., Xiao, Y.Y., Stoleru, G.L., Theos, A.C., 2017. Dysfunctional autophagy in RPE, a contributing factor in age-related macular degeneration. Cell Death Dis. 8.

Gonzalez, V.H., Campbell, J., Holekamp, N.M., Kiss, S., Loewenstein, A., Augustin, A.J., Ma, J., Ho, A.C., Patel, V., Whitcup, S.M., Dugel, P.U., 2016. Early and Long-Term Responses to Anti–Vascular Endothelial Growth Factor Therapy in Diabetic Macular Edema: Analysis of Protocol I Data. Am. J. Ophthalmol. 172, 72–79.

Gragoudas, E.S., Adamis, A.P., Cunningham, E.T., Feinsod, M., Guyer, D.R., 2004. Pegaptanib for Neovascular Age-Related Macular Degeneration. N. Engl. J. Med. 351, 2805–2816.

Gross, J.G., Glassman, A.R., Jampol, L.M., Inusah, S., Aiello, L.P., Antoszyk, A.N., Baker, C.W., Berger, B.B., Bressler, N.M., Browning, D., Elman, M.J., Ferris, F.L., Friedman, S.M., Marcus, D.M., Melia, M., Stockdale, C.R., Sun, J.K., Beck, R.W., 2015. Panretinal Photocoagulation vs Intravitreous Ranibizumab for Proliferative Diabetic Retinopathy. JAMA 314, 2137.

Guariguata, L., Whiting, D.R., Hambleton, I., Beagley, J., Linnenkamp, U., Shaw, J.E., 2014. Global estimates of diabetes prevalence for 2013 and projections for 2035. Diabetes Res. Clin. Pract. 103, 137–149.

Guidry, C., 2010. Proliferative vitreoretinopathy, in: Ocular Disease. Elsevier, pp. 612–617.

Gupta, V., Gupta, V.B., Chitranshi, N., Gangoda, S., Vander Wall, R., Abbasi, M., Golzan, M., Dheer, Y., Shah, T., Avolio, A., Chung, R., Martins, R., Graham, S., 2016. One protein, multiple pathologies: multifaceted involvement of amyloid β in neurodegenerative disorders of the brain and retina. Cell. Mol. Life Sci. 73, 4279–4297.

Halle, A., Hornung, V., Petzold, G.C., Stewart, C.R., Monks, B.G., Reinheckel, T., Fitzgerald, K.A., Latz, E., Moore, K.J., Golenbock, D.T., 2008. The NALP3 inflammasome is involved in the innate immune response to amyloid-β. Nat. Immunol. 9, 857–865.

Haque, A., Polcyn, R., Matzelle, D., Banik, N.L., 2018. New insights into the role of neuron-specific enolase in neuro-inflammation, neurodegeneration, and neuroprotection. Brain Sci. 8.

Harhaj, N.S., Felinski, E.A., Wolpert, E.B., Sundstrom, J.M., Gardner, T.W., Antonetti, D.A., 2006. VEGF activation of protein kinase C stimulates occludin phosphorylation and contributes to endothelial permeability. Investig. Ophthalmol. Vis. Sci. 47, 5106–5115.

Haurigot, V., Villacampa, P., Ribera, A., Llombart, C., Bosch, A., Nacher, V., Ramos, D., Ayuso, E., Segovia, J.C., Bueven, J.A., Ruberte, J., Bosch, F., 2009. Increased intraocular insulin-like growth factor-I triggers blood-retinal barrier breakdown. J. Biol. Chem. 284, 22961–22969.

Heier, J.S., Brown, D.M., Chong, V., Korobelnik, J.-F., Kaiser, P.K., Nguyen, Q.D., Kirchhof, B., Ho, A., Ogura, Y., Yancopoulos, G.D., Stahl, N., Vitti, R., Berliner, A.J., Soo, Y., Anderesi, M., Groetzbach, G., Sommerauer, B., Sandbrink, R., Simader, C., Schmidt-Erfurth, U., 2012. Intravitreal Aflibercept (VEGF Trap-Eye) in Wet Age-related Macular Degeneration. Ophthalmology 119, 2537–2548.

Hernández-Zimbrón, L.F., Zamora-Alvarado, R., Ochoa-De La Paz, L., Velez-Montoya, R., Zenteno, E., Gulias-Cañizo, R., Quiroz-Mercado, H., Gonzalez-Salinas, R., 2018. Age-Related Macular Degeneration: New Paradigms for Treatment and Management of AMD. Oxid. Med. Cell. Longev. 2018.

Hernández, C., Burgos, R., Cantón, A., García-Arumí, J., Segura, R.M., Simó, R., 2001. Vitreous levels of vascular cell adhesion molecule and vascular endothelial growth factor in patients with proliferative diabetic retinopathy: A case-control study. Diabetes Care 24, 516–521.

Hernández, C., Simó-Servat, A., Bogdanov, P., Simó, R., 2017. Diabetic retinopathy: new therapeutic perspectives based on pathogenic mechanisms. J. Endocrinol. Invest. 40, 925–935.

Hiscott, P., Sheridan, C., Magee, R.M., Grierson, I., 1999. Matrix and the retinal pigment epithelium in proliferative retinal disease. Prog. Retin. Eye Res. 18, 167–190.

Holekamp, N.M., 2010. The Vitreous Gel: More than Meets the Eye. Am. J. Ophthalmol. 149, 32-36.e1.

Holekamp, N.M., Bouck, N., Volpert, O., 2002. Pigment epithelium-derived factor is deficient in the vitreous of patients with choroidal neovascularization due to age-related macular degeneration. Am. J. Ophthalmol. 134, 220–227.

Huber, M., Wachtlin, J., 2012. Vitreous levels of proteins implicated in angiogenesis are modulated in patients with retinal or choroidal neovascularization. Ophthalmologica 228, 188–193.

Hussain, A.A., Lee, Y., Zhang, J.J., Marshall, J., 2011. Disturbed matrix metalloproteinase activity of Bruch's membrane in age-related macular degeneration. Investig. Ophthalmol. Vis. Sci. 52, 4459–4466.

Hyttinen, J.M.T., Błasiak, J., Niittykoski, M., Kinnunen, K., Kauppinen, A., Salminen, A., Kaarniranta, K., 2017. DNA damage response and autophagy in the degeneration of retinal pigment epithelial cells—Implications for age-related macular degeneration (AMD). Ageing Res. Rev. 36, 64–77.

Idrees, S., Sridhar, J., Kuriyan, A.E., 2019. Proliferative vitreoretinopathy: A review. Int. Ophthalmol. Clin. 59, 221–240.

Iglicki, M., Busch, C., Zur, D., Okada, M., Mariussi, M., Chhablani, J.K., Cebeci, Z., Fraser-Bell, S., Chaikitmongkol, V., Couturier, A., Giancipoli, E., Lupidi, M., Rodríguez-Valdés, P.J., Rehak, M., Fung, A.T., Goldstein, M., Loewenstein, A., 2019. Dexamethasone Implant for Diabetic Macular Edema in Naïve compared with Refractory Eyes. Retina 39, 44–51.

Ioachim, E., Stefaniotou, M., Gorezis, S., Tsanou, E., Psilas, K., Agnantis, N.J., 2005. Immunohistochemical study of extracellular matrix components in epiretinal membranes of vitreoproliferative retinopathy and proliferative diabetic retinopathy. Eur. J. Ophthalmol. 15, 384–391.

Ishizaki, E., Takai, S., Ueki, M., Maeno, T., Maruichi, M., Sugiyama, T., Oku, H., Ikeda, T., Miyazaki, M., 2006. Correlation between angiotensin-converting enzyme, vascular endothelial growth factor, and matrix metalloproteinase-9 in the vitreous of eyes with diabetic retinopathy. Am. J. Ophthalmol. 141.

Iyer, S.S., Pulskens, W.P., Sadler, J.J., Butter, L.M., Teske, G.J., Ulland, T.K., Eisenbarth, S.C., Florquin, S., Flavell, R.A., Leemans, J.C., Sutterwala, F.S., 2009. Necrotic cells trigger a sterile inflammatory response through the Nlrp3 inflammasome. Proc. Natl. Acad. Sci. U. S. A. 106, 20388–20393.

Izuta, H., Chikaraishi, Y., Adachi, T., Shimazawa, M., Sugiyama, T., Ikeda, T., Hara, H., 2009. Extracellular SOD and VEGF are increased in vitreous bodies from proliferative diabetic retinopathy patients. 2663–2672.

Izuta, H., Matsunaga, N., Shimazawa, M., Sugiyama, T., Ikeda, T., Hara, H., 2010. Proliferative diabetic retinopathy and relations among antioxidant activity, oxidative stress, and VEGF in the vitreous body. Mol. Vis. 16, 130–6.

Jager, R.D., Mieler, W.F., Miller, J.W., 2008. Age-Related Macular Degeneration. N. Engl. J. Med. 358, 2606–2617.

Jarrett, S.G., Boulton, M.E., 2012. Consequences of oxidative stress in age-related macular degeneration. Mol. Aspects Med. 33, 399–417.

Jay, N.L., Gillies, M., 2012. Proteomic analysis of ophthalmic disease. Clin. Experiment. Ophthalmol. 40, 755–763.

Jeganathan, V.S.E., Wang, J.J., Wong, T.Y., 2008. Ocular associations of diabetes other than diabetic retinopathy. Diabetes Care 31, 1905–1912.

Jin, M., Kashiwagi, K., Iizuka, Y., Tanaka, Y., Imai, M., Tsukahara, S., 2001. Matrix metalloproteinases in human diabetic and nondiabetic vitreous. Retina 21, 28–33.

Jonas, J.B., Hayler, J.K., Söfker, A., Panda-Jonas, S., 2001. Intravitreal injection of crystalline cortisone as adjunctive treatment of proliferative diabetic retinopathy. Am. J. Ophthalmol. 131, 468–471.

Joshi, M., Agrawal, S., Christoforidis, J.B., 2013. Inflammatory mechanisms of idiopathic epiretinal membrane formation. Mediators Inflamm. 2013.

Joussen, A.M., Poulaki, V., Le, M.L., Koizumi, K., Esser, C., Janicki, H., Schraermeyer, U., Kociok, N., Fauser, S., Kirchhof, B., Kern, T.S., Adamis, A.P., 2004. A central role for inflammation in the pathogenesis of diabetic retinopathy. FASEB J. 18, 1450–1452.

Jünemann, A.G.M., Rejdak, R., Huchzermeyer, C., Maciejewski, R., Grieb, P., Kruse, F.E., Zrenner, E., Rejdak, K., Petzold, A., 2015. Elevated vitreous body glial fibrillary acidic protein in retinal diseases. Graefe's Arch. Clin. Exp. Ophthalmol. 253, 2181–2186.

Kaemmerer, E., Schutt, F., Krohne, T.U., Holz, F.G., Kopitz, J., 2007. Effects of lipid peroxidation-related protein modifications on RPE lysosomal functions and POS phagocytosis. Investig. Ophthalmol. Vis. Sci. 48, 1342–1347.

Kandarakis, S.A., Piperi, C., Topouzis, F., Papavassiliou, A.G., 2014. Emerging role of advanced glycation-end products (AGEs) in the pathobiology of eye diseases. Prog. Retin. Eye Res. 42, 85–102.

Kang, G.Y., Bang, J.Y., Choi, A.J., Yoon, J., Lee, W.C., Choi, S., Yoon, S., Kim, H.C., Baek, J.H., Park, H.S., Lim, H.J., Chung, H., 2014. Exosomal proteins in the aqueous humor as novel biomarkers in patients with neovascular age-related macular degeneration. J. Proteome Res. 13, 581–595.

Kannan, R., Sreekumar, P.G., Hinton, D.R., 2012. Novel roles for α-crystallins in retinal function and disease. Prog. Retin. Eye Res. 31, 576–604.

Karkhur, S., Hasanreisoglu, M., Vigil, E., Halim, M.S., Hassan, M., Plaza, C., Nguyen, N. V., Afridi, R., Tran, A.T., Do, D. V., Sepah, Y.J., Nguyen, Q.D., 2019. Interleukin-6 inhibition in the management of non-infectious uveitis and beyond. J. Ophthalmic Inflamm. Infect. 9.

Kaur, C., Foulds, W.S., Ling, E.A., 2008. Blood-retinal barrier in hypoxic ischaemic conditions: Basic concepts, clinical features and management. Prog. Retin. Eye Res. 27, 622–647.

Kayama, M., Nakazawa, T., Thanos, A., Morizane, Y., Murakami, Y., Theodoropoulou, S., Abe, T., Vavvas, D., Miller, J.W., 2011. Heat shock protein 70 (HSP70) is critical for the photoreceptor stress response after retinal detachment via modulating anti-apoptotic Akt kinase. Am. J. Pathol. 178, 1080–1091.

Kern, T.S., 2007. Contributions of inflammatory processes to the development of the early stages of diabetic retinopathy. Exp. Diabetes Res. 2007, 95103.

Kertes, P.J., 2004. Photodynamic therapy of subfoveal choroidal neovascularization with verteporfin. Evidence-Based Eye Care 5, 10–12.

Kim, K., Kim, S.J., Yu, H.G., Yu, J., Park, K.S., Jang, I.J., Kim, Y., 2010. Verification of biomarkers for diabetic retinopathy by multiple reaction monitoring. J. Proteome Res. 9, 689–699.

Kim, S.J., Kim, S., Park, J., Lee, H.K., Park, K.S., Yu, H.G., Kim, Y., 2006. Differential Expression of Vitreous Proteins in Proliferative Diabetic Retinopathy. Curr. Eye Res. 31, 231–240.

Kim, T., Sang, J.K., Kim, K., Kang, U.B., Lee, C., Kyong, S.P., Hyeong, G.Y., Kim, Y., 2007. Profiling of vitreous proteomes from proliferative diabetic retinopathy and nondiabetic patients. Proteomics 7, 4203–4215.

Kimura, K., Orita, T., Liu, Y., Yang, Y., Tokuda, K., Kurakazu, T., Noda, T., Yanai, R., Morishige, N., Takeda, A., Ishibashi, T., Sonoda, K.-H.H., 2015. Attenuation of EMT in RPE cells and subretinal fibrosis by an RAR-γ agonist. J. Mol. Med. 93, 749–758.

Kita, T., Clermont, A.C., Murugesan, N., Zhou, Q., Fujisawa, K., Ishibashi, T., Aiello, L.P., Feener, E.P., 2015. Plasma kallikrein-kinin system as a VEGF-independent mediator of diabetic macular edema. Diabetes 64, 3588–3599.

Kita, T., Hata, Y., Arita, R., Kawahara, S., Miura, M., Nakao, S., Mochizuki, Y., Enaida, H., Goto, Y., Shimokawa, H., Hafezi-Moghadam, A., Ishibashi, T., 2008. Role of TGF-β in proliferative vitreoretinal diseases and ROCK as a therapeutic target. Proc. Natl. Acad. Sci. U. S. A. 105, 17504–17509.

Klaassen, I., de Vries, E.W., Vogels, I.M.C., van Kampen, A.H.C., Bosscha, M.I., Steel, D.H.W., Van Noorden, C.J.F., Lesnik-Oberstein, S.Y., Schlingemann, R.O., 2017. Identification of proteins associated with clinical and pathological features of proliferative diabetic retinopathy in vitreous and fibrovascular membranes. PLoS One 12, e0187304.

Klaassen, I., van Geest, R.J., Kuiper, E.J., van Noorden, C.J.F., Schlingemann, R.O., 2015. The role of CTGF in diabetic retinopathy. Exp. Eye Res. 133, 37–48.

Klaassen, I., Van Noorden, C.J.F., Schlingemann, R.O., 2013. Molecular basis of the inner blood-retinal barrier and its breakdown in diabetic macular edema and other pathological conditions. Prog. Retin. Eye Res. 34, 19–48.

Klein, M.L., Ferris, F.L., Armstrong, J., Hwang, T.S., Chew, E.Y., Bressler, S.B., Chandra, S.R., 2008. Retinal Precursors and the Development of Geographic Atrophy in Age-Related Macular Degeneration. Ophthalmology 115, 1026–1031.

Ko, J.A., Sotani, Y., Ibrahim, D.G., Kiuchi, Y., 2017. Role of macrophage migration inhibitory factor (MIF) in the effects of oxidative stress on human retinal pigment epithelial cells. Cell Biochem. Funct. 35, 426–432.

Köberlein, J., Beifus, K., Schaffert, C., Finger, R.P., 2013. The economic burden of visual impairment and blindness: A systematic review. BMJ Open 3.

Kodama, M., Matsuura, T., Hara, Y., 2013. Structure of vitreous body and its relationship with liquefaction. J. Biomed. Sci. Eng. 06, 739–745.

Kon, C.H., Tranos, P., Aylward, G.W., 2005. Risk Factors in Proliferative Vitreoretinopathy, in: Vitreo-Retinal Surgery. Springer-Verlag, Berlin/Heidelberg, pp. 121–134.

Korpos, E., Wu, C., Sorokin, L., 2009. Multiple Roles of the Extracellular Matrix in Inflammation. Curr. Pharm. Des. 15, 1349–1357.

Koskela, U.E., Kuusisto, S.M., Nissinen, A.E., Savolainen, M.J., Liinamaa, M.J., 2013. High vitreous concentration of IL-6 and IL-8, but not of adhesion molecules in relation to plasma concentrations in proliferative diabetic retinopathy. Ophthalmic Res. 49, 108–114.

Koss, M.J., Hoffmann, J., Nguyen, N., Pfister, M., Mischak, H., Mullen, W., Husi, H., Rejdak, R., Koch, F., Jankowski, J., Krueger, K., Bertelmann, T., Klein, J., Schanstra, J.P., Siwy, J., 2014. Proteomics of vitreous humor of patients with exudative age-related macular degeneration. PLoS One 9, 1–11.

Koss, M.J., Pfister, M., Koch, F.H., 2011. Inflammatory and Angiogenic Protein Detection in the Human Vitreous: Cytometric Bead Assay. J. Ophthalmol. 2011, 1–4.

Kovacs, K., Marra, K. V., Yu, G., Wagley, S., Ma, J., Teague, G.C., Nandakumar, N., Lashkari, K., Arroyo, J.G., 2015. Angiogenic and inflammatory vitreous biomarkers associated with increasing levels of retinal ischemia. Investig. Ophthalmol. Vis. Sci. 56, 6523–6530.

Kowluru, R.A., Kowluru, A., Mishra, M., Kumar, B., 2015. Oxidative stress and epigenetic modifications in the pathogenesis of diabetic retinopathy. Prog. Retin. Eye Res. 48, 40–61.

Kowluru, R.A., Zhong, Q., Santos, J.M., 2012. Matrix metalloproteinases in diabetic retinopathy: Potential role of MMP-9. Expert Opin. Investig. Drugs 21, 797–805.

Krohne, T.U., Stratmann, N.K., Kopitz, J., Holz, F.G., 2010. Effects of lipid peroxidation products on lipofuscinogenesis and autophagy in human retinal pigment epithelial cells. Exp. Eye Res. 90, 465–471.

Kroll, P., Büchele Rodrigues, E., Hoerle, S., 2007. Pathogenesis and classification of proliferative diabetic vitreoretinopathy. Ophthalmologica 221, 78–94.

Kroll, P., Rodrigues, E.B., Meyer, C.H., 2014. III.L. Proliferative Diabetic Vitreoretinopathy, in: Vitreous. Springer New York, New York, NY, pp. 421–434.

Kruk, J., Kubasik-Kladna, K., Y. Aboul-Enein, H., 2015. The Role Oxidative Stress in the Pathogenesis of Eye Diseases: Currnt Status and a Dual Role of Physical Activity. Mini-Reviews Med. Chem. 16, 241–257.

Kubay, O. V., Charteris, D.G., Newland, H.S., Raymond, G.L., 2005. Retinal detachment neuropathology and potential strategies for neuroprotection. Surv. Ophthalmol. 50, 463–475.

Kuiper, E.J., De Smet, M.D., Van Meurs, J.C., Tan, H.S., Tanck, M.W.T., Oliver, N., Van Nieuwenhoven, F.A., Goldschmeding, R., Schlingemann, R.O., 2006. Association of connective tissue growth factor with fibrosis in vitreoretinal disorders in the human eye. Arch. Ophthalmol. 124, 1457–1462.

Kuiper, E.J., Van Nieuwenhoven, F.A., de Smet, M.D., van Meurs, J.C., Tanck, M.W., Oliver, N., Klaassen, I., Van Noorden, C.J.F., Goldschmeding, R., Schlingemann, R.O., 2008. The angio-fibrotic switch of VEGF and CTGF in proliferative diabetic retinopathy. PLoS One 3, 1–7.

Kusuhara, S., Fukushima, Y., Ogura, S., Inoue, N., Uemura, A., 2018. Pathophysiology of diabetic retinopathy: The old and the new. Diabetes Metab. J. 42, 364–376.

Kutty, R.K., Samuel, W., Boyce, K., Cherukuri, A., Duncan, T., Jaworski, C., Nagineni, C.N., Redmond, T.M., 2016. Proinflammatory cytokines decrease the expression of genes critical for RPE function. Mol. Vis. 22, 1156–1168.

Kwon, O.W., Roh, M.I., Song, J.H., 2010. Retinal detachment and proliferative vitreoretinopathy, in: Retinal Pharmacotherapy. Elsevier, pp. 147–151.

Kwon, Y.H., Kim, Y.A., Yoo, Y.H., 2017. Loss of Pigment Epithelial Cells Is Prevented by Autophagy, 11th ed, Autophagy: Cancer, Other Pathologies, Inflammation, Immunity, Infection, and Aging. Elsevier Inc.

Lambert, N.G., ElShelmani, H., Singh, M.K., Mansergh, F.C., Wride, M.A., Padilla, M., Keegan, D., Hogg, R.E., Ambati, B.K., 2016. Risk factors and biomarkers of age-related macular degeneration. Prog. Retin. Eye Res. 54, 64–102.

Lambert, V., Wielockx, B., Munaut, C., Galopin, C., Jost, M., Itoh, T., Werb, Z., Baker, A., Libert, C., Krell, H.-W., Foidart, J.-M., Noël, A., Rakic, J.-M., 2003. MMP-2 and MMP-9 synergize in promoting choroidal neovascularization. FASEB J. 17, 2290–2292.

Lawler, P.R., Lawler, J., 2012. Molecular basis for the regulation of angiogenesis by thrombospondin-1 and -2. Cold Spring Harb. Perspect. Med. 2, a006627–a006627.

Le Goff, M.M., Bishop, P.N., 2008. Adult vitreous structure and postnatal changes. Eye 22, 1214–1222.

Lechner, J., O'Leary, O.E., Stitt, A.W., 2017. The pathology associated with diabetic retinopathy. Vision Res. 139, 7–14.

Lee, R., Wong, T.Y., Sabanayagam, C., 2015. Epidemiology of diabetic retinopathy, diabetic macular edema and related vision loss. Eye Vis. 2, 17.

Lei, H., Velez, G., Cui, J., Samad, A., Maberley, D., Matsubara, J., Kazlauskas, A., 2010. N-acetylcysteine suppresses retinal detachment in an experimental model of proliferative vitreoretinopathy. Am. J. Pathol. 177, 132–140.

Lei, H., Velez, G., Hovland, P., Hirose, T., Gilbertson, D., Kazlauskas, A., 2009. Growth factors outside the PDGF family drive experimental PVR. Investig. Ophthalmol. Vis. Sci. 50, 3394–3403.

Lewis, G.P., Fisher, S.K., 2003. Up-Regulation of Glial Fibrillary Acidic Protein in Response to Retinal Injury: Its Potential Role in Glial Remodeling and a Comparison to Vimentin Expression. Int. Rev. Cytol. 230, 263–290.

Li, J., Lu, Q., Lu, P., 2018. Quantitative proteomics analysis of vitreous body from type 2 diabetic patients with proliferative diabetic retinopathy. BMC Ophthalmol. 18, 151.

Lim, L.S., Mitchell, P., Seddon, J.M., Holz, F.G., Wong, T.Y., 2012. Age-related macular degeneration. Lancet 379, 1728–1738.

Limb, G.A., Chignell, A.H., 1999. Vitreous levels of intercellular adhesion molecule 1 (ICAM-1) as a risk indicator of proliferative vitreoretinopathy. Br. J. Ophthalmol. 83, 953–956.

Liu, R.T., Gao, J., Cao, S., Sandhu, N., Cui, J.Z., Chou, C.L., Fang, E., Matsubara, J.A., 2013. Inflammatory mediators induced by amyloid-beta in the retina and RPE In Vivo: Implications for inflammasome activation in age-related macular degeneration. Investig. Ophthalmol. Vis. Sci. 54, 2225–2237.

Liu, X., Ye, F., Xiong, H., Hu, D.N., Limb, G.A., Xie, T., Peng, L., Zhang, P., Wei, Y., Zhang, W., Wang, J., Wu, H., Lee, P., Song, E., Zhang, D.Y., 2015. IL-1β Induces IL-6 production in retinal Müller cells predominantly through the activation of P38 MAPK/NF-κB signaling pathway. Exp. Cell Res. 331, 223–231.

Lo, A.C.Y., Woo, T.T.Y., Wong, R.L.M., Wong, D., 2011. Apoptosis and other cell death mechanisms after retinal detachment: Implications for photoreceptor rescue. Ophthalmologica 226, 10–17.

Loukovaara, S., Nurkkala, H., Tamene, F., Gucciardo, E., Liu, X., Repo, P., Lehti, K., Varjosalo, M., 2015. Quantitative Proteomics Analysis of Vitreous Humor from Diabetic Retinopathy Patients. J. Proteome Res. 14, 5131–5143.

Loyet, K.M., DeForge, L.E., Katschke, K.J., Diehl, L., Graham, R.R., Pao, L., Sturgeon, L., Lewin-Koh, S.C., Hollyfield, J.G., Campagne, M. van L., 2012. Activation of the alternative complement pathway in vitreous is controlled by genetics in age-related macular degeneration. Investig. Ophthalmol. Vis. Sci. 53, 6628–6637.

Lu, M., Perez, V.L., Ma, N., Miyamoto, K., Peng, H.B., Liao, J.K., Adamis, A.P., 1999. VEGF increases retinal vascular ICAM-1 expression in vivo. Invest. Ophthalmol. Vis. Sci. 40, 1808–12.

Lu, P., Takai, K., Weaver, V.M., Werb, Z., 2011. Extracellular Matrix Degradation and Remodeling in Development and Disease. Cold Spring Harb. Perspect. Biol. 3, a005058–a005058.

Luibl, V., Isas, J.M., Kayed, R., Glabe, C.G., Langen, R., Chen, J., 2006. Drusen deposits associated with aging and age-related macular degeneration contain nonfibrillar amyloid oligomers. J. Clin. Invest. 116, 378–385.

Macular Photocoagulation Study Group, 1994. Laser photocoagulation for juxtafoveal choroidal neovascularization. Five-year results from randomized clinical trials. Macular Photocoagulation Study Group. Arch. Ophthalmol. 112, 500–9.

Macular Photocoagulation Study Group, 1993. Laser Photocoagulation of Subfoveal Neovascular Lesions of Age-Related Macular Degeneration. Arch. Ophthalmol. 111, 1200.

Madeira, M.H., Boia, R., Santos, P.F., Ambrósio, A.F., Santiago, A.R., 2015. Contribution of microglia-mediated neuroinflammation to retinal degenerative diseases. Mediators Inflamm. 2015.

Madsen-Bouterse, S.A., Kowluru, R.A., 2008. Oxidative stress and diabetic retinopathy: Pathophysiological mechanisms and treatment perspectives. Rev. Endocr. Metab. Disord. 9, 315–327.

Mahajan, V.B., Skeie, J.M., 2014. Translational vitreous proteomics. Proteomics. Clin. Appl. 8, 204–8.

Maier, R., Weger, M., Haller-Schober, E.-M., El-Shabrawi, Y., Wedrich, A., Theisl, A., Aigner, R., Barth, A., Haas, A., 2008. Multiplex bead analysis of vitreous and serum concentrations of inflammatory and proangiogenic factors in diabetic patients. Mol. Vis. 14, 637–643.

Maik-Rachline, G., Seger, R., 2006. Variable phosphorylation states of pigment-epithelium-derived factor differentially regulate its function. Blood 107, 2745–2752.

Maik-Rachline, G., Shaltiel, S., Seger, R., 2005. Extracellular phosphorylation converts pigment epithelium-derived factor from a neurotrophic to an antiangiogenic factor. Blood 105, 670–678.

Mancino, R., Di Pierro, D., Varesi, C., Cerulli, A., Feraco, A., Cedrone, C., Pinazo-Duran, M.D., Coletta, M., Nucci, C., 2011. Lipid peroxidation and total antioxidant capacity in vitreous, aqueous humor, and blood samples from patients with diabetic retinopathy. Mol. Vis. 17, 1298–304.

Mandal, N., Heegaard, S., Prause, J.U., Honoré, B., Vorum, H., 2010. Ocular proteomics with emphasis on two-dimensional gel electrophoresis and mass spectrometry. Biol. Proced. Online 12, 56–88.

Marmorstein, L.Y., Munier, F.L., Arsenijevic, Y., Schorderet, D.F., Mclaughlin, P.J., Chung, D., Traboulsi, E., Marmorstein, A.D., 2002. Aberrant accumulation of EFEMP1 underlies drusen formation in Malattia Leventinese and age-related macular degeneration. Proc. Natl. Acad. Sci. 99, 13067–13072.

Matsuo, T., 1998. TIMP-1 and TIMP-2 Levels in Vitreous and Subretinal Fluid. Jpn. J. Ophthalmol. 42, 377–380.

Maugeri, A., Barchitta, M., Mazzone, M.G., Giuliano, F., Agodi, A., 2018. Complement system and age-related macular degeneration: Implications of gene-environment interaction for preventive and personalized medicine. Biomed Res. Int. 2018.

Medeiros, N.E., Curcio, C.A., 2001. Preservation of ganglion cell layer neurons in age-related macular degeneration. Investig. Ophthalmol. Vis. Sci. 42, 795–803.

Mekjavic, P.J., Kraut, A., Urbancic, M., Lenassi, E., Hawlina, M., 2011. Efficacy of 12-month treatment of neovascular age-related macular degeneration with intravitreal bevacizumab based on individually determined injection strategies after three consecutive monthly injections. Acta Ophthalmol. 89, 647–653.

Mesquita, J., Castro-de-Sousa, J.P., Vaz-Pereira, S., Neves, A., Passarinha, L.A., Tomaz, C.T., 2018a. Evaluation of the growth factors VEGF-a and VEGF-B in the vitreous and serum of patients with macular and retinal vascular diseases. Growth Factors 36, 48–57.

Mesquita, J., Castro-de-Sousa, J.P., Vaz-Pereira, S., Neves, A., Passarinha, L.A., Tomaz, C.T., 2018b. Vascular endothelial growth factors and placenta growth factor in retinal vasculopathies: Current research and future perspectives. Cytokine Growth Factor Rev. 39, 102–115.

Mesquita, J., Castro de Sousa, J., Vaz-Pereira, S., Neves, A., Tavares-Ratado, P., M. Santos, F., A. Passarinha, L., T. Tomaz, C., 2017. VEGF-B Levels in the Vitreous of Diabetic and Non-Diabetic Patients with Ocular Diseases and Its Correlation with Structural Parameters. Med. Sci. 5, 17.

Minamoto, A., Yamane, K., Yokoyama, T., Thongboonkerd, V., 2007. Proteomics of vitreous fluid. Proteomics Hum. Body Fluids Princ. Methods, Appl. 495–507.

Miyamoto, K., Khosrof, S., Bursell, S.E., Moromizato, Y., Aiello, L.P., Ogura, Y., Adamis, A.P., 2000. Vascular endothelial growth factor (VEGF)-induced retinal vascular permeability is mediated by intercellular adhesion molecule-1 (ICAM-1). Am. J. Pathol. 156, 1733–1739.

Monteiro, J.P., Santos, F.M., Rocha, A.S., Castro-de-Sousa, J.P., Queiroz, J.A., Passarinha, L.A., Tomaz, C.T., 2015. Vitreous humor in the pathologic scope: Insights from proteomic approaches. PROTEOMICS - Clin. Appl. 9, 187–202.

Morescalchi, F., Duse, S., Gambicorti, E., Romano, M.R., Costagliola, C., Semeraro, F., 2013. Proliferative Vitreoretinopathy after eye injuries: An overexpression of growth factors and cytokines leading to a retinal keloid. Mediators Inflamm. 2013.

Mori, Keisuke, Duh, E., Gehlbach, P., Ando, A., Takahashi, K., Pearlman, J., Mori, Keiko, Yang, H.S., Zack, D.J., Ettyreddy, D., Brough, D.E., Wei, L.L., Campochiaro, P.A., 2001. Pigment epithelium-derived factor inhibits retinal and choroidal neovascularization. J. Cell. Physiol. 188, 253–263.

Moysidis, S.N., Thanos, A., Vavvas, D.G., 2012. Mechanisms of inflammation in proliferative vitreoretinopathy: From bench to bedside. Mediators Inflamm. 2012.

Mukai, R., Okunuki, Y., Husain, D., Kim, C.B., Lambris, J.D., Connor, K.M., 2018. The complement system is critical in maintaining retinal integrity during aging. Front. Aging Neurosci. 10, 1–12.

Mukherjee, S., Guidry, C., 2007. The insulin-like growth factor system modulates retinal pigment epithelial cell tractional force generation. Investig. Ophthalmol. Vis. Sci. 48, 1892–1899.

Mullins, R.F., Schoo, D.P., Sohn, E.H., Flamme-Wiese, M.J., Workamelahu, G., Johnston, R.M., Wang, K., Tucker, B.A., Stone, E.M., 2014. The membrane attack complex in aging human choriocapillaris: Relationship to macular degeneration and choroidal thinning. Am. J. Pathol. 184, 3142–3153.

Murakami, Y., Notomi, S., Hisatomi, T., Nakazawa, T., Ishibashi, T., Miller, J.W., Vavvas, D.G., 2013. Photoreceptor cell death and rescue in retinal detachment and degenerations. Prog. Retin. Eye Res. 37, 114–140.

Mysona, B.A., Matragoon, S., Stephens, M., Mohamed, I.N., Farooq, A., Bartasis, M.L., Fouda, A.Y., Shanab, A.Y., Espinosa-Heidmann, D.G., El-Remessy, A.B., 2015. Imbalance of the Nerve Growth Factor and Its Precursor as a Potential Biomarker for Diabetic Retinopathy. Biomed Res. Int. 2015, 1–12.

Nakanishi, T., Koyama, R., Ikeda, T., Shimizu, A., 2002. Catalogue of soluble proteins in the human vitreous humor: Comparison between diabetic retinopathy and macular hole. J. Chromatogr. B Anal. Technol. Biomed. Life Sci. 776, 89–100.

Nakazawa, T., Takeda, M., Lewis, G.P., Cho, K.S., Jiao, J., Wilhelmsson, U., Fisher, S.K., Pekny, M., Chen, D.F., Miller, J.W., 2007. Attenuated glial reactions and photoreceptor degeneration after retinal detachment in mice deficient in glial fibrillary acidic protein and vimentin. Investig. Ophthalmol. Vis. Sci. 48, 2760–2768.

Navaratna, D., McGuire, P.G., Menicucci, G., Das, A., 2007. Proteolytic Degradation of VE-Cadherin Alters the Blood-Retinal Barrier in Diabetes. Diabetes 56, 2380–2387.

Nawaz, I.M., Rezzola, S., Cancarini, A., Russo, A., Costagliola, C., Semeraro, F., Presta, M., 2019. Human vitreous in proliferative diabetic retinopathy: Characterization and translational implications. Prog. Retin. Eye Res. 109, 110–119.

Nebbioso, M., Federici, M., Rusciano, D., Evangelista, M., Pescosolido, N., 2012. Oxidative Stress in Preretinopathic Diabetes Subjects and Antioxidants. Diabetes Technol. Ther. 14, 257–263.

Nentwich, M.M., 2015. Diabetic retinopathy - ocular complications of diabetes mellitus. World J. Diabetes 6, 489.

Nian, S., C.Y. Lo, A., 2019. Protecting the Aging Retina, in: Neuroprotection. IntechOpen, p. 13.

Nobl, M., Reich, M., Dacheva, I., Siwy, J., Mullen, W., Schanstra, J.P., Choi, C.Y., Kopitz, J., Kretz, F.T.A., Auffarth, G.U., Koch, F., Koss, M.J., 2016. Proteomics of vitreous in neovascular age-related macular degeneration. Exp. Eye Res. 146, 107–117.

Nourinia, R., Borna, F., Rahimi, A., Bonyadi, M.H.J., Amizadeh, Y., Daneshtalab, A., Kheiri, B., Ahmadieh, H., 2019. Repeated injection of methotrexate into silicone oil-filled eyes for grade c proliferative vitreoretinopathy: A pilot study. Ophthalmologica 242, 113–117.

Ortiz, G., Salica, J.P., Chuluyan, E.H., Gallo, J.E., 2014. Diabetic retinopathy: Could the alpha-1 antitrypsin be a therapeutic option? Biol. Res. 47, 1–9.

Osborne, N.N., Chidlow, G., Wood, J.P.M., Schmidt, K.-G., Casson, R., Melena, J., 2001. Expectations in the treatment of retinal diseases: Neuroprotection. Curr. Eye Res. 22, 321–332.

Park, K., Jin, J., Hu, Y., Zhou, K., Ma, J.X., 2011. Overexpression of pigment epithelium-derived factor inhibits retinal inflammation and neovascularization. Am. J. Pathol. 178, 688–698.

Pastor, J.C., Rojas, J., Pastor-Idoate, S., Di Lauro, S., Gonzalez-Buendia, L., Delgado-Tirado, S., 2016. Proliferative vitreoretinopathy: A new concept of disease pathogenesis and practical consequences. Prog. Retin. Eye Res. 51, 125–155.

Patel, J.I., Tombran-Tink, J., Hykin, P.G., Gregor, Z.J., Cree, I.A., 2006. Vitreous and aqueous concentrations of proangiogenic, antiangiogenic factors and other cytokines in diabetic retinopathy patients with macular edema: Implications for structural differences in macular profiles. Exp. Eye Res. 82, 798–806.

Paulus, Y.M., Campbell, J.P., 2015. Neuroprotection and retinal diseases. Dev. Ophthalmol. 55, 322–329.

Pennock, S., Haddock, L.J., Mukai, S., Kazlauskas, A., 2014. Vascular endothelial growth factor acts primarily via platelet-derived growth factor receptor α to promote proliferative vitreoretinopathy. Am. J. Pathol. 184, 3052–3068.

Pennock, S., Kim, D., Mukai, S., Kuhnle, M., Chun, D.W., Matsubara, J., Cui, J., Ma, P., Maberley, D., Samad, A., Van Geest, R.J., Oberstein, S.L., Schlingemann, R.O., Kazlauskas, A., 2013. Ranibizumab Is a Potential Prophylaxis for Proliferative Vitreoretinopathy, a Nonangiogenic Blinding Disease. Am. J. Pathol. 182, 1659–1670.

Pennock, S., Rheaume, M.A., Mukai, S., Kazlauskas, A., 2011. A novel strategy to develop therapeutic approaches to prevent Proliferative vitreoretinopathy. Am. J. Pathol. 179, 2931–2940.

Pinazo-Durán, M.D., Gallego-Pinazo, R., García-Medina, J.J., Zanón-Moreno, V., Nucci, C., Dolz-Marco, R., Martínez-Castillo, S., Galbis-Estrada, C., Marco-Ramírez, C., López-Gálvez, M.I., Galarreta, D.J., Díaz-Llópis, M., 2014. Oxidative stress and its downstream signaling in aging eyes. Clin. Interv. Aging 9, 637–652.

Ponnalagu, M., Subramani, M., Jayadev, C., Shetty, R., Das, D., 2017. Retinal pigment epithelium-secretome: A diabetic retinopathy perspective. Cytokine 95, 126–135.

Ponsioen, T.L., Hooymans, J.M.M., Los, L.I., 2010. Remodelling of the human vitreous and vitreoretinal interface - A dynamic process. Prog. Retin. Eye Res. 29, 580–595.

Pulley, J.M., Rhoads, J.P., Jerome, R.N., Challa, A.P., Erreger, K.B., Joly, M.M., Lavieri, R.R., Perry, K.E., Zaleski, N.M., Shirey-Rice, J.K., Aronoff, D.M., 2020. Using What We Already Have: Uncovering New Drug Repurposing Strategies in Existing Omics Data. Annu. Rev. Pharmacol. Toxicol. 60, annurev-pharmtox-010919-023537.

Qazi, Y., Maddula, S., Ambati, B.K., 2009. Mediators of ocular angiogenesis. J. Genet. 88, 495–515.

Ramke, J., Gilbert, C.E., 2017. Universal eye health: are we getting closer? Lancet Glob. Heal. 5:e843–e844.

Rangasamy, S., McGuire, P.G., Nitta, C.F., Monickaraj, F., Oruganti, S.R., Das, A., 2014. Chemokine mediated monocyte trafficking into the retina: Role of inflammation in alteration of the blood-retinal barrier in diabetic retinopathy. PLoS One 9, 1–10.

Rashid, K., Akhtar-Schaefer, I., Langmann, T., 2019. Microglia in retinal degeneration. Front. Immunol. 10, 1–19.

Rashid, K., Wolf, A., Langmann, T., 2018. Microglia Activation and Immunomodulatory Therapies for Retinal Degenerations. Front. Cell. Neurosci. 12, 1–8.

Ratnayaka, J.A., Serpell, L.C., Lotery, A.J., 2015. Dementia of the eye: the role of amyloid beta in retinal degeneration. Eye 29, 1013–1026.

Reibaldi, M., Russo, A., Longo, A., Bonfiglio, V., Uva, M.G., Gagliano, C., Toro, M.D., Avitabile, T., 2013. Rhegmatogenous retinal detachment with a high risk of proliferative vitreoretinopathy treated with episcleral surgery and an intravitreal dexamethasone 0.7-mg implant. Case Rep. Ophthalmol. 4, 79–83.

Reverter, J.L., Nadal, J., Fernández-Novell, J.M., Ballester, J., Ramió-Lluch, L., Rivera, M.M., Elizalde, J., Abengoechea, S., Guinovart, J.J., Rodríguez-Gil, J.E., 2009. Tyrosine phosphorylation of vitreous inflammatory and angiogenic peptides and proteins in diabetic retinopathy. Investig. Ophthalmol. Vis. Sci. 50, 1378–1382.

Richer, S., Ulanski, L., Popenko, N.A., Pratt, S.G., Hitchmoth, D., Chous, P., Patel, S., Sockanathan, S., Sardi, B., 2016. Age-related Macular Degeneration Beyond the Age-related Eye Disease Study II. Adv. Ophthalmol. Optom. 1, 335–369.

Ricker, L.J.A.G., Dieudonné, S.C., Kessels, A.G.H., Rennel, E.S., Berendschot, T.T.J.M., Hendrikse, F., Kijlstra, A., La Heij, E.C., 2012. Antiangiogenic isoforms of vascular endothelial growth factor predominate in subretinal fluid of patients with rhegmatogenous retinal detachment and proliferative vitreoretinopathy. Retina 32, 54–59.

Rivera, J.C., Dabouz, R., Noueihed, B., Omri, S., Tahiri, H., Chemtob, S., 2017. Ischemic retinopathies: Oxidative stress and inflammation. Oxid. Med. Cell. Longev. 2017.

Robbins, S.G., Mixon, R.N., Wilson, D.J., Hart, C.E., Robertson, J.E., Westra, I., Planck, S.R., Rosenbaum, J.T., 1994. Platelet-derived growth factor ligands and receptors immunolocalized in proliferative retinal diseases. Investig. Ophthalmol. Vis. Sci. 35, 3649–3663.

Rocha, A.S., Santos, F.M., Monteiro, J.P., Castro-de-Sousa, J.P., Queiroz, J.A., Tomaz, C.T., Passarinha, L.A., 2014. Trends in proteomic analysis of human vitreous humor samples. Electrophoresis 35, 2495–2508.

Rodrigues, M., Xin, X., Jee, K., Babapoor-Farrokhran, S., Kashiwabuchi, F., Ma, T., Bhutto, I., Hassan, S.J., Daoud, Y., Baranano, D., Solomon, S., Lutty, G., Semenza, G.L., Montaner, S., Sodhi, A., 2013. VEGF secreted by hypoxic Müller cells induces MMP-2 expression and activity in endothelial cells to promote retinal neovascularization in proliferative diabetic retinopathy. Diabetes 62, 3863–3873.

Rodríguez De La Rúa, E., Pastor, J.C., Aragón, J., Mayo-Iscar, A., Martínez, V., García-Arumí, J., Giraldo, A., Sanabria-Ruiz Colmenares, M.R., Miranda, I., 2005. Interaction between surgical procedure for repairing retinal detachment and clinical risk factors for proliferative vitreoretinopathy. Curr. Eye Res. 30, 147–153.

Romero-Aroca, P., Reyes-Torres, J., Baget-Bernaldiz, M., Blasco-Sune, C., 2014. Laser Treatment for Diabetic Macular Edema in the 21st Century. Curr. Diabetes Rev. 10, 100–112.

Rosenfeld, P.J., Brown, D.M., Heier, J.S., Boyer, D.S., Kaiser, P.K., Chung, C.Y., Kim, R.Y., 2006. Ranibizumab for Neovascular Age-Related Macular Degeneration. N. Engl. J. Med. 355, 1419–1431.

Roybal, C.N., Velez, G., Toral, M.A., Tsang, S.H., Bassuk, A.G., Mahajan, V.B., 2018. Personalized Proteomics in Proliferative Vitreoretinopathy Implicate Hematopoietic Cell Recruitment and mTOR as a Therapeutic Target. Am. J. Ophthalmol. 186, 152–163.

Rübsam, A., Parikh, S., Fort, P.E., 2018. Role of inflammation in diabetic retinopathy. Int. J. Mol. Sci. 19, 1–31.

Rudnicka, A.R., Jarrar, Z., Wormald, R., Cook, D.G., Fletcher, A., Owen, C.G., 2012. Age and gender variations in age-related macular degeneration prevalence in populations of European ancestry: A meta-analysis. Ophthalmology 119, 571–580.

Rutar, M., Valter, K., Natoli, R., Provis, J.M., 2014. Synthesis and propagation of complement C3 by microglia/monocytes in the aging retina. PLoS One 9.

Saaddine, J.B., Honeycutt, A.A., Narayan, K.M.V., Zhang, X., Klein, R., Boyle, J.P., 2008. Projection of diabetic retinopathy and other major eye diseases among people with diabetes mellitus: United States, 2005-2050. Arch. Ophthalmol. (Chicago, Ill. 1960) 126, 1740–7.

Sabanayagam, C., Cheng, C.-Y., 2017. Global causes of vision loss in 2015: are we on track to achieve the Vision 2020 target? Lancet Glob. Heal. 5, e1164–e1165.

Saccà, S.C., Roszkowska, A.M., Izzotti, A., 2013. Environmental light and endogenous antioxidants as the main determinants of non-cancer ocular diseases. Mutat. Res. - Rev. Mutat. Res. 752, 153–171.

Saika, S., 2006. TGFβ pathobiology in the eye. Lab. Investig. 86, 106–115.

Salzmann, J., Limb, G.A., Khaw, P.T., Gregor, Z.J., Webster, L., Chignell, A.H., Charteris, D.G., 2000. Matrix metalloproteinases and their natural inhibitors in fibrovascular membranes of proliferative diabetic retinopathy. Br. J. Ophthalmol. 84, 1091–1096.

SanGiovanni, J.P., 2008. The Relationship of Dietary ω-3 Long-Chain Polyunsaturated Fatty Acid Intake With Incident Age-Related Macular Degeneration. Arch. Ophthalmol. 126, 1274.

Santiago, A.R., Boia, R., Aires, I.D., Ambrósio, A.F., Fernandes, R., 2018. Sweet Stress: Coping With Vascular Dysfunction in Diabetic Retinopathy. Front. Physiol 9, 820.

Santos, A.R., Ribeiro, L., Bandello, F., Lattanzio, R., Egan, C., Frydkjaer-Olsen, U., García-Arumí, J., Gibson, J., Grauslund, J., Harding, S.P., Lang, G.E., Massin, P., Midena, E., Scanlon, P., Aldington, S.J., Simão, S., Schwartz, C., Ponsati, B., Porta, M., Costa, M.A., Hernández, C., Cunha-Vaz, J., Simó, R., 2017. Functional and structural findings of neurodegeneration in early stages of diabetic retinopathy: Cross-sectional analyses of baseline data of the EUROCONDOR project. Diabetes 66, 2503–2510.

Santos, F.M., Albuquerque, T., Gaspar, L.M., Dias, J.M.L., Castro e Sousa, J.P., Paradela, A., Tomaz, C.T., Passarinha, L.A., 2019. Refinement of two-dimensional electrophoresis for vitreous proteome profiling using an artificial neural network. Anal. Bioanal. Chem. 411, 5115–5126.

Santos, F.M., Gaspar, L.M., Ciordia, S., Rocha, A.S., Castro e Sousa, J., Paradela, A., Passarinha, L.A., Tomaz, C.T., 2018. iTRAQ Quantitative Proteomic Analysis of Vitreous from Patients with Retinal Detachment. Int. J. Mol. Sci. 19, 1157.

Sapieha, P., Hamel, D., Shao, Z., Rivera, J.C., Zaniolo, K., Joyal, J.S., Chemtob, S., 2010. Proliferative retinopathies: Angiogenesis that blinds. Int. J. Biochem. Cell Biol. 42, 5–12.

Sato, K., Takeda, A., Hasegawa, E., Jo, Y.J., Arima, M., Oshima, Y., Ryoji, Y., Nakazawa, T., Yuzawa, M., Nakashizuka, H., Shimada, H., Kimura, K., Ishibashi, T., Sonoda, K.H., 2018. Interleukin-6 plays a crucial role in the development of subretinal fibrosis in a mouse model. Immunol. Med. 41, 23–29.

Schaub, F., Hoerster, R., Schiller, P., Felsch, M., Kraus, D., Zarrouk, M., Kirchhof, B., Fauser, S., 2018. Prophylactic intravitreal 5-fluorouracil and heparin to prevent proliferative vitreoretinopathy in high-risk patients with retinal detachment: study protocol for a randomized controlled trial. Trials 19, 384.

Schmidt, J.C., Mennel, S., Meyer, C.H., Kroll, P., 2008. Posterior Vitreomacular Adhesion: A Potential Risk Factor for Exudative Age-related Macular Degeneration. Am. J. Ophthalmol. 145, 1107.

Schmidt, K.-G., Bergert, H., Funk, R., 2008. Neurodegenerative Diseases of the Retina and Potential for Protection and Recovery. Curr. Neuropharmacol. 6, 164–178.

Schori, C., Trachsel, C., Grossmann, J., Zygoula, I., Barthelmes, D., Grimm, C., 2018. The Proteomic Landscape in the Vitreous of Patients With Age-Related and Diabetic Retinal Disease. Invest. Ophthalmol. Vis. Sci. 59, AMD31–AMD40.

Sebag, J., 2010. Vitreous Anatomy, Aging, and Anomalous Posterior Vitreous Detachment, in: Encyclopedia of the Eye. Elsevier, pp. 307–315.

Sebag, J., 2009. Vitreous: The resplendent enigma. Br. J. Ophthalmol. 93, 989–991.

Seddon, J.M., 2006. Cigarette Smoking, Fish Consumption, Omega-3 Fatty Acid Intake, and Associations With Age-Related Macular Degeneration. Arch. Ophthalmol. 124, 995.

Semba, R.D., Enghild, J.J., Venkatraman, V., Dyrlund, T.F., Van Eyk, J.E., 2013. The Human Eye Proteome Project: Perspectives on an emerging proteome. Proteomics 13, 2500–2511.

Semenza, G.L., 2001. Hypoxia-inducible factor 1: Control of oxygen homeostasis in health and disease. Pediatr. Res. 49, 614–617.

Sethi, C.S., Lewis, G.P., Fisher, S.K., Leitner, W.P., Mann, D.L., Luthert, P.J., Charteris, D.G., 2005. Glial remodeling and neural plasticity in human retinal detachment with proliferative vitreoretinopathy. Investig. Ophthalmol. Vis. Sci. 46, 329–342.

Shahulhameed, S., Vishwakarma, S., Chhablani, J., Tyagi, M., Pappuru, R.R., Jakati, S., Chakrabarti, S., Kaur, I., 2020. A Systematic Investigation on Complement Pathway Activation in Diabetic Retinopathy. Front. Immunol. 11, 1–14.

Sharma, T., Fong, A., Lai, T.Y., Lee, V., Das, S., Lam, D., 2016. Surgical treatment for diabetic vitreoretinal diseases: a review. Clin. Exp. Ophthalmol. 44, 340–354.

Shitama, T., Hayashi, H., Noge, S., Uchio, E., Oshima, K., Haniu, H., Takemori, N., Komori, N., Matsumoto, H., 2008. Proteome profiling of vitreoretinal diseases by cluster analysis. Proteomics - Clin. Appl. 2, 1265–1280.

Simó-Servat, O., Hernández, C., Simó, R., 2012. Usefulness of the Vitreous Fluid Analysis in the Translational Research of Diabetic Retinopathy. Mediators Inflamm. 2012, 1–11.

Simó, R., Higuera, M., García-Ramírez, M., Canals, F., García-Arumí, J., Hernández, C., 2008. Elevation of apolipoprotein A-I and apolipoprotein H levels in the vitreous fluid and overexpression in the retina of diabetic patients. Arch. Ophthalmol. 126, 1076–1081.

Simó, R., Lecube, A., Segura, R.M., García Arumí, J., Hernández, C., 2002. Free insulin growth factor-I and vascular endothelial growth factor in the vitreous fluid of patients with proliferative diabetic retinopathy. Am. J. Ophthalmol. 134, 376–82.

Simó, R., Stitt, A.W., Gardner, T.W., 2018. Neurodegeneration in diabetic retinopathy: does it really matter? Diabetologia 61, 1902–1912.

Singh, M., Tyagi, S.C., 2017. Metalloproteinases as mediators of inflammation and the eyes: Molecular genetic underpinnings governing ocular pathophysiology. Int. J. Ophthalmol. 10, 1308–1318.

Sinha, D., Valapala, M., Shang, P., Hose, S., Grebe, R., Lutty, G.A., Zigler, J.S., Kaarniranta, K., Handa, J.T., 2016. Lysosomes: Regulators of autophagy in the retinal pigmented epithelium. Exp. Eye Res. 144, 46–53.

Skei, J.M., Fingert, J.H., Russell, S.R., Stone, E.M., Mullins, R.F., 2010. Complement component C5a activates ICAM-1expression on human choroidal endothelial cells. Investig. Ophthalmol. Vis. Sci. 51, 5336–5342.

Skeie, J.M., Roybal, C.N., Mahajan, V.B., 2015. Proteomic insight into the molecular function of the vitreous. PLoS One 10, 1–19.

Slakter, J.S., Bochow, T., D'Amico, D.J., Marks, B., Jerdan, J., Sullivan, E.K., 2006. Anecortave acetate (15 milligrams) versus photodynamic therapy for treatment of subfoveal neovascularization in age-related macular degeneration. Ophthalmology 113, 3–13.

Sonoda, T., Sugahara, K.-H., Mochizuki, M., Enaida, Y., 2009. Comprehensive Analysis of Inflammatory Immune Mediators in Vitreoretinal Diseases. PLoS One 4, 8158.

Sorokin, L., 2010. The impact of the extracellular matrix on inflammation. Nat. Rev. Immunol. 10, 712–723.

Sottile, J., 2004. Regulation of angiogenesis by extracellular matrix. Biochim. Biophys. Acta - Rev. Cancer 1654, 13–22.

Spooren, A., Kolmus, K., Laureys, G., Clinckers, R., De Keyser, J., Haegeman, G., Gerlo, S., 2011. Interleukin-6, a mental cytokine. Brain Res. Rev. 67, 157–183.

Srividya, G., Jain, M., Mahalakshmi, K., Gayathri, S., Raman, R., Angayarkanni, N., 2018. A novel and less invasive technique to assess cytokine profile of vitreous in patients of diabetic macular oedema. Eye 32, 820–829.

Stitt, A.W., 2001. Advanced glycation: An important pathological event in diabetic and age related ocular disease. Br. J. Ophthalmol. 85, 746–753.

Stitt, A.W., Curtis, T.M., Chen, M., Medina, R.J., McKay, G.J., Jenkins, A., Gardiner, T.A., Lyons, T.J., Hammes, H.P., Simó, R., Lois, N., 2016. The progress in understanding and treatment of diabetic retinopathy. Prog. Retin. Eye Res. 51, 156–186.

Strauss, O., 2005. The Retinal Pigment Epithelium in Visual Function. Physiol. Rev. 85, 845–881.

Subramanyam, M., Goyal, J., 2016. Translational biomarkers: from discovery and development to clinical practice. Drug Discov. Today Technol. 21–22, 3–10.

Supuran, C.T., 2019. Agents for the prevention and treatment of age-related macular degeneration and macular edema: a literature and patent review. Expert Opin. Ther. Pat. 29, 761–767.

Suzuki, M., Tsujikawa, M., Itabe, H., Du, Z.J., Xie, P., Matsumura, N., Fu, X., Zhang, R., Sonoda, K.H., Egashira, K., Hazen, S.L., Kamei, M., 2012. Chronic photo-oxidative stress and subsequent MCP-1 activation as causative factors for age-related macular degeneration. J. Cell Sci. 125, 2407–2415.

Suzuki, Y., Nakazawa, M., Suzuki, K., Yamazaki, H., Miyagawa, Y., 2011. Expression profiles of cytokines and chemokines in vitreous fluid in diabetic retinopathy and central retinal vein occlusion. Jpn. J. Ophthalmol. 55, 256–263.

Sweigard, J.H., Matsumoto, H., Smith, K.E., Kim, L.A., Paschalis, E.I., Okonuki, Y., Castillejos, A., Kataoka, K., Hasegawa, E., Yanai, R., Husain, D., Lambris, J.D., Vavvas, D., Miller, J.W., Connor, K.M., 2015. Inhibition of the alternative complement pathway preserves photoreceptors after retinal injury. Sci. Transl. Med. 7, 21–24.

Sydorova, M., Lee, M.S., 2005. Vascular endothelial growth factor levels in vitreous and serum of patients with either proliferative diabetic retinopathy or proliferative vitreoretinopathy. Ophthalmic Res. 37, 188–190.

Symeonidis, C., Diza, E., Papakonstantinou, E., Souliou, E., Dimitrakos, S.A., Karakiulakis, G., 2007. Correlation of the Extent and Duration of Rhegmatogenous Retinal Detachment With the Expression of Matrix Metalloproteinases in the Vitreous. Retina 27, 1279–1285.

Symeonidis, C., Papakonstantinou, E., Androudi, S., Rotsos, T., Diza, E., Brazitikos, P., Karakiulakis, G., Dimitrakos, S.A., 2011a. Interleukin-6 and the matrix metalloproteinase response in the vitreous during proliferative vitreoretinopathy. Cytokine 54, 212–217.

Symeonidis, C., Papakonstantinou, E., Souliou, E., Karakiulakis, G., Dimitrakos, S.A., Diza, E., 2011b. Correlation of matrix metalloproteinase levels with the grade of proliferative vitreoretinopathy in the subretinal fluid and vitreous during rhegmatogenous retinal detachment. Acta Ophthalmol. 89, 339–345.

Szklarczyk, D., Gable, A.L., Lyon, D., Junge, A., Wyder, S., Huerta-Cepas, J., Simonovic, M., Doncheva, N.T., Morris, J.H., Bork, P., Jensen, L.J., Von Mering, C., 2019. STRING v11: Protein-protein association networks with increased coverage, supporting functional discovery in genome-wide experimental datasets. Nucleic Acids Res. 47, D607–D613.

Tamiya, S., Liu, L.H., Kaplan, H.J., 2010. Epithelial-mesenchymal transition and proliferation of retinal pigment epithelial cells initiated upon loss of cell-cell contact. Investig. Ophthalmol. Vis. Sci. 51, 2755–2763.

Tang, J., Kern, T.S., 2011. Inflammation in diabetic retinopathy. Prog. Retin. Eye Res. 30, 343–358.

Taylor, A.W., 2009. Ocular immune privilege. Eye 23, 1885–1889.

Ting, D.S.W., Cheung, G.C.M., Wong, T.Y., 2016. Diabetic retinopathy: global prevalence, major risk factors, screening practices and public health challenges: a review. Clin. Exp. Ophthalmol. 44, 260–277.

Tong, Y., Zhou, Y.L., Wang, Y.X., Zhao, P.Q., Wang, Z.Y., 2016. Retinal pigment epithelium cell-derived exosomes: Possible relevance to CNV in wet-age related macular degeneration. Med. Hypotheses 97, 98–101.

Toomey, C.B., Johnson, L. V., Bowes Rickman, C., 2018. Complement factor H in AMD: Bridging genetic associations and pathobiology. Prog. Retin. Eye Res. 62, 38–57.

Tosi, G.M., Neri, G., Caldi, E., Fusco, F., Bacci, T., Tarantello, A., Nuti, E., Marigliani, D., Baiocchi, S., Traversi, C., Barbarino, M., Eandi, C.M., Parolini, B., Mundo, L., Santucci, A., Orlandini, M., Galvagni, F., 2018a. TGF-β concentrations and activity are down-regulated in the aqueous humor of patients with neovascular age-related macular degeneration. Sci. Rep. 8, 1–9.

Tosi, G.M., Orlandini, M., Galvagni, F., 2018b. The Controversial Role of TGF-β in Neovascular Age-Related Macular Degeneration Pathogenesis. Int. J. Mol. Sci. 19, 1–16.

Tsai, T., Kuehn, S., Tsiampalis, N., Vu, M.-K., Kakkassery, V., Stute, G., Dick, H.B., Joachim, S.C., 2018. Anti-inflammatory cytokine and angiogenic factors levels in vitreous samples of diabetic retinopathy patients. PLoS One 13, e0194603.

Tsutsumi, C., Sonoda, K., Egashira, K., Qiao, H., Hisatomi, T., Nakao, S., Ishibashi, M., Charo, I.F., Sakamoto, T., Murata, T., Ishibashi, T., 2003. The critical role of ocular-infiltrating macrophages in the development of choroidal neovascularization. J. Leukoc. Biol. 74, 25–32.

Vadlapatla, R.K., Vadlapudi, A.D., Mitra, A.K., 2013. Hypoxia-inducible factor-1 (HIF-1): a potential target for intervention in ocular neovascular diseases. Curr. Drug Targets 14, 919–935.

Van Geest, R.J., Klaassen, I., Lesnik-Oberstein, S.Y., Tan, H.S., Mura, M., Goldschmeding, R., Van Noorden, C.J.F., Schlingemann, R.O., 2013. Vitreous TIMP-1 levels associate with neovascularization and TGF-β2 levels but not with fibrosis in the clinical course of proliferative diabetic retinopathy. J. Cell Commun. Signal. 7, 1–9.

Van Geest, R.J., Lesnik-Oberstein, S.Y., Tan, H.S., Mura, M., Goldschmeding, R., Van Noorden, C.J.F., Klaassen, I., Schlingemann, R.O., 2012. A shift in the balance of vascular endothelial growth factor and connective tissue growth factor by bevacizumab causes the angiofibrotic switch in proliferative diabetic retinopathy. Br. J. Ophthalmol. 96, 587–590.

van Karnebeek, C.D.M., Wortmann, S.B., Tarailo-Graovac, M., Langeveld, M., Ferreira, C.R., van de Kamp, J.M., Hollak, C.E., Wasserman, W.W., Waterham, H.R., Wevers, R.A., Haack, T.B., Wanders, R.J.A., Boycott, K.M., 2018. The role of the clinician in the multi-omics era: are you ready? J. Inherit. Metab. Dis. 41, 571–582.

Vaughan-Thomas, A., Gilbert, S.J., Duance, V.C., 2000. Elevated levels of proteolytic enzymes in the aging human vitreous. Investig. Ophthalmol. Vis. Sci. 41, 3299–3304.

Velez, G., Tang, P.H., Cabral, T., Cho, G.Y., Machlab, D.A., Tsang, S.H., Bassuk, A.G., Mahajan, V.B., 2018. Personalized Proteomics for Precision Health: Identifying Biomarkers of Vitreoretinal Disease. Transl. Vis. Sci. Technol. 7, 12.

Verardo, M.R., Lewis, G.P., Takeda, M., Linberg, K.A., Byun, J., Luna, G., Wilhelmsson, U., Pekny, M., Chen, D.F., Fisher, S.K., 2008. Abnormal reactivity of Müller cells after retinal detachment in mice deficient in GFAP and vimentin. Investig. Ophthalmol. Vis. Sci. 49, 3659–3665.

Vinores, S.A., Xiao, W.-H., Shen, J., Campochiaro, P.A., 2007. TNF-α is critical for ischemia-induced leukostasis, but not retinal neovascularization nor VEGF-induced leakage. J. Neuroimmunol. 182, 73–79.

Vizin, T., Kos, J., 2015. Gamma-enolase: A well-known tumour marker, with a less-known role in cancer. Radiol. Oncol. 49, 217–226.

Walia, S., Clermont, A.C., Gao, B.-B.B., Aiello, L.P., Feener, E.P., 2010. Vitreous proteomics and diabetic retinopathy. Semin. Ophthalmol. 25, 289–294.

Wang, A.L., Lukas, T.J., Yuan, M., Du, N., Tso, M.O., Neufeld, A.H., 2009. Autophagy and Exosomes in the Aged Retinal Pigment Epithelium: Possible Relevance to Drusen Formation and Age-Related Macular Degeneration. PLoS One 4, e4160.

Wang, H., Feng, L., Hu, J., Xie, C., Wang, F., 2013. Differentiating vitreous proteomes in proliferative diabetic retinopathy using high-performance liquid chromatography coupled to tandem mass spectrometry. Exp. Eye Res. 108, 110–119.

Wang, H., Feng, L., Hu, J.W., Xie, C.L., Wang, F., 2012. Characterisation of the vitreous proteome in proliferative diabetic retinopathy. Proteome Sci. 10, 1–11.

Wang, J., Chen, S., Jiang, F., You, C., Mao, C., Yu, J., Han, J., Zhang, Z., Yan, H., 2014. Vitreous and plasma VEGF levels as predictive factors in the progression of proliferative diabetic retinopathy after vitrectomy. PLoS One 9, 1–8.

Wang, K., Li, H., Sun, R., Liu, C., Luo, Y., Fu, S., Ying, Y., 2018. Emerging roles of transforming growth factor β signaling in wet age-related macular degeneration. Acta Biochim. Biophys. Sin. (Shanghai). 51, 1–8.

Wang, S., Park, J.K., Duh, E.J., 2012. Novel targets against retinal angiogenesis in diabetic retinopathy. Curr. Diab. Rep. 12, 355–363.

Wang, W., Lo, A.C.Y., 2018. Diabetic retinopathy: Pathophysiology and treatments. Int. J. Mol. Sci. 19.

Wang, X., Ma, W., Han, S., Meng, Z., Zhao, L., Yin, Y., Wang, Y., Li, J., 2017. TGF-β participates choroid neovascularization through Smad2/3-VEGF/TNF-α signaling in mice with Laser-induced wet age-related macular degeneration. Sci. Rep. 7, 1–13.

Wei, Q., Zhang, T., Jiang, R., Chang, Q., Zhang, Y., Huang, X., Gao, X., Jin, H., Xu, G., 2017. Vitreous fibronectin and fibrinogen expression increased in eyes with proliferative diabetic retinopathy after intravitreal anti-VEGF therapy. Investig. Ophthalmol. Vis. Sci. 58, 5783–5791.

Whitcup, S.M., Sodhi, A., Atkinson, J.P., Holers, V.M., Sinha, D., Rohrer, B., Dick, A.D., 2013. The role of the immune response in age-related macular degeneration. Int. J. Inflam. 2013.

Whitmore, S.S., Sohn, E.H., Chirco, K.R., Drack, A. V., Stone, E.M., Tucker, B.A., Mullins, R.F., 2015. Complement activation and choriocapillaris loss in early AMD: Implications for pathophysiology and therapy. Prog. Retin. Eye Res. 45, 1–29.

Wiedemann, P., 1992. Growth factors in retinal diseases: Proliferative vitreoretinopathy, proliferative diabetic retinopathy, and retinal degeneration. Surv. Ophthalmol. 36, 373–384.

Wiedemann, P., Yandiev, Y., Hui, Y.-N., Wang, Y., 2013. Pathogenesis of Proliferative Vitreoretinopathy, in: Ryan, S.J., Hinton, D.R., Wiedemann, P. (Eds.), Retina. Elsevier, pp. 1640–1646.

Witmer, A.N., Vrensen, G.F.J.M., Van Noorden, C.J.F., Schlingemann, R.O., 2003. Vascular endothelial growth factors and angiogenesis in eye disease. Prog. Retin. Eye Res. 22, 1–29.

Wladis, E.J., Falk, N.S., Iglesias, B. V., Beer, P.M., Gosselin, E.J., 2013. Analysis of the molecular biologic milieu of the vitreous in proliferative vitreoretinopathy. Retina 33, 807–811.

Wong, T.Y., Cheung, C.M.G., Larsen, M., Sharma, S., Simó, R., 2016. Diabetic retinopathy. Nat. Rev. Dis. Prim. 2, 16012.

Wong, W.L., Su, X., Li, X., Cheung, C.M.G., Klein, R., Cheng, C.Y., Wong, T.Y., 2014. Global prevalence of age-related macular degeneration and disease burden projection for 2020 and 2040: A systematic review and meta-analysis. Lancet Glob. Heal. 2, e106–e116.

Wooff, Y., Man, S.M., Aggio-Bruce, R., Natoli, R., Fernando, N., 2019. IL-1 family members mediate cell death, inflammation and angiogenesis in retinal degenerative diseases. Front. Immunol. 10, 1–21.

World Health Organization, 2019. World report on vision, World health Organization.

Wormald, R, Evans, J., Smeeth, L., Henshaw, K., 2005. Photodynamic therapy for neovascular age-related macular degeneration, in: Wormald, Richard (Ed.), Cochrane Database of Systematic Reviews. John Wiley & Sons, Ltd, Chichester, UK, pp. 61–67.

Wu, Z., Ding, N., Yu, M., Wang, K., Luo, S., Zou, W., Zhou, Y., Yan, B., Jiang, Q., 2016. Identification of potential biomarkers for rhegmatogenous retinal detachment associated with choroidal detachment by vitreous iTRAQ-based proteomic profiling. Int. J. Mol. Sci. 17.

Wynn, T. a, 2007. Common and unique mechanisms regulate fibrosis in various fibroproliferative diseases. J. Clin. Invest. 117, 524–529.

X. Shaw, P., Stiles, T., Douglas, C., Ho, D., Fan, W., Du, H., Xiao, X., 2016. Oxidative stress, innate immunity, and age-related macular degeneration. AIMS Mol. Sci. 3, 196–221.

Xu, J., Chen, L.J., Yu, J., Wang, H.J., Zhang, F., Liu, Q., Wu, J., 2018. Involvement of Advanced Glycation End Products in the Pathogenesis of Diabetic Retinopathy. Cell. Physiol. Biochem. 48, 705–717.

Yamane, K., Minamoto, A., Yamashita, H., Takamura, H., Miyamoto-Myoken, Y., Yoshizato, K., Nabetani, T., Tsugita, A., Mishima, H.K., 2003. Proteome Analysis of Human Vitreous Proteins. Mol. Cell. Proteomics 2, 1177–1187.

Yang, I.H., Lee, J.J., Wu, P.C., Kuo, H.K., Kuo, Y.H., Huang, H.M., 2020. Oxidative stress enhanced the transforming growth factor-β2-induced epithelial-mesenchymal transition through chemokine ligand 1 on ARPE-19 cell. Sci. Rep. 10, 1–10.

Yang, M.M., Wang, J., Ren, H., Sun, Y.D., Fan, J.J., Teng, Y., Li, Y.B., 2016. Genetic Investigation of Complement Pathway Genes in Type 2 Diabetic Retinopathy: An Inflammatory Perspective. Mediators Inflamm. 2016.

Yau, J.W.Y., Rogers, S.L., Kawasaki, R., Lamoureux, E.L., Kowalski, J.W., Bek, T., Chen, S.J., Dekker, J.M., Fletcher, A., Grauslund, J., Haffner, S., Hamman, R.F., Ikram, M.K., Kayama, T., Klein, B.E.K., Klein, R., Krishnaiah, S., Mayurasakorn, K., O'Hare, J.P., Orchard, T.J., Porta, M., Rema, M., Roy, M.S., Sharma, T., Shaw, J., Taylor, H., Tielsch, J.M., Varma, R., Wang, J.J., Wang, N., West, S., Zu, L., Yasuda, M., Zhang, X., Mitchell, P., Wong, T.Y., 2012. Global prevalence and major risk factors of diabetic retinopathy. Diabetes Care 35, 556–564.

Yonekawa, Y., Miller, J., Kim, I., 2015. Age-Related Macular Degeneration: Advances in Management and Diagnosis. J. Clin. Med. 4, 343–359.

Yoshida, S., Nakama, T., Ishikawa, K., Nakao, S., Sonoda, K., Ishibashi, T., 2017. Periostin in vitreoretinal diseases. Cell. Mol. Life Sci. 74, 4329–4337.

Yu, B., Egbejimi, A., Dharmat, R., Xu, P., Zhao, Z., Long, B., Miao, H., Chen, R., Wensel, T.G., Cai, J., Chen, Y., 2018. Phagocytosed photoreceptor outer segments activate mTORC1 in the retinal pigment epithelium. Sci. Signal. 11, eaag3315.

Yu, J., Liu, F., Cui, S.J., Liu, Y., Song, Z.Y., Cao, H., Chen, F.E., Wang, W.J., Sun, T., Wang, F., 2008. Vitreous proteomic analysis of proliferative vitreoretinopathy. Proteomics 8, 3667–3678.

Yu, J., Peng, R., Chen, H., Cui, C., Ba, J., 2012. Elucidation of the pathogenic mechanism of rhegmatogenous retinal detachment with proliferative vitreoretinopathy by proteomic analysis. Investig. Ophthalmol. Vis. Sci. 53, 8146–8153.

Yu, J., Peng, R., Chen, H., Cui, C., Ba, J., Wang, F., 2014. Kininogen 1 and insulin-like growth factor binding protein 6: Candidate serum biomarkers of proliferative vitreoretinopathy. Clin. Exp. Optom. 97, 72–79.

Zafar, S., Sachdeva, M., Frankfort, B.J., Channa, R., 2019. Retinal Neurodegeneration as an Early Manifestation of Diabetic Eye Disease and Potential Neuroprotective Therapies. Curr. Diab. Rep. 19.

Zhang, H., Liu, Z.L., 2012. Transforming growth factor-β neutralizing antibodies inhibit subretinal fibrosis in a mouse model. Int. J. Ophthalmol. 5, 307–311.

Zhang, M., Jiang, N., Chu, Y., Postnikova, O., Varghese, R., Horvath, A., Cheema, A.K., Golestaneh, N., 2020. Dysregulated metabolic pathways in age-related macular degeneration. Sci. Rep. 10, 1–14.

Zhao, C., Yasumura, D., Li, X., Matthes, M., Lloyd, M., Nielsen, G., Ahern, K., Snyder, M., Bok, D., Dunaief, J.L., LaVail, M.M., Vollrath, D., 2011. mTOR-mediated dedifferentiation of the retinal pigment epithelium initiates photoreceptor degeneration in mice. J. Clin. Invest. 121, 369–383.

Zhao, M., Bai, Y., Xie, W., Shi, X., Li, F., Yang, F., Sun, Y., Huang, L., Li, X., 2015. Interleukin-1β Level Is Increased in Vitreous of Patients with Neovascular Age-Related Macular Degeneration (nAMD) and Polypoidal Choroidal Vasculopathy (PCV). PLoS One 10, e0125150.

Zheng, L., Kågedal, K., Dehvari, N., Benedikz, E., Cowburn, R., Marcusson, J., Terman, A., 2009. Oxidative stress induces macroautophagy of amyloid β-protein and ensuing apoptosis. Free Radic. Biol. Med. 46, 422–429.

Zhou, P., Kannan, R., Spee, C., Sreekumar, P.G., Dou, G., Hinton, D.R., 2014. Protection of Retina by αB Crystallin in Sodium Iodate Induced Retinal Degeneration. PLoS One 9, e98275.

Zou, C., Han, C., Zhao, M., Yu, J., Bai, L., Yao, Y., Gao, S., Cao, H., Zheng, Z., 2018. Change of ranibizumab-induced human vitreous protein profile in patients with proliferative diabetic retinopathy based on proteomics analysis. Clin. Proteomics 15, 12.

Chapter 2

Global aims

In middle-income and industrialized countries, AMD and DR have emerged as priority eye diseases due to the exacerbated growth and aging of the world population and increasing prevalence of diabetes mellitus. Despite the multiple options available for the management of these diseases, there is still progression to visual impairment and blindness in proliferative etiology. Considering the multifactorial nature of AMD and DR, multi-omics approaches, such as proteomics, could help to understand the pathophysiologic processes underlying these diseases. Therefore, in this doctoral project, several approaches were developed and applied for the study of the vitreous proteome. Considering that changes in vitreous structure and on the vitreoretinal interface are underling the pathogenesis of RD, the study of vitreous in RD was also establish as an intermediate task. Although the study of the vitreous proteome in retinal detachment was not initially one of the goals set, the results obtained in this intermediate task shown to be promising.

This Ph.D. thesis was developed based on two main general objectives. The first aim was the development of a straightforward approach for the analysis of the proteome of human vitreous. So, several gel-based and gel-free techniques were implemented for the study of the vitreous proteome in different vitreoretinal diseases. The second aim was to gain new insights into the understanding of pathological mechanisms underlying RD, DR, and AMD and, potentially find new vitreous biomarkers. For this purpose, the vitreous collected from patients suffering from these vitreoretinal diseases were analyzed by quantitative gel-free proteomics approaches.

To fulfill the main objectives of this doctoral thesis, specific goals were defined and performed throughout this project, including:

1. Application of an artificial neural network (ANN) for the refinement of sample preparation and experimental conditions for vitreous proteome profiling by 2DE (**Paper III**).

2. Development of iTRAQ-based proteomics strategy for the analysis of the proteome of vitreous collected from patients with RRD in comparison to macular epiretinal membranes (MEM). Validation of potential biomarkers of RRD by Western blot analysis (**Paper IV**).

3. Development of a label-free proteomics strategy for the analysis of the proteome of vitreous collected from patients with DR and AMD compared to MEM. Potential biomarkers were validated in vitreous collected from patients with DR, AMD, RD, and ERM by MRM, Receiver Operating Characteristic (ROC) analysis, and Western blot (**Paper V**).

Chapter 3

Section 1 – Paper III

Refinement of two-dimensional electrophoresis for vitreous proteome profiling using an artificial neural network

Fátima M. Santos, Tânia Albuquerque, Leonor M. Gaspar, João M. L. Dias, João P. Castro e Sousa, Alberto Paradela, Cândida T. Tomaz, Luís A. Passarinha

Analytical and Bioanalytical Chemistry, 411 (20): 5115-5126, May 2015
(DOI: 10.1007/s00216-019-01887-y)

This paper reports the application of an artificial neural network (ANN) for the refinement of sample preparation and experimental conditions for vitreous proteome profiling by 2DE. Using ANN, both the protein recovery and the number of spots detected in 2DE gels were significantly improved. The optimized response (580 spots) represents a 2.4-fold improvement over the standard initial conditions of the experimental design. After the removal of albumin and IgG, the analysis of vitreous using the optimized protocol resulted in an additional 1.3-fold increment in protein detection over the optimal output, with an average of 761 spots detected in vitreous from different vitreoretinopathies. Our results clearly indicate the importance of combining the appropriate amount of solubilizing agents with suitable control of the temperature and voltage to obtain high-resolved gels.

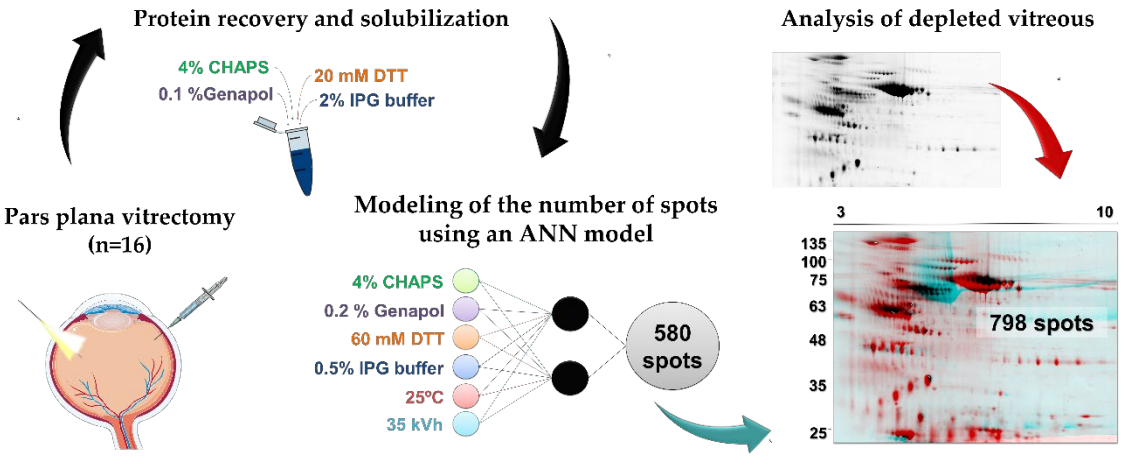

The supplementary material of this article is available in (https://doi.org/10.1007/s00216-019-01887-y) and in the Appendix.

Analytical and Bioanalytical Chemistry
https://doi.org/10.1007/s00216-019-01887-y

RESEARCH PAPER

Refinement of two-dimensional electrophoresis for vitreous proteome profiling using an artificial neural network

Fátima M. Santos[1,2,3,4] · Tânia Albuquerque[1] · Leonor M. Gaspar[1,2] · João M. L. Dias[5] · João P. Castro e Sousa[1,6] · Alberto Paradela[7] · Cândida T. Tomaz[1,2] · Luís A. Passarinha[1,4]

Received: 6 March 2019 / Revised: 18 April 2019 / Accepted: 30 April 2019

Abstract

Despite technological advances, two-dimensional electrophoresis (2DE) of biological fluids, such as vitreous, remains a major challenge. In this study, artificial neural network was applied to optimize the recovery of vitreous proteins and its detection by 2DE analysis through the combination of several solubilizing agents (CHAPS, Genapol, DTT, IPG buffer), temperature, and total voltage. The highest protein recovery (94.9% ± 4.5) was achieved using 4% (*w*/*v*) CHAPS, 0.1% (*v*/v) Genapol, 20 mM DTT, and 2% (*v*/*v*) IPG buffer. Two iterations were required to achieve an optimized response (580 spots) using 4% (*w*/*v*) CHAPS, 0.2% (*v*/*v*) Genapol, 60 mM DTT, and 0.5% (*v*/*v*) IPG buffer at 35 kVh and 25 °C, representing a 2.4-fold improvement over the standard initial conditions of the experimental design. The analysis of depleted vitreous using the optimized protocol resulted in an additional 1.3-fold increment in protein detection over the optimal output, with an average of 761 spots detected in vitreous from different vitreoretinopathies. Our results clearly indicate the importance of combining the appropriate amount of solubilizing agents with a suitable control of the temperature and voltage to obtain high-quality gels. The high-throughput of this model provides an effective starting point for the optimization of 2DE protocols. This experimental design can be adapted to other types of matrices.

Keywords Artificial neural network · Gel-based proteomics · Ocular pathologies · Two-dimensional gel electrophoresis · Vitreous

Abbreviations

2DE	Two-dimensional electrophoresis
ANN	Artificial neural networks
HMW	High-molecular-weight
IAA	Iodoacetamide
IEF	Isoelectric focusing
kVh	Kilovolts hour
LMW	Low-molecular-weight
MMW	Medium-molecular-weight

Electronic supplementary material The online version of this article (https://doi.org/10.1007/s00216-019-01887-y) contains supplementary material, which is available to authorized users.

✉ Luís A. Passarinha
lpassarinha@fcsaude.ubi.pt; lapp@ubi.pt

[1] CICS-UBI—Health Sciences Research Centre, University of Beira Interior, 6201-506 Covilhã, Portugal

[2] Chemistry Department, Faculty of Sciences, University of Beira Interior, 6201-001 Covilhã, Portugal

[3] Laboratory of Pharmacology and Toxicology—UBIMedical, University of Beira Interior, 6200-284 Covilhã, Portugal

[4] UCIBIO@REQUIMTE, Departamento de Química, Faculdade de Ciências e Tecnologia, Universidade Nova de Lisboa, 2829-516 Caparica, Portugal

[5] Cancer Molecular Diagnostics Laboratory, National Institute for Health Research, Biomedical Research Centre, University of Cambridge, Cambridge, England, UK

[6] Department of Ophthalmology, Centro Hospitalar de Leiria, 2410-197 Leiria, Portugal

[7] Unidad de Proteomica, Centro Nacional de Biotecnología, CSIC, Calle Darwin 3, Campus de Cantoblanco, 28049 Madrid, Spain

Published online: 31 May 2019

Introduction

Ocular proteomics has emerged as an opportunity for discovering new biomarkers, which could help to unveil the pathophysiology of many ocular diseases and anticipate its progression [1, 2]. Vitreous is an ocular fluid localized between the inner retina and lens, and, as it is less complex than other ocular matrices, it could be an excellent source of biological material for the identification of subtle changes in protein expression [2, 3]. As its proteome is affected by the physiological and pathological conditions of the retina, the study of vitreous has been a mean of indirectly understanding the vitreoretinal interface underlying many retinal diseases [4, 5]. Therefore, a comprehensive characterization of the vitreous proteome has been made to achieve this goal [6–19]. Gel-free techniques such as LC-MS and CE-MS have emerged as an alternative for the characterization of vitreous proteome [8–10, 19]; however, gel-based proteomic techniques are still widely used for in-depth proteome analyses [20, 21].

Two-dimensional electrophoresis (2DE) combined with identification by MALDI-TOF/TOF mass spectrometry has been widely used for the analysis of vitreous proteome [6, 7, 12–16]. If combined with more sensitive detection techniques, refined gel image processing, and proper sample preparation, 2DE is a valuable tool for routine and high-resolution analysis of proteoforms [22, 23]. Sample preparation has been the main focus in the optimization of 2DE protocols [24–26]. Protein extraction, enrichment, and solubilization should be adapted for each specific sample to improve the detection of protein diversity, removal of interfering substances, and interactions between polypeptides, without jeopardizing the yield and reproducibility [27, 28]. Moreover, the solubilizing agents must be compatible with isoelectric focusing (IEF) and preserve the protein solubilization at critical steps, e.g., at the sample entry into the gel and/or when protein achieves its isoelectric point [29]. Nevertheless, other strategies should be considered to avoid gel-to-gel variation, including the refinement and tuning of protein separation by isoelectric point (pI) [30–34] and by molecular weight (MW) [33, 35, 36].

In this work, a careful combination of physicochemical factors that influence both sample preparation and separation by pI was considered for the analysis of vitreous proteins by 2DE. In addition, an artificial neural network (ANN) was developed to maximize the number of protein spots detected in 2DE gels by combining different solubilizing agents (CHAPS, Genapol, DTT, IPG buffer) with the temperature and total voltage of IEF. Furthermore, ANN was used to improve protein recovery and solubilization from vitreous samples by combining the four solubilizing agents. By mimicking the structure and functional aspects of biological neural networks, ANN can be trained "by example" from a set of cases (inputs) to recognize patterns and to accurately predict responses (outputs) [37, 38].

Materials and methods

Materials

Solutions were prepared with ultrapure water obtained with a Milli-Q system (Millipore/Waters). Chemicals are commercially available and were used without further purification. 2DE QUANT kit, HiTrap™ Albumin & IgG Depletion 1 mL column, immobilized pH gradient (IPG) strips, IPG buffer 3-10, iodoacetamide (IAA), and thiourea were obtained from GE Healthcare Life Sciences (Uppsala, Sweden). Genapol X-100, urea, alpha-cyano-4-hydroxycinnamic acid, bromophenol blue, Tris, ammonium bicarbonate, trypsin from porcine pancreas, and TFA were purchased from Sigma-Aldrich (St. Louis, MO, USA). DTT was obtained from Himedia (Mumbai, India). HPLC grade solvents (methanol and chloroform), LC-MS grade solvents (water and acetonitrile), glycerol, and Coomassie Brilliant Blue G-250 were acquired from Fluka Chemika (Buchs, Switzerland). CALMix was acquired from AB Sciex (Framingham, MA, USA). Acrylamide 4K solution 40% was obtained from PanReac AppliChem (Darmstadt, Germany) and CHAPS was obtained from Amresco (OH, USA). Sodium phosphate, sodium chloride, and glycine were obtained from Fisher Scientific (Loughborough, UK).

Patients and controls

Vitreous samples were collected via pars plana vitrectomy, over a year period, at the Ophthalmology Service of Leiria-Pombal Hospital, Portugal. The protocol for sample collection was approved by the hospital ethics committee (Code: CHL-15481) and informed consent from all patients was obtained in agreement with the Declaration of Helsinki. Samples were collected from 16 patients with vitreomacular traction syndrome, of which 11 were diabetics and 5 non-diabetics. Patients included 4 females and 12 males, with ages comprised between 62 and 84 years. For the analysis of depleted samples, vitreous was collected from 3 individuals: a 68-year-old woman diagnosed with proliferative diabetic retinopathy, a 70-year-old man diagnosed with rhegmatogenous retinal detachment, and a 65-year-old woman with cortical fragments. Vitreous samples were transferred to sterile cryogenic vials after collection and frozen at − 80 °C until further processing.

Experimental design

A set of 30 exploratory experiments were designed using the Screening option in MODDE 12.1 based on a factorial design at three levels (L27) with three central points. Six factors that influence the extraction, solubilization, and separation by IEF of vitreous proteins were considered for maximizing the detection of spots in 2DE gels, including solubilizing agents and

physical parameters. The solubilizing agents comprised detergents (CHAPS at 0, 2, and 4% (*w*/*v*) and/or Genapol at 0, 0.1, and 0.2% (*v*/*v*)), DTT (20, 40, and 60 mM), and IPG buffer (0.5, 1, and 2% (*v*/*v*)). The physical parameters were the total voltage (35, 40, and 45 kilovolts hour (kVh)) and temperature (15, 20, and 25 °C). Table S1 (see Electronic Supplementary Material, ESM) lists the physical-chemical parameters and respective ranges combined for the experimental design, the model development, and the optimization by ANN.

Extraction and solubilization of vitreous proteins

Individual vitreous samples were centrifuged at 18,620×*g* for 10 min at 4 °C, and the resultant supernatants from 16 patients were pooled for further analysis. The pool was quantified using 2DE Quant kit (GE Healthcare Life Sciences). Proteins were extracted from vitreous using chloroform/methanol precipitation, as previously described [10, 18]. Briefly, 800 μL methanol, 200 μl chloroform, and 600 μL Milli-Q water were added to 200 μL of sample. The mixture was centrifuged at 15,000×*g* for 5 min at 4 °C, and the aqueous layer was removed. After centrifugation, 800 μL of methanol was added, and the protein pellet was recovered after centrifugation at 18,620×*g* for 10 min. The pellet was solubilized with a buffer composed of 7 M urea, 2 M thiourea, and 0.002% (*w*/*v*) bromophenol blue and supplemented with CHAPS, Genapol, DTT, and IPG buffer, according to the experimental design (ESM Table S1). All samples were prepared at least in triplicate for each run.

Two-dimensional gel electrophoresis

IPG strips (pH 3–10, 24 cm) were rehydrated, according to experimental design, for 14 h at room temperature. According to optimized conditions, 250 μg of vitreous proteins was applied by cup loading and separated by isoelectric focusing in an Ettan IPGphor III device (GE Healthcare Life Sciences) for a total of 35, 40, or 45 kVh, with temperatures ranging between 15, 20, and 25 °C (ESM Table S2). Technical duplicates were performed for each experiment. IPG strips were incubated for 15 min with equilibration buffer (6 M urea, 75 mM Tris-HCl buffer, 29.3% (*v*/*v*) glycerol, 2% (*w*/*v*) SDS, 0.02% (*w*/*v*) bromophenol blue) supplemented with 1% (*w*/*v*) DTT, and, subsequently, for 15 min with equilibration buffer supplemented with 2.5% (*w*/*v*) IAA. The second dimension was performed on 10% acrylamide gels, using Ettan DALTSIX Large Vertical System (GE Healthcare Life Sciences, Sweden). Gels were initially run at 1.5 mA/gel for 45 min and, then, at 17 mA/gel to separate the proteins by MW. Gels were stained using a colloidal Coomassie Brilliant Blue solution [18, 39] and scanned using ImageScanner III (GE Healthcare Life Sciences, Sweden). The spots were automatically detected using the ImageMaster 2D Platinum v7.0 (GE Healthcare) software. The detection was performed using the following parameters, smooth = 3, minimum area = 5, and saliency = 15, and artifacts (e.g., dust, bubbles, among others) and edges of the images were manually removed. The total number of proteins spots, volume, intensity, and saliency was assessed for each experiment.

Artificial neural network

A feed-forward ANN was applied to predict the number of protein spots detected in 2DE gels as a function of the solubilizing conditions (CHAPS, Genapol, DTT, IPG buffer), total voltage, and temperature. The ANN tool was implemented in MATLAB™ using the Neural Network Toolbox and the "newff" function. The ANN structure, comprising a total of 17 parameters, was designed with an input layer with six neurons (one for each input variables), an output layer with one neuron (number of detected spots), and one hidden layer with two neurons (6/2/1). The transfer functions for the input and output layers were defined by the linear function "purelin" and for the hidden layer by the log-sigmoid function "logsig." The ANN model training was performed with Levenberg-Marquardt back-propagation method "trainlm," up to 1000 epochs, using the "train" function with the performance function "mse" goal set at 1×10^{-10}. The remaining training parameters were set at their default values. The parameter optimization for each model was carried out until either the maximum number of epochs or the performance goal was reached. A randomly selected dataset, containing 25% of the total number of experiments, was left aside for model validation. The outliers were discarded from the dataset using the modified Thompson Tau test for a Student's *t* critical value (based on an alpha level of 0.075) with two degrees of freedom. The model selection process was repeated until the coefficient of determination (R^2) for the selected set (excluding the outliers) of observed versus the predicted number of protein spots has exceeded 0.925. The optimized ANN inner parameters are present in ESM Table S2.

Analysis of depleted vitreous using 2DE optimal operation conditions

Human serum albumin and IgG were depleted from individual vitreous samples using a HiTrap™ Albumin & IgG Depletion 1 mL column (GE Healthcare, Uppsala, Sweden), as previously performed by our group [18]. The depletion was performed at room temperature in an ÄKTA avant FPLC system with UNICORN software (GE Healthcare, Uppsala, Sweden) equipped with a 1-mL injection loop. All buffers were prepared with Milli-Q system water, filtered through a 0.20-μm pore size membrane (Schleicher Schuell, Dassel, Germany) and degassed ultrasonically. The flow-through fraction containing low-abundant non-bound proteins was collected, desalted using Vivaspin 6, 3 kDa MWCO (GE Healthcare), and precipitated as described before. The pellet obtained was solubilized in a

buffer composed of 7 M urea, 2 M thiourea, 4% (*w*/*v*) CHAPS, 0.1% (*v*/*v*) Genapol, 20 mM DTT, and 2% (*v*/*v*) IPG buffer. IEF was performed with an IPG strip rehydrated with 7 M urea, 2 M thiourea, 4% (*w*/*v*) CHAPS, 0.2% (*v*/*v*) Genapol, 60 mM DTT, and 0.5% (*v*/*v*) IPG buffer. A total of 250 μg was focused at 35 kVh and 25 °C, as previously performed.

Protein identification

Protein spots were manually excised from 2DE gels, destained (50% (*v*/*v*) acetonitrile in 50 mM ammonium bicarbonate), reduced (10 mM DTT, 1 h at 37 °C), and alkylated (55 mM IAA, 30 min at room temperature). Then, spots were rehydrated for 1 h with 30 μL of 10 ng/μL of trypsin solution at 4 °C and digested overnight at 37 °C. Tryptic peptides were extracted and salts washed with Zip-tip pipette tips C18 0.1–10 μL pipette tips (Millipore®, Molsheim, France), as previously described [18]. MS and MS/MS spectra were acquired on a 4800 plus MALDI-TOF/TOF mass analyzer (AB Sciex, Framingham, MA, USA), equipped with a 355-nm laser. MALDI-TOF/TOF was initially calibrated, using the CALMix 1/CALMix 2 calibration mixture that includes the following components: des-arg-bradykinin (904.4681 *m*/*z*), angiotensin I (1296.6853 *m*/*z*), Glu-fibrinopeptide B (1570.6774 *m*/*z*), and ACTH (2093.0867 *m*/*z*). Tryptic peptides corresponding to individual spots were mixed with 5 mg/mL of alpha-cyano-4-hydroxycinnamic acid in proportion 1:1 and spotted on a MALDI plate. All spots were acquired in positive MS reflector mode in the range 800 to 4000 *m*/*z* by averaging 1500 laser spots. The eight more intense MS ions per spot that satisfied the precursor criteria (200 ppm fraction-to-fraction precursor exclusion, *S*/*N* ratio > 25) were selected for subsequent MS/MS analysis. MS/MS analysis was performed using 1 keV collision energy of 1 kV with a total of 1500 laser shots per spectrum. Raw data were searched using the MASCOT search engine from ProteinPilot™ Software 4.5 (AB Sciex, Framingham, MA, USA) against the *Homo sapiens* UniProtKB reviewed database (20,360 entries, 9th of July 2018). Search parameters were set as follows: enzyme—trypsin, fixed modifications—carboxymethyl (C), variable modifications—oxidation (M), peptide mass tolerance ± 100 ppm, fragment mass tolerance ± 0.3 Da, missed cleavages 2. Protein scores of 56 were used as a cutoff for protein identification using MASCOT ($p < 0.05$).

Results

Experimental design and artificial neural network modeling

For the design of the ANN, both solubilizing agents and physical parameters were selected as inputs variables. The inputs variables and respective range levels were selected according to previous studies in the literature [3, 6, 12–14, 16] and to preliminary results from our research group. According to the literature, CHAPS (0, 2, and 4% (*w*/*v*)), DTT (20, 40, and 60 mM), and IPG buffer (0.5, 1, and 2% (*v*/*v*)) were selected as inputs. Additionally, the non-ionic detergent Genapol (0, 0.1, and 0.2% (*v*/*v*)) was included in this study because of its good performance in protein recovery from vitreous samples [40]. Chaotropic agents were not selected as inputs, but 7 M urea/2 M thiourea were included in all the buffers used for extraction and solubilization of vitreous proteins. Temperatures between 15 and 25 °C were tested, according to the results obtained by Görg and colleagues [41]. Total voltage was 35 to 45 kVh for 24 cm IPG strips pH 3–10, according to the manufacturer. According to this, the inputs variables and respective code levels were defined for the experimental design, as shown in ESM Table S1. The 30 experiments defined by CCD for the optimization of the number of proteins spots detected in the 2DE analysis are listed in ESM Table S2.

Improvement of protein extraction based on the ANN model

The first goal of this study was to establish a cost-effective protocol for the extraction and solubilization of vitreous proteins for 2DE analysis. Preliminary results showed that acetone precipitation leads to an unreproducible recovery of proteins from vitreous, with poor recovery yields (59% ± 27). TCA/acetone precipitation was remarkably more efficient than acetone alone, with recovery yields of 84% ± 18, similar to the results (> 90%) obtained with 2-D Clean-Up Kit (GE Healthcare). Nevertheless, the cost makes inconceivable its use for the preparation of many samples. The choice turned out to be a methanol/chloroform precipitation due to its easy and fast handling, efficiency, and cost-effectiveness. The effect of the four solubilizing components (CHAPS, Genapol, DTT, IPG buffer) on the protein solubilization was studied using the ANN experimental design (ESM Table S1). Table 1 shows the recovery yields obtained in the solubilization of vitreous proteins combining distinct solubilizing agents, with values ranging between 72.7% ± 5.4 and 94.9% ± 4.5. We found that CHAPS showed the greatest improvement on protein solubilization, with recovery yield increases from 78.2 to 87.2% by varying its concentration from 0 to 4% (*w*/*v*). The effect of Genapol on the protein solubilization was more evident at low percentages of CHAPS. Therefore, such high concentrations of Genapol are not required in the presence of CHAPS. IPG buffer did not have a relevant impact on recovery yields, but best results were obtained at 2% (*v*/*v*). Lower concentrations of DTT (20–40 mM) increased protein recovery. Combining all factors, the highest protein recovery (94.9% ± 4.5) was achieved combining 4% (*w*/*v*) CHAPS, 0.1% (*v*/*v*) Genapol, 20 mM DTT, and 2% (*v*/*v*) IPG buffer.

Table 1 Recovery yields obtained in the solubilization of vitreous proteins with different combinations of solubilizing agents

Experiment number	Solubilizing agents				Output
	CHAPS (% *w/v*)	Genapol (% *v/v*)	DTT (mM)	IPG buffer (% *v/v*)	Protein recovery per buffer (%)
1, 2, 3	0	0.0	20	0.5	80.1 ± 5.9
4, 5, 6	0	0.1	40	1.0	81.9 ± 14.3
7, 8, 9	0	0.2	60	2.0	72.7 ± 5.4
10, 11, 12	2	0.0	40	2.0	90.0 ± 5.3
13, 14, 15	2	0.1	60	0.5	87.1 ± 4.8
16, 17, 28	2	0.2	20	1.0	81.7 ± 7.0
19, 20, 21	4	0.0	60	1.0	84.5 ± 10.0
22, 23, 24	4	0.1	20	2.0	94.9 ± 4.5
25, 26, 27	4	0.2	40	0.5	86.3 ± 5.4
28, 29, 30	2	0.1	40	1.0	84.4 ± 11.7
31, 32	4	0.2	60	0.5	83.2 ± 12.0

Modeling of the number of spots detected in 2DE analysis using an ANN model

Experimental conditions for vitreous proteome profiling by 2DE were optimized by ANN modeling using a stepwise process to maximize the number of detected protein spots. The ANN model is slightly biased with a slope and intercept of 0.91 and 20.49, respectively, and an R^2 of the fitting between the measured and predicted output of 0.925 (Fig. 1a). Two iterations were required to achieve an optimal response (580 spots) under the optimal conditions (4% (*w/v*) CHAPS, 0.2% (*v/v*) Genapol, 60 mM DTT, 0.5% (*v/v*) IPG buffer at 35 kVh and 25 °C). Figure 1 b depicts the contour plots from the ANN model for the two-factor interaction between the solubilizing agents (CHAPS, Genapol, DTT, and IPG buffer) and the physical parameters (temperature and total voltage), respectively. The optimal run (experiment 32) showed a 20.6% (1.2-fold) and 134.7% (2.4-fold) improvement over the best (experiment 25) and the more standard (experiment 21) conditions performed in the experimental design. The two-factor interaction between Genapol and CHAPS (Fig. 1b) evidences an abrupt reduction in the response (less than 200 spots) when lower concentrations of detergents are applied. Percentages of Genapol above 0.15% (*v/v*) promote a positive outcome, which is reinforced in the presence of CHAPS. Genapol has a positive effect on the spot detection, even without CHAPS, but the opposite situation is not verified. In fact, less than 200 spots are detected without Genapol, even at higher concentrations of CHAPS. Higher outcomes are also accomplished with 60 mM DTT and 0.5% (*v/v*) IPG buffer (Fig. 1b). Good responses are obtained combining 20 mM of DTT and 0.15% (*v/v*) Genapol but, as the detergent concentration rises, increasing the DTT concentration is also required. According to that, the best results were obtained in experiments 25 and 32 using 0.5% (*v/v*) IPG buffer, in which 514 and 584 spots were detected in 2DE gels.

Concerning the physical parameters, optimal results are obtained with high temperatures (25 °C) and lower total voltages (35 kVh) (Fig. 1b). The effect of physical parameters in protein detection appears to be highly influenced by the levels of Genapol and DTT but not by the concentration of CHAPS and IPG buffer (Fig. 1b). As Genapol percentage increases, higher temperatures and lower voltages are required to maintain an effective detection level. Indeed, temperature, voltage, and DTT should be carefully maintained close to the optimal values to obtain the best outcome. Also, the set voltage was not reached in some experiences, especially in those that combined higher concentrations of DTT and/or IPG buffer with higher voltages.

Effect of ANN factors in the quality of 2DE gels

After validation, the gels were visually inspected, and several protein spots were manually excised and identified by mass spectrometry to confirm the robustness of the established ANN model. Furthermore, parameters such as intensity, area, saliency, and volume of the spots were measured in gel images using the ImageMaster 2D Platinum v7.0 software (ESM Table S2). Visual inspection of gels with increasing concentrations of detergents allowed us to detect changes in spot patterns throughout the experimental optimization. Figure 2 shows the contour plot of two-factor interaction between CHAPS and Genapol and the representative 2DE gels obtained at different conditions (experiments 2 (a), 7 (b), 13 (b), 21 (e), and 25 (d) from ESM Table S2). The spots identified by MALDI-TOF/TOF are shown in detail in the 2DE gel from experiment 32 (Fig. 3a) and the complete list of identified proteins and peptides are listed in ESM Table S3. The 3D visualization of high-MW (HMW), medium-MW (MMW), and low-MW (LMW)

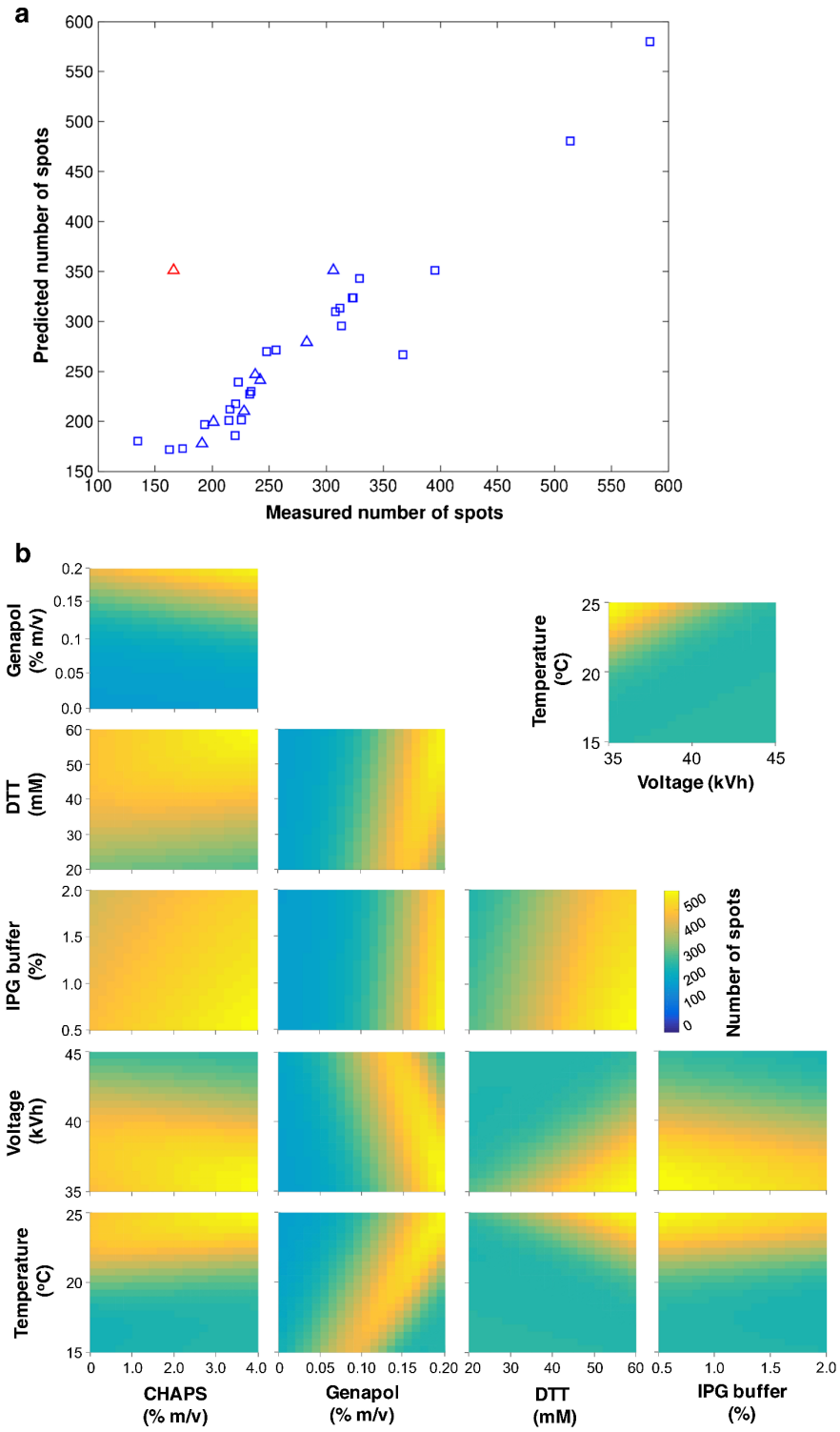
a
Predicted number of spots
Measured number of spots
b
Genapol (% m/v)
DTT (mM)
IPG buffer (%)
Voltage (kVh)
Temperature (ºC)
CHAPS (% m/v)
Genapol (% m/v)
DTT (mM)
IPG buffer (%)
Number of spots

◀ **Fig. 1** (**a**) Artificial neural network model fitting comparing the experimental and predicted number of spots detected in two-dimensional gels. The experiments used for the training (squares) and the validation (triangles) of the experimental design are represented in blue and the outliers (experiment 30) in red. (**b**) Contour plots obtained from the ANN model for the two-factor interaction between solubilizing agents and physical parameters (temperature and total voltage)

areas from representative 2DE gels obtained throughout the experimental optimization is shown in Fig. 3b.

In gels with the highest number of spots (e.g., experiment 25 in Fig. 2d), the volume/area occupied by high-abundant protein spots is lower, compared with the gels with fewer spots (e.g., experiment 2 in Fig. 2a). A close look at highly abundant vitreous proteins such as alpha-1-antitrypsin, serotransferrin, and albumin (spots 5, 6, and 7 in Fig. 3a) showed a significant increase in intensity/saliency with the improvement of experimental conditions, but a decrease in the percentage of occupied volume. The number of proteins ranging between 48 and 75 kDa did not increase so significantly through the optimization, but this increase was significant for high- and low-molecular-weight proteins. Up to 81 HMW and 42 LMW proteins were found in gels with lower number spots (e.g., experiments 2, 7, and 13), but 173 high- and 69 low-mass proteins were detected using optimal conditions (ESM Table S2). As shown in Figs. 2 and 3, it is evident the positive effect of Genapol on the detection of these proteins. For example, HMW proteins, such as retinol-binding protein (spot 1) and ceruloplasmin (spots 2), or LMW proteins, such as immunoglobulin light chains (spots 14 and 15), were barely visible in the first experiments but showed a substantial increase in its intensity/saliency through the optimization process (ESM Table S2). Spot resolution was also increased, particularly in experiments using 40–60 mM of DTT (Fig. 3b). DTT led to a more significant increase in protein detection in ranges between 35 and 75 kDa than at HMW and LMW ranges (ESM Table S2). Furthermore, it was verified that spot resolution is negatively affected by lower temperatures and high voltages. At these conditions, the gels present distorted protein patterns with poorly resolved spots and an extensive horizontal and vertical streaking. These effects are attenuated by the presence of Genapol and/or DTT, as seen in experiments 7 (Fig. 2b), 18, and 20.

Analysis of depleted vitreous using 2DE optimal operation conditions

Despite the improvement of the experimental conditions, an extensive vertical and horizontal streaking pattern is visible in the gels run on undepleted samples. To improve the quality of

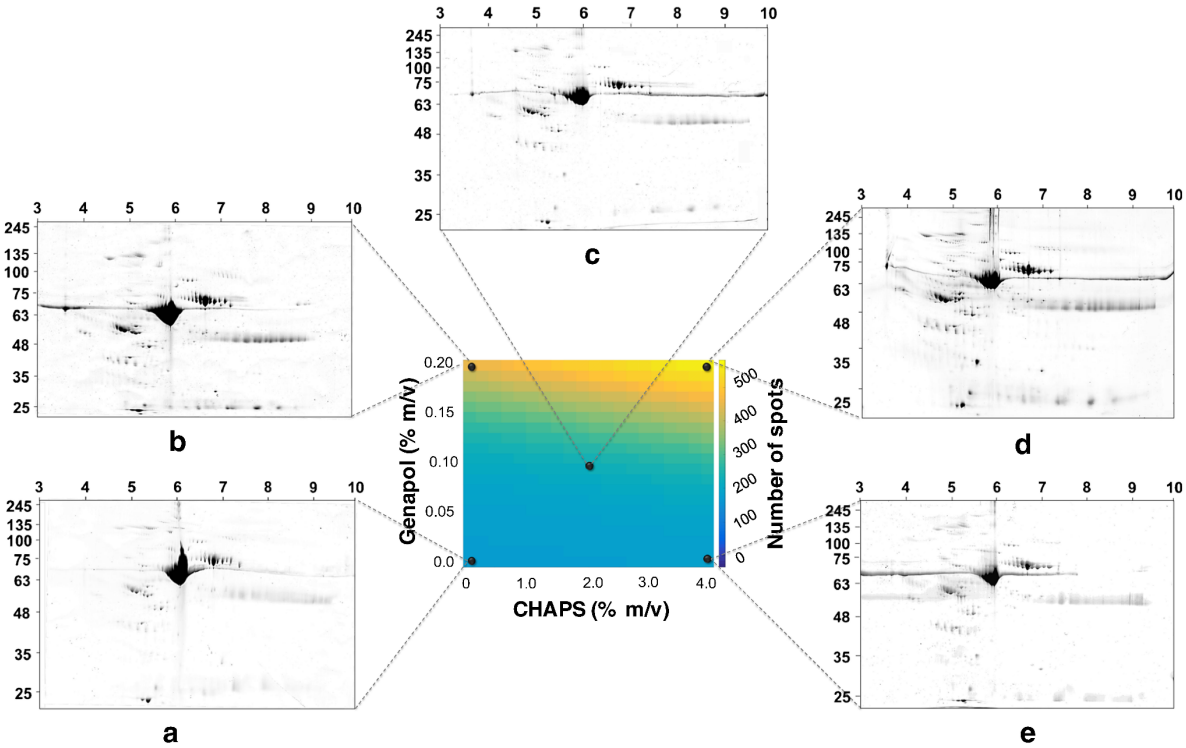

Fig. 2 Contour plot of two-factor interaction between the detergents CHAPS and Genapol and the representative 2DE gels for the experiments (**a**) 2, (**b**) 7, (**c**) 13, (**d**) 25, and (**e**) 21. The concentration of CHAPS and Genapol used in each experiment is represented in the contour plot by black spots

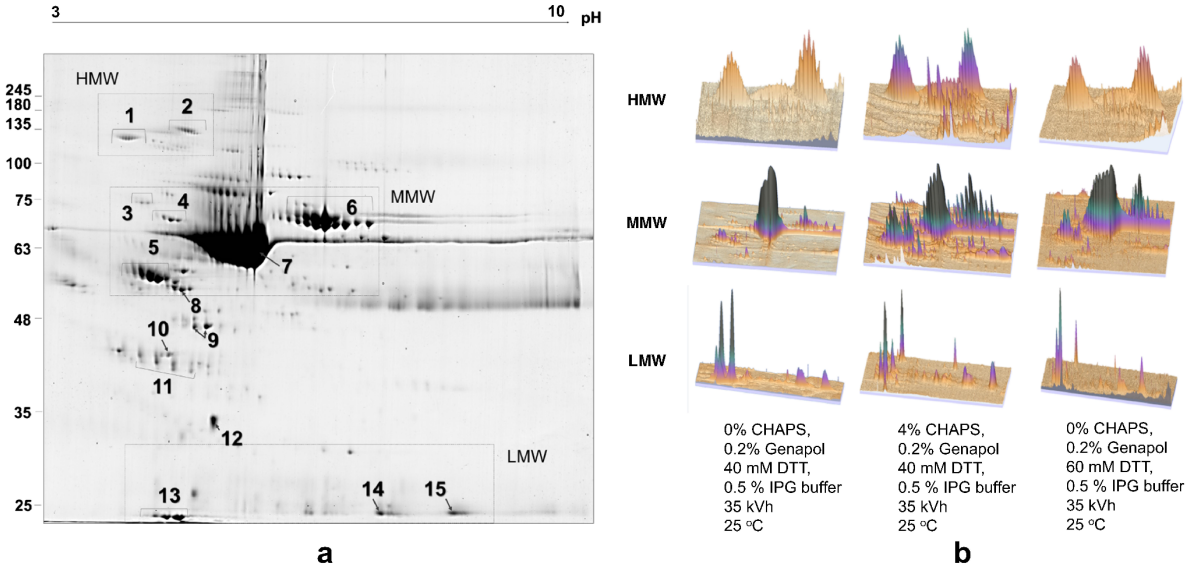

Fig. 3 (**a**) Representative 2DE gels from the analysis of vitreous in experiments 32 using 4% (*w*/*v*) CHAPS, 0.2% (*v*/*v*) Genapol, 60 mM DTT, and 0.5% (*v*/*v*) IPG buffer at 35 kVh and 25 °C. The numbered spots were identified was 1: retinol-binding protein 3, 2: ceruloplasmin, 3: prothrombin, 4: alpha-1B-glycoprotein, 5: alpha-1-antitrypsin, 6: serotransferrin, 7: serum albumin, 8: vitamin D–binding protein, 9: pigment epithelium–derived factor, 10: apolipoprotein A-IV, 11: haptoglobin, 12: transthyretin, 13: apolipoprotein A-I, 14: immunoglobulin kappa constant, 15: immunoglobulin kappa light chain. (**b**) 3D visualization of high-molecular-weight (HMW), medium-molecular-weight (MMW), and low-molecular-weight (LMW) regions of 2DE gels obtained throughout the experimental optimization

gels, albumin and IgG were removed using HiTrap™ Albumin & IgG Depletion 1 mL column and depleted vitreous samples were analyzed by 2DE using the optimized protocol. For this purpose, vitreous was collected from three different samples, including a woman with cortical fragments in vitreous (HV 24), a woman diagnosed with PDR (HV 26), and a man diagnosed with rhegmatogenous retinal detachment (HV 580). Depletion of high-abundant proteins resulted in a substantial increase in the number of protein spots detected in the gels, with 798, 701, and 785 spots detected in HV 24, HV 580, and HV 26, respectively (Fig. 4a–c). On average, this represents an increase of 23.1% (1.3-fold) in global protein detection over the optimal output of the ANN model. Overlap analysis of the 2DE gels from experiment 32 (blue) and depleted vitreous (red) 24 indicated new spots (black) detected in regions previously occupied by albumin and IgG (Fig. 4d). At these conditions, it was possible to identify 445 spots in MMW region, compared with the 353 spots previously detected in experiment 32. Also, more 42 LMW proteins and 33 HMW proteins were detected, and other spots become more visible in the gels after albumin and IgG removal.

Discussion

2DE remains a valuable tool for the high-resolution analysis of vitreous proteome [6, 7, 12–16] due to its affordable price, robustness, and high-resolution. Nevertheless, both proteome complexity and wide dynamic range of vitreous samples hinder its analysis by 2DE. The present work aimed to establish a cost-effective experimental protocol for the analysis of vitreous by 2DE considering some parameters with potential impact on its solubilization, extraction, and detection. In the first approach, the extraction method was selected using the traditional one-factor-at-a-time approach. Although this methodology is useful for a preliminary screening, it is extremely time-consuming and it is not efficient to evaluate in an objective manner the interaction between inputs in multifactorial systems [42–44]. Considering the substantial number of factors under study, multivariate statistical methodologies were applied to evaluate the effect of multiple factors in the final response. Response surface methodology (RSM), which includes factorial design and regression analysis, is useful to optimize significant factors to maximize the response [43], but this model would have 28 parameters compared with 17 parameters of our ANN model. According to that, a set of 30 exploratory experiments were designed based on a factorial design at three levels (L27) with three central points. ANN was used to explore the effect of the combination of six factors that influence vitreous protein analysis by 2DE, including solubilizing agents (CHAPS, Genapol, DTT, IPG buffer) and physical parameters (total voltage and temperature). We found that optimal conditions (run 32) included 4% (*w*/*v*) CHAPS, 0.2% (*v*/*v*) Genapol, 60 mM DTT, and 0.5% (*v*/*v*) IPG buffer

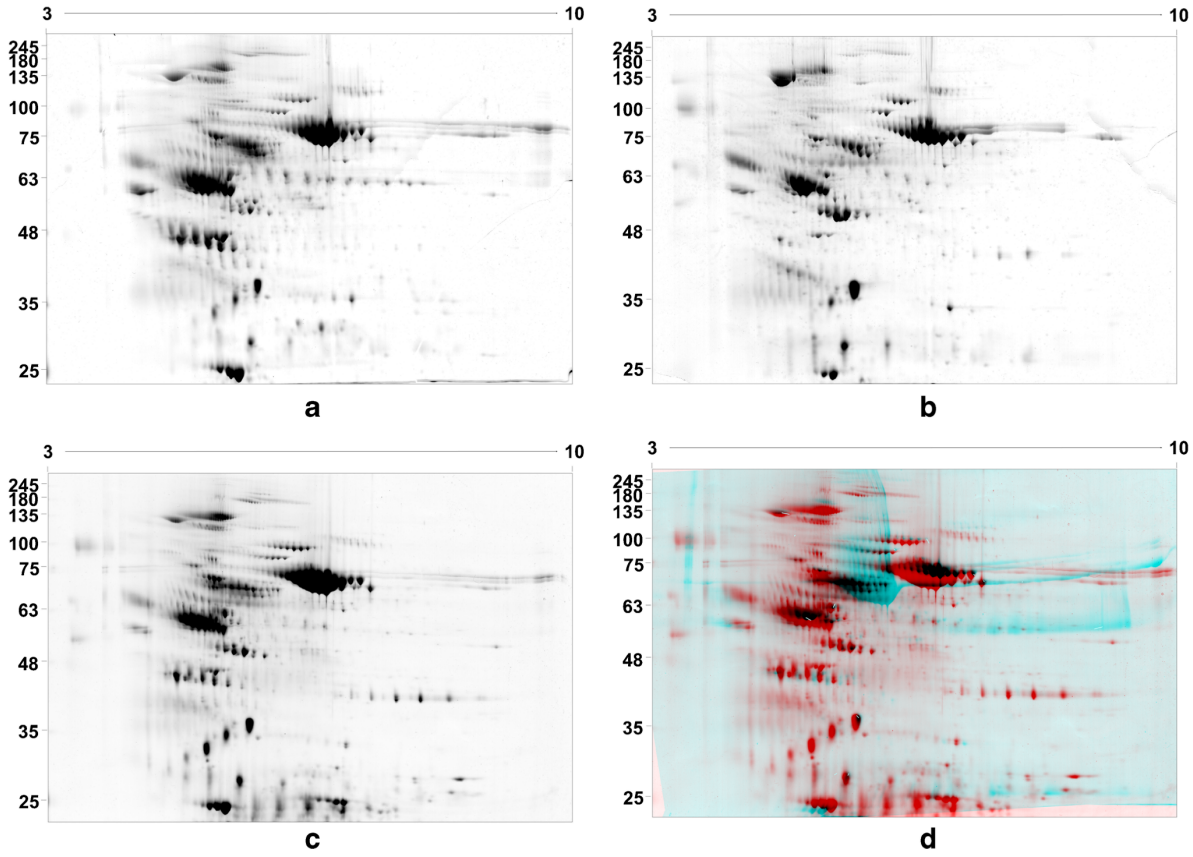

Fig. 4 Representative 2DE gels from the analysis of depleted vitreous collected from (**a**) a patient diagnosed with PDR (HV 26), (**b**) a patient diagnosed with rhegmatogenous retinal detachment (HV 580), and (**c**) a patient with cortical fragments in vitreous (HV 24). (**d**) Image representing the overlapping of representative 2DE gels from the analysis of depleted vitreous HV 24 (colored at red) and the 2DE gels from the analysis of vitreous in experiments 32 (colored at blue). The black spots correspond to overlapping spots between the two gels

at 35 kVh. These conditions allowed us to detect 580 spots, representing a 1.2-fold/2.4-fold improvement over the best/standard conditions performed in the experimental design. For maximizing the protein recovery yield (94.9% ± 4.5), the conditions were similar, but it was preferable to decrease the concentration of DTT to 20 mM and of Genapol to 0.1% (*v*/*v*).

CHAPS is the most commonly used surfactant in 2DE protocols due to its greater solubilizing power [45]. In this work, CHAPS allowed recoveries greater than 80% and promoted the detection of more than 200 spots. Although the performance of CHAPS was reasonable, it has been reported that it is worst for the extraction of challenging proteins (e.g., hydrophobic and/or HMW proteins) [29]. To increase its solubilizing power, the buffer was complemented with Genapol, a non-ionic detergent that demonstrated high efficiency for the extraction of vitreous proteins [40]. In fact, Genapol has a positive effect on the detection of protein spots, even in the absence of CHAPS. DTT showed superior performance at increasing concentrations, which can be related to its potential interference with IEF. DTT becomes deprotonated as it moves towards the anode, which increases the conductivity in IEF and diminishes the reducing power at the cathode region. At these conditions, proteins become less soluble and tend to precipitate, causing horizontal streaking and poor resolution in the second dimension of 2DE [46]. Best results were obtained with 60 mM DTT combined with reduced voltages (35 kVh) to avoid potential interferences in long runs. Besides, the combination of high concentration of DTT/IPG buffer with lower temperatures/high voltages results in poor focusing of vitreous proteins. At these conditions, the gels present distorted protein patterns with poorly resolved spots and an extensive horizontal and vertical streaking. Temperature is a critical parameter since it largely affects pI values, with variations up to 0.6 pH units between 4 and 25 °C [28, 41]. Although the temperature of 20 °C is the most recommended for IEF, our results indicate that a slight increase to 25 °C can benefit the quality of vitreous analysis by 2DE. As previously reported by Görg and co-workers, the entry and

mobility of proteins in IPG strips are improved with a slighter increase in the temperature, and, consequently, clearer background gels with well-defined spots are obtained [41]. Considering that, it must be kept in mind that physical parameters such as temperature and voltage have an enormous impact on the final quality of gels and, thus, should be recorded and controlled during the IEF.

Despite the meticulous refinement of several parameters, high-abundant proteins, such as albumin, cause an extensive vertical and the horizontal streaking, which hampers the detection of less abundant proteins. The complexity and wide dynamic concentration range of biological fluids exceed the high resolving power of 2DE, and, therefore, it is highly recommended to reduce the complexity of the sample previously to 2DE analysis [3, 20]. In this study, the depletion of abundant proteins including albumin and IgG allowed an increase of 23.1% (1.3-fold) in the number of proteins detected over the optimal conditions performed without depletion. Although the depletion of abundant proteins can lead to the co-depletion of important proteins, it seems to be a suitable approach to increase the coverage of vitreous proteome.

Conclusions

Despite technological advances, the 2DE analysis of biological fluids, such as vitreous, remains a major challenge. In this work, an ANN was developed to maximize the extraction of vitreous proteins and its detection in 2DE gels by combining solubilizing agents (CHAPS, Genapol, DTT, and IPG buffer) at different temperatures and total voltages. The best protein recovery was obtained using 4% (*w*/*v*) CHAPS, 0.1% (*v*/*v*) Genapol, 20 mM of DTT, and 2% (*v*/*v*) IPG buffer, with recoveries of 94.9% ± 4.5, but it was required to increase the DTT and Genapol concentration and to decrease the percentage of IPG buffer to maximize the protein detection in gels. In these conditions, 580 spots were detected in 2DE gels, showing a 2.4-fold improvement over the standard conditions of the experimental design. Our results clearly indicate that it is crucial to combine appropriate amounts of chaotropes, detergents, ampholytes, and reducing reagents to improve protein extraction and detection and to obtain well-resolved gels. Beyond the complexity of maintaining protein solubility in IEF, it must be kept in mind that physical parameters have a relevant role and should be recorded and controlled during the experimental procedure. Finally, when working with biological fluids, it is important to reduce sample complexity before 2DE analysis to facilitate the access to the low-abundant proteins, and to increase the proteome coverage. Besides obtaining optimal conditions for the extraction and analysis of vitreous proteins by 2DE, the ANN is helpful to understand how different parameters can affect the visual aspect of gels and resolution of protein spots. This experimental design and model can be adapted to other types of samples, depending on the characteristics of proteins to be solubilized and the parameters that influence its solubilization.

Funding information This project was supported by the University of Beira Interior—Health Sciences Research Centre (CICS). Santos FM received a fellowship (CENTRO-07-ST24-FEDER-002014) and a doctoral fellowship (SFRH/BD/112526/2015) from FCT. Gaspar LM received a fellowship from Novartis Farma-Produtos Farmacêuticos, SA. This work is supported by FEDER funds through the POCI—COMPETE 2020—Operational Programme Competitiveness and Internationalisation in Axis I—Strengthening research, technological development and innovation Project (POCI-01-0145-FEDER-007491) and National Funds by FCT—Foundation for Science and Technology Project (UID/Multi/00709/2013). This work was also supported by the Applied Molecular Biosciences Unit- UCIBIO which is financed by national funds from FCT/MCTES (UID/Multi/04378/2019). CNB-CSIC proteomics lab is a member of Proteored, PRB2-ISCIII and is supported by grant PT13/0001, of the PE I +D+i 2013–2016, funded by ISCIII and FEDER.

Compliance with ethical standards

Conflict of interest The authors declare that they have no conflict of interest.

Research involving human participants and/or animals The protocol for sample collection was approved by the Ethics Committee of Leiria-Pombal Hospital, Portugal (Code: CHL-15481). An informed consent from all patients was obtained in agreement with the Declaration of Helsinki.

References

1. Semba RD, Enghild JJ, Venkatraman V, Dyrlund TF, Van Eyk JE. The Human Eye Proteome Project: perspectives on an emerging proteome. Proteomics. 2013;13:2500–11.
2. Jay NL, Gillies M. Proteomic analysis of ophthalmic disease. Clin Exp Ophthalmol. 2012;40:755–63. https://doi.org/10.1111/j.1442-9071.2012.02788.x.
3. Rocha AS, Santos FM, Monteiro JP, Castro-de-Sousa JP, Queiroz JA, Tomaz CT, et al. Trends in proteomic analysis of human vitreous humor samples. Electrophoresis. 2014;35:2495–508. https://doi.org/10.1002/elps.201400049.
4. Monteiro JP, Santos FM, Rocha AS, Castro-de-Sousa JP, Queiroz JA, Passarinha LA, et al. Vitreous humor in the pathologic scope: insights from proteomic approaches. PROTEOMICS Clin Appl. 2015;9:187–202. https://doi.org/10.1002/prca.201400133.
5. Mahajan VB, Skeie JM. Translational vitreous proteomics. Proteomics Clin Appl. 2014;8:204–8. https://doi.org/10.1002/prca.201300062.
6. Sang JK, Kim S, Park J, Hong KL, Kyong SP, Hyeong GY, et al. Differential expression of vitreous proteins in proliferative diabetic retinopathy. Curr Eye Res. 2006;31:231–40. https://doi.org/10.1080/02713680600557030.
7. Nakanishi T, Koyama R, Ikeda T, Shimizu A. Catalogue of soluble proteins in the human vitreous humor: comparison between diabetic retinopathy and macular hole. J Chromatogr B Anal Technol Biomed Life Sci. 2002;776:89–100. https://doi.org/10.1016/S1570-0232(02)00078-8.
8. Koss MJ, Hoffmann J, Nguyen N, Pfister M, Mischak H, Mullen W, et al. Proteomics of vitreous humor of patients with exudative

age-related macular degeneration. PLoS One. 2014;9:1–11. https://doi.org/10.1371/journal.pone.0096895.
9. Loukovaara S, Nurkkala H, Tamene F, Gucciardo E, Liu X, Repo P, et al. Quantitative proteomics analysis of vitreous humor from diabetic retinopathy patients. J Proteome Res. 2015;14:5131–43. https://doi.org/10.1021/acs.jproteome.5b00900.
10. Santos FM, Gaspar LM, Ciordia S, Rocha AS, Castro e Sousa J, Paradela A, et al. iTRAQ quantitative proteomic analysis of vitreous from patients with retinal detachment. Int J Mol Sci. 2018;19:1157. https://doi.org/10.3390/ijms19041157.
11. Öhman T, Tamene F, Göös H, Loukovaara S, Varjosalo M. Systems pathology analysis identifies neurodegenerative nature of age-related vitreoretinal interface diseases. Aging Cell. 2018;17. https://doi.org/10.1111/acel.12809.
12. Shitama T, Hayashi H, Noge S, Uchio E, Oshima K, Haniu H, et al. Proteome profiling of vitreoretinal diseases by cluster analysis. Proteomics Clin Appl. 2008;2:1265–80. https://doi.org/10.1002/prca.200800017.
13. Yamane K, Minamoto A, Yamashita H, Takamura H, Miyamoto-Myoken Y, Yoshizato K, et al. Proteome analysis of human vitreous proteins. Mol Cell Proteomics. 2003;2:1177–87. https://doi.org/10.1074/mcp.M300038-MCP200.
14. Kim T, Sang JK, Kim K, Kang UB, Lee C, Kyong SP, et al. Profiling of vitreous proteomes from proliferative diabetic retinopathy and nondiabetic patients. Proteomics. 2007;7:4203–15. https://doi.org/10.1002/pmic.200700745.
15. Neal RE, Bettelheim FA, Lin C, Winn KC, Garland DL, Zigler JS. Alterations in human vitreous humour following cataract extraction. Exp Eye Res. 2005;80:337–47. https://doi.org/10.1016/j.exer.2004.09.015.
16. Sugioka K, Saito A, Kusaka S, Kuniyoshi K, Shimomura Y. Identification of vitreous proteins in retinopathy of prematurity. Biochem Biophys Res Commun. 2017;488:483–8. https://doi.org/10.1016/j.bbrc.2017.05.067.
17. Gao B-B, Chen X, Timothy N, Aiello LP, Feener EP. Characterization of the vitreous proteome in diabetes without diabetic retinopathy and diabetes with proliferative diabetic retinopathy. J Proteome Res. 2008;7:2516–25. https://doi.org/10.1021/pr800112g.
18. Gaspar LM, Santos FM, Albuquerque T, Castro-de-Sousa JP, Passarinha LA, Tomaz CT. Proteome analysis of vitreous humor in retinal detachment using two different flow-charts for protein fractionation. J Chromatogr B Anal Technol Biomed Life Sci. 2017;1061–1062:334–41. https://doi.org/10.1016/j.jchromb.2017.07.049.
19. Reich M, Dacheva I, Siwy J, Mullen W, Schanstra JP, Choi CY, et al. Proteomics of vitreous in neovascular age-related macular degeneration. Exp Eye Res. 2016;146:107–17. https://doi.org/10.1016/j.exer.2016.01.001.
20. Rogowska-Wrzesinska A, Le Bihan MC, Thaysen-Andersen M, Roepstorff P. 2D gels still have a niche in proteomics. J Proteome. 2013;88:4–13. https://doi.org/10.1016/j.jprot.2013.01.010.
21. Oliveira BM, Coorssen JR, Martins-de-Souza D. 2DE: the phoenix of proteomics. J Proteome. 2014;104:140–50. https://doi.org/10.1016/j.jprot.2014.03.035.
22. Gauci V, Wright E, Coorssen J. Quantitative proteomics: assessing the spectrum of in-gel protein detection methods. J Chem Biol. 2011;4:3–29. https://doi.org/10.1007/s12154-010-0043-5.
23. Magdeldin S, Enany S, Yoshida Y, Xu B, Zhang Y, Zureena Z, et al. Basics and recent advances of two dimensional- polyacrylamide gel electrophoresis. Clin Proteomics. 2014;11:16. https://doi.org/10.1186/1559-0275-11-16.
24. Valente KN, Choe LH, Lenhoff AM, Lee KH. Optimization of protein sample preparation for two-dimensional electrophoresis. Electrophoresis. 2012;33:1947–57. https://doi.org/10.1002/elps.201100659.
25. Chen CPC, Hsu CC, Yeh WL, Lin HC, Hsieh SY, Lin SC, et al. Optimizing human synovial fluid preparation for two-dimensional gel electrophoresis. Proteome Sci. 2011;9. https://doi.org/10.1186/1477-5956-9-65.
26. Saraygord-Afshari N, Naderi-Manesh H, Naderi M. Increasing proteome coverage for gel-based human tear proteome maps: towards a more comprehensive profiling. Biomed Chromatogr. 2015;29:1056–67. https://doi.org/10.1002/bmc.3392.
27. Westermeier R. Looking at proteins from two dimensions: a review on five decades of 2D electrophoresis. Arch Physiol Biochem. 2014;120:168–72. https://doi.org/10.3109/13813455.2014.945188.
28. López JL. Two-dimensional electrophoresis in proteome expression analysis. J Chromatogr B Anal Technol Biomed Life Sci. 2007;849:190–202. https://doi.org/10.1016/j.jchromb.2006.11.049.
29. Rabilloud T, Lelong C. Two-dimensional gel electrophoresis in proteomics: a tutorial. J Proteome. 2011;74:1829–41. https://doi.org/10.1016/j.jprot.2011.05.040.
30. Guo C-G, Li S, Wang H-Y, Zhang D, Li G-Q, Zhang J, et al. Study on stability mechanism of immobilized pH gradient in isoelectric focusing via the Svensson–Tiselius differential equation and moving reaction boundary. Talanta. 2013;111:20–7. https://doi.org/10.1016/J.TALANTA.2013.03.026.
31. Cao C-X. Moving chemical reaction boundary and isoelectric focusing I. Conditional equations for Svensson-Tiselius' differential equation of solute concentration distribution in idealized isoelectric focusing at steady state. 1998.
32. Slibinskas R, Ražanskas R, Zinkevičiute R, Čiplys E. Comparison of first dimension IPG and NEPHGE techniques in two-dimensional gel electrophoresis experiment with cytosolic unfolded protein response in Saccharomyces cerevisiae. Proteome Sci. 2013;11. https://doi.org/10.1186/1477-5956-11-36.
33. Hanneken M, Šlais K, König S. pI-Control in comparative fluorescence gel electrophoresis (CoFGE) using amphoteric azo dyes. EuPA Open Proteomics. 2015;8:36–9. https://doi.org/10.1016/j.euprot.2015.03.003.
34. Guo C-G, Shang Z, Yan J, Li S, Li G-Q, Liu R-Z, et al. A tunable isoelectric focusing via moving reaction boundary for two-dimensional gel electrophoresis and proteomics. Talanta. 2015;137:197–203. https://doi.org/10.1016/J.TALANTA.2015.01.038.
35. Moche M, Albrecht D, Maaß S, Hecker M, Westermeier R, Büttner K. The new horizon in 2D electrophoresis: new technology to increase resolution and sensitivity. Electrophoresis. 2013;34:1510–8. https://doi.org/10.1002/elps.201200618.
36. Hanneken M, König S. Horizontal comparative fluorescence two-dimensional gel electrophoresis for improved spot coordinate detection. Electrophoresis. 2014;35:1118–21. https://doi.org/10.1002/elps.201300507.
37. Khan J, Wei JS, Ringnér M, Saal LH, Ladanyi M, Westermann F, et al. Classification and diagnostic prediction of cancers using gene expression profiling and artificial neural networks. Nat Med. 2001;7:673–9. https://doi.org/10.1038/89044.
38. Lancashire LJ, Lemetre C, Ball GR. An introduction to artificial neural networks in bioinformatics - application to complex microarray and mass spectrometry datasets in cancer studies. Brief Bioinform. 2009;10:315–29. https://doi.org/10.1093/bib/bbp012.
39. Candiano G, Bruschi M, Musante L, Santucci L, Ghiggeri GM, Carnemolla B, et al. Blue silver: a very sensitive colloidal Coomassie G-250 staining for proteome analysis. Electrophoresis. 2004;25:1327–33. https://doi.org/10.1002/elps.200305844.
40. Patel N, Solanki E, Picciani R, Cavett V, Caldwell-Busby JA, Bhattacharya SK. Strategies to recover proteins from ocular tissues for proteomics. Proteomics. 2008;8:1055–70. https://doi.org/10.1002/pmic.200700856.

41. Görg A, Postel W, Friedrich C, Kuick R, Strahler JR, Hanash SM. Temperature-dependent spot positional variability in two-dimensional polypeptide patterns. Electrophoresis. 1991;12:653–8. https://doi.org/10.1002/elps.1150120910.
42. Nor NM, Mohamed MS, Loh TC, Foo HL, Rahim RA, Tan JS, et al. Comparative analyses on medium optimization using one-factor-at-a-time , response surface methodology, and artificial neural network for lysine–methionine biosynthesis by Pediococcus pentosaceus RF-1. Biotechnol Biotechnol Equip. 2017;31:935–47. https://doi.org/10.1080/13102818.2017.1335177.
43. Pedro AQ, Martins LM, Dias JML, Bonifácio MJ, Queiroz JA, Passarinha LA. An artificial neural network for membrane-bound catechol-O-methyltransferase biosynthesis with Pichia pastoris methanol-induced cultures. Microb Cell Factories. 2015;14:113. https://doi.org/10.1186/s12934-015-0304-7.
44. Brown SR, Staff M, Lee R, Love J, Parker DA, Aves SJ, et al. Design of experiments methodology to build a multifactorial statistical model describing the metabolic interactions of alcohol dehydrogenase isozymes in the ethanol biosynthetic pathway of the yeast Saccharomyces cerevisiae. ACS Synth Biol. 2018;7:1676–84. https://doi.org/10.1021/acssynbio.8b00112.
45. Padula M, Berry I, O'Rourke M, Raymond B, Santos J, Djordjevic SP. A comprehensive guide for performing sample preparation and top-down protein analysis. Proteomes. 2017;5:11. https://doi.org/10.3390/proteomes5020011.
46. Görg A, Boguth G, Obermaier C, Posch A, Weiss W. Two-dimensional polyacrylamide gel electrophoresis with immobilized pH gradients in the first dimension (IPG-Dalt): the state of the art and the controversy of vertical versus horizontal systems. Electrophoresis. 1995;16:1079–86.

Section 2 – Paper IV

iTRAQ Quantitative Proteomic Analysis of Vitreous from Patients with Retinal Detachment

Fátima M. Santos, Leonor M.Gaspar, Sergio Ciordia, Ana S. Rocha 1,2, João Paulo Castro e Sousa, Alberto Paradela, Luís A. Passarinha, Cândida Teixeira Tomaz

International Journal of Molecular Sciences, 19 (4): 1–22, April 2018.
(DOI: 10.3390/ijms19041157)

In this paper, vitreous samples collected from patients with RRD were compared with MEM using iTRAQ-based quantitative analysis. As a result, 1030 proteins were identified, of those a total of 150 proteins were found differentially expressed in the vitreous of patients with RRD, including 96 overexpressed and 54 underexpressed. The accumulation of photoreceptor proteins, including phosducin, rhodopsin, and s-arrestin, and vimentin in vitreous may indicate that photoreceptor degeneration occurs in RRD. Nevertheless, the proteins found differentially expressed in RRD suggest that different protective mechanisms (e.g. HIF-1 signaling pathway) are activated after RRD to promote the survival of retinal cells through complex cellular responses.

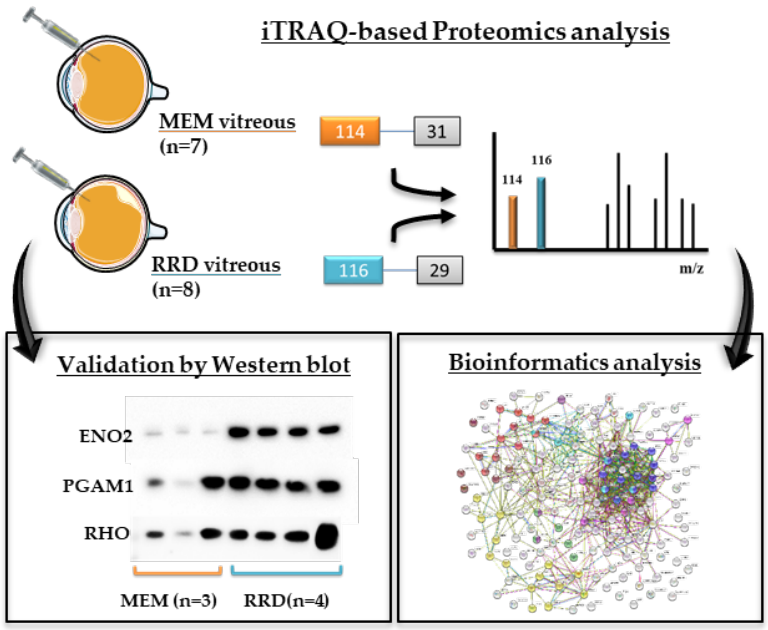

The supplementary material of this article is available in (https://www.mdpi.com/1422-0067/19/4/1157/s1) and in the Appendix.

International Journal of
Molecular Sciences

MDPI

Article

iTRAQ Quantitative Proteomic Analysis of Vitreous from Patients with Retinal Detachment

Fátima Milhano Santos [1,2,3], Leonor Mesquita Gaspar [1,2], Sergio Ciordia [4], Ana Sílvia Rocha [1,2], João Paulo Castro e Sousa [1,5], Alberto Paradela [4], Luís António Passarinha [1,3] and Cândida Teixeira Tomaz [1,2,*]

1 CICS-UBI—Health Sciences Research Centre, University of Beira Interior, 6201-506 Covilhã, Portugal; ftxsantos@gmail.com (F.M.S.); leonormgaspar@gmail.com (L.M.G.); asilviarocha@gmail.com (A.S.R.); jpcastrosousa@netcabo.pt (J.P.C.e.S.); lpassarinha@fcsaude.ubi.pt (L.A.P.)
2 Chemistry Department, Faculty of Sciences, University of Beira Interior, 6201-001 Covilhã, Portugal
3 Laboratory of Pharmacology and Toxicology—UBIMedical, University of Beira Interior, 6200-284 Covilhã, Portugal
4 Unidad de Proteomica, Centro Nacional de Biotecnología, CSIC, Calle Darwin 3, Campus de Cantoblanco, 28049 Madrid, Spain; sciordia@cnb.csic.es (S.C.); Alberto.Paradela@cnb.csic.es (A.P.)
5 Hospital Center Leiria-Pombal, 3100-462 Pombal, Portugal
* Correspondence: ctomaz@ubi.pt; Tel.: +351-275-242-021

Received: 8 February 2018; Accepted: 8 April 2018; Published: 11 April 2018

Abstract: Rhegmatogenous retinal detachment (RRD) is a potentially blinding condition characterized by a physical separation between neurosensory retina and retinal pigment epithelium. Quantitative proteomics can help to understand the changes that occur at the cellular level during RRD, providing additional information about the molecular mechanisms underlying its pathogenesis. In the present study, iTRAQ labeling was combined with two-dimensional LC-ESI-MS/MS to find expression changes in the proteome of vitreous from patients with RRD when compared to control samples. A total of 150 proteins were found differentially expressed in the vitreous of patients with RRD, including 96 overexpressed and 54 underexpressed. Several overexpressed proteins, several such as glycolytic enzymes (fructose-bisphosphate aldolase A, gamma-enolase, and phosphoglycerate kinase 1), glucose transporters (GLUT-1), growth factors (metalloproteinase inhibitor 1), and serine protease inhibitors (plasminogen activator inhibitor 1) are regulated by HIF-1, which suggests that HIF-1 signaling pathway can be triggered in response to RRD. Also, the accumulation of photoreceptor proteins, including phosducin, rhodopsin, and s-arrestin, and vimentin in vitreous may indicate that photoreceptor degeneration occurs in RRD. Also, the accumulation of photoreceptor proteins, including phosducin, rhodopsin, and s-arrestin, and vimentin in vitreous may indicate that photoreceptor degeneration occurs in RRD. Nevertheless, the differentially expressed proteins found in this study suggest that different mechanisms are activated after RRD to promote the survival of retinal cells through complex cellular responses.

Keywords: iTRAQ; quantitative proteomics; retinal detachment; vitreous proteome

1. Introduction

Retinal Detachment (RD) is a potentially blinding disease characterized by a physical separation between the neurosensory retina (NSR) and the underlying retinal pigment epithelium (RPE) [1,2]. Modifications in adhesion between the NSR and RPE and the degradation of interphotoreceptor matrix glue can be involved in the onset of RD [3,4]. Risk factors such as age, the level of oxygenation, and other ocular diseases (e.g., myopia, vitreoretinal degeneration) contribute to reducing the retinal adhesion, and therefore to the development of RD [3–5]. The most common type of RD

is rhegmatogenous, with an incidence of 6.3–17.9 per 100,000 people per year. Its pathogenesis is manifested by the presence of a full-thickness retinal break [1,4,6]. Rhegmatogenous retinal detachment (RRD) may be triggered by vitreous syneresis, a liquefaction of gel caused by age or by trauma, which reduces the vitreoretinal adhesion and results in deflation and relaxation of the collagen network and in the accumulation of vitreous fluid in subretinal space [3,4,7]. Subsequently, vitreous falls upon itself causing the physical separation between the NSR and the RPE of the retina, leading to severe and permanent loss of vision [4,5,7].

The treatment of RD has dramatically improved over the past decades. Surgical procedures including scleral buckling, pars plana vitrectomy, and pneumatic retinopexy have been successfully used for the treatment of RRD, with primary success rates of up to 90% [6,8,9]. However, when RRD is associated with macular detachment, choroidal detachment (RRDCD) or PVR, the patients experience poor visual recovery and low reattachment rates [10,11]. Besides the structural changes that occur in the retina, the complex biomolecular mechanisms that are activated following RRD can also play an important role in its pathogenesis. As matter of fact, numerous cytokines, and pro-inflammatory and growth factors are released in vitreous after RD. It was proposed that these molecules have a relevant role in the reparative wound-healing process and retinal photoreceptor apoptosis in RRD, and consequently, may improve the post-surgical visual outcomes [12]. Also, the proteome and biochemical properties of vitreous are directly affected by physiological and pathological conditions of the retina [13–15]. So, vitreous is a suitable matrix for studying the pathophysiological mechanisms in the RRD.

Quantitative proteomics provides an additional approach to understand the global proteomic dynamics by identifying and comparing quantitatively several proteins in ocular fluids [16,17]. Although the application of proteomics technology in ophthalmic research is becoming increasingly common [15,18,19], the published information about vitreous proteome in RD is scarce. Indeed, the majority of these studies are focused on PVR [14,20–22] with the application of different proteomic techniques. In the current study, isobaric tags for relative and absolute quantitation (iTRAQ) labeling was combined with two-dimensional LC-ESI-MS/MS (2DE-LC-MS/MS) to find expression changes in the proteome of vitreous from patients with RRD when compared to macular epiretinal membranes (MEM). This work was focused in RRD, the most common but less severe type of RD, in order to understand the complex biological processes that are activated after RD.

2. Results

2.1. Characterization of Patients and Vitreous Samples

Demographic and clinical characteristics of patients enrolled in the study and the description of the corresponding vitreous samples are summarized in Table 1. The study groups consisted of 15 patients, 9 women, and 6 men, with ages comprised between 52 and 84 years. The RRD group included 8 patients and the control group was composed of 7 patients with MEM. From these, 8 patients were selected for the analysis of the differentially expressed proteins using iTRAQ-based analysis. Specifically, vitreous collected from 4 patients (1 male, 3 females) with RRD were analyzed and compared to the vitreous collected from 4 patients (2 males, 2 females) with MEM. In the RRD group, the 4 patients had macula-off RRD, with an extension of detachment of 2 (n = 2), 3 (n = 1) and 4 (n = 1) quadrants. Seven patients were selected for the validation of protein biomarkers by Western blotting (WB), 4 with RRD (2 males, 2 females) and 3 with MEM (1 male, 2 females). From these patients, 3 had macula-in RRD and 1 macula-off RRD, with an extension of detachment of 1 (n = 3) and 3 (n = 1) quadrants. Both groups were similar in age and gender, but the patients with RRD had a lower median age, 64 ± 7 years, compared to a median of 76 ± 5 from the patients of the control group. The protein concentration was slightly higher in vitreous from patients with RRD, averaging 3.12 ± 2.96 μg/μL, than in MEM group, with average concentrations of 2.66 ± 1.63 μg/μL. In patients with RRD, the total

protein concentration in vitreous increases with the extension of RD (number of quadrants) and in the macula-off RRD.

Table 1. Demographic and clinical characteristics of patients involved in the study and description of corresponding vitreous samples collected via pars plana vitrectomy.

Demographic and Clinical Characteristics		RRD [1] (n = 8)	MEM [1] (n = 7)
Demographic characteristics of patients	Gender [2]	M = 3; F = 5	M = 3; F = 4
	Age (MD ± SD)	64 ± 7	76 ± 5
	Age (range)	52–69	69–84
	Eye Submitted to PPV [3]	LE = 3; RE = 5	LE = 5; RE = 2
Characterization of retinal detachment	Macula-off/Macula-in	5/3	
	Extent of retinal detachment (n/n_{total}) [4]		
	1 quadrant	3/8	
	2 quadrants	2/8	
	3 quadrants	2/8	
	4 quadrants	1/8	
	Multiple detachments (n/n_{total}) [4]	4/8	
Characterization of vitreous samples	Protein concentration (µg/µL, MD ± SD)	3.12 ± 2.96	2.66 ± 1.63
	iTRAQ label	116 (n = 4)	114 (n = 4)
	Validation by Western blotting	n = 4	n = 3

[1] RRD: Rhegmatogenous retinal detachment; MEM: Macular epiretinal membranes; [2] F: Female; M: Male; [3] PPV: Pars plana vitrectomy; RE: right eye; LE: left eye; [4] Number of samples/number total of samples.

2.2. Vitreous Proteome in Rhegmatogenous Retinal Detachment (RRD)

By combining iTRAQ labeling with 2D-nano-LC-MS/MS, 1030 proteins were identified with 6078 peptides, of which 2613 correspond to unique peptides (Supplementary Table S1). To recognize which proteins were newly found in the present study, the identified proteins were compared to previous vitreous proteomics reports [19,23–35], as seen in Supplementary Table S2.

From the identified proteins, 150 were found differentially expressed in RRD versus MEM, including 96 overexpressed and 54 underexpressed (Supplementary Table S3). In literature, iTRAQ ratios >1.2 (overexpressed) or <0.82 (underexpressed), with a p-value < 0.01, were considered significant fold changes in terms of protein expression [20]. In this study, iTRAQ ratios between 221.22 and 2.06 were reported for the overexpressed proteins, and iTRAQ ratios between 0.00 and 0.52 were reported for the underexpressed, with p-values below 0.01 (Supplementary Table S3). As shown in Table 2, some plasma proteins were significantly decreased in RRD, including retinol-binding protein 4 (RBP4) and apolipoprotein A-IV (APOA4). Proteins displaying highest overexpression include photoreceptor proteins, such as phosducin (PDC), rhodopsin (RHO), and s-arrestin (SAG).

Table 2. List of proteins found differentially expressed in vitreous of patients with rhegmatogenous retinal detachment (RRD) in comparison with macular epiretinal membranes (MEM), with FDR ≈ 0.

Accession	Description	Gene	Score	Number of Peptides (Total/Unique)	Coverage	RRD/MEM Ratio [1]
P06727	Apolipoprotein A-IV	APOA4	2834	119/3	49.7	0.002 ***
P02753	Retinol-binding protein 4	RBP4	222	10/1	10.4	0.003 ***
O95447	Lebercilin-like protein	LCA5L	25	2/0	2.2	0.003 ***
P50213	Isocitrate dehydrogenase [NAD] subunit alpha, mitochondrial	IDH3A	35	2/0	2.7	0.004 ***
Q96BN8	Ubiquitin thioesterase otulin	FAM105B	28	2/0	2.0	0.005 ***
Q8NBP7	Proprotein convertase subtilisin/kexin type 9	PCSK9	32	2/0	3.2	0.038 ***
P01011	Alpha-1-antichymotrypsin	SERPINA3	1786	63/2	23.4	0.040 ***
P02748	Complement component C9	C9	1126	47/3	13.4	0.058 ***
P02655	Apolipoprotein C-II	APOC2	214	6/2	20.4	0.110 ***
P02656	Apolipoprotein C-III	APOC3	319	10/1	26.3	0.139 ***
Q9HAZ2	PR domain zinc finger protein 16	PRDM16	28	2/0	0.5	0.162 ***
P43652	Afamin	AFM	1336	45/7	13.2	0.162 ***
P02750	Leucine-rich alpha-2-glycoprotein	LRG1	1108	39/5	24.6	0.177 ***
Q6UXB8	Peptidase inhibitor 16	PI16	234	11/3	4.7	0.211 ***
P13646	Keratin, type I cytoskeletal 13	KRT13	440	12/5	16.0	0.230 ***
P35542	Serum amyloid A-4 protein	SAA4	129	4/1	13.9	0.241 ***
Q15166	Serum paraoxonase/lactonase 3	PON3	109	5/0	4.5	0.255 ***
P20941	Phosducin	PDC	47	2/0	5.3	221.22 ***
P14550	Alcohol dehydrogenase [NADP(+)]	AKR1A1	67	2/2	11.1	173.64 ***
P08100	Rhodopsin	RHO	432	15/1	11.1	23.646 ***
P10523	S-arrestin	SAG	1469	56/5	30.5	16.032 ***
P18545	Retinal rod rhodopsin-sensitive cGMP 3,5-cyclic phosphodiesterase subunit gamma	PDE6G	32	2/0	10.3	15.606 ***
P11488	Guanine nucleotide-binding protein G(t) subunit alpha-1	GNAT1	62	2/0	4.3	15.144 ***
Q9UHI8	A disintegrin and metalloproteinase with thrombospondin motifs 1	ADAMTS1	188	4/1	2.2	14.086 ***
O00560	Syntenin-1	SDCBP	496	19/1	20.1	14.012 ***
P11166	Solute carrier family 2, facilitated glucose transporter member 1	SLC2A1	49	3/1	5.1	13.116 ***
Q17R60	Interphotoreceptor matrix proteoglycan 1	IMPG1	1108	35/8	9.5	11.116 ***
O43490	Prominin-1	PROM1	304	11/5	5.4	10.761 ***
P69905	Hemoglobin subunit alpha	HBA1	417	14/3	24.1	10.528 ***
P51674	Neuronal membrane glycoprotein M6-a	GPM6A	133	4/2	7.6	9.061 ***
P62873	Guanine nucleotide-binding protein G(I)/G(S)/G(T) subunit beta-1	GNB1	332	13/6	11.2	8.579 ***
P12277	Creatine kinase B-type	CKB	415	12/5	12.7	8.576 ***
Q9BZV3	Interphotoreceptor matrix proteoglycan 2	IMPG2	302	15/1	4.0	8.451 ***
P16499	Rod cGMP-specific 3′,5′-cyclic phosphodiesterase subunit alpha	PDE6A	243	11/5	2.8	8.274 ***
P43320	Beta-crystallin B2	CRYBB2	775	26/4	37.4	7.078 ***
P62979	Ubiquitin-40S ribosomal protein S27a	RPS27A	247	5/1	10.3	6.897 ***

Table 2. *Cont.*

Accession	Description	Gene	Score	Number of Peptides (Total/Unique)	Coverage	RRD/MEM Ratio [1]
P68871	Hemoglobin subunit beta	HBB	343	13/1	32.3	6.812 ***
P09104	Gamma-enolase	ENO2	720	24/0	14.4	6.478 ***
P02489	Alpha-crystallin A chain	CRYAA	122	5/1	27.7	6.345 ***
P31025	Lipocalin-1	LCN1	192	7/1	16.1	6.178 ***
P07900	Heat shock protein HSP 90-alpha	HSP90AA1	414	12/3	5.6	6.171 ***
P02511	Alpha-crystallin B chain	CRYAB	108	3/1	22.3	5.648 ***
P02042	Hemoglobin subunit delta	HBD	173	7/2	23.8	5.595 ***
P09467	Fructose-1,6-bisphosphatase 1	FBP1	55	3/1	4.7	5.308 ***
P63104	14-3-3 protein zeta/delta	YWHAZ	455	11/6	10.5	5.127 ***
Q12931	Heat shock protein 75 kDa, mitochondrial	TRAP1	87	3/0	2.0	5.027 ***
P18669	Phosphoglycerate mutase 1	PGAM1	310	12/5	16.6	4.998 ***
P09455	Retinol-binding protein 1	RBP1	50	2/0	8.9	4.680 ***
P36222	Chitinase-3-like protein 1	CHI3L1	1472	55/5	27.1	4.635 ***
Q06830	Peroxiredoxin-1	PRDX1	234	9/3	8.8	4.531 ***
P37837	Transaldolase	TALDO1	116	5/3	10.4	4.388 ***
P09972	Fructose-bisphosphate aldolase C	ALDOC	818	28/6	24.3	4.286 ***
P31949	Protein S100-A11	S100A11	38	2/0	8.6	4.258 ***

[1] Fold changes >1 are considered for overexpressed proteins and <1 for underexpressed proteins with significant differences (*** p-value < 0.0001) between RRD and MEM.

The 150 proteins found differentially expressed in vitreous of RRD compared to MEM were classified according to the related GO (Gene Ontology) terms for biological process, molecular function and cellular component, using STRAP (Software Tool for Rapid Annotation of Proteins), as seen in Figure 1 and in Supplementary Table S4. According to STRAP classification for biological processes (Figure 1), the differentially expressed proteins in RRD vitreous were related to regulation (n = 116) or cellular processes (n = 109). Biological processes, such as signal transduction, apoptosis, cell proliferation, gene expression, and/or RHO mediated signaling pathway were primarily regulated by the proteins found overexpressed in RRD. The regulation of complement activation was found to be mediated by proteins underexpressed in RRD. Regarding cellular processes, various proteins (19 overexpressed, 2 underexpressed) were involved in neutrophil degranulation. A significant part of differentially expressed proteins also participates in metabolic processes, such as gluconeogenesis or proteolysis. Regarding the analysis of molecular function (Figure 1), both overexpressed and underexpressed proteins were mainly binding proteins (n = 117) or/and with catalytic activity (n = 56). Moreover, many of the differentially expressed proteins in RRD were extracellular matrix structural constituents, and a significant part of overexpressed proteins were identified as structural constituents of the eye lens. The categorization according to cellular component (Figure 1) showed that these proteins were largely found in extracellular space (n = 129) and are classified as extracellular matrix components (n = 21) or as blood particles (n = 25). On the other hand, differentially expressed proteins were also localized intracellularly, namely in the cytoplasm (n = 65), nucleus (n = 49), plasma membrane (n = 47), and in other intracellular organelles (n = 58).

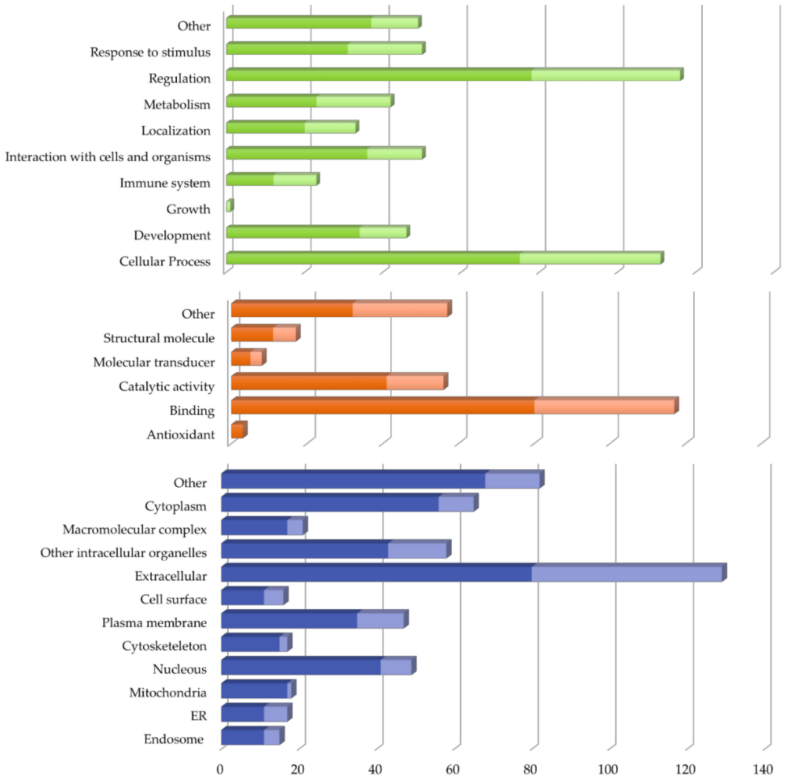

Figure 1. Classification of the 150 proteins found differentially expressed in vitreous of patients with rhegmatogenous retinal detachment in comparison with macular epiretinal membranes samples according to Gene Ontology (GO) terms using STRAP 1.5. GO annotation for biological process, molecular function, and cellular component are represented by green, orange, and blue bars, respectively.

Further analyses were made by STRING database (Search Tool for the Retrieval of Interacting Genes/Proteins) to generate an overall protein-protein interaction network (PPI) based on interaction evidence, with high confidence (0.70). The network is enriched in 231 interactions between the 150 proteins found differentially expressed in RRD, with a PPI enrichment p-value $< 1.0 \times 10^{-16}$. The PPI network was grouped into 11 relevant protein clusters using the Markov Cluster Algorithm (MCL) clustering option provided by STRING, as shown in Figure 2 and Supplementary Table S4. Many of the clusters share interactions among them, indicating that these molecules play key roles in diverse pathways. To infer the functional associations, the clusters were classified according to Reactome and Kyoto encyclopedia of genes and genomes (KEGG) (Supplementary Table S4).

Cluster 1 (red) is the larger and is associated with carbon metabolism (glycolysis/gluconeogenesis and pentose phosphate pathway), biosynthesis of amino acids, and transcriptional regulator hypoxia-inducible factor-1 (HIF-1) signaling pathway. Carbon metabolism proteins were found overexpressed in this study, including isomerases (TPI1, GPI), aldolases (TALDO1, ALDOA, ALDOC), and other proteins, such as AKR1A1, phosphoglycerate mutase 1 (PGAM1), fructose-1,6-bisphosphatase 1 (FBP1), and phosphoglycerate kinase 1 (PGK1). Glycolytic enzymes (ALDOA, ENO2, and PGK1), metalloproteinase inhibitor 1 (TIMP1), and plasminogen activator inhibitor 1 (SERPINE1) are related to HIF-1 signaling pathway.

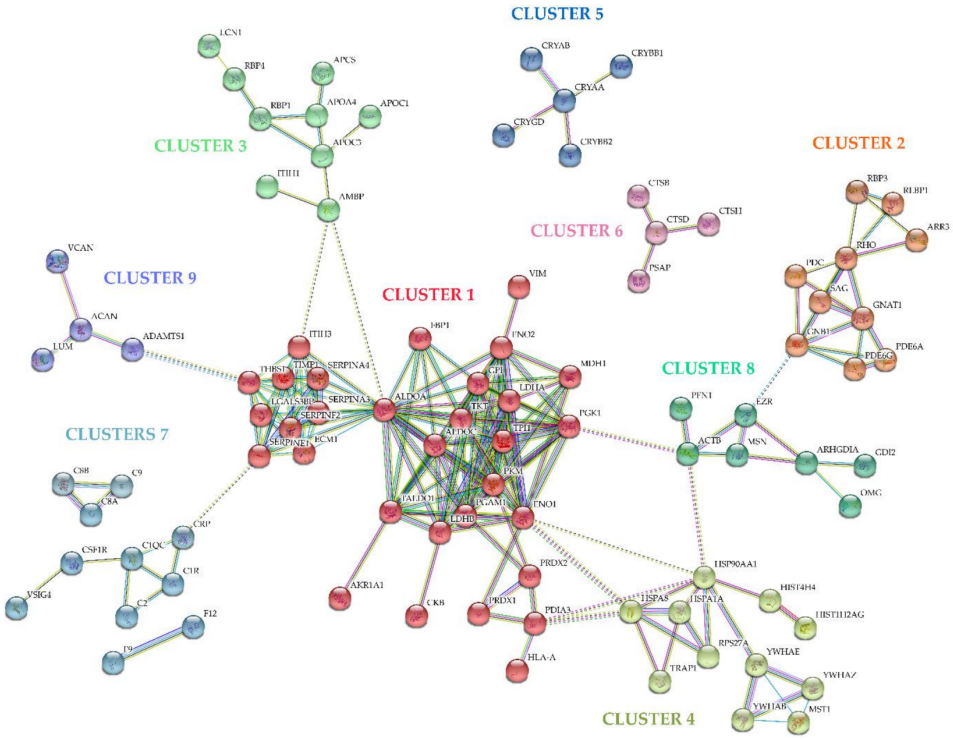

Figure 2. Protein-protein interaction network of the proteins found differentially expressed in RRD, based on interaction evidence, predicted using STRING 10. The protein-protein interaction network (PPI) network was grouped into 11 relevant protein clusters using the ECM clustering option provided by STRING.

Cluster 2 (orange) represents proteins specifically involved in phototransduction, including PDC, RHO, SAG, retinaldehyde-binding protein 1 (RLBP1), retinal phosphodiesterase subunits (PDE6A, PDE6G) and transducin subunits (GNAT1, GNB1). It is important to evidence that high levels of these specific proteins were found in RRD, with iTRAQ ratios between 3.45 and 221.22. Likewise, other

proteins essential for eye function can be found in other clusters. In cluster 3 (light green), in which are included plasma apolipoproteins (APOA4, APOC2, APOC3), the only overexpressed proteins are retinol-binding proteins (RBP1, RBP3) and retinaldehyde-binding protein 1 (RLBP1), related to retinoid metabolism and transport, and consequently, to phototransduction. The custer 5 (dark cyan) is composed of the structural components of the lens, alpha-crystallins (CRYAA, CRYAB), and beta-crystallins (CRYBB1, CRYBB2), also overexpressed in RRD.

The Cluster 4 interactions (olive) showed a significant enrichment to PI3K-Akt signaling pathway, Hippo signaling pathway, and HSF1 activation. So, upregulated proteins such as heat shock proteins (HSPA1A, HSP90AA1, and TRAP1), 14-3-3 proteins (YWHAE, YWHAB, and YWHAZ), and Ubiquitin-40S ribosomal protein S27a (RPS27A) are related to cellular responses to heat stress and the regulation of apoptotic signaling. Cathepsins (CTSB, CTSD, and CTSH) and prosaposin (PSAP) are lysosomal enzymes, grouped into cluster 6 (pink), and found overexpressed in RRD vitreous proteome when compared with MEM samples. Proteins involved in complement and coagulation cascades pathways and defense response were grouped into three clusters, denominated clusters 7, colored with cyan. Complement components (C1R, C2, C8A, C8B, C9), coagulation factors (F9, F12), and C-reactive protein (CRP) were found underexpressed in RRD but macrophage colony-stimulating factor 1 receptor (CSF1R), v-set and immunoglobulin domain-containing protein 4 (VSIG4), and complement C1q subcomponent subunit C (C1QC) were found overexpressed. Cluster 8 (see green) is mainly composed of components of myelin sheath, some of them involved in the regulation of actin cytoskeleton. The proteins from cluster 9 (purple) are proteinaceous components of extracellular matrix that participate in glycosaminoglycan biosynthesis and turnover.

2.3. Protein Validation by Western Blotting

For the validation of quantitative results, WB analysis was performed to confirm the overexpression of some proteins in RRD vitreous. Thus, ENO2, PGAM1, and RHO were randomly chosen and detected in RRD (n = 4) and MEM (n = 3) vitreous samples by WB analysis. Changes in protein abundance were highly consistent with the results obtained using iTRAQ (Figure 3). Mann–Whitney *U* test showed a highly significant increase in the levels of a native form of ENO2 (78 kDa) in RRD versus MEM, and this difference is consistent among samples of the same study group. Analysis of PGAM1 and RHO also confirms that these proteins are overexpressed in RRD, but the difference is less significant ($p < 0.05$). The expression of PGAM1 and RHO in the vitreous of patient HV237 (MEM) is similar to the RRD group. RHO is also highly expressed in vitreous of patient HV 629 when compared to the other RRD samples.

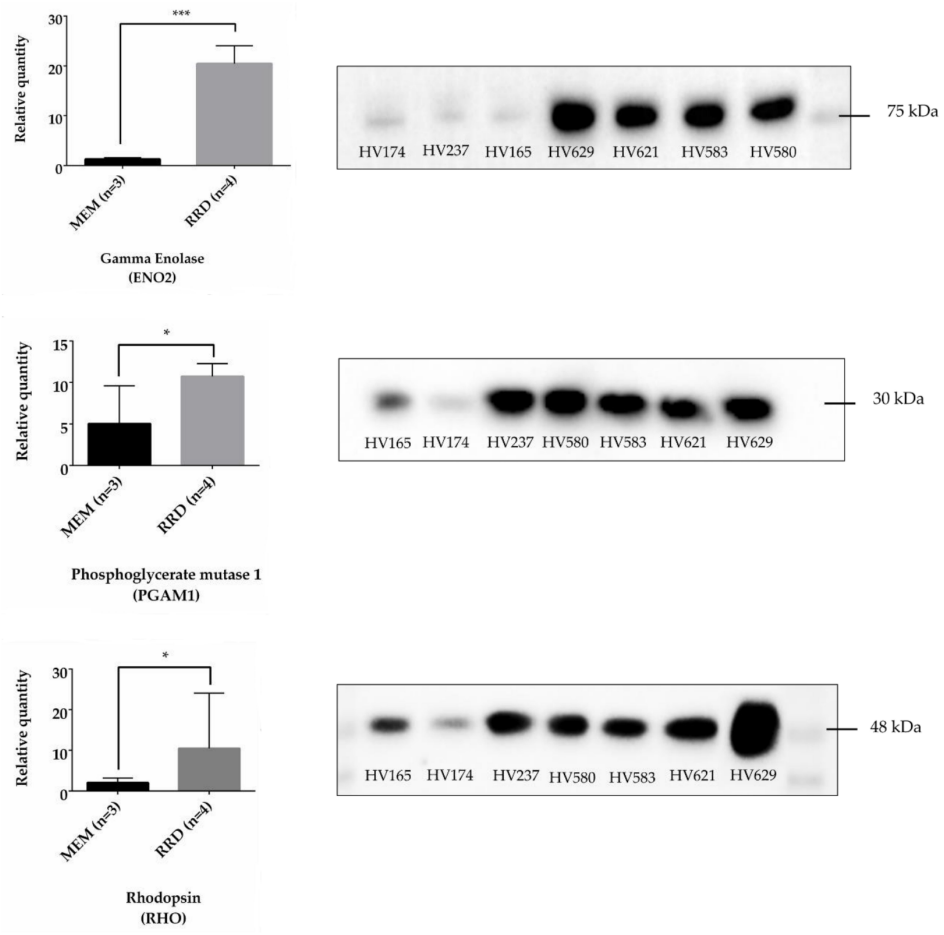

Figure 3. Western blot analyses of ENO2, PGAM1, and RHO in vitreous samples from patients with MEM (HV165, 174 and 237) and RRD (HV580, 583, 621 and 629). Statistics analysis were performed using Mann–Whitney U test, with * and *** representing $p < 0.05$ and $p = 0.0007$, respectively.

3. Discussion

In recent years, effort has been made for the characterization of the complete vitreous proteome, either through analysis of post-mortem samples or samples obtained by vitrectomy. Recently, Loukovaara and co-workers identified the larger set of proteins so far found in human vitreous, using MS-based label-free quantitative proteomics analysis [5]. Indeed, many authors have contributed to the enrichment of our knowledge about human vitreous proteome, [1–9,24–29] proving that no individual technology can cover completely this proteome. In the present study, 1030 proteins were identified with 6078 peptides, of which 2613 correspond to unique peptides. These proteins were compared to previous vitreous proteomics reports (Supplementary Table S2), including twelve studies in which vitreous were collected by pars plana vitrectomy [19,23–33,35] and one study in which vitreous core was aspirated from post-mortem healthy eyes [34]. Table 3 displays the total number of proteins identified in the vitreous using distinct experimental set-ups, including the number of proteins found exclusively in each study. Most of the identified proteins (808 proteins) have been previously described in vitreous proteome, establishing the validity of the data from the current study. To the best of our knowledge, 222 of the identified proteins were exclusively found in this study, compared to previous reports [19,23–34].

Table 3. Comparison of proteins identified in vitreous using different experimental set-ups.

Experimental Set-up	Number of Identified Proteins [1]	Number of Proteins Exclusively Identified	Reference
HAPs depletion 2D-LC-MS/MS (TripleTOF 5600)	1030	222	Present study
HAPs depletion IEX, SDS-PAGE, MALDI-TOF/TOF	127	63	[19]
CE-MS (micro-TOF MS)	101	-	[35]
CE-MS (micro-TOF MS)	94	-	[33]
2D-LC-MS/MS (LTQ Velos)	1575 [2]	653 [2]	[34]
RP-LC-ESI-MS/MS (Orbitrap Elite hybrid MS)	2482	1696	[32]
CE-MS (micro-TOF MS)	96	-	[31]
HAPs depletion SCX, SDS-PAGE, and OFFGEL, RP-LC-MS/MS (LTQ-OrbitrapVelos)	1201	324	[30]
SDS-PAGE and IEF, RP-LC-MS/MS (LTQ-Orbitrap XL MS)	1110	302	[29]
SDS-PAGE, LC-MS/MS (LTQ)	249	13	[28]
HAPs depletion 2DE, MALDI-TOF SDS-PAGE, LC-MALDI-TOF/TOF, and LC-MS/MS	455	54	[27]
2DE, LC-Q-TOF/TOF (QTOF2)	13	-	[26]
SDS-PAGE, MALDI-TOF	12	-	[25]
2DE, LC-Q-TOF/TOF, and MALDI-TOF	18	-	[24]
2DE, MALDI-TOF, and LC-MS/MS (LCQ DECA) IEX, LC-MS/MS (LCQ DECA)	54	19	[23]

[1] In all these studies, protein isoforms were referred as a single protein; [2] Only non-redundant proteins were considered.

Few studies have been published regarding the vitreous proteome in RD and the majority of them were focused in PVR, one of the most common causes of failure to correct RRD [14,20–22]. Shitama and colleagues found higher expression levels of pigment-epithelium derived factor and apolipoprotein A1 in RD, compared to other ocular diseases [14]. Yu and colleagues found 516 proteins in vitreous of RRD patients with PVR using SDS-PAGE and reversed-phase liquid chromatography-tandem mass spectrometry [22]. iTRAQ combined with liquid chromatography-electrospray ion trap-mass spectrometry-mass spectrometry (LC-ESI-MS/MS)was used by Wu and co-workers to identify 103 proteins differentially expressed, including 54 up-regulated and 49 down-regulated proteins, in RRDCD when compared with RD [11]. More recently, our research group identified 127 proteins in vitreous of RD patients, of which 68 had not yet been found in previous studies, by combining ion exchange chromatography, SDS-PAGE and MALDI-TOF/TOF analysis [19]. In the current study, iTRAQ labeling was combined with 2DE-LC-MS/MS to find expression changes in the proteome of vitreous from patients with RRD, the most common type of RD. Using this technique, 150 proteins (96 overexpressed and 54 underexpressed) were found differentially expressed in these patients. WB analysis confirmed that the levels of ENO2, PGAM1, and RHO were up-regulated which is consistent with the iTRAQ-based proteomics results. Functional enrichment analyses of the differentially expressed proteins were also applied using STRAP and STRING to better elucidate the molecular mechanism underlying RRD pathogenesis.

Carbon metabolism is the most basic aspect of life since it comprises various pathways essential to obtain energy for cell function and survival. In this study, many of the proteins found differentially expressed in RRD are related to carbon metabolism and to glycolysis. Proteins such as TPI1, GPI, ALDOA, ALDOC, AKR1A1, PGAM1, ENO2, FBP1, PGK1, L-lactate dehydrogenase, pyruvate kinase, as well as the solute carrier family 2, facilitated glucose transporter member 1 (SLC2A1) were found

overexpressed. Glycolytic enzymes may be upregulated in RRD in an effort to obtain more energy through glycolysis to compensate the metabolic "stress" state of the retina. Indeed, the function and maintenance of retinal cells require high levels of energy in the form of ATP that are mainly generated from glucose by both anaerobic and aerobic glycolysis [36,37]. Mandal and co-workers already found increased levels of α-enolase in retinal extracts after RD in rabbits, suggesting an upregulation of the glycolytic process, but ALDOA were found underexpressed in that study [38]. Additionally, pentose phosphate pathway, fructose and mannose metabolism, and biosynthesis of amino acids were found upregulated in RDD, suggesting that the retinal cells may consume alternative energy substrates. The pentose phosphate pathway, besides increasing the production of NADPH, may also have a protective role through the regeneration of reduced glutathione [39]. S-transferase (GSTP1), overexpressed in this study, is an intracellular detoxification enzyme that catalyzes the reduction of electrophiles in retina, iris, and cornea [40–42]. Another hypothesis is that increase of carbon metabolism may help to prevent the death of photoreceptors during RRD. The function and survival of photoreceptors and other retinal cells depends on the diffusion of nutrients and oxygen from choroidal circulation [36]. During RRD, this supply is compromised by the physical separation between NSR and RPE, creating an intraretinal environment with starvation of oxygen and glucose. So, the upregulation of enzymes involved in aerobic and anaerobic glycolysis may protect the retinal cells face to hypoglycemia and hypoxia [36,43,44]. Nevertheless, there is some evidence that the glycolytic process is also affected by more severe states of disease, such PVR, where the glycolysis metabolism seems to be significantly reduced [21]. Yu and co-workers found that enolases (ENO2), aldolases (ALDOA, ALDOC), kinases (PGK1, PKM) and other glycolytic proteins (PGAM1, triosephosphate isomerase (TPI1), GPI, LDHB) were significantly down-regulated in moderate PVR [21]. Indeed, some of them disappeared in severe PVR vitreous or were only detected in vitreous from normal human eyes. Other authors found that TPI1 was downregulated in the vitreous from patients with RRDCD [11]. Metabolic analysis of vitreous confirms that the glycolytic profile of vitreous is different between RRD and PVR [45]. Li and colleagues found increased expression levels of D-glyceraldehyde and glycerate in RRD [45], which are metabolites catalyzed by TPI1 and PGK1/PGAM, respectively. These data suggest that glycolysis process is initially upregulated to compensate the metabolic stress of retinal cells after RD, but glycolytic proteins are lost in the progression to more severe conditions.

The fact that some protective mechanisms are triggered during RRD is also suggested by the upregulation of proteins involved in cellular responses to heat stress and the regulation of apoptotic signaling. Another interesting fact is that many of these proteins are associated with HIF-1 signaling pathway. HIF-1 is a transcriptional regulator that mediates the cellular responses to reduced oxygen levels through changes in gene expression [46,47]. Thus, glycolytic enzymes (ALDOA, ENO2, and PGK1), glucose transporters (SLC2A1), growth factors (TIMP1), and SERPINE1 appear to be upregulated in response to HIF-1. So, HIF-1 may act as a regulator of retinal hypoxia after DDR by controlling cellular anaerobic metabolism, angiogenesis, and cell survival. Proteins such as α-crystallins, β-crystallins, 14-3-3 isoforms and heat shock proteins may also have a protective role in RRD. Despite the role of α-crystallin in retinal and vitreous function has not been fully described [48], most of studies suggest that it has a protective role in degeneration, inflammation, and other retinal stress conditions [49]. Heat shock proteins are a family of proteins that are expressed in response to ocular stress or injury, e.g., ischemia, and participate in folding and repair of damaged proteins [50–52]. Particularly, HSP90 seems to have an anti-apoptotic effect mediated by different molecular partners, including the phosphorylated serine/threonine kinase Akt that inhibits the apoptosis though NF-κB (factor nuclear kappa B) [50]. Kayama and colleagues found high levels of HSP70 after RD in mice and rats, which were associated with phosphorylated Akt to avoid its dephosphorylation and further activation of apoptosis [51]. Curiously, other proteins found overexpressed in RRD (PROM1, CHI3L1, YWHAB, CSF1R) were associated with Akt signaling pathways. Specifically, 14-3-3s are small proteins that modulate cell growth and differentiation, regulation of apoptosis and cell cycle. Although the specific role of these proteins in retinal biology is not yet recognized, YWHAQ and YWHAE are

the 14-3-3s proteins most highly expressed in the mouse retina and high levels of YWHAE are present in Rod photoreceptors [53]. Curiously, 14-3-3 proteins were found to interact with PDC, after its light-dependent phosphorylation, indicating that these may participate in facilitating the dark adaptation of the photoreceptor [53,54].

Lysosomal enzymes are widely distributed in ocular tissues and their involvement was suggested in the pathogenesis of several diseases, including RD [55]. The RPE is the main responsible for the phagocytosis of photoreceptor outer segments and by its consecutive lysosomal degradation [55,56]. Lysosomal proteins were previously found augmented in the vitreous and subretinal fluid, and their levels were related to RRD duration [57,58]. More recently, higher expression levels of cathepsin D were found in vitreous from patients with PVR [14,21], confirming our results. So, it was suggested that the increase of lysosomal digestion is a later event in RD, contributing to the photoreceptor degeneration and inflammation [57]. Also, considering the role of vitreous liquefaction in RD onset [3,4,7], it has been suggested that lysosomal enzymes, mainly cathepsin D, may be involved in the degradation of glycosaminoglycans, and collagen molecules, of rod outer segments and RHO [55,58,59]. Finally, increased cathepsin A activity in the subretinal fluid was associated with retinal degradation in RD [59]. Another hypothesis is that lysosomal enzymes have a protective effect in the eye, maintaining the health of the neural components of the retina [59].

Phototransduction is a biochemical process essential for vision by which retinal rod outer segment (ROS) capture and convert photons into electrical signals [60,61]. This biochemical cascade is initiated by Rho, a G-protein-coupled receptor found in ROS disks whose structure suffers conformational changes induced by photon absorption [60,62,63]. Transducin is a heterotrimeric G protein that binds the activated Rho, triggering the exchange of GDP by GTP in the α subunit of transducin (GNAT1) and its dissociation from β (GNB1) and γ subunits [60,64]. In its turn, GNAT1 activates phosphodiesterase (PDE6), which is composed of two large catalytic subunits (PDE6A and PDE6B) and two PDE6G subunits, triggering cGMP hydrolysis. Reduction of cGMP levels leads to the closure of the cGMP-gated cation channels in the plasma membrane and to rod cell hyperpolarization [60]. SAG is responsible by regulation of the phototransduction cascade through capture and regeneration of phosphorylated Rho [30]. PDC is a small binding protein found abundantly in photoreceptors that may be responsible for the regulation light sensitivity in the ROS through interaction with the subunits G$\beta\gamma$ of transducin [54]. Considering the specific localization of these proteins in ROS and its relevance to eye function, its accumulation in vitreous implies that the death of photoreceptors occurs after RRD [65–67]. The increase of vimentin (VIM) levels found in RRD vitreous also suggest that high levels of retinal stress are induced by the detachment. Vimentin is expressed in retinal astrocytes and Müller cells in the healthy retina but, when RD occurs, the "stress" induces a progressive increase of vimentin in the cell over time, thus becoming the predominant intermediate filament [68,69]. Mandal and co-workers confirmed by 2D-PAGE and immunocytochemistry analysis that the Müller cell hypertrophy is accompanied by an increased expression of intracellular vimentin. This suggests that vimentin and other structural proteins may reinforce the structure of Müller cells in response to RD [63]. Indeed, the lack of vimentin limits the growth of these cells into subretinal space, avoiding the formation of subretinal membrane into this cavity that could jeopardize the photoreceptor regeneration even after successful retinal reattachment surgery. So, this fact can explain the reduced levels of photoreceptor degeneration after RD in in vimentin-deficient mice [70,71]. Another indicator of retinal stress is the highly significant increase (6.5-fold) of the levels of ENO2 in RRD versus MEM, which was confirmed by WB analysis. ENO2 is a cellular damage marker released after retinal neuron injury. High levels of ENO2 were detected in the subretinal fluid, vitreous, and aqueous after RD. In fact, ENO2 appears to be an effective biomarker of retinal damage [72,73]. The maintenance of retinal structure and homeostasis is crucial for healthy vision [74]. Thus, RPE and NSR separation, by reducing the influx of nutrients and oxygen into the retina, induces retinal stress, causing the death of retinal photoreceptors and structural changes in retinal glial cells.

Although biological events, such as inflammation, immune responses, and coagulation/fibrinolysis have been associated with RD, in this study, only a few proteins related to inflammatory responses were found overexpressed in RRD. Chitinase-3-like protein 1, previously detected in severe PVR vitreous [21], and thrombospondin-1 are positive regulators of inflammatory responses, while SERPINE1 is a negative regulator of fibrinolysis (Supplementary Table S4). Surprisingly, many proteins involved in acute inflammatory response and in complement and coagulation cascades were found underexpressed in RRD. Interestingly, only the components of C1 (C1QC, C1R), the first component of the serum complement system, were found upregulated in RRD. However, previous transcriptomic analysis of human retinal samples reveals that genes related to an inflammatory process are up-regulated in RD, including complement pathway proteins and members of the major histocompatibility complex [5]. So, it is suggested that at the beginning of RRD low levels of plasma proteins are present in vitreous, including inflammatory proteins, complement components, and coagulation factors. This may result from the decrease of the influx of plasma proteins from choroid into vitreous, after the RD, or by the migration of these proteins to the subretinal fluid. It is well known that with the increase of the duration of RRD, the composition of the subretinal fluid becomes more similar to plasma [75]. The blood-retinal barrier (BRB) breakdown, which only occurs later in RD, may also explain the changes in the composition of eye fluids. BRB breakdown and the accentuated levels of inflammatory proteins appear to have a central role in the evolution of RD to more severe pathologies [5,11,22,75]. As a matter of fact, the influx of blood, serum proteins, and vitreal cells through the retinal break is enough to stimulate the PVR development [76]. After the BRB breakdown, the direct influx of cells (RPE cells, fibroblasts, myofibroblasts, among others) into vitreous causes chemotaxis of inflammatory cells [76,77]. For this reason, most of the studies concerning PVR report high levels of plasma protein in vitreous. Albumin, transferrin, apolipoproteins, complement components, members of the serpin family, growth factors and other plasma components were found upregulated in vitreous from patients with PVR [14,21,22,78] and with RRDCD [11]. To fully understanding these findings, it would be extremely relevant to evaluate the variations in the vitreous proteome along the course of the RRD and to compare with other progressive forms of the ocular diseases. In fact, the goal must be to find vitreous biomarkers whose expression levels are correlated with DR severity, i.e., proteins that can act as specific indicators of the disease progression. Although the vitreous levels may better reflect the molecular changes in the eye, the measurement of these biomarkers in body fluids, such as serum or plasma is more accessible for clinical purposes [79]. Therefore, the best strategy is to find the specific disease biomarkers in the vitreous, and, then, try to measure and correlate its levels in serum or plasma. Some authors found a relationship in the levels of kininogen 1 and insulin-like growth factor binding protein 6 between vitreous and plasma in PVR [21,78], but for many other biomarkers, no correlation was found [21,80,81]. In a study of Yu and colleagues, only kininogen 1, among 102 PVR-specific proteins, was specifically detected in both vitreous and serum [21]. Different studies have tried to find a correlation between serum and vitreous in other ocular diseases [82–84], including our research group that analyzed the levels of placental growth factor, and vascular endothelial growth factors A (VEGF-A) and B (VEGF-B) [85,86]. In our study, VEGF-A and VEGF-B concentrations were higher in proliferative ocular diseases compared to non-proliferative ocular diseases [86], but no correlation between vitreous vs. serum VEGF-A and VEGF-B was observed. Also, no correlation between vitreous and serum levels of placental growth factor was found in patients with diabetic retinopathy [85]. Comparing to other ocular pathologies, there are few studies in DRR/PVR, which may also explain the lack of biomarkers significantly correlated between serum and vitreous.

4. Materials and Methods

4.1. Demographics and Clinical Variables

Undiluted vitreous samples were collected via pars plana vitrectomy on the Ophthalmology service of Leiria-Pombal Hospital (Leiria, Portugal), according to the protocol for sample collection

approved by the hospital ethics committee (Code: CHL-15481) [87]. An informed consent from all patients was obtained after an explanation of the purpose of this study, which adhered to the tenets of the Declaration of Helsinki. Vitreous samples contaminated with plasma and/or associated with other diseases were excluded, as well as samples from patients subjected to previous intraocular surgeries. The patients had not undergone previous vitrectomies. After exclusion, vitreous collected from 4 patients (1 male, 3 females) diagnosed with RRD were included in the study group, and vitreous collected from 4 patients (2 males, 2 females) diagnosed with MEM were included in the control group. For the validation of iTRAQ results, vitreous from 7 patients were analyzed by WB: 4 patients (2 males, 2 females) diagnosed with RRD and 3 patients (1 male, 2 females) with MEM. Demographic characteristics of patients enrolled in this study and the description of corresponding vitreous samples are summarized in Table 1. Upon collection, vitreous samples were transferred to sterile cryogenic vials and frozen at −80 °C, until further processing.

4.2. Vitreous Samples Handling

Vitreous samples were centrifuged at 14,000 rpm for 10 min at 4 °C to separate the soluble proteins from structural components. The protein concentration was determined using a Micro BCA™ Protein Assay Kit (Thermo-Scientific, Porto Salvo, Portugal) and equal volumes of individual vitreous samples were combined according to the study group (RRD vs. MEM), as seen in Table 1. Seppro® IgY14 LC5 and SuperMix LC2 columns (Sigma-Aldrich, St. Louis, MO, USA) were used in tandem for removing abundant plasma proteins from pooled vitreous samples, including albumin and IgG, according to the manufacturer's instructions. The flow-through fractions were concentrated and desalted using Amicon Ultra-15 3 K Centrifugal Filter Unit (Merck Millipore, Madrid, Spain) and precipitated by chloroform–methanol (4/1, *v/v*). The pellet was resuspended in a buffer with 7 M urea, 2 M thiourea, and 100 mM triethylammonium bicarbonate (TEAB), compatible with iTRAQ labeling. Samples were quantified using RC DC™ Protein Assay (BioRad, Madrid, Spain), according to the manufacturer's instructions.

4.3. In-Solution Digestion and iTRAQ Labeling

After reduction and alkylation, 25 µg of sample was combined with trypsin from porcine pancreas (Sigma-Aldrich) at a final trypsin:protein ratio of 1:10 and digested overnight at 37 °C. Tryptic peptides were dried by vacuum centrifugation, reconstituted in 80 µL labeling buffer (70% ethanol/25 mM TEAB) and labeled with iTRAQ reagents, according to the manufacturer's protocol (ABSciex, Framingham, MA, USA). Specifically, pooled samples from RRD group (n = 4) and from the control group (n = 4) were incubated with the reagents 116 and 114, respectively, over 2 h at RT. Labeling was confirmed by MS/MS analysis using 4800 MALDI TOF/TOF analyzer (ABSciex, Framingham, MA, USA).

4.4. 2D-Nano-LC-ESI-MS/MS Analysis

After labeling, samples were combined and fractionated in an RP column (100 × 2.1 mm, 5 µm particle size, Fortis Technologies, Neston, UK) using a Knauer Smartline HPLC system with UV detection at 214 nm. Peptides fractionation was performed at a flow rate of 150 µL/min with 95% of buffer A (10 mM NH4OH, pH 9.4) for 10 min, followed by a linear increase to 25% buffer B (10 mM NH4OH, 80% of methanol, pH 9.4) for 10 min, to 75% B for 40 min, and, finally, to 100% B. Fractions were collected, pooled into 5 fractions that were dried by vacuum centrifugation and desalted using a SEP-PAK C18 Cartridges (Waters, Milford, MA, USA) [88,89].

Tryptic peptides (5 µL) were desalted onto a trap column C18 PepMap (100 µm × 2 cm, 5 µm, 100 Å, Dionex) using solvent A (0.1% formic acid in water) at 2 µL/min, using an Ultra 2D Plus (Eksigent, Dublin, CA, USA) system coupled to TripleTOF 5600 System via a Nanospray III source (AB Sciex). After desalting, trap column was switched online with an RP nanoACQUITY UPLC analytical column (75 µm × 15 cm, 1.7 µm, Waters). Peptides were eluted at a flow rate of 250 nL/min,

using the following conditions: a 110 min linear gradient from 4.8%–30% B (0.1% formic acid in ACN), followed by two linear gradients, 10 min from 30%–40% B and 5 min from 40%–90% B. Two technical replicates were performed for each fraction. TripleTOF 5600 system was operated in positive ion mode with the capillary voltage set at 1500 V, curtain gas of 25 and nebulizer gas of 10. System was operated in an information-dependent acquisition mode with a TOF/MS survey scan (350–1250 m/z) with an accumulation time of 250 ms. Each MS/MS spectrum was accumulated for 150 ms (100–1800 m/z) and only the parent ions with a charge state from +2 to +5 were included in the MS/MS fragmentation. Dynamic exclusion allowed that former target ions were excluded for a period of 12 s. The MS/MS spectra were acquired in high sensitivity mode with 'adjust collision energy when using iTRAQ reagent' settings.

4.5. MS/MS Data Analysis

Raw data files were converted to mgf. files and searched against *Homo sapiens* UniProtKB reviewed database [90] downloaded from Swiss-Prot at 22nd March 2014 and its corresponding reversed database. Database searches were performed using a licensed version of Mascot v.2.2.04 (Matrix science, London, UK). Search parameters were set as follows: enzyme: trypsin allowed missed cleavages: 1; fixed modifications: methythio (C) and iTRAQ4plex; variable modifications: acetyl (Protein N-term), deaminated (NQ) and oxidation (M); peptide mass tolerance: $\pm$25 ppm for precursors and 0.05 Da for fragment masses.

Relative abundance of the proteins in RRD versus MEM was computed as a weighted average of ratios of the reporter ions (116 vs. 114). Finally, ratios were normalized by dividing each protein ratio by the median value of the tag and the obtained value was log2-transformed. Log2 peptide ratios followed a normal distribution that was fitted using least squares regression. FDR of $\leq$1% at peptide level was manually assessed using Excel 2010 by applying a target-Decoy approach. Using this strategy, MS/MS data were searched against both the target database and the decoy sequence database, a consciously incorrect database containing reversed shuffled peptide sequences [23]. The peptides identified in this decoy database search result in an incorrect identification, and thus are considered false-positives (FP). Then, FDR is calculated according to the number of FP above a threshold divided by the total number of peptide matches above that threshold. For the selection of differentially expressed proteins, the requirements were (i) identification in both technical replicates, (ii) identification with more than one unique peptide and (iii) the assessed protein ratio was required to be in the 5% most extreme region of a Gaussian distribution fit on all ratios (FDR < 0.05) for both technical replicates.

4.6. Bioinformatic Analysis

Differentially expressed proteins were analyzed according to GO terms for biological process, cellular component and molecular function using STRAP 1.5 (Software Tool for Rapid Annotation of Proteins) at November 2017. To assess functional associations between proteins, differentially expressed in RDD, the online tool STRING 10 was applied with a high confidence (0.70) [91,92]. Protein clusters were defined with MCL clustering using an inflation parameter of 1.3. Pathways enrichment of proteins clusters were performed according to Reactome pathway knowledgebase [93] and KEGG pathway database [94].

4.7. Validation by Western Blotting

ENO2, PGAM1, and RHO were randomly chosen from the proteins found differentially expressed in RRD for the validation by WB. Briefly, equal amounts of proteins (15 µg) for each sample were loaded on a 12.5% sodium dodecyl sulfate polyacrylamide gel. Proteins were then transferred from the gel to a PVDF membrane using Trans-Blot Turbo™ Transfer System (Bio-Rad Laboratories, Hercules, CA, USA) for 45 min. After blocking with a solution of 5% of powdered milk in 0.1% Tween-20, the membranes were incubated overnight at 4 °C with monoclonal antibodies prepared in 5% of BSA. The antibodies applied for the validation and respective dilutions are as follows: γ Enolase Antibody

(NSE-P1) (sc-21738; Santa Cruz, CA, USA) at 1:500, anti-PGAM1/4 (D-5) (sc-365677; Santa Cruz, CA, USA) at 1:300, and anti-rhodopsin (RET-P1) (sc-57433; Santa Cruz, CA, USA) at 1:300. After the incubation with the primary antibodies, membranes were incubated with an anti-Mouse IgG (Fab specific)–Peroxidase antibody (A3682; Sigma, St. Louis, MO, USA) at 1:10,000. Protein bands were visualized using the Clarity™ Western ECL Substrate (Biorad, Hercules, CA, USA). The detection and relative quantification of the bands was done using Image lab 5.0 software (Biorad, Hercules, CA, USA). Data processing and statistical analyses (Mann-Whitney *U* test, $p < 0.05$) were performed using GraphPad Prism Software (San Diego, CA, USA).

5. Conclusions

A total of 1030 proteins were identified using iTRAQ labelling combined with two-dimensional LC-ESI-MS/MS, and 150 proteins were found differentially expressed between RRD and MEM control (96 overexpressed and 54 underexpressed proteins). These proteins were analyzed regarding their molecular function, biological process and KEGG pathways, to better elucidate the molecular mechanism underlying RRD pathogenesis. It is interesting to note that in RRD, there appears to be a balance between death and survival of retinal cells. HIF-1 signaling pathway seems to have a crucial role in the response to retinal stress after RD, promoting the retinal cell survival through the up-regulation of glycolytic enzymes, glucose transporters, and growth factors. The increased levels of molecular chaperones (alpha-crystallins, beta-crystallins) and heat shock proteins (HSP90AA1, HSPA1A, HSPA8) can be related to a protective role in RRD. On the other hand, the accumulation of proteins from photoreceptor cells, NSE, and vimentin in vitreous indicate that the death of photoreceptors occurs in RRD. Lysosomal degradation appears to be up-regulated in RRD, but it is not known whether it has a beneficial or a hazard effect on the survival of retinal cells. Surprisingly, many proteins involved in acute inflammatory response and in complement and coagulation cascades were found underexpressed in RRD. So, processes such as inflammation, coagulation, and fibrosis can be later events in RRD pathogenesis. Vitreous seems to play a key role in the onset of RRD but one must bear in mind that levels of protein in vitreous are an indirect measurement of the events that take place in the retina. Although more studies will be required to fully understand some of these findings, the obtained results provide a basis for new insights in RRD investigation.

Supplementary Materials: Four supplementary tables are provided as supplementary materials at http://www.mdpi.com/1422-0067/19/4/1157/s1. Table S1.1—Protein list corresponding to proteins only identified in technical replicate 1 and 2 with an FDR of 1% at the peptide level. FDR and p-value displayed in the table are related to quantification analysis using iTRAQ labeling and not to protein identification. Proteins highlighted in gray, red and green correspond, respectively to the non-differentially expressed, underexpressed and overexpressed in RRD (116) when compared with MEM control samples (114). Table S1.2—Peptide list corresponding to proteins identified in technical replicate 1 and 2 with an FDR of 1% at the peptide level. Cells highlighted in light pink and blue correspond to peptides identified in replicates 1 and 2, respectively. Unique peptides are highlighted at green. Table S2.1—Comparison of published proteins found in vitreous humor proteome in previous reports with the list of proteins identified in the current study. Table S2.2—List of proteins of vitreous humor proteome newly identified in the current study. Table S3.1—Proteins found differentially expressed, which were identified in technical replicate 1 and 2 with a FDR of 1% at the peptide level. FDR and p-value displayed in the table are related to quantification analysis using iTRAQ labeling and not to protein identification. Proteins highlighted in gray, red and green correspond, respectively to non-differentially expressed, underexpressed and overexpressed proteins in RRD (116) when compared with MEM control samples (114). Table S3.2—Protein list corresponding to the proteins found differentially expressed, which were identified in technical replicate 1 and 2 with a FDR of 1% at the peptide level. FDR and p-value displayed in table are related to quantification analysis using iTRAQ labeling and not to protein identification. Proteins highlighted in gray, red and green correspond, respectively to non-differentially expressed, underexpressed and overexpressed proteins in RRD (116) when compared with MEM control samples (114). Table S4.1—Results of STRAP bioinformatics analysis of differentially expressed proteins found in vitreous humor proteome of RRD patients compared with MEM control samples. Proteins are classified according their function, catalytic activity and gene Ontology (Go terms for biological process, cellular component and molecular function. Table S4.2—Classification of differentially expressed proteins found in vitreous humor proteome of RRD vs MEM according to biological processes using STRAP. Table S4.3—Classification of differentially expressed proteins found in vitreous humor proteome of RRD vs MEM according to molecular function using STRAP. Table S4.4—Clusters in the protein-protein interaction network of the proteins found differentially expressed in RRD. The clusters were predicted using the ECM clustering option provided by STRING. Table S4.5—Pathways

enrichment of proteins clusters according to KEGG pathway database. Table S4.6—Pathways enrichment of proteins clusters according to Reactome pathway knowledgebase.

Acknowledgments: This project was supported by University of Beira Interior—Health Sciences Research Centre (CICS). Santos FM acknowledges a fellowship [CENTRO-07-ST24-FEDER-002014] and a doctoral fellowship [SFRH/BD/112526/2015] from FCT. Gaspar LM acknowledges a fellowship from Novartis Farma-Produtos Farmacêuticos, SA. Rocha AS acknowledges PhD fellowship of Sciences Faculty financed by ICI and Santander Totta. This work is supported by FEDER funds through the POCI—COMPETE 2020—Operational Programme Competitiveness and Internationalisation in Axis I—Strengthening research, technological development and innovation Project [POCI-01-0145-FEDER-007491] and National Funds by FCT—Foundation for Science and Technology Project [UID/Multi/00709/2013]. CNB-CSIC proteomics lab is a member of ProteoRed, supported by PRB2-ISCIII grant [PT13/0001].

Author Contributions: Fátima M. Santos conceived, designed and performed the experiments, analyzed the data, and wrote the manuscript. Leonor M. Gaspar analyzed the data and wrote the manuscript. Sergio Ciordia conceived, designed, and performed the experiments and analyzed the data. Ana S. Rocha conceived, designed, and performed some of the experiments. João P. Castro-de-Sousa collected vitreous samples during PPV, and collected and analyzed the data. Alberto Paradela supervised the experiments, analyzed the data, and proof read. Luís A. Passarinha and Cândida T. Tomaz designed the experiments, analyzed the data, and proof read. All authors read and approved the final manuscript.

Conflicts of Interest: The authors declare no conflict of interest.

Abbreviations

2D-LC-MS/MS	Two-dimensional liquid chromatography-electrospray tandem mass spectrometry
AKR1A1	Alcohol dehydrogenase [NADP(+)]
ALDOA	Fructose-bisphosphate aldolase A
ALDOC	Fructose-bisphosphate aldolase C
APOA4	Apolipoprotein A-IV
APOC2	Apolipoprotein C-II
APOC3	Apolipoprotein C-III
BRB	Blood-retinal barrier
C1R	Complement component 1
C8A	Complement component 8
C8B	Complement component 8
C9	Complement component 9
ENO2	Enolase 2
F12	Coagulation factor XII
F9	Coagulation factor IX
FBP1	Fructose-1,6-bisphosphatase 1
GO	Gene ontology
GPI	Glucose-6-phosphate isomerase
GSTP1	Gstp1
HIF-1	Transcriptional regulator hypoxia-inducible factor-1
iTRAQ	Isobaric tags for relative and absolute quantitation
KEGG	Kyoto encyclopedia of genes and genomes
LC-ESI-MS/MS	Liquid chromatography-electrospray ion trap-mass spectrometry-mass spectrometry
LDHB	L-lactate dehydrogenase
MALDI-TOF/TOF	Matrix-assisted laser desorption/ionization-tandem time-of-flight mass spectrometry
MEM	Macular epiretinal membranes
NSR	Neurosensory retina
PDC	Phosducin
PDE6G	Retinal rod rhodopsin-sensitive cgmp 3~,5~-cyclic phosphodiesterase
PGAM1	Phosphoglycerate mutase 1
PGK1	Phosphoglycerate kinase 1
PKM	Pyruvate kinase
PVR	Proliferative vitreoretinopathy
RBP1	Retinol-binding protein 1
RBP3	Retinol-binding protein 3
RBP4	Retinol-binding protein 4
RD	Retinal detachment
RD	Retinal detachment
RHO	Rhodopsin
RLBP1	Retinaldehyde-binding protein 1

ROS	Retinal rod outer segment
RPE	Retinal pigment epithelium
RRD	Rhegmatogenous retinal detachment
RRDCD	Rhegmatogenous retinal detachment associated with choroidal detachment
SAG	S-arrestin
SLC2A1	solute carrier family 2, facilitated glucose transporter member 1
STRAP	Software Tool for Rapid Annotation of Proteins
STRING	Search Tool for the Retrieval of Interacting Genes/Proteins
TALDO1	Transaldolase
TPI1	Triosephosphate isomerase
VEGF-A	Vascular endothelial growth factor A
VEGF-B	Vascular endothelial growth factor B
WB	Western blotting

References

1. Mitry, D.; Charteris, D.G.; Fleck, B.W.; Campbell, H.; Singh, J. The epidemiology of rhegmatogenous retinal detachment: Geographical variation and clinical associations. *Br. J. Ophthalmol.* **2010**, *94*, 678–684. [CrossRef] [PubMed]
2. Kang, H.K.; Luff, A.J. Management of retinal detachment: A guide for non-ophthalmologists. *BMJ* **2008**, *336*, 1235–1240. [CrossRef] [PubMed]
3. Ghazi, N.G.; Green, W.R. Pathology and pathogenesis of retinal detachment. *Eye* **2002**, *16*, 411–421. [CrossRef] [PubMed]
4. Kuhn, F.; Aylward, B. Rhegmatogenous retinal detachment: A reappraisal of its pathophysiology and treatment. *Ophthalmic Res.* **2014**, *51*, 15–31. [CrossRef] [PubMed]
5. Delyfer, M.-N.; Raffelsberger, W.; Mercier, D.; Korobelnik, J.-F.; Gaudric, A.; Charteris, D.G.; Tadayoni, R.; Metge, F.; Caputo, G.; Barale, P.-O.; et al. Transcriptomic Analysis of Human Retinal Detachment Reveals Both Inflammatory Response and Photoreceptor Death. *PLoS ONE* **2011**, *6*, e28791. [CrossRef] [PubMed]
6. Nemet, A.; Moshiri, A.; Yiu, G.; Loewenstein, A.; Moisseiev, E. A Review of Innovations in Rhegmatogenous Retinal Detachment Surgical Techniques. *J. Ophthalmol.* **2017**, *2017*, 1–5. [CrossRef] [PubMed]
7. Mitry, D.; Fleck, B.W.; Wright, A.F.; Campbell, H.; Charteris, D.G. Pathogenesis of rhegmatogenous retinal detachment: Predisposing anatomy and cell biology. *Retina* **2010**, *30*, 1561–1572. [CrossRef] [PubMed]
8. Haugstad, M.; Moosmayer, S.; Bragadóttir, R. Primary rhegmatogenous retinal detachment—Surgical methods and anatomical outcome. *Acta Ophthalmol.* **2017**, *95*, 247–251. [CrossRef] [PubMed]
9. Sahanne, S.; Tuuminen, R.; Haukka, J.; Loukovaara, S. A retrospective study comparing outcomes of primary rhegmatogenous retinal detachment repair by scleral buckling and pars plana vitrectomy in Finland. *Clin. Ophthalmol.* **2017**, *11*, 503–509. [CrossRef] [PubMed]
10. Feltgen, N.; Walter, P. Rhegmatogenous retinal detachment—An ophthalmologic emergency. *Dtsch. Arztebl. Int.* **2014**, *111*, 12–22. [CrossRef] [PubMed]
11. Wu, Z.; Ding, N.; Yu, M.; Wang, K.; Luo, S.; Zou, W.; Zhou, Y.; Yan, B.; Jiang, Q. Identification of Potential Biomarkers for Rhegmatogenous Retinal Detachment Associated with Choroidal Detachment by Vitreous iTRAQ-Based Proteomic Profiling. *Int. J. Mol. Sci.* **2016**, *17*, 2052. [CrossRef] [PubMed]
12. Tuuminen, R.; Haukka, J.; Loukovaara, S. Statins in rhegmatogenous retinal detachment are associated with low intravitreal angiopoietin-2, VEGF and MMP-2 levels, and improved visual acuity gain in vitrectomized patients. *Graefes Arch. Clin. Exp. Ophthalmol.* **2015**, *253*, 1685–1693. [CrossRef] [PubMed]
13. Angi, M.; Kalirai, H.; Coupland, S.E.; Damato, B.E.; Semeraro, F.; Romano, M.R. Proteomic Analyses of the Vitreous Humour. *Mediat. Inflamm.* **2012**, *2012*, 1–7. [CrossRef] [PubMed]
14. Shitama, T.; Hayashi, H.; Noge, S.; Uchio, E.; Oshima, K.; Haniu, H.; Takemori, N.; Komori, N.; Matsumoto, H. Proteome Profiling of Vitreoretinal Diseases by Cluster Analysis. *Proteom. Clin. Appl.* **2008**, *2*, 1265–1280. [CrossRef] [PubMed]
15. Rocha, A.S.; Santos, F.M.; Monteiro, J.P.; Castro-de-Sousa, J.P.; Queiroz, J.A.; Passarinha, L.P. Trends in proteomic analysis of human vitreous humor samples. *Electrophoresis* **2014**, *35*, 2495–2508. [CrossRef] [PubMed]

16. Pollreisz, A.; Funk, M.; Breitwieser, F.F.P.F.; Parapatics, K.; Sacu, S.; Georgopoulos, M.; Dunavoelgyi, R.; Zlabinger, G.J.; Colinge, J.; Bennett, K.L.; et al. Quantitative proteomics of aqueous and vitreous fluid from patients with idiopathic epiretinal membranes. *Exp. Eye Res.* **2013**, *108*, 48–58. [CrossRef] [PubMed]
17. Silberring, J.; Ciborowski, P. Biomarker discovery and clinical proteomics. *TrAC Trends Anal. Chem.* **2010**, *29*, 128–140. [CrossRef] [PubMed]
18. Monteiro, J.P.J.P.; Santos, F.M.F.M.; Rocha, A.S.A.S.; Castro-de-Sousa, J.P.J.P.; Queiroz, J.A.J.A.; Passarinha, L.A.L.A.; Tomaz, C.T.C.T. Vitreous humor in the pathologic scope: Insights from proteomic approaches. *Proteom. Clin. Appl.* **2015**, *9*, 187–202. [CrossRef] [PubMed]
19. Gaspar, L.M.; Santos, F.M.; Albuquerque, T.; Castro-de-Sousa, J.P.; Passarinha, L.A.; Tomaz, C.T. Proteome analysis of vitreous humor in retinal detachment using two different flow-charts for protein fractionation. *J. Chromatogr. B Anal. Technol. Biomed. Life Sci.* **2017**, *1061–1062*, 334–341. [CrossRef] [PubMed]
20. Kuo, H.-K.; Chen, Y.-H.; Huang, F.; Wu, Y.-C.; Shiea, J.; Wu, P.-C. The upregulation of zinc finger protein 670 and prostaglandin D2 synthase in proliferative vitreoretinopathy. *Graefes Arch. Clin. Exp. Ophthalmol.* **2016**, *254*, 205–213. [CrossRef] [PubMed]
21. Yu, J.; Liu, F.; Cui, S.-J.; Liu, Y.; Song, Z.-Y.; Cao, H.; Chen, F.-E.; Wang, W.-J.; Sun, T.; Wang, F. Vitreous proteomic analysis of proliferative vitreoretinopathy. *Proteomics* **2008**, *8*, 3667–3678. [CrossRef] [PubMed]
22. Yu, J.; Peng, R.; Chen, H.; Cui, C.; Ba, J. Elucidation of the Pathogenic Mechanism of Rhegmatogenous Retinal Detachment with Proliferative Vitreoretinopathy by Proteomic Analysis. *Investig. Opthalmol. Vis. Sci.* **2012**, *53*, 8146. [CrossRef] [PubMed]
23. Nakanishi, T.; Koyama, R.; Ikeda, T.; Shimizu, A. Catalogue of soluble proteins in the human vitreous humor: Comparison between diabetic retinopathy and macular hole. *J. Chromatogr. B Anal. Technol. Biomed. Life Sci.* **2002**, *776*, 89–100. [CrossRef]
24. Yamane, K.; Minamoto, A.; Yamashita, H.; Takamura, H.; Miyamoto-Myoken, Y.; Yoshizato, K.; Nabetani, T.; Tsugita, A.; Mishima, H.K. Proteome analysis of human vitreous proteins. *Mol. Cell. Proteom.* **2003**, *2*, 1177–1187. [CrossRef] [PubMed]
25. Wu, C.W.; Sauter, J.L.; Johnson, P.K.; Chen, C.-D.; Olsen, T.W. Identification and localization of major soluble vitreous proteins in human ocular tissue. *Am. J. Ophthalmol.* **2004**, *137*, 655–661. [CrossRef] [PubMed]
26. Ouchi, M.; West, K.; Crabb, J.W.; Kinoshita, S.; Kamei, M. Proteomic analysis of vitreous from diabetic macular edema. *Exp. Eye Res.* **2005**, *81*, 176–182. [CrossRef] [PubMed]
27. Kim, T.; Kim, S.J.; Kim, K.; Kang, U.-B.; Lee, C.; Park, K.S.; Yu, H.G.; Kim, Y. Profiling of vitreous proteomes from proliferative diabetic retinopathy and nondiabetic patients. *Proteomics* **2007**, *7*, 4203–4215. [CrossRef] [PubMed]
28. Gao, B.B.-B.B.; Chen, X.; Timothy, N.; Aiello, L.P.; Feener, E.P. Characterization of the vitreous proteome in diabetes without diabetic retinopathy and diabetes with proliferative diabetic retinopathy. *J. Proteome Res.* **2008**, *7*, 2516–2525. [CrossRef] [PubMed]
29. Aretz, S.; Krohne, T.U.; Kammerer, K.; Warnken, U.; Hotz-Wagenblatt, A.; Bergmann, M.; Stanzel, B.V.; Kempf, T.; Holz, F.G.; Schnölzer, M.; et al. In-depth mass spectrometric mapping of the human vitreous proteome. *Proteome Sci.* **2013**, *11*, 10. [CrossRef] [PubMed]
30. Murthy, K.R.; Goel, R.; Subbannayya, Y.; Jacob, H.K.; Murthy, P.R.; Manda, S.; Patil, A.H.; Sharma, R.; Sahasrabuddhe, N.A.; Parashar, A.; et al. Proteomic analysis of human vitreous humor. *Clin. Proteom.* **2014**, *11*, 29. [CrossRef] [PubMed]
31. Koss, M.J.; Hoffmann, J.; Nguyen, N.; Pfister, M.; Mischak, H.; Mullen, W.; Husi, H.; Rejdak, R.; Koch, F.; Jankowski, J.; et al. Proteomics of vitreous humor of patients with exudative age-related macular degeneration. *PLoS ONE* **2014**, *9*, 1–11. [CrossRef] [PubMed]
32. Loukovaara, S.; Nurkkala, H.; Tamene, F.; Gucciardo, E.; Liu, X.; Repo, P.; Lehti, K.; Varjosalo, M. Quantitative Proteomics Analysis of Vitreous Humor from Diabetic Retinopathy Patients. *J. Proteome Res.* **2015**, *14*, 5131–5143. [CrossRef] [PubMed]
33. Reich, M.; Dacheva, I.; Nobl, M.; Siwy, J.; Schanstra, J.P.; Mullen, W.; Koch, F.H.J.J.; Kopitz, J.; Kretz, F.T.A.A.; Auffarth, G.U.; et al. Proteomic Analysis of Vitreous Humor in Retinal Vein Occlusion. *PLoS ONE* **2016**, *11*, e0158001. [CrossRef] [PubMed]
34. Skeie, J.M.; Roybal, C.N.; Mahajan, V.B. Proteomic insight into the molecular function of the vitreous. *PLoS ONE* **2015**, *10*, 1–19. [CrossRef] [PubMed]

35. Nobl, M.; Reich, M.; Dacheva, I.; Siwy, J.; Mullen, W.; Schanstra, J.P.; Choi, C.Y.; Kopitz, J.; Kretz, F.T.A.; Auffarth, G.U.; et al. Proteomics of vitreous in neovascular age-related macular degeneration. *Exp. Eye Res.* **2016**, *146*, 107–117. [CrossRef] [PubMed]
36. Stone, J.; Maslim, J.; Valter-Kocsi, K.; Mervin, K.; Bowers, F.; Chu, Y.; Barnett, N.; Provis, J.; Lewis, G.; Fisher, S.K.; et al. Mechanisms of photoreceptor death and survival in mammalian retina. *Prog. Retin. Eye Res.* **1999**, *18*, 689–735. [CrossRef]
37. Narayan, D.S.; Chidlow, G.; Wood, J.P.M.; Casson, R.J. Glucose metabolism in mammalian photoreceptor inner and outer segments. *Clin. Exp. Ophthalmol.* **2017**, *45*, 730–741. [CrossRef] [PubMed]
38. Mandal, N.; Lewis, G.P.; Fisher, S.K.; Heegaard, S.; Prause, J.U.; la Cour, M.; Vorum, H.; Honoré, B. Protein changes in the retina following experimental retinal detachment in rabbits. *Mol. Vis.* **2011**, *17*, 2634–2648. [PubMed]
39. Bolaños, J.P.; Almeida, A.; Moncada, S. Glycolysis: A bioenergetic or a survival pathway? *Trends Biochem. Sci.* **2010**, *35*, 145–149. [CrossRef] [PubMed]
40. Ganea, E.; Harding, J.J. Glutathione-related enzymes and the eye. *Curr. Eye Res.* **2006**, *31*, 1–11. [CrossRef] [PubMed]
41. Bhosale, P.; Larson, A.J.; Frederick, J.M.; Southwick, K.; Thulin, C.D.; Bernstein, P.S. Identification and characterization of a Pi isoform of glutathione S-transferase (GSTP1) as a zeaxanthin-binding protein in the macula of the human eye. *J. Biol. Chem.* **2004**, *279*, 49447–49454. [CrossRef] [PubMed]
42. Lee, W.-H.; Joshi, P.; Wen, R. Glutathione S-Transferase Pi Isoform (GSTP1) expression in murine retina increases with developmental maturity. In *Advances in Experimental Medicine and Biology*; Bowes Rickman, C., LaVail, M.M., Anderson, R.E., Grimm, C., Hollyfield, J., Ash, J., Eds.; Springer: Cham, Switzerland, 2014; Volume 854, pp. 23–30. ISBN 978-3-319-17120-3.
43. Aït-Ali, N.; Fridlich, R.; Millet-Puel, G.; Clérin, E.; Delalande, F.; Jaillard, C.; Blond, F.; Perrocheau, L.; Reichman, S.; Byrne, L.C.; et al. Rod-derived cone viability factor promotes cone survival by stimulating aerobic glycolysis. *Cell* **2015**, *161*, 817–832. [CrossRef] [PubMed]
44. Chertov, A.O.; Holzhausen, L.; Kuok, I.T.; Couron, D.; Parker, E.; Linton, J.D.; Sadilek, M.; Sweet, I.R.; Hurley, J.B. Roles of glucose in photoreceptor survival. *J. Biol. Chem.* **2011**, *286*, 34700–34711. [CrossRef] [PubMed]
45. Li, M.; Li, H.; Jiang, P.; Liu, X.; Xu, D.; Wang, F. Investigating the pathological processes of rhegmatogenous retinal detachment and proliferative vitreoretinopathy with metabolomics analysis. *Mol. Biosyst.* **2014**, *10*, 1055–1062. [CrossRef] [PubMed]
46. Vadlapatla, R.K.; Vadlapudi, A.D.; Mitra, A.K. Hypoxia-inducible factor-1 (HIF-1): A potential target for intervention in ocular neovascular diseases. *Curr. Drug Targets* **2013**, *14*, 919–935. [CrossRef] [PubMed]
47. Semenza, G.L. Hypoxia-inducible factor 1: Control of oxygen homeostasis in health and disease. *Pediatr. Res.* **2001**, *49*, 614–617. [CrossRef] [PubMed]
48. Kannan, R.; Sreekumar, P.G.; Hinton, D.R. Novel roles for α-crystallins in retinal function and disease. *Prog. Retin. Eye Res.* **2012**, *31*, 576–604. [CrossRef] [PubMed]
49. Yao, J.; Liu, X.; Yang, Q.; Zhuang, M.; Wang, F.; Chen, X.; Hang, H.; Zhang, W.; Liu, Q. Proteomic analysis of the aqueous humor in patients with wet age-related macular degeneration. *Proteom. Clin. Appl.* **2013**, *7*, 550–560. [CrossRef] [PubMed]
50. Garrido, C.; Gurbuxani, S.; Ravagnan, L.; Kroemer, G. Heat Shock Proteins: Endogenous Modulators of Apoptotic Cell Death. *Biochem. Biophys. Res. Commun.* **2001**, *286*, 433–442. [CrossRef] [PubMed]
51. Kayama, M.; Nakazawa, T.; Thanos, A.; Morizane, Y.; Murakami, Y.; Theodoropoulou, S.; Abe, T.; Vavvas, D.; Miller, J.W. Heat shock protein 70 (HSP70) is critical for the photoreceptor stress response after retinal detachment via modulating anti-apoptotic Akt kinase. *Am. J. Pathol.* **2011**, *178*, 1080–1091. [CrossRef] [PubMed]
52. Urbak, L.; Vorum, H. Heat Shock Proteins in the Human Eye. *Int. J. Proteom.* **2010**, *2010*, 1–8. [CrossRef] [PubMed]
53. Inamdar, S.M.; Lankford, C.K.; Laird, J.G.; Novbatova, G.; Tatro, N.; Whitmore, S.S.; Scheetz, T.E.; Baker, S.A. Analysis of 14-3-3 isoforms expressed in photoreceptors. *Exp. Eye Res.* **2018**, *170*, 108–116. [CrossRef] [PubMed]
54. Nakano, K.; Chen, J.; Tarr, G.E.; Yoshida, T.; Flynn, J.M.; Bitensky, M.W. Rethinking the role of phosducin: Light-regulated binding of phosducin to 14-3-3 in rod inner segments. *Proc. Natl. Acad. Sci. USA* **2001**, *98*, 4693–4698. [CrossRef] [PubMed]

55. Hayasaka, S. Lysosomal enzymes in ocular tissues and diseases. *Surv. Ophthalmol.* **1983**, *27*, 245–258. [CrossRef]
56. Mahon, G.J.; Anderson, H.R.; Gardiner, T.A.; McFarlane, S.; Archer, D.B.; Stitt, A.W. Chloroquine causes lysosomal dysfunction in neural retina and RPE: Implications for retinopathy. *Curr. Eye Res.* **2004**, *28*, 277–284. [CrossRef] [PubMed]
57. Quintyn, J.C.; Brasseur, G. Subretinal fluid in primary rhegmatogenous retinal detachment: Physiopathology and composition. *Surv. Ophthalmol.* **2004**, *49*, 96–108. [CrossRef] [PubMed]
58. Hayasaka, S.; Hara, S.; Mizuno, K. Lysosomal Enzymes in Subretinal Fluid. *Albrecht Graefes Arch. Klin. Exp. Ophthalmol.* **1976**, *20*, 13–20. [CrossRef]
59. Im, E.; Kazlauskas, A. The role of cathepsins in ocular physiology and pathology. *Exp. Eye Res.* **2007**, *84*, 383–388. [CrossRef] [PubMed]
60. Molday, R.S.; Moritz, O.L. Photoreceptors at a glance. *J. Cell Sci.* **2015**, *128*, 4039–4045. [CrossRef] [PubMed]
61. Wensel, T.G. Signal transducing membrane complexes of photoreceptor outer segments. *Vis. Res.* **2008**, *48*, 2052–2061. [CrossRef] [PubMed]
62. Zhou, X.E.; Melcher, K.; Xu, H.E. Structure and activation of rhodopsin. *Acta Pharmacol. Sin.* **2012**, *33*, 291–299. [CrossRef] [PubMed]
63. Ridge, K.D.; Palczewski, K. Visual rhodopsin sees the light: Structure and mechanism of G protein signaling. *J. Biol. Chem.* **2007**, *282*, 9297–9301. [CrossRef] [PubMed]
64. Clack, J.W.; Springmeyer, M.L.; Clark, C.R.; Witzmann, F.A. Transducin subunit stoichiometry and cellular distribution in rod outer segments. *Cell Biol. Int.* **2006**, *30*, 829–835. [CrossRef] [PubMed]
65. Murakami, Y.; Notomi, S.; Hisatomi, T.; Nakazawa, T.; Ishibashi, T.; Miller, J.W.; Vavvas, D.G. Photoreceptor cell death and rescue in retinal detachment and degenerations. *Prog. Retin. Eye Res.* **2013**, *37*, 114–140. [CrossRef] [PubMed]
66. Arroyo, J.G.; Yang, L.; Bula, D.; Chen, D.F. Photoreceptor apoptosis in human retinal detachment. *Am. J. Ophthalmol.* **2005**, *139*, 605–610. [CrossRef] [PubMed]
67. Lo, A.C.Y.; Woo, T.T.Y.; Wong, R.L.M.; Wong, D. Apoptosis and other cell death mechanisms after retinal detachment: Implications for photoreceptor rescue. *Ophthalmologica* **2011**, *226*, 10–17. [CrossRef] [PubMed]
68. Okada, M.; Matsumura, M.; Ogino, N.; Honda, Y. Müller cells in detached human retina express glial fibrillary acidic protein and vimentin. *Graefes Arch. Clin. Exp. Ophthalmol.* **1990**, *228*, 467–474. [CrossRef] [PubMed]
69. Lewis, G.P.; Fisher, S.K. Up-Regulation of Glial Fibrillary Acidic Protein in Response to Retinal Injury: Its Potential Role in Glial Remodeling and a Comparison to Vimentin Expression. *Int. Rev. Cytol.* **2003**, *230*, 263–290. [CrossRef] [PubMed]
70. Nakazawa, T.; Takeda, M.; Lewis, G.P.; Cho, K.-S.; Jiao, J.; Wilhelmsson, U.; Fisher, S.K.; Pekny, M.; Chen, D.F.; Miller, J.W. Attenuated Glial Reactions and Photoreceptor Degeneration after Retinal Detachment in Mice Deficient in Glial Fibrillary Acidic Protein and Vimentin. *Investig. Opthalmol. Vis. Sci.* **2007**, *48*, 2760. [CrossRef] [PubMed]
71. Verardo, M.R.; Lewis, G.P.; Takeda, M.; Linberg, K.A.; Byun, J.; Luna, G.; Wilhelmsson, U.; Pekny, M.; Chen, D.F.; Fisher, S.K. Abnormal reactivity of Müller cells after retinal detachment in mice deficient in GFAP and vimentin. *Investig. Ophthalmol. Vis. Sci.* **2008**, *49*, 3659–3665. [CrossRef] [PubMed]
72. Quintyn, J.C.; Pereira, F.; Hellot, M.F.; Brasseur, G.; Coquerel, A. Concentration of neuron-specific enolase and S100 protein in the subretinal fluid of rhegmatogenous retinal detachment. *Graefes Arch. Clin. Exp. Ophthalmol.* **2005**, *20*, 20. [CrossRef] [PubMed]
73. Dunker, S.; Sadun, A.A.; Sebag, J. Neuron specific enolase in retinal detachment. *Curr. Eye Res.* **2001**, *23*, 382–385. [CrossRef] [PubMed]
74. Athanasiou, D.; Aguilà, M.; Bevilacqua, D.; Novoselov, S.S.; Parfitt, D.A.; Cheetham, M.E. The cell stress machinery and retinal degeneration. *FEBS Lett.* **2013**, *587*, 2008–2017. [CrossRef] [PubMed]
75. Sebag, J. *Vitreous*; Sebag, J., Ed.; Springer: New York, NY, USA, 2014; ISBN 978-1-4939-1086-1.
76. Morescalchi, F.; Duse, S.; Gambicorti, E.; Romano, M.R.; Costagliola, C.; Semeraro, F. Proliferative Vitreoretinopathy after eye injuries: An overexpression of growth factors and cytokines leading to a retinal keloid. *Mediat. Inflamm.* **2013**, *2013*. [CrossRef] [PubMed]
77. Sadaka, A.; Giuliari, G.P. Proliferative vitreoretinopathy: Current and emerging treatments. *Clin. Ophthalmol.* **2012**, *6*, 1325–1333. [CrossRef] [PubMed]

78. Yu, J.; Peng, R.; Chen, H.; Cui, C.; Ba, J.; Wang, F. Kininogen 1 and insulin-like growth factor binding protein 6: Candidate serum biomarkers of proliferative vitreoretinopathy. *Clin. Exp. Optom.* **2014**, *97*, 72–79. [CrossRef] [PubMed]
79. Kersten, E.; Paun, C.C.; Schellevis, R.L.; Hoyng, C.B.; Delcourt, C.; Lengyel, I.; Peto, T.; Ueffing, M.; Klaver, C.C.W.; Dammeier, S.; et al. Systemic and ocular fluid compounds as potential biomarkers in age-related macular degeneration. *Surv. Ophthalmol.* **2017**, 1–31. [CrossRef] [PubMed]
80. Sydorova, M.; Lee, M.S. Vascular Endothelial Growth Factor Levels in Vitreous and Serum of Patients with either Proliferative Diabetic Retinopathy or Proliferative Vitreoretinopathy. *Ophthalmic Res.* **2005**, *37*, 188–190. [CrossRef] [PubMed]
81. Yoshimura, T.; Sonoda, K.; Sugahara, M.; Mochizuki, Y.; Enaida, H.; Oshima, Y.; Ueno, A.; Hata, Y.; Yoshida, H.; Ishibashi, T. Comprehensive analysis of inflammatory immune mediators in vitreoretinal diseases. *PLoS ONE* **2009**, *4*, e8158. [CrossRef] [PubMed]
82. Shao, J.; Xin, Y.; Li, R.; Fan, Y. Vitreous and serum levels of transthyretin (TTR) in high myopia patients are correlated with ocular pathologies. *Clin. Biochem.* **2011**, *44*, 681–685. [CrossRef] [PubMed]
83. Maier, R.; Weger, M.; Haller-Schober, E.-M.; El-Shabrawi, Y.; Wedrich, A.; Theisl, A.; Aigner, R.; Barth, A.; Haas, A. Multiplex bead analysis of vitreous and serum concentrations of inflammatory and proangiogenic factors in diabetic patients. *Mol. Vis.* **2008**, *14*, 637–643. [PubMed]
84. Zheng, B.; Li, T.; Chen, H.; Xu, X.; Zheng, Z. Correlation between ficolin-3 and vascular endothelial growth factor-to-pigment epithelium-derived factor ratio in the vitreous of eyes with proliferative diabetic retinopathy. *Am. J. Ophthalmol.* **2011**, *152*, 1039–1043. [CrossRef] [PubMed]
85. Mesquita, J.; Castro Sousa, J.P.; Tavares-Ratado, P.; Vaz-Pereira, S.; Neves, A.; Rocha, A.S.; Santos, F.; Passarinha, L.; Tomaz, C. Comparison of serum and vitreous PlGF in diabetic retinopathy patients and non-diabetic patients. *Investig. Ophthalmol. Vis. Sci.* **2015**, *56*, 5179.
86. Mesquita, J.; e Sousa, J.P.C.; Vaz-Pereira, S.; Neves, A.; Passarinha, L.; Tomaz, C. Quantitative analysis and correlation of VEGF-A and VEGF-B in serum and vitreous humor of patients with proliferative vs non-proliferative ocular disease. *Investig. Ophthalmol. Vis. Sci.* **2017**, *58*, 604.
87. Mesquita, J.; Castro de Sousa, J.; Vaz-Pereira, S.; Neves, A.; Tavares-Ratado, P.; Santos, F.M.; Passarinha, L.A.; Tomaz, C.T. VEGF-B Levels in the Vitreous of Diabetic and Non-Diabetic Patients with Ocular Diseases and Its Correlation with Structural Parameters. *Med. Sci.* **2017**, *5*, 17. [CrossRef] [PubMed]
88. Paradela, A.; Mariscotti, J.F.; Navajas, R.; Ramos-Fernández, A.; Albar, J.P.; García-del Portillo, F. Inverse regulation in the metabolic genes pckA and metE revealed by proteomic analysis of the Salmonella RcsCDB regulon. *J. Proteome Res.* **2011**, *10*, 3386–3398. [CrossRef] [PubMed]
89. Mateos, J.; Carneiro, I.; Corrales, F.; Elortza, F.; Paradela, A.; del Pino, M.S.; Iloro, I.; Marcilla, M.; Mora, M.I.; Valero, L.; et al. Multicentric study of the effect of pre-analytical variables in the quality of plasma samples stored in biobanks using different complementary proteomic methods. *J. Proteom.* **2017**, *150*, 109–120. [CrossRef] [PubMed]
90. Uniprot. Available online: http://www.uniprot.org/ (accessed on 22 March 2014).
91. STRING: Functional Protein Association Networks. Available online: https://string-db.org/ (accessed on 27 November 2017).
92. Szklarczyk, D.; Franceschini, A.; Wyder, S.; Forslund, K.; Heller, D.; Huerta-Cepas, J.; Simonovic, M.; Roth, A.; Santos, A.; Tsafou, K.P.; Kuhn, M.; et al. STRING v10: Protein–protein interaction networks, integrated over the tree of life. *Nucleic Acids Res.* **2015**, *43*, D447–D452. [CrossRef] [PubMed]
93. Reactome Pathway Database. Available online: https://reactome.org/ (accessed on 26 March 2018).
94. KEGG: Kyoto Encyclopedia of Genes and Genomes. Available online: http://www.kegg.jp/kegg/ (accessed on 26 March 2018).

Section 3 – Paper V

Differentiating the Vitreous Proteome in Age-Related Macular Degeneration and Diabetic Retinopathy by Label-Free Relative Quantification and Multiple Reaction Monitoring

Fátima M. Santos, Sergio Ciordia, Alberto Paradela, João Paulo Castro de Sousa, Marta Garcia-Flores, Cândida T. Tomaz, Luís A. Passarinha

(Manuscript in preparation)

In this paper, a label-free quantitative (LFQ) method was applied to compare the vitreous proteome in PDR (n=4), dry AMD (n=4), and ERM (n=4). For this purpose, we implemented an LFQ method that combines a fractionation by short SDS–polyacrylamide gel electrophoresis and analysis by LC-MS/MS. Using this strategy, a total of 680 proteins were identified, of which 586 were identified using the software search engine MASCOT and 580 using MaxQuant. Post hoc tests revealed that 96 of these proteins are capable of differentiating among the different groups, whereas 118 proteins (17 up- and 101 down-regulated) were found differentially regulated in PDR compared to ERM and 95 proteins (10 up- and 85 down-regulated) in PDR compared to dry AMD. Functional enrichment analysis indicates that these differentially expressed proteins are correlated to pathways/ biological processes such as complement and coagulation cascades, ECM organization, platelet degranulation, lysosomal degradation, cell adhesion, and central nervous system development. Finally, some potential biomarkers were selected according to iTRAQ and LFQ experiments and validated by multiple reaction monitoring (MRM) in a larger set of vitreous samples. Of the 35 proteins analyzed, complement and coagulation components (C6, C8B, prothrombin), acute-phase proteins (alpha-1-antichymotrypsin), adhesion molecules (galectin-3-binding protein), ECM components (opticin), and neurodegeneration biomarkers (beta-amyloid, amyloid-like protein 2) stand out as the more efficient biomarkers to discriminate among the different disease groups.

The supplementary material of this article is available in the Appendix.

Original research manuscript

Differentiating the Vitreous Proteome in Age-Related Macular Degeneration and Diabetic Retinopathy by Label-Free Relative Quantification and Multiple Reaction Monitoring

Fátima M. Santos[1,2,3], Sergio Ciordia[4], Alberto Paradela[4], João Paulo Castro de Sousa[1,5], Cândida T. Tomaz[1,2], Luís A. Passarinha[1,3,6]*

[1] CICS-UBI – Centro de Investigação em Ciências da Saúde, Universidade da Beira Interior, 6201001 Covilhã, Portugal.

[2] Chemistry Department, Faculty of Sciences, University of Beira Interior, 6201-001 Covilhã, Portugal

[3] UCIBIO – Applied Molecular Biosciences Unit, Departamento de Química, Faculdade de Ciências e Tecnologia, Universidade NOVA de Lisboa, 2829-516 Caparica, Portugal

[4] Unidad de Proteómica, Centro Nacional de Biotecnología, CSIC, Calle Darwin 3, Campus de Cantoblanco, 28049 Madrid, Spain.

[5] Department of Ophthalmology, Centro Hospitalar de Leiria, 2410-197 Leiria, Portugal.

[6] Laboratory of Pharmacology and Toxicology—UBIMedical, University of Beira Interior, 6200-284 Covilhã, Portugal.

Abstract

Diabetic retinopathy (DR) and age-related macular degeneration (AMD) are leading causes of visual impairment and blindness in people aged 50 years or older in middle-income and industrialized countries. Although Anti-VEGF therapies have improved the management of neovascular AMD (nAMD) and proliferative DR (PDR), no treatment options exist for the highly prevalent dry form of AMD. To unravel the biological mechanism processes underlying these pathologies and to find new potential biomarkers, a label-free quantitative (LFQ) method was applied to analyze the vitreous proteome in PDR (n=4), AMD (n=4) compared to idiopathic epiretinal membranes (ERM) (n=4). Post hoc tests revealed that 96 proteins are capable of differentiating among the different groups, whereas 118 proteins (17 up- and 101 down-) were found differentially regulated in PDR compared to ERM and 95 proteins (10 up- and 85 down-) in PDR compared to dry AMD. The pathway analysis indicates that mediators of complement and coagulation cascades and acute phase responses are enriched in PDR vitreous, whilst proteins highly correlated to the extracellular matrix (ECM) organization, platelet degranulation, lysosomal degradation, cell adhesion, and central nervous system development were found underexpressed. According to these results, 35 proteins were selected and validated by MRM-based (multiple reaction monitoring) targeted proteomics in a larger set of vitreous samples from patients with ERM (n=21), DR/PDR (n=20), AMD (n=11), and retinal detachment/proliferative

* **Corresponding Author**: UCIBIO, Departmento de Química, Faculdade de Ciências e Tecnologia, Universidade Nova de Lisboa, 2829-516 Caparica, Portugal; Tel.: +351 275 329 069; Fax: +351 275 329 099; Email address: lpassarinha@fcsaude.ubi.pt,lapp@ubi.pt.

vitreoretinopathy (n=13). From the 26 potential biomarkers capable of differentiating between the different groups, complement and coagulation components (C6, C8B, prothrombin), acute-phase mediators (alpha-1-antichymotrypsin), adhesion molecules (galectin-3-binding protein), ECM components (opticin), and neurodegeneration biomarkers (beta-amyloid, amyloid-like protein 2) stand out efficiently to discriminate the disease groups under study.

Keywords: Age-related macular degeneration, Biomarkers, Complement and coagulation cascades, Neurodegeneration, Proliferative Diabetic Retinopathy, Vitreous proteomics.

1. Introduction

Despite improvements achieved in the prevention and control of ocular diseases in the past 30 years, the public health burden of visual impairment and blindness is expected to increase in the next years as a result of the dramatic growth and aging of the world population and increase in the prevalence of chronic diseases such as diabetes mellitus [1–3]. Diabetic retinopathy (DR) and age-related macular degeneration (AMD) are leading causes of visual impairment and blindness in people aged 50 years or older in middle-income and industrialized countries and, therefore, they are considered priority eye diseases by World Health Organization [4–6]. DR is a microvascular complication that develops in patients with diabetes [7, 8]. In the non-proliferative stage, early clinical features include the presence of microaneurysms, basement membrane thickening, and loss of pericytes, although increasing evidence suggests that microvascular changes may be preceded by neuroglial degeneration [2, 8–11]. AMD is a multifactorial disease characterized by the accumulation of soft drusen between the retinal pigment epithelium (RPE) and the degeneration of photoreceptors and RPE [12–14]. From this early stage, AMD can progress to a “dry” or non-exudative form that features an extensive macular degeneration (geographic atrophy) and hyperpigmentation of RPE, or to neovascular AMD (nAMD) [14–16]. In the most severe cases, deregulation of ocular angiogenesis leads both AMD and DR to progress to their proliferative etiology. Neovascularization in proliferative DR (PDR) occurs along the surface of the inner retina and into the posterior vitreous in response to sustained hypoxia, whereas in nAMD the choroidal vessels compromise the outer blood-retinal barrier and invade the subretinal space [17, 18].

Vascular Endothelial Growth Factor (VEGF) signaling plays a key role in vascular development and stimulation of ocular angiogenesis [18–20]. So, anti-VEGF drugs are currently used as first-line therapy for the management of PDR [21–23] and nAMD [24–26]. Nevertheless, anti-VEGF therapy requires frequent and costly intravitreal injections and has been associated with local side

Abbreviations: AACT, alpha-1-antichymotrypsin; AAT, alpha-1-antitrypsin; AMD, Age-Related Macular Degeneration; APLP2, Amyloid-like protein 2; APP, Beta-Amyloid; BCAN, Brevican core protein; C2, Complement 2; C5, Complement 5; C6, Complement 6; C8B, component C8 beta chain; CDH2, neural cadherin; CE, collision energy; CFH, complement factor H; CHGA, chromogranin-A; CLU, Clusterin; CST3, Cystatin-C; CSTN1, Calsyntenin-1; CTSZ, Cathepsin Z; DP, Declustering Potential; DR, Diabetic Retinopathy; ECM, Extracellular Matrix; ERM, Epiretinal Membranes; F2, Prothrombin; F9, Coagulation Factor IX; GNS, N-acetylglucosamine-6-sulfatase; IDA, Information-dependent acquisition.

effects (e.g. endophthalmitis, cataracts, retinal detachment, vitreous hemorrhage, and increased ocular pressure) [2, 27, 28]. Furthermore, some patients exhibit only a moderate to poor response with continued intensive anti-VEGF treatment [29, 30]. Besides that, therapies for "dry" AMD are still an unmet requirement and its management relies only on the prevention of risk factors (e.g. reducing cigarette consumption) and increased consumption of vitamins and oxidants [15, 31, 32]. Therefore, a better knowledge of the pathological mechanisms underlying the disease onset or progression could be helpful to explore cost-effective therapeutic alternatives for the management of these proliferative eye diseases [2, 5, 15, 33, 34].

So far, the characterization of the proteome of the vitreous humor in DR/PDR has contributed extensively to the recognition of target pathways and to identify candidate biomarkers for its diagnosis and treatment [35–38]. However, the validation of these potential biomarkers in a larger number of samples is frequently an unfulfilled requirement for the discovery of reliable vitreous biomarkers. On the other hand, few studies have focused on the characterization of vitreous proteomics in AMD [39–41]. To further elucidate some of these pathological mechanisms, we have applied a label-free quantitative (LFQ) proteomics approach for the understanding of the vitreous proteome in PDR and AMD compared to idiopathic epiretinal membranes (ERM) samples. A scheduled multiple reaction monitoring (MRM) method was designed for potential biomarker validation in a larger set of human vitreous samples.

2. Materials and methods

2.1. Collection of vitreous samples by pars plana vitrectomy

Vitreous samples were collected on the Ophthalmology Service of Leiria-Pombal Hospital, Portugal, as described previously [42], according to a protocol approved by the hospital ethics committee (Code: CHL-15481). All patients included in this study gave their informed consent, which adhered to the tenets of the Declaration of Helsinki. Vitreous samples were collected in sterile cryogenic vials at the beginning of pars plana vitrectomy by aspiration into a 2 mL syringe attached to the vitreous cutter. Upon collection, vitreous samples were placed immediately on ice and frozen at -80 oC until further analysis. The medical history of the patients was assessed to confirm the diagnosis, baseline characteristics, and associated diseases. Demographic characteristics and the description of corresponding vitreous samples are summarized in Table 1 and a more detailed version is given in supplementary table 1. Samples from patients subjected to intraocular surgeries or intravitreal drug treatments 3 months prior were excluded from the study. Most patients underwent surgery for ERM removal due to the marked decrease in visual acuity. For label-free proteomic analysis, 12 patients (7 women and 5 men) with the diagnosis of PDR (n=4), dry AMD (n=4), and ERM (n=4). Older patients or with other serious illnesses associated (e.g. neoplasia) were removed from the study. For MRM, more samples (n=65) were used, including some of the samples previously analyzed in the LFQ experiment. MRM experiments were performed on vitreous samples from patients with ERM (n=21), DR/PDR (n=20), AMD (n=11), rhegmatogenous retinal detachment (RRD) with and without proliferative vitreoretinopathy (PVR) (n=13). Finally, 27 patients were selected for Western Blot (WB) analysis,

including patients with ERM (n=5), PDR (n=9), AMD (n=6), and RRD (n=7), from which 3 patients have PVR.

2.2. Preparation of vitreous samples

Vitreous samples were centrifuged at 18 400 x g for 15 min at 4ºC and supernatant protein concentration was determined using a colorimetric assay (Pierce 660 nm protein assay, Thermo Fisher Scientific, Massachusetts, USA), according to manufacturer's instructions. For the removal of high-abundant proteins in vitreous, 400 µg of protein was depleted using High Select™ Top14 Abundant Protein Depletion Mini Spin Columns (Thermo Fischer Scientific, Massachusetts, USA), Briefly, 300 µl of sample was mixed with the resin by inverting the column several times until completely homogeneous and incubated for 10 min at room temperature. Depleted vitreous samples were recovered by centrifugation at 1000 x g for 2 min and concentrated using Nanosep® Centrifugal Devices 10K (Pall, Madrid, Spain). Then, samples were solubilized with loading sample buffer, denaturized at 60 ºC for 10 min, loaded, and concentrated in a 12% sodium dodecyl sulfate-polyacrylamide gel electrophoresis (SDS-PAGE) gel. After Quick Coomassie staining, protein bands were manually excised, cut into cubes (1 mm^2), and deposited in 96-well plates. Tryptic digestion was processed automatically in a Proteineer DP robot (Bruker Daltonics, Bremen, Germany), as previously described [43]. Tryptic peptides were extracted by adding 1% formic acid in 50% acetonitrile, collected from wells, dried by speed-vacuum centrifugation, and frozen at -20ºC until further processing.

2.3. LC-MS/MS quantitative analysis and database search

LC-MS/MS analyses were performed using a nanoLC Ultra 1D plus (Eksigent Technologies, AB SCIEX, Foster City, CA) coupled to a TripleTOF 5600 System via a Nanospray III source. Tryptic peptides were solubilized using solvent A (2% ACN, 0.1% FA) and the concentration was determined using Qubit assay (Thermo Fisher), according to manufacturer's instructions. Tryptic peptides (1 µg) were loaded onto a C18 Acclaim PepMapTM 100 trapping column (Thermo Scientific, 100 µm I.D. × 2 cm, 5 µm particle diameter, 100 Å) using solvent A at 2 µL/min and, after desalting, switched online with an Acquity UPLC® M-Class Peptide BEH C18 analytical Column (Waters, 75 µm × 15 cm, 1.7 µm, 130 Å). Peptides were fractionated at a flow rate of 250 nL/min in a 250 min gradient with concentrations of ACN ranging from 2% to 90%. TripleTOF 5600 system was operated in positive ion mode with an ion spray voltage of 2300 V, curtain gas (CUR) of 35, interface heater temperature (IHT) of 150ºC, ion source gas 1 (GS1) of 25 and, declustering potential (DP) of 100 V. Data was acquired in information-dependent acquisition (IDA) mode with Analyst TF 1.7 software (SCIEX, USA). IDA parameters were: survey scan in the mass range of 350–1250 m/z, accumulation time of 250 ms, followed by MS^2 spectrum accumulation for 100 ms (100–1800 m/z) in a cycle of 4.04 sec. The criteria for MS/MS fragmentation were defined for ions greater than 350 and smaller than 1250 m/z with a charge state of 2–5 and an abundance threshold greater than 90 counts. Dynamic exclusion was allowed

for a period of 15s. IDA rolling collision energy (CE) parameter script was used for automatically controlling the CE.

MaxQuant (http://maxquant.org/, Version 1.6.5.0) was used to generate peak lists from raw files, peptide and protein identification after database search, and for LFQ intensity and intensity-based absolute quantification (iBAQ) algorithm. Andromeda search engine was used to search the acquired MS/MS spectra against the Homo sapiens UniProtKB reviewed database (20418 protein sequences). Search parameters were set as follows: carbamidomethyl (C) as a fixed modification, oxidation (M), acetyl (Protein N-term), Gln->pyro-Glu and, Glu->pyro-Glu as variable modifications, trypsin/P as protease allowing up to 2 missed cleavages. Precursor mass tolerances were set at 20 ppm and the fragment mass tolerance at 0.01 Da. Proteins identified only with modified peptides ("only by site"), reversed sequences, and potential contaminants were removed from the reported identified protein groups. For LFQ, multiplicity was set at 1, LFQ min ratio counts at 2, and the options "iBAQ" and "match between runs" (time window of 0.7 min and alignment of 20 min) were picked. The false discovery rate (FDR) of peptides and proteins was set at 1%.

Additionally, mgf. files were generated using Peak View (AB SCIEX) and searched against homo sapiens UniProtKB reviewed database, which included 20418 protein sequences and corresponding reversed sequences, using Mascot v.2.2.04. Search parameters were identical to those previously described but peptide mass tolerance was set as 25 ppm and MS/MS fragment tolerance as 0.05 Da. FDR of ≤1% at peptide level was assessed applying a target-Decoy approach, in which MS/MS data were searched against both the target database and the decoy sequence database, containing reversed shuffled peptide sequences [44].

2.4. Bioinformatics and statistical analysis

The protein normalized intensity lists of the 12 vitreous samples from PDR (n=4), nAMD (n=4), and ERM (n=4) groups were processed using Perseus software (version 1.6.10.0). The normalized intensity was calculated by dividing the intensity of each protein by the sum of the intensity of all proteins detected in that sample and multiplying it by the median of the sum of the intensity of all proteins detected in vitreous samples. Depleted proteins, potential contaminants, reversed and proteins only identified by site were removed. Data were logarithmized (Log2), filtered by valid values (min 70% of valid values), and missing values were imputed with random numbers from a normal distribution (width=0.3, shift=1.8). Multi scatter plots and histograms were applied to evaluate data quality. Post hoc tests, hierarchical clustering, principal component analysis (PCA), and two-sample t-tests were performed for differentiating the three groups in terms of protein expression based on intensity differences. A permutation-based method was used to correct for multiple hypothesis testing with the number of randomizations set to 250 and an FDR<5%. Differentially expressed proteins were analyzed using DAVID Bioinformatics website (https://david.ncifcrf.gov/) [45], and ClueGO (version 2.5.7) [46] for functional enrichment based on gene ontology (GO) analyses and pathways/reactions (KEGG and REACTOME databases). Protein-protein association networks were assessed using the online tool STRING 11 (http://string-db.org), with high confidence (0.75) and based on the molecular action [47].

2.5. Validation by multiple reaction monitoring

MRM based targeted proteomics analysis was designed in Skyline v. 4.2.0.19009 and performed in a nanoLC Ultra 1D plus Ultra 2D Plus system (Eksigent Technologies, AB SCIEX, Foster City, CA) coupled to a 5500 QTRAP triple quadrupole mass spectrometer (Sciex, Massachusetts, USA) via a Nanospray III source. A scheduled method was designed for the relative quantitation of 35 proteins, using 2-3 prototypic peptides per protein and 3-4 transitions per peptide (332 transitions in total), based on the in-silico digestion of protein sequences of database and MS^2 spectrums from shotgun experiments. The Homo sapiens UniProtKB reviewed database was used as background proteome. The selected enzyme was trypsin/P [KR |-] and the peptide parameters were: length range 8 to 25 amino acids, charged 2+ and 3+, no miscleavages, and potentially modified residues such as methionine (Met, M) and cysteine (Cys, C). When possible, peptides were selected from distinct regions of the protein sequence. For sample preparation, 10 µg of non-depleted vitreous samples were loaded on a SDS-PAGE gel and in-gel digested, as previously described. The peptide concentration was determined using Qubit assay (Thermo Fisher), according to the manufacturer's instructions, and 1 µg of tryptic peptides was loaded onto a C18 Acclaim PepMapTM 100 column (Thermo Scientific, 300 µm I.D. × 5 cm, 5 µm particle diameter, 100 Å) using solvent A (2%B ACN, 0.1% formic acid in water) at 2 µL/min. After desalting, trap column was switched online with a C18 BioSphere column (Nano-separations, 75 µm I.D. × 15 cm, 3 µm particle diameter, 120 Å) and peptides were fractionated in a 30 min gradient to 90 % of mobile phase B (100% ACN, 0.1% formic acid) at 300 nL/min, followed by 15 min of equilibration. The 5500 QTRAP system was operated in positive polarity and the MRM scan mode, with an ion spray voltage of 2800 V, IHT of 150 ºC, CUR of 20, GS1 of 25, medium collision gas, and DP of 80 V. Scheduled mode was enabled and detection window set at 300 sec. Collision energy and the expected retention time for each transition were defined in Skyline, according to the preliminary data. Beta-galactosidase standards and a pool of vitreous samples were injected alternately with the vitreous samples to monitor unwanted changes in the MS signal and in the retention time. Raw MS data were imported into Skyline and the automatically selected chromatographic peaks were manually revised considering both the expected retention times and the distribution of the signal strength of the transitions. The total area, which corresponds to the sum of the intensity of all transitions per peptide and all peptides of a specific protein, was used for further statistical analysis. The total area of each protein was normalized by dividing it by the total area of digested beta-galactosidase injected between each sample to correct the augment of the signal of MS equipment over time. GraphPad Prism Software (San Diego, CA, USA) was applied for statistical analysis (Kruskal-Wallis tests, q-value<0.05) with the correction for multiple comparisons and to generate receiver operating characteristic (ROC) curves.

2.6. Validation by Western Blotting

For Western blot analysis, equal amounts of proteins (15 µg) were separated by SDS-PAGE and transferred to a PVDF membrane using the Trans-Blot Turbo™ Transfer System (Bio-Rad Laboratories, Hercules, CA, USA). After blocking with 5% of powdered milk in 0.1% Tween-20,

the membranes were incubated overnight at 4 ◦C with distinct antibodies in 5% of BSA, including 1:3000-diluted polyclonal rabbit anti-human chromogranin-A (CHGA) antibody (A0430; Dako), 1:500-diluted polyclonal rabbit anti-tissue inhibitor of metalloproteinase inhibitor 2 (TIMP2) antibody (ab74216; Abcam), 1:1000-diluted monoclonal mouse anti-β-Amyloid (APP) antibody (A5213, Sigma-Aldrich), and 1:500-diluted monoclonal mouse anti-cystatin C (CST3) antibody (sc-515732; Santa Cruz Biotechnology). PVDF membranes were incubated with a 1:100000 dilution of anti-mouse IgG (Fab specific)–Peroxidase antibody (A3682; Sigma-Aldrich) or anti-Rabbit IgG (whole molecule)–Peroxidase antibody (A0545; Sigma-Aldrich). Protein bands were visualized using the Clarity Western ECL Substrate (Biorad, Hercules, CA, USA). Band detection and relative quantification were performed using Image lab 5.0 software (Biorad, Hercules, CA, USA). Statistical analyses (Kruskal-Wallis tests, q-value<0.05) were performed using GraphPad Prism Software (San Diego, CA, USA).

3. Results

3.1. Vitreous proteome in diabetic retinopathy and age-related macular degeneration

For the discovery phase, a LFQ strategy was applied to analyze the proteome of vitreous collected from patients with DR (n=4), dry AMD (n=4), and ERM (n=4). Using two different strategies for protein database search, a total of 680 proteins were identified, of which 586 proteins were identified by MASCOT and 580 proteins by MaxQuant (corresponding to 474 protein groups) (supplementary table 2). A total number of 195 protein groups were detected in all the samples. An average of 366 ± 31 protein groups was identified in control ERM vitreous, 361 ± 46 protein groups in dry AMD, and 310 ± 14 protein groups in PDR. Multiple scatter plots (supplementary figure 1) were applied to assess data reproducibility and correlation within and between disease groups. The analysis of multiple scatter plots showed high data reproducibility. The best correlation values between replicates and within groups were found for PDR samples (average 0.89 ± 0.02), but samples from dry AMD and ERM groups also showed good correlation values between groups (average 0.87 ± 0.05). Sample correlation was higher within than between groups, except for the dry AMD group. One of the samples collected from a patient with dry AMD (VH 219) showed a poorer correlation (< 0.8) with other samples within the same disease group and a higher correlation with samples from the PDR group (> 0.87). So, this sample was removed from quantitative analysis, improving within-group Pearson correlation values from an average of 0.84 ± 0.06 to 0.90 ± 0.01 (supplementary figure 1).

Subsequently, post hoc tests and hierarchical clustering were performed to differentiate the three groups in terms of protein expression based on intensity differences. Post hoc tests revealed that 96 proteins are differentially expressed among the three disease groups. Specifically, 83 proteins distinguished between PDR and ERM groups while 79 proteins did so between PDR and dry AMD groups (supplementary table 3). Hierarchical clustering analysis of these 96 proteins is represented in heatmap based on its intensities normalized to log base 2 (Figure 1A). Figure 1A reveals that most of these proteins are down-regulated in PDR compared to ERM and dry AMD

groups (blue cluster), except for a small cluster (orange cluster) composed mainly of complement (C5, C2, CFH) and coagulation factors such as prothrombin (F2), among other proteins. Only inter-alpha-trypsin inhibitor heavy chain H3 (ITIH3) differentiates the dry AMD from ERM control samples in hierarchical clustering, as represented in a pink cluster (Figure 1A).

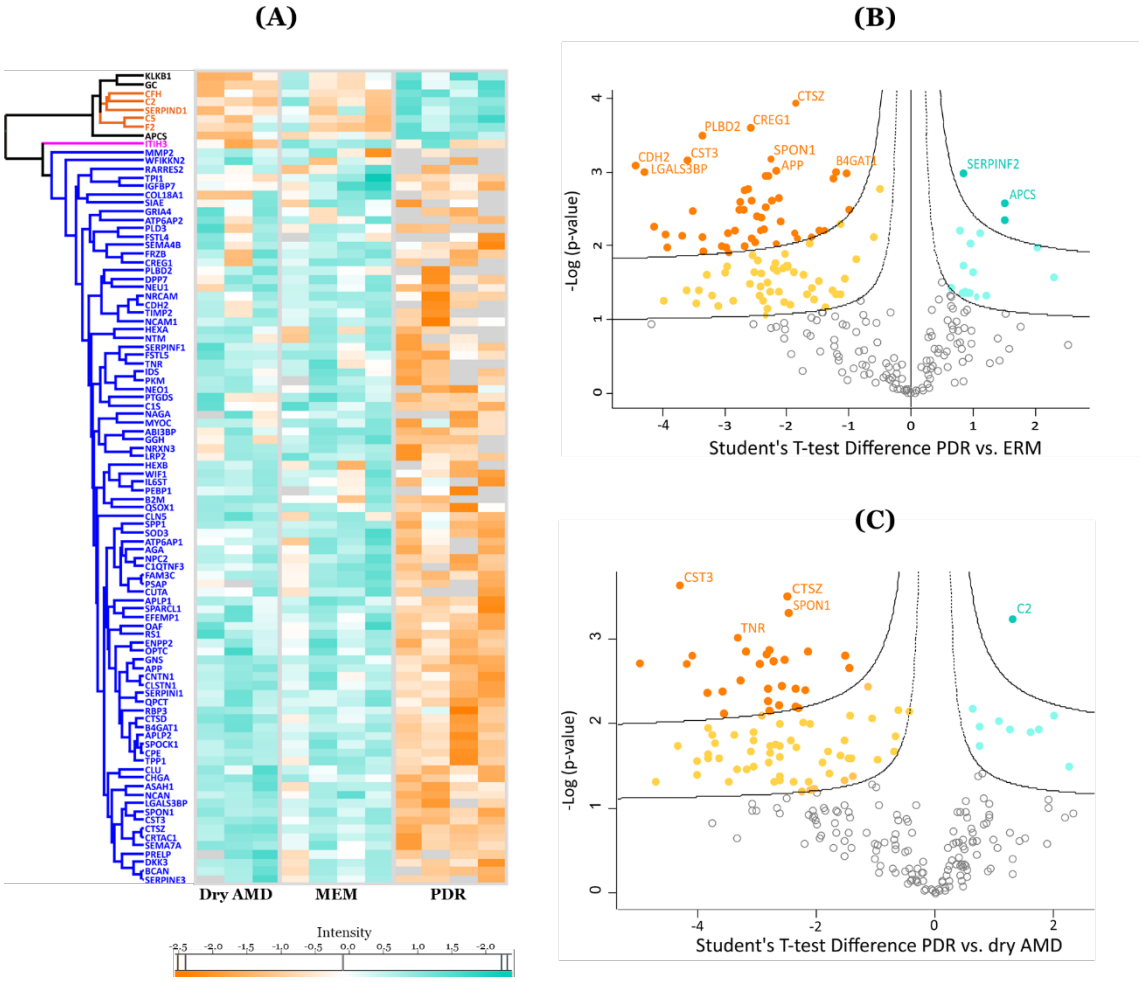

Fig. 1 - (A) Heatmap representing the intensities normalized to log base 2 and analyzed by hierarchical clustering of 96 proteins found differentially expressed among the three disease groups in post hoc tests. Hawaii plots display the proteins found up-regulated (blue-green) and down-regulated (orange) in proliferative diabetic retinopathy (PDR) compared to patients with (B) epiretinal membranes (ERM) and with (C) dry age-related macular degeneration (dry AMD).

Furthermore, multiple t-tests with an FDR cutoff of 5% were performed to identify differentially expressed proteins in PDR versus dry AMD and PDR versus ERM (Figure 1B/C and supplementary table 3). We found 118 significantly regulated proteins (17 up- and 101 down-) and 95 proteins (10 up- and 85 down-) in PDR relative to the ERM and dry AMD groups, respectively (Fig. 2C/D). Most proteins (5 up- and 76 down-regulated proteins) were found differentially expressed in PDR relative to the other two disease groups, but 14 proteins were found exclusively by comparison with dry AMD group and 37 proteins by comparison with ERM group. Fetuin-B, keratin, type II cytoskeletal 2 epidermal and serum amyloid P-component showed the highest levels of expression in PDR (FDR<0.001), while the more significant down-regulated proteins were protein CREG1, neural cadherin (CDH2), galectin-3-binding protein (LGALS3BP), Putative

phospholipase B-like 2, and CST3. LGALS3BP and CST3 were also significantly downregulated in PDR versus dry AMD, as well as cathepsin Z (CTSZ), spondin-1 (SPON1), and tenascin-R (TNR). Complement C2 (C2) was the protein that showed the highest levels of expression in the PDR group compared to dry AMD with an FDR lower than 0.001 (Figure 1C). Some complement factors (e.g. CFB, C8B), acute-phase response proteins (e.g. F2, alpha-2-antiplasmin), and proteins related to lysosomal degradation (e.g. Alpha-N-acetylgalactosaminidase, Prosaposin, Cathepsin L1) and ECM organization (metalloproteinase inhibitor 1 (TIMP1)) only show differential expression in PDR compared to ERM. Although some proteins such as ProSAAS, neurosecretory protein VGF, or phosphoglycerate mutase 1 were exclusively detected in dry AMD samples, no differential proteins were found compared to ERM controls with an FDR<5%.

3.2. Vitreous Functional enrichment of differentially expressed proteins

To gain insights into the biological roles and pathways of the differentially expressed proteins, the proteins were analyzed using a combination of bioinformatics tools such as DAVID, ClueGo (Cytoscape app), and STRING. Functional enrichment indicates that underexpressed proteins in PDR are highly correlated and share common biological processes/pathways such as extracellular matrix (ECM) disassembly and organization, platelet degranulation, lysosomal degradation, cell adhesion, and central nervous system development (e.g. regulation of axon regeneration) (Figure 2A/B and supplementary table 4). Decreased levels of proteins involved in chondroitin sulfate catabolic process and keratan sulfate catabolic process, including beta-hexosaminidase (HEXA, HEXB) and N-acetylglucosamine-6-sulfatase (GNS). Furthermore, some of the proteins involved in these processes also participate in cell adhesion and ECM organization, including brevican core protein (BCAN) and neurocan core protein (NCAN), or are ECM components such as prolargin. In turn, proteins related to acute-phase responses and fibrin clot formation are only found upregulated in PDR compared to ERM, whereas complement and coagulation proteins are up-regulated in PDR in both comparisons. According to GO classification for molecular function (Figure 2D), both up- and down-regulated proteins in PDR have serine-type endopeptidase activity (7.0- and 6.0-fold enrichment), serine-type endopeptidase (18.5- and 17.6-fold) and metalloendopeptidase inhibitor activities (46.7- and 35.6-fold), or binding function (e.g. heparin and calcium). On the other hand, down-regulated proteins have serine-type carboxypeptidase activity (32.0- and 54.2-fold), binding functions, or are ECM structural constituents (13.4- and 14.2-fold). According to GO classification for cellular components (Figure 2E), most of the differentially expressed proteins are localized extracellularly, and, curiously, many of them are associated with extracellular exosomes (87 proteins). A significant part of downregulated proteins in PDR compared to ERM and dry AMD are in the basement membrane (13.7- and 7.3-fold enrichment), the lysosomal lumen (25.4- and 33.9-fold enrichment), and secretory vesicles, such as platelet dense granule (44.1 and 41.1-fold enrichment), whereas overexpressed proteins are mainly blood microparticles. ECM-related proteins were mainly found underexpressed in PDR with fold enrichment of 11.0 and 9.7 comparing to ERM and dry AMD, respectively. Although with less significance, many underregulated proteins are localized in the neuronal cell body, axons, node of Ranvier, perineuronal nets, and postsynaptic membranes. Differentially expressed

proteins were also analyzed based on the Genetic Association Database using the DAVID bioinformatics tool (supplementary table 4). Proteins involved in pathways, such as complement and coagulation cascades, lysosomal degradation, ECM organization, and regulation of inflammatory response, were found associated with type 2 diabetes and macular edema, whereas the pigment epithelium-derived factor (PEDF) and serine protease HTRA1 were found specifically related to DR. These two proteins, as well as complement components (e.g. CFH, C2), regulators of complement cascades (clusterin (CLU)) and amyloidosis proteins (amyloid-beta precursor protein [APP], CST3) are also associated to macular degeneration and pathological processes, such as choroidal neovascularization, geographic atrophy, and retinal drusen.

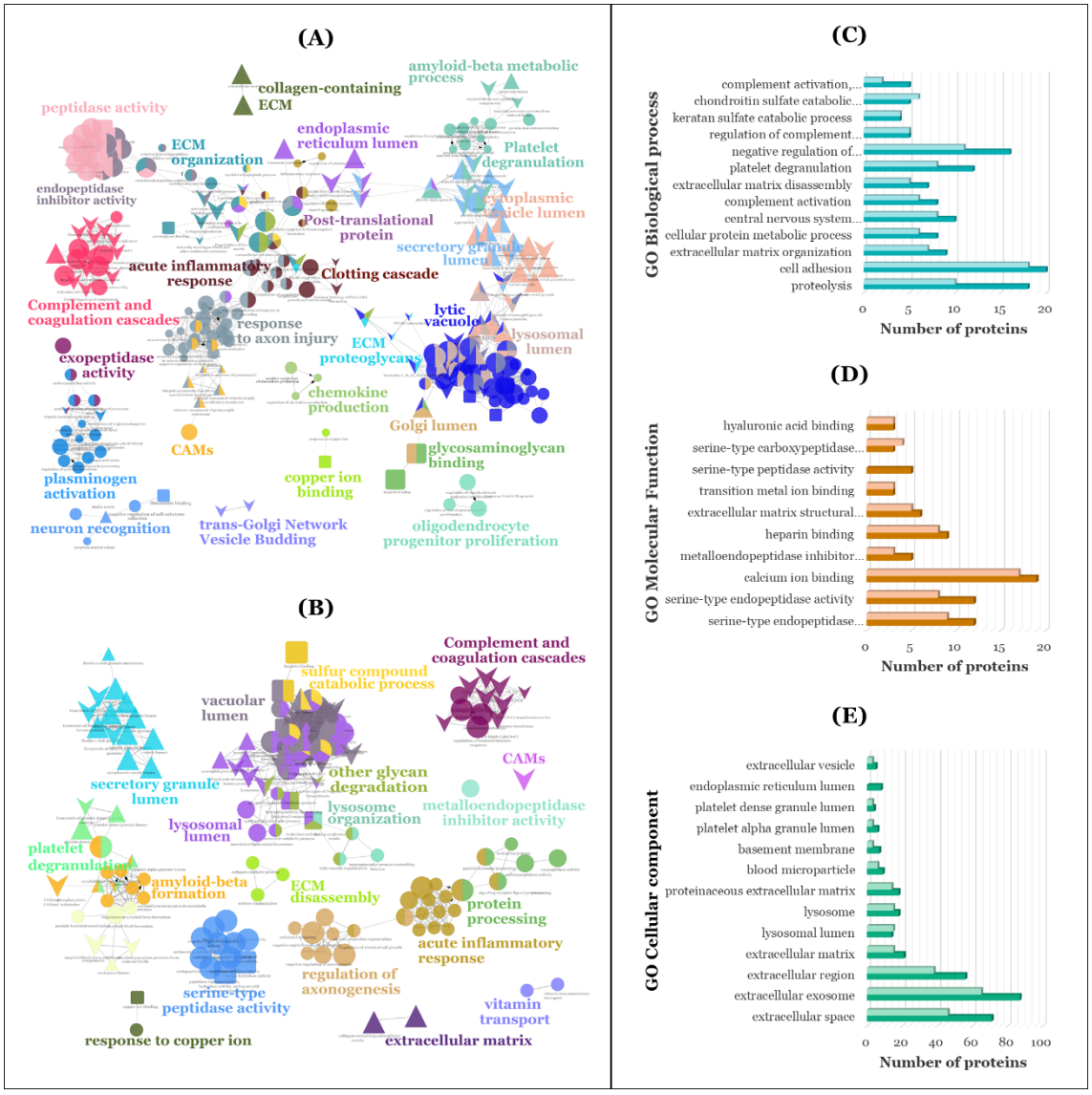

Fig. 2 - Functionally grouped network of enriched categories generated in ClueGO (Cytoscape) for the proteins found differentially expressed in proliferative diabetic retinopathy (PDR) compared to patients with (A) epiretinal membranes (ERM) and with (B) dry age-related macular degeneration (dry AMD). These proteins were also classified according to gene ontology (GO) terms using DAVID Bioinformatics tool and ClueGo for (C) biological process, (D) molecular function, and (E) cellular component with the darkest colors representing proteins differentially expressed in PDR versus ERM, and lightest colors representing proteins differentially expressed in PDR versus dry AMD. ECM – extracellular matrix; CAMs - Cell adhesion molecules.

In addition, STRING was used to generate high confidence (0.70) overall protein-protein interaction network between 118 differentially expressed proteins in PDR versus ERM (Figure 3A) and 95 proteins in PDR versus dry AMD (Figure 3B). Some biological processes/pathways stand out in both interaction networks, including multicellular organism and nervous system development, myeloid leukocyte activation, regulation of proteolysis, and cell adhesion, as well as proteins associated with lysosomes. These data reinforce that ECM organization, complement and coagulation cascades, and inflammatory responses are implicated in these diseases. Specific pathways/terms such as regulation of insulin-like growth factor (IGFs) transport and uptake by insulin-like growth factor binding proteins (IGFBPs), amyloidosis, neurodegeneration, metabolism of angiotensinogen to angiotensin, post-translational modifications (e.g phosphorylation), and regulation of Wnt signaling and MAPK cascades were also found associated to differentially expressed proteins. Remarkably, several proteins, including APP, CLU, CST3, CTSZ, osteopontin (SPP1), TIMP2, and lecticans (versican core protein (VCAN), NCAN, BCAN), play key roles in multiple pathways, as seen in Figure 3.

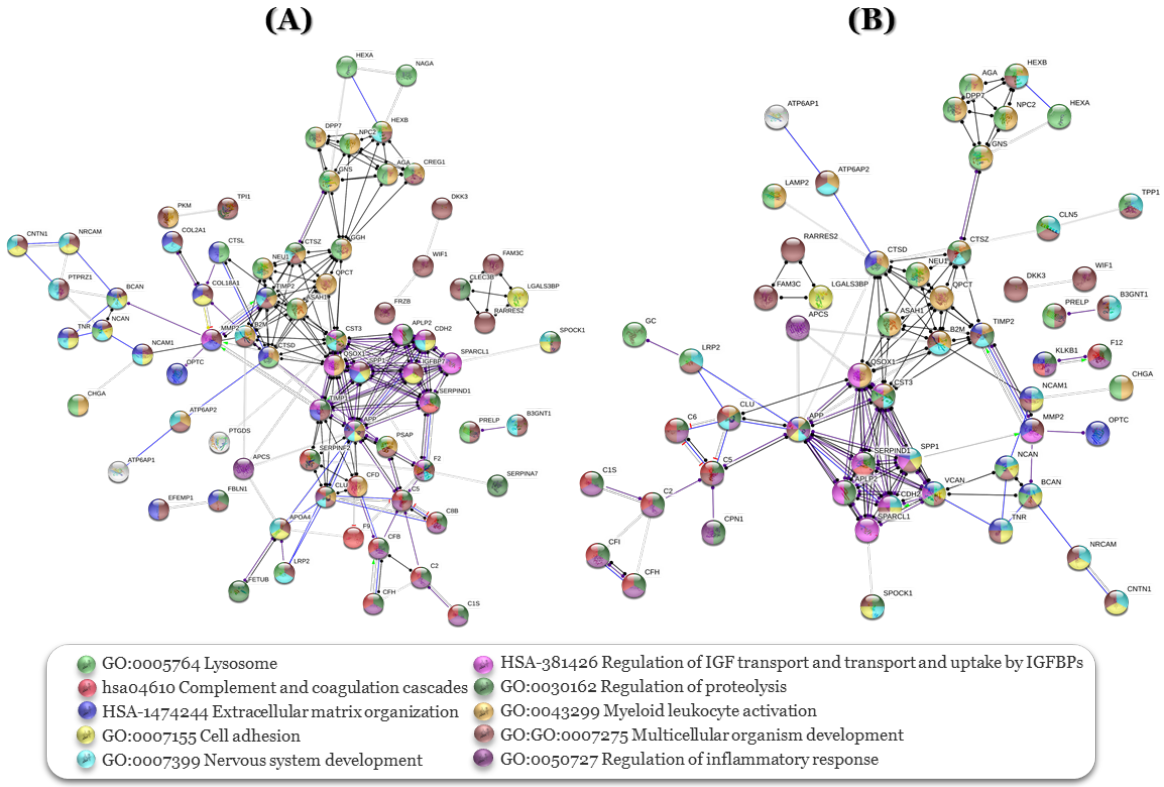

Fig. 3 - Protein-protein interaction network between (A) 118 differentially expressed proteins in proliferative diabetic retinopathy (PDR) versus epiretinal membranes (ERM), and (B) 95 differentially expressed proteins in PDR versus dry age-related macular degeneration based on molecular action with high confidence (0.70). Some biological processes/pathways stand out in both interaction networks, including complement and coagulation cascades, lysosomal degradation, cell adhesion, extracellular matrix organization, multicellular organism, and nervous system development, among others, as represented by colored nodes.

3.3. Vitreous Functional enrichment of differentially expressed proteins

Some potential biomarkers were selected for further validation by targeted proteomics (MRM). Potential biomarkers were selected based on their differential levels of expression in the LFQ experiment and statistical significance, their interaction levels with other proteins considering the STRING interaction network, and the pathways in which they are involved (e.g complement and coagulation cascades). Proteins were also selected according to the number of detected peptides (specifically, unique peptides) for each protein and the signal-noise ratio in the fragmentation spectrum to ensure that proteins were detectable by MRM in non-depleted vitreous samples. It was also taken into consideration if these proteins were reported in previously published proteomics studies. For example, alpha-1-antitrypsin (AAT), which was depleted in our experiment, is an acute-phase protein highly abundant in vitreous and was selected as a potential biomarker according to the previous vitreous proteomics studies in AMD [39], RD/PVR [48–50], and DR/PDR [48, 51–55]. Some proteins found differentially expressed in LFQ experiment already have been reported in our previous study [56], including retinoschisin (RS1) and LGALS3BP that were found upregulated in rhegmatogenous retinal detachment (RRD) compared to ERM, while coagulation factor IX (F9) complement, component C8 beta chain (C8B) and C2 were found downregulated. For the validation, we also took into consideration two more proteins found differentially expressed in that study, the alpha-1-antichymotrypsin (AACT) and complement component C9 (C9). For this reason, a group of patients with RRD, without and with PVR, were included in the MRM experiment. The final scheduled method with the list of potential biomarkers and the corresponding peptides and transitions monitored, as well as other parameters, is detailed in the supplementary table 5.1. MRM experiments were performed on vitreous samples from patients with ERM (n=21), DR/PDR (n=20), AMD (n=11), and RRD/PVR (n=13).

Out of the 35 analyzed proteins, 26 proteins potentially differentiate between the different groups. MRM results of potential candidate biomarkers and respective ROC curves are displayed in supplementary figures 2, 3, and 4. Among these, LGALS3BP and F2 are the proteins with more potential to differentiate the disease groups (p-value<0.0001). F2 showed higher efficiency for distinguishing the DR/PDR and AMD groups from RRD/PVR with an area under the curve (AUC) higher than 0.9 and p-value lower than 0.001, whereas LGALS3BP allowed to differentiate DR/PDR from AMD and RRD/PVR groups. In contrast, the differences verified for the levels of neural cell adhesion molecule 1 (NCAM1), TNR, AAT, CTSZ, myocilin, nucleobindin-1, and neuroserpin were no statistically significant, according to Kruskal-Wallis tests (supplementary figure 4). As in previous reports, our results indicate that AAT is increased in DR/PDR, AMD, and RRD/PVR groups in comparison to ERM controls but these differences are non-significant. Analysis results of TIMP2 and CHGA by MRM were not taken into consideration for quantitation because their signal was very poor. CHGA was undetected in many of the samples, whereas in the case of TIMP2 only a peptide was detected with a few transitions. Also, LFQ data were confirmed by WB analysis (supplementary figure 5), showing that CHGA is down-regulated in patients with PDR compared to the ones with AMD, but this result could not be verified for the comparison

with ERM controls. On the other hand, TIMP2 MRM levels are increased in PDR comparing to ERM and AMD groups, contrary to the LFQ results. Furthermore, the levels of TIMP2 are significantly lower in RRD/PVR group and it was not even detected in two samples (HV 500 and HV 785).

Complement and coagulation components were significantly higher in DR/PDR and AMD groups, and distinguish between patients with these diseases from ERM patients, and RRD with high sensitivity and specificity (AUC > 0.7, p-value<0.05). Complement factor 3 (C3) and F2 are the only ones capable of differentiating the RRD/PVR and ERM groups, with lower levels being found in RRD/PVR than in ERM (only significant differences for F2 levels). As reported previously, complement components (e.g. C8B, C9, F9) are downregulated in RRD [56], although the differences are more significant when compared to DR/PDR and AMD groups. F2 also discriminated very efficiently patients with DR/PDR (AUC=0.9346, p-value<0.0001) and AMD (AUC=0.9301, p-value=0.0004) from RRD/PVR, whilst complement 6 (C6) and coagulation factor IX (F9) could be used as reliable biomarkers for distinguishing patients with DR/PDR from ERM controls (AUC=0.8024, p-value=0.0009) and RRD/PVR (AUC=0.8538, p-value=0.0007), respectively. In turn, as the levels of complement and coagulation components are very similar in these two pathologies, they do not distinguish the DR/PDR and AMD groups. Proteins such as C2, C8B, and CFH seem to be more effective in distinguishing AMD and ERM groups (AUC>0.8) than DR/PDR and ERM (AUC<0.77). MRM data also confirmed the down-regulation of several adhesion molecules in PDR compared to ERM and AMD groups, except for neurexin-3 (NRX3A) whose levels were found higher in the PDR group than in ERM (supplementary figure 3). From the analyzed adhesion molecules, NRX3A is the only one capable of differentiating between AMD and ERM groups (AUC=0.7835, p-value=0.0094). Calsyntenin-1 (CSTN1), LGALS3BP, CDH2, RS1 discriminated between PDR and AMD. Nevertheless, CSTN1 and LGALS3BP showed better efficacy with AUC of 0.8136 (p-value=0.0044) and 0.9 (p-value=0.0003), respectively. The high levels of LGALS3BP found in RRD/PVR in MRM analysis confirms our previous data [56] and allowed this candidate biomarker to distinguish proficiently these patients from the ones with ERM (AUC=0.7875, p-value=0.0054) and DR/PDR (AUC=0.9385, p-value<0.0001). In turn, the low levels of SPON1 and NRX3A found in this pathology indicate that these can be good biomarkers to differentiate it from the AMD group, with an AUC of 0.8182 (p-value = 0.0084) and 0.9021 (p-value =0.0009), respectively. MRM analysis also confirmed the LFQ data concerning the underexpression in PDR of vitreous anti-angiogenic factors (opticin [OPTC], PEDF), lysosomal enzymes (GNS) and proteins involved in insulin processing (Carboxypeptidase E) and detoxification of reactive oxygen species (Extracellular superoxide dismutase [Cu-Zn] [SOD3]). All of these proteins were capable of differentiating DR from ERM and AMD groups (AUC>0.7, p-value<0.05), whereas OPTC, PEDF, and SOD3 also can discriminate patients with DR from patients with RRD/PVR.

In contrast, MRM results did not confirm the downregulation of AACT in the DRR group [56]. Instead, the highest levels of AACT were found in RRD/PVR group, followed by AMD and DR/PDR, strengthening the role of inflammation in these pathologies. Our MRM results neither

confirmed the downregulation of SPP1 and protein FAM3C in PDR but they show to be good biomarkers to distinguish RRD/PVR and DR/PDR groups with AUC>0.8 and p-value≤0.001. SPP1 also showed great efficacy to distinguish RRD/PVR from ERM (AUC>0.8315, p-value<0.0013) and AMD (AUC>0.9231, p-value<0.0013) groups, whereas FAM3C differentiate the DR/PDR from ERM (AUC=0.8548, p-value<0.0001). Proteins related to amyloidosis, including the CST3, APP, and amyloid-like protein 2 (APLP2), have been validated by MRM (supplementary figures 2 and Figure 4). Curiously, changes in expression levels of APP and APLP2 are quite similar. The highest levels were found in AMD, and such variance is highly significant when compared with DR/PDR and RRD/PVR groups, where the levels are the lowest. The analysis of CST3 by MRM confirmed its significant downregulation in PDR compared to ERM and AMD groups, as well as to RRD/PVR. The levels of APP and CST3 were also confirmed by WB analysis (Figure 4), showing downregulation of both proteins in PDR compared to AMD, but not to ERM controls. Interestingly, the APP precursor was not detected in WB analysis but two bands corresponding to APP fragments, a strong band at 25 kDa (APP fragment), and a faint band between 48 kDa and 63 kDa (supplementary figure 6).

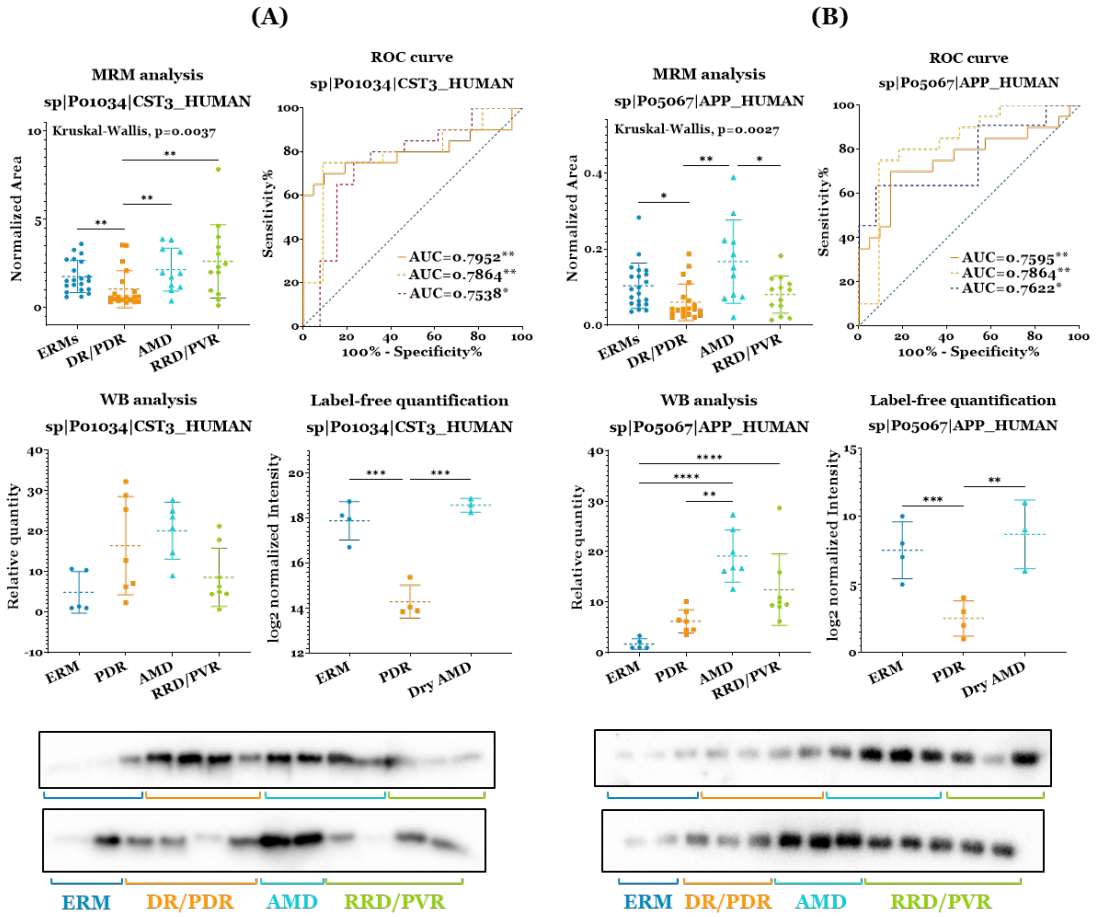

Fig. 4 - Comparison of the results of the analysis of (A) cystatin-C (CST3) and amyloid-beta (APP) by label-free quantitation (LFQ), multiple reaction monitoring (MRM) and Western blot (WB), and respective ROC curves.

4. Discussion

In the last years, the study of the vitreous proteome gained growing interest as a means of understanding the pathophysiological mechanisms that occur in eye diseases. Many researchers have contributed to the characterization of the human vitreous proteome in pathologies, such as DR [51–55, 57–65], AMD [39–41], retinal detachment [56, 66], and PVR [49, 50, 67], and ERM [68–71]. Although the study of the vitreous proteome is promising to elucidate some of the pathogenesis underlying many vitreoretinal diseases, the demand for reliable vitreous biomarkers in ocular disease has not been completely successful so far [72, 73]. In this work, a LFQ method was applied in the discovery phase to compare the vitreous proteome in patients with PDR, dry AMD, and ERM, which could shed some light on the pathophysiological mechanisms of these diseases. LQF experiment allowed to identify 118 proteins (17 up- and 101 down-) differentially expressed in PDR compared to ERM patients, whereas 95 proteins (10 up- and 85 down-) were found differentially expressed in PDR compared to nAMD patients. Functional enrichment analyses indicate that up-regulated proteins in PDR are mainly associated with immune system biological processes such as complement and coagulation cascades and acute-phase responses. The analysis of downregulated proteins shows that vitreous from patients with ERM and nAMD is enriched in adhesion and neuronal proteins, lysosomal proteases, and other proteolytic enzymes, and ECM components compared to patients with PDR. In turn, no significant differences were observed comparing the vitreous of patients with AMD and ERM (only ITIH3 differentiates these diseases), which suggests that these diseases share the same pathophysiological mechanisms. Moreover, one of the samples from a patient with dry AMD showed a higher correlation with samples from the PDR group than with the other samples of its disease group. This suggests that, at an earlier stage, AMD pathogenesis share some molecular mechanisms with ERM, but with its progression to a proliferative etiology, it begins to share more clinical features with PDR. Based on these assumptions, differences found in the vitreous proteome in the LFQ experiment were considered a source of potential biomarkers for differentiating these eye diseases. Consequently, several candidate biomarkers were selected and validated by MRM. From the 35 candidate biomarkers, 26 proteins involved in several biological processes have been shown the potential to differentiate between the disease groups, as discussed below.

The low activation levels of complement and coagulation cascades in the eye are characteristic of its immune-privileged status, which contributes to retinal homeostasis and integrity [74–76]. Chronic activation of complement and coagulation has been implicated in a variety of pathophysiological features, including increased vascular permeability [77, 78], loss and activation of choriocapillaris endothelial cells [79, 80], inflammation [80, 81], and loss of photoreceptors [75]. Therefore, complement and coagulation have been implicated in DR/PDR [41, 48, 52, 53, 55, 57, 60, 64, 65, 82], AMD [41, 83], and RD/PVR [49, 50, 84, 85]. Furthermore, genetic polymorphisms in complement genes, such as C3, CFH, and CFB, are considered a risk factor for AMD [83, 86]. In this study, complement and coagulation components were found significantly up-regulated in DR/PDR and AMD, which reinforces their role in these diseases.

Interestingly, C2 and CFH were found up-regulated in PDR compared to nAMD in the LFQ experiment, but the levels of these proteins were higher in AMD than DR/PDR group when a larger set of samples (including a few patients with nAMD) were analyzed by MRM. Schori and co-workers also reported the enrichment of complement cascade components in PDR vitreous but found reduced levels of CFH in nAMD [41]. This suggests that levels of these factors increase gradually in vitreous with the progression from a non-proliferative to a proliferative etiology. Indeed, higher levels of complement and coagulation factors were detected in more severe forms of DR and AMD associated with neovascularization, fibrovascular proliferation, vitreous-macular traction syndrome, macular edema, and vitreous hemorrhage. In contrast, complement and coagulation were found downregulated in RRD/PVR compared to other pathologies under study, such as in our previous study [56]. The influx of plasma proteins into the retina and vitreous cavity increases with the duration of RRD as the result of the breakdown of the BRB [87, 88]. Therefore, the intravitreal levels of plasma proteins, including inflammatory proteins and complement and coagulation factors are expected to increase with the progression of the disease to PVR [56]. Although the number of samples is low to assess the statistical differences between vitreous from RRD and PVR patients, the higher levels of complement and coagulation components were found in a patient with re-detachment associated with PVR. Therefore, the increase of these proteins in the vitreous is non-specific for a particular disease but could be a suitable predictor of its progression to a proliferative etiology. Indeed, complement and coagulation seem to be involved in pathological processes shared by DR/PDR, AMD, and RRD/PVR.

In the LQF experiment, a significant number of adhesion molecules, nervous system development proteins, and ECM components were found up-regulated in dry AMD and ERM, pointing toward the neurodegenerative nature of these pathologies as reported previously [40, 69, 71]. Retinal endothelial cells constitutively express high levels of adhesion molecules, which are further increased in pathological conditions. The expression of adhesion molecules supports retinal leukocytosis and, if leukocyte activation is sustained, it may predispose the retina to inflammation and degeneration of endothelial cells and pericytes [89]. Cell adhesion molecules participate in a wide number of biological processes in central nervous system development and retina, including neurogenesis, neuronal cell migration, and differentiation, formation and regeneration of axons, and formation of synapse and complex of glial networks synapse [90, 91]. MRM results confirmed the up-regulation in AMD and ERM of molecules involved in neuronal cell adhesion (CSTN1, CDH2, SPON1), in cell-cell adhesion in the retina (RS1), and integrin-mediated cell adhesion (LGALS3BP), and suggest that these proteins are potential biomarkers for discriminating between PDR and AMD. In particular, LGALS3BP showed to be an efficient biomarker capable of differentiating all the disease groups, with the higher levels found in RRD/PVR and lowest in PDR, which is coherent with previous reports [49, 56, 60]. The role of adhesion molecules is supported by ECM that provides a scaffolding via ECM–integrin-binding for cell migration [92]. Besides controlling basic cellular activities [93, 94], ECM remodeling modulates pathological features of vitreoretinal diseases like neovascularization [95, 96], inflammation [97, 98], and fibrosis [99, 100]. The degradation of ECM components by metalloproteinases (MMPs) provides scaffolding zones that facilitate cell adhesion and migration and change the bioavailability of

factors sequestered in ECM, including growth factors, chemoattractant, and other signaling molecules [93, 95, 96]. Here, MMP2 and TIMP2 were found downregulated in PDR compared to ERM and dry AMD, but TIMP1 was only found downregulated compared to ERM. Indeed, some of these molecules were not detected in some PDR vitreous samples. However, higher levels of TIMP2 were found in DR/PDR group and AMD by Western blot analysis (supplementary figure 5). It has been suggested that TIMP-2 is constitutively expressed by the human retina at physiological conditions, but TIMPs levels suffer concomitant changes in response to a pathological stimulus [101]. Nevertheless, Zou and co-workers recently reported that TIMP2 is downregulated in PDR and its levels increase after the treatment with ranibizumab, which confirms its relevance as an inhibitor of angiogenesis [60]. SPP1 is a matricellular protein, existing as a soluble cytokine or as an immobilized ECM compound that mediates cell migration, cell-matrix adhesion, and survival of many cell types, inflammatory responses, angiogenesis, and tissue remodeling [102, 103]. SPP1 was found downregulated in PDR in the LFQ experiment, which is according to previous reports [41, 58, 60], but these results were not confirmed by MRM, where the levels were only found downregulated in DRR/PVR group. Higher intravitreal levels of SPP1 have been reported in PDR compared to RD, especially in patients with active PDR, suggesting a role of these proteins in angiogenesis [104]. OPTC is another ECM component found downregulated in PDR both in LFQ and MRM experiments. OPTC is a glycoprotein highly abundant in vitreous that exerts anti-angiogenic activity by regulating adhesion characteristics of ECM components through its competitive binding to collagen, inhibiting endothelial cell interactions, and preventing the strong adhesions required for pro-angiogenic signaling [105]. Therefore, the decrease of the levels of OPTC in the vitreous, which was verified in PDR and AMD groups, may conduce to an angiogenic environment in the eye. This fact is reinforced by the downregulation of PEDF in PDR compared to ERM and AMD, although these differences were not significant in the MRM analysis. PEDF is mainly secreted by the RPE and is a potent inhibitor of angiogenesis, even though it participates in other processes such as neuronal differentiation in retinoblastoma cells, inhibits retinal inflammation, and protects retinal neurons from light-induced damages, oxidative stress, and excitotoxicity [106, 107]. PEDF levels in the vitreous of patients are controversial because there is no consistency across studies in PDR [52, 54, 55, 57, 58, 64, 65, 108] and nAMD [40, 109, 110]. Nevertheless, anti-angiogenic and neurotrophic activities of PEDF are not only controlled by its expression levels, but also by phosphorylation levels [111, 112], which explains some of the discrepancies. The antioxidant enzyme SOD3 was found downregulated in all disease groups, compared to ERM controls in LQF and MRM analysis, even these changes are more significant when we compare DR/PDR to ERM. It has been suggested that SOD3 is locally sequestered in vitreous ECM by binding heparan sulfate proteoglycans, such as heparin, in areas of oxidative stress to prevent superoxide radical-induced damages in neighboring structures such as the inner retina, ciliary body, and lens [113]. Therefore, the antioxidant potential of SOD3 may provide a protective mechanism of the retina and surrounding tissues, since impaired redox balance in vitreous has been implicated in DR [114–118], AMD [110, 119], and PVR [118]. Although the protective effect of SOD3 is mediated by the removal of superoxide radicals, it has been suggested that it also promotes the survival of starving

photoreceptor cells by enhancing glucose availability [120], and stabilizes the retinal vasculature, and reduced vessel leakage through the stabilization of hypoxia-inducible factors [121].

Our data also suggests that lysosomal enzymes are accumulated in vitreous from patients with AMD and ERM. In part, the accumulation of lysosomal enzymes can be related to the activation of leukocytes, resulting in the stimulation of phagocytosis and respiratory burst, the release of lysosomal enzymes, inflammatory mediators, and adhesion molecules [122]. On the other hand, lysosomal dysfunction, one of the pathological mechanisms that lead to the death of neurons and RPE cells, was related to AMD [123–126], DR [125], and PVR [126]. Lysosomal turnover is essential for retinal homeostasis, which is maintained actively by RPE through phagocytosis (e.g. photoreceptor outer segment phagocytosis) and autophagy [124, 127]. Impaired autophagy and exosome-mediated release of intracellular proteins contribute to the accumulation of lipofuscin and drusen in Bruch's membrane [123, 128], which creates a physical barrier to the influx of oxygen and nutrients to the photoreceptors and the waste removal between RPE and choroid [129]. Furthermore, it has been suggested that lysosomal enzymes (e.g. cathepsin D) contribute to the pathogenesis of ocular diseases through the degradation of ECM components and/or regulation of angiogenesis [130]. Autophagy is upregulated in the RPE as a protective mechanism against retinal stress. However, prolonged stress downregulates autophagy, which leads to increased debris, mitochondrial injury, and RPE atrophy, and eventually to metabolic reprogramming [131]. GNS, a lysosomal enzyme physiologically required for the degradation of heparan sulfate [132], was selected and validated as a biomarker of lysosomal function. Higher levels of these enzymes were found in AMD and ERM compared to DR/PDR and RRD/PVR groups, which confirms our LFQ data.

Interestingly, APP and related proteins (e.g. CST3, CLSTN1, SPP1, APLP2) seem to form a central cluster in a protein-protein interaction network that integrates multiple pathways (Figure 3). APP is a membrane glycoprotein mainly produced by retinal ganglion cells and the RPE that performs physiological functions in neurite growth, neuronal adhesion, and axonogenesis. Amyloid processing results in the accumulation of several fragments in the eye, in particular in drusen, which have been associated with neurodegeneration in retinal diseases such as AMD and glaucoma [133–135]. The increased phagocytic capacity of microglia and the expression of APP degrading enzymes is suggested to contribute to the amyloid-beta clearance in physiological conditions. Notwithstanding, the generation of APP peptides and the associated neurotoxicity seems to be mediated by its intralysosomal accumulation through macroautophagy, and consequent lysosomal membrane permeabilization, which eventually promotes the neuroinflammation by the induction of pro-inflammatory cytokines and NLRP3 inflammasome [136–138]. Furthermore, APP peptides can induce mitochondrial dysfunction, oxidative stress, the activation of the complement cascade, and changes in vascular endothelium in the retina [135, 139]. In this work, APP and APP-like proteins (e.g. APLP2) were found upregulated in AMD in comparison to DR/PDR, PDR, and RRD/PVR, which was confirmed by LFQ and MRM analysis. Several authors report the underexpression of these proteins in PDR [41, 52, 53, 60], whereas Yu and co-workers detected them in moderate PVR, but not in severe PVR and in healthy controls

[49], which confirms our data. Considering that APP is an integral membrane protein, these quantitative results must correspond to APP fragments, which was confirmed by WB analysis. Two bands corresponding to APP fragments were detected, a faint band between 48 kDa and 63 kDa and a 25 kDa strong band that may correspond, respectively, to amyloid fragments such Aβ40 and Aβ42 [140] and c-terminal fragments of APP resultant from proteolytic processing by η-secretase [141]. This APP fragment showed to be highly abundant in vitreous from AMD patients, suggesting that it could be a potential biomarker of neurodegenerative vitreoretinal diseases. Also associated with amyloidosis, CST3 was also found upregulated in AMD compared to DR/PDR, but the higher levels were found in RRD/PVR. CST3 is a potent inhibitor of lysosomal and extracellular cysteine proteinases ubiquitously expressed by all mammalian tissues and present in all body fluids. In the eye, it is particularly abundant in RPE [142]. Mutations in CST3 genes were associated with a high risk of developing nAMD [143], and hereditary cerebral hemorrhage with amyloidosis-Icelandic type [144]. Mutant variants of CST3 are found co-deposited with APP peptides in senile plaques and arteriolar walls in the brain of AD patients, suggesting a role in amyloidosis [142, 143]. On the other hand, it has suggested the involvement of CST3 in several neuroprotective mechanisms by inhibition of cysteine proteases and induction of autophagy, induction of neurogenesis, and inhibition of oligomerization and amyloid fibril formation [145]. Another interesting outcome from our study was the high levels of CST3 found in DRR/PVR, which was previously reported by Yu and co-workers [49]. To the best of our knowledge, there are no studies regarding the role of CST3 in RRD/PVR, but some evidence indicates that it is capable of inhibiting epithelial-mesenchymal transition, a clinical feature of PVR that occurs in RPE cells, in mammary epithelial cells [146].

5. Conclusions

The characterization of the proteome of vitreous humor has contributed extensively to the recognition of pathways involved in several vitreoretinal diseases. Nevertheless, the lack of validation of these potential biomarkers in a larger number of samples may explain why the demand for suitable vitreous biomarkers has not been successful so far. In this work, a LFQ method was applied to analyze the vitreous proteome in PDR and AMD compared to ERM. Our findings reinforce the involvement of complement and coagulation cascades in the pathogenesis of PDR and nAMD, indicating that these proteins are non-specific biomarkers for a particular disease, but could be a suitable predictor of its progression to a proliferative etiology. Furthermore, a significant number of adhesion molecules, nervous system development proteins, lysosomal proteins, and ECM components were found up-regulated in dry AMD and ERM, pointing toward the neurodegenerative nature of these pathologies. This indicates that the results should be reviewed carefully since most studies, including ours, use this pathology (or macular holes) as a control. Although the functional analysis did not highlight proteins related to angiogenesis, the downregulation of anti-angiogenic factors, such as OPTC and PEDF in PDR and AMD may suggest that vitreous is conduced to an angiogenic environment in these pathologies. Perhaps, the most interesting outcome is the important role of APP in neurodegeneration in vitreoretinal diseases in which it integrates multiple pathways, emphasizing the multifactor

nature of these diseases. Finally, we provide a list of potential biomarkers capable of discriminating several vitreoretinal diseases, including DR/PDR, AMD, DDR/PVR, and ERM. According to ROC curves, complement and coagulation components (C6, C8B, prothrombin), acute-phase mediators (AACT), adhesion molecules (LGALS3BP), ECM components (OPTC), and neurodegeneration biomarkers (APP, amyloid-like protein 2, FAM3C) stand out, based in our results, as the more efficient to discriminate different disease groups. In conclusion, our study shed some light on the mechanisms underlying the PDR and AMD, besides providing fundamental information regarding potential biomarkers in vitreous. These proteins could be assessed in samples obtained as part of the clinical routine to the prognosis of the patient's disease evolution and proper response to treatment or could be seen as target candidates for the development of new pharmaceutical drugs.

Acknowledgments

FM Santos acknowledges a doctoral fellowship [SFRH/BD/112526/2015] from FCT. This project was supported by the University of Beira Interior—Health Sciences Research Centre (CICS-UBI) supported by FEDER funds through the POCI—COMPETE 2020—Operational Programme Competitiveness and Internationalisation in Axis I—Strengthening research, technological development and innovation Project (POCI-01-0145-FEDER-007491) and National Funds by FCT—Foundation for Science and Technology Project (UID/Multi/ 00709/2013). This work was also supported by the Applied Molecular Biosciences Unit- UCIBIO which is financed by national funds from FCT/MCTES (UID/Multi/04378/2019). CNB-CSIC proteomics lab is a member ofProteored, PRB2-ISCIII and is supported by grant PT13/0001, of the PE I +D+i 2013–2016, funded by ISCIII and FEDER. The authors also acknowledge CICS-UBI researchers Daniela Talhada, Catarina Ferreira, Telma Quintela, Catarina Duarte, and Professora Elisa Cairrão for providing some of the antibodies used in the validation of biomarkers by Western blot.

Conflicts of Interest: The authors declare no conflict of interest.

References

1. Guariguata L, Whiting DR, Hambleton I, et al (2014) Global estimates of diabetes prevalence for 2013 and projections for 2035. Diabetes Res Clin Pract 103:137–149.

2. Duh EJ, Sun JK, Stitt AW (2017) Diabetic retinopathy: current understanding, mechanisms, and treatment strategies. JCI insight 2:1–13.

3. Wong WL, Su X, Li X, et al (2014) Global prevalence of age-related macular degeneration and disease burden projection for 2020 and 2040: A systematic review and meta-analysis. Lancet Glob Heal 2:e106–e116.

4. Jaki Mekjavić P, Jūratė Balčiūnienė V, Ćeklić L, et al (2019) The Burden of Macular Diseases in Central and Eastern Europe—Implications for Healthcare Systems. Value Heal Reg Issues 19:1–6.

5. Amadio M, Kaarniranta K, Xu H, et al (2018) Molecular Mechanisms Underlying Age-Related Ocular Diseases. Oxid Med Cell Longev 2018:8476164.

6. Ramasamy K, Ramasamy K, Kuppamuthu D, Jayapal JM (2019) Proteomics of Neurodegenerative Disorders of the Eye. pp 393–402

7. Nentwich MM (2015) Diabetic retinopathy - ocular complications of diabetes mellitus. World J Diabetes 6:489.

8. Wang W, Lo ACY (2018) Diabetic retinopathy: Pathophysiology and treatments. Int J Mol Sci 19:.9.

9. Lechner J, O'Leary OE, Stitt AW (2017) The pathology associated with diabetic retinopathy. Vision Res 139:7–14.

10. Wong TY, Cheung CMG, Larsen M, et al (2016) Diabetic retinopathy. Nat Rev Dis Prim 2:16012.

11. Kusuhara S, Fukushima Y, Ogura S, et al (2018) Pathophysiology of diabetic retinopathy: The old and the new. Diabetes Metab J 42:364–376.

12. Ardeljan D, Chan CC (2013) Aging is not a disease: Distinguishing age-related macular degeneration from aging. Prog Retin Eye Res 37:68–89.

13. Jager RD, Mieler WF, Miller JW (2008) Age-Related Macular Degeneration. N Engl J Med 358:2606–2617.

14. Ambati J, Atkinson JP, Gelfand BD (2013) Immunology of age-related macular degeneration. Nat Rev Immunol 13:438–451. https://doi.org/10.1038/nri3459

15. Yonekawa Y, Miller J, Kim I (2015) Age-Related Macular Degeneration: Advances in Management and Diagnosis. J Clin Med 4:343–359.

16. Klein ML, Ferris FL, Armstrong J, et al (2008) Retinal Precursors and the Development of Geographic Atrophy in Age-Related Macular Degeneration. Ophthalmology 115:1026–1031.

17. Sapieha P, Hamel D, Shao Z, et al (2010) Proliferative retinopathies: Angiogenesis that blinds. Int J Biochem Cell Biol 42:5–12.

18. Amadio M, Govoni S, Pascale A (2016) Targeting VEGF in eye neovascularization: What's new?: A comprehensive review on current therapies and oligonucleotide-based interventions under development. Pharmacol Res 103:253–269.

19. Mesquita J, Castro-de-Sousa JP, Vaz-Pereira S, et al (2018) Vascular endothelial growth factors and placenta growth factor in retinal vasculopathies: Current research and future perspectives. Cytokine Growth Factor Rev 39:102–115.

20. Mesquita J, Castro-de-Sousa JP, Vaz-Pereira S, et al (2018) Evaluation of the growth factors VEGF-a and VEGF-B in the vitreous and serum of patients with macular and retinal vascular diseases. Growth Factors 36:48–57.

21. Gross JG, Glassman AR, Jampol LM, et al (2015) Panretinal Photocoagulation vs Intravitreous Ranibizumab for Proliferative Diabetic Retinopathy. JAMA 314:2137.

22. Bressler SB, Liu D, Glassman AR, et al (2017) Change in diabetic retinopathy through 2 years secondary analysis of a randomized clinical trial comparing aflibercept, bevacizumab, and ranibizumab. JAMA Ophthalmol 135:558–568.

23. Cai S, Bressler NM (2015) Aflibercept, Bevacizumab, or Ranibizumab for Diabetic Macular Edema. N Engl J Med 372:1193–1203.

24. Mekjavic PJ, Kraut A, Urbancic M, et al (2011) Efficacy of 12-month treatment of neovascular age-related macular degeneration with intravitreal bevacizumab based on individually determined injection strategies after three consecutive monthly injections. Acta Ophthalmol 89:647–653.

25. Rosenfeld PJ, Brown DM, Heier JS, et al (2006) Ranibizumab for Neovascular Age-Related Macular Degeneration. N Engl J Med 355:1419–1431.

26. Heier JS, Brown DM, Chong V, et al (2012) Intravitreal Aflibercept (VEGF Trap-Eye) in Wet Age-related Macular Degeneration. Ophthalmology 119:2537–2548.

27. Wirostko B, Wong TY, Simó R (2008) Vascular endothelial growth factor and diabetic complications. Prog Retin Eye Res 27:608–621.

28. Bressler SB, Almukhtar T, Bhorade A, et al (2015) Repeated intravitreous ranibizumab injections for diabetic macular edema and the risk of sustained elevation of intraocular pressure OR the need for ocular hypotensive treatment. JAMA Ophthalmol 133:589–597.

29. Gonzalez VH, Campbell J, Holekamp NM, et al (2016) Early and Long-Term Responses to Anti–Vascular Endothelial Growth Factor Therapy in Diabetic Macular Edema: Analysis of Protocol I Data. Am J Ophthalmol 172:72–79.

30. Wykoff CC, Brown DM, Maldonado ME, Croft DE (2014) Aflibercept treatment for patients with exudative age-related macular degeneration who were incomplete responders to multiple ranibizumab injections (TURF trial). Br J Ophthalmol 98:951–955.

31. Richer S, Ulanski L, Popenko NA, et al (2016) Age-related Macular Degeneration Beyond the Age-related Eye Disease Study II. Adv Ophthalmol Optom 1:335–369.

32. Holz FG, Schmitz-Valckenberg S, Fleckenstein M (2014) Recent developments in the treatment of age-related macular degeneration. J Clin Invest 124:1430–1438.

33. Stitt AW, Curtis TM, Chen M, et al (2016) The progress in understanding and treatment of diabetic retinopathy. Prog Retin Eye Res 51:156–186.

34. Hernández C, Simó-Servat A, Bogdanov P, Simó R (2017) Diabetic retinopathy: new therapeutic perspectives based on pathogenic mechanisms. J Endocrinol Invest 40:925–935.

35. Walia S, Clermont AC, Gao B-BB, et al (2010) Vitreous proteomics and diabetic retinopathy. Semin Ophthalmol 25:289–294.

36. Simó-Servat O, Hernández C, Simó R (2012) Usefulness of the Vitreous Fluid Analysis in the Translational Research of Diabetic Retinopathy. Mediators Inflamm 2012:1–11.

37. Nawaz IM, Rezzola S, Cancarini A, et al (2019) Human vitreous in proliferative diabetic retinopathy: Characterization and translational implications. Prog Retin Eye Res 109:110–119.

38. Csősz É, Deák E, Kalló G, et al (2017) Diabetic retinopathy: Proteomic approaches to help the differential diagnosis and to understand the underlying molecular mechanisms. J Proteomics 150:351–358.

39. Koss MJ, Hoffmann J, Nguyen N, et al (2014) Proteomics of vitreous humor of patients with exudative age-related macular degeneration. PLoS One 9:1–11.

40. Nobl M, Reich M, Dacheva I, et al (2016) Proteomics of vitreous in neovascular age-related macular degeneration. Exp Eye Res 146:107–117.

41. Schori C, Trachsel C, Grossmann J, et al (2018) The Proteomic Landscape in the Vitreous of Patients With Age-Related and Diabetic Retinal Disease. Invest Ophthalmol Vis Sci 59:AMD31–AMD40.

42. Mesquita J, Castro de Sousa J, Vaz-Pereira S, et al (2017) VEGF-B Levels in the Vitreous of Diabetic and Non-Diabetic Patients with Ocular Diseases and Its Correlation with Structural Parameters. Med Sci 5:17.

43. Sorokin DiY, Messina E, Smedile F, et al (2017) Discovery of anaerobic lithoheterotrophic haloarchaea, ubiquitous in hypersaline habitats. ISME J 11:1245–1260.

44. Käll L, Storey JD, MacCoss MJ, Noble WS (2008) Assigning Significance to Peptides Identified by Tandem Mass Spectrometry Using Decoy Databases. J Proteome Res 7:29–34.

45. Jiao X, Sherman BT, Huang DW, et al (2012) DAVID-WS: A stateful web service to facilitate gene/protein list analysis. Bioinformatics 28:1805–1806.

46. Bindea G, Mlecnik B, Hackl H, et al (2009) ClueGO: A Cytoscape plug-in to decipher functionally grouped gene ontology and pathway annotation networks. Bioinformatics 25:1091–1093.

47. Szklarczyk D, Gable AL, Lyon D, et al (2019) STRING v11: Protein-protein association networks with increased coverage, supporting functional discovery in genome-wide experimental datasets. Nucleic Acids Res 47:D607–D613.

48. Shitama T, Hayashi H, Noge S, et al (2008) Proteome profiling of vitreoretinal diseases by cluster analysis. Proteomics - Clin Appl 2:1265–1280.

49. Yu J, Liu F, Cui SJ, et al (2008) Vitreous proteomic analysis of proliferative vitreoretinopathy. Proteomics 8:3667–3678.

50. Yu J, Peng R, Chen H, et al (2012) Elucidation of the pathogenic mechanism of rhegmatogenous retinal detachment with proliferative vitreoretinopathy by proteomic analysis. Investig Ophthalmol Vis Sci 53:8146–8153.

51. Nakanishi T, Koyama R, Ikeda T, Shimizu A (2002) Catalogue of soluble proteins in the human vitreous humor: Comparison between diabetic retinopathy and macular hole. J Chromatogr B Anal Technol Biomed Life Sci 776:89–100.

52. Gao B-B, Chen X, Timothy N, et al (2008) Characterization of the Vitreous Proteome in Diabetes without Diabetic Retinopathy and Diabetes with Proliferative Diabetic Retinopathy. J Proteome Res 7:2516–2525.

53. Loukovaara S, Nurkkala H, Tamene F, et al (2015) Quantitative Proteomics Analysis of Vitreous Humor from Diabetic Retinopathy Patients. J Proteome Res 14:5131–5143.

54. Kim SJ, Kim S, Park J, et al (2006) Differential Expression of Vitreous Proteins in Proliferative Diabetic Retinopathy. Curr Eye Res 31:231–240.

55. Wang H, Feng L, Hu J, et al (2013) Differentiating vitreous proteomes in proliferative diabetic retinopathy using high-performance liquid chromatography coupled to tandem mass spectrometry. Exp Eye Res 108:110–119.

56. Santos FM, Gaspar LM, Ciordia S, et al (2018) iTRAQ Quantitative Proteomic Analysis of Vitreous from Patients with Retinal Detachment. Int J Mol Sci 19:1157.

57. Yamane K, Minamoto A, Yamashita H, et al (2003) Proteome Analysis of Human Vitreous Proteins. Mol Cell Proteomics 2:1177–1187.

58. Minamoto A, Yamane K, Yokoyama T, Thongboonkerd V (2007) Proteomics of vitreous fluid. Proteomics Hum Body Fluids Princ Methods, Appl 495–507.

59. Kim T, Sang JK, Kim K, et al (2007) Profiling of vitreous proteomes from proliferative diabetic retinopathy and nondiabetic patients. Proteomics 7:4203–4215.

60. García-Ramírez M, Canals F, Hernández C, et al (2007) Proteomic analysis of human vitreous fluid by fluorescence-based difference gel electrophoresis (DIGE): A new strategy for identifying potential candidates in the pathogenesis of proliferative diabetic retinopathy. Diabetologia 50:1294–1303.

61. Simó R, Higuera M, García-Ramírez M, et al (2008) Elevation of apolipoprotein A-I and apolipoprotein H levels in the vitreous fluid and overexpression in the retina of diabetic patients. Arch Ophthalmol 126:1076–1081.

62. Wang H, Feng L, Hu JW, et al (2012) Characterisation of the vitreous proteome in proliferative diabetic retinopathy. Proteome Sci 10:1–11.

63. Balaiya S, Zhou Z, Chalam K V. (2017) Characterization of vitreous and aqueous proteome in humans with proliferative diabetic retinopathy and its clinical correlation. Proteomics Insights 8:1–10.

64. Li J, Lu Q, Lu P (2018) Quantitative proteomics analysis of vitreous body from type 2 diabetic patients with proliferative diabetic retinopathy. BMC Ophthalmol 18:151.

65. Zou C, Han C, Zhao M, et al (2018) Change of ranibizumab-induced human vitreous protein profile in patients with proliferative diabetic retinopathy based on proteomics analysis. Clin Proteomics 15:12.

66. Gaspar LM, Santos FM, Albuquerque T, et al (2017) Proteome analysis of vitreous humor in retinal detachment using two different flow-charts for protein fractionation. J Chromatogr B 1061–1062:334–341.

67. Roybal CN, Velez G, Toral MA, et al (2018) Personalized Proteomics in Proliferative Vitreoretinopathy Implicate Hematopoietic Cell Recruitment and mTOR as a Therapeutic Target. Am J Ophthalmol 186:152–163.

68. Mandal N, Kofod M, Vorum H, et al (2013) Proteomic analysis of human vitreous associated with idiopathic epiretinal membrane. Acta Ophthalmol 91:333–334.

69. Pollreisz A, Funk M, Breitwieser FP, et al (2013) Quantitative proteomics of aqueous and vitreous fluid from patients with idiopathic epiretinal membranes. Exp Eye Res 108:48–58.

70. Yu J, Feng L, Wu Y, et al (2014) Vitreous proteomic analysis of idiopathic epiretinal membranes. Mol Biosyst 10:2558–2566.

71. Öhman T, Tamene F, Göös H, et al (2018) Systems pathology analysis identifies neurodegenerative nature of age-related vitreoretinal interface diseases. Aging Cell 17:e12809.

72. Rocha AS, Santos FM, Monteiro JP, et al (2014) Trends in proteomic analysis of human vitreous humor samples. Electrophoresis 35:2495–2508.

73. Angi M, Kalirai H, Coupland SE, et al (2012) Proteomic analyses of the vitreous humour. Mediators Inflamm 2012:.

74. Mukai R, Okunuki Y, Husain D, et al (2018) The complement system is critical in maintaining retinal integrity during aging. Front Aging Neurosci 10:1–12.

75. Sweigard JH, Matsumoto H, Smith KE, et al (2015) Inhibition of the alternative complement pathway preserves photoreceptors after retinal injury. Sci Transl Med 7:21–24.

76. Clark SJ, Bishop PN (2018) The eye as a complement dysregulation hotspot. Semin Immunopathol 40:65–74.

77. Gao BB, Clermont A, Rook S, et al (2007) Extracellular carbonic anhydrase mediates hemorrhagic retinal and cerebral vascular permeability through prekallikrein activation. Nat Med 13:181–188.

78. Abdulaal M, Haddad NMN, Sun JK, Silva PS (2016) The role of plasma kallikrein-kinin pathway in the development of diabetic retinopathy: Pathophysiology and therapeutic approaches. Semin Ophthalmol 31:19–24.

79. Whitmore SS, Sohn EH, Chirco KR, et al (2015) Complement activation and choriocapillaris loss in early AMD: Implications for pathophysiology and therapy. Prog Retin Eye Res 45:1–29.

80. Skei JM, Fingert JH, Russell SR, et al (2010) Complement component C5a activates ICAM-1expression on human choroidal endothelial cells. Investig Ophthalmol Vis Sci 51:5336–5342.

81. Bastiaans J, Van Meurs JC, Van Holten-Neelen C, et al (2013) Factor Xa and thrombin stimulate proinflammatory and profibrotic mediator production by retinal pigment epithelial cells: A role in vitreoretinal disorders? Graefe's Arch Clin Exp Ophthalmol 251:1723–1733.

82. Shahulhameed S, Vishwakarma S, Chhablani J, et al (2020) A Systematic Investigation on Complement Pathway Activation in Diabetic Retinopathy. Front Immunol 11:1–14.

83. Loyet KM, DeForge LE, Katschke KJ, et al (2012) Activation of the alternative complement pathway in vitreous is controlled by genetics in age-related macular degeneration. Investig Ophthalmol Vis Sci 53:6628–6637.

84. Wu Z, Ding N, Yu M, et al (2016) Identification of potential biomarkers for rhegmatogenous retinal detachment associated with choroidal detachment by vitreous iTRAQ-based proteomic profiling. Int J Mol Sci 17:.

85. Mulder VC, Bastiaans J, van Leuven CJM, et al (2018) Thrombin Generation in Vitreous and Subretinal Fluid of Patients with Retinal Detachment. Ophthalmologica 240:23–28.

86. Toomey CB, Johnson L V., Bowes Rickman C (2018) Complement factor H in AMD: Bridging genetic associations and pathobiology. Prog Retin Eye Res 62:38–57.

87. Cunha-Vaz J (2009) The Blood–Retinal Barrier in Retinal Disease. Eur Ophthalmic Rev 03:105.

88. Campochiaro PA, Bryan JA, Conway BP, Jaccoma EH (1986) Intravitreal Chemotactic and Mitogenic Activity: Implication of Blood-Retinal Barrier Breakdown. Arch Ophthalmol 104:1685–1687.

89. Bharadwaj AS, Appukuttan B, Wilmarth PA, et al (2013) Role of the retinal vascular endothelial cell in ocular disease. Prog Retin Eye Res 32:102–180.

90. Togashi H, Sakisaka T, Takai Y (2009) Cell adhesion molecules in the central nervous system. Cell Adhes Migr 3:29–35.

91. Missaire M, Hindges R (2015) The role of cell adhesion molecules in visual circuit formation: From neurite outgrowth to maps and synaptic specificity. Dev Neurobiol 75:569–583.

92. Ridley AJ, Schwartz MA, Burridge K, et al (2003) Cell Migration: Integrating Signals from Front to Back. Science (80-) 302:1704–1709.

93. Lu P, Takai K, Weaver VM, Werb Z (2011) Extracellular Matrix Degradation and Remodeling in Development and Disease. Cold Spring Harb Perspect Biol 3:a005058–a005058.

94. Frantz C, Stewart KM, Weaver VM (2010) The extracellular matrix at a glance. J Cell Sci 123:4195–4200.

95. Sottile J (2004) Regulation of angiogenesis by extracellular matrix. Biochim Biophys Acta - Rev Cancer 1654:13–22.

96. Bishop PN (2015) The role of extracellular matrix in retinal vascular development and preretinal neovascularization. Exp Eye Res 133:30–36.

97. Sorokin L (2010) The impact of the extracellular matrix on inflammation. Nat Rev Immunol 10:712–723.

98. Singh M, Tyagi SC (2017) Metalloproteinases as mediators of inflammation and the eyes: Molecular genetic underpinnings governing ocular pathophysiology. Int J Ophthalmol 10:1308–1318.

99. Chaudhary R, Scott RAH, Wallace G, et al (2020) Inflammatory and fibrogenic factors in proliferative vitreoretinopathy development. Transl Vis Sci Technol 9:1–17.

100. Wynn T a (2007) Common and unique mechanisms regulate fibrosis in various fibroproliferative diseases. J Clin Invest 117:524–529.

101. Das A, Navaratna D, McGuire PG (2008) Beyond VEGF – Other Factors Important in Retinal Neovascularization: Potential Targets in Proliferative Diabetic Retinopathy. In: Diabetic Retinopathy. Humana Press, Totowa, NJ, pp 375–398.

102. Chowdhury UR, Jea SY, Oh DJ, et al (2011) Expression profile of the matricellular protein osteopontin in primary open-angle glaucoma and the normal human eye. Investig Ophthalmol Vis Sci 52:6443–6451.

103. Lund SA, Giachelli CM, Scatena M (2009) The role of osteopontin in inflammatory processes. J Cell Commun Signal 3:311–322.

104. Abu El-Asrar AM, Imtiaz Nawaz M, Kangave D, et al (2012) Osteopontin and Other Regulators of Angiogenesis and Fibrogenesis in the Vitreous from Patients with Proliferative Vitreoretinal Disorders. Mediators Inflamm 2012:1–8.

105. Le Goff MM, Sutton MJ, Slevin M, et al (2012) Opticin Exerts Its Anti-angiogenic Activity by Regulating Extracellular Matrix Adhesiveness. J Biol Chem 287:28027–28036.

106. Park K, Jin J, Hu Y, et al (2011) Overexpression of pigment epithelium-derived factor inhibits retinal inflammation and neovascularization. Am J Pathol 178:688–698.

107. Barnstable CJ, Tombran-Tink J (2004) Neuroprotective and antiangiogenic actions of PEDF in the eye: Molecular targets and therapeutic potential. Prog Retin Eye Res 23:561–577.

108. Duh EJ, Yang HS, Haller JA, et al (2004) Vitreous levels of pigment epithelium-derived factor and vascular endothelial growth factor: Implications for ocular angiogenesis. Am J Ophthalmol 137:668–674.

109. Huber M, Wachtlin J (2012) Vitreous levels of proteins implicated in angiogenesis are modulated in patients with retinal or choroidal neovascularization. Ophthalmologica 228:188–193.

110. Holekamp NM, Bouck N, Volpert O (2002) Pigment epithelium-derived factor is deficient in the vitreous of patients with choroidal neovascularization due to age-related macular degeneration. Am J Ophthalmol 134:220–227.

111. Maik-Rachline G, Seger R (2006) Variable phosphorylation states of pigment-epithelium-derived factor differentially regulate its function. Blood 107:2745–2752.

112. Maik-Rachline G, Shaltiel S, Seger R (2005) Extracellular phosphorylation converts pigment epithelium-derived factor from a neurotrophic to an antiangiogenic factor. Blood 105:670–678.

113. Wert KJ, Velez G, Cross MR, et al (2018) Extracellular superoxide dismutase (SOD3) regulates oxidative stress at the vitreoretinal interface. Free Radic Biol Med 124:408–419.

114. Izuta H, Matsunaga N, Shimazawa M, et al (2010) Proliferative diabetic retinopathy and relations among antioxidant activity, oxidative stress, and VEGF in the vitreous body. Mol Vis 16:130–6.

115. Brzović-Šarić V, Landeka I, Šarić B, et al (2015) Levels of selected oxidative stress markers in the vitreous and serum of diabetic retinopathy patients. Mol Vis 21:649–64.

116. Nebbioso M, Federici M, Rusciano D, et al (2012) Oxidative Stress in Preretinopathic Diabetes Subjects and Antioxidants. Diabetes Technol Ther 14:257–263.

117. Mancino R, Di Pierro D, Varesi C, et al (2011) Lipid peroxidation and total antioxidant capacity in vitreous, aqueous humor, and blood samples from patients with diabetic retinopathy. Mol Vis 17:1298–304.

118. Cicik E, Tekin H, Akar S, et al (2003) Interleukin-8, nitric oxide and glutathione status in proliferative vitreoretinopathy and proliferative diabetic retinopathy. Ophthalmic Res 35:251–255.

119. Berra A, Ferreira S, Stanga P, Llesuy S (2002) Age-related antioxidant capacity of the vitreous and its possible relationship with simultaneous changes in photoreceptors, retinal pigment epithelium and Bruchs' membrane in human donors' eyes. Arch Gerontol Geriatr 34:371–377.

120. Brown EE, DeWeerd AJ, Ildefonso CJ, et al (2019) Mitochondrial oxidative stress in the retinal pigment epithelium (RPE) led to metabolic dysfunction in both the RPE and retinal photoreceptors. Redox Biol 24:101201.

121. Mira E, Carmona-Rodríguez L, Pérez-Villamil B, et al (2018) SOD3 improves the tumor response to chemotherapy by stabilizing endothelial HIF-2α. Nat Commun 9:575.

122. CAMPBELL PA (1990) The neutrophil, a professional killer of bacteria, may be controlled by T cells. Clin Exp Immunol 79:141–143.

123. Hyttinen JMT, Błasiak J, Niittykoski M, et al (2017) DNA damage response and autophagy in the degeneration of retinal pigment epithelial cells—Implications for age-related macular degeneration (AMD). Ageing Res Rev 36:64–77.

124. Sinha D, Valapala M, Shang P, et al (2016) Lysosomes: Regulators of autophagy in the retinal pigmented epithelium. Exp Eye Res 144:46–53.

125. Abcouwer SF, Gardner TW (2014) Diabetic retinopathy: Loss of neuroretinal adaptation to the diabetic metabolic environment. Ann N Y Acad Sci 1311:174–190.

126. Feng H, Zhao X, Guo Q, et al (2019) Autophagy resists EMT process to maintain retinal pigment epithelium homeostasis. Int J Biol Sci 15:507–521.

127. Kwon YH, Kim YA, Yoo YH (2017) Loss of Pigment Epithelial Cells Is Prevented by Autophagy. In: Autophagy: Cancer, Other Pathologies, Inflammation, Immunity, Infection, and Aging, 11th ed. Elsevier, pp 105–117

128. Wang AL, Lukas TJ, Yuan M, et al (2009) Autophagy and Exosomes in the Aged Retinal Pigment Epithelium: Possible Relevance to Drusen Formation and Age-Related Macular Degeneration. PLoS One 4:e4160.

129. Marmorstein LY, Munier FL, Arsenijevic Y, et al (2002) Aberrant accumulation of EFEMP1 underlies drusen formation in Malattia Leventinese and age-related macular degeneration. Proc Natl Acad Sci 99:13067–13072.

130. Im E, Kazlauskas A (2007) The role of cathepsins in ocular physiology and pathology. Exp Eye Res 84:383–388.

131. Lakkaraju A, Umapathy A, Tan LX, et al (2020) The cell biology of the retinal pigment epithelium. Prog Retin Eye Res 100846.

132. Mok A, Cao H, Hegele RA (2003) Genomic basis of mucopolysaccharidosis type IIID (MIM 252940) revealed by sequencing of GNS encoding N-acetylglucosamine-6-sulfatase. Genomics 81:1–5.

133. Ratnayaka JA, Serpell LC, Lotery AJ (2015) Dementia of the eye: the role of amyloid beta in retinal degeneration. Eye 29:1013–1026.

134. Luibl V, Isas JM, Kayed R, et al (2006) Drusen deposits associated with aging and age-related macular degeneration contain nonfibrillar amyloid oligomers. J Clin Invest 116:378–385.

135. Gupta V, Gupta VB, Chitranshi N, et al (2016) One protein, multiple pathologies: multifaceted involvement of amyloid β in neurodegenerative disorders of the brain and retina. Cell Mol Life Sci 73:4279–4297.

136. Gold M, El Khoury J (2015) β-amyloid, microglia, and the inflammasome in Alzheimer's disease. Semin Immunopathol 37:607–611.

137. Cuenca N, Fernández-Sánchez L, Campello L, et al (2014) Cellular responses following retinal injuries and therapeutic approaches for neurodegenerative diseases. Prog Retin Eye Res 43:17–75.

138. Zheng L, Kågedal K, Dehvari N, et al (2009) Oxidative stress induces macroautophagy of amyloid β-protein and ensuing apoptosis. Free Radic Biol Med 46:422–429.

139. Salminen A, Ojala J, Kauppinen A, et al (2009) Inflammation in Alzheimer's disease: Amyloid-β oligomers trigger innate immunity defence via pattern recognition receptors. Prog Neurobiol 87:181–194.

140. Prakasam A, Muthuswamy A, Ablonczy Z, et al (2010) Differential Accumulation of Secreted AβPP Metabolites in Ocular Fluids. J Alzheimer's Dis 20:1243–1253.

141. García-Ayllón MS, Lopez-Font I, Boix CP, et al (2017) C-Terminal fragments of the amyloid precursor protein in cerebrospinal fluid as potential biomarkers for Alzheimer disease. Sci Rep 7:1–7.

142. Paraoan L, Hiscott P, Gosden C, Grierson I (2010) Cystatin C in macular and neuronal degenerations: Implications for mechanism(s) of age-related macular degeneration. Vision Res 50:737–742.

143. Zurdel J (2002) CST3 genotype associated with exudative age-related macular degeneration. Br J Ophthalmol 86:214–219.

144. Palsdottir A, Snorradottir AO, Thorsteinsson L (2006) Hereditary cystatin C amyloid angiopathy: genetic, clinical, and pathological aspects. Brain Pathol. 16:55–59.

145. Gauthier S, Kaur G, Mi W, et al (2011) Protective mechanisms by cystatin C in neurodegenerative diseases. Front Biosci - Sch 3 S:541–554.

146. Sokol JP, Neil JR, Schiemann BJ, Schiemann WP (2005) The use of cystatin C to inhibit epithelial-mesenchymal transition and morphological transformation stimulated by transforming growth factor-β. Breast Cancer Res 7:R844.

Chapter 4

General Discussion

Besides the associated economic costs, VI and blindness cause a significant social-economic burden in modern society, highly impairing the quality of life of the patients [59, 60]. Despite improvements achieved in the prevention and control of ocular diseases in the past 30 years, the public health burden of VI and blindness is expected to increase in the future [270]. As a result of the dramatic growth and aging of the world population and the increase in the prevalence of chronic diseases such as diabetes mellitus [270–273], pathologies such as AMD and DR have emerged as priority eye diseases in middle-income and industrialized countries [274, 275]. Rhegmatogenous retinal detachment (RRD) is a potentially blinding disease and ophthalmologic emergency characterized by a physical separation between the neurosensory retina and the underlying RPE [276–278]. If left untreated, RRD can progress to PVR, a major complication characterized by the growth and contraction of cellular membranes on both surfaces of the detached retina and within the vitreous cavity [279, 280]. Despite the multiple treatment options available, some of these patients still progress to visual impairment and blindness [66]. Besides that, therapies for "dry" AMD are still an unmet requirement and its management relies only on the prevention of risk factors [281–284]. Thus, it is necessary to globally strengthen the eye health care system, but also to find new strategies to prevent and treat chronic eye diseases [62]. Ocular proteomics has emerged as an opportunity for discovering new biomarkers, which could help to unveil the pathophysiology of many ocular diseases and anticipate their progressive states [66, 87, 285]. In the last years, a comprehensive characterization of the proteome of vitreous has been made to achieve this goal [31, 92, 97, 109, 114, 115, 117, 120, 124, 129, 139, 140]. So far, the characterization of the proteome of the vitreous humor in DR/PDR has contributed extensively to the recognition of pathways involved in this pathology and to identify candidate biomarkers for its treatment [98, 175, 286, 287]. The lack of validation of these potential biomarkers in a larger number of samples may explain the lack of suitable vitreous biomarkers so far. To our best knowledge, few studies have focused on the characterization of vitreous proteomics in AMD [125–127] and RRD [107, 131, 132, 288]. Therefore, several gel-based and gel-free techniques were developed in this thesis to be applied for the analysis of vitreous proteome in these vitreoretinal pathologies.

In the first task of this Ph.D. thesis, we established a cost-effective experimental protocol for the analysis of vitreous by 2DE considering some parameters with potential impact on its solubilization, extraction, and detection. Firstly, a cost-effective protocol for the

extraction of vitreous proteins was established using the traditional one-factor-at-a-time approach. Protocols such as acetone precipitation, TCA/acetone precipitation, methanol/chloroform precipitation, and a 2-D Clean-Up Kit (GE Healthcare) were evaluated for protein extraction from the vitreous matrix. The choice turned out to be a methanol/chloroform precipitation due to its easy and fast handling, efficiency, and overall cost-effectiveness. This protocol was applied, not only for the preparation of vitreous samples for 2DE analysis but also in the iTRAQ experiment. Although the one-factor-at-a-time approach was useful for preliminary screening, it is extremely time-consuming and it is not efficient to evaluate accurately the interaction between inputs in multifactorial systems [289–291]. Therefore, an ANN was applied to explore the effect of the combination of factors that influence vitreous protein analysis by 2DE, including solubilizing agents (CHAPS, Genapol, DTT, IPG buffer) and physical parameters (total voltage and temperature). Using this strategy, we optimized the protocol for the extraction and solubilization of proteins from vitreous samples (protein recovery yields of 94.9% ± 4.5) and obtained optimal results in its analysis by 2DE (580 spots). These data reinforce the importance of combining appropriate amounts of solubilizing agents to improve the extraction, solubilization, and detection of vitreous proteins, and to obtain well-resolved gels. Beyond that, our results indicate that physical parameters have a significant influence on isoelectric focusing and, thereby, should be adjusted and monitored. Despite the meticulous refinement of several parameters, high abundant proteins, such as albumin, still cause extensive vertical and horizontal streaking, which hampers the detection of less abundant proteins. The complexity and wide dynamic concentration range of biological fluids exceed the high resolving power of 2DE, and, therefore, it is highly recommended to reduce the complexity of the sample previously to 2DE analysis [165, 167]. For this purpose, albumin and IgG were removed from samples before their analysis using the optimized protocol. As a result, there was a substantial increase in the number of protein spots detected in the gels, with an average of 761 spots in vitreous from different vitreoretinopathies. Therefore, after the depletion of abundant proteins, the proposed methodology offers an efficient protocol for high-resolution profiling of vitreous proteome, which can be advantageous for the analysis of specific proteoforms, including different isoforms and post-translational modified proteins. However, after the removal of the most abundant vitreous proteins, it is still possible to detect highly intense spots, which correspond to serotransferrin, alpha-1-antitrypsin, alpha-1B-glycoprotein, TTR, or haptoglobin. Considering these findings, more in-depth depletion methods were applied in further proteomics analysis, instead of only removing albumin and IgG.

Gel-free techniques offer a promising alternative for the characterization of the vitreous proteome [25], [110], [125], [126], [135], [195], and, therefore, in the second task of this Ph.D. project, an iTRAQ labeling based technique was applied for the analysis of vitreous proteome. This task was initially thought to analyze and compare the proteome of vitreous collected from patients with PDR to ERM and MH, two diseases widely used as controls in proteomics studies. As previously referred, the collection of vitreous is restricted to patients suffering from vitreoretinal diseases. So, obtaining samples from healthy eyes to serve as controls in proteomics studies is not possible for ethical reasons [22, 41, 66]. Our preliminary iTRAQ data showed few differences between the vitreous proteome in macular epimacular membranes (MEM) and MH (only 13 differentially expressed proteins), but 74 proteins were found differentially expressed (34 overexpressed and 40 underexpressed) in PDR in comparison to these conditions (data not published). Functional enrichment analysis revealed that the majority of these overexpressed proteins are related to complement and coagulation cascades, whereas many of the underexpressed proteins take part in the regulation of the central nervous system, neurogenesis, and ECM remodeling. Nevertheless, the most promising results were obtained comparing the proteome of vitreous collected from patients with RRD to MEM using the same approach. Of the 1030 proteins identified, 150 proteins were found differentially expressed in the vitreous of patients with RRD, including 96 overexpressed and 54 underexpressed. Several overexpressed proteins, such as glycolytic enzymes (fructose-bisphosphate aldolase A, gamma-enolase, and phosphoglycerate kinase), glucose transporters (GLUT-1), growth factors (metalloproteinase inhibitor), and serine protease inhibitors (plasminogen activator inhibitor) are regulated by HIF-1, a transcriptional regulator that mediates the cellular responses to reduced oxygen levels through changes in gene expression [292, 293]. So, this suggests that the HIF-1 signaling pathway may act as a regulator of retinal hypoxia after DDR by controlling cellular anaerobic metabolism, and cell survival. In turn, the accumulation of photoreceptor proteins, including phosducin, rhodopsin (RHO), and S-arrestin, and vimentin in vitreous may indicate that photoreceptor degeneration occurs in RRD. Nevertheless, the overexpression of proteins of carbon metabolism or molecular chaperones, among others, suggests that different protective mechanisms are activated after RRD. Therefore, the activation of mechanisms, such as the HIF-1 signaling pathway, may promote the survival of retinal cells. Lysosomal degradation appears to be up-regulated in RRD, but it is not known whether it has beneficial or hazardous effects on the survival of retinal cells. Finally, we validated three potential biomarkers (gamma-enolase, phosphoglycerate mutase 1, and RHO) in RRD by Western blot. Whilst gamma-enolase

and RHO are markers of retinal damage, phosphoglycerate mutase 1 is a glycolytic protein that may be upregulated in response to HIF-1.

Several studies have compared labeling and label-free methods and the majority of them consider that label-free is more accurate and yields higher proteome coverage [250, 254, 259, 260]. However, the performance of label-free based on SC is worse than labeling-based approaches [294]. In turn, stable isotope labeling approaches exhibited greater consistency between replicates, resulting in higher quantification precision and higher statistical significance [250, 260]. Nevertheless, the use of complementary approaches is beneficial to gain proteome coverage [259, 260]. Therefore, although the results obtained in the iTRAQ strategy showed to be promising, a label-free quantitative (LFQ) method was optimized to analyze the vitreous proteome in PDR and dry AMD. For the optimization of the methodology, several sample preparation strategies were evaluated. Firstly, we tested the performance of two depletion mini-columns for the removal of high-abundant proteins in vitreous. Specifically, high Select™ HSA/Immunoglobulin Depletion Mini Spin Column (colored blue) allowed to remove only albumin and IgG, while High Select™ Top14 Abundant Protein Depletion Mini Spin Columns (colored yellow) removed 14 high-abundant proteins (Figure 9). The performance of these columns was evaluated by the analysis of depleted samples by SDS-PAGE and LC-MS/MS. The SDS-PAGE results showed that more bands are visible after the depletion of 14 high-abundant proteins in vitreous and, although the majority of the proteins was

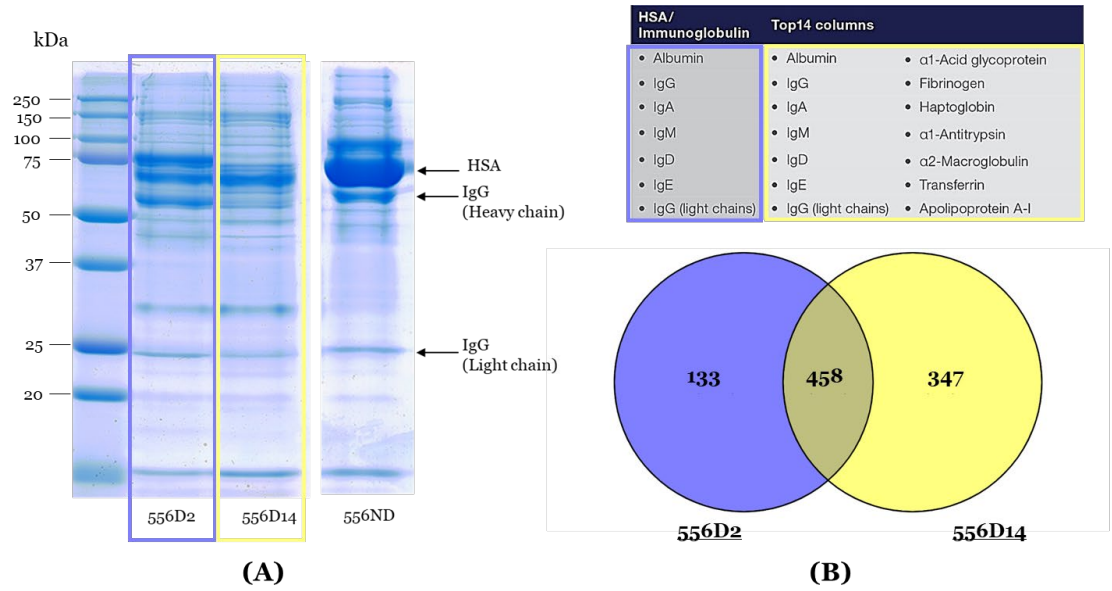

Figure 9 - (A) SDS-PAGE analysis of non-depleted vitreous (556ND) and the flow-through obtained after the depletion of albumin and IgG (556D2) and 14 high-abundant proteins (556D14). (B) Venn graph represents the number of proteins identified after the depletion with an FDR<1%.

identified in both methods, another 347 proteins were identified using a more in-depth depletion strategy. This confirms our previous results regarding the analysis of vitreous proteome by 2DE (Paper III) showing that despite albumin is the more abundant protein in vitreous, the depletion of further proteins is required to improve proteome coverage. So, vitreous collected from patients with PDR (n=4), dry AMD (n=4), and ERM (n=4) was depleted using high Select™ Top14 Abundant Protein Depletion columns, followed by the digestion using s-trap columns, according to the manufacturer's instructions, and analysis by LC-MS/MS. However, some samples increased the back pressure of pre-column, making the system unstable. This can induce changes in the chromatographic profiles, which would jeopardize the extraction of intensity values from chromatographic profiles, and, as a result, the quantitation accuracy. Thus, digested samples were filtered to try to remove the interferents (e.g. poorly digested proteins) that increase the pressure of the chromatographic system. Although this strategy showed to be fruitful in solving backpressure problems, the chromatographic profiles of the analysis of vitreous by LC-MS/MS before and after filtration were quite distinct. While 771 proteins were identified initially, only 556 were detected in the same vitreous sample after filtration.

Therefore, a distinct strategy that combines fractionation by short SDS–polyacrylamide gel electrophoresis and analysis by LC-MS/MS was implemented for the analysis of vitreous proteome collected from patients with PDR (n=4) compared to dry AMD (n=4) and ERM (n=4). As this methodology applies in-gel digestion, the gel acts as a filter, which prevents the recovering of poorly digested proteins. A total of 680 proteins were identified, 586 by the software search engine MASCOT and 580 using MaxQuant (corresponding to 474 protein groups). Subsequently, post hoc tests, hierarchical clustering, and multiple t-tests were performed for differentiating the three disease groups in terms of protein expression based on their intensity. Of these proteins, 83 can distinguish between PDR and ERM groups, while 79 proteins can discriminate between PDR and dry AMD groups. Furthermore, this LQF experiment allowed to identify 118 proteins (17 up- and 101 down-) differentially expressed in PDR compared to ERM patients, whereas 95 proteins (10 up- and 85 down-) were found differentially expressed in PDR compared to nAMD. Functional enrichment evidence that the underexpressed proteins are correlated to pathways/ biological processes, such as ECM disassembly and organization, platelet degranulation, lysosomal degradation, cell adhesion, and central nervous system development. In turn, mediators of complement and coagulation cascades and acute-phase inflammatory responses were found enriched in PDR vitreous, reinforcing the role of these pathways in the pathogenesis of PDR.

For last, some potential biomarkers were selected for further validation by targeted proteomics (MRM) based on their differential levels of expression in the LFQ and iTRAQ experiments and statistical significance, their interaction levels (based on STRING protein-protein interaction network), and on the pathways in which they are involved. It was also taken into consideration if these proteins were reported in the literature. The final scheduled method with the list of potential biomarkers and the corresponding peptides and transitions monitored, as well as other parameters, is detailed in the supplementary material table 5 from Paper V. MRM experiments were performed in a larger set of samples, including vitreous collected from patients with ERM (n=21), DR/PDR (n=20), AMD (n=11), and RRD/PVR (n=13) to conciliate the results from iTRAQ and LFQ experiments. Out of the 35 analyzed proteins, 26 proteins potentially differentiate between the distinct groups according to the MRM results and respective receiver operating characteristic curves (Paper V). Complement and coagulation components (C6, C8B, prothrombin), acute-phase proteins (alpha-1-antichymotrypsin), adhesion molecules (galectin-3-binding protein), ECM components (OPTC), and neurodegeneration biomarkers (beta-amyloid, amyloid-like protein 2) stand out as the more efficient biomarkers to discriminate among the different disease groups. Overall, complement and coagulation components were found significantly up-regulated in DR/PDR and AMD compared to ERM and RRD, which confirms the iTRAQ and LFQ data. Our results also suggest that the increase of complement and coagulation in vitreous is non-specific for a particular disease but could be a suitable predictor of its progression to a proliferative etiology, since complement and coagulation seem to be involved in pathological processes shared by DR/PDR, AMD, and RRD/PVR. On the other hand, a significant number of adhesion molecules, nervous system development proteins, and ECM components were found up-regulated in dry AMD and ERM in LFQ, pointing toward the neurodegenerative nature of these pathologies, as reported previously [102, 126, 142]. Additionally, changes in the levels of both cell adhesion molecules and ECM components indicate that some pathological events in these diseases can be mediated by the migration of cells upon the ECM remodeling [142]. The role of neurodegeneration in the AMD is reinforced by the upregulation of amyloid-beta in the vitreous, which were confirmed by LFQ, MRM, and Western blot analysis. The results obtained in iTRAQ and LFQ also shown that the levels of lysosomal proteins are changed in these pathologies. So, the lysosomal enzyme GNS was selected and validated as a biomarker of lysosomal function, with the higher levels found in AMD and ERM compared to DR/PDR and RRD/PVR groups, which confirms our LFQ data. Lysosomal turnover is essential for retinal homeostasis, which is maintained essentially by RPE due to its very active processes of phagocytosis (e.g. photoreceptor outer segment

phagocytosis) and autophagy [295, 296]. As a result, lysosomal dysfunction seems to be one of the pathological mechanisms that lead to the death of neurons and RPE cells, which was correlated to AMD [295, 297–299], DR [298], and PVR [299].

Chapter 5

Concluding remarks and future perspectives

In conclusion, several gel-based and gel-free strategies were developed and implemented for the analysis of vitreous proteome in different vitreoretinal diseases. Concerning the gel-based method, a mathematical model created by ANN provided an effective 2DE protocol for high-resolution analysis of vitreous proteome, which can be advantageous for specific proteoforms, including different isoforms and post-translational modified proteins. On the other hand, high-throughput methods, such as iTRAQ and LFQ, provided a more in-depth analysis of vitreous proteome. Using these techniques, we identified 1030 proteins by iTRAQ and 985 by LFQ, some of them that have not been previously identified.

More relevant is the fact that vitreous analysis using these methodologies provided new insights on the pathogenesis of RRD, PDR, and AMD. Complement and coagulation have been implicated in these pathologies, but the increase of the levels of these proteins is non-specific for a particular disease but could be a suitable predictor of its progression to a proliferative etiology. Our results also reinforce the neurodegenerative nature of AMD and ERM, whereas the detection of markers of cell damage in vitreous from RRD patients suggests that degeneration of photoreceptors occurs in this pathology. Although we have not found proteins related to angiogenesis, which are relevant in neovascular pathologies, such as nAMD and PDR, the downregulation of anti-angiogenic factors, such as OPTC and PEDF, may suggest that vitreous is conduced to an angiogenic environment in these diseases. Highlighting iTRAQ achievements, some protection mechanisms including the HIF-1 signaling pathway seem to be triggered in response to retinal stress after the DRR to promote the survival of retinal cells. Although further studies are required to understand some of our findings, the obtained results provide a scientific basis for new insights into the pathogenesis of PDR, AMD, and RRD. Beyond that, these discovery proteomics experiments afford fundamental information regarding potential biomarkers, with the successful validation of 26 proteins by MRM. According to ROC curves, complement and coagulation components (C6, C8B, prothrombin), acute-phase mediators (alpha-1-antichymotrypsin), adhesion molecules (galectin-3-binding protein), ECM components (OPTC), and neurodegeneration biomarkers (beta-amyloid, amyloid-like protein 2, FAM3C) stand out as the more efficient to discriminate different disease groups. Nevertheless, it must be taken into consideration that vitreous biomarkers cannot be used for regular diagnosis due to invasive sampling. However, they can be candidates for new pharmaceutical targets and, when the samples are obtained as

part of the clinical routine, be used for the prognosis of the patient's disease evolution and/or to predict the proper response to treatment.

Although the main aims of this Ph.D. thesis were fulfilled, the obtained results open up new future perspectives. In the first place, it would be interesting to develop a multiplex method, considering the biomarkers validated in this work, capable of optimally correlate specific proteins/signaling pathways with the progression of vitreoretinal diseases and their clinical features. Of course, the development of a reliable diagnosis method that could be incorporated into the clinical routine will require a larger number of samples collected from different stages of the pathology. Nevertheless, vitreous is mainly collected in the more advanced stages of the pathologies (e.g. ERM and vitreous hemorrhage), which hinders the obtention of vitreous samples from the earliest stages of the disease. Thus, it must be taken into account the challenging nature of this objective, and further studies should be performed to address it. In this sense, proteomics data should be supplemented with functional studies, and other -omics analysis (e.g. genomics and metabolomics), and *in vitro* and *in vivo* experiments. In particular, genomics analysis could be relevant in nAMD, since this disorder has a significant genetic component. Also, some work has been developed in the stimulation of retinal cell culture (e.g. RPE) with vitreous samples to understand the changes induced at the molecular and morphological levels, which could be an interesting complement for future studies.

Finally, for the development of more specific and effective therapies we need to successfully target specific proteoforms. Several authors reported the presence of different isoforms, and proteins with PTMs and dual function in vitreous. Therefore, it is important to validate the specific proteoforms that are involved in the events underlying vitreoretinal pathologies. For this purpose, it would be interesting to combine the new 2DE protocol with a Western blot to enable the high-resolution analysis of these proteoforms.

References

References

1. Siggers JH, Ethier CR (2012) Fluid Mechanics of the Eye. Annu Rev Fluid Mech 44:347–372. https://doi.org/10.1146/annurev-fluid-120710-101058.

2. Tripathi RC, Tripathi BJ (1984) Anatomy of the Human Eye, Orbit, and Adnexa. In: Davson H (ed) The Eye, 3rd Editio. Elsevier, pp 1–268.

3. Willoughby CE, Ponzin D, Ferrari S, et al (2010) Anatomy and physiology of the human eye: Effects of mucopolysaccharidoses disease on structure and function - a review. Clin Exp Ophthalmol 38:2–11. https://doi.org/10.1111/j.1442-9071.2010.02363.x.

4. Ding SLS, Kumar S, Mok PL (2017) Cellular reparative mechanisms of mesenchymal stem cells for retinal diseases. Int J Mol Sci 18:. https://doi.org/10.3390/ijms18081406.

5. Riordan-Eva P (2008) Anatomy & Embryology of the Eye: Introduction. In: Riordan-Eva P, Whitcher JP (eds) Vaughan and Asbury's General Ophthalmology, 17th edition, 17th ed. McGraw Hill.

6. Liebovitch LS (2006) Why the Eye Is Round. In: Fischbarg J (ed) The Biology of the Eye, 1st Editio. Elsevier Ltd., pp 1–19.

7. Bishop PN (2000) Structural macromolecules and supramolecular organisation of the vitreous gel. Prog Retin Eye Res 19:323–344. https://doi.org/10.1016/S1350-9462(99)00016-6.

8. Kodama M, Matsuura T, Hara Y (2013) Structure of vitreous body and its relationship with liquefaction. J Biomed Sci Eng 06:739–745. https://doi.org/10.4236/jbise.2013.67091.

9. Chirila T V., Hong Y (2016) Chapter C2 The Vitreous Humor. In: Handbook of Biomaterial Properties. Springer New York, New York, NY, pp 125–134.

10. Sebag J (2010) Vitreous Anatomy, Aging, and Anomalous Posterior Vitreous Detachment. In: Encyclopedia of the Eye. Elsevier, pp 307–315.

11. Le Goff MM, Bishop PN (2008) Adult vitreous structure and postnatal changes. Eye 22:1214–1222. https://doi.org/10.1038/eye.2008.21.

12. Ihanamäki T, Pelliniemi LJ, Vuorio E (2004) Collagens and collagen-related matrix components in the human and mouse eye. Prog Retin Eye Res 23:403–434. https://doi.org/10.1016/J.PRETEYERES.2004.04.002.

13. Scott JE (1975) Composition and structure of the pericellular environment. Physiological function and chemical composition of pericellular proteoglycan (an evolutionary view). Philos Trans R Soc London Ser B Biol Sci 271:135–142. https://doi.org/10.1098/rstb.1975.0047.

14. Kingston ZS, Provis JM, Madigan MC (2014) II.A. Development and Developmental Disorders of Vitreous. In: Vitreous. Springer New York, New York, NY, pp 95–111.

15. Sebag J, Sebag J (1989) Embryology of the Vitreous. In: The Vitreous. Springer New York, New York, NY, pp 7–16.

16. Ponsioen TL, Hooymans JMM, Los LI (2010) Remodelling of the human vitreous and vitreoretinal interface - A dynamic process. Prog Retin Eye Res 29:580–595. https://doi.org/10.1016/j.preteyeres.2010.07.001.

17. Mglinets V (2016) The genetic basis of the formation, structure, and functions of the vitreous body. Biol Bull Rev 6:519. https://doi.org/10.1134/S2079086416060049.

18. Sebag J, Silverman RH, Coleman DJ (2014) To see the invisible: The quest of imaging vitreous. Vitr Heal Dis 193–219. https://doi.org/10.1007/978-1-4939-1086-1_12.

19. Sebag J (2014) The underlying anatomy of vitreous and its role in retinal disease. Retin Today MAR:2–5. https://doi.org/10.1080/02699931.2017.1303452.

20. De Smet MD, Gad Elkareem AM, Zwinderman AH (2013) The vitreous, the retinal interface in ocular health and disease. Ophthalmologica 230:165–178. https://doi.org/10.1159/000353447.

21. Skeie JM, Mahajan VB (2011) Dissection of human vitreous body elements for proteomic analysis. J Vis Exp 47:5–8. https://doi.org/10.3791/2455.

22. Angi M, Kalirai H, Coupland SE, et al (2012) Proteomic analyses of the vitreous humour. Mediators Inflamm 2012:. https://doi.org/10.1155/2012/148039.

23. Theocharis AD, Papageorgakopoulou N, Feretis E, Theocharis DA (2002) Occurrence and structural characterization of versican-like proteoglycan in human vitreous. Biochimie 84:1237–1243. https://doi.org/10.1016/S0300-9084(02)00015-9.

24. Foster WJ (2008) Vitreous substitutes. Expert Rev Ophthalmol 3:211–218. https://doi.org/10.1586/17469899.3.2.211.

25. Skeie JM, Roybal CN, Mahajan VB (2015) Proteomic insight into the molecular function of the vitreous. PLoS One 10:1–19. https://doi.org/10.1371/journal.pone.0127567.

26. Liu Y, Bouhenni RA, Dufresne CP, et al (2016) Differential Expression of Vitreous Proteins in Young and Mature New Zealand White Rabbits. PLoS One 11:1–15. https://doi.org/10.1371/journal.pone.0153560.

27. Bernal A, Parel JM, Manns F (2006) Evidence for posterior zonular fiber attachment on the anterior hyaloid membrane. Investig Ophthalmol Vis Sci 47:4708–4713. https://doi.org/10.1167/iovs.06-0441.

28. Mitry D, Fleck BW, Wright AF, et al (2010) PATHOGENESIS OF RHEGMATOGENOUS RETINAL DETACHMENT. Retina 30:1561–1572. https://doi.org/10.1097/IAE.0b013e3181f669e6.

29. Tozer K, Johnson MW, Sebag J (2014) II.C. Vitreous Aging and Posterior Vitreous Detachment. In: Vitreous. Springer New York, New York, NY, pp 131–150.

30. Bishop PN (2014) I.A. Vitreous Proteins. In: Vitreous. Springer New York, New York, NY, pp 3–12.

31. Aretz S, Krohne TU, Kammerer K, et al (2013) In-depth mass spectrometric mapping of the human vitreous proteome. Proteome Sci 11:5956. https://doi.org/10.1186/1477-5956-11-22.

32. Grus FH, Joachim SC, Pfeiffer N (2007) Proteomics in ocular fluids. Proteomics - Clin Appl 1:876–888. https://doi.org/10.1002/prca.200700105.

33. Clausen R, Weller M, Wiedemann P, et al (2004) An immunochemical quantitative analysis of the protein pattern in physiologic and pathologic vitreous. Graefe's Arch Clin Exp Ophthalmol 229:186–190. https://doi.org/10.1007/BF00170555.

34. Filas BA, Zhang Q, Okamoto RJ, et al (2014) Enzymatic degradation identifies components responsible for the structural properties of the vitreous body. Investig Ophthalmol Vis Sci 55:55–63. https://doi.org/10.1167/iovs.13-13026.

35. Foulds WS (1987) Is your vitreous really necessary?: The role of the vitreous in the eye with particular reference to retinal attachment, detachment and the mode of action of vitreous substitutes. Eye 1:641–664. https://doi.org/10.1038/eye.1987.107.

36. Bishop PN, Takanosu M, Le Goff M, Mayne R (2002) The role of the posterior ciliary body in the biosynthesis of vitreous humour. Eye 16:454–460. https://doi.org/10.1038/sj.eye.6700199.

37. Halfter W, Dong S, Dong A, et al (2008) Origin and turnover of ECM proteins from the inner limiting membrane and vitreous body. Eye 22:1207–1213. https://doi.org/10.1038/eye.2008.19.

38. Halfter W, Dong S, Schurer B, et al (2005) Embryonic synthesis of the inner limiting membrane and vitreous body. Investig Ophthalmol Vis Sci 46:2202–2209. https://doi.org/10.1167/iovs.04-1419.

39. Ponsioen TL, van Luyn MJA, van der Worp RJ, et al (2008) Human retinal Müller cells synthesize collagens of the vitreous and vitreoretinal interface in vitro. Mol Vis 14:652–60.

40. Yee KMP, Feener EP, Madigan M, et al (2015) Proteomic analysis of embryonic and young human vitreous. Investig Ophthalmol Vis Sci 56:7036–7042. https://doi.org/10.1167/iovs.15-16809.

41. Monteiro JP, Santos FM, Rocha AS, et al (2015) Vitreous humor in the pathologic scope: Insights from proteomic approaches. PROTEOMICS - Clin Appl 9:187–202. https://doi.org/10.1002/prca.201400133.

42. Ahmad MT, Zhang P, Dufresne C, et al (2018) The Human Eye Proteome Project: Updates on an Emerging Proteome. Proteomics 18:1–31. https://doi.org/10.1002/pmic.201700394.

43. Ankamah E, Sebag J, Ng E, Nolan JM (2019) Vitreous Antioxidants, Degeneration, and Vitreo-Retinopathy: Exploring the Links. Antioxidants 9:7. https://doi.org/10.3390/antiox9010007.

44. Sebag J (2014) Vitreous. Springer New York, New York, NY.

45. Sebag J (2009) Vitreous: The resplendent enigma. Br J Ophthalmol 93:989–991. https://doi.org/10.1136/bjo.2009.157313.

46. Alovisi C, Panico C, De Sanctis U, Eandi CM (2017) Vitreous Substitutes: Old and New Materials in Vitreoretinal Surgery. https://doi.org/10.1155/2017/3172138.

47. Holekamp NM (2010) The Vitreous Gel: More than Meets the Eye. Am J Ophthalmol 149:32-36.e1. https://doi.org/10.1016/j.ajo.2009.07.036.

48. Shui Y-B (2009) The Gel State of the Vitreous and Ascorbate-Dependent Oxygen Consumption. Arch Ophthalmol 127:475. https://doi.org/10.1001/archophthalmol.2008.621.

49. Patz A, Brem S, Finkelstein D, et al (1978) A New Approach to the Problem of Retinal Neovascularization. Ophthalmology 85:626–637. https://doi.org/10.1016/S0161-6420(78)35640-2.

50. Lutty GA, Thompson DC, Gallup JY, et al (1983) Vitreous: An inhibitor of retinal extract-induced neovascularization. Investig Ophthalmol Vis Sci 24:52–56.

51. Felton SM, Brown GC, Felberg NT, Federman JL (1979) Vitreous Inhibition of Tumor Neovascularization. Arch Ophthalmol 97:1710–1713. https://doi.org/10.1001/archopht.1979.01020020278019.

52. Brem S, Preis I, Langer R, et al (1977) Inhibition of neovascularization by an extract derived from vitreous. Am J Ophthalmol 84:323–325. https://doi.org/10.1016/0002-9394(77)90672-9.

53. Dawson DW (1999) Pigment Epithelium-Derived Factor: A Potent Inhibitor of Angiogenesis. Science 285:245–248. https://doi.org/10.1126/science.285.5425.245

54. Mori K, Duh E, Gehlbach P, et al (2001) Pigment epithelium-derived factor inhibits retinal and choroidal neovascularization. J Cell Physiol 188:253–263. https://doi.org/10.1002/jcp.1114.

55. Park K, Jin J, Hu Y, et al (2011) Overexpression of pigment epithelium-derived factor inhibits retinal inflammation and neovascularization. Am J Pathol 178:688–698. https://doi.org/10.1016/j.ajpath.2010.10.014.

56. Bishop PN (2015) The role of extracellular matrix in retinal vascular development and preretinal neovascularization. Exp Eye Res 133:30–36. https://doi.org/10.1016/j.exer.2014.10.021.

57. Lawler PR, Lawler J (2012) Molecular basis for the regulation of angiogenesis by thrombospondin-1 and -2. Cold Spring Harb Perspect Med 2:a006627–a006627. https://doi.org/10.1101/cshperspect.a006627.

58. Schmidt JC, Mennel S, Meyer CH, Kroll P (2008) Posterior Vitreomacular Adhesion: A Potential Risk Factor for Exudative Age-related Macular Degeneration. Am J Ophthalmol 145:1107. https://doi.org/10.1016/j.ajo.2008.03.011.

59. Sabanayagam C, Cheng C-Y (2017) Global causes of vision loss in 2015: are we on track to achieve the Vision 2020 target? Lancet Glob Heal 5:e1164–e1165. https://doi.org/10.1016/S2214-109X(17)30412-6.

60. Bourne RRA, Flaxman SR, Braithwaite T, et al (2017) Magnitude, temporal trends, and projections of the global prevalence of blindness and distance and near vision impairment: a systematic review and meta-analysis. Lancet Glob Heal 5:e888–e897. https://doi.org/10.1016/S2214-109X(17)30293-0.

61. Flaxman SR, Bourne RRA, Resnikoff S, et al (2017) Global causes of blindness and distance vision impairment 1990–2020: a systematic review and meta-analysis. Lancet Glob Heal 5:e1221–e1234. https://doi.org/10.1016/S2214-109X(17)30393-5.

62. Ramke J, Gilbert CE (2017) Universal eye health: are we getting closer? Lancet Glob Heal 5:e843–e844. https://doi.org/10.1016/S2214-109X(17)30302-9.

63. Keeffe J, Resnikoff S (2019) Prevalence and Causes of Vision Impairment and Blindness: The Global Burden of Disease. In: Khanna RC, Rao GN, Marmamula S (eds) Innovative Approaches in the Delivery of Primary and Secondary Eye Care. Springer International Publishing, Cham, pp 7–20.

64. Bourne RRA, Stevens GA, White RA, et al (2013) Causes of vision loss worldwide, 1990-2010: A systematic analysis. Lancet Glob Heal 1:e339–e349. https://doi.org/10.1016/S2214-109X(13)70113-X.

65. Fricke TR, Tahhan N, Resnikoff S, et al (2018) Global Prevalence of Presbyopia and Vision Impairment from Uncorrected Presbyopia. Ophthalmology 125:1492–1499. https://doi.org/10.1016/j.ophtha.2018.04.013.

66. Semba RD, Enghild JJ, Venkatraman V, et al (2013) The Human Eye Proteome Project: Perspectives on an emerging proteome. Proteomics 13:2500–2511. https://doi.org/10.1002/pmic.201300075.

67. Rao GN (2019) VISION 2020: Past, Present and Future. In: Khanna RC, Rao GN, Marmamula S (eds). Springer International Publishing, Cham, pp 1–5.

68. World Health Organization (2019) World report on vision.

69. Subramanyam M, Goyal J (2016) Translational biomarkers: from discovery and development to clinical practice. Drug Discov Today Technol 21–22:3–10. https://doi.org/10.1016/j.ddtec.2016.10.001.

70. van Karnebeek CDM, Wortmann SB, Tarailo-Graovac M, et al (2018) The role of the clinician in the multi-omics era: are you ready? J Inherit Metab Dis 41:571–582. https://doi.org/10.1007/s10545-017-0128-1.

71. Kersten E, Paun CC, Schellevis RL, et al (2018) Systemic and ocular fluid compounds as potential biomarkers in age-related macular degeneration. Surv Ophthalmol 63:9–39. https://doi.org/10.1016/j.survophthal.2017.05.003.

72. Petalcorin MF, Shafqat N, Lu ZH, Petalcorin MIR (2019) Clinical Proteomics. In: Encyclopedia of Bioinformatics and Computational Biology. Elsevier, Totowa, NJ, pp 911–925.

73. Wilkins MR, Sanchez JC, Gooley AA, et al (1996) Progress with proteome projects: Why all proteins expressed by a genome should be identified and how to do it. Biotechnol Genet Eng Rev 13:19–50. https://doi.org/10.1080/02648725.1996.10647923.

74. Marko-Varga G (2004) Proteomics principles and challenges. Pure Appl Chem 76:829–837. https://doi.org/10.1351/pac200476040829.

75. Zhang Y, Fonslow BR, Shan B, et al (2013) Protein analysis by shotgun/bottom-up proteomics. Chem Rev 113:2343–2394. https://doi.org/10.1021/cr3003533.

76. McDonald WH, Yates JR (2002) Shotgun proteomics and biomarker discovery. Dis Markers 18:99–105. https://doi.org/10.1155/2002/505397.

77. Shi Y, Xiang R, Horváth C, Wilkins JA (2004) The role of liquid chromatography in proteomics. J Chromatogr A 1053:27–36. https://doi.org/10.1016/j.chroma.2004.07.044.

78. Neverova I, Van Eyk JE (2005) Role of chromatographic techniques in proteomic analysis. J Chromatogr B Anal Technol Biomed Life Sci 815:51–63. https://doi.org/10.1016/j.jchromb.2004.11.009.

79. Schulze WX, Usadel B (2010) Quantitation in Mass-Spectrometry-Based Proteomics. Annu Rev Plant Biol 61:491–516. https://doi.org/10.1146/annurev-arplant-042809-112132.

80. America AHP, Cordewener JHG (2008) Comparative LC-MS: A landscape of peaks and valleys. Proteomics 8:731–749. https://doi.org/10.1002/pmic.200700694.

81. Aebersold R, Mann M (2016) Mass-spectrometric exploration of proteome structure and function. Nature 537:347–355. https://doi.org/10.1038/nature19949.

82. Gedela S, Medicherla NR (2007) Chromatographic Techniques for the Separation of Peptides: Application to Proteomics. Chromatographia 65:511–518. https://doi.org/10.1365/s10337-007-0215-9.

83. Ponomarenko EA, Poverennaya E V, Ilgisonis E V, et al (2016) The Size of the Human Proteome: The Width and Depth. Int J Anal Chem 2016:1–6. https://doi.org/10.1155/2016/7436849.

84. Schmit PO, Vialaret J, Wessels HJCT, et al (2018) Towards a routine application of Top-Down approaches for label-free discovery workflows. J Proteomics 175:12–26. https://doi.org/10.1016/j.jprot.2017.08.003.

85. Deracinois B, Flahaut C, Duban-Deweer S, Karamanos Y (2013) Comparative and Quantitative Global Proteomics Approaches: An Overview. Proteomes 1:180–218. https://doi.org/10.3390/proteomes1030180.

86. Nilsson T, Mann M, Aebersold R, et al (2010) Mass spectrometry in high-throughput proteomics: Ready for the big time. Nat Methods 7:681–685. https://doi.org/10.1038/nmeth0910-681.

87. Jay NL, Gillies M (2012) Proteomic analysis of ophthalmic disease. Clin Experiment Ophthalmol 40:755–763. https://doi.org/10.1111/j.1442-9071.2012.02788.x.

88. Velez G, Tang PH, Cabral T, et al (2018) Personalized Proteomics for Precision Health: Identifying Biomarkers of Vitreoretinal Disease. Transl Vis Sci Technol 7:12. https://doi.org/10.1167/tvst.7.5.12.

89. Banerjee S (2006) A review of developments in the management of retinal diseases. J R Soc Med 99:125–127. https://doi.org/10.1258/jrsm.99.3.125.

90. Chaudhry NA, Cohen KA, Flynn HW, Murray TG (2004) Combined pars plana vitrectomy and lens management in complex vitreoretinal disease. Semin Ophthalmol 18:132–141. https://doi.org/10.1080/08820530390899178.

91. Wang H, Feng L, Hu JW, et al (2012) Characterisation of the vitreous proteome in proliferative diabetic retinopathy. Proteome Sci 10:1–11. https://doi.org/10.1186/1477-5956-10-15.

92. Wu CW, Sauter JL, Johnson PK, et al (2004) Identification and localization of major soluble vitreous proteins in human ocular tissue. Am J Ophthalmol 137:655–61. https://doi.org/10.1016/j.ajo.2003.11.009.

93. Cehofski LJ, Mandal N, Honoré B, Vorum H (2014) Analytical platforms in vitreoretinal proteomics. Bioanalysis 6:3051–3066. https://doi.org/10.4155/bio.14.227

94. Sonoda T, Sugahara K-H, Mochizuki M, Enaida Y (2009) Comprehensive Analysis of Inflammatory Immune Mediators in Vitreoretinal Diseases. PLoS One 4:8158. https://doi.org/10.1371/journal.pone.0008158.

95. Mahajan VB, Skeie JM (2014) Translational vitreous proteomics. Proteomics Clin Appl 8:204–8. https://doi.org/10.1002/prca.201300062.

96. Sjöstrand J, Karlsson J -O, Andersson A -K (1992) Changes in the soluble protein of the human vitreous in vitreoretinal disease. Acta Ophthalmol 70:814–819. https://doi.org/10.1111/j.1755-3768.1992.tb04893.x.

97. Murthy KR, Goel R, Subbannayya Y, et al (2014) Proteomic analysis of human vitreous humor. Clin Proteomics 11:29. https://doi.org/10.1186/1559-0275-11-29

98. Simó-Servat O, Hernández C, Simó R (2012) Usefulness of the Vitreous Fluid Analysis in the Translational Research of Diabetic Retinopathy. Mediators Inflamm 2012:1–11. https://doi.org/10.1155/2012/872978.

99. Skeie JM, Mahajan VB (2013) Proteomic interactions in the mouse vitreous-retina complex. PLoS One 8:1–14. https://doi.org/10.1371/journal.pone.0082140

100. Rauh M (2012) LC–MS/MS for protein and peptide quantification in clinical chemistry. J Chromatogr B 883–884:59–67. https://doi.org/10.1016/j.jchromb.2011.09.030.

101. Mandal N, Heegaard S, Prause JU, et al (2010) Ocular proteomics with emphasis on two-dimensional gel electrophoresis and mass spectrometry. Biol Proced Online 12:56–88. https://doi.org/10.1007/s12575-009-9019-7.

102. Pollreisz A, Funk M, Breitwieser FP, et al (2013) Quantitative proteomics of aqueous and vitreous fluid from patients with idiopathic epiretinal membranes. Exp Eye Res 108:48–58. https://doi.org/10.1016/j.exer.2012.11.010.

103. Cottrell JS (2011) Protein identification using MS/MS data. J Proteomics 74:1842–1851. https://doi.org/10.1016/j.jprot.2011.05.014.

104. Bose U, Wijffels G, Howitt CA, Colgrave ML (2019) Proteomics: Tools of the Trade. In: Capelo-Martínez J-L (ed). Springer International Publishing, Cham, pp 1–22

105. Zhao Y, Weber SR, Lease J, et al (2018) Liquid Biopsy of Vitreous Reveals an Abundant Vesicle Population Consistent With the Size and Morphology of Exosomes. Transl Vis Sci Technol 7:6. https://doi.org/10.1167/tvst.7.3.6.

106. Skeie JM, Brown EN, Martinez HD, et al (2012) Proteomic analysis of vitreous biopsy techniques. Retina 32:2141–2149. https://doi.org/10.1097/IAE.0b013e3182562017.

107. Shitama T, Hayashi H, Noge S, et al (2008) Proteome profiling of vitreoretinal diseases by cluster analysis. Proteomics - Clin Appl 2:1265–1280. https://doi.org/10.1002/prca.200800017.

108. Tamburro D, Facchiano F, Petricoin EF, et al (2010) Mass spectrometry-based characterization of the vitreous phosphoproteome. Proteomics - Clin Appl 4:839–846. https://doi.org/10.1002/prca.201000032.

109. Nakanishi T, Koyama R, Ikeda T, Shimizu A (2002) Catalogue of soluble proteins in the human vitreous humor: Comparison between diabetic retinopathy and macular hole. J Chromatogr B Anal Technol Biomed Life Sci 776:89–100. https://doi.org/10.1016/S1570-0232(02)00078-8.

110. Loukovaara S, Nurkkala H, Tamene F, et al (2015) Quantitative Proteomics Analysis of Vitreous Humor from Diabetic Retinopathy Patients. J Proteome Res 14:5131–5143. https://doi.org/10.1021/acs.jproteome.5b00900.

111. Balaiya S, Zhou Z, Chalam K V. (2017) Characterization of vitreous and aqueous proteome in humans with proliferative diabetic retinopathy and its clinical correlation. Proteomics Insights 8:1–10. https://doi.org/10.1177/1178641816686078.

112. Li J, Lu Q, Lu P (2018) Quantitative proteomics analysis of vitreous body from type 2 diabetic patients with proliferative diabetic retinopathy. BMC Ophthalmol 18:151. https://doi.org/10.1186/s12886-018-0821-3.

113. Zou C, Han C, Zhao M, et al (2018) Change of ranibizumab-induced human vitreous protein profile in patients with proliferative diabetic retinopathy based on proteomics analysis. Clin Proteomics 15:12. https://doi.org/10.1186/s12014-018-9187-z.

114. Yamane K, Minamoto A, Yamashita H, et al (2003) Proteome Analysis of Human Vitreous Proteins. Mol Cell Proteomics 2:1177–1187. https://doi.org/10.1074/mcp.M300038-MCP200.

115. Kim SJ, Kim S, Park J, et al (2006) Differential Expression of Vitreous Proteins in Proliferative Diabetic Retinopathy. Curr Eye Res 31:231–240. https://doi.org/10.1080/02713680600557030.

116. Minamoto A, Yamane K, Yokoyama T, Thongboonkerd V (2007) Proteomics of vitreous fluid. Proteomics Hum Body Fluids Princ Methods, Appl 495–507. https://doi.org/10.1007/978-1-59745-432-2_23.

117. Kim T, Sang JK, Kim K, et al (2007) Profiling of vitreous proteomes from proliferative diabetic retinopathy and nondiabetic patients. Proteomics 7:4203–4215. https://doi.org/10.1002/pmic.200700745.

118. García-Ramírez M, Canals F, Hernández C, et al (2007) Proteomic analysis of human vitreous fluid by fluorescence-based difference gel electrophoresis (DIGE): A new strategy for identifying potential candidates in the pathogenesis of proliferative diabetic retinopathy. Diabetologia 50:1294–1303. https://doi.org/10.1007/s00125-007-0627-y

119. Simó R, Higuera M, García-Ramírez M, et al (2008) Elevation of apolipoprotein A-I and apolipoprotein H levels in the vitreous fluid and overexpression in the retina of diabetic patients. Arch Ophthalmol 126:1076–1081. https://doi.org/10.1001/archopht.126.8.1076.

120. Gao B-B, Chen X, Timothy N, et al (2008) Characterization of the Vitreous Proteome in Diabetes without Diabetic Retinopathy and Diabetes with Proliferative Diabetic Retinopathy. J Proteome Res 7:2516–2525. https://doi.org/10.1021/pr800112g.

121. Wang H, Feng L, Hu J, et al (2013) Differentiating vitreous proteomes in proliferative diabetic retinopathy using high-performance liquid chromatography coupled to tandem mass spectrometry. Exp Eye Res 108:110–119. https://doi.org/10.1016/j.exer.2012.11.023.

122. Hernández C, García-Ramírez M, Colomé N, et al (2013) Identification of new pathogenic candidates for diabetic macular edema using fluorescence-based difference gel electrophoresis analysis. Diabetes Metab Res Rev 29:499–506. https://doi.org/10.1002/dmrr.2419.

123. Hernández C, García-Ramírez M, Colomé N, et al (2010) New pathogenic candidates for diabetic macular edema detected by proteomic analysis. Diabetes Care 33:2010. https://doi.org/10.2337/dc10-0232.

124. Ouchi M, West K, Crabb JW, et al (2005) Proteomic analysis of vitreous from diabetic macular edema. Exp Eye Res 81:176–182. https://doi.org/10.1016/j.exer.2005.01.020.

125. Koss MJ, Hoffmann J, Nguyen N, et al (2014) Proteomics of vitreous humor of patients with exudative age-related macular degeneration. PLoS One 9:1–11. https://doi.org/10.1371/journal.pone.0096895.

126. Nobl M, Reich M, Dacheva I, et al (2016) Proteomics of vitreous in neovascular age-related macular degeneration. Exp Eye Res 146:107–117. https://doi.org/10.1016/j.exer.2016.01.001.

127. Schori C, Trachsel C, Grossmann J, et al (2018) The Proteomic Landscape in the Vitreous of Patients With Age-Related and Diabetic Retinal Disease. Invest Ophthalmol Vis Sci 59:AMD31–AMD40. https://doi.org/10.1167/iovs.18-24122.

128. Mirzaei M, Gupta VBVKVB, Chick JM, et al (2017) Age-related neurodegenerative disease associated pathways identified in retinal and vitreous proteome from human glaucoma eyes. Sci Rep 7:1–16. https://doi.org/10.1038/s41598-017-12858-7.

129. Gaspar LM, Santos FM, Albuquerque T, et al (2017) Proteome analysis of vitreous humor in retinal detachment using two different flow-charts for protein fractionation. J Chromatogr B 1061–1062:334–341. https://doi.org/10.1016/j.jchromb.2017.07.049.

130. Roybal CN, Velez G, Toral MA, et al (2018) Personalized Proteomics in Proliferative Vitreoretinopathy Implicate Hematopoietic Cell Recruitment and mTOR as a Therapeutic Target. Am J Ophthalmol 186:152–163. https://doi.org/10.1016/j.ajo.2017.11.025.

131. Yu J, Peng R, Chen H, et al (2012) Elucidation of the pathogenic mechanism of rhegmatogenous retinal detachment with proliferative vitreoretinopathy by proteomic analysis. Investig Ophthalmol Vis Sci 53:8146–8153. https://doi.org/10.1167/iovs.12-10079.

132. Yu J, Liu F, Cui SJ, et al (2008) Vitreous proteomic analysis of proliferative vitreoretinopathy. Proteomics 8:3667–3678. https://doi.org/10.1002/pmic.200700824.

133. Velez G, Yang J, Li AS, et al (2019) Proteomic insight into the pathogenesis of CAPN5-vitreoretinopathy. Sci Rep 9:7608. https://doi.org/10.1038/s41598-019-44031-7.

134. Naru J, Aggarwal R, Singh U, et al (2016) Proteomic analysis of differentially expressed proteins in vitreous humor of patients with retinoblastoma using iTRAQ-coupled ESI-MS/MS approach. Tumor Biol 37:13915–13926. https://doi.org/10.1007/s13277-016-5162-3.

135. Reich M, Dacheva I, Nobl M, et al (2016) Proteomic Analysis of Vitreous Humor in Retinal Vein Occlusion. PLoS One 11:e0158001. https://doi.org/10.1371/journal.pone.0158001.

136. Zhang P, Zhu M, Zhao Y, et al (2017) A proteomic approach to understanding the pathogenesis of idiopathic macular hole formation. Clin Proteomics 14:1–10. https://doi.org/10.1186/s12014-017-9172-y.

137. Yu J, Feng L, Wu Y, et al (2014) Vitreous proteomic analysis of idiopathic epiretinal membranes. Mol Biosyst 10:2558–2566. https://doi.org/10.1039/c4mb00240g.

138. Mandal N, Kofod M, Vorum H, et al (2013) Proteomic analysis of human vitreous associated with idiopathic epiretinal membrane. Acta Ophthalmol 91:333–334. https://doi.org/10.1111/aos.12075.

139. Neal RE, Bettelheim FA, Lin C, et al (2005) Alterations in human vitreous humour following cataract extraction. Exp Eye Res 80:337–47. https://doi.org/10.1016/j.exer.2004.09.015.

140. Sugioka K, Saito A, Kusaka S, et al (2017) Identification of vitreous proteins in retinopathy of prematurity. Biochem Biophys Res Commun 488:483–488. https://doi.org/10.1016/j.bbrc.2017.05.067.

141. Kasudhan KS, Sarkar S, Gupta V, et al (2018) Identification of unique proteins in vitreous fluid of patients with noninfectious uveitis. Acta Ophthalmol 96:e989–e1003. https://doi.org/10.1111/aos.13801.

142. Öhman T, Tamene F, Göös H, et al (2018) Systems pathology analysis identifies neurodegenerative nature of age-related vitreoretinal interface diseases. Aging Cell 17:e12809. https://doi.org/10.1111/acel.12809.

143. Kito K, Ito T (2008) Mass Spectrometry-Based Approaches Toward Absolute Quantitative Proteomics. Curr Genomics 9:263–274. https://doi.org/10.2174/138920208784533647.

144. Hernandez P, Binz P-A, Wilkins MR Protein Identification in Proteomics. In: Proteome Research. Springer Berlin Heidelberg, Berlin, Heidelberg, pp 41–67.

145. Corthals GL, Rose K (2007) Quantitation in Proteomics. In: Proteome Research. Springer Berlin Heidelberg, Berlin, Heidelberg, pp 69–93.

146. Aebersold R, Mann M (2003) Mass spectrometry-based proteomics. Nature 422:198–207. https://doi.org/10.1038/nature01511.

147. Cañas Montalvo B, López-Ferrer D, Ramos-Fernández A, et al (2006) Mass spectrometry technologies for proteomics. Briefings Funct Genomics Proteomics 4:295–320. https://doi.org/10.1093/bfgp/eli002.

148. Veenstra TD (2007) Global and targeted quantitative proteomics for biomarker discovery. J Chromatogr B Anal Technol Biomed Life Sci 847:3–11. https://doi.org/10.1016/j.jchromb.2006.09.004.

149. Anjo SI, Santa C, Manadas B (2017) SWATH-MS as a tool for biomarker discovery: From basic research to clinical applications. Proteomics 17:3–4. https://doi.org/10.1002/pmic.201600278.

150. Doerr A (2016) Proteomics: The human proteome on target. Nat Methods 13:712. https://doi.org/10.1038/nmeth.3987.

151. Peterson AC, Russell JD, Bailey DJ, et al (2012) Parallel Reaction Monitoring for High Resolution and High Mass Accuracy Quantitative, Targeted Proteomics. Mol Cell Proteomics 11:1475–1488. https://doi.org/10.1074/mcp.O112.020131.

152. Bodzon-Kulakowska A, Bierczynska-Krzysik A, Dylag T, et al (2007) Methods for samples preparation in proteomic research. J Chromatogr B 849:1–31. https://doi.org/10.1016/j.jchromb.2006.10.040.

153. Cañas B, Piñeiro C, Calvo E, et al (2007) Trends in sample preparation for classical and second generation proteomics. J Chromatogr A 1153:235–258. https://doi.org/10.1016/j.chroma.2007.01.045.

154. Feist P, Hummon AB (2015) Proteomic challenges: Sample preparation techniques for Microgram-Quantity protein analysis from biological samples. Int J Mol Sci 16:3537–3563. https://doi.org/10.3390/ijms16023537.

155. Len ACL, Powner MB, Zhu L, et al (2012) Pilot application of iTRAQ to the retinal disease macular telangiectasia. J Proteome Res 11:537–553. https://doi.org/10.1021/pr200889t.

156. Yan Q, Clark JI, Sage EH (2000) Expression and characterization of SPARC in human lens and in the aqueous and vitreous humors. Exp Eye Res 71:81–90. https://doi.org/10.1006/exer.2000.0853.

157. Izuta H, Chikaraishi Y, Adachi T, et al (2009) Extracellular SOD and VEGF are increased in vitreous bodies from proliferative diabetic retinopathy patients. Mol Vis 15:2663–72.

158. Klaassen I, de Vries EW, Vogels IMC, et al (2017) Identification of proteins associated with clinical and pathological features of proliferative diabetic retinopathy in vitreous and fibrovascular membranes. PLoS One 12:e0187304. https://doi.org/10.1371/journal.pone.0187304.

159. Koyama R, Nakanishi T, Ikeda T, Shimizu A (2003) Catalogue of soluble proteins in human vitreous humor by one-dimensional sodium dodecyl sulfate–polyacrylamide gel electrophoresis and electrospray ionization mass spectrometry including seven angiogenesis-regulating factors. J Chromatogr B 792:5–21. https://doi.org/10.1016/S1570-0232(03)00133-8.

160. Mysona BA, Matragoon S, Stephens M, et al (2015) Imbalance of the Nerve Growth Factor and Its Precursor as a Potential Biomarker for Diabetic Retinopathy. Biomed Res Int 2015:1–12. https://doi.org/10.1155/2015/571456.

161. GE Healthcare (2004) 2-D Electrophoresis - Principles and Methods. GE Healthcare.

162. Görg A, Weiss W, Dunn MJ (2004) Current two-dimensional electrophoresis technology for proteomics. Proteomics 4:3665–3685. https://doi.org/10.1002/pmic.200401031.

163. Wessel D, Flügge UI (1984) A method for the quantitative recovery of protein in dilute solution in the presence of detergents and lipids. Anal Biochem 138:141–143. https://doi.org/10.1016/0003-2697(84)90782-6.

164. Jiang L, He L, Fountoulakis M (2004) Comparison of protein precipitation methods for sample preparation prior to proteomic analysis. J Chromatogr A 1023:317–320. https://doi.org/10.1016/j.chroma.2003.10.029.

165. Rocha AS, Santos FM, Monteiro JP, et al (2014) Trends in proteomic analysis of human vitreous humor samples. Electrophoresis 35:2495–2508. https://doi.org/10.1002/elps.201400049.

166. Ahmed N, Rice GE (2005) Strategies for revealing lower abundance proteins in two-dimensional protein maps. J Chromatogr B Anal Technol Biomed Life Sci 815:39–50. https://doi.org/10.1016/j.jchromb.2004.10.070.

167. Rogowska-Wrzesinska A, Le Bihan MC, Thaysen-Andersen M, Roepstorff P (2013) 2D gels still have a niche in proteomics. J. Proteomics 88:4–13.

168. Rabilloud T, Chevallet M, Luche S, Lelong C (2010) Two-dimensional gel electrophoresis in proteomics: Past, present and future. J Proteomics 73:2064–2077. https://doi.org/10.1016/j.jprot.2010.05.016.

169. Gardner TW, Sundstrom JM (2017) A proposal for early and personalized treatment of diabetic retinopathy based on clinical pathophysiology and molecular phenotyping. Vision Res 139:153–160. https://doi.org/10.1016/j.visres.2017.03.006.

170. Chandramouli K, Qian P-Y (2009) Proteomics: Challenges, Techniques and Possibilities to Overcome Biological Sample Complexity. Hum Genomics Proteomics 1:22. https://doi.org/10.4061/2009/239204.

171. Baracat-Pereira MC, de Oliveira Barbosa M, Magalhães MJ, et al (2012) Separomics applied to the proteomics and peptidomics of low-abundance proteins: Choice of methods and challenges - A review. Genet Mol Biol 35:283–291. https://doi.org/10.1590/S1415-47572012000200009.

172. Gundry RL, White MY, Murray CI, et al (2009) Preparation of Proteins and Peptides for Mass Spectrometry Analysis in a Bottom-Up Proteomics Workflow. In: Current Protocols in Molecular Biology. John Wiley & Sons, Inc., Hoboken, NJ, USA, pp 342–355.

173. Reverter JL, Nadal J, Fernández-Novell JM, et al (2009) Tyrosine phosphorylation of vitreous inflammatory and angiogenic peptides and proteins in diabetic retinopathy. Investig Ophthalmol Vis Sci 50:1378–1382. https://doi.org/10.1167/iovs.08-2736.

174. Mukai N, Nakanishi T, Shimizu A, et al (2008) Identification of phosphotyrosyl proteins in vitreous humours of patients with vitreoretinal diseases by sodium dodecyl sulphate-polyacrylamide gel electrophoresis/Western blotting/matrix-assisted laser desorption time-of-flight mass spectrometry. Ann Clin Biochem 45:307–312. https://doi.org/10.1258/acb.2007.007151.

175. Nawaz IM, Rezzola S, Cancarini A, et al (2019) Human vitreous in proliferative diabetic retinopathy: Characterization and translational implications. Prog Retin Eye Res 109:110–119. https://doi.org/10.1016/j.preteyeres.2019.03.002.

176. Klingeborn M, Dismuke WM, Bowes Rickman C, Stamer WD (2017) Roles of exosomes in the normal and diseased eye. Prog Retin Eye Res 59:158–177. https://doi.org/10.1016/j.preteyeres.2017.04.004.

177. Laemmli UK (1970) Cleavage of Structural Proteins during the Assembly of the Head of Bacteriophage T4. Nature 227:680–685. https://doi.org/10.1038/227680a0.

178. Hoch H (1949) A differential method for the detection of small differences in mobility of colloids in electrophoresis. Biochem J 45:285–294. https://doi.org/10.1042/bj0450285.

179. Abdallah C, Dumas-Gaudot E, Renaut J, Sergeant K (2012) Gel-based and gel-free quantitative proteomics approaches at a glance. Int J Plant Genomics 2012:. https://doi.org/10.1155/2012/494572.

180. Jafari M, Primo V, Smejkal GB, et al (2012) Comparison of in-gel protein separation techniques commonly used for fractionation in mass spectrometry-based proteomic profiling. Electrophoresis 33:2516–2526. https://doi.org/10.1002/elps.201200031.

181. Tsuji F (2012) Biomarker Identification of Vitreous Fluid for Diabetic Retinopathy. J Postgenomics Drug Biomark Dev 02: https://doi.org/10.4172/2153-0769.1000e120.

182. Ong SE, Pandey A (2001) An evaluation of the use of two-dimensional gel electrophoresis in proteomics. Biomol Eng 18:195–205. https://doi.org/11911086

183. Pomastowski P, Buszewski B (2014) Two-dimensional gel electrophoresis in the light of new developments. TrAC - Trends Anal Chem 53:167–177. https://doi.org/10.1016/j.trac.2013.09.010.

184. O'Farrell PH (1975) High resolution two-dimensional electrophoresis of proteins. J Biol Chem 250:4007–21. https://doi.org/10.1016/j.bbi.2008.05.010.

185. Issaq HJ, Veenstra TD (2008) Two-dimensional polyacrylamide gel electrophoresis (2D-PAGE): Advances and perspectives. Biotechniques 44:697–700. https://doi.org/10.2144/000112823.

186. Harper S, W. Speicher D (2019) Comparing Complex Protein Samples Using Two-Dimensional Polyacrylamide Gels. Curr Protoc Protein Sci. https://doi.org/10.1002/cpps.87.

187. Beranova-Giorgianni S (2003) Proteome analysis by two-dimensional gel electrophoresis and mass spectrometry: Strengths and limitations. TrAC - Trends Anal Chem 22:273–281. https://doi.org/10.1016/S0165-9936(03)00508-9.

188. Chevalier F (2010) Highlights on the capacities of "Gel-based" proteomics. Proteome Sci 8:23. https://doi.org/10.1186/1477-5956-8-23.

189. Carrette O, Burkhard PR, Sanchez J, Hochstrasser DF (2006) State-of-the-art two-dimensional gel electrophoresis: a key tool of proteomics research. Nat Protoc 1:812–23. https://doi.org/10.1038/nprot.2006.104.

190. Gauci V, Wright E, Coorssen J (2011) Quantitative proteomics: assessing the spectrum of in-gel protein detection methods. J Chem Biol 4:3–29. https://doi.org/10.1007/s12154-010-0043-5.

191. Magdeldin S, Enany S, Yoshida Y, et al (2014) Basics and recent advances of two dimensional- polyacrylamide gel electrophoresis. Clin Proteomics 11:16. https://doi.org/10.1186/1559-0275-11-16.

192. Zhu W, Smith JW, Huang CM (2010) Mass spectrometry-based label-free quantitative proteomics. J Biomed Biotechnol 2010:. https://doi.org/10.1155/2010/840518.

193. Wasinger VC, Zeng M, Yau Y (2013) Current Status and Advances in Quantitative Proteomic Mass Spectrometry. Int J Proteomics 2013:1–12. https://doi.org/10.1155/2013/180605.

194. Finoulst I, Pinkse M, Van Dongen W, Verhaert P (2011) Sample preparation techniques for the untargeted LC-MS-based discovery of peptides in complex biological matrices. J Biomed Biotechnol 2011:. https://doi.org/10.1155/2011/245291.

195. Mitulovic G, Mechtler K (2006) HPLC techniques for proteomics analysis--a short overview of latest developments. Brief Funct Genomic Proteomic 5:249–60. https://doi.org/10.1093/bfgp/ell034.

196. Ma Y, Yang C, Tao Y, et al (2013) Recent technological developments in proteomics shed new light on translational research on diabetic microangiopathy. FEBS J 280:5668–5681. https://doi.org/10.1111/febs.12369.

197. Padula M, Berry I, O'Rourke M, et al (2017) A Comprehensive Guide for Performing Sample Preparation and Top-Down Protein Analysis. Proteomes 5:11. https://doi.org/10.3390/proteomes5020011.

198. Smith RD, Wahl JH, Goodlett DR, Hofstadler SA (1993) Capillary electrophoresis/mass spectrometry. Anal Chem 65:574A-584A. https://doi.org/10.1021/ac00061a001.

199. Desiderio C, Rossetti DV, Iavarone F, et al (2010) Capillary electrophoresis-mass spectrometry: Recent trends in clinical proteomics. J Pharm Biomed Anal 53:1161–1169. https://doi.org/10.1016/j.jpba.2010.06.035.

200. Mischak H, Vlahou A, Ioannidis JPA (2013) Technical aspects and inter-laboratory variability in native peptide profiling: The CE-MS experience. Clin Biochem 46:432–443. https://doi.org/10.1016/j.clinbiochem.2012.09.025.

201. Kolch W, Neusüß C, Pelzing M, Mischak H (2005) Capillary electrophoresis-mass spectrometry as a powerful tool in clinical diagnosis and biomarker discovery. Mass Spectrom Rev 24:959–977. https://doi.org/10.1002/mas.20051.

202. Stalmach A, Albalat A, Mullen W, Mischak H (2013) Recent advances in capillary electrophoresis coupled to mass spectrometry for clinical proteomic applications. Electrophoresis 34:1452–1464. https://doi.org/10.1002/elps.201200708.

203. Mischak H, Coon JJ, Novak J, et al (2009) Capillary electrophoresis-mass spectrometry as a powerful tool in biomarker discovery and clinical diagnosis: An update of recent developments. Mass Spectrom Rev 28:703–724. https://doi.org/10.1002/mas.20205.

204. Theodorescu D, Wittke S, Ross MM, et al (2006) Discovery and validation of new protein biomarkers for urothelial cancer: A prospective analysis. Lancet Oncol 7:230–240. https://doi.org/10.1016/S1470-2045(06)70584-8.

205. Silberring J, Ciborowski P (2010) Biomarker discovery and clinical proteomics. TrAC - Trends Anal Chem 29:128–140. https://doi.org/10.1016/j.trac.2009.11.007.

206. Bantscheff M, Schirle M, Sweetman G, et al (2007) Quantitative mass spectrometry in proteomics: a critical review. Anal Bioanal Chem 389:1017–1031. https://doi.org/10.1007/s00216-007-1486-6.

207. Xie F, Liu T, Qian W-J, et al (2011) Liquid Chromatography-Mass Spectrometry-based Quantitative Proteomics. J Biol Chem 286:25443–25449. https://doi.org/10.1074/jbc.R110.199703

208. Hauck SM, Hofmaier F, Dietter J, et al (2012) Label-free LC-MSMS analysis of vitreous from autoimmune uveitis reveals a significant decrease in secreted Wnt signalling inhibitors DKK3 and SFRP2. J Proteomics 75:4545–4554. https://doi.org/10.1016/j.jprot.2012.04.052.

209. Zhou L, Liu X, Koh SK, et al (2011) Quantitative Proteomic Analysis of Retina in Oxygen-Induced Retinopathy Mice using iTRAQ with 2D NanoLC-nanoESI-MS/MS. J Integr OMICS 1:226–235. https://doi.org/10.5584/jiomics.v1i2.36.

210. Chen W, Lu Q, Lu L, Guan H (2017) Increased levels of alphaB-crystallin in vitreous fluid of patients with proliferative diabetic retinopathy and correlation with vascular endothelial growth factor. Clin Exp Ophthalmol 45:379–384. https://doi.org/10.1111/ceo.12891.

211. Simó R, Lecube A, Segura RM, et al (2002) Free insulin growth factor-I and vascular endothelial growth factor in the vitreous fluid of patients with proliferative diabetic retinopathy. Am J Ophthalmol 134:376–82.

212. Yan Y, Zhu L, Hong L, et al (2016) The impact of ranibizumab on the level of intercellular adhesion molecule type 1 in the vitreous of eyes with proliferative diabetic retinopathy. Acta Ophthalmol 94:358–364. https://doi.org/10.1111/aos.12806.

213. Shao J, Xin Y, Li R, Fan Y (2011) Vitreous and serum levels of transthyretin (TTR) in high myopia patients are correlated with ocular pathologies. Clin Biochem 44:681–685. https://doi.org/10.1016/j.clinbiochem.2011.03.032.

214. Liu X-Y, Li L, Yao J-Q, et al (2011) Osteopontin expression in vitreous and proliferative retinal membranes of patients with proliferative vitreous retinopathy. Int J Ophthalmol 4:. https://doi.org/10.3980/j.issn.2222-3959.2011.04.17.

215. Li J, Hu W, Song H, et al (2016) Increased Vitreous Chemerin Levels Are Associated with Proliferative Diabetic Retinopathy. Ophthalmologica 236:61–66. https://doi.org/10.1159/000447752.

216. Shao J, Xin Y, Yao Y (2011) Correlation of misfolded transthyretin in abnormal vitreous and high myopia related ocular pathologies. Clin Chim Acta 412:2117–2121. https://doi.org/10.1016/j.cca.2011.07.021.

217. Mesquita J, Castro de Sousa J, Vaz-Pereira S, et al (2017) VEGF-B Levels in the Vitreous of Diabetic and Non-Diabetic Patients with Ocular Diseases and Its Correlation with Structural Parameters. Med Sci 5:17. https://doi.org/10.3390/medsci5030017.

218. Mesquita J, Castro-de-Sousa JP, Vaz-Pereira S, et al (2018) Evaluation of the growth factors VEGF-a and VEGF-B in the vitreous and serum of patients with macular and retinal vascular diseases. Growth Factors 36:48–57. https://doi.org/10.1080/08977194.2018.1477140.

219. Jünemann AGM, Rejdak R, Huchzermeyer C, et al (2015) Elevated vitreous body glial fibrillary acidic protein in retinal diseases. Graefe's Arch Clin Exp Ophthalmol 253:2181–2186. https://doi.org/10.1007/s00417-015-3127-7.

220. Hernández C, Garcia-Ramírez M, Simó R (2013) Overexpression of hemopexin in the diabetic eye: A new pathogenic candidate for diabetic macular edema. Diabetes Care 36:2815–2821. https://doi.org/10.2337/dc12-2634.

221. Zhao M, Bai Y, Xie W, et al (2015) Interleukin-1β Level Is Increased in Vitreous of Patients with Neovascular Age-Related Macular Degeneration (nAMD) and Polypoidal Choroidal Vasculopathy (PCV). PLoS One 10:e0125150. https://doi.org/10.1371/journal.pone.0125150.

222. Praidou A, Papakonstantinou E, Androudi S, et al (2011) Vitreous and serum levels of vascular endothelial growth factor and platelet-derived growth factor and their correlation in patients with non-proliferative diabetic retinopathy and clinically significant macula oedema. Acta Ophthalmol 89:248–254. https://doi.org/10.1111/j.1755-3768.2009.01661.x.

223. Abu El-Asrar AM, Mohammad G, Nawaz MI, et al (2013) Relationship between vitreous levels of matrix metalloproteinases and vascular endothelial growth factor in proliferative diabetic retinopathy. PLoS One 8:1–11. https://doi.org/10.1371/journal.pone.0085857.

224. Koskela UE, Kuusisto SM, Nissinen AE, et al (2013) High vitreous concentration of IL-6 and IL-8, but not of adhesion molecules in relation to plasma concentrations in proliferative diabetic retinopathy. Ophthalmic Res 49:108–114. https://doi.org/10.1159/000342977.

225. Srividya G, Jain M, Mahalakshmi K, et al (2018) A novel and less invasive technique to assess cytokine profile of vitreous in patients of diabetic macular oedema. Eye 32:820–829. https://doi.org/10.1038/eye.2017.285.

226. Maier R, Weger M, Haller-Schober E-M, et al (2008) Multiplex bead analysis of vitreous and serum concentrations of inflammatory and proangiogenic factors in diabetic patients. Mol Vis 14:637–43.

227. Ghodasra DH, Fante R, Gardner TW, et al (2016) Safety and Feasibility of Quantitative Multiplexed Cytokine Analysis From Office-Based Vitreous Aspiration. Investig Opthalmology Vis Sci 57:3017. https://doi.org/10.1167/iovs.15-18721.

228. Ehlken C, Grundel B, Michels D, et al (2015) Increased expression of angiogenic and inflammatory proteins in the vitreous of patients with ischemic central retinal vein occlusion. PLoS One 10:1–15. https://doi.org/10.1371/journal.pone.0126859.

229. Murugeswari P, Shukla D, Kim R, et al (2014) Angiogenic potential of vitreous from proliferative diabetic retinopathy and Eales' disease patients. PLoS One 9:1–8. https://doi.org/10.1371/journal.pone.0107551.

230. Jakobsson G, Sundelin K, Zetterberg H, Zetterberg M (2015) Increased levels of inflammatory immune mediators in vitreous from pseudophakic eyes. Investig Ophthalmol Vis Sci 56:3407–3414. https://doi.org/10.1167/iovs.15-16837.

231. Velez G, Bassuk AG, Colgan D, et al (2017) Therapeutic drug repositioning using personalized proteomics of liquid biopsies. JCI Insight 2:1–10. https://doi.org/10.1172/jci.insight.97818.

232. Kim K, Kim SJ, Yu HG, et al (2010) Verification of biomarkers for diabetic retinopathy by multiple reaction monitoring. J Proteome Res 9:689–699. https://doi.org/10.1021/pr901013d.

233. Ong S-E, Blagoev B, Kratchmarova I, et al (2002) Stable Isotope Labeling by Amino Acids in Cell Culture, SILAC, as a Simple and Accurate Approach to Expression Proteomics. Mol Cell Proteomics 1:376–386. https://doi.org/10.1074/mcp.M200025-MCP200.

234. Gygi SP, Rist B, Gerber SA, et al (1999) Quantitative analysis of complex protein mixtures using isotope-coded affinity tags. Nat Biotechnol 17:994–999. https://doi.org/10.1038/13690.

235. Schmidt A, Kellermann J, Lottspeich F (2005) A novel strategy for quantitative proteomics using isotope-coded protein labels. Proteomics 5:4–15. https://doi.org/10.1002/pmic.200400873.

236. Yao X, Freas A, Ramirez J, et al (2001) Proteolytic 18O labeling for comparative proteomics: Model studies with two serotypes of adenovirus. Anal Chem 73:2836–2842. https://doi.org/10.1021/ac001404c.

237. Kirkpatrick DS, Gerber SA, Gygi SP (2005) The absolute quantification strategy: A general procedure for the quantification of proteins and post-translational modifications. Methods 35:265–273. https://doi.org/10.1016/j.ymeth.2004.08.018.

238. Thompson A, Schäfer J, Kuhn K, et al (2003) Tandem mass tags: A novel quantification strategy for comparative analysis of complex protein mixtures by MS/MS. Anal Chem 75:1895–1904. https://doi.org/10.1021/ac0262560.

239. Ross PL, Huang YN, Marchese JN, et al (2004) Multiplexed Protein Quantitation in Saccharomyces cerevisiae Using Amine-reactive Isobaric Tagging Reagents. Mol Cell Proteomics 3:1154–1169. https://doi.org/10.1074/mcp.M400129-MCP200.

240. Sap KA, Demmers JAA (2012) Labeling Methods in Mass Spectrometry Based Quantitative Proteomics. In: Leung H-C, Man TK, Flores R (eds) Integrative Proteomics. IntechOpen, pp 111–132.

241. Wu Z, Ding N, Yu M, et al (2016) Identification of potential biomarkers for rhegmatogenous retinal detachment associated with choroidal detachment by vitreous iTRAQ-based proteomic profiling. Int J Mol Sci 17:. https://doi.org/10.3390/ijms17122052.

242. Kowalczuk L, Matet A, Dor M, et al (2018) Proteome and Metabolome of Subretinal Fluid in Central Serous Chorioretinopathy and Rhegmatogenous Retinal Detachment: A Pilot Case Study. Transl Vis Sci Technol 7:3. https://doi.org/10.1167/tvst.7.1.3.

243. Song X, Bandow J, Sherman J, et al (2008) iTRAQ experimental design for plasma biomarker discovery. J Proteome Res 7:2952–2958. https://doi.org/10.1021/pr800072x.

244. Savitski MM, Mathieson T, Zinn N, et al (2013) Measuring and managing ratio compression for accurate iTRAQ/TMT quantification. J Proteome Res 12:3586–3598. https://doi.org/10.1021/pr400098r.

245. Fuller, R. H, Morris, E. G (2012) Quantitative Proteomics Using iTRAQ Labeling and Mass Spectrometry. Integr Proteomics 442. https://doi.org/10.5772/31469.

246. Sandberg AS, Branca RMM, Lehtiö J, Forshed J (2014) Quantitative accuracy in mass spectrometry based proteomics of complex samples: The impact of labeling and precursor interference. J Proteomics 96:133–144. https://doi.org/10.1016/j.jprot.2013.10.035.

247. Beck F, Burkhart JM, Geiger J, et al (2012) Robust Workflow for iTRAQ-Based Peptide and Protein Quantification. In: Marcus K (ed). Humana Press, Totowa, NJ, pp 101–113.

248. Searle BC, Yergey AL (2019) An efficient solution for resolving iTRAQ and TMT channel cross-talk. J Mass Spectrom 0–1. https://doi.org/10.1002/jms.4354.

249. Wong Y-K, Zhang J, Hua Z-C, et al (2017) Recent advances in quantitative and chemical proteomics for autophagy studies. https://doi.org/10.1080/15548627.2017.1313944.

250. Ahrné E, Glatter T, Viganò C, et al (2016) Evaluation and improvement of quantification accuracy in isobaric mass tag-based protein quantification experiments. J Proteome Res 15:2537–2547. https://doi.org/10.1021/acs.jproteome.6b00066.

251. Moulder R, Bhosale SD, Goodlett DR, Lahesmaa R (2018) Analysis of the plasma proteome using iTRAQ and TMT-based isobaric labelling. Mass Spectrom Rev 37:583–606. https://doi.org/10.1002/mas.21550.

252. Casey TM, Khan JM, Bringans SD, et al (2017) Analysis of Reproducibility of Proteome Coverage and Quantitation Using Isobaric Mass Tags (iTRAQ and TMT). J Proteome Res 16:384–392. https://doi.org/10.1021/acs.jproteome.5b01154.

253. Chee SG, Poh KC, Trong KP, Wright PC (2007) Technical, experimental, and biological variations in isobaric tags for relative and absolute quantitation (iTRAQ). J Proteome Res 6:821–827. https://doi.org/10.1021/pr060474i.

254. Trinh H V., Grossmann J, Gehrig P, et al (2013) iTRAQ-Based and Label-Free Proteomics Approaches for Studies of Human Adenovirus Infections. Int J Proteomics 2013:1–16. https://doi.org/10.1155/2013/581862.

255. Distler U, Kuharev J, Navarro P, Tenzer S (2016) Label-free quantification in ion mobility-enhanced data-independent acquisition proteomics. Nat Protoc 11:795–812. https://doi.org/10.1038/nprot.2016.042.

256. Vowinckel J, Capuano F, Campbell K, et al (2014) The beauty of being (label)-free: sample preparation methods for SWATH-MS and next-generation targeted proteomics. F1000Research 1–26. https://doi.org/10.12688/f1000research.2-272.v2.

257. Tate S, Larsen B, Bonner R, Gingras AC (2013) Label-free quantitative proteomics trends for protein-protein interactions. J Proteomics 81:91–101. https://doi.org/10.1016/j.jprot.2012.10.027.

258. Nahnsen S, Bielow C, Reinert K, Kohlbacher O (2013) Tools for Label-free Peptide Quantification. Mol Cell Proteomics 12:549–556. https://doi.org/10.1074/mcp.R112.025163.

259. Megger DA, Bracht T, Meyer HE, Sitek B (2013) Label-free quantification in clinical proteomics. Biochim Biophys Acta - Proteins Proteomics 1834:1581–1590. https://doi.org/10.1016/j.bbapap.2013.04.001.

260. Neilson KA, Ali NA, Muralidharan S, et al (2011) Less label, more free: Approaches in label-free quantitative mass spectrometry. Proteomics 11:535–553. https://doi.org/10.1002/pmic.201000553.

261. Bubis JA, Levitsky LI, Ivanov M V., et al (2017) Comparative evaluation of label-free quantification methods for shotgun proteomics. Rapid Commun Mass Spectrom 31:606–612. https://doi.org/10.1002/rcm.7829.

262. Lundgren DH, Hwang S-I, Wu L, Han DK (2010) Role of spectral counting in quantitative proteomics. Expert Rev Proteomics 7:39–53. https://doi.org/10.1586/epr.09.69.

263. Old WM, Meyer-Arendt K, Aveline-Wolf L, et al (2005) Comparison of Label-free Methods for Quantifying Human Proteins by Shotgun Proteomics. Mol Cell Proteomics 4:1487–1502. https://doi.org/10.1074/mcp.M500084-MCP200.

264. Zhang B, † BZ, VerBerkmoes NC, et al (2006) Detecting Differential and Correlated Protein Expression in Label-Free Shotgun Proteomics. J Proteome Res 1–10. https://doi.org/10.1021/pr0600273.

265. Ishihama Y, Oda Y, Tabata T, et al (2005) Exponentially modified protein abundance index (emPAI) for estimation of absolute protein amount in proteomics by the number of sequenced peptides per protein. Mol Cell Proteomics 4:1265–1272. https://doi.org/10.1074/mcp.M500061-MCP200.

266. Zybailov B, Mosley AL, Sardiu ME, et al (2006) Statistical analysis of membrane proteome expression changes in Saccharomyces cerevisiae. J Proteome Res 5:2339–2347. https://doi.org/10.1021/pr060161n.

267. Lu P, Vogel C, Wang R, et al (2007) Absolute protein expression profiling estimates the relative contributions of transcriptional and translational regulation. Nat Biotechnol 25:117–124. https://doi.org/10.1038/nbt1270.

268. Sardiu ME, Washburn MP (2010) Enriching quantitative proteomics with SIN. Nat Biotechnol 28:40–42. https://doi.org/10.1038/nbt0110-40.

269. Moulder R, Goo YA, Goodlett DR (2016) Label-free quantitation for clinical proteomics. In: Sechi S (ed) Methods in Molecular Biology. Springer New York, New York, NY, pp 65–76.

270. Ackland P, Resnikoff S, Bourne R (2018) World blindness and visual impairment: despite many successes, the problem is growing. Community eye Heal 30:71–73.

271. Guariguata L, Whiting DR, Hambleton I, et al (2014) Global estimates of diabetes prevalence for 2013 and projections for 2035. Diabetes Res Clin Pract 103:137–149. https://doi.org/10.1016/j.diabres.2013.11.002.

272. Duh EJ, Sun JK, Stitt AW (2017) Diabetic retinopathy: current understanding, mechanisms, and treatment strategies. JCI insight 2:1–13. https://doi.org/10.1172/jci.insight.93751.

273. Wong WL, Su X, Li X, et al (2014) Global prevalence of age-related macular degeneration and disease burden projection for 2020 and 2040: A systematic review and meta-analysis. Lancet Glob Heal 2:e106–e116. https://doi.org/10.1016/S2214-109X(13)70145-1.

274. Jaki Mekjavić P, Jūratė Balčiūnienė V, Ćeklić L, et al (2019) The Burden of Macular Diseases in Central and Eastern Europe—Implications for Healthcare Systems. Value Heal Reg Issues 19:1–6. https://doi.org/10.1016/j.vhri.2018.11.002.

275. Amadio M, Kaarniranta K, Xu H, et al (2018) Molecular Mechanisms Underlying Age-Related Ocular Diseases. Oxid Med Cell Longev 2018:8476164. https://doi.org/10.1155/2018/8476164.

276. Mitry D, Charteris DG, Fleck BW, et al (2010) The epidemiology of rhegmatogenous retinal detachment: Geographical variation and clinical associations. Br J Ophthalmol 94:678–684. https://doi.org/10.1136/bjo.2009.157727.

277. Kang HK, Luff AJ (2008) Management of retinal detachment: A guide for non-ophthalmologists. Bmj 336:1235–1240. https://doi.org/10.1136/bmj.39581.525532.47.

278. Sahanne S, Tuuminen R, Haukka J, Loukovaara S (2017) A retrospective study comparing outcomes of primary rhegmatogenous retinal detachment repair by scleral buckling and pars plana vitrectomy in Finland. Clin Ophthalmol 11:503–509. https://doi.org/10.2147/OPTH.S128746.

279. Idrees S, Sridhar J, Kuriyan AE (2019) Proliferative vitreoretinopathy: A review. Int Ophthalmol Clin 59:221–240. https://doi.org/10.1097/IIO.0000000000000258.

280. Pastor JC, Rojas J, Pastor-Idoate S, et al (2016) Proliferative vitreoretinopathy: A new concept of disease pathogenesis and practical consequences. Prog Retin Eye Res 51:125–155. https://doi.org/10.1016/j.preteyeres.2015.07.005.

281. Richer S, Ulanski L, Popenko NA, et al (2016) Age-related Macular Degeneration Beyond the Age-related Eye Disease Study II. Adv Ophthalmol Optom 1:335–369. https://doi.org/10.1016/j.yaoo.2016.03.018.

282. Lim LS, Mitchell P, Seddon JM, et al (2012) Age-related macular degeneration. Lancet 379:1728–1738. https://doi.org/10.1016/S0140-6736(12)60282-7.

283. Yonekawa Y, Miller J, Kim I (2015) Age-Related Macular Degeneration: Advances in Management and Diagnosis. J Clin Med 4:343–359. https://doi.org/10.3390/jcm4020343.

284. Holz FG, Schmitz-Valckenberg S, Fleckenstein M (2014) Recent developments in the treatment of age-related macular degeneration. J Clin Invest 124:1430–1438. https://doi.org/10.1172/JCI71029.

285. Cryan LLM, O'Brien C (2008) Proteomics as a research tool in clinical and experimental ophthalmology. 2:. https://doi.org/10.1002/prca.200780094.

286. Walia S, Clermont AC, Gao B-BB, et al (2010) Vitreous proteomics and diabetic retinopathy. Semin Ophthalmol 25:289–294. https://doi.org/10.3109/08820538.2010.518912.

287. Csősz É, Deák E, Kalló G, et al (2017) Diabetic retinopathy: Proteomic approaches to help the differential diagnosis and to understand the underlying molecular mechanisms. J Proteomics 150:351–358. https://doi.org/10.1016/j.jprot.2016.06.034.

288. Kuo HK, Chen YH, Huang F, et al (2016) The upregulation of zinc finger protein 670 and prostaglandin D2 synthase in proliferative vitreoretinopathy. Graefe's Arch Clin Exp Ophthalmol 254:205–213. https://doi.org/10.1007/s00417-015-3022-2.

289. Nor NM, Mohamed MS, Loh TC, et al (2017) Comparative analyses on medium optimization using one-factor-at-a-time, response surface methodology, and artificial neural network for lysine–methionine biosynthesis by Pediococcus pentosaceus RF-1. Biotechnol Biotechnol Equip 31:935–947. https://doi.org/10.1080/13102818.2017.1335177.

290. Pedro AQ, Martins LM, Dias JML, et al (2015) An artificial neural network for membrane-bound catechol-O-methyltransferase biosynthesis with Pichia pastoris methanol-induced cultures. Microb Cell Fact 14:113. https://doi.org/10.1186/s12934-015-0304-7.

291. Brown SR, Staff M, Lee R, et al (2018) Design of Experiments Methodology to Build a Multifactorial Statistical Model Describing the Metabolic Interactions of Alcohol Dehydrogenase Isozymes in the Ethanol Biosynthetic Pathway of the Yeast Saccharomyces cerevisiae. ACS Synth Biol 7:1676–1684. https://doi.org/10.1021/acssynbio.8b00112.

292. Wang H, Zang C, Liu XS, Aster JC (2015) The Role of Notch Receptors in Transcriptional Regulation. J Cell Physiol 230:982–988. https://doi.org/10.1002/jcp.24872.

293. Semenza GL (2001) Hypoxia-inducible factor 1: Control of oxygen homeostasis in health and disease. Pediatr Res 49:614–617. https://doi.org/10.1203/00006450-200105000-00002.

294. Li Z, Adams RM, Chourey K, et al (2012) Systematic comparison of label-free, metabolic labeling, and isobaric chemical labeling for quantitative proteomics on LTQ orbitrap velos. J Proteome Res 11:1582–1590. https://doi.org/10.1021/pr200748h.

295. Sinha D, Valapala M, Shang P, et al (2016) Lysosomes: Regulators of autophagy in the retinal pigmented epithelium. Exp Eye Res 144:46–53. https://doi.org/10.1016/j.exer.2015.08.018.

296. Kwon YH, Kim YA, Yoo YH (2017) Loss of Pigment Epithelial Cells Is Prevented by Autophagy. In: Autophagy: Cancer, Other Pathologies, Inflammation, Immunity, Infection, and Aging, 11th ed. Elsevier, pp 105–117.

297. Hyttinen JMT, Błasiak J, Niittykoski M, et al (2017) DNA damage response and autophagy in the degeneration of retinal pigment epithelial cells—Implications for age-related macular degeneration (AMD). Ageing Res Rev 36:64–77. https://doi.org/10.1016/j.arr.2017.03.006.

298. Abcouwer SF, Gardner TW (2014) Diabetic retinopathy: Loss of neuroretinal adaptation to the diabetic metabolic environment. Ann N Y Acad Sci 1311:174–190. https://doi.org/10.1111/nyas.12412.

299. Feng H, Zhao X, Guo Q, et al (2019) Autophagy resists EMT process to maintain retinal pigment epithelium homeostasis. Int J Biol Sci 15:507–521. https://doi.org/10.7150/ijbs.30575.

Appendix

Appendix I - Supplementary material of the Paper II

Table S1.1 - Proteins found differentially expressed in vitreous collected from patients with Diabetic retinopathy (DR) and proliferative diabetic retinopathy (PDR). The abbreviations MH and ERM correspond to the control groups of patients with macular holes and epiretinal membranes. respectively. whereas ND corresponds to non-diabetic patients. In the studies performed by Zou. Loukovaara and respective co-workers. the group of patients treated with intravitreal injection of Ranibizumab and Avastin. respectively. were defined as IVR. Symbols ↑ and ↓ correspond to the up-regulated and down-regulated proteins. respectively.

								Shitama. *et. al.*. (2008)			Gao. *et. al.*. (2008) (p-value<0.05)	
Uniprot Acess	**Description**	**Nakanishi.** *et.* al.. (2002) DR/MH	**Yamane.** *et. al.*. (2003) PDR/MH	**Kim.** *et. al.*. (2006) PDR/MH	**Minamoto.** *et. al.*. (2007) DR/MH	**García-Ramírez.** *et. al.*. (2007) log2 (PDR/MH)	**Simó.** *et. al.*. (2008) PDR/MH	**PDR/MH**	**NPDR/MH**	**PDR/NPDR**	**log2 (PDR/ND)**	**log2 (PDR/Diabetic)**
P63104	14-3-3 protein zetavsdelta											ND PDR
P62736	Actin. aortic smooth muscle										1.54	
P02763	Alpha-1-acid glycoprotein 1										3.36	
P01011	Alpha-1-antichymotrypsin										3.77	
P01009	Alpha-1-antitrypsin	↑		↓				↑	↑		2.63	
P04217	Alpha-1B-glycoprotein				↑			↑	↑		2.06	
P02765	Alpha-2-HS-glycoprotein	↑									1.10	
P01023	Alpha-2-macroglobulin				↑							
P05067	Amyloid-beta precursor protein											ND PDR
Q06481	Amyloid-like protein 2										ND PDR	ND PDR
P01019	Angiotensinogen										1.47	0.71
P01008	Antithrombin-III										1.82	
P02647	Apolipoprotein A-I					1.43	↑		↑	↓	3.36	
P02652	Apolipoprotein A-II										2.47	
P06727	Apolipoprotein A-IV			↓	↑			↑	↑			
P02656	Apolipoprotein C-III										3.83	
P02649	Apolipoprotein E				↑							
P98160	Basement membrane-specific heparan sulfate proteoglycan core protein										3.51	
P02749	Beta-2-glycoprotein 1					2.16	↑					
P61769	Beta-2-microglobulin										1.86	
O94985	Calsyntenin-1											-1.18
P00915	Carbonic anhydrase 1										ND ND	
P04040	Catalase		↑		↑							
P07339	Cathepsin D				↑							
P00450	Ceruloplasmin				↑							
P36222	Chitinase-3-like protein 1										3.53	
P25940	Collagen alpha-3(V) chain										ND PDR	
P01024	Complement C3				↑	1.64	↑	↑	↑	↓	2.03	
P0C0L4	Complement C4-A	↑			↑							
P0C0L5	Complement C4-B	↑			↑	1.57	↑					
P02748	Complement component C9					1.62	↑					

P00751	Complement factor B					1.90	↑					
P00746	Complement factor D				↑							
P05156	Complement factor I				↑						2.19	
Q13822	Ectonucleotide pyrophosphatase/phosphodiesterase family member 2											-2.14
P08294	Extracellular superoxide dismutase [Cu-Zn]											ND PDR
P02671	Fibrinogen alpha chain					6.23	↑					
P02679	Fibrinogen gamma chain							↑	↑	↑		
P09972	Fructose-bisphosphate aldolase C											ND PDR
P09104	Gamma-enolase		↑		↑							
P06396	Gelsolin										1.36	
P69905	Hemoglobin subunit alpha										ND ND	
P02042	Hemoglobin subunit delta										ND ND	
P04196	Histidine-rich glycoprotein										1.93	
P01876	Immunoglobulin heavy constant alpha 1				↑							
P01857	Immunoglobulin heavy constant gamma 1	↑									2.69	
P06312	Immunoglobulin kappa variable 4-1										4.13	
P19823	Inter-alpha-trypsin inhibitor heavy chain H2					-2.58	↓					
Q9BZV3	Interphotoreceptor matrix proteoglycan 2											ND PDR
P01042	Kininogen-1				↑							
P02750	Leucine-rich alpha-2-glycoprotein										2.74	
P00338	L-lactate dehydrogenase A chain											ND PDR
P08571	Monocyte differentiation antigen CD14										4.15	
Q8IVL0	Neuron navigator 3										ND PDR	
Q99574	Neuroserpin											ND PDR
Q06830	Peroxiredoxin-1										ND ND	
P36955	Pigment epithelium-derived factor			↑		-2.67	↓				1.66	
P41222	Prostaglandin-H2 D-isomerase			↑								
P02760	Protein AMBP			↑	↑							
P00734	Prothrombin				↑						2.09	
P09455	Retinol-binding protein 1						↓					
P10745	Retinol-binding protein 3					-2.77						-2.86
P02753	Retinol-binding protein 4										4.69	
P02787	Serotransferrin							↑	↑			
P02768	Serum albumin							↑	↑		2.15	
Q9NRC6	Spectrin beta chain. non-erythrocytic 5			↓								
Q9HCB6	Spondin-1										-2.29	
P02766	Transthyretin										2.19	
P35030	Trypsin-3										-2.06	
P02774	Vitamin D-binding protein							↑	↑		1.69	
Q15904	V-type proton ATPase subunit S1											ND PDR
P25311	Zinc-alpha-2-glycoprotein				↑	1.72	↑	↑				

Table S1.1 – (continued)

Uniprot Acess	Description	Maier. *et.* al.. (2008) log2 (DR/ND)	Kim. *et. al*..(2010) PDR/MH	Kim. *et. al*..(2010) NPDR/MH	Suzuki. et.al.. (2011) log2 (DR/Control)	Wang. et.al.. (2012) average log2(PDR/control)	Wang. et.al.. (2013) log2 (PDR/control)	Koskela. et.al.. (2013) log2 (PDR/ND)	Loukovaara. *et.al*..(2015) (p-value<0.005) (q-value<0.01) log2 (PDR/DR)	Loukovaara. *et.al*..(2015) (p-value<0.005) (q-value<0.01) log2 (PDR/IVR)
O94851	[F-actin]-monooxygenase MICAL2						2.96			
Q9UJ83	2-hydroxyacyl-CoA lyase 1								0.90	
P50914	60S ribosomal protein L14						3.99			
P83731	60S ribosomal protein L24						3.54			
Q8WXS8	A disintegrin and metalloproteinase with thrombospondin motifs 14								0.72	
P62736	Actin. aortic smooth muscle						2.59			
O14639	Actin-binding LIM protein 1								1.25	
O43306	Adenylate cyclase type 6								-1.32	
P51828	Adenylate cyclase type 7								1.28	
Q8WXG9	Adhesion G-protein coupled receptor V1								2.48	
Q96AP0	Adrenocortical dysplasia protein homolog								0.92	1.77
P43652	Afamin								0.90	1.77
Q5JQC9	A-kinase anchor protein 4								1.34	
P02763	Alpha-1-acid glycoprotein 1						3.30		0.70	
P19652	Alpha-1-acid glycoprotein 2						13.00		1.02	
P01011	Alpha-1-antichymotrypsin						64.56		1.05	
P01009	Alpha-1-antitrypsin						-2.40		1.04	
P04217	Alpha-1B-glycoprotein						-2.93		0.78	
P08697	Alpha-2-antiplasmin								0.76	
P02765	Alpha-2-HS-glycoprotein								0.77	
P01023	Alpha-2-macroglobulin						-3.65		0.61	
P02489	Alpha-crystallin A chain						-3.39			
P02511	Alpha-crystallin B chain					-26.80				
P06733	Alpha-enolase						-1.64			
P05067	Amyloid-beta precursor protein								-1.02	
Q8NI99	Angiopoietin-related protein 6						1.90			
P01019	Angiotensinogen								1.91	
Q9NQW6	Anillin						-3.59			
O75179	Ankyrin repeat domain-containing protein 17									2.64
Q96NW4	Ankyrin repeat domain-containing protein 27								0.76	1.80
Q8WWH4	Ankyrin repeat. SAM and basic leucine zipper domain-containing protein 1								0.71	
Q01484	Ankyrin-2								1.58	
Q5XXA6	Anoctamin-1								2.12	
P01008	Antithrombin-III						-7.90		1.44	
O14617	AP-3 complex subunit delta-1								1.89	
P02647	Apolipoprotein A-I						2.12		0.66	
P02652	Apolipoprotein A-II								1.55	
P06727	Apolipoprotein A-IV						-2.91		0.78	
Q0VD83	Apolipoprotein B receptor									2.55
P04114	Apolipoprotein B-100								2.51	
P02654	Apolipoprotein C-I								1.38	
P02655	Apolipoprotein C-II								0.84	
P02656	Apolipoprotein C-III								2.13	
P02649	Apolipoprotein E						-3.23			

O95445	Apolipoprotein M								0.95	
Q96NN9	Apoptosis-inducing factor 3									2.36
Q13625	Apoptosis-stimulating of p53 protein 2								0.71	
Q7Z6K5	Arpin								0.95	
P17174	Aspartate aminotransferase. cytoplasmic						-1.59			
O15265	Ataxin-7								1.47	
P08183	ATP-dependent translocase ABCB1								1.09	
Q13490	Baculoviral IAP repeat-containing protein 2								3.02	
O95817	BAG family molecular chaperone regulator 3									2.51
Q6W2J9	BCL-6 corepressor								1.64	1.73
P02749	Beta-2-glycoprotein 1						-4.92		1.25	1.47
Q562R1	Beta-actin-like protein 2						-2.84			
P05813	Beta-crystallin A3					-164.16	2.99			
P53673	Beta-crystallin A4					-5.70	-2.19			
P53674	Beta-crystallin B1					-3.74	-6.84			
P43320	Beta-crystallin B2					-15.21				0.80
B7Z1M9	C2 calcium-dependent domain-containing protein 4D									1.43
Q9Y426	C2 domain-containing protein 2									2.56
P05937	Calbindin						2.89			
P98194	Calcium-transporting ATPase type 2C member 1								1.38	
Q13557	Calciumvscalmodulin-dependent protein kinase type II subunit delta									3.51
O94985	Calsyntenin-1						-1.80			
Q9UDT6	CAP-Gly domain-containing linker protein 2									1.90
P00918	Carbonic anhydrase 2					3.26				
Q96IY4	Carboxypeptidase B2								1.43	
O75976	Carboxypeptidase D								0.58	
P22792	Carboxypeptidase N subunit 2								1.06	
Q8N3K9	Cardiomyopathy-associated protein 5								1.10	0.92
Q8WXE0	Caskin-2								1.48	
P04040	Catalase								0.84	
P07339	Cathepsin D					-3.05			0.53	
Q8NEC5	Cation channel sperm-associated protein 1						3.10			
P13500	C-C motif chemokine 2	0.69			1.69					
P13236	C-C motif chemokine 4				1.08					
Q9UKZ1	CCR4-NOT transcription complex subunit 11									3.12
P16070	CD44 antigen								0.69	
Q7Z7A1	Centriolin								1.10	1.84
Q9HC77	Centromere protein J								1.41	
Q8TEP8	Centrosomal protein of 192 kDa								-1.20	
Q9BV73	Centrosome-associated protein CEP250								0.79	
P00450	Ceruloplasmin						2.08		0.81	
Q494V2	Cilia- and flagella-associated protein 100									1.81
Q8N1V2	Cilia- and flagella-associated protein 52								1.13	
Q0VF96	Cingulin-like protein 1									2.31
O75153	Clustered mitochondria protein homolog									1.07
P10909	Clusterin					-2.87	-2.87			
P12259	Coagulation factor V								1.12	
P00748	Coagulation factor XII								1.43	
P23528	Cofilin-1						-7.06			
Q8N3U4	Cohesin subunit SA-2									5.72
Q5VVM6	Coiled-coil domain-containing protein 30						2.30			
P02462	Collagen alpha-1(IV) chain									2.96
Q8IZC6	Collagen alpha-1(XXVII) chain								1.11	
P08572	Collagen alpha-2(IV) chain								1.45	
P12111	Collagen alpha-3(VI) chain								2.00	

P02746	Complement C1q subcomponent subunit B								0.54	
P06681	Complement C2								2.11	
P01024	Complement C3						-3.44		1.63	
P0C0L4	Complement C4-A						-4.01			
P0C0L5	Complement C4-B						8.04		1.18	
P01031	Complement C5								0.71	
P10643	Complement component C7								1.20	
P07357	Complement component C8 alpha chain								0.69	
P07358	Complement component C8 beta chain								1.27	
P07360	Complement component C8 gamma chain								0.78	
P02748	Complement component C9								1.84	
P00751	Complement factor B								0.88	
P00746	Complement factor D								0.75	
P08603	Complement factor H								0.87	
Q03591	Complement factor H-related protein 1								1.30	
P05156	Complement factor I					2.29			1.25	
Q9H9E3	Conserved oligomeric Golgi complex subunit 4								1.23	
Q02246	Contactin-2									1.77
P08185	Corticosteroid-binding globulin								0.87	
P12277	Creatine kinase B-type						-7.17			
Q92793	CREB-binding protein						2.20			
Q8IWT3	Cullin-9								1.14	
P02778	C-X-C motif chemokine 10	1.69			2.77					
Q9NYV4	Cyclin-dependent kinase 12								1.37	
P01034	Cystatin-C						-1.85		-0.77	
Q6ZWL3	Cytochrome P450 4V2								1.63	
Q8NCM8	Cytoplasmic dynein 2 heavy chain 1								0.80	
O00154	Cytosolic acyl coenzyme A thioester hydrolase					-7.16				
P0CG12	Decreased expression in renal and prostate cancer protein								1.12	
Q96N67	Dedicator of cytokinesis protein 7								0.62	
Q8NF50	Dedicator of cytokinesis protein 8						-4.49			
Q9BTZ2	Dehydrogenasevsreductase SDR family member 4						2.87			
P49366	Deoxyhypusine synthase									2.79
Q9UBP4	Dickkopf-related protein 3						-1.91			
Q16555	Dihydropyrimidinase-related protein 2						-2.63			
Q9P265	Disco-interacting protein 2 homolog B									3.06
O95886	Disks large-associated protein 3								0.97	
Q9Y485	DmX-like protein 1								1.08	
Q9UBS4	DnaJ homolog subfamily B member 11									2.19
O60469	Down syndrome cell adhesion molecule								0.64	
Q96DT5	Dynein heavy chain 11. axonemal								1.24	
O95714	E3 ubiquitin-protein ligase HERC2								0.76	
Q7Z6Z7	E3 ubiquitin-protein ligase HUWE1								1.27	
Q86YJ5	E3 ubiquitin-protein ligase MARCHF9								0.79	
O75592	E3 ubiquitin-protein ligase MYCBP2								2.04	
Q8NG27	E3 ubiquitin-protein ligase Praja-1									2.18
Q16206	Ecto-NOX disulfide-thiol exchanger 2						5.91			
Q9HCE0	Ectopic P granules protein 5 homolog						2.37			
Q12926	ELAV-like protein 2								1.45	
Q9BXR3	Endogenous retrovirus group K member 6 Pol protein									3.12
P54760	Ephrin type-B receptor 4								1.49	
P58107	Epiplakin								0.67	
P16581	E-selectin							1.24		
P03372	Estrogen receptor						4.89			
O15372	Eukaryotic translation initiation factor 3 subunit H								1.56	3.82

P02671	Fibrinogen alpha chain								0.89	
P02675	Fibrinogen beta chain						-3.11		0.89	
P02679	Fibrinogen gamma chain								1.40	
P02751	Fibronectin								0.70	
Q14315	Filamin-C								0.75	1.57
Q12778	Forkhead box protein O1								1.27	
B1AJZ9	Forkhead-associated domain-containing protein 1								2.12	
P04075	Fructose-bisphosphate aldolase A						4.48			
P09972	Fructose-bisphosphate aldolase C						-1.66			
P07315	Gamma-crystallin C					-147.83				
P22914	Gamma-crystallin S					-27.42	-4.63			
P09104	Gamma-enolase					-25.63	-3.16			
Q92820	Gamma-glutamyl hydrolase		↑	↓						
P06396	Gelsolin								1.11	
O60318	Germinal-center associated nuclear protein								0.66	
Q6ZMI3	Gliomedin								0.95	
Q2KHR3	Glutamine and serine-rich protein 1								1.19	2.48
P22352	Glutathione peroxidase 3					-2.49				
P04406	Glyceraldehyde-3-phosphate dehydrogenase		↑	↑		-30.90				
Q5SZD4	Glycine N-acyltransferase-like protein 3						-4.81			
Q8NBJ4	Golgi membrane protein 1								1.98	
Q6Y7W6	GRB10-interacting GYF protein 2								1.07	1.82
Q9C091	GREB1-like protein								0.70	
Q5VVW2	GTPase-activating Rap/Ran-GAP domain-like protein 3								0.80	
P62873	Guanine nucleotide-binding protein								1.13	
Q9BVP2	Guanine nucleotide-binding protein-like 3									2.21
Q9H0R5	Guanylate-binding protein 3						-10.73			
P14317	Hematopoietic lineage cell-specific protein								0.76	
P68871	Hemoglobin subunit beta						1.86			
P02042	Hemoglobin subunit delta						4.55			
P02790	Hemopexin					3.31				
P05546	Heparin cofactor 2								1.17	
Q04756	Hepatocyte growth factor activator		↑	↑						
P82970	High mobility group nucleosome-binding domain-containing protein 5								1.59	
P04196	Histidine-rich glycoprotein						-1.58			
O14686	Histone-lysine N-methyltransferase 2D									1.92
Q86X24	HORMA domain-containing protein 1									2.27
O75330	Hyaluronan mediated motility receptor						5.94			
Q14520	Hyaluronan-binding protein 2								1.74	
Q9Y4L1	Hypoxia up-regulated protein 1								1.50	
P01876	Immunoglobulin heavy constant alpha 1					0.65			1.08	
P01877	Immunoglobulin heavy constant alpha 2								1.01	
P01857	Immunoglobulin heavy constant gamma 1						1.83			
P01859	Immunoglobulin heavy constant gamma 2						4.39		0.76	
P01860	Immunoglobulin heavy constant gamma 3								1.00	
P01871	Immunoglobulin heavy constant mu								2.60	
P01766	Immunoglobulin heavy variable 3-13					-6.14				
P01619	Immunoglobulin kappa variable 3-20						2.19			
P01842	Immunoglobulin lambda constant 1					-2.61				
P0DOY3	Immunoglobulin lambda constant 3									1.69
Q14164	Inhibitor of nuclear factor kappa-B kinase subunit epsilon								0.81	
Q14573	Inositol 1.4.5-trisphosphate receptor type 3								1.21	
P18065	Insulin-like growth factor-binding protein 2									1.10
Q16270	Insulin-like growth factor-binding protein 7									1.43
P19827	Inter-alpha-trypsin inhibitor heavy chain H1								1.05	

P19823	Inter-alpha-trypsin inhibitor heavy chain H2								0.76	
Q06033	Inter-alpha-trypsin inhibitor heavy chain H3								1.85	
Q14624	Inter-alpha-trypsin inhibitor heavy chain H4								1.11	
P05362	Intercellular adhesion molecule 1							3.11		
Q53G44	Interferon-induced protein 44-like									2.03
P22301	Interleukin-10				0.65			1.45		
P35225	Interleukin-13				0.97					
P05231	Interleukin-6				3.01			6.09		
P10145	Interleukin-8				3.65			6.47		
Q9NSE4	Isoleucine--tRNA ligase. mitochondrial								2.02	
Q9P266	Junctional protein associated with coronary artery disease								-1.61	
O60229	Kalirin								0.53	
P29622	Kallistatin		↑	↑					2.40	
Q9P2N6	KAT8 regulatory NSL complex subunit 3								2.49	
Q2M2I5	Keratin. type I cytoskeletal 24								0.61	
P35527	Keratin. type I cytoskeletal 9					-2.20				
P35908	Keratin. type II cytoskeletal 2 epidermal					0.10				
P02538	Keratin. type II cytoskeletal 6A					3.23				
O60938	Keratocan								1.65	
Q7Z4S6	Kinesin-like protein KIF21A									3.88
P01042	Kininogen-1								1.13	
Q14968	Leukocyte platelet-activating factor receptor						2.03			
Q86UK5	Limbin									1.97
P07195	L-lactate dehydrogenase B chain						1.99			
Q9NZR2	Low-density lipoprotein receptor-related protein 1B								0.55	
P51884	Lumican								1.48	1.67
P40925	Malate dehydrogenase. cytoplasmic					-4.74				
O43451	Maltase-glucoamylase. intestinal								1.09	
O75448	Mediator of RNA polymerase II transcription subunit 24								1.36	
P16035	Metalloproteinase inhibitor 2								0.72	
Q9UPN3	Microtubule-actin cross-linking factor 1. isoforms 1/2/3/5								1.82	
P46821	Microtubule-associated protein 1B								1.18	
Q96JE9	Microtubule-associated protein 6								0.82	
Q99683	Mitogen-activated protein kinase kinase kinase 5								2.37	
Q9Y4K4	Mitogen-activated protein kinase kinase kinase kinase 5								0.51	
P08571	Monocyte differentiation antigen CD14								1.39	
Q96T58	Msx2-interacting protein								0.81	
P33527	Multidrug resistance-associated protein 1									2.51
Q9P2K5	Myelin expression factor 2								1.63	
P35749	Myosin-11								0.57	
O94760	N(G).N(G)-dimethylarginine dimethylaminohydrolase 1					-6.74				
Q96PD5	N-acetylmuramoyl-L-alanine amidase								1.10	
P20929	Nebulin								1.41	
Q8WXH0	Nesprin-2								0.59	
Q9ULJ8	Neurabin-1									2.00
Q8NFP9	Neurobeachin								1.37	
O14594	Neurocan core protein								0.53	
Q14112	Nidogen-2						1.81			
P29475	Nitric oxide synthase. brain								1.21	
P48552	Nuclear receptor-interacting protein 1								0.52	
Q02818	Nucleobindin-1								0.86	
O60287	Nucleolar pre-ribosomal-associated protein 1								0.86	1.93
P12270	Nucleoprotein TPR								2.64	
Q96RS6	NudC domain-containing protein 1									4.80
Q9UBM4	Opticin						-2.48			

O15018	PDZ domain-containing protein 2								0.56	
P62937	Peptidyl-prolyl cis-trans isomerase A						-4.79			
P45877	Peptidyl-prolyl cis-trans isomerase C								1.54	
P32119	Peroxiredoxin-2								1.52	
P30041	Peroxiredoxin-6								0.83	
Q03181	Peroxisome proliferator-activated receptor delta								1.00	
Q5SV97	PGC-1 and ERR-induced regulator in muscle protein 1								0.74	2.58
P30086	Phosphatidylethanolamine-binding protein 1					-39.30				
Q9Y2H2	Phosphatidylinositide phosphatase SAC2								1.72	
P00558	Phosphoglycerate kinase 1						-2.44		1.57	
P55058	Phospholipid transfer protein								0.67	
O15067	Phosphoribosylformylglycinamidine synthase								2.00	
P36955	Pigment epithelium-derived factor					-3.08	-6.47			
Q99959	Plakophilin-2								0.72	
P03952	Plasma kallikrein								1.86	
P05155	Plasma protease C1 inhibitor						-2.92		1.99	
P00747	Plasminogen								0.91	
P16284	Platelet endothelial cell adhesion molecule							1.11		
P01127	Platelet-derived growth factor subunit B				1.06					
Q86SQ0	Pleckstrin homology-like domain family B member 2								2.73	
Q13310	Polyadenylate-binding protein 4									4.08
Q15022	Polycomb protein SUZ12								0.61	
Q9NTG1	Polycystic kidney disease and receptor for egg jelly-related protein								1.16	
Q9UQ05	Potassium voltage-gated channel subfamily H member 4								3.08	
P54707	Potassium-transporting ATPase alpha chain 2								1.04	1.14
P20742	Pregnancy zone protein						-2.96			
Q15751	Probable E3 ubiquitin-protein ligase HERC1								1.85	
Q15031	Probable leucine--tRNA ligase. mitochondrial								2.14	
Q14005	Pro-interleukin-16								1.19	
Q9P2B2	Prostaglandin F2 receptor negative regulator								1.19	
P41222	Prostaglandin-H2 D-isomerase					-2.53	-12.33			
P02760	Protein AMBP								0.75	
Q9UPA5	Protein bassoon								1.30	
Q9NQ89	Protein C12orf4								3.31	
P0CF97	Protein FAM200B									2.47
Q92520	Protein FAM3C								-1.52	
Q5TBA9	Protein furry homolog									2.07
P54198	Protein HIRA								1.10	
Q96ST2	Protein IWS1 homolog									2.17
Q7L590	Protein MCM10 homolog						7.55			
Q86WI3	Protein NLRC5								-1.44	
Q86U86	Protein polybromo-1									1.96
Q9Y520	Protein PRRC2C						-5.68			
P04271	Protein S100-B						1.56			
Q13796	Protein Shroom2								1.21	
Q99497	Protein/nucleic acid deglycase DJ-1						-1.69			
P00734	Prothrombin						-1.50		2.87	
Q6V0I7	Protocadherin Fat 4								0.90	1.46
Q9HCL0	Protocadherin-18									1.79
Q8IZP2	Putative protein FAM10A4								1.12	
P14618	Pyruvate kinase PKM						-7.71			
Q4ADV7	RAB6A-GEF complex partner protein 1								1.09	
Q6GYQ0	Ral GTPase-activating protein subunit alpha-1								1.30	
Q96PV0	Ras/Rap GTPase-activating protein SynGAP								0.76	
P60602	Reactive oxygen species modulator 1								1.79	

P10745	Retinol-binding protein 3						-3.14			
Q9HCM1	Retroelement silencing factor 1									1.57
Q8NET4	Retrotransposon Gag-like protein 9									2.58
Q8N392	Rho GTPase-activating protein 18								2.37	
Q9P227	Rho GTPase-activating protein 23								0.61	
O43182	Rho GTPase-activating protein 6								1.11	
Q13464	Rho-associated protein kinase 1								1.37	
Q5TZA2	Rootletin								0.93	1.79
P21817	Ryanodine receptor 1								0.64	
P10523	S-arrestin						-1.61			
Q86VW0	SEC14 domain and spectrin repeat-containing protein 1								0.78	3.29
Q8WXD2	Secretogranin-3								1.34	
Q13523	Serine/threonine-protein kinase PRP4 homolog								1.10	
P02787	Serotransferrin						-4.17			
P02768	Serum albumin						-2.29/-1.51		0.96	
P02743	Serum amyloid P-component								1.43	
Q9UBL3	Set1/Ash2 histone methyltransferase complex subunit ASH2									3.61
P98077	SHC-transforming protein 2								-1.63	
Q9H7L9	Sin3 histone deacetylase corepressor complex component SDS3									2.13
Q8N300	Small vasohibin-binding protein									2.11
Q9UBP0	Spastin								0.76	
Q9H6E5	Speckle targeted PIP5K1A-regulated pol									5.97
Q9P2P6	StAR-related lipid transfer protein 9								2.73	
Q14683	Structural maintenance of chromosomes protein 1A									4.59
Q96SB8	Structural maintenance of chromosomes protein 6								2.53	
P55809	Succinyl-CoA:3-ketoacid coenzyme A transferase 1. mitochondrial								2.30	
Q9UBS9	SUN domain-containing ossification factor						-1.84			
Q7Z4L5	Tetratricopeptide repeat protein 21B								0.73	1.72
P05543	Thyroxine-binding globulin		↑	↑						
Q8IUC6	TIR domain-containing adapter molecule 1								0.67	
Q9H497	Torsin-3A								0.84	
P31629	Transcription factor HIVEP2								1.17	
Q2LD37	Transmembrane protein KIAA1109								1.58	
P02766	Transthyretin						-5.70			
O14773	Tripeptidyl-peptidase 1									1.86
P68363	Tubulin alpha-1B chain					2.36				
Q9BQE3	Tubulin alpha-1C chain						-2.27			
P0DPH7	Tubulin alpha-3C chain						-4.60			
P68366	Tubulin alpha-4A chain						-4.96			
P07437	Tubulin beta chain						-4.80			
Q9H4B7	Tubulin beta-1 chain						-3.00			
Q13509	Tubulin beta-3 chain						-3.40			
P23458	Tyrosine-protein kinase JAK1								1.22	
Q70CQ4	Ubiquitin carboxyl-terminal hydrolase 31								0.69	
Q70EK9	Ubiquitin carboxyl-terminal hydrolase 51									1.90
P40818	Ubiquitin carboxyl-terminal hydrolase 8								1.12	
Q16763	Ubiquitin-conjugating enzyme E2 S								1.04	
Q6P1W5	Uncharacterized protein C1orf94								1.28	
Q9ULV0	Unconventional myosin-Vb								0.50	
Q9HD67	Unconventional myosin-X								0.74	
Q96JP2	Unconventional myosin-XVB								0.37	
A7E2U8	UPF0602 protein C4orf47								0.65	
Q7Z7G8	Vacuolar protein sorting-associated protein 13B								0.62	
P19320	Vascular cell adhesion protein 1							1.88		
P15692	Vascular endothelial growth factor A	4.66			4.97					

Q6EMK4	Vasorin									1.49
P13611	Versican core protein						2.20			
O15195	Villin-like protein								0.91	
P08670	Vimentin						-2.30			
P02774	Vitamin D-binding protein						-4.48		0.92	
P07225	Vitamin K-dependent protein S								0.89	
P04004	Vitronectin								1.17	
P04275	von Willebrand factor		↑	↑						
P38606	V-type proton ATPase catalytic subunit A						3.98			
Q9Y5W5	Wnt inhibitory factor 1						-1.54			
Q5SVQ8	Zinc finger and BTB domain-containing protein 41									3.23
P17040	Zinc finger and SCAN domain-containing protein 20								0.70	
O14978	Zinc finger protein 263								1.45	
Q8TB69	Zinc finger protein 519									4.54
Q9UC06	Zinc finger protein 70									2.54
Q8N4W9	Zinc finger protein 808								1.04	
Q92784	Zinc finger protein DPF3								2.34	
A7E2V4	Zinc finger SWIM domain-containing protein 8									1.77
P25311	Zinc-alpha-2-glycoprotein					3.72				

Table S1.1 – (continued)

Uniprot Acess	Description	Balaiya. et.al.. (2017) PDR/Control	Klaassen. et.al.. (2017) log2 (PDR/control)	Schori. et.al.. (2018) log2 (PDR/ERM)	Zou. *et.al.*.(2018) (p-value<0.05) log2 (PDR/MH)	Zou. *et.al.*.(2018) (p-value<0.05) log2 (PDR/IVR)2	Srividya. *et.al.*.(2018) (p-value<0.05) log2 (DME/MH)	Srividya. *et.al.*.(2018) (p-value<0.05) log2 (PDR/MH)	Tsai. et.al..(2018) log2 (DR/MH) (p-value<0.05)
P62258	14-3-3 protein epsilon					ND PDR			
P61981	14-3-3 protein gamma			6.54					
Q9BRK5	45 kDa calcium-binding protein				ND PDR				
P17643	5.6-dihydroxyindole-2-carboxylic acid oxidase			-4.31					
P10809	60 kDa heat shock protein. mitochondrial				ND MH	ND IVR			
P52209	6-phosphogluconate dehydrogenase. decarboxylating			3.09					
P08253	72 kDa type IV collagenase			1.64					
Q9UHI8	A disintegrin and metalloproteinase with thrombospondin motifs 1			2.69					
Q13510	Acid ceramidase			-1.79	ND PDR				
P63261	Actin. cytoplasmic 2			2.63					
Q15848	Adiponectin		1.98						
O00468	Agrin				ND PDR				
P02763	Alpha-1-acid glycoprotein 1	ND PDR							
P19652	Alpha-1-acid glycoprotein 2	ND PDR			0.16				
P01011	Alpha-1-antichymotrypsin			2.37					
P04217	Alpha-1B-glycoprotein			2.16					
P08697	Alpha-2-antiplasmin			1.97					
P02765	Alpha-2-HS-glycoprotein			4.49					
P01023	Alpha-2-macroglobulin				-0.74				
P02489	Alpha-crystallin A chain			4.90	ND MH	ND IVR			
P02511	Alpha-crystallin B chain				ND MH	ND IVR			
P17050	Alpha-N-acetylgalactosaminidase			-2.72					
P05067	Amyloid-beta precursor protein	ND control		-1.71	-3.22				
P51693	Amyloid-like protein 1			-2.70	-3.38				
Q06481	Amyloid-like protein 2	ND PDR		-3.35	-2.58				
P03950	Angiogenin			1.93					

Q15389	Angiopoietin-1		1.45						
P01019	Angiotensinogen			1.74					
Q01484	Ankyrin-2				ND MH	ND IVR			
P01008	Antithrombin-III	ND PDR							
P02652	Apolipoprotein A-II				0.34	-0.37			
P06727	Apolipoprotein A-IV			3.78					
P04114	Apolipoprotein B-100				ND MH	ND IVR			
P02654	Apolipoprotein C-I				0.30	1.01			
P15289	Arylsulfatase A			-2.10					
P15848	Arylsulfatase B			-2.24					
O75882	Attractin				-0.78				
O43505	Beta-1.4-glucuronyltransferase 1				-1.60				
P02749	Beta-2-glycoprotein 1			2.44					
P61769	Beta-2-microglobulin			2.81					
Q96KN2	Beta-Ala-His dipeptidase				ND PDR				
P05813	Beta-crystallin A3				ND MH	ND IVR			
P53673	Beta-crystallin A4				ND MH	ND IVR			
P53674	Beta-crystallin B1				ND MH	ND IVR			
P43320	Beta-crystallin B2				ND MH	ND IVR			
P43251	Biotinidase				-0.93				
P07738	Bisphosphoglycerate mutase			10.37		ND PDR			
P12643	Bone morphogenetic protein 2		0.70						
Q96GW7	Brevican core protein			-3.13					
Q8IZJ3	C3 and PZP-like alpha-2-macroglobulin domain-containing protein 8				ND PDR				
P04003	C4b-binding protein alpha chain					ND PDR			
P12830	Cadherin-1			5.37					
P19022	Cadherin-2				ND PDR				
P27797	Calreticulin				ND PDR				
O94985	Calsyntenin-1			-1.89	-1.50				
P00915	Carbonic anhydrase 1			47.75		ND PDR			
P00918	Carbonic anhydrase 2			17.83					
P16870	Carboxypeptidase E				-2.81				
Q9Y646	Carboxypeptidase Q				ND PDR				
Q9NQ79	Cartilage acidic protein 1				ND PDR				
P04040	Catalase			18.02		ND PDR			
P07858	Cathepsin B				ND PDR				
P07339	Cathepsin D	ND PDR			-0.95				
Q9UBR2	Cathepsin Z				ND PDR				
P13500	C-C motif chemokine 2							2.43	
P10147	C-C motif chemokine 3						0.67	1.02	
P13236	C-C motif chemokine 4						0.40	1.57	
P48745	CCN family member 3		0.80						
P16070	CD44 antigen			2.23					
P13987	CD59 glycoprotein				ND PDR				
Q8N3J6	Cell adhesion molecule 2			-1.98					
Q4KMG0	Cell adhesion molecule-relatedvsdown-regulated by oncogenes			-1.78					
O75503	Ceroid-lipofuscinosis neuronal protein 5			-1.68					
P00450	Ceruloplasmin			2.10	-0.37	0.87			
Q9BU40	Chordin-like protein 1				ND MH	ND IVR			
P10645	Chromogranin-A				ND MH	ND IVR			
P10909	Clusterin				-0.90				
Q15846	Clusterin-like protein 1				ND PDR				
P02458	Collagen alpha-1(II) chain	ND PDR			ND PDR				
P20849	Collagen alpha-1(IX) chain				ND PDR				
P12109	Collagen alpha-1(VI) chain				ND PDR				

P12107	Collagen alpha-1(XI) chain	ND PDR							
P08123	Collagen alpha-2(I) chain				ND PDR				
Q14055	Collagen alpha-2(IX) chain	ND PDR			ND PDR				
Q14050	Collagen alpha-3(IX) chain	ND PDR							
P02745	Complement C1q subcomponent subunit A					ND PDR			
Q9BXJ4	Complement C1q tumor necrosis factor-related protein 3				ND PDR				
P00736	Complement C1r subcomponent				-1.42	ND PDR			
P06681	Complement C2			2.25	ND MH	ND IVR			
P0C0L4	Complement C4-A				-0.35				
P0C0L5	Complement C4-B				-0.30				
P01031	Complement C5			2.05					
P10643	Complement component C7			2.39					
P07358	Complement component C8 beta chain				ND MH	ND IVR			
P02748	Complement component C9			3.16					
P00751	Complement factor B			2.23					
P00746	Complement factor D			4.73					
P36980	Complement factor H-related protein 2			1.90					
P05156	Complement factor I	ND control		1.97	-0.61				
Q02246	Contactin-2			-2.56					
Q9UHC6	Contactin-associated protein-like 2			-2.71					
P08185	Corticosteroid-binding globulin			2.04					
P02741	C-reactive protein			5.55					
P02778	C-X-C motif chemokine 10						1.92	4.87	
P01034	Cystatin-C				-0.82				
Q14204	Cytoplasmic dynein 1 heavy chain 1				ND MH	ND IVR			
P13716	Delta-aminolevulinic acid dehydratase			34.67					
P81605	Dermcidin				ND MH	ND IVR			
Q9UBP4	Dickkopf-related protein 3				0.51	1.25			
Q9UHL4	Dipeptidyl peptidase 2			-2.07	ND PDR				
P09172	Dopamine beta-hydroxylase			2.13					
Q13822	Ectonucleotide pyrophosphatasevsphosphodiesterase family member 2				-1.79				
Q12805	EGF-containing fibulin-like extracellular matrix protein 1	ND control			-0.67				
P51671	Eotaxin						0.58	0.98	
P02794	Ferritin heavy chain					ND PDR			
Q9UGM5	Fetuin-B			2.21					
P35555	Fibrillin-1				ND PDR				
P02671	Fibrinogen alpha chain	ND control		5.23	1.34	0.30			
P02675	Fibrinogen beta chain	ND control		16.38	ND MH	ND IVR			
P02679	Fibrinogen gamma chain	ND control		14.47					
P09038	Fibroblast growth factor 2						0.29	0.76	
P23142	Fibulin-1				-1.77				
P20930	Filaggrin				ND MH	ND IVR			
P30043	Flavin reductase					ND PDR			
Q6MZW2	Follistatin-related protein 4			-2.31	ND PDR				
P04075	Fructose-bisphosphate aldolase A					ND PDR			
Q08380	Galectin-3-binding protein				ND PDR				
P17900	Ganglioside GM2 activator				ND PDR				
P06396	Gelsolin			2.85	-0.45				
P14314	Glucosidase 2 subunit beta				ND PDR				
P48058	Glutamate receptor 4				ND PDR				
Q16769	Glutaminyl-peptide cyclotransferase				ND PDR				
O00461	Golgi integral membrane protein 4			-2.29					
P09919	Granulocyte colony-stimulating factor						1.20	1.31	
O95390	Growth/differentiation factor 11			-1.87					
Q99988	Growth/differentiation factor 15		1.40						

P62826	GTP-binding nuclear protein Ran					ND PDR			
Q02747	Guanylin			16.14					
P00738	Haptoglobin				ND MH	ND IVR			
P04792	Heat shock protein beta-1			-1.84					
P69905	Hemoglobin subunit alpha	ND control			ND PDR	-2.29			
P68871	Hemoglobin subunit beta	ND control		107.83		-1.51			
P69891	Hemoglobin subunit gamma-1					ND PDR			
P69892	Hemoglobin subunit gamma-2					ND PDR			
P02790	Hemopexin				-0.31				
P05546	Heparin cofactor 2			2.14					
P14210	Hepatocyte growth factor		1.67						
P04196	Histidine-rich glycoprotein	ND control		2.23	-0.18				
Q96S86	Hyaluronan and proteoglycan link protein 3			-4.07					
Q14520	Hyaluronan-binding protein 2			2.26					
P22304	Iduronate 2-sulfatase			-1.74	ND PDR				
P01876	Immunoglobulin heavy constant alpha 1				0.39	0.92			
P01877	Immunoglobulin heavy constant alpha 2				0.88	1.52			
A0A0A0MS15	Immunoglobulin heavy variable 3-49				ND MH	ND IVR			
P01767	Immunoglobulin heavy variable 3-53					ND PDR			
A0A0B4J1V6	Immunoglobulin heavy variable 3-73				ND MH	ND IVR			
A0A0B4J1X5	Immunoglobulin heavy variable 3-74				3.14	3.59			
P01602	Immunoglobulin kappa variable 1-5				-0.40				
A0A0C4DH72	Immunoglobulin kappa variable 1-6					ND PDR			
A2NJV5	Immunoglobulin kappa variable 2-29				ND MH	ND IVR			
A0A075B6S2	Immunoglobulin kappa variable 2D-29				ND MH	ND IVR			
P01619	Immunoglobulin kappa variable 3-20	ND PDR				ND PDR			
P06312	Immunoglobulin kappa variable 4-1				ND MH	ND IVR			
P0DOY2	Immunoglobulin lambda constant 2				ND PDR				
A0M8Q6	Immunoglobulin lambda constant 7				ND MH	ND IVR			
A0A075B6J0	Immunoglobulin lambda variable 1-40					ND PDR			
P01700	Immunoglobulin lambda variable 1-47					ND PDR			
P08833	Insulin-like growth factor-binding protein 1		3.31						
P18065	Insulin-like growth factor-binding protein 2		0.56	1.52					
P17936	Insulin-like growth factor-binding protein 3		4.23						
P24592	Insulin-like growth factor-binding protein 6				-1.04				
Q16270	Insulin-like growth factor-binding protein 7				-1.11				
Q06033	Inter-alpha-trypsin inhibitor heavy chain H3				ND MH	ND IVR			
Q14624	Inter-alpha-trypsin inhibitor heavy chain H4			1.97					
Q86UX2	Inter-alpha-trypsin inhibitor heavy chain H5				ND PDR				
P05362	Intercellular adhesion molecule 1		2.43	2.14					
P01579	Interferon gamma						0.88	0.88	0.71
P01584	Interleukin-1 beta						1.07	0.84	1.24
P18510	Interleukin-1 receptor antagonist protein						5.83	1.92	
P22301	Interleukin-10						0.42	1.10	
P29460	Interleukin-12 subunit beta							1.41	
P35225	Interleukin-13						0.88	3.35	
P40933	Interleukin-15							0.93	
Q16552	Interleukin-17A						0.29	0.45	
P60568	Interleukin-2							0.62	
P05112	Interleukin-4						0.88	0.87	
P05113	Interleukin-5						0.76	0.90	
P05231	Interleukin-6						1.42	3.61	
P13232	Interleukin-7						3.79	4.56	
P10145	Interleukin-8						1.51	5.13	
P15248	Interleukin-9						0.51	0.96	

P29622	Kallistatin			1.89					
P13646	Keratin. type I cytoskeletal 13				ND MH	ND IVR			
P08779	Keratin. type I cytoskeletal 16				ND MH	ND IVR			
P04264	Keratin. type II cytoskeletal 1			-3.10	0.13	2.03			
P48668	Keratin. type II cytoskeletal 6C				ND MH	ND IVR			
P01042	Kininogen-1	ND control		2.42	ND PDR				
Q14767	Latent-transforming growth factor beta-binding protein 2				ND MH	ND IVR			
P02750	Leucine-rich alpha-2-glycoprotein			3.35					
Q9P2V4	Leucine-rich repeat. immunoglobulin-like domain and transmembrane domain-containing protein 1			-2.12					
Q9NT99	Leucine-rich repeat-containing protein 4B			-3.23					
P05451	Lithostathine-1-alpha			5.40					
P00338	L-lactate dehydrogenase A chain					ND PDR			
P07195	L-lactate dehydrogenase B chain					ND PDR			
P08637	Low affinity immunoglobulin gamma Fc region receptor III-A			2.34					
P98164	Low-density lipoprotein receptor-related protein 2				ND PDR				
P51884	Lumican			2.11					
P10253	Lysosomal alpha-glucosidase				ND PDR				
P10619	Lysosomal protective protein			-1.51					
P61626	Lysozyme C			3.23	ND MH	ND IVR			
P07333	Macrophage colony-stimulating factor 1 receptor			1.78					
P40121	Macrophage-capping protein			2.09					
P01033	Metalloproteinase inhibitor 1			2.39		ND PDR			
P16035	Metalloproteinase inhibitor 2					-2.81			
Q13228	Methanethiol oxidase					ND PDR			
P55083	Microfibril-associated glycoprotein 4				ND PDR				
P26038	Moesin			3.50					
P08571	Monocyte differentiation antigen CD14			2.16					
Q7Z7M0	Multiple epidermal growth factor-like domains protein 8			-1.81	ND PDR				
P13533	Myosin-6				ND MH	ND IVR			
P12883	Myosin-7				ND MH	ND IVR			
P20933	N(4)-(beta-N-acetylglucosaminyl)-L-asparaginase				ND PDR				
P15586	N-acetylglucosamine-6-sulfatase			-1.81	ND PDR				
Q96PD5	N-acetylmuramoyl-L-alanine amidase			2.19					
P13591	Neural cell adhesion molecule 1				ND MH	ND IVR			
P32004	Neural cell adhesion molecule L1			-2.19					
O00533	Neural cell adhesion molecule L1-like protein				ND PDR				
Q9ULB1	Neurexin-1			-4.08					
Q9Y4C0	Neurexin-3				ND PDR				
Q9HDB5	Neurexin-3-beta			-1.89					
Q09666	Neuroblast differentiation-associated protein AHNAK					ND PDR			
O14594	Neurocan core protein			-11.29					
P05408	Neuroendocrine protein 7B2				ND PDR				
P12036	Neurofilament heavy polypeptide				ND MH	ND IVR			
Q92823	Neuronal cell adhesion molecule			-2.09	ND PDR				
O15240	Neurosecretory protein VGF			-2.18	ND PDR				
Q99574	Neuroserpin			-2.08	ND PDR				
Q9P121	Neurotrimin			-2.05	ND PDR				
P59665	Neutrophil defensin 1					1.61			
P59666	Neutrophil defensin 3					1.61			
P61916	NPC intracellular cholesterol transporter 2				ND MH	ND IVR			
P23515	Oligodendrocyte-myelin glycoprotein			-2.51	ND PDR				
Q9UBM4	Opticin	ND PDR			-1.10				
P10451	Osteopontin	ND PDR		-1.85	-2.03				
O95428	Papilin				ND PDR				
P62937	Peptidyl-prolyl cis-trans isomerase A					ND PDR			

P30041	Peroxiredoxin-6					ND PDR			
P30086	Phosphatidylethanolamine-binding protein 1					ND PDR			
Q96S96	Phosphatidylethanolamine-binding protein 4				ND PDR				
P55058	Phospholipid transfer protein					ND PDR			
P36955	Pigment epithelium-derived factor	ND PDR							
P49763	Placenta growth factor		5.84						8.59
Q9BTY2	Plasma alpha-L-fucosidase				ND PDR				
P03952	Plasma kallikrein				ND MH	ND IVR			
P05155	Plasma protease C1 inhibitor				ND PDR				
P05154	Plasma serine protease inhibitor			1.73	-0.07	1.71			
P00747	Plasminogen				-0.49				
P13796	Plastin-2			2.66					
P04085	Platelet-derived growth factor subunit A		2.60						
P01127	Platelet-derived growth factor subunit B		2.05				0.45	0.98	
P21246	Pleiotrophin				ND PDR				
Q6UX71	Plexin domain-containing protein 2			-1.93	ND PDR				
P0CG47	Polyubiquitin-B					ND PDR			
P0CG48	Polyubiquitin-C					ND PDR			
Q6S8J3	POTE ankyrin domain family member E				ND MH	ND IVR			
Q15113	Procollagen C-endopeptidase enhancer 1			5.68					
P51888	Prolargin				ND PDR				
Q07954	Prolow-density lipoprotein receptor-related protein 1			-1.73					
Q02297	Pro-neuregulin-1. membrane-bound isoform		1.63						
P07602	Prosaposin				-1.77				
P02760	Protein AMBP	ND control		5.33					
O60888	Protein CutA			-2.35	ND PDR				
Q92520	Protein FAM3C			-1.98					
Q99497	Protein/nucleic acid deglycase DJ-1			5.40					
P00734	Prothrombin	ND control							
P20396	Pro-thyrotropin-releasing hormone				ND MH	ND IVR			
P00491	Purine nucleoside phosphorylase					ND PDR			
P48741	Putative heat shock 70 kDa protein 7			-19.67					
Q8NHP8	Putative phospholipase B-like 2			-2.41					
P50395	Rab GDP dissociation inhibitor beta			3.08					
Q9BSG5	Retbindin	ND control			-1.16				
P00352	Retinal dehydrogenase 1			8.50					
P10745	Retinol-binding protein 3	ND PDR			-1.24				
P02753	Retinol-binding protein 4			2.70					
O15537	Retinoschisin			-3.41	ND PDR				
P34096	Ribonuclease 4			2.48					
P13489	Ribonuclease inhibitor			24.70					
P07998	Ribonuclease pancreatic	ND control							
Q86VB7	Scavenger receptor cysteine-rich type 1 protein M130			2.02					
Q92765	Secreted frizzled-related protein 3				-0.70				
Q6FHJ7	Secreted frizzled-related protein 4			2.91					
P05060	Secretogranin-1			-1.98	ND PDR				
P13521	Secretogranin-2			-2.25	ND PDR				
Q8WXD2	Secretogranin-3				ND PDR				
Q9BYH1	Seizure 6-like protein			-1.92					
Q53EL9	Seizure protein 6 homolog				ND PDR				
O75326	Semaphorin-7A			-2.56					
Q92743	Serine protease HTRA1				ND PDR				
P02787	Serotransferrin				-1.08				
A8MV23	Serpin E3			-4.28					
P02768	Serum albumin				-0.40				

P0DJI8	Serum amyloid A-1 protein			26.88					
P04278	Sex hormone-binding globulin			2.48					
O75368	SH3 domain-binding glutamic acid-rich-like protein			5.34					
Q9HAT2	Sialate O-acetylesterase				ND PDR				
P01241	Somatotropin		1.18						
P09486	SPARC				ND PDR				
Q14515	SPARC-like protein 1				-2.97				
O00391	Sulfhydryl oxidase 1				ND PDR				
P00441	Superoxide dismutase [Cu-Zn]				ND MH	ND IVR			
Q7Z7G0	Target of Nesh-SH3			-2.58					
Q92752	Tenascin-R			-1.93	ND PDR				
P22105	Tenascin-X			-2.79					
Q08629	Testican-1			-2.07					
Q92563	Testican-2			-3.86	ND PDR				
Q9BQ16	Testican-3			-4.16					
P07996	Thrombospondin-1		3.37						
P05543	Thyroxine-binding globulin			2.42					
Q8WZ42	Titin					ND PDR			
P37837	Transaldolase					ND PDR			
Q14956	Transmembrane glycoprotein NMB			2.60					
P02766	Transthyretin	ND PDR							
P60174	Triosephosphate isomerase					ND PDR			
O14773	Tripeptidyl-peptidase 1				ND PDR				
P01375	Tumor necrosis factor						0.80	0.98	
P08138	Tumor necrosis factor receptor superfamily member 16		0.85						
O95407	Tumor necrosis factor receptor superfamily member 6B		1.70						
P62979	Ubiquitin-40S ribosomal protein S27a		1.78			ND PDR			
P62987	Ubiquitin-60S ribosomal protein L40					ND PDR			
O75752	UDP-GalNAc:beta-1.3-N-acetylgalactosaminyltransferase 1			-3.04					
P19320	Vascular cell adhesion protein 1			2.74					
P15692	Vascular endothelial growth factor A		5.68	1.59	1.46	1.29		1.18	5.92/7.95
P08670	Vimentin				ND MH	ND IVR			
P02774	Vitamin D-binding protein			2.72					
P07225	Vitamin K-dependent protein S				-1.17				
P04004	Vitronectin	ND control		2.03					
Q9Y279	V-set and immunoglobulin domain-containing protein 4			4.34					
Q15904	V-type proton ATPase subunit S1				ND PDR				
Q9Y5W5	Wnt inhibitory factor 1				-1.58				
P12955	Xaa-Pro dipeptidase			1.84					
A4UGR9	Xin actin-binding repeat-containing protein 2				ND MH	ND IVR			
Q86Y38	Xylosyltransferase 1			-3.46					
Q8NB15	Zinc finger protein 511			2.25					
P25311	Zinc-alpha-2-glycoprotein	ND control		2.18					

Table S1.2 - Proteins found differentially expressed in vitreous collected from patients with age-related macular degeneration (AMD) and neovascular age-related macular degeneration (nAMD). Nobl and co-workers compared nAMD with choroidal neovascularization without signs of bleeding (CNVwvsoB). nAMD with signs of bleeding (CNVwB) and nAMD with hemorrhagic choroidal neovascularization (hCNV) to idiopathic vitreous floaters (iVF).

				Nobl. *et. al.*. (2016)			Schori. *et. al.*. (2018)	
Uniprot	Description	Huber. et. al.. (2012) log2 (nAMD/Control)	Koss. et. al.. (2014) log2 (AMD/control)	log2 (CNVw/oB/iVF)	log2 (CNVwB/iVF)	log2 (hCNV/iVF)	log2 (dry AMD/control)	log2 (nAMD/control)
P61981	14-3-3 protein gamma							6.00
P63261	Actin. cytoplasmic 2						-1.95	
P43652	Afamin		1.71					
P19652	Alpha-1-acid glycoprotein 2		1.37					
P01009	Alpha-1-antitrypsin		0.79					
P15144	Aminopeptidase N						-6.66	
O15123	Angiopoietin-2	0.92						
P01008	Antithrombin-III		2.46					
P02647	Apolipoprotein A-I		1.20					
P05090	Apolipoprotein D						-3.20	
P61769	Beta-2-microglobulin							1.92
Q13867	Bleomycin hydrolase							-7.76
P33151	Cadherin-5						-2.20	
P07858	Cathepsin B							2.07
Q9UBR2	Cathepsin Z							1.36
P36222	Chitinase-3-like protein 1							3.17
P06276	Cholinesterase						1.68	
P10909	Clusterin			0.96	1.23	1.37		
P00740	Coagulation factor IX						-2.72	
P03951	Coagulation factor XI						-3.46	
Q02388	Collagen alpha-			-3.65	-2.43	-2.57		
Q14050	Collagen alpha-			-0.37	0.59	1.27		
P28838	Cytosol aminopeptidase						-12.16	
P13716	Delta-aminolevulinic acid dehydratase						5.52	
Q14118	Dystroglycan							1.54
P14625	Endoplasmin							1.97
Q9UNN8	Endothelial protein C receptor							-9.96
Q16610	Extracellular matrix protein 1						-2.25	
P02794	Ferritin heavy chain							4.25
P02671	Fibrinogen alpha chain		1.54					
P02751	Fibronectin						-2.85	
P04075	Fructose-bisphosphate aldolase A						-2.31	
P09972	Fructose-bisphosphate aldolase C							1.96
P13284	Gamma-interferon-inducible lysosomal thiolreductase							3.21
P17900	Ganglioside GM2 activator						-1.74	
P14314	Glucosidase 2 subunit beta							1.78
P22352	Glutathione peroxidase 3		2.09					
P00390	Glutathione reductase. mitochondrial							3.07
P00738	Haptoglobin		1.55					
P68871	Hemoglobin subunit beta			5.32	3.26	5.79		
P26927	Hepatocyte growth factor-like protein						-3.34	
P04196	Histidine-rich glycoprotein		3.44					

P30501	HLA class I histocompatibility antigen. C alpha chain						-6.96	
P01876	Immunoglobulin heavy constant alpha 1		5.14					
P01857	Immunoglobulin heavy constant gamma 1		1.65					
P01859	Immunoglobulin heavy constant gamma 2			0.11	-1.27	-1.30		
P01834	Immunoglobulin kappa constant		2.71					
P0DOY2	Immunoglobulin lambda constant 2		2.19	0.93	1.25	0.79		
B9A064	Immunoglobulin lambda-like polypeptide 5			1.26	2.48	0.48		
P19827	Inter-alpha-trypsin inhibitor heavy chain H1		1.23					
P05362	Intercellular adhesion molecule 1						-2.05	
P13598	Intercellular adhesion molecule 2						-2.35	
Q9NPH3	Interleukin-1 receptor accessory protein						-2.53	
O75874	Isocitrate dehydrogenase [NADP] cytoplasmic						-6.79	
P02788	Lactotransferrin						-3.23	
Q99538	Legumain						-3.06	
P05451	Lithostathine-1-alpha						-1.71	
P10619	Lysosomal protective protein						-1.94	
P13473	Lysosome-associated membrane glycoprotein 2							1.58
P04156	Major prion protein							2.05
O00187	Mannan-binding lectin serine protease 2							2.44
P16519	Neuroendocrine convertase 2							2.07
O15240	Neurosecretory protein VGF						-2.27	
P61916	NPC intracellular cholesterol transporter 2							1.86
Q5VST9	Obscurin			-0.75	-2.31	-2.32		
Q9UBM4	Opticin			-1.20	-1.71	-1.66		
O95497	Pantetheinase						-1.81	
O75594	Peptidoglycan recognition protein 1							2.10
P30086	Phosphatidylethanolamine-binding protein 1							1.64
P15259	Phosphoglycerate mutase 2							2.27
P36955	Pigment epithelium-derived factor	-3.06		0.88	1.18	0.91		
P15151	Poliovirus receptor						-2.00	
Q9H3G5	Probable serine carboxypeptidase CPVL						2.13	1.91
Q9UHG2	ProSAAS						-2.14	
P07602	Prosaposin							1.92
P41222	Prostaglandin-H2 D-isomerase		0.72	0.59	0.78	0.22		
Q9UK55	Protein Z-dependent protease inhibitor						-2.45	
Q99497	Protein/nucleic acid deglycase DJ-1							2.50
P00352	Retinal dehydrogenase 1							4.60
P10745	Retinol-binding protein 3		1.48					
Q53RT3	Retroviral-like aspartic protease 1							-4.64
P34096	Ribonuclease 4						-1.77	
P07998	Ribonuclease pancreatic						2.43	1.69
Q86VB7	Scavenger receptor cysteine-rich type 1 protein M130						-2.48	
Q13275	Semaphorin-3F							1.75
P02787	Serotransferrin		0.80					
P02768	Serum albumin		0.93					
Q99519	Sialidase-1							1.94
P02549	Spectrin alpha chain. erythrocytic 1							-1.48
Q9HCB6	Spondin-1							1.95
P00441	Superoxide dismutase [Cu-Zn]							1.57
Q9BQ16	Testican-3						-3.05	
P02766	Transthyretin		0.80					
P78324	Tyrosine-protein phosphatase non-receptor type substrate 1							1.55
P17948	Vascular endothelial growth factor receptor 1	0.95						8.23
P35968	Vascular endothelial growth factor receptor 2						-1.96	

Table S1.3 - Proteins found differentially expressed in vitreous collected from patients with retinal detachment (RD) and proliferative vitreoretinopathy (PVR). The abbreviations MH and ERM correspond to the control groups of patients with macular holes and epiretinal membranes. respectively. PVR-C-D corresponds to patients with severe PVR (grade C or D). whereas PVR-B corresponds to patients with moderate PVR (grade B). Symbols ↑ and ↓ correspond to the up-regulated and down-regulated proteins. respectively.

			Shitama. *et. al.* (2008)			Yu. *et. al.* (2008)			
Uniprot	**Description**	**Banerjee. et. al. (2007) log2(PVR/ERM)**	**PVR/MH**	**RD/MH**	**PVR/RD**	**log2 (PVR-B/control)**	**log2 (PVR-C-D/control)**	**log2 (PVR-C-D/PVR-B)**	**Yu. *et. al.* (2012) PVR/control**
Q92665	28S ribosomal protein S31. mitochondrial						ND control	ND PVR-B	
Q9UHI8	A disintegrin and metalloproteinase with thrombospondin motifs 1					ND control		ND PVR-C/D	
P68032	Actin. alpha cardiac muscle 1								↓
P68133	Actin. alpha skeletal muscle								↓
P60709	Actin. cytoplasmic 1								↓
P63261	Actin. cytoplasmic 2								↓
P01009	Alpha-1-antitrypsin		↑	↑	↑	2.19	3.19		↑
P04217	Alpha-1B-glycoprotein					2.66	3.74		↑
P02765	Alpha-2-HS-glycoprotein					1.51	3.19	1.68	↑
P01023	Alpha-2-macroglobulin						ND control	ND PVR-B	
P06733	Alpha-enolase					-2.72			
P05067	Amyloid-beta precursor protein					ND control		ND PVR-C/D	
Q06481	Amyloid-like protein 2					ND control		ND PVR-C/D	
P01019	Angiotensinogen						ND control	ND PVR-B	
P01008	Antithrombin-III		↑				3.00		
P02647	Apolipoprotein A-I							2.00	
P06727	Apolipoprotein A-IV		↑	↑	↑				
P02749	Beta-2-glycoprotein 1						ND control	ND PVR-B	
P13929	Beta-enolase					ND PVR-B	ND PVR-C/D		
Q6UXY1	Brain-specific angiogenesis inhibitor 1-associated protein 2-like protein 2						ND control	ND PVR-B	
Q5T5Y3	Calmodulin-regulated spectrin-associated protein 1						ND control	ND PVR-B	
O94985	Calsyntenin-1					ND control		ND PVR-C/D	
P07339	Cathepsin D			↑			1.32	1.74	
P13500	C-C motif chemokine 2	3.76							
P10147	C-C motif chemokine 3	ND control							
P13236	C-C motif chemokine 4	ND control							
P13501	C-C motif chemokine 5	ND control							
Q02224	Centromere-associated protein E						ND control	ND PVR-B	
Q9BSQ5	Cerebral cavernous malformations 2 protein						ND control	ND PVR-B	
P00450	Ceruloplasmin					1.32	1.81		
Q13976	cGMP-dependent protein kinase 1						ND control	ND PVR-B	
P36222	Chitinase-3-like protein 1						ND control	ND PVR-B	
P10909	Clusterin		↑	↑	↓				
P01024	Complement C3					2.81	4.32	1.51	
P0C0L4	Complement C4-A							2.26	
P0C0L5	Complement C4-B							2.14	↑
P00751	Complement factor B							3.00	↑
Q03591	Complement factor H-related protein 1						ND control	ND PVR-B	
P01034	Cystatin-C						1.42	1.68	

Q14008	Cytoskeleton-associated protein 5						ND control	ND PVR-B	
Q92608	Dedicator of cytokinesis protein 2						ND control	ND PVR-B	
Q9UBP4	Dickkopf-related protein 3					ND control		ND PVR-C/D	
Q14194	Dihydropyrimidinase-related protein 1					ND PVR-B	ND PVR-C/D		
Q16555	Dihydropyrimidinase-related protein 2					-3.46			
Q9ULT8	E3 ubiquitin-protein ligase HECTD1						ND control	ND PVR-B	
Q12805	EGF-containing fibulin-like extracellular matrix protein 1					ND control		ND PVR-C/D	
Q14494	Endoplasmic reticulum membrane sensor NFE2L1						ND control	ND PVR-B	
P51671	Eotaxin	ND control							
O15372	Eukaryotic translation initiation factor 3 subunit H						ND control	ND PVR-B	
A0A1B0GW35	Exocyst complex component 1-like						ND control	ND PVR-B	
P08294	Extracellular superoxide dismutase [Cu-Zn]						ND control	ND PVR-B	
Q5VZK9	F-actin-uncapping protein LRRC16A						ND control	ND PVR-B	
P05230	Fibroblast growth factor 1	ND control							
P09972	Fructose-bisphosphate aldolase C					ND PVR-B	ND PVR-C/D		
Q08380	Galectin-3-binding protein						ND control	ND PVR-B	
P09104	Gamma-enolase					-1.70			
P15104	Glutamine synthetase					ND PVR-B	ND PVR-C/D		
P22352	Glutathione peroxidase 3						ND control	ND PVR-B	
P04406	Glyceraldehyde-3-phosphate dehydrogenase					-2.32			
P09919	Granulocyte colony-stimulating factor	ND control							
Q8IWJ2	GRIP and coiled-coil domain-containing protein 2						ND control	ND PVR-B	
P00738	Haptoglobin						ND control	ND PVR-B	
P00739	Haptoglobin-related protein						ND control	ND PVR-B	
P11142	Heat shock cognate 71 kDa protein					ND PVR-B	ND PVR-C/D		
P69905	Hemoglobin subunit alpha						ND control	ND PVR-B	
P68871	Hemoglobin subunit beta					ND control		ND PVR-C/D	
P02790	Hemopexin					3.09	3.00		↑
P05546	Heparin cofactor 2						ND control	ND PVR-B	
P04196	Histidine-rich glycoprotein							3.00	
Q9NR48	Histone-lysine N-methyltransferase ASH1L						ND control	ND PVR-B	
A6NJT0	Homeobox protein unc-4 homolog						ND control	ND PVR-B	
Q9Y6R7	IgGFc-binding protein					ND control		ND PVR-C/D	
P19823	Inter-alpha-trypsin inhibitor heavy chain H2						ND control	ND PVR-B	
P01579	Interferon gamma	ND control							
P22301	Interleukin-10	ND control							
P29460	Interleukin-12 subunit beta	ND control							
P05231	Interleukin-6	7.34							
P10145	Interleukin-8	3.67							
P51884	Lumican					ND control		ND PVR-C/D	
P07199	Major centromere autoantigen B						ND control	ND PVR-B	
Q96PG2	Membrane-spanning 4-domains subfamily A member 10						ND control	ND PVR-B	
P08571	Monocyte differentiation antigen CD14						ND control	ND PVR-B	
Q86VD1	MORC family CW-type zinc finger protein 1						ND control	ND PVR-B	
Q96PD5	N-acetylmuramoyl-L-alanine amidase						ND control	ND PVR-B	
P22894	Neutrophil collagenase						ND control	ND PVR-B	
Q9Y2I6	Ninein-like protein						ND control	ND PVR-B	
Q53F19	Nuclear cap-binding protein subunit 3						ND control	ND PVR-B	
O75376	Nuclear receptor corepressor 1						ND control	ND PVR-B	
P19338	Nucleolin					ND PVR-B	ND PVR-C/D		
Q9UBM4	Opticin						-2.32		↓
Q6GQQ9	OTU domain-containing protein 7B						ND control	ND PVR-B	
O95153	Peripheral-type benzodiazepine receptor-associated protein 1						ND control	ND PVR-B	

Q06830	Peroxiredoxin-1					ND PVR-B	ND PVR-C/D		
P32119	Peroxiredoxin-2					ND PVR-B	ND PVR-C/D		
P00558	Phosphoglycerate kinase 1					ND PVR-B	ND PVR-C/D		
P36955	Pigment epithelium-derived factor		↑	↑	↓		1.39	1.84	
P05155	Plasma protease C1 inhibitor						3.81	2.22	↑
Q8NCW6	Polypeptide N-acetylgalactosaminyltransferase 11						ND control	ND PVR-B	
Q9H0S4	Probable ATP-dependent RNA helicase DDX47						ND control	ND PVR-B	
P41222	Prostaglandin-H2 D-isomerase						2.00	2.42	↑
P02760	Protein AMBP					ND control		ND PVR-C/D	
Q5SWX8	Protein odr-4 homolog						ND control	ND PVR-B	
Q99497	Protein/nucleic acid deglycase DJ-1					ND PVR-B	ND PVR-C/D		
P14618	Pyruvate kinase PKM					-4.58			
P18433	Receptor-type tyrosine-protein phosphatase alpha					ND control		ND PVR-C/D	
Q9BSG5	Retbindin						ND control	ND PVR-B	
P02753	Retinol-binding protein 4		↑				ND control	ND PVR-B	
P02787	Serotransferrin		↑	↑					
Q9UIV8	Serpin B13						ND control	ND PVR-B	
P48594	Serpin B4						ND control	ND PVR-B	
P02768	Serum albumin		↑	↑	↓		2.28	2.15	
P02743	Serum amyloid P-component		↑	↑	↑				
Q9BX66	Sorbin and SH3 domain-containing protein 1						ND control	ND PVR-B	
Q9NRC6	Spectrin beta chain. non-erythrocytic 5						ND control	ND PVR-B	
P00441	Superoxide dismutase [Cu-Zn]					ND PVR-B	ND PVR-C/D		
Q5SRN2	Testis-expressed basic protein 1						ND control	ND PVR-B	
P46100	Transcriptional regulator ATRX						ND control	ND PVR-B	
Q8TDI8	Transmembrane channel-like protein 1						ND control	ND PVR-B	
P02766	Transthyretin		↑	↑	↓		2.36	1.93	
P60174	Triosephosphate isomerase					ND PVR-B	ND PVR-C/D		
A6NHL2	Tubulin alpha chain-like 3					ND PVR-B	ND PVR-C/D		
Q71U36	Tubulin alpha-1A chain					ND PVR-B	ND PVR-C/D		
P68363	Tubulin alpha-1B chain					ND PVR-B	ND PVR-C/D		
Q9BQE3	Tubulin alpha-1C chain					ND PVR-B	ND PVR-C/D		
P0DPH7	Tubulin alpha-3C chain					ND PVR-B	ND PVR-C/D		
P0DPH8	Tubulin alpha-3D chain					ND PVR-B	ND PVR-C/D		
Q6PEY2	Tubulin alpha-3E chain					ND PVR-B	ND PVR-C/D		
P68366	Tubulin alpha-4A chain					ND PVR-B	ND PVR-C/D		
Q9NY65	Tubulin alpha-8 chain					ND PVR-B	ND PVR-C/D		
P07437	Tubulin beta chain					ND control		ND PVR-C/D	
Q9H4B7	Tubulin beta-1 chain					ND PVR-B	ND PVR-C/D		
Q13885	Tubulin beta-2A chain					-3.06			
Q9BVA1	Tubulin beta-2B chain					ND control		ND PVR-C/D	
Q13509	Tubulin beta-3 chain					-3.00			
P04350	Tubulin beta-4A chain					ND PVR-B	ND PVR-C/D		
P68371	Tubulin beta-4B chain					-3.25			
Q9BUF5	Tubulin beta-6 chain					ND PVR-B	ND PVR-C/D		
Q3ZCM7	Tubulin beta-8 chain					ND PVR-B	ND PVR-C/D		
P01375	Tumor necrosis factor	ND control							
P50591	Tumor necrosis factor ligand superfamily member 10						ND control	ND PVR-B	
P15692	Vascular endothelial growth factor A	ND control							
Q9UL36	Zinc finger protein 236					ND control		ND PVR-C/D	
P25311	Zinc-alpha-2-glycoprotein		↑						

Table S1.3 – (continued)

		Wladis. *et. al.*.(2012)		Yu. *et. al.*.(2014)			Roybal. *et. al.*.*(2018)*				
Uniprot	**Description**	**log2 (PVR/Control)**	**log2 (PVR/RD)**	**PVR/control**	**PVR-C-D/PVR-B**	**log2 (PVR-C-D/PVR-B)**	**PVR-A-B/ERM**	**PVR-C/ERM**	**log2 (PVR-C/ERM)**	**log2 (PVR-C/PVR-A)**	**log2 (PVR-C/PVR-B)**
Q16627	C-C motif chemokine 14							↑			
O15467	C-C motif chemokine 16							↑			
P55773	C-C motif chemokine 23							↑			
Q9Y258	C-C motif chemokine 26						↑				
Q9Y4X3	C-C motif chemokine 27						↑				
Q9NRJ3	C-C motif chemokine 28						↑				
P10147	C-C motif chemokine 3	1.73	0.93					↑	2.018196211		
P13236	C-C motif chemokine 4								3.240654628		
P80075	C-C motif chemokine 8							↑			
Q9Y240	C-type lectin domain family 11 member A	0.65	1.51								
P02778	C-X-C motif chemokine 10	1.46	1.02					↑	1.714814819		
O14625	C-X-C motif chemokine 11						↑				
P42830	C-X-C motif chemokine 5						↑				
Q07325	C-X-C motif chemokine 9							↑			
O94907	Dickkopf-related protein 1							↑			
P09919	Granulocyte colony-stimulating factor	5.25	3.28					↑			
P04141	Granulocyte-macrophage colony-stimulating factor	-0.13	-0.73								
P17936	Insulin-like growth factor-binding protein 3									3.207754371	
P24592	Insulin-like growth factor-binding protein 6			ND control	↑	0.29					
P05362	Intercellular adhesion molecule 1								2.01477257		
P01579	Interferon gamma						↑				
Q8IU54	Interferon lambda-1						↑				
P35225	Interleukin-13						↑				
P40933	Interleukin-15	0.90	0.82								
Q16552	Interleukin-17A						↑				
Q96PD4	Interleukin-17F						↑				
P60568	Interleukin-2						↑				
Q6EBC2	Interleukin-31						↑				
P05112	Interleukin-4	0.51	0.31								
P05113	Interleukin-5	2.49	2.04								
P05231	Interleukin-6	4.53	2.07							1.784322393	2.150248752
P13232	Interleukin-7						↑				
P10145	Interleukin-8							↑			
P15248	Interleukin-9						↑				
P01042	Kininogen-1			ND control	↑	0.24					
P21583	Kit ligand	0.53	0.88								
P15018	Leukemia inhibitory factor						↑				
P47992	Lymphotactin						↑				
Q99733	Nucleosome assembly protein 1-like 4							↑			
P49763	Placenta growth factor								5.597713998		
P02776	Platelet factor 4							↑			
P48061	Stromal cell-derived factor 1							↑			
P15692	Vascular endothelial growth factor A								8.541237602		
P04004	Vitronectin			ND control	↑						

Table S2.1 - List of the differentially expressed proteins analyzed in STRING. AMD - Age-related macular degeneration; DR - Diabetic Retinopathy. nAMD - Neovascular age-related macular degeneration; N/D - Non-differential/Not detected; RD - Retinal Detachment; PDR - Proliferative Diabetic Retinopathy; PVR - Proliferative Vitreoretinopathy.

		DR/PDR			AMD		PVR/RD			
Uniprot	Protein name	DR or PDR/control	PDR/DR or diabetic	PDR/IVR	nAMD/control	dry AMD/control	PVR/control	RD/control	PVR-C/D/PVR-B/A	PVR/RD
P61981	14-3-3 protein gamma	1 ↑; 0 ↓	0 ↑; 0 ↓	0 ↑; 0 ↓	1 ↑; 0 ↓	0 ↑; 0 ↓	N/D	N/D	N/D	N/D
Q9UHI8	A disintegrin and metalloproteinase with thrombospondin motifs 1	1 ↑; 0 ↓	0 ↑; 0 ↓	0 ↑; 0 ↓	N/D	N/D	1 ↑; 0 ↓	0 ↑; 0 ↓	0 ↑; 1 ↓	0 ↑; 0 ↓
P63261	Actin. cytoplasmic 2	1 ↑; 0 ↓	0 ↑; 0 ↓	0 ↑; 0 ↓	0 ↑; 1 ↓	0 ↑; 0 ↓	0 ↑; 0 ↓	0 ↑; 0 ↓	0 ↑; 1 ↓	0 ↑; 0 ↓
P43652	Afamin	0 ↑; 0 ↓	1 ↑; 0 ↓	1 ↑; 0 ↓	1 ↑; 0 ↓	0 ↑; 0 ↓	N/D	N/D	N/D	N/D
P19652	Alpha-1-acid glycoprotein 2	2 ↑; 1 ↓	1 ↑; 0 ↓	0 ↑; 0 ↓	1 ↑; 0 ↓	0 ↑; 0 ↓	N/D	N/D	N/D	N/D
P01009	Alpha-1-antitrypsin	3 ↑; 2 ↓	1 ↑; 0 ↓	0 ↑; 0 ↓	1 ↑; 0 ↓	0 ↑; 0 ↓	2 ↑; 0 ↓	1 ↑; 0 ↓	1 ↑; 0 ↓	1 ↑; 0 ↓
P04217	Alpha-1B-glycoprotein	4 ↑; 1 ↓	1 ↑; 0 ↓	0 ↑; 0 ↓	N/D	N/D	1 ↑; 0 ↓	0 ↑; 0 ↓	1 ↑; 0 ↓	0 ↑; 0 ↓
P02765	Alpha-2-HS-glycoprotein	3 ↑; 0 ↓	1 ↑; 0 ↓	0 ↑; 0 ↓	N/D	N/D	1 ↑; 0 ↓	0 ↑; 0 ↓	2 ↑; 0 ↓	0 ↑; 0 ↓
P01023	Alpha-2-macroglobulin	1 ↑; 2 ↓	1 ↑; 0 ↓	0 ↑; 0 ↓	N/D	N/D	1 ↑; 0 ↓	0 ↑; 0 ↓	1 ↑; 0 ↓	0 ↑; 0 ↓
P06733	Alpha-enolase	0 ↑; 1 ↓	0 ↑; 0 ↓	0 ↑; 0 ↓	N/D	N/D	0 ↑; 1 ↓	0 ↑; 0 ↓	0 ↑; 0 ↓	0 ↑; 0 ↓
P05067	Amyloid-beta precursor protein	1 ↑; 2 ↓	0 ↑; 2 ↓	0 ↑; 0 ↓	N/D	N/D	1 ↑; 0 ↓	0 ↑; 0 ↓	0 ↑; 1 ↓	0 ↑; 0 ↓
Q06481	Amyloid-like protein 2	0 ↑; 4 ↓	0 ↑; 1 ↓	0 ↑; 0 ↓	N/D	N/D	1 ↑; 0 ↓	0 ↑; 0 ↓	0 ↑; 1 ↓	0 ↑; 0 ↓
P01019	Angiotensinogen	2 ↑; 0 ↓	2 ↑; 0 ↓	0 ↑; 0 ↓	N/D	N/D	1 ↑; 0 ↓	0 ↑; 0 ↓	1 ↑; 0 ↓	0 ↑; 0 ↓
P01008	Antithrombin-III	1 ↑; 2 ↓	1 ↑; 0 ↓	0 ↑; 0 ↓	1 ↑; 0 ↓	0 ↑; 0 ↓	2 ↑; 0 ↓	0 ↑; 0 ↓	0 ↑; 0 ↓	0 ↑; 0 ↓
P02647	Apolipoprotein A-I	6 ↑; 0 ↓	1 ↑; 1 ↓	0 ↑; 0 ↓	1 ↑; 0 ↓	0 ↑; 0 ↓	0 ↑; 0 ↓	0 ↑; 0 ↓	1 ↑; 0 ↓	0 ↑; 0 ↓
P06727	Apolipoprotein A-IV	3 ↑; 2 ↓	1 ↑; 0 ↓	0 ↑; 0 ↓	N/D	N/D	1 ↑; 0 ↓	1 ↑; 0 ↓	0 ↑; 0 ↓	1 ↑; 0 ↓
P02749	Beta-2-glycoprotein 1	3 ↑; 1 ↓	1 ↑; 0 ↓	1 ↑; 0 ↓	N/D	N/D	1 ↑; 0 ↓	0 ↑; 0 ↓	1 ↑; 0 ↓	0 ↑; 0 ↓
P61769	Beta-2-microglobulin	2 ↑; 0 ↓	0 ↑; 0 ↓	0 ↑; 0 ↓	1 ↑; 0 ↓	0 ↑; 0 ↓	N/D	N/D	N/D	N/D
O94985	Calsyntenin-1	0 ↑; 3 ↓	0 ↑; 1 ↓	0 ↑; 0 ↓	N/D	N/D	1 ↑; 0 ↓	0 ↑; 0 ↓	0 ↑; 1 ↓	0 ↑; 0 ↓
P07858	Cathepsin B	0 ↑; 1 ↓	0 ↑; 0 ↓	0 ↑; 0 ↓	1 ↑; 0 ↓	0 ↑; 0 ↓	N/D	N/D	N/D	N/D
P07339	Cathepsin D	1 ↑; 3 ↓	1 ↑; 0 ↓	0 ↑; 0 ↓	N/D	N/D	1 ↑; 0 ↓	1 ↑; 0 ↓	1 ↑; 0 ↓	0 ↑; 0 ↓
Q9UBR2	Cathepsin Z	0 ↑; 1 ↓	0 ↑; 0 ↓	0 ↑; 0 ↓	1 ↑; 0 ↓	0 ↑; 0 ↓	N/D	N/D	N/D	N/D
P13500	C-C motif chemokine 2	3 ↑; 0 ↓	0 ↑; 0 ↓	0 ↑; 0 ↓	N/D	N/D	1 ↑; 0 ↓	0 ↑; 0 ↓	0 ↑; 0 ↓	0 ↑; 0 ↓
P10147	C-C motif chemokine 3	1 ↑; 0 ↓	0 ↑; 0 ↓	0 ↑; 0 ↓	N/D	N/D	3 ↑; 0 ↓	0 ↑; 0 ↓	0 ↑; 0 ↓	1 ↑; 0 ↓
P13236	C-C motif chemokine 4	2 ↑; 0 ↓	0 ↑; 0 ↓	0 ↑; 0 ↓	N/D	N/D	1 ↑; 0 ↓	0 ↑; 0 ↓	0 ↑; 0 ↓	0 ↑; 0 ↓
P00450	Ceruloplasmin	3 ↑; 1 ↓	1 ↑; 0 ↓	1 ↑; 0 ↓	N/D	N/D	1 ↑; 0 ↓	0 ↑; 0 ↓	0 ↑; 0 ↓	0 ↑; 0 ↓
P36222	Chitinase-3-like protein 1	1 ↑; 0 ↓	0 ↑; 0 ↓	0 ↑; 0 ↓	1 ↑; 0 ↓	0 ↑; 0 ↓	1 ↑; 0 ↓	0 ↑; 0 ↓	1 ↑; 0 ↓	0 ↑; 0 ↓
P10909	Clusterin	0 ↑; 3 ↓	0 ↑; 0 ↓	0 ↑; 0 ↓	1 ↑; 0 ↓	0 ↑; 0 ↓	1 ↑; 0 ↓	1 ↑; 0 ↓	0 ↑; 0 ↓	0 ↑; 1 ↓
Q14050	Collagen alpha-3(IX) chain	0 ↑; 1 ↓	0 ↑; 0 ↓	0 ↑; 0 ↓	1 ↑; 0 ↓	0 ↑; 0 ↓	N/D	N/D	N/D	N/D
P01024	Complement C3	5 ↑; 1 ↓	1 ↑; 1 ↓	0 ↑; 0 ↓	N/D	N/D	1 ↑; 0 ↓	0 ↑; 0 ↓	1 ↑; 0 ↓	0 ↑; 0 ↓
P0C0L4	Complement C4-A	2 ↑; 2 ↓	0 ↑; 0 ↓	0 ↑; 0 ↓	N/D	N/D	0 ↑; 0 ↓	0 ↑; 0 ↓	1 ↑; 0 ↓	0 ↑; 0 ↓
P0C0L5	Complement C4-B	5 ↑; 1 ↓	1 ↑; 0 ↓	0 ↑; 0 ↓	N/D	N/D	0 ↑; 0 ↓	0 ↑; 0 ↓	2 ↑; 0 ↓	0 ↑; 0 ↓
P00751	Complement factor B	3 ↑; 0 ↓	1 ↑; 0 ↓	0 ↑; 0 ↓	N/D	N/D	0 ↑; 0 ↓	0 ↑; 0 ↓	2 ↑; 0 ↓	0 ↑; 0 ↓
Q03591	Complement factor H-related protein 1	0 ↑; 0 ↓	1 ↑; 0 ↓	0 ↑; 0 ↓	N/D	N/D	1 ↑; 0 ↓	0 ↑; 0 ↓	1 ↑; 0 ↓	0 ↑; 0 ↓
P02778	C-X-C motif chemokine 10	3 ↑; 0 ↓	0 ↑; 0 ↓	0 ↑; 0 ↓	N/D	N/D	2 ↑; 0 ↓	0 ↑; 0 ↓	0 ↑; 0 ↓	1 ↑; 0 ↓
P01034	Cystatin-C	0 ↑; 2 ↓	0 ↑; 1 ↓	0 ↑; 0 ↓	N/D	N/D	1 ↑; 0 ↓	0 ↑; 0 ↓	1 ↑; 0 ↓	0 ↑; 0 ↓
P13716	Delta-aminolevulinic acid dehydratase	1 ↑; 0 ↓	0 ↑; 0 ↓	0 ↑; 0 ↓	1 ↑; 0 ↓	0 ↑; 0 ↓	N/D	N/D	N/D	N/D
Q9UBP4	Dickkopf-related protein 3	1 ↑; 1 ↓	0 ↑; 0 ↓	1 ↑; 0 ↓	N/D	N/D	1 ↑; 0 ↓	0 ↑; 0 ↓	0 ↑; 1 ↓	0 ↑; 0 ↓
Q16555	Dihydropyrimidinase-related protein 2	0 ↑; 1 ↓	0 ↑; 0 ↓	0 ↑; 0 ↓	N/D	N/D	0 ↑; 1 ↓	0 ↑; 0 ↓	0 ↑; 0 ↓	0 ↑; 0 ↓
Q12805	EGF-containing fibulin-like extracellular matrix protein 1	1 ↑; 1 ↓	0 ↑; 0 ↓	0 ↑; 0 ↓	N/D	N/D	1 ↑; 0 ↓	0 ↑; 0 ↓	0 ↑; 1 ↓	0 ↑; 0 ↓
P51671	Eotaxin	1 ↑; 0 ↓	0 ↑; 0 ↓	0 ↑; 0 ↓	N/D	N/D	1 ↑; 0 ↓	0 ↑; 0 ↓	0 ↑; 0 ↓	0 ↑; 0 ↓
O15372	Eukaryotic translation initiation factor 3 subunit H	0 ↑; 0 ↓	1 ↑; 0 ↓	1 ↑; 0 ↓	N/D	N/D	1 ↑; 0 ↓	0 ↑; 0 ↓	1 ↑; 0 ↓	0 ↑; 0 ↓
P08294	Extracellular superoxide dismutase [Cu-Zn]	0 ↑; 0 ↓	0 ↑; 1 ↓	0 ↑; 0 ↓	N/D	N/D	1 ↑; 0 ↓	0 ↑; 0 ↓	1 ↑; 0 ↓	0 ↑; 0 ↓
P02794	Ferritin heavy chain	0 ↑; 0 ↓	0 ↑; 0 ↓	0 ↑; 1 ↓	1 ↑; 0 ↓	0 ↑; 0 ↓	N/D	N/D	N/D	N/D

P02671	Fibrinogen alpha chain	5 ↑; 0 ↓	1 ↑; 0 ↓	1 ↑; 0 ↓	1 ↑; 0 ↓	0 ↑; 0 ↓	N/D	N/D	N/D	N/D
P02751	Fibronectin	0 ↑; 0 ↓	1 ↑; 0 ↓	0 ↑; 0 ↓	0 ↑; 1 ↓	0 ↑; 0 ↓	N/D	N/D	N/D	N/D
P04075	Fructose-bisphosphate aldolase A	1 ↑; 0 ↓	0 ↑; 0 ↓	0 ↑; 1 ↓	0 ↑; 1 ↓	0 ↑; 0 ↓	N/D	N/D	N/D	N/D
P09972	Fructose-bisphosphate aldolase C	0 ↑; 1 ↓	0 ↑; 1 ↓	0 ↑; 0 ↓	1 ↑; 0 ↓	0 ↑; 0 ↓	0 ↑; 1 ↓	0 ↑; 0 ↓	0 ↑; 0 ↓	0 ↑; 0 ↓
Q08380	Galectin-3-binding protein	0 ↑; 1 ↓	0 ↑; 0 ↓	0 ↑; 0 ↓	N/D	N/D	1 ↑; 0 ↓	0 ↑; 0 ↓	1 ↑; 0 ↓	0 ↑; 0 ↓
P09104	Gamma-enolase	2 ↑; 2 ↓	0 ↑; 0 ↓	0 ↑; 0 ↓	N/D	N/D	0 ↑; 1 ↓	0 ↑; 0 ↓	0 ↑; 0 ↓	0 ↑; 0 ↓
P17900	Ganglioside GM2 activator	0 ↑; 1 ↓	0 ↑; 0 ↓	0 ↑; 0 ↓	0 ↑; 1 ↓	0 ↑; 0 ↓	N/D	N/D	N/D	N/D
P14314	Glucosidase 2 subunit beta	0 ↑; 1 ↓	0 ↑; 0 ↓	0 ↑; 0 ↓	1 ↑; 0 ↓	0 ↑; 0 ↓	N/D	N/D	N/D	N/D
P22352	Glutathione peroxidase 3	0 ↑; 1 ↓	0 ↑; 0 ↓	0 ↑; 0 ↓	1 ↑; 0 ↓	0 ↑; 0 ↓	1 ↑; 0 ↓	0 ↑; 0 ↓	1 ↑; 0 ↓	0 ↑; 0 ↓
P04406	Glyceraldehyde-3-phosphate dehydrogenase	1 ↑; 1 ↓	0 ↑; 0 ↓	0 ↑; 0 ↓	N/D	N/D	0 ↑; 1 ↓	0 ↑; 0 ↓	0 ↑; 0 ↓	0 ↑; 0 ↓
P09919	Granulocyte colony-stimulating factor	1 ↑; 0 ↓	0 ↑; 0 ↓	0 ↑; 0 ↓	N/D	N/D	3 ↑; 0 ↓	0 ↑; 0 ↓	0 ↑; 0 ↓	1 ↑; 0 ↓
P00738	Haptoglobin	1 ↑; 0 ↓	0 ↑; 0 ↓	1 ↑; 0 ↓	1 ↑; 0 ↓	0 ↑; 0 ↓	1 ↑; 0 ↓	0 ↑; 0 ↓	1 ↑; 0 ↓	0 ↑; 0 ↓
P69905	Hemoglobin subunit alpha	2 ↑; 1 ↓	0 ↑; 0 ↓	0 ↑; 1 ↓	N/D	N/D	1 ↑; 0 ↓	0 ↑; 0 ↓	1 ↑; 0 ↓	0 ↑; 0 ↓
P68871	Hemoglobin subunit beta	3 ↑; 0 ↓	0 ↑; 0 ↓	0 ↑; 1 ↓	1 ↑; 0 ↓	0 ↑; 0 ↓	1 ↑; 0 ↓	0 ↑; 0 ↓	0 ↑; 1 ↓	0 ↑; 0 ↓
P02790	Hemopexin	1 ↑; 1 ↓	0 ↑; 0 ↓	0 ↑; 0 ↓	N/D	N/D	1 ↑; 0 ↓	0 ↑; 0 ↓	1 ↑; 0 ↓	0 ↑; 0 ↓
P05546	Heparin cofactor 2	1 ↑; 0 ↓	1 ↑; 0 ↓	0 ↑; 0 ↓	N/D	N/D	1 ↑; 0 ↓	0 ↑; 0 ↓	1 ↑; 0 ↓	0 ↑; 0 ↓
P04196	Histidine-rich glycoprotein	3 ↑; 2 ↓	0 ↑; 0 ↓	0 ↑; 0 ↓	1 ↑; 0 ↓	0 ↑; 0 ↓	0 ↑; 0 ↓	0 ↑; 0 ↓	1 ↑; 0 ↓	0 ↑; 0 ↓
P01876	Immunoglobulin heavy constant alpha 1	3 ↑; 0 ↓	1 ↑; 0 ↓	1 ↑; 0 ↓	1 ↑; 0 ↓	0 ↑; 0 ↓	N/D	N/D	N/D	N/D
P01857	Immunoglobulin heavy constant gamma 1	3 ↑; 0 ↓	0 ↑; 0 ↓	0 ↑; 0 ↓	1 ↑; 0 ↓	0 ↑; 0 ↓	N/D	N/D	N/D	N/D
P01859	Immunoglobulin heavy constant gamma 2	1 ↑; 0 ↓	1 ↑; 0 ↓	0 ↑; 0 ↓	0 ↑; 1 ↓	0 ↑; 0 ↓	N/D	N/D	N/D	N/D
P0DOY2	Immunoglobulin lambda constant 2	0 ↑; 1 ↓	0 ↑; 0 ↓	0 ↑; 0 ↓	N/D	N/D	N/D	N/D	N/D	N/D
P17936	Insulin-like growth factor-binding protein 3	1 ↑; 0 ↓	0 ↑; 0 ↓	0 ↑; 0 ↓	N/D	N/D	0 ↑; 0 ↓	0 ↑; 0 ↓	1 ↑; 0 ↓	0 ↑; 0 ↓
P24592	Insulin-like growth factor-binding protein 6	0 ↑; 1 ↓	0 ↑; 0 ↓	0 ↑; 0 ↓	N/D	N/D	1 ↑; 0 ↓	0 ↑; 0 ↓	1 ↑; 0 ↓	0 ↑; 0 ↓
P19827	Inter-alpha-trypsin inhibitor heavy chain H1	0 ↑; 0 ↓	1 ↑; 0 ↓	0 ↑; 0 ↓	1 ↑; 0 ↓	0 ↑; 0 ↓	N/D	N/D	N/D	N/D
P19823	Inter-alpha-trypsin inhibitor heavy chain H2	0 ↑; 2 ↓	1 ↑; 0 ↓	0 ↑; 0 ↓	N/D	N/D	1 ↑; 0 ↓	0 ↑; 0 ↓	1 ↑; 0 ↓	0 ↑; 0 ↓
P05362	Intercellular adhesion molecule 1	3 ↑; 0 ↓	0 ↑; 0 ↓	0 ↑; 0 ↓	0 ↑; 1 ↓	0 ↑; 0 ↓	1 ↑; 0 ↓	0 ↑; 0 ↓	0 ↑; 0 ↓	0 ↑; 0 ↓
P01579	Interferon gamma	2 ↑; 0 ↓	0 ↑; 0 ↓	0 ↑; 0 ↓	N/D	N/D	2 ↑; 0 ↓	0 ↑; 0 ↓	0 ↑; 0 ↓	0 ↑; 0 ↓
P22301	Interleukin-10	3 ↑; 0 ↓	0 ↑; 0 ↓	0 ↑; 0 ↓	N/D	N/D	1 ↑; 0 ↓	0 ↑; 0 ↓	0 ↑; 0 ↓	0 ↑; 0 ↓
P29460	Interleukin-12 subunit beta	1 ↑; 0 ↓	0 ↑; 0 ↓	0 ↑; 0 ↓	N/D	N/D	1 ↑; 0 ↓	0 ↑; 0 ↓	0 ↑; 0 ↓	0 ↑; 0 ↓
P35225	Interleukin-13	2 ↑; 0 ↓	0 ↑; 0 ↓	0 ↑; 0 ↓	N/D	N/D	1 ↑; 0 ↓	0 ↑; 0 ↓	0 ↑; 0 ↓	0 ↑; 0 ↓
P40933	Interleukin-15	1 ↑; 0 ↓	0 ↑; 0 ↓	0 ↑; 0 ↓	N/D	N/D	1 ↑; 0 ↓	0 ↑; 0 ↓	0 ↑; 0 ↓	1 ↑; 0 ↓
Q16552	Interleukin-17A	1 ↑; 0 ↓	0 ↑; 0 ↓	0 ↑; 0 ↓	N/D	N/D	1 ↑; 0 ↓	0 ↑; 0 ↓	0 ↑; 0 ↓	0 ↑; 0 ↓
P60568	Interleukin-2	1 ↑; 0 ↓	0 ↑; 0 ↓	0 ↑; 0 ↓	N/D	N/D	1 ↑; 0 ↓	0 ↑; 0 ↓	0 ↑; 0 ↓	0 ↑; 0 ↓
P05112	Interleukin-4	1 ↑; 0 ↓	0 ↑; 0 ↓	0 ↑; 0 ↓	N/D	N/D	1 ↑; 0 ↓	0 ↑; 0 ↓	0 ↑; 0 ↓	1 ↑; 0 ↓
P05113	Interleukin-5	1 ↑; 0 ↓	0 ↑; 0 ↓	0 ↑; 0 ↓	N/D	N/D	1 ↑; 0 ↓	0 ↑; 0 ↓	0 ↑; 0 ↓	1 ↑; 0 ↓
P05231	Interleukin-6	3 ↑; 0 ↓	0 ↑; 0 ↓	0 ↑; 0 ↓	N/D	N/D	2 ↑; 0 ↓	0 ↑; 0 ↓	2 ↑; 0 ↓	1 ↑; 0 ↓
P13232	Interleukin-7	1 ↑; 0 ↓	0 ↑; 0 ↓	0 ↑; 0 ↓	N/D	N/D	1 ↑; 0 ↓	0 ↑; 0 ↓	0 ↑; 0 ↓	0 ↑; 0 ↓
P10145	Interleukin-8	3 ↑; 0 ↓	0 ↑; 0 ↓	0 ↑; 0 ↓	N/D	N/D	2 ↑; 0 ↓	0 ↑; 0 ↓	0 ↑; 0 ↓	0 ↑; 0 ↓
P15248	Interleukin-9	1 ↑; 0 ↓	0 ↑; 0 ↓	0 ↑; 0 ↓	N/D	N/D	1 ↑; 0 ↓	0 ↑; 0 ↓	0 ↑; 0 ↓	0 ↑; 0 ↓
P01042	Kininogen-1	3 ↑; 1 ↓	1 ↑; 0 ↓	0 ↑; 0 ↓	N/D	N/D	1 ↑; 0 ↓	0 ↑; 0 ↓	1 ↑; 0 ↓	0 ↑; 0 ↓
P05451	Lithostathine-1-alpha	1 ↑; 0 ↓	0 ↑; 0 ↓	0 ↑; 0 ↓	0 ↑; 1 ↓	0 ↑; 0 ↓	N/D	N/D	N/D	N/D
P51884	Lumican	1 ↑; 0 ↓	1 ↑; 0 ↓	1 ↑; 0 ↓	N/D	N/D	1 ↑; 0 ↓	0 ↑; 0 ↓	0 ↑; 1 ↓	0 ↑; 0 ↓
P10619	Lysosomal protective protein	0 ↑; 1 ↓	0 ↑; 0 ↓	0 ↑; 0 ↓	0 ↑; 1 ↓	0 ↑; 0 ↓	N/D	N/D	N/D	N/D
P08571	Monocyte differentiation antigen CD14	2 ↑; 0 ↓	1 ↑; 0 ↓	0 ↑; 0 ↓	N/D	N/D	1 ↑; 0 ↓	0 ↑; 0 ↓	1 ↑; 0 ↓	0 ↑; 0 ↓
Q96PD5	N-acetylmuramoyl-L-alanine amidase	1 ↑; 0 ↓	1 ↑; 0 ↓	0 ↑; 0 ↓	N/D	N/D	1 ↑; 0 ↓	0 ↑; 0 ↓	1 ↑; 0 ↓	0 ↑; 0 ↓
O15240	Neurosecretory protein VGF	0 ↑; 2 ↓	0 ↑; 0 ↓	0 ↑; 0 ↓	0 ↑; 1 ↓	0 ↑; 0 ↓	N/D	N/D	N/D	N/D
P61916	NPC intracellular cholesterol transporter 2	1 ↑; 0 ↓	0 ↑; 0 ↓	1 ↑; 0 ↓	1 ↑; 0 ↓	0 ↑; 0 ↓	N/D	N/D	N/D	N/D
Q9UBM4	Opticin	0 ↑; 3 ↓	0 ↑; 0 ↓	0 ↑; 0 ↓	0 ↑; 1 ↓	0 ↑; 0 ↓	0 ↑; 1 ↓	0 ↑; 0 ↓	0 ↑; 1 ↓	0 ↑; 0 ↓
Q06830	Peroxiredoxin-1	1 ↑; 0 ↓	0 ↑; 0 ↓	0 ↑; 0 ↓	N/D	N/D	0 ↑; 1 ↓	0 ↑; 0 ↓	0 ↑; 0 ↓	0 ↑; 0 ↓
P32119	Peroxiredoxin-2	0 ↑; 0 ↓	1 ↑; 0 ↓	0 ↑; 0 ↓	N/D	N/D	0 ↑; 1 ↓	0 ↑; 0 ↓	0 ↑; 0 ↓	0 ↑; 0 ↓
P30086	Phosphatidylethanolamine-binding protein 1	0 ↑; 1 ↓	0 ↑; 0 ↓	0 ↑; 1 ↓	1 ↑; 0 ↓	0 ↑; 0 ↓	N/D	N/D	N/D	N/D
P00558	Phosphoglycerate kinase 1	0 ↑; 1 ↓	1 ↑; 0 ↓	0 ↑; 0 ↓	N/D	N/D	0 ↑; 1 ↓	0 ↑; 0 ↓	0 ↑; 0 ↓	0 ↑; 0 ↓
P36955	Pigment epithelium-derived factor	2 ↑; 5 ↓	0 ↑; 0 ↓	0 ↑; 0 ↓	2 ↑; 1 ↓	0 ↑; 0 ↓	2 ↑; 0 ↓	1 ↑; 0 ↓	1 ↑; 0 ↓	0 ↑; 1 ↓
P49763	Placenta growth factor	2 ↑; 0 ↓	0 ↑; 0 ↓	0 ↑; 0 ↓	N/D	N/D	1 ↑; 0 ↓	0 ↑; 0 ↓	0 ↑; 0 ↓	0 ↑; 0 ↓
P05155	Plasma protease C1 inhibitor	0 ↑; 2 ↓	1 ↑; 0 ↓	0 ↑; 0 ↓	N/D	N/D	1 ↑; 0 ↓	0 ↑; 0 ↓	2 ↑; 0 ↓	0 ↑; 0 ↓

P07602	Prosaposin	0 ↑; 1 ↓	0 ↑; 0 ↓	0 ↑; 0 ↓	1 ↑; 0 ↓	0 ↑; 0 ↓	N/D	N/D	N/D	N/D
P41222	Prostaglandin-H2 D-isomerase	1 ↑; 2 ↓	0 ↑; 0 ↓	0 ↑; 0 ↓	2 ↑; 0 ↓	0 ↑; 0 ↓	1 ↑; 0 ↓	0 ↑; 0 ↓	2 ↑; 0 ↓	0 ↑; 0 ↓
P02760	Protein AMBP	4 ↑; 0 ↓	1 ↑; 0 ↓	0 ↑; 0 ↓	N/D	N/D	1 ↑; 0 ↓	0 ↑; 0 ↓	0 ↑; 1 ↓	0 ↑; 0 ↓
Q99497	Protein/nucleic acid deglycase DJ-1	1 ↑; 1 ↓	0 ↑; 0 ↓	0 ↑; 0 ↓	1 ↑; 0 ↓	0 ↑; 0 ↓	0 ↑; 1 ↓	0 ↑; 0 ↓	0 ↑; 0 ↓	0 ↑; 0 ↓
P14618	Pyruvate kinase PKM	0 ↑; 1 ↓	0 ↑; 0 ↓	0 ↑; 0 ↓	N/D	N/D	0 ↑; 1 ↓	0 ↑; 0 ↓	0 ↑; 0 ↓	0 ↑; 0 ↓
Q9BSG5	Retbindin	1 ↑; 1 ↓	0 ↑; 0 ↓	0 ↑; 0 ↓	N/D	N/D	1 ↑; 0 ↓	0 ↑; 0 ↓	1 ↑; 0 ↓	0 ↑; 0 ↓
P00352	Retinal dehydrogenase 1	1 ↑; 0 ↓	0 ↑; 0 ↓	0 ↑; 0 ↓	1 ↑; 0 ↓	0 ↑; 0 ↓	N/D	N/D	N/D	N/D
P10745	Retinol-binding protein 3	0 ↑; 4 ↓	0 ↑; 1 ↓	0 ↑; 0 ↓	1 ↑; 0 ↓	0 ↑; 0 ↓	N/D	N/D	N/D	N/D
P02753	Retinol-binding protein 4	2 ↑; 0 ↓	0 ↑; 0 ↓	0 ↑; 0 ↓	N/D	N/D	2 ↑; 0 ↓	0 ↑; 0 ↓	1 ↑; 0 ↓	0 ↑; 0 ↓
P34096	Ribonuclease 4	1 ↑; 0 ↓	0 ↑; 0 ↓	0 ↑; 0 ↓	0 ↑; 1 ↓	0 ↑; 0 ↓	N/D	N/D	N/D	N/D
P07998	Ribonuclease pancreatic	1 ↑; 0 ↓	0 ↑; 0 ↓	0 ↑; 0 ↓	2 ↑; 0 ↓	0 ↑; 0 ↓	N/D	N/D	N/D	N/D
Q86VB7	Scavenger receptor cysteine-rich type 1 protein M130	1 ↑; 0 ↓	0 ↑; 0 ↓	0 ↑; 0 ↓	0 ↑; 1 ↓	0 ↑; 0 ↓	N/D	N/D	N/D	N/D
P02787	Serotransferrin	1 ↑; 2 ↓	0 ↑; 0 ↓	0 ↑; 0 ↓	1 ↑; 0 ↓	0 ↑; 0 ↓	1 ↑; 0 ↓	1 ↑; 0 ↓	0 ↑; 0 ↓	0 ↑; 0 ↓
P02768	Serum albumin	2 ↑; 2 ↓	1 ↑; 0 ↓	0 ↑; 0 ↓	1 ↑; 0 ↓	0 ↑; 0 ↓	2 ↑; 0 ↓	1 ↑; 0 ↓	1 ↑; 0 ↓	0 ↑; 1 ↓
P02743	Serum amyloid P-component	0 ↑; 0 ↓	1 ↑; 0 ↓	0 ↑; 0 ↓	N/D	N/D	1 ↑; 0 ↓	1 ↑; 0 ↓	0 ↑; 0 ↓	1 ↑; 0 ↓
Q9NRC6	Spectrin beta chain. non-erythrocytic 5	0 ↑; 1 ↓	0 ↑; 0 ↓	0 ↑; 0 ↓	N/D	N/D	1 ↑; 0 ↓	0 ↑; 0 ↓	1 ↑; 0 ↓	0 ↑; 0 ↓
Q9HCB6	Spondin-1	0 ↑; 1 ↓	0 ↑; 0 ↓	0 ↑; 0 ↓	1 ↑; 0 ↓	0 ↑; 0 ↓	N/D	N/D	N/D	N/D
P00441	Superoxide dismutase [Cu-Zn]	1 ↑; 0 ↓	0 ↑; 0 ↓	1 ↑; 0 ↓	1 ↑; 0 ↓	0 ↑; 0 ↓	0 ↑; 1 ↓	0 ↑; 0 ↓	0 ↑; 0 ↓	0 ↑; 0 ↓
Q9BQ16	Testican-3	0 ↑; 1 ↓	0 ↑; 0 ↓	0 ↑; 0 ↓	0 ↑; 1 ↓	0 ↑; 0 ↓	N/D	N/D	N/D	N/D
P02766	Transthyretin	1 ↑; 2 ↓	0 ↑; 0 ↓	0 ↑; 0 ↓	1 ↑; 0 ↓	0 ↑; 0 ↓	2 ↑; 0 ↓	1 ↑; 0 ↓	1 ↑; 0 ↓	0 ↑; 1 ↓
P60174	Triosephosphate isomerase	0 ↑; 0 ↓	0 ↑; 0 ↓	0 ↑; 1 ↓	N/D	N/D	0 ↑; 1 ↓	0 ↑; 0 ↓	0 ↑; 0 ↓	0 ↑; 0 ↓
P68363	Tubulin alpha-1B chain	1 ↑; 0 ↓	0 ↑; 0 ↓	0 ↑; 0 ↓	N/D	N/D	0 ↑; 1 ↓	0 ↑; 0 ↓	0 ↑; 0 ↓	0 ↑; 0 ↓
Q9BQE3	Tubulin alpha-1C chain	0 ↑; 1 ↓	0 ↑; 0 ↓	0 ↑; 0 ↓	N/D	N/D	0 ↑; 1 ↓	0 ↑; 0 ↓	0 ↑; 0 ↓	0 ↑; 0 ↓
P0DPH7	Tubulin alpha-3C chain	0 ↑; 1 ↓	0 ↑; 0 ↓	0 ↑; 0 ↓	N/D	N/D	0 ↑; 1 ↓	0 ↑; 0 ↓	0 ↑; 0 ↓	0 ↑; 0 ↓
P68366	Tubulin alpha-4A chain	0 ↑; 1 ↓	0 ↑; 0 ↓	0 ↑; 0 ↓	N/D	N/D	0 ↑; 1 ↓	0 ↑; 0 ↓	0 ↑; 0 ↓	0 ↑; 0 ↓
P07437	Tubulin beta chain	0 ↑; 1 ↓	0 ↑; 0 ↓	0 ↑; 0 ↓	N/D	N/D	1 ↑; 0 ↓	0 ↑; 0 ↓	0 ↑; 1 ↓	0 ↑; 0 ↓
Q9H4B7	Tubulin beta-1 chain	0 ↑; 1 ↓	0 ↑; 0 ↓	0 ↑; 0 ↓	N/D	N/D	0 ↑; 1 ↓	0 ↑; 0 ↓	0 ↑; 0 ↓	0 ↑; 0 ↓
Q13509	Tubulin beta-3 chain	0 ↑; 1 ↓	0 ↑; 0 ↓	0 ↑; 0 ↓	N/D	N/D	0 ↑; 1 ↓	0 ↑; 0 ↓	0 ↑; 0 ↓	0 ↑; 0 ↓
P01375	Tumor necrosis factor	1 ↑; 0 ↓	0 ↑; 0 ↓	0 ↑; 0 ↓	N/D	N/D	1 ↑; 0 ↓	0 ↑; 0 ↓	0 ↑; 0 ↓	0 ↑; 0 ↓
P15692	Vascular endothelial growth factor A	7 ↑; 0 ↓	0 ↑; 0 ↓	1 ↑; 0 ↓	N/D	N/D	1 ↑; 0 ↓	0 ↑; 0 ↓	0 ↑; 0 ↓	0 ↑; 0 ↓
P04004	Vitronectin	2 ↑; 0 ↓	1 ↑; 0 ↓	0 ↑; 0 ↓	N/D	N/D	1 ↑; 0 ↓	0 ↑; 0 ↓	1 ↑; 0 ↓	0 ↑; 0 ↓
P25311	Zinc-alpha-2-glycoprotein	7 ↑; 0 ↓	0 ↑; 0 ↓	0 ↑; 0 ↓	N/D	N/D	1 ↑; 0 ↓	0 ↑; 0 ↓	0 ↑; 0 ↓	0 ↑; 0 ↓

Appendix II - Supplementary material of the Paper III[1]

Table S1 - List of experiments performed to improving the protein recovery and solubilization from vitreous proteins based on CCD and ANN modeling.

Number of experiment	Recovery per experiment (%)	Standard deviation (%)	Recovery per buffer (%)	Standard deviation (%)	Input (4 factors) CHAPS (% m/v)	Genapol (% v/v)	DTT (mM)	IPG buffer (% v/v)
1	81.0	7.64	80.1	5.9	0	0	20	0.5
2	76.6	6.93			0	0	20	0.5
3	84.8	8.66			0	0	20	0.5
4	84.5	5.40	81.9	14.3	0	0.1	40	1
5	58.6	2.10			0	0.1	40	1
6	94.6	9.80			0	0.1	40	1
7	68.9	2.80	72.7	5.4	0	0.2	60	2
8	70.6	1.95			0	0.2	60	2
9	77.5	5.72			0	0.2	60	2
10	87.5	4.90	90.0	5.3	2	0	40	2
11	86.4	6.58			2	0	40	2
12	94.9	1.84			2	0	40	2
13	91.0	3.97	87.1	4.8	2	0.1	60	0.5
14	87.4	3.03			2	0.1	60	0.5
15	83.0	4.74			2	0.1	60	0.5
16	82.8	5.84	81.7	7.0	2	0.2	20	1
17	88.0	2.23			2	0.2	20	1
18	74.3	3.64			2	0.2	20	1
19	86.2	5.82	84.5	10.0	4	0	60	1
20	74.7	6.74			4	0	60	1
21	92.5	5.24			4	0	60	1
22	96.6	4.83	94.9	4.5	4	0.1	20	2
23	91.2	1.79			4	0.1	20	2
24	97.9	2.79			4	0.1	20	2
25	86.6	6.68	86.3	5.4	4	0.2	40	0.5
26	90.2	3.78			4	0.2	40	0.5
27	84.1	3.46			4	0.2	40	0.5
28	74.5	5.22	84.4	11.7	2	0.1	40	1
29	90.3	8.66			2	0.1	40	1
30	93.2	6.21			2	0.1	40	1
31	85.0	22.06	83.2	12.0	4	0.2	60	0.5
32	78.0	9.31			4	0.2	60	0.5

[1] Due to the high amount of supplementary information available in Paper III. only the more relevant part is available in this thesis.

The complete supplementary material of this article is available in (https://doi.org/10.1007/s00216-019-01887-y).

Table S2 - List of experiments performed to maximize the number of protein spots detected in the analysis of vitreous by 2DE electrophoresis based on CCD and ANN modeling. Input variables are represented by the corresponding coded levels. The predicted values for the number of protein spots detected in 2DE gels are those obtained in the last optimization iteration.

	Inputs						Number of spots		Improvement in the response (comparison with optimal inputs)	
Experiment	CHAPS (% m/v)	Genapol (% m/v)	DTT (mM)	IPG buffer (% v/v)	Voltage hour (KVh)	Temperature (ºC)	Observed (average)	Predicted by the ANN model	Percentage (%)	Increase fold
1	0	0	20	0.5	35	15	233	227	155.0	2.5
2	0	0	20	0.5	40	20	228	210	176.2	2.8
3	0	0	20	0.5	45	25	194	197	194.7	2.9
4	0	0.1	40	1	35	15	242	241	140.5	2.4
5	0	0.1	40	1	40	20	323	324	79.2	1.8
6	0	0.1	40	1	45	25	324	324	79.2	1.8
7	0	0.2	60	2	35	15	221	218	166.3	2.7
8	0	0.2	60	2	40	20	226	201	188.1	2.9
9	0	0.2	60	2	45	25	216	212	173.7	2.7
10	2	0	40	2	35	20	220	186	212.1	3.1
11	2	0	40	2	40	25	135	180	221.4	3.2
12	2	0	40	2	45	15	174	173	235.3	3.4
13	2	0.1	60	0.5	35	20	329	343	69.1	1.7
14	2	0.1	60	0.5	40	25	314	296	96.1	2.0
15	2	0.1	60	0.5	45	15	201	199	190.8	2.9
16	2	0.2	20	1	35	20	223	239	142.5	2.4
17	2	0.2	20	1	40	25	234	230	151.9	2.5
18	2	0.2	20	1	45	15	256	272	113.4	2.1
19	4	0	60	1	35	25	191	178	225.7	3.3
20	4	0	60	1	40	15	283	279	107.6	2.1
21	4	0	60	1	45	20	238	247	134.7	2.3
22	4	0.1	20	2	35	25	312	313	85.1	1.9
23	4	0.1	20	2	40	15	215	201	188.8	2.9
24	4	0.1	20	2	45	20	163	172	237.7	3.4
25	4	0.2	40	0.5	35	25	514	480	20.7	1.2
26	4	0.2	40	0.5	40	15	248	270	114.9	2.1
27	4	0.2	40	0.5	45	20	367	267	117.3	2.2
28	2	0.1	40	1	40	20	395	351	65.1	1.7
29	2	0.1	40	1	40	20	306	351	65.1	1.7
30	2	0.1	40	1	40	20	166	351	65.1	1.7
B1	4	0.2	44	0.5	35	25	354			
B2	0	0.2	44	0.5	35	25	390			
B3	4	0.2	48	0.5	35	25	431			
B4	0	0.2	40	0.5	35	25	372			
C1	4	0.2	60	0.8	35	20	246			
C9	4	0.2	20	0.5	44.5	25	264			
31	4	0.2	60	0.5	35	20	308	310	87.2	1.9
32	4	0.2	60	0.5	35	25	584	580		

Appendix III - Supplementary material of the Paper IV[1]

Table S3 - Proteins found differentially expressed, which were identified in technical replicate 1 and 2 with an FDR of 1% at peptide level. FDR and p-value displayed in table are related to quantification analysis using iTRAQ labeling and not to protein identification. Proteins highlighted in gray, red, and green correspond, respectively, to non-differentially expressed, underexpressed, and overexpressed proteins in RRD (116) when compared with MEM control samples (114).

Uniprot Access	Description	Prot score	Coverage	116vs114	Log2 ratio	p-value	FDR
P20941	Phosducin	46.77	5.3	221.22	5.84	0	0
P14550	Alcohol dehydrogenase [NADP(+)]	66.54	11.1	173.64	4.67	0	0
P08100	Rhodopsin	432.23	11.1	23.65	4.54	0	0
P10523	S-arrestin	1469.05	30.5	16.03	4.00	0	0
P18545	Retinal rod rhodopsin-sensitive cGMP 3~.5~-cyclic phosphodiesterase subunit gamma	31.72	10.3	15.61	3.86	0	0
P11488	Guanine nucleotide-binding protein G(t) subunit alpha-1	62.23	4.3	15.14	3.92	0	0
Q9UHI8	A disintegrin and metalloproteinase with thrombospondin motifs 1	187.64	2.2	14.09	2.82	0	0
O00560	Syntenin-1	496.08	20.1	14.01	3.79	0	0
P11166	Solute carrier family 2. facilitated glucose transporter member 1	49.04	5.1	13.12	3.71	0	0
Q17R60	Interphotoreceptor matrix proteoglycan 1	1107.5	9.5	11.12	3.47	0	0
O43490	Prominin-1	303.56	5.42	10.76	3.41	0	0
P69905	Hemoglobin subunit alpha	416.77	24.1	10.53	3.27	0	0
P51674	Neuronal membrane glycoprotein M6-a	132.63	7.6	9.06	3.17	6.21725E-15	1.24898E-13
P62873	Guanine nucleotide-binding protein G(I)/G(S)/G(T) subunit beta-1	332.03	11.2	8.58	3.06	2.66454E-15	5.47441E-14
P12277	Creatine kinase B-type	415.31	12.7	8.58	3.09	1.17684E-14	2.57314E-13
Q9BZV3	Interphotoreceptor matrix proteoglycan 2	302.27	4.0	8.45	3.06	1.68754E-14	3.31638E-13
P16499	Rod cGMP-specific 3~.5~-cyclic phosphodiesterase subunit alpha	242.94	2.8	8.27	3.05	2.84661E-13	6.06029E-12
P43320	Beta-crystallin B2	775.32	37.4	7.08	2.82	2.96174E-11	5.32455E-10
P62979	Ubiquitin-40S ribosomal protein S27a	246.95	10.3	6.90	2.78	8.18146E-12	1.5759E-10
P68871	Hemoglobin subunit beta	343.01	32.3	6.81	2.75	4.83191E-12	8.5648E-11
P09104	Gamma-enolase	720.34	14.4	6.48	2.68	2.25324E-11	3.63738E-10
P02489	Alpha-crystallin A chain	122.31	27.7	6.35	2.64	4.7915E-12	9.45445E-11
P31025	Lipocalin-1	192.19	16.05	6.18	2.63	5.75596E-10	8.78599E-09
P07900	Heat shock protein HSP 90-alpha	413.73	5.6	6.17	2.50	5.73763E-13	1.05853E-11
P02511	Alpha-crystallin B chain	107.78	22.3	5.65	2.44	8.473E-12	1.59411E-10
P02042	Hemoglobin subunit delta	173.16	23.8	5.59	2.38	1.18925E-11	1.99089E-10
P09467	Fructose-1.6-bisphosphatase 1GN=FBP1	55.42	4.7	5.31	2.36	7.33478E-11	1.18677E-09
P63104	14-3-3 protein zeta/delta	455.32	10.52	5.13	2.29	6.42153E-11	1.10532E-09
Q12931	Heat shock protein 75 kDa. mitochondrial	87.08	2	5.03	2.07	6.7184E-12	1.16797E-10
P18669	Phosphoglycerate mutase 1	309.92	16.575	5.00	2.31	2.52214E-09	3.51795E-08
P09455	Retinol-binding protein 1	50.09	8.9	4.68	2.23	1.58033E-07	1.80068E-06
P36222	Chitinase-3-like protein 1	1471.73	27.1	4.64	2.21	1.07036E-07	1.40232E-06
Q06830	Peroxiredoxin-1	233.99	8.76	4.53	2.17	1.2379E-07	1.55425E-06
P37837	Transaldolase	115.65	10.4	4.39	2.13	4.51245E-07	5.22981E-06
P09972	Fructose-bisphosphate aldolase C	818.41	24.3	4.29	2.09	1.48189E-07	1.83511E-06
P31949	Protein S100-A11	37.76	8.6	4.26	2.05	1.16409E-08	1.44885E-07
P00338	L-lactate dehydrogenase A chain	71.59	12.7	4.23	1.97	1.42227E-09	2.05467E-08
P08107	Heat shock 70 kDa protein 1A/1B	135.07	4.7	4.03	1.99	7.81391E-08	9.16153E-07
P01033	Metalloproteinase inhibitor 1	367	12.6	4.00	2.00	2.19613E-06	2.30849E-05
P11142	Heat shock cognate 71 kDa protein	428.64	8.0	3.89	1.95	7.73678E-07	8.12864E-06
P40925	Malate dehydrogenase. cytoplasmic	248.35	8.6	3.77	1.86	2.398E-07	2.89038E-06
P15311	Ezrin	58.76	5.1	3.69	1.88	4.31079E-06	4.23582E-05
P62258	14-3-3 protein epsilon	305.48	15.7	3.64	1.86	5.64482E-06	5.37149E-05

[1] Due to the high amount of supplementary information available in Paper IV only the more relevant is available in this thesis.

The complete supplementary material of this article is available in (https://doi.org/10.1007/s00216-019-01887-y).

P10745	Retinol-binding protein 3	6908.85	38.3	3.55	1.83	1.37126E-05	0.000123261
P05121	Plasminogen activator inhibitor 1	62.9	5.7	3.46	1.79	2.21469E-05	0.000194749
P12271	Retinaldehyde-binding protein 1	56.94	10.1	3.45	1.66	6.26011E-08	7.55885E-07
P31946	14-3-3 protein beta/alpha	211.96	13.2	3.40	1.74	4.31784E-06	4.19713E-05
Q14956	Transmembrane glycoprotein NMB	183.02	3	3.38	1.74	6.69255E-06	6.30215E-05
Q14019	Coactosin-like protein	274.97	19.6	3.32	1.72	1.19993E-05	0.000107399
P52565	Rho GDP-dissociation inhibitor 1	70.66	7.4	3.25	1.70	3.15003E-05	0.00026825
Q9H299	SH3 domain-binding glutamic acid-rich-like protein 3	55.67	22.05	3.25	1.70	7.70571E-05	0.000599683
P26038	Moesin	346.42	6.7	3.23	1.69	1.85771E-05	0.000165153
P00558	Phosphoglycerate kinase 1	42.46	8.6	3.17	1.60	1.20147E-06	1.21499E-05
P60174	Triosephosphate isomerase	870.92	20.0	3.17	1.66	6.50058E-05	0.000506597
P53674	Beta-crystallin B1	374.51	16.2	3.12	1.63	1.18248E-05	0.000109957
P07339	Cathepsin D	2674.43	31.2	3.12	1.64	9.71686E-05	0.000720003
P32119	Peroxiredoxin-2	410.45	13.9	3.08	1.61	4.25438E-05	0.00035284
P50395	Rab GDP dissociation inhibitor beta	119.5	7.8	3.05	1.56	3.36799E-06	3.28277E-05
P60709	Actin. cytoplasmic 1	456.66	17.6	3.03	1.60	0.00013614	0.000969058
P04439	HLA class I histocompatibility antigen. A-3 alpha chain	65.8	3.8	3.01	1.49	3.65161E-06	3.66784E-05
O15537	Retinoschisin	270.83	11.9	2.98	1.58	0.000223928	0.001477596
P06733	Alpha-enolase	541.52	17.6	2.93	1.55	0.000127155	0.000970455
Q96JP9	Cadherin-related family member 1	852.8	7.6	2.91	1.54	0.000103999	0.000808994
P04075	Fructose-bisphosphate aldolase A	475.47	18.0	2.89	1.53	0.000204617	0.001491307
Q6EMK4	Vasorin	408.31	4.9	2.88	1.53	0.000287851	0.001990353
P07602	Prosaposin	698.09	9.1	2.88	1.53	0.000328853	0.002198694
P40121	Macrophage-capping protein	135.96	5.3	2.87	1.52	0.00036049	0.002333093
P06744	Glucose-6-phosphate isomerase	178.38	6.5	2.84	1.50	0.00015665	0.001184393
P08670	Vimentin	531.03	12.1	2.82	1.49	0.000204426	0.001400005
P36575	Arrestin-C	97.27	12.4	2.81	1.49	0.000192401	0.001428007
P29401	Transketolase	253.2	5.2	2.75	1.44	8.74755E-05	0.000693801
Q08380	Galectin-3-binding protein	1119.8	11.0	2.64	1.40	0.001042991	0.006070359
P30740	Leukocyte elastase inhibitor	67.44	4.2	2.54	1.34	0.000944829	0.005656457
Q99538	Legumain	122.94	3.9	2.50	1.32	0.000901228	0.005440993
P0C0S8	Histone H2A type 1	107.48	14.6	2.49	1.31	0.001475684	0.008290476
P62805	Histone H4	31.09	21.4	2.45	1.24	0.000206962	0.001396224
Q9Y279	V-set and immunoglobulin domain-containing protein 4	92.3	7.8	2.38	1.25	0.003142339	0.015522814
Q15846	Clusterin-like protein 1	308.98	8.6	2.37	1.24	0.001992877	0.010893498
P00736	Complement C1r subcomponent	1092.66	13.7	2.36	1.23	0.001752679	0.00943108
Q99784	Noelin	269.73	6.8	2.36	1.24	0.002731275	0.014255493
Q14574	Desmocollin-3	36.14	1.2	2.32	1.20	0.001531626	0.00844262
P07858	Cathepsin B	424.19	13.9	2.30	1.20	0.005502328	0.025508229
P30101	Protein disulfide-isomerase A3	256.5	4.4	2.29	1.19	0.004467714	0.02151417
Q13822	Ectonucleotide pyrophosphatase/phosphodiesterase family member 2	2385.2	19.0	2.28	1.19	0.004219249	0.020439355
P14618	Pyruvate kinase PKM	362.17	8.4	2.28	1.19	0.002712379	0.014248795
P07195	L-lactate dehydrogenase B chain	103.39	9.3	2.28	1.17	0.001151577	0.006654471
P07737	Profilin-1	237.2	22.5	2.27	1.18	0.006030145	0.027671325
P07333	Macrophage colony-stimulating factor 1 receptor	362.05	2.48	2.20	1.13	0.003183568	0.015641009
P54802	Alpha-N-acetylglucosaminidase	574.25	6.05	2.19	1.12	0.002511389	0.013279174
P08581	Hepatocyte growth factor receptor	170.78	2	2.19	1.13	0.007642421	0.032886802
P09211	Glutathione S-transferase P	290.66	10.06	2.14	1.10	0.011979267	0.04908465
P02747	Complement C1q subcomponent subunit C	196.32	14.82	2.13	1.09	0.009937038	0.041588346
P07996	Thrombospondin-1	80.42	2	2.13	1.09	0.00468343	0.022287616
P09668	Pro-cathepsin H	147.08	5.5	2.08	1.05	0.006171491	0.027432617
P00918	Carbonic anhydrase 2	242.68	9.4	2.06	1.04	0.009494939	0.039800031
P09382	Galectin-1	153.03	11.9	2.06	1.04	0.012425793	0.04926718
P26927	Hepatocyte growth factor-like protein	381.24	7.7	0.52	-0.94	0.006445267	0.028338157
A8MV23	Serpin E3	131.01	6.1	0.51	-0.99	0.003325409	0.016709662
Q92563	Testican-2	435.73	13.2	0.50	-0.99	0.008301962	0.036789087
Q9BQ16	Testican-3	98.42	6.7	0.50	-1.01	0.003302301	0.016136651
P51884	Lumican	1079.81	25.7	0.49	-1.03	0.008566911	0.036097037
Q16610	Extracellular matrix protein 1	418.1	9.8	0.49	-1.04	0.007050897	0.030667611
P06681	Complement C2	1582.12	15.7	0.48	-1.06	0.007978934	0.034153215
P22792	Carboxypeptidase N subunit 2	339.48	8.4	0.47	-1.09	0.001163106	0.00674005
Q9UNN8	Endothelial protein C receptor	131.34	9.7	0.47	-1.09	0.003607164	0.017903043
P08697	Alpha-2-antiplasmin	369.08	7.3	0.47	-1.10	0.002923473	0.014601215
Q96PD5	N-acetylmuramoyl-L-alanine amidase	1311.14	19.9	0.46	-1.12	0.002900636	0.014946591
Q04756	Hepatocyte growth factor activator	350.97	5.5	0.46	-1.13	0.002751922	0.013897976
P07357	Complement component C8 alpha chain	96.87	5.5	0.45	-1.16	0.000654619	0.004042648
Q9NPH3	Interleukin-1 receptor accessory protein	120.59	4.2	0.44	-1.21	0.000121235	0.000876768
Q96S86	Hyaluronan and proteoglycan link protein 3	116.45	8.5	0.44	-1.20	0.000443542	0.002847823
P02654	Apolipoprotein C	219.36	32.5	0.44	-1.19	0.00196032	0.010363331
P00748	Coagulation factor XII	339.2	8.1	0.43	-1.21	0.001837501	0.009771183
P13611	Versican core protein	659.94	1.7	0.42	-1.24	0.001692132	0.009159804
P07358	Complement component C8 beta chain	526.6	7.8	0.41	-1.27	0.000965156	0.00569935
P25311	Zinc-alpha-2-glycoprotein	2193.61	44.0	0.41	-1.27	0.001235197	0.007022753
P19827	Inter-alpha-trypsin inhibitor heavy chain H1	2000.36	13.8	0.41	-1.32	3.80217E-05	0.00032123

Q06033	Inter-alpha-trypsin inhibitor heavy chain H3	625.13	6.6	0.39	-1.37	0.000280363	0.001989594
P08185	Corticosteroid-binding globulin	1105.39	15.4	0.386	-1.38	0.000311476	0.001996978
P16112	Aggrecan core protein	92.3	0.7	0.375	-1.43	6.87003E-05	0.000526314
P05543	Thyroxine-binding globulin	1354.13	26.7	0.371	-1.43	0.000176951	0.00124003
P05546	Heparin cofactor 2	1432.83	25.5	0.363	-1.47	0.000127579	0.000915327
P29622	Kallistatin	1287.7	17.8	0.362	-1.48	5.48526E-05	0.000442739
P15169	Carboxypeptidase N catalytic chain	296.49	10.9	0.354	-1.50	0.000105606	0.000769904
P02760	Protein AMBP	1222.89	22.2	0.353	-1.52	2.3469E-05	0.000204155
P02741	C-reactive protein	212.05	8.1	0.330	-1.64	1.64059E-06	1.83098E-05
P27169	Serum paraoxonase/arylesterase 1	1267.05	23.4	0.314	-1.67	2.98351E-05	0.000256866
P07320	Gamma-crystallin D	25.81	5.7	0.313	-1.69	3.15041E-06	3.23633E-05
P02743	Serum amyloid P-component	452.43	12.2	0.308	-1.70	1.01737E-05	9.38469E-05
P00740	Coagulation factor IX	361.35	6.3	0.282	-1.85	2.49005E-07	2.92339E-06
Q07507	Dermatopontin	45.01	5.5	0.274	-2.03	5.28876E-11	8.24317E-10
P18428	Lipopolysaccharide-binding protein	195.73	3.6	0.258	-1.97	9.78062E-08	1.13036E-06
P23515	Oligodendrocyte-myelin glycoprotein	544.3	7.7	0.257	-1.96	1.25443E-06	1.25288E-05
Q15166	Serum paraoxonase/lactonase 3	109.39	4.5	0.255	-2.01	7.63148E-09	9.64667E-08
P35542	Serum amyloid A-4 protein	128.69	13.9	0.241	-2.08	7.42E-09	9.52822E-08
P13646	Keratin. type I cytoskeletal 13	439.68	16.0	0.230	-4.47	3.66983E-77	1.50797E-75
Q6UXB8	Peptidase inhibitor 16	233.57	4.7	0.211	-2.26	1.98348E-09	2.75856E-08
P02750	Leucine-rich alpha-2-glycoprotein	1107.55	24.6	0.177	-2.50	5.85938E-10	8.77822E-09
P43652	Afamin	1335.89	13.2	0.162	-2.62	7.02063E-11	1.15912E-09
Q9HAZ2	PR domain zinc finger protein 16	27.71	0.5	0.162	-2.63	6.49335E-11	1.0944E-09
P02656	Apolipoprotein C-III	318.53	26.3	0.139	-2.85	3.05583E-13	5.75516E-12
P02655	Apolipoprotein C-II	213.85	20.4	0.110	-5.26	2.15529E-87	9.74191E-86
P02748	Complement component C9	1126.39	13.4	0.058	-4.14	1.47604E-26	3.42138E-25
P01011	Alpha-1-antichymotrypsin	1785.94	23.4	0.040	-5.46	1.39215E-66	4.50498E-65
Q8NBP7	Proprotein convertase subtilisin/kexin type 9	31.97	3.2	0.038	-4.73	6.45423E-33	1.63171E-31
Q96BN8	Ubiquitin thioesterase otulin	27.79	2	0.005	-8.46	9.445E-132	5.8777E-130
P50213	Isocitrate dehydrogenase [NAD] subunit alpha. mitochondrial	34.88	2.7	0.004	-7.86	2.84888E-81	1.22637E-79
O95447	Lebercilin-like protein	25.3	2.2	0.003	-8.31	1.561E-104	7.4286E-103
P02753	Retinol-binding protein 4	222.38	10.4	0.003	-8.49	3.7602E-115	2.028E-113
P06727	Apolipoprotein A-IV	2833.63	49.7	0.002	-9.15	3.8646E-113	2.9113E-111

Appendix IV - Supplementary material of the Paper V

Table S1 - Demographic characteristics of patients involved in the study and description of corresponding vitreous samples collected via pars plana vitrectomy. Abbreviations: M - Male; F - Female; VMT - vitreous-macula traction syndrome; ERM - Epiretinal membranes; NVI - neovascularization of the iris; CNV - Choroidal neovascularization; SCH - Subconjunctival hemorrhage; CNVM - choroidal neovascular membrane; NVD - Neovascularization of the disc.

	Experiment								
Sample	**LFQ**	**MRM**	**WB**	**Age**	**Gender**	**Disease group**	**Eye**	**Diagnosis**	**Protein concentration (µg/µl. MD ± SD)**
11		x	x	59	F	DR/PDR	LE	PDR with fibrovascular proliferation	9.54
13		x	x	81	M	AMD	LE	nAMD with ERM	1.56
32			x	79	M	DR/PDR	RE	PDR with vitreous hemorrage	4.01
60		x		67	M	DR/PDR	LE	PDR with VMT	2.96
61		x		76	M	DR/PDR	RE	PDR with asteroid hyalosis	2.77
128		x		39	M	DR/PDR	RE	PDR with vitreous hemorrage	0.92
141		x		60	M	DR/PDR	RE	PDR with vitreous hemorrage	0.21
147		x		58	M	DR/PDR	LE	PDR with asteroid hyalosis and ERMs	2.77
152		x		70	F	AMD	LE	AMD with ERM (diabetic)	0.21
170		x	x	77	F	AMD	RE	AMD with ERM	0.56
181	x	x		81	F	AMD	LE	AMD with ERM	0.60
201		x		74	F	AMD	RE	AMD with ERM	0.55
217		x		74	F	DR/PDR	LE	Diabetic macular edema	4.75
219	x		x	75	F	AMD	LE	AMD with ERM	0.73
220		x		92	F	AMD	RE	CNV with SCH	0.47
255			x	80	M	ERM	LE	Senil cataract with ERM	3.16
259		x		63	M	ERM	LE	Cataract with ERM	0.44
263		x		80	F	ERM	LE	ERM	0.34
272		x		71	M	ERM	LE	ERM	2.08
273	x		x	77	F	ERM	LE	ERM	0.75
296		x		44	F	DR/PDR	RE	Diabetic macular hemorrage	3.09
309		x		39	M	DR/PDR	LE	DR	0.50
312		x	x	64	F	DR/PDR	RE	PDR with ERM	1.08
329		x	x	69	F	DR/PDR	LE	PDR with vitreous hemorrage	2.67
337		x		67	M	DR/PDR	RE	PDR with synchisis and ERM	0.58
342		x		76	M	DR/PDR	LE	PDR with ERM	0.63
361	x			77	F	ERM	RE	ERM	0.33
363			x	81	M	ERM	RE	ERM	0.66
373		x		81	F	ERM	RE	ERM	0.31
405		x		72	M	DR/PDR	RE	PDR with VMT	0.73
415		x		67	M	ERM	LE	ERM	0.55
429	x	x	x	75	M	ERM	RE	ERM	0.83
439		x		68	M	ERM	LE	ERM	0.50
445	x	x		74	M	ERM	RE	ERM	0.41
446		x		41	F	RRD/PVR	RE	RRD	1.81
456		x		79	M	ERM	RE	ERM	0.79
458		x	x	82	M	AMD	RE	AMD with ERM	2.04
460		x		82	M	ERM	RE	ERM	0.97
466		x	x	77	M	AMD	RE	AMD with ERM	1.79
473		x	x	76	F	RRD/PVR	LE	RRD with PVR (diabetic)	5.23
479		x	x	74	M	ERM	LE	ERM	1.89
498		x		65	M	ERM	RE	ERM	0.24
500			x	58	F	RRD/PVR	LE	Re-RRD with PVR	2.25
504		x		85	M	ERM	RE	ERM	0.10
506		x	x	63	M	DR/PDR	LE	PDR with PVR	0.87
514	x	x	x	28	F	DR/PDR	LE	PDR with CNVM and NVD	1.58

515	x	x		71	F	AMD	RE	AMD with ERM	0.39
517		x		88	F	ERM	RE	ERM	0.82
520		x		73	M	ERM	LE	ERM	2.64
526		x		71	M	ERM	RE	ERM	0.51
527		x		85	F	ERM	RE	ERM	1.07
528		x		77	M	ERM	LE	ERM	2.78
530	x	x	x	79	M	AMD	LE	AMD with ERM and VMT	0.66
532		x		83	M	ERM	RE	ERM	2.37
535		x		9	M	ERM	RE	ERM	0.09
536		x		79	M	AMD	LE	AMD with VMT	3.87
542		x		62	M	ERM	RE	ERM	0.15
546		x	x	66	M	RRD/PVR	RE	RRD	0.87
548	x	x	x	74	M	DR/PDR	LE	PDR with ERM	1.25
551		x		66	M	DR/PDR	RE	PDR with vitreous hemorrage	0.90
555		x	x	70	M	RRD/PVR	RE	RRD with PVR	0.56
556		x	x	87	M	RRD/PVR	LE	RRD	2.56
558		x		82	F	RRD/PVR	LE	RRD	0.09
560		x	x	65	M	RRD/PVR	LE	RRD	2.81
567		x		74	F	RRD/PVR	RE	RRD	0.19
579		x		67	M	RRD/PVR	LE	RRD	0.60
590		x		57	M	RRD/PVR	LE	RRD	0.49
723	x	x	x	22	F	DR/PDR	RE	PDR	1.84
726		x				RRD/PVR	LE	RRD	0.17
728		x		94		RRD/PVR	RE	RRD	0.20
770	x	x	x		M	DR/PDR	RE	PDR with NVI	1.43
785		x	x			RRD/PVR	RE	RRD	0.70

Table S2.1 - Protein list corresponding to proteins identified in vitreous samples using MASCOT with an FDR of 1% at peptide level. The protein score. number of peptides. and coverage (cover) represent the best values obtained in the identification of these proteins.

				PSMs_AMD				PSMs_ERM				PSMs_PDR			
Main Protein	Score	# Peptides	Cover. (%)	181	219	515	530	273	361	429	445	514	548	723	770
sp|P62258	102.49	2	18.8	1			2	1	1		2	1	1	1	1
sp|P63104	124.17	3	21.6	2			3	1			3		1	1	1
sp|Q9BRK5	290.63	7	22.7	7		2	6		2	3	1				
sp|P08195	237.58	5	13.7	2	1	6	5	2	3	4	3	1		1	
sp|P08253	773.33	16	38	16	8	13	19	11	20	8	13	8	11	3	2
sp|Q9UHI8	83.52	2	5.3	2				1	2	1	3		1	1	
sp|P22303	111.21	2	14.5	1		2	1		2	1	1				
sp|Q13510	664.84	13	43	13	6	9	24	10	17	12	19	2	7	2	3
sp|Q92484	199.49	5	9.5	3	2	2	5	1	4	2	3	1		1	1
sp|P62736	439.59	9	24.1								15				
sp|P60709	835.58	15	45.9	15	19	14	14	13	8	8	25	12	20	16	9
sp|Q15848	101.99	2	12.3	2	1	1	1		1			1	1	1	2
sp|P43652	2544.38	42	59.8	52	144	74	80	95	87	60	64	92	116	98	74
sp|P16112	117.19	2	0.8	3	1	2	2		1	2		2		1	
sp|O00468	494.93	10	8.6	2	2	2	11	1	8	3	3	2	2	1	1
sp|Q09328	207.07	4	9	3	1	2	6	1	2	2	1	1		1	1
sp|P02763	341.37	5	27.4	7	1	9	3	4	1	7	3	4	3	3	8
sp|P19652	322.58	6	28.9	7		8	5	5		5	2	4	2	4	9
sp|P01011	4181.79	59	64.1	499	295	361	333	244	277	333	275	351	334	361	401
sp|P01009	2524.07	39	67.5	138	147	145	116	91	115	96	77	155	111	123	107
sp|P04217	2943.46	43	65.5	147	194	171	143	184	175	147	130	245	182	239	169
sp|P08697	2274.1	34	69.2	65	96	74	73	60	57	67	54	96	66	93	84
sp|P02765	2495.51	34	55.3	113	181	108	144	101	117	105	117	169	172	125	119
sp|P01023	1472.77	25	27.1	35	14	12	10	25	23	20	16	21	30	19	9
sp|P06733	288.62	4	13.6	2		2	4	2	1	1	5		3	2	2
sp|P49641	78.28	2	3.6	1		1	2		1						
sp|P17050	347.2	6	19.7	8	1	8	10	4	6	7	8	1	2	1	1
sp|P54802	438.98	8	20.2	6	2	2	5	2	9		1	2	2		
sp|P05067	1180.25	22	27.9	43	16	39	51	33	48	31	43	15	18	9	13
sp|P51693	922.74	17	23.1	32	12	27	29	28	30	25	34	13	16	20	9
sp|Q06481	2524.7	38	40	104	30	96	93	74	117	82	90	26	41	6	28
sp|O43827	72.27	2	6.9					2			1				
sp|P01019	3038.8	40	62.9	105	120	123	123	98	123	101	107	360	149	178	98
sp|P01008	3957	62	70.7	251	372	371	340	243	326	284	245	428	396	358	437
sp|Q8N7J2	38.74	1	1	3	5	3	4	3	2	3	4	3	7	3	5
sp|P02647	3348.21	54	80.5	105	132	113	179	116	152	171	166	168	163	140	102
sp|P02652	617.68	12	69	5	6	9	9	9	6	11	11	21	12	16	6
sp|P06727	3282.13	53	72.5	93	113	73	151	87	77	91	100	136	132	173	134
sp|P04114	1969.07	41	16.7	46								2			
sp|P02656	191.37	2	16.2									2		4	
sp|P05090	534.14	10	34.4	17	26	10	23	21	13	14	24	14	21	20	22
sp|P02649	2807.49	39	77	114	62	69	141	41	90	79	141	91	65	112	60
sp|O14791	400.03	8	28.9	1	7	2	3	2	1			11	3		2
sp|O95445	125.44	2	17.6	2	2	1	2	1	2	2	3	3	3	3	2
sp|P08519	297.12	4	0.8		4	3	5	4	3		3	5		3	4
sp|P53367	39.38	1	1.9	2	2	1	5	1	2	2	6	1	2	1	1
sp|Q8NEN0	54.1	1	1.8	1	2	1		2	1		1	1		2	1
sp|P15289	157.57	3	14	1		3	4		6		6				
sp|P15848	86.88	2	6.6	2		2	1		2	1	2				
sp|P17174	299.66	6	25.4	1	2	5	6	2		1	5		1	2	2
sp|Q5T9A4	44.73	1	2.5	1	1	2	3	2	1	1	3	5	3	4	4
sp|O75882	652.18	12	10.4	5	13	15	8	10	8	9	9	8	15	12	7
sp|P98160	1114.13	21	7.7	11	6	12	12	12	17	11	27	24	15	25	17
sp|Q8NES3	90.93	2	10	1			2	1	1	1	3		1		
sp|P15291	430.83	6	30.4	8	2	3	6	2	4	4	4	2	3	1	1
sp|O43286	55.66	1	2.1	2	1	1	2	2	2	2	2	1	1	1	1
sp|O43505	1186.12	20	56.1	44	17	43	49	24	41	29	42	24	17	25	16
sp|P02749	1897.85	30	67.8	66	64	58	78	52	36	43	63	109	93	46	78
sp|P61769	127.83	3	42.9	6		3	5	3	4	3	5			1	2
sp|Q562R1	176.11	3	11.2		4	1	4						2		
sp|Q96KN2	667.9	12	31.8	14	22	27	14	12	17	13	12	16	15	17	9
sp|P43320	190.97	4	25.9	5		4	1		4						
sp|P13929	171.43	2	7.6					2	1		3		2		
sp|P06865	912.78	17	36.7	26	5	21	18	10	21	9	15	4	7	3	1
sp|P07686	694.77	15	37.1	19	3	17	15	3	23	10	26	2	4	3	
sp|O00462	345.1	8	12.5	8		3	11		9	3	4	1	1		
sp|P21810	188.93	3	15.8											6	
sp|P43251	998.55	15	32.8	37	26	30	30	21	42	26	28	15	20	22	19
sp|Q9BUH8	48.47	1	1.2	7	4	5	4	4	7	6	8	2	2	2	3
sp|Q96GW7	615.92	13	13.6	14	3	7	26	2	14	7	8	4	2	2	1
sp|Q8IZJ3	1394.75	25	25.9	12	15	24	16	10	36	17	24	11	12	7	14

sp|P04003	694.6	13	26.3	23								3	1	1	2
sp|P19022	472.67	8	11	18		9	11	4	13	13	17		1		
sp|P33151	183.08	4	8.9		6	1		1	1		2	3	4	3	3
sp|P55285	72.43	2	2.7										2		
sp|Q96JP9	587.66	9	16.9	18		1	6	3	3	2		1			
sp|P27797	333.81	8	27.6	9	3	10	6	3	10	6	9	2	3		3
sp|O94985	3031.8	48	53.4	111	54	106	117	101	149	69	107	49	47	28	25
sp|Q9H4D0	170.38	4	4.5	2		1	1	1	4		4				
sp|Q9BQT9	214.08	4	9.5	4		4	4	2	4		2	1			
sp|P00915	793.02	11	55.9	14								13		20	
sp|Q9ULX7	118.16	2	8.3	2		1	2		3	1	3				
sp|P00918	256.52	5	33.8				7	1	3	2	6	1			
sp|Q9NS85	192.3	3	12.8	3		2	6	3	1	4	1		1		
sp|Q96IY4	648.97	12	37.4	14	15	17	15	10	12	8	12	21	14	12	19
sp|P16870	1651.75	27	63.7	54	18	53	53	38	66	46	69	17	16	15	11
sp|P15169	273.29	6	26.2	1	3	1	3	1	1			2	3	9	4
sp|P22792	433.52	8	34.1	8	9	3	2	10	2	2	1	4	7	11	7
sp|Q9Y646	525.55	7	23.5	9	1	11	12	3	11	7	11	2	5	1	
sp|Q8N3K9	33.62	1	0.9	1	2		2		4	4	2	3		2	
sp|Q9NQ79	1241.43	21	41.5	37	24	39	32	27	44	27	34	18	11	10	16
sp|P49747	95.06	2	6.1		2	1	1	1	1	1	1	1	2		
sp|P04040	134.42	3	12.1											3	
sp|P07858	643.82	11	38.1	10	3	8	9	4	14	7	16	2	8	6	5
sp|P07339	2887.45	43	65.3	137	52	116	129	81	131	84	102	83	101	60	62
sp|Q9UBX1	336.36	7	26.9	9	3	7	7	6	5	4	3		1		
sp|P07711	411.95	7	29.7	12	2	12	11	7	11	12	9	4	5	4	4
sp|P43234	132.59	3	10.9	1			5	1	1	2	3				
sp|Q9UBR2	288.94	6	22.1	7	2	7	9	5	6	6	7	4	4	3	2
sp|P16070	133.51	2	4.2	2	2	2	2	2	3	2	3	2	4	2	2
sp|P13987	75.68	1	6.2	2		2	2	1	2	3	3	1	2	1	
sp|Q9BY67	480.92	8	32.4	10	1	10	7	4	12	3	7	1	2	1	3
sp|Q8N3J6	188.24	4	12.9	4	1	1	2	1	4		2		1		1
sp|Q8NFZ8	132.33	2	8.5	2		2			1		2		1	1	
sp|Q4KMG0	131.33	2	3.9	1	1	1	2	1	2	1	1	1			
sp|P43121	97.86	2	6.5		2		1	1				1	1		2
sp|Q8TEP8	46.25	1	0.9	2	1						1				2
sp|O15078	35.25	1	2			1	1	2	1			1	2		
sp|P23435	108.58	2	10.4			1	2		1	1	2		1		
sp|Q8IUK8	114.74	2	8.9	1		1	1		3		2				
sp|O75503	236.55	5	14.5	7		7	7	4	6	3	6	1	1		1
sp|P00450	8739.85	124	80.7	470	482	441	407	502	485	288	376	581	541	421	537
sp|P36222	1844.82	25	61.6	70	26	64	67	45	59	39	69	38	52	29	66
sp|Q13231	308.31	6	18.2	12							2	5	4		2
sp|P06276	157.14	4	16.3	3	1	1	1		1		1	1		5	2
sp|Q9BU40	206.34	3	10.9	1		1	1		1		3				
sp|P10645	380.95	7	26.7	7	1	9	8	5	10	9	4	5	2	2	
sp|P26992	70.8	2	4.8	1		1	1		2		1				
sp|P10909	3059.03	45	50.1	282	161	202	400	239	229	256	318	206	214	201	140
sp|Q15846	528.63	10	27.7	14			3		1	1		1	1		
sp|P00740	318.45	6	23.9	3	4	3	1	4	3	2	2	9	3	3	5
sp|P12259	499.68	12	7.8		1	2	2	5	7	5	12	1	6	1	
sp|P00742	264.76	5	16	5	6	6	7	7	4	3	6	9	8	6	7
sp|P03951	265.03	5	12.3		3			2		1	1	4	1	5	1
sp|P00748	1108.56	19	35.3	17	17	18	14	26	17	11	20	23	21	36	26
sp|P00488	108.31	2	7.8	2	2			2				1	2	1	2
sp|P05160	242.04	5	11	1	2		1	2	1			5	3	3	3
sp|Q4G0X9	61.83	2	2.6	2			2		1						
sp|P02452	300.37	5	5.9							2		4		12	2
sp|P02458	464.85	7	4.8	11	4	11	9	10	9	8	13	5	8	3	5
sp|P02461	138.74	3	4.8											5	
sp|P20849	145.81	3	2.4			1	2		3		2				
sp|P20908	130.5	2	1.6	2											
sp|P12109	694.35	14	26.2	15	4	13	18	11	23	10	15	7	4	12	7
sp|P39060	490.17	9	7.1	8		3	9	7	6	9	13		2	3	
sp|P08123	375.27	7	5.7						1		1	1		8	
sp|Q14055	302.01	4	5.7	1	2	5	8	3	8	3	6	1	3	1	2
sp|P12111	409.13	9	6.3	1			1	2				1	1	10	2
sp|Q5KU26	98.92	2	3.6	2		2	2	1	3		3				
sp|P02745	217.2	4	18	9	3	1	7	4	4	5	5	4	6	7	1
sp|P02746	607.5	9	37.2	21	12	7	13	12	11	15	19	12	13	12	10
sp|P02747	507.51	8	34.7	20	13	7	12	12	11	12	17	10	16	12	8
sp|Q9BXJ4	200.85	4	16.3	20	6	8	18	9	22	12	18	7	8	7	1
sp|Q9BXJ0	122.22	2	11.5	3		1	1	1	1	2	2			1	
sp|P00736	1482.48	26	47.7	45	22	18	33	29	28	18	33	11	26	17	19
sp|Q9NZP8	362.56	6	15.6	5	8	8	10	7	8	7	5	8	9	8	7
sp|P09871	1053.66	17	36.2	33	20	21	25	23	29	15	24	9	23	14	13
sp|P06681	1551.3	26	44.4	44	52	40	46	53	34	33	30	67	61	71	60
sp|P01024	17465.46	253	87.9	849	1551	950	1071	1071	835	876	777	1276	1501	1151	1048
sp|P0C0L4	11152.69	167	74	635	579	365	314	455	671	539	781	534	711	896	396
sp|P0C0L5	11615.82	172	74.8	646	587	361	303	473	669	549	784	545	713	898	395
sp|P01031	3535.09	64	49.5	85	116	62	77	83	65	58	50	92	113	93	94
sp|P13671	1280.14	21	31.2	20	35	25	32	30	17	16	18	27	35	29	29

sp|P10643	1649.36	30	42.8	32	46	24	28	31	23	9	25	17	51	35	25
sp|P07357	1041.91	18	30.1	17	17	13	15	10	10	16	12	23	20	28	22
sp|P07358	1151.3	20	39.4	33	30	32	31	18	18	27	25	37	40	36	31
sp|P07360	709.66	10	54	16	16	11	14	10	10	15	16	20	24	16	17
sp|P02748	1794.79	28	43.6	73	73	51	65	56	44	62	43	70	77	78	76
sp|P00751	4335.2	71	63.1	124	229	142	147	159	152	141	100	222	196	195	180
sp|P00746	615.06	11	55.3	12	7	6	18	11	11	8	12	6	8	3	8
sp|P08603	3418.39	54	54.8	53	107	54	44	75	52	53	49	99	115	91	104
sp|Q03591	995.24	15	57.3	17	25	16	19	25	20	9	27	28	30	15	22
sp|P36980	647.75	9	48.9	14	17	10	13	18	13	9	20	19	18	7	12
sp|Q02985	220.47	4	12.7	3	6			3							6
sp|Q9BXR6	112.82	1	3.5			1			2		3	1	2	1	2
sp|P05156	1857.37	29	47.3	75	63	66	74	68	69	53	76	66	76	66	70
sp|Q12860	1477.85	25	33	25	12	29	29	22	42	15	28	7	12	9	8
sp|Q02246	435.6	8	12.6	1		4	3	3	9	4	2		1		
sp|Q8IWV2	331.45	6	9.1	3	3	6	7	5	8	4	6	1	5	3	
sp|Q9UHC6	224.56	5	6.4			1	2	3	5						
sp|Q9C0A0	74.59	2	4.1						2						
sp|P08185	1850.14	25	69.6	42	71	57	47	44	47	42	41	129	64	68	66
sp|P02741	334.06	6	25.4	4	4	5	2	3	1	4		8	2	18	4
sp|Q9NYV4	38.39	1	1.1					2	1						
sp|Q14004	38.39	1	1.2					2	1						
sp|P50750	38.39	1	2.4					2	1						
sp|P01034	1061.89	15	56.8	56	2	63	42	14	74	26	57	9	5	9	6
sp|Q96BY6	42.57	1	0.6		2	1	2	1	2	2	1	2	2		1
sp|O00115	86.76	2	11.1	1		2	1		1	2	2			1	
sp|P17661	103.31	2	5.7	3											
sp|Q14126	79.09	2	2.1				1		2		1		1		
sp|Q9UBP4	1439.12	22	45.4	94	37	74	82	58	91	66	82	66	54	67	36
sp|Q01459	213.56	3	18.7	3	1	2	4	2	3	2	2	1	3	1	
sp|Q9UHL4	789.31	14	48.6	8	3	11	11	12	22	15	21	8	3	5	2
sp|Q9P0K1	85.41	2	2.4	1			1	1		2					
sp|Q5FWF4	50.87	1	1.6		2	1	1	1	2	2	2	2	1	1	1
sp|P09172	112.71	2	3.9											2	
sp|Q14118	403.86	6	11.3	3		6	10	4	4	7	8	2	3	2	1
sp|Q5XPI4	48.85	1	0.5	1			1	1				2	1		1
sp|P53804	37.2	1	0.9								1	1		1	4
sp|Q93070	38.95	1	2.2					1	5		1	1			
sp|Q13822	1954.83	35	49.7	73	53	69	62	60	89	46	61	39	50	31	28
sp|Q12805	1485.99	21	42.8	63	53	57	58	53	65	44	60	37	58	39	36
sp|O95967	186.89	4	13.8	5	1				2	3			1		
sp|Q9NZ08	359.14	7	17.2	7		1	3	1	4	1					1
sp|P11021	220.41	4	17.7	3		4	5	2	4	1	1			2	2
sp|P14625	119.52	3	6.1	3			1	1	2			1		3	
sp|Q9UNN8	115.2	2	16.4					1		1					2
sp|Q9Y2E5	141.58	2	3			1	1		3		1				
sp|Q16610	461.68	8	31.5	9	10	9	6	14	12	3	7	7	11	7	12
sp|P08294	794.16	11	62.5	12	12	11	12	15	16	14	22	6	8	7	6
sp|Q9Y2M0	39.36	1	1.5	1			2			1	1	2			
sp|Q14CZ7	43.25	1	1.1	1	6	3		3	2	3	1	2	6	1	1
sp|Q9UKT5	46.27	1	2.6	2	1	1		1	1	2		1	1	2	2
sp|Q5SYB0	44.33	1	1.1		2				2		2				
sp|P02794	228.61	4	36.1	3					1		1			5	
sp|P02792	644.23	10	46.9	13		3					2	4	7	23	4
sp|Q9UGM5	422.8	7	33.5	7	8	13	5	9	5	5	6	20	9	8	8
sp|P02671	1487.76	28	29.8	53		2	1	1	1	6		5	10	15	
sp|P02675	2774.75	40	66.4	93	4	8	3	6	2	3	2	7	13	18	3
sp|P02679	1729.92	28	67.5	83	4	10	6	5	5	10	2	10	20	19	2
sp|P11362	56.75	1	1.6				2	1	1						
sp|P02751	2845.58	45	31.9	28	19	3	12	28	8	17	7	42	23	85	10
sp|P23142	611.89	11	23.8	13	15	11	18	17	19	9	12	5	21	6	9
sp|P98095	62.3	2	3.4											2	
sp|Q12841	310.13	7	21.4	9	3	10	10	7	11	5	12	6	5	5	4
sp|Q6MZW2	920.26	15	25.7	23		10	17	8	17	2	9	1		1	1
sp|Q8N475	1719.53	29	41.9	44	2	21	29	28	50	5	17	2	6	2	
sp|P00883	160.22	3	17.3		1	3		1	1	1		3	3	3	
sp|P04075	218.52	4	21.4	2		3	4				4				5
sp|P05062	149.11	3	16.8											4	
sp|P09972	368.71	7	27.5	1		2	9		2	4	2		1		2
sp|P16930	85.15	2	10											2	
sp|Q08380	1006.94	17	33	31	12	22	32	19	36	18	20	1	2	4	3
sp|P07315	158.02	4	31			4									
sp|P07320	48.31	1	9.8	1		2	2		2	1	2				
sp|P22914	370.84	7	59	2		15	9		7	2	4				
sp|P09104	520.37	8	29.5	3		4	8		2	2	3		1	1	2
sp|Q92820	573.16	11	48.1	3	6	7	10	5	9	6	15	5	4	2	3
sp|P17900	241.8	5	41.5	7	1	3	4	1	6	6	7	3	3		1
sp|P06396	3835.48	53	72.1	171	132	116	139	127	146	117	151	122	152	95	112
sp|P14136	78.09	1	4.9					2	4			2	2	2	
sp|P06744	82.61	2	5.6			2			1					2	
sp|P14314	109.66	2	7.8	1		1	2	1	4	1	2				
sp|P04062	122.54	3	10.6	1		1	3		1		1				

sp|P48058	356.43	6	10.6	8	5	7	7	2	7	5	8	2	3	2	
sp|Q16769	250.62	5	30.2	7	1	9	8	4	7	7	10	2	2	3	3
sp|P22352	1059.08	18	60.2	83	59	77	96	58	85	64	113	74	84	76	60
sp|P09211	100.66	2	14.8				2				2			1	
sp|P04406	600.63	10	37.3	11	3	7	14	7	6	10	14	4	9	9	6
sp|P35052	249.48	6	14.2	3		1	2	2	4	2	6		1		
sp|O00461	265.59	4	6	1		2	4	2	2	1	2				
sp|Q8NCC3	109.4	2	7.5	2	1		1		1	1	2				
sp|Q14393	212	3	8.6	3	1	3		3	4	1	3	1		2	
sp|O95390	92.05	2	5.9	2								1	1		
sp|O14793	209.46	4	27.5	4		2	5	2	2	3	4			2	
sp|P00738	733.34	13	39.7		4	14	5		2	23			11		2
sp|P00739	384	7	22.7			8				13			6		
sp|P48723	489.93	9	31	9	1	9	12	1	5	5	6	3	2		
sp|P54652	79.03	2	5.5	1		1					2			1	
sp|P69905	644.17	11	91.5	10								25		35	
sp|P68871	1042.79	17	89.8	14								37		51	
sp|P02042	590.12	9	48.3	7								27		28	
sp|P02790	4566.54	69	81.1999999999999	339	440	395	378	304	377	299	300	430	419	272	399
sp|P05546	1519.1	28	57.7	38	69	46	44	44	35	55	40	102	66	60	57
sp|Q04756	359.11	6	11	2	7		4	4	2		1	2	5	4	4
sp|P26927	133.21	3	4.9				1	2					3		1
sp|O95568	60.47	1	4.6			7			7	8	8	11			10
sp|P04196	1668.53	26	42.3	46	93	56	54	46	55	68	68	53	80	63	66
sp|P01891	133.41	2	9.3			2				1					2
sp|Q86YZ3	41.21	1	1.3				1	1	1			2	1	1	
sp|P10915	101.63	2	5.1				3			1					
sp|Q96S86	673	13	50.6	4		1	21		1	5	4	1			
sp|Q86UW8	53.32	1	5.5				2								
sp|Q14520	394.47	8	17.1	6	5	5	7	6	4	5	3	10	4	9	7
sp|Q9Y4L1	129.12	3	2.7	2			3		1		1	1	1	1	
sp|O75144	96.9	2	6.6	2	2		1	1	2	1		1	1		
sp|P22304	785.83	14	34	17	2	11	11	10	22	9	8	4	3	3	1
sp|Q9Y6R7	5890.62	90	22.6	195	139	60	154	84	73	89	107	84	116	145	46
sp|P01876	790.91	12	51.8	21	11	20	7	7	9	14	16	11	16	22	7
sp|P01877	382.26	6	28.5	11		11		4	7	8	10		5	12	
sp|P01857	861.88	14	60.3	20	37	14	23	24	24	26	14	22	35	21	18
sp|P01859	612.96	11	31.6	9	12	11	20	8	10	22	11	12	24	13	7
sp|P01860	498.24	10	30.8	12	19	11	16	12	12	16	11	13	26	13	10
sp|P01861	454.56	7	30	10	14	8	11	9	9	12	6	14	16	10	6
sp|A0A0B4J1V1	106.52	2	15.4											2	
sp|P01834	833.32	10	81.3	10	28	8	19	16	18	25	19	6	21	20	13
sp|P01619	151.03	2	21.6	1	1		1		1		2				
sp|A0A0C4DH25	133.7	2	19.8					1		2					1
sp|P0DOY2	349.36	6	82.1	6	7	1	2	3	3	5	5	2	14	5	2
sp|A0A075B6I4	49.21	1	6	2	1		1				1		1		
sp|B9A064	221.91	4	30.8		3					1		2	8	4	
sp|O14498	209.23	4	11.2	3	2	3	2	1	3	1	5		1		2
sp|Q8N3Z0	29.17	1	1.7				1		2						
sp|Q14643	39.38	1	0.8					1		1	1	1		3	
sp|P18065	76.05	2	15.4	2						1	1	2	1	1	1
sp|P24593	104.79	2	5.1	1		2	1	1	1	1	1				2
sp|P24592	317.24	5	15.8	2	1	2	5	3	3	6	6	3	4	1	3
sp|Q16270	389.27	7	24.5	4	5	6	4	4	7	10	12	5	4	1	1
sp|P35858	1225.91	20	43.3	18	23	20	25	24	28	14	13	34	15	31	28
sp|P19827	2866.09	42	49.5	40	88	30	40	77	50	67	43	58	107	59	27
sp|P19823	2097	35	42.5	31	94	32	47	93	54	60	50	36	115	49	32
sp|Q06033	1016.39	19	35.1	6	26	3	6	11	8	5	6	3	11	6	2
sp|Q14624	3413.22	52	58.8	109	146	91	105	153	102	88	80	145	117	115	127
sp|Q86UX2	664.37	14	26.8	12	4	8	10	7	17	5	12	10	8	3	1
sp|P05362	98.78	2	4.5										1	2	
sp|Q9NPH3	86.24	2	3.7	2		2	1		2		1	3	1		
sp|P40189	308.32	6	17.8	10		2	6	4	8	6	3	2	3	5	2
sp|Q17R60	123.77	3	5.9	3		1	2		1	1				1	
sp|Q9UBX7	109.64	2	6.4			1	2								
sp|P29622	1628.77	27	64.2	32	44	58	55	47	43	40	55	71	65	46	69
sp|Q14525	51.95	1	3.5				5				2				
sp|Q92764	51.97	1	3.5	2	3	3	5	2	3	3	2	2	3	3	5
sp|O76013	45.38	1	3					2							
sp|O76015	51.97	1	3.3	2	3	3	5	2	3	3	2	2	3	3	5
sp|P13645	2326.58	34	57.5	45	44	35	79	34	44	30	36	42	49	56	75
sp|Q99456	100.35	2	5.9		3	3	5	2	3			5	3		6
sp|P13646	227.03	4	9.4		6	3	6	3			3	5	6	7	7
sp|P02533	657.54	11	41.7	10	15	9	22	6	9	10	12	11	11	14	21
sp|O77727	251.33	5	10.4		7		11	5			6			10	12
sp|P19012	239.33	5	10.3								8		9	9	14
sp|P08779	461.5	9	24.5		15		19				11			10	18
sp|Q04695	339.78	6	15.7								9				15
sp|P05783	51.97	1	3.7	2							2				5
sp|P08727	187.37	4	7.8							7	8				
sp|Q2M2I5	108.67	2	4.8									3			6
sp|Q7Z3Z0	124.1	2	5.6			1						3			5

sp|Q7Z3Y8	166.93	4	5.9				4	3	4						
sp|P35527	2362.42	31	65.7	39	38	23	69	23	39	18	14	35	28	40	44
sp|Q9NSB2	42.49	1	4.3	2	1								1		3
sp|P04264	2401.86	34	52.3	72	68	49	93	46	62	42	36	64	60	76	91
sp|Q7Z794	178.99	3	6.6	5	7	3	14	2	4	2	1	7	7	5	12
sp|P35908	2227.01	33	69.8	43	44	25	75	19	38	22	30	38	48	43	57
sp|Q01546	221.22	5	8.9	5	5	1	8	1			3	5			9
sp|P12035	96.87	2	9.7	1	1		4		2			2			4
sp|P19013	175.26	3	7.3	6	5	2	7	2	6	2	4	5	5	5	9
sp|P13647	794.12	16	33.2	9	14	6	26	7	10	6	8	12	13	13	20
sp|P02538	643.16	13	25	10	19	5	23	5	9	6	7	11	12	14	19
sp|P04259	562.96	11	19.5	12	17	7	24	7	14	7	8	12	15	17	20
sp|P08729	114.56	2	7.5	5	3		5					3			
sp|Q86Y46	136.33	3	9.8	1		1	4	1			1	2	3	2	
sp|Q7RTS7	100.17	2	6.6					1				2	3	2	5
sp|O95678	259.97	5	13.1							2		6			10
sp|Q8N1N4	57.95	1	2.7										2		2
sp|Q5XKE5	173.41	3	11.2	3	5		12	2	4		2				7
sp|P05787	171.82	3	8.9	6	4	3	6	3	5	2	2	4	4	4	8
sp|Q6KB66	78.09	1	8.2	3	2	2	3	2	4		2	2	2	2	3
sp|Q5T011	28.54	1	0.5	1			1	1	1	1	2		1		
sp|P01042	2516.1	36	41.3	86	144	103	91	75	92	80	71	151	120	122	102
sp|Q08431	118.25	2	14.7	1		2	3		1		2				
sp|P02788	109.98	2	4.9	3									1		
sp|P55268	121.41	2	1.2	1			1		2						
sp|Q14767	308.29	7	7.4					6	2	2	1		7	6	3
sp|O00292	197.85	4	27.9				1				1	4	2	4	
sp|Q99538	274.1	5	14.3	2	1	2	1		5	1	1				
sp|P02750	1616.01	22	57.1	102	82	73	63	60	60	75	56	95	62	95	85
sp|P0C6S8	85.53	2	8.1					1	2	1					
sp|Q9HBL6	80.76	2	5.5	1		1	1	1		2					
sp|Q9P2V4	207.31	4	7.5	3		1	6	2	2	3	5	1		1	
sp|Q9NT99	171.95	4	13.6				4		5		3				
sp|Q13449	430.35	7	33.7	14	2	17	19	8	18	12	11	9	7	12	2
sp|P31025	295.16	5	46					1							13
sp|P18428	524.61	9	19.5	12	8	8	11	5		7	3	15	8	6	4
sp|P00338	308.57	5	22.6	2	1	3	6	2	3	3	6	4	4	5	6
sp|P07195	311.6	5	23.1	2	3	1	3		4	2	5	3	3	3	3
sp|P08637	71.43	2	7.1	1	1						1	2		1	1
sp|P98164	701.49	13	3.8	13	12	14	13	18	20	9	19	3	12	10	4
sp|P14151	51.35	1	12.9	1	2	1	1	1	1	1	1	1	1	2	1
sp|P51884	1154.59	19	46.7	35	46	32	30	30	40	27	25	27	48	24	39
sp|P11117	163.87	3	9	3		3	3	1	3	3	1		1		
sp|P10253	308.31	5	7.9	4	1	2	1	3	2	2	6		2		
sp|P10619	199.75	2	10.8	1		3	4	1	2	1	2				
sp|P42785	140.94	2	13.7			1	3		1					1	
sp|Q9UMR5	86.45	2	13.2	1		2			1	1	2				
sp|P11279	82.46	2	4.8	2		2	1	2	1	1	1			1	
sp|P13473	103.37	2	4.9		4		2		2	2	2		3	3	2
sp|P07333	154.9	3	8	3	2		1		1				2	2	
sp|P04156	93.87	2	9.1	1				1	1		2				
sp|P40925	217.47	4	20.4		1	3	4	1	2	2	3		1	2	
sp|Q9UM22	199.88	4	22.3	2	2	4	5	2	7	6	4		2		
sp|O00187	102.25	2	4.2										2		
sp|P33908	442.08	8	16.4	10	2	7	11	6	7	4	7	2	4	2	5
sp|Q9NR34	227.81	5	14.8	5	1	2	4	2	4	4	4	1	3	1	1
sp|P14780	143.47	3	8.9									3			
sp|P01033	271.18	4	40.6	8	3	3	7	7	12	6	10	3	5	7	6
sp|P16035	441.2	7	50.5	5	3	8	9	7	5	6	11	2	4	1	
sp|Q9UJH8	70.79	2	11.3	2			2		1		2				
sp|Q13228	157.8	3	8.5	2	1	2	1	3	2	1	5			1	
sp|P55083	105.73	2	14.5	2		1	2	1	1	2	3		1		1
sp|P20774	86.32	2	8.7		1		2	2	1		1		2		
sp|P26038	76.76	2	5.5	2							1	1	1	2	
sp|P08571	1108.78	15	47.2	38	29	21	30	20	25	20	20	26	27	26	20
sp|O60568	73.75	2	9.6	2			1		1	1					
sp|Q9H8L6	50.24	1	0.9	1	1	1	1		1	1	1	2	1	1	1
sp|Q7Z7M0	262.7	5	3.6	1			2	5	2	2	1	2	3	6	
sp|Q9UNW1	182.96	4	16.4	6	3	4	5	5	4	3	5	6	4	2	3
sp|Q99972	847.25	16	45	23	4	14	16	19	21	7	25	5	15	1	7
sp|Q8NEV4	33.67	1	1.6	1	1	2	1			1	1		1		
sp|P20933	327.25	6	32.1	7	4	8	6	2	7	8	11	1	5	4	
sp|P34059	88.61	2	6.1	1		1	1		2		2				
sp|P15586	602.77	11	22.1	14	5	16	16	11	24	14	15	2	8	5	3
sp|Q9NY97	71.57	2	5.3	2		1									
sp|Q96PD5	1739.77	24	54.9	35	46	30	40	37	45	39	40	41	54	32	49
sp|Q15223	70.7	2	6.4	1		1	1		1		2	1			
sp|Q92859	461.8	9	10.9	10	2	5	12	8	10	6	5	3	3	3	1
sp|P13591	1113.93	20	31.7	26	8	19	24	17	34	17	19	11	15	11	8
sp|P32004	131.27	3	5.9			1	2		3	1					
sp|O00533	1174.49	19	25.4	25	15	18	22	17	27	18	23	16	18	24	8
sp|Q9ULB1	293.26	7	8.3	5		4	4	6	9	4	5				

sp|Q9P2S2	230.83	4	5.4			2	4	2	7	2	4				
sp|Q9Y4C0	1448.81	26	28.2	19	7	20	24	21	38	20	23	3	10	9	3
sp|P41271	55.39	1	3.9	1	1	2	2	2	2	2	3		1	1	1
sp|O14594	642.11	13	11.4	22	4	10	23	5	21	22	11	5	5	2	4
sp|P16519	261.41	4	9.6	5	1	4	7	1	3	4	6		1		
sp|O94856	353.93	8	9.9	4		4		3	8	2	2	2	2		1
sp|P12036	99.33	2	2		2	1	2	1			1	1	2		2
sp|Q9NZ94	76.45	2	3.1	2											
sp|Q92823	1703.74	29	32.6	32	11	26	50	22	51	24	36	16	17	18	8
sp|Q7Z3B1	272.11	5	22.3	2		4	7	1	6	5	3		1		
sp|Q15818	118.2	2	9.7	1		1	2		1	2	1				
sp|P47972	145.06	3	6	2			4		1		2				
sp|O14786	160.55	3	5.5	3	1	1	3	2	2		1		1	1	
sp|O15240	213.95	4	9.3	2		1	4	1	1	1	1				
sp|Q99574	1110.15	20	51.7	24	12	40	25	22	32	23	33	14	11	7	4
sp|Q9P121	269.13	4	19.2	6		5	2	1	7	5	5	1	5	1	1
sp|P80188	178.22	3	23.2	1	1			3	1	1	1		1		2
sp|Q99784	120.69	2	6.6	4	1	2	3	1	4	2	2	2	3	1	
sp|O95897	141.15	3	5.7	5	2	2	3	1	2	2	2	2	2	2	1
sp|P61916	599.81	12	51.7	18	8	13	16	10	17	18	23	6	7	7	8
sp|Q02818	160.57	2	11.1	3		1	3	2	1	1	2	1	1	1	1
sp|Q8NGL6	40.53	1	2.3	1						1				2	
sp|P23515	537.15	11	20.2	16	8	12	26	1	8	11	8	8	3	5	4
sp|Q14982	84.79	2	13	2		1	1		1		1		1		
sp|Q9UBM4	1263.58	17	50.6	33	22	50	36	33	44	20	41	28	26	17	21
sp|Q99983	138.7	3	9.5		1	2		1	4		1		2		
sp|P10451	473.3	6	25.2	12	4	9	20	9	11	15	14	7	6	12	5
sp|Q86UD1	501.07	8	42.1	12	7	7	16	5	12	6	14	9	8	8	3
sp|P50897	304.5	6	26.1	6		4	3	4	7	4	6	1	1	1	
sp|O95497	361.93	6	25.9	2	10			1	1	1	1	1	4	5	
sp|O95428	350.27	7	11.3	5	1	2	4	3	8	4	3		3	1	
sp|Q9BXP8	571.33	12	9.9	8	7	8	7	12	11	8	8	14	12	11	4
sp|P26022	184.48	3	12.9	2			2		1	4					
sp|Q6UXB8	279.56	6	9.9	1	8	1	1	2	3	4	3	1	10		1
sp|P19021	502.29	9	14.5	11	2	4	11	5	6	8	13	3	3	2	1
sp|P23284	170.6	3	25.9	1			1		1		3				
sp|Q15063	279.59	4	15.8											4	
sp|P41219	41.17	1	4.7	2											
sp|Q06830	116.68	2	9.5	1	1		2				2				
sp|P32119	250.09	5	27.3	5	2	1	2		3	3	3	2	1	7	2
sp|P30086	224.3	4	26.7	2		2	5	1	2	3	6		1	1	1
sp|Q96S96	598.02	9	51.1	6	6	9	13	3	11	9	20	3	3	2	5
sp|P80108	558.36	10	15.4	9	6	3	10	10	7	2	2	9	15	2	4
sp|P00558	146.47	2	11.5	2	2	1	2	1	1	1	1	1	2	2	3
sp|P07205	146.47	2	12.5	1	1	1	1	1		1			1	1	3
sp|P18669	147.88	3	22				3								
sp|Q96FE7	89.79	2	9.9	1		1	1	2	1	1	1		1		1
sp|Q8IV08	201.17	4	16.7	7	1	3	4	5	5	5	2		2	2	1
sp|P55058	784.83	16	37.7	34	14	12	25	9	16	13	16	16	17	16	7
sp|P36955	4810.67	72	86.4	633	373	639	729	437	753	542	550	384	369	401	362
sp|Q63HQ2	138.61	2	3.1	3		3	1		2	2	2				
sp|Q9BTY2	191.41	4	24.2		1	5	1	1	4	2	1				
sp|P03952	815.86	15	28.8	9	14	7	10	8	9	5	7	24	15	23	15
sp|P05155	2293.45	34	45.4	159	144	128	142	176	172	89	131	123	158	148	121
sp|P05154	1023.65	17	43.3	33	26	26	35	36	20	27	33	43	38	39	28
sp|P00747	3225.8	53	65.2	76	92	68	92	103	93	43	82	138	111	77	94
sp|Q15195	83.11	2	27.1										3		
sp|Q02325	141	3	30.2	4				6	5		5	5	7		
sp|P13796	220.85	4	14.8	1	7	4	3	4	1		3	3	4	4	4
sp|Q8IUK5	193.35	3	14.8	1		3	3		3	1					
sp|Q6UX71	391.42	7	23.4	8	2	3	5	3	9	4	6	1	4	5	2
sp|O15031	509.78	10	7.7	6	1	6	1	6	11	7	11	1	6	2	
sp|P15151	80.56	2	5		2	1	1					1			
sp|Q86SR1	136.59	4	9.5	2	1		4		1	1				1	
sp|Q10471	109.22	2	8.2	2		1	2	1	1		1		1	1	1
sp|Q6S8J3	304.86	6	6.2	8										8	
sp|A5A3E0	343.2	6	6.5			5	6	6							7
sp|P0CG38	261.07	5	4.8		5				4						
sp|P20742	951.74	20	21	8	2	4	2	6	2	2		21	4	2	2
sp|O94913	35.66	1	1	2		1		2							
sp|Q8N0Y7	88.46	2	9.4	2					1	1				1	
sp|Q9H3G5	278.77	6	22.5	1	2	2	9	1	6	3	6	1	1		
sp|P09668	154.36	3	14				1		1	2	3				
sp|Q15113	202.94	4	14	2	1	1		4	2	3	4	1	5		1
sp|Q02809	151.9	3	7.8	4	1	2	2	2	1	2	2		1		
sp|P51888	358.02	8	29.1	7	3	8	9	6	5	8	11	2	2	2	1
sp|Q07954	118.74	3	1.3	3			1	2	2		2		1		
sp|Q12884	47.99	1	2.2	3	3										
sp|Q9UHG2	206.99	2	10.4	2			2			1				1	
sp|P07602	380.58	7	14.9	11		9	6	5	13	11	13		4		
sp|P41222	1728.38	22	73.7	288	124	199	254	188	419	219	367	117	130	97	125
sp|P02760	1100.26	16	50.6	49	54	23	39	38	28	33	51	56	64	43	58

sp|O75629	174.61	4	34.1	2	1	2	5	3	9	7	7		1		
sp|O60888	205.09	4	22.9	1	1	3	2	1	3	2	7	2	2	2	
sp|P30101	90.96	2	5.7	1		1			1		2				
sp|Q92520	846.58	12	48.9	18	2	15	19	9	22	19	26	5	3	8	1
sp|Q0P6D2	161.91	3	11.7	4		5	5		2	1	5		1		1
sp|Q99435	137.32	3	6.9	2	1	2	1	1	4	2	2	1	2		
sp|Q9UK55	303.54	5	17.3	1	6	2	2	1	2	2	1	6	7	7	6
sp|Q99497	103.39	3	22.8	1			2		2	2	4				
sp|P00734	2950.71	45	59.2	72	91	58	74	80	55	38	56	101	87	104	82
sp|Q6P1N9	39.41	1	5.7	1		2	1	1	1		2		2		1
sp|P48741	65.85	2	6	1		2	1				1	1		1	
sp|Q8NHP8	299.35	7	18.7	4	1	4	6	4	8	4	9				
sp|P14618	532.71	10	30.5	11	2	4	7	3	8	3	8	1	3	2	2
sp|P23468	141.06	4	2.2	1		2	3	3	4		3	1	1		
sp|P10586	471.26	9	7.9	4	1	3	9	6	10	1	3		1		
sp|P23470	182.44	4	3.5	4		3	3		4	2	1	1		1	
sp|Q13332	518.66	9	10.7	10	2	5	7	8	9	3	3	2	2	3	1
sp|P23471	527.34	9	4.5	14	4	10	17	7	16	8	13	3	7	5	2
sp|P78509	205.26	5	2.1	2	1	1	5	5	1	2	1		1		
sp|O75787	583.54	10	33.1	18	1	6	9	5	7	8	16	2	6		1
sp|Q9BSG5	322.35	5	23.6	9	1	1	3		4	4	6		1	1	
sp|P49788	173.43	3	18	1	4	7	4	3	8	2	3		2	2	3
sp|Q99969	285.88	6	55.8	7		6	5	1	5	6	7		1		
sp|P10745	9631.17	126	82.8	705	414	535	621	504	732	425	521	418	653	271	376
sp|P02753	1418.82	21	78.6	85	84	47	86	48	70	69	88	111	100	70	99
sp|O15537	537.69	9	44.2	24	14	15	16	14	25	10	16	7	9	4	10
sp|P07998	227.07	4	48.1	5	2	6	12	1	10	3	9	4	4	1	2
sp|O00584	215.65	4	21.9	5	2	5	6	5	5	6	7	3	4	4	1
sp|P10523	344.75	7	30.4	4	1		14		2		4				
sp|Q86VB7	237.87	6	5.8	4	5	1	2	2	3	1	2	3	6	3	1
sp|Q92765	650.03	10	26.2	22	8	12	23	13	13	14	22	7	10	7	4
sp|P05060	183.92	3	6.5	1		1	4		2	1				1	
sp|Q8WXD2	474.74	9	31.4	3		6	13	5	5	6	5	1	2	5	
sp|Q6UXD5	224.24	4	14.7	2			3		4	2					
sp|Q9BYH1	230.12	4	8.5	4		4	6	3	4	6	3	1	4	3	
sp|Q53EL9	442.88	7	11.4	11	2	11	15	11	15	7	10	7	6	7	2
sp|P49908	317	6	18.1	4	7	4	4	3	5	3	7	5	8	4	6
sp|Q14563	208.02	4	10.8	5		5	4	4	5	3	6	1	3	1	2
sp|Q13214	204.18	4	10.7	4	1	3	4	3	4	2	4	1	1		
sp|Q13275	346.79	7	10.4	8		3	1	1	4	3	3		1	1	1
sp|Q9NPR2	305.79	7	13.5	8		4	3	3	6	1	1	1	1	2	2
sp|Q9H2E6	111.01	3	3.7	1		1	1		3		1				
sp|O75326	1705.94	27	50.6	54	19	45	37	28	55	31	34	16	22	23	23
sp|Q92743	514.32	9	29.2	11		1	7	2	4	2	5		2	2	
sp|P02787	3536.02	59	66.5	107	72	111	78	58	124	87	73	70	65	96	48
sp|A8MV23	546.81	11	20	1	5	3	10	6	13	7	6	3	2		
sp|P02769	3488.31	55	74	107	186	137	159	129	282	182	160	133	157	126	134
sp|P02768	9989.69	142	88	837	1474	1157	1146	974	1237	1316	1159	932	1355	905	1041
sp|P35542	141.14	2	20			1	1		1		2		1		1
sp|P02743	548.24	8	31.8	7	11		12	7	6	14	11	16	16	16	17
sp|P27169	927.23	16	59.4	8	29	12	20	22	12	14	15	30	33	8	20
sp|Q15166	100.9	2	4.5	2	4	3	3	4	1	2	3	4	6	2	4
sp|P04278	516.57	9	45.8	8	9	4	4	5	3	4	4	17	9	5	6
sp|Q9HAT2	477.19	9	14.3	10	2	13	14	4	13	8	9	2	2	3	1
sp|Q99519	303.53	6	19.8	2	1	6	6	7	3	5	10	2	3		
sp|Q5TFQ8	138.28	3	8.3	2			1		4		1			1	
sp|Q9H156	66.62	2	3.8						2		1				
sp|O75093	31.77	1	1						1		2				
sp|P09486	234.98	5	23.4	6		5	8	3	3	2	3	7	1	4	1
sp|Q14515	1693.74	26	38.9	22	11	35	23	20	40	17	27	13	14	20	8
sp|P17405	61.77	1	1.6	1					2		1	1			
sp|Q9HCB6	1358.73	23	37.3	39	15	43	40	31	41	29	46	21	23	16	10
sp|O76061	81.1	2	10.3					2		2		1			1
sp|O00391	957.59	18	28.5	23	11	19	23	24	30	9	19	12	11	10	12
sp|Q8TAQ9	45.73	1	2.2	1			1	1		1	1		1	2	1
sp|P00441	266.17	4	58.4	2		5	4	1	2	2	5	1	1	1	
sp|Q7Z7G0	993.51	17	23.3	9	5	31	22	10	32	21	21	4	9	9	6
sp|P24821	768.21	13	10	8		3	11	5	1	15	6	1	8	16	
sp|Q92752	1001.48	16	17.4	10	6	12	11	8	18	12	4	2	2	3	1
sp|P22105	151.02	3	1.6					1				1		3	
sp|Q8IZW8	45.57	1	1.4	1				1	1	2					
sp|Q08629	318.01	6	16.4	12	7	13	18	10	18	15	13	8	10	4	3
sp|Q92563	198.5	3	10.8	2		3	5	3	5	2	1				
sp|Q9BQ16	229.14	4	10.3	6		4	3		11	3					
sp|P05452	896.75	13	62.4	10	18	14	20	13	19	13	29	8	16	6	11
sp|O00142	40.64	1	2.6					1							2
sp|P05543	1447.19	23	57.6	39	75	52	37	42	53	40	36	65	54	49	57
sp|P04066	183.94	4	12.7	1		4	2	1	1	2	2			2	
sp|P37837	112.39	2	9.2											2	
sp|P02786	86.86	2	4.6			2	1							1	2
sp|Q15582	682.34	14	38.9	17	18	6	11	18	7	4	7	9	8	9	17
sp|Q14956	60.14	2	3.3	2	1				1		1		1		

sp|Q24JP5	216.84	3	9	4		1	3	2	4		1		1		
sp|P02766	3336.44	38	80.3	664	310	446	674	482	704	523	624	375	460	514	554
sp|P60174	663.47	10	72	4	3	6	9	5	10	6	13	1	5	3	2
sp|O14773	1864.11	25	48.8	59	18	52	40	24	63	47	42	15	16	9	13
sp|P00761	112.3	2	7.8	7	9	7	8	7	7	11	9	7	8	9	8
sp|Q9GZX9	44.78	1	6.7	1		1	1	1	1	1	2	1	1		1
sp|P30530	131.39	3	3.4	3		2	3		2	2	1	2	2	4	1
sp|O75752	151.74	3	17.2	3		4	4		3	1	2				
sp|Q8N8K9	41.78	1	1.1	2	1	1	2		4	2	1		2	1	1
sp|P17948	92.58	2	4	2			1	1	1						
sp|Q6EMK4	684.21	9	21	12	8	6	11	14	12	7	9	6	10	10	11
sp|P13611	923.02	14	6.1	27	18	31	51	4	30	36	27	22	6	26	18
sp|Q12907	228.91	5	25.3	5		2	6		4	1	7	1	1	3	2
sp|P08670	285.19	6	21.2	7							1			1	
sp|P02774	5561.03	79	80.2	237	287	247	290	284	264	206	258	476	338	305	354
sp|P04070	116.08	3	13.2				1	1		1	1	3	2		1
sp|P07225	1432.89	21	31.7	39	15	20	23	25	23	20	22	22	26	20	18
sp|P04004	1261.38	21	34.1	31	75	36	41	54	33	48	34	78	51	71	53
sp|P04275	116.05	2	1.8	1				1				2	2	4	1
sp|Q8WY21	354.67	7	10.4	1		1	1	2	8	1	1				
sp|Q15904	449.47	7	20.6	11	1	4	11	7	9	10	12	2	3	1	
sp|Q5VU97	129.62	4	5.8	1			2		4		1	1			
sp|Q8TEU8	223.42	4	13.9	3	9	4	2	3	1	2	3		2		
sp|Q9Y5W5	973.49	15	36.7	49	9	52	37	27	45	33	67	17	23	10	6
sp|P12955	124.02	3	10.8	1	4	2	2	2	2	1	2	2	1	2	2
sp|Q86Y38	179.57	4	7.4	1			2	1	1	5			1		
sp|P25311	2260.71	34	64.1	108	121	97	131	90	72	105	126	137	108	140	178

Table S2.2 - Protein list corresponding to proteins identified in vitreous samples using MaxQuant with a 1% FDR.

Main Protein	Protein group	Number of proteins	Peptides	Razor + unique peptides	Unique peptides	Cover. [%]	Score
A8MV23	**A8MV23**	**1**	9	9	9	17.7	71.251
O00115	**O00115**	**1**	3	3	3	9.2	28.192
O00391	**O00391**	**1**	17	17	17	28	164.08
O00461	**O00461**	**1**	3	3	3	5.6	32.127
O00462	**O00462;Q9NQW7**	**2**	8	8	8	11.5	63.023
O00468	**O00468**	**1**	10	10	10	5.7	70.408
O00533	**O00533**	**1**	22	22	22	26.5	219.46
O00584	**O00584**	**1**	3	3	3	16.8	34.776
O14498	**O14498**	**1**	4	4	4	11.2	24.882
O14594	**O14594**	**1**	13	13	12	11.6	110.1
O14773	**O14773**	**1**	17	17	17	45.6	323.31
O14786	**O14786**	**1**	2	2	2	2.9	19.077
O14791	**O14791**	**1**	4	4	4	11.8	36.265
O14793	**O14793**	**1**	3	3	3	9.1	18.957
O15031	**O15031**	**1**	9	9	9	7	77.94
O15240	**O15240**	**1**	3	3	3	6	18.718
O15537	**O15537**	**1**	9	9	9	41.5	112.65
O43505	**O43505**	**1**	20	20	20	51.6	323.31
O60568	**O60568**	**1**	2	2	2	4.1	12.035
O60888	**O60888**	**1**	3	3	3	25.7	50.85
O75144	**O75144**	**1**	2	2	2	6.6	12.557
O75326	**O75326**	**1**	26	26	26	43.7	323.31
O75503	**O75503**	**1**	4	4	4	10.6	28.497
O75629	**O75629**	**1**	4	4	4	25	32.84
O75752	**O75752**	**1**	3	3	3	10	34.321
O75787	**O75787**	**1**	11	11	11	36.6	96.165
O75882	**O75882**	**1**	17	17	17	13	279.73
O94856	**O94856**	**1**	3	3	3	3.1	26.611
O94985	**O94985**	**1**	41	41	41	47.9	323.31
O95428	**O95428**	**1**	6	6	6	7.1	70.294
O95497	**O95497;Q9NY84**	**2**	6	6	6	14.4	44.976
O95897	**O95897**	**1**	2	2	2	4	15.135
P00338	**P00338;Q6ZMR3;P07864**	**3**	5	5	4	15.1	34.143
P00441	**P00441**	**1**	4	4	4	37	94.995
P00450	**P00450**	**1**	79	79	79	74.9	323.31
P00558	**P00558**	**1**	2	2	2	8.4	15.651
P00734	**P00734**	**1**	38	38	38	56.1	323.31
P00736	**P00736**	**1**	23	23	22	36.7	276.77
P00738	**P00738;P00739**	**2**	8	8	8	21.2	69.98
P00740	**P00740**	**1**	6	6	6	19.1	63.07
P00742	**P00742**	**1**	5	5	5	13.1	37.71
P00746	**P00746**	**1**	11	11	11	53	184.96
P00747	**P00747;Q15195;Q02325**	**3**	49	49	47	57.4	323.31
P00748	**P00748**	**1**	12	12	12	27.6	136.03
P00751	**P00751**	**1**	57	57	57	59.2	323.31
P00883	**P00883;P04075**	**2**	5	5	5	16.2	32.658
P00915	**P00915**	**1**	9	9	9	50.6	140.89
P00918	**P00918;P00921**	**2**	3	3	3	13.1	17.375
P01008	**P01008**	**1**	42	42	42	72	323.31
P01009	**P01009**	**1**	34	34	34	67.7	323.31
P01011	**P01011**	**1**	38	38	38	64.1	323.31
P01019	**P01019**	**1**	28	28	28	70.7	323.31
P01023	**P01023**	**1**	28	28	23	24.7	323.31
P01024	**P01024;O95568**	**2**	177	177	177	85	323.31
P01031	**P01031**	**1**	67	67	67	46.5	323.31
P01033	**P01033**	**1**	6	6	6	44.4	77.585
P01034	**P01034**	**1**	9	9	9	56.8	283.09
P01042	**P01042**	**1**	29	29	29	35.6	323.31
P01619	**P01619;A0A0C4DH25**	**2**	3	3	3	27.6	46.286
P01834	**P01834;P0DOX7**	**2**	8	8	8	82.2	323.31
P0DOX5	**P0DOX5;P01857**	**2**	12	12	5	34.5	225.38
P01859	**P01859**	**1**	9	6	3	30.7	74.246

P01876	**P01876**	**1**	11	11	6	39.4	123.98
P01877	**P01877;P0DOX2**	**2**	7	2	2	29.7	16.617
P02452	**P02452**	**1**	4	4	4	3.8	33.769
P02458	**P02458**	**1**	9	9	9	6.1	122.97
P02533	**P02533;Q04695;P08727;P19012;Q99456;P02534;Q14525;Q15323;P35900;P05783;Q14532;O76014;Q92764;O76015;O76013;Q7Z3Y9**	**16**	16	12	7	34.5	96.916
P02538	**P02538;P48668;O95678**	**3**	10	3	2	18.4	19.704
P02647	**P02647**	**1**	42	42	42	83.1	323.31
P02649	**P02649**	**1**	27	27	27	74.1	323.31
P02652	**P02652**	**1**	7	7	7	64	87.701
P02656	**P02656**	**1**	1	1	1	16.2	21.907
P02671	**P02671**	**1**	20	20	20	21.9	280.22
P02675	**P02675**	**1**	27	27	27	58	323.31
P02679	**P02679**	**1**	17	17	17	46.8	323.31
P02741	**P02741**	**1**	5	5	5	17.4	34.773
P02743	**P02743**	**1**	9	9	9	34.1	144.12
P02745	**P02745**	**1**	4	4	4	16.3	43.494
P02746	**P02746**	**1**	8	8	8	28.5	123.32
P02747	**P02747**	**1**	7	7	7	35.5	178.58
P02748	**P02748;REV__Q4AC99;Q96BY6**	**3**	25	25	25	41.9	323.31
P02749	**P02749**	**1**	21	21	21	67.8	323.31
P02750	**P02750**	**1**	19	19	19	53.3	323.31
P02751	**P02751**	**1**	34	34	34	22.3	323.31
P02753	**P02753**	**1**	14	14	14	75.1	323.31
P02760	**P02760**	**1**	17	17	17	50.6	323.31
P02763	**P02763**	**1**	6	6	4	27.9	43.234
P02765	**P02765**	**1**	22	22	22	62.9	323.31
P02766	**P02766**	**1**	19	19	19	80.3	323.31
P02768	**P02768**	**1**	90	90	83	88.7	323.31
P02769	**P02769**	**1**	42	35	35	69.2	323.31
P02774	**P02774**	**1**	50	50	50	81.9	323.31
P02787	**P02787**	**1**	53	53	53	68.5	323.31
P02790	**P02790**	**1**	44	44	44	76.2	323.31
P02792	**P02792**	**1**	7	7	7	43.4	68.264
P02794	**P02794**	**1**	3	3	3	16.9	20.556
P03951	**P03951**	**1**	4	4	4	6.2	25.198
P03952	**P03952;P20718**	**2**	17	17	17	31.2	157.4
P04003	**P04003**	**1**	4	4	4	6.7	39.576
P04004	**P04004**	**1**	14	14	14	33.1	323.31
P04062	**P04062**	**1**	3	3	3	6.5	17.816
P04066	**P04066**	**1**	3	3	3	8.8	18.031
P04114	**P04114**	**1**	17	17	17	4.4	108.36
P04196	**P04196**	**1**	22	22	22	39.4	323.31
P04217	**P04217**	**1**	29	29	29	65.3	323.31
P04264	**P04264**	**1**	36	36	32	55.7	323.31
P04275	**P04275**	**1**	3	3	3	1.5	18.361
P04278	**P04278**	**1**	10	10	10	40.5	102.9
P04406	**P04406;O14556**	**2**	11	11	11	42.1	126.64
P05062	**P05062**	**1**	3	3	3	11.3	29.837
P05067	**P05067**	**1**	22	20	20	27.3	323.31
P05090	**P05090**	**1**	10	10	10	40.2	164.93
P05154	**P05154**	**1**	15	15	15	40.4	323.31
P05155	**P05155**	**1**	26	26	26	43.8	323.31
P05156	**P05156**	**1**	28	28	28	44.4	323.31
P05160	**P05160**	**1**	4	4	4	7.3	24.888
P05452	**P05452**	**1**	8	8	8	47	259.09
P05543	**P05543**	**1**	21	21	21	54.5	323.31
P05546	**P05546**	**1**	23	23	23	47.5	263.45
P06396	**P06396;REV__Q6TDU7**	**2**	45	45	45	56.8	323.31
P06681	**P06681**	**1**	29	29	29	39.9	323.31
P06727	**P06727**	**1**	45	45	45	67.4	323.31
P06733	**P06733**	**1**	4	3	3	14.3	20.718
P06865	**P06865**	**1**	14	14	14	27	127.82
P07195	**P07195**	**1**	4	3	3	13.8	19.795
P07225	**P07225**	**1**	17	17	17	24.6	253.76
P07333	**P07333**	**1**	2	2	2	2.7	12.523
P07339	**P07339**	**1**	28	28	28	65.3	323.31
P07357	**P07357**	**1**	16	16	16	29.8	273.3
P07358	**P07358**	**1**	20	20	20	39.4	267.77

P07360	**P07360**	**1**	9	9	9	61.9	280.57
P07602	**P07602**	**1**	6	6	6	13	43.229
P07686	**P07686**	**1**	13	13	13	26.4	100.57
P07711	**P07711;Q5NE16;P43235;O60911**	**4**	7	7	7	28.2	90.95
P07858	**P07858**	**1**	10	10	10	38.1	117.32
P07998	**P07998**	**1**	4	4	4	48.1	53.295
P08123	**P08123**	**1**	5	5	5	4.2	56.604
P08185	**P08185**	**1**	17	17	17	56.8	323.31
P08195	**P08195**	**1**	6	6	6	14	53.342
P08253	**P08253**	**1**	16	16	16	29.7	129.6
P08294	**P08294**	**1**	8	8	8	42.9	178.74
P08519	**P08519**	**1**	4	2	2	1	20.279
P08571	**P08571**	**1**	14	14	14	45.6	323.31
P08603	**P08603;Q02985**	**2**	58	58	53	53.5	323.31
P08637	**P08637;O75015**	**2**	2	2	2	7.1	12.744
P08670	**P08670;P17661**	**2**	2	2	2	4.7	29.286
P08697	**P08697**	**1**	25	25	25	66.6	323.31
P09104	**P09104;P13929**	**2**	4	4	3	12.4	26.915
P09486	**P09486**	**1**	6	6	6	23.4	46.491
P09871	**P09871**	**1**	18	18	18	33.4	312.58
P09972	**P09972**	**1**	4	4	4	17	91.06
P0C0L4	**P0C0L4**	**1**	117	6	6	65.9	139.81
P0C0L5	**P0C0L5**	**1**	119	119	8	66.5	323.31
P0C6S8	**P0C6S8**	**1**	2	2	2	3.9	12.444
P0DOY3	**P0DOY3;P0DOY2;P0DOX8;P0CG04;B9A064;P0CF74;A0M8Q6**	**7**	6	6	6	82.1	54.371
P10253	**P10253**	**1**	4	4	4	5.4	27.544
P10451	**P10451**	**1**	8	8	8	34.1	172.05
P10523	**P10523**	**1**	7	7	7	27.7	49.213
P10586	**P10586**	**1**	7	7	6	3.8	44.795
P10619	**P10619**	**1**	2	2	2	5.6	17.985
P10643	**P10643;Q12884**	**2**	31	31	31	42.8	323.31
P10645	**P10645**	**1**	11	11	11	26.5	115.52
P10745	**P10745**	**1**	68	68	68	80.4	323.31
P10909	**P10909**	**1**	27	27	27	46.5	323.31
P11021	**P11021**	**1**	4	4	4	9	30.875
P11117	**P11117**	**1**	4	4	4	9	26.53
P12109	**P12109**	**1**	13	13	13	19.4	129.04
P12111	**P12111**	**1**	4	4	4	1.9	25.557
P12259	**P12259**	**1**	8	8	8	5	53.15
P12955	**P12955**	**1**	2	2	2	4.3	12.218
P13591	**P13591**	**1**	15	15	15	24.6	177.26
P13611	**P13611**	**1**	13	13	13	4.5	323.31
P13645	**P13645;O77727;Q7Z3Y7;Q7Z3Z0;Q7Z3Y8;Q2M2I5**	**6**	30	30	24	56.3	323.31
P13647	**P13647;P05787;Q7RTS7;Q86Y46;P08729;Q14CN4;Q8N1N4;Q3SY84;Q9NSB2;P12036**	**10**	13	9	7	21.4	82.354
P13671	**P13671**	**1**	20	20	20	26.1	314.65
P13796	**P13796;P13797**	**2**	5	5	5	10.4	30.004
P14618	**P14618;P30613**	**2**	9	9	9	22.4	66.316
P14625	**P14625**	**1**	4	4	4	5.2	23.362
P15169	**P15169**	**1**	8	8	8	23.8	71.539
P15291	**P15291**	**1**	5	5	5	23.4	36.128
P15586	**P15586**	**1**	8	8	8	14.9	77.803
P16035	**P16035**	**1**	6	6	6	23.6	112.77
P16070	**P16070**	**1**	2	2	2	3	18.091
P16112	**P16112**	**1**	2	2	2	1	12.486
P16519	**P16519**	**1**	6	6	6	11.8	42.129
P16870	**P16870**	**1**	25	25	25	54.2	323.31
P17050	**P17050**	**1**	6	6	6	19.7	60.187
P17174	**P17174**	**1**	7	7	7	22.5	44.729
P17900	**P17900**	**1**	6	6	6	29.5	41.949
P18428	**P18428**	**1**	8	8	8	22	60.525
P18669	**P18669;P15259;Q8N0Y7**	**3**	3	3	3	17.7	18.895
P19021	**P19021**	**1**	12	12	12	14.8	85.238
P19022	**P19022**	**1**	9	9	9	12	88.982
P19652	**P19652**	**1**	5	3	3	24.4	28.643
P19823	**P19823**	**1**	28	28	28	35.2	323.31
P19827	**P19827**	**1**	30	30	30	44.8	323.31
P20742	**P20742**	**1**	17	12	12	13	92.385
P20933	**P20933**	**1**	4	4	4	19.7	46.326

P21810	**P21810**	**1**	2	2	2	8.7	14.091
P22304	**P22304**	**1**	8	8	8	18.2	72.055
P22352	**P22352**	**1**	14	14	14	47.3	323.31
P22792	**P22792**	**1**	10	10	10	21.5	92.899
P22914	**P22914**	**1**	5	5	5	34.3	43.747
P23142	**P23142**	**1**	12	12	12	20.3	155.02
P23284	**P23284**	**1**	2	2	2	9.3	12.051
P23435	**P23435**	**1**	3	3	3	13	16.923
P23468	**P23468**	**1**	4	3	3	2.2	17.23
P23470	**P23470**	**1**	4	4	4	3.5	34.685
P23471	**P23471**	**1**	10	10	10	4.9	93.27
P23515	**P23515**	**1**	9	9	9	21.4	142.83
P24592	**P24592**	**1**	3	3	3	15.8	31.252
P24821	**P24821**	**1**	13	13	13	8	101.41
P25311	**P25311**	**1**	24	24	24	61.1	323.31
P26022	**P26022**	**1**	3	3	3	9.4	19.478
P26927	**P26927;Q2TV78**	**2**	3	3	3	5.1	19.035
P26992	**P26992**	**1**	2	2	2	4.8	12.329
P27169	**P27169**	**1**	14	14	14	47.6	190.09
P27797	**P27797**	**1**	7	7	7	21.3	48.895
P29622	**P29622**	**1**	27	27	27	66.5	323.31
P30086	**P30086**	**1**	7	7	7	56.7	63.438
P30530	**P30530**	**1**	2	2	2	2.6	17.186
P31025	**P31025;Q5VSP4**	**2**	5	5	5	34.7	43.397
P32004	**P32004**	**1**	2	2	2	2	13.316
P32119	**P32119;Q06830**	**2**	6	6	6	27.3	40.544
P33151	**P33151**	**1**	6	6	6	8.9	38.289
P33908	**P33908**	**1**	9	9	9	14.4	55.708
P35052	**P35052**	**1**	5	5	5	10.4	34.109
P35443	**P35443**	**1**	3	2	2	4.1	12.47
P35527	**P35527**	**1**	23	22	22	49.9	323.31
P35542	**P35542**	**1**	2	2	2	20	14.678
P35858	**P35858**	**1**	19	19	19	38	323.31
P35908	**P35908;Q01546;Q5XKE5;P19013;Q7Z794;P12035**	**6**	28	26	22	50.2	323.31
P36222	**P36222**	**1**	21	21	21	57.2	323.31
P36955	**P36955**	**1**	49	49	49	78.7	323.31
P36980	**P36980**	**1**	9	3	3	48.9	36.669
P39060	**P39060**	**1**	11	11	11	8.8	114
P40189	**P40189**	**1**	8	8	8	11	64.563
P40925	**P40925**	**1**	2	2	2	6.6	13.028
P41222	**P41222**	**1**	15	15	15	70.5	323.31
P42785	**P42785**	**1**	3	3	3	7.7	25.298
P43234	**P43234**	**1**	3	3	3	8.1	16.602
P43251	**P43251**	**1**	14	14	14	30.9	323.31
P43320	**P43320**	**1**	5	5	5	31.2	34.314
P43652	**P43652**	**1**	39	39	39	57.9	323.31
P48058	**P48058**	**1**	7	7	7	7.5	73.95
P48723	**P48723**	**1**	9	9	9	26.3	58.471
P49747	**P49747**	**1**	3	3	2	6.1	17.343
P49788	**P49788**	**1**	4	4	4	13.6	28.762
P49908	**P49908**	**1**	5	5	5	16	41.068
P50897	**P50897**	**1**	4	4	4	18.3	39.678
P51693	**P51693**	**1**	14	14	14	21.5	263.73
P51884	**P51884**	**1**	18	18	18	45.3	323.31
P51888	**P51888**	**1**	9	9	9	28	81.049
P54802	**P54802**	**1**	6	6	6	12.4	39.01
P55058	**P55058**	**1**	16	16	16	47.5	152.75
P55083	**P55083**	**1**	2	2	2	9.8	32.265
P60174	**P60174**	**1**	10	10	10	47.2	83.8
P63261	**P63261;P60709;P63267;P68133;P68032;P62736;Q6S8J3;A5A3E0;P0CG38;Q9BYX7;Q562R1;P0CG39**	**12**	13	13	13	42.9	201.45
P61769	**P61769**	**1**	3	3	3	35.3	26.221
P61916	**P61916**	**1**	10	10	10	51.7	104.8
P68871	**P68871;P02042;P69892;P69891;P02100**	**5**	14	14	14	95.2	244.74
P69905	**P69905**	**1**	7	7	7	71.1	97.17
P78509	**P78509**	**1**	2	2	2	0.6	13.438
P80108	**P80108**	**1**	11	11	11	17.1	95.996
P80188	**P80188**	**1**	3	3	3	21.7	49.482

P98160	**P98160**	**1**	30	30	30	8.7	283.07
P98164	**P98164**	**1**	14	14	14	3.2	107.24
Q01459	**Q01459**	**1**	3	3	3	11.4	43.689
Q02246	**Q02246**	**1**	11	11	11	15.1	71.677
Q02809	**Q02809**	**1**	7	7	7	13.1	42.181
Q02818	**Q02818**	**1**	5	5	5	13	31.594
Q03591	**Q03591;Q9BXR6**	**2**	14	9	4	57.3	249.82
Q04756	**Q04756**	**1**	5	5	5	9.2	49.864
Q06033	**Q06033**	**1**	17	17	17	26.2	181.94
Q06481	**Q06481**	**1**	32	32	30	40.5	323.31
Q08380	**Q08380**	**1**	14	14	14	27.7	280.9
Q08431	**Q08431**	**1**	2	2	2	7.5	20.344
Q08629	**Q08629;Q9BQ16**	**2**	5	5	5	11.6	46.054
Q09328	**Q09328**	**1**	3	3	3	6.7	25.374
Q0P6D2	**Q0P6D2**	**1**	2	2	2	4.3	13.409
Q10471	**Q10471**	**1**	2	2	2	3.9	12.209
Q12805	**Q12805**	**1**	19	19	19	44.2	323.31
Q12841	**Q12841**	**1**	7	7	7	21.4	54.387
Q12860	**Q12860**	**1**	24	24	24	27.4	273.15
Q12907	**Q12907**	**1**	5	5	5	22.5	35.476
Q13214	**Q13214**	**1**	3	3	3	3.9	23.228
Q13231	**Q13231**	**1**	5	5	5	14.4	30.247
Q13275	**Q13275**	**1**	4	4	4	5.7	25.274
Q13332	**Q13332**	**1**	11	11	11	9.8	146.1
Q13449	**Q13449**	**1**	8	8	8	31.4	69.712
Q13510	**Q13510**	**1**	11	11	11	31.4	114.47
Q13822	**Q13822**	**1**	36	36	36	46.6	323.31
Q14050	**Q14050**	**1**	3	3	3	6.4	18.702
Q14055	**Q14055**	**1**	2	2	2	3.9	38.055
Q14118	**Q14118**	**1**	7	7	7	10.9	91.471
Q14393	**Q14393**	**1**	3	3	3	5	20.288
Q14515	**Q14515**	**1**	25	25	25	43.2	323.31
Q14520	**Q14520**	**1**	7	7	7	12.7	61.129
Q14563	**Q14563**	**1**	4	4	4	7.1	39.374
Q14624	**Q14624**	**1**	45	45	45	54.8	323.31
Q14767	**Q14767**	**1**	6	6	6	4.1	36.818
Q15063	**Q15063**	**1**	3	3	3	5.5	21.029
Q15113	**Q15113**	**1**	4	4	4	12.7	28.338
Q15223	**Q15223**	**1**	3	3	3	8.1	18.881
Q15582	**Q15582**	**1**	19	19	19	37.6	144.17
Q15818	**Q15818**	**1**	5	5	5	11.1	30.755
Q15846	**Q15846**	**1**	6	6	6	19.5	81.814
Q15848	**Q15848**	**1**	2	2	2	12.3	18.112
Q15904	**Q15904**	**1**	7	7	7	18.5	131.26
Q16270	**Q16270**	**1**	7	7	7	24.5	72.759
Q16610	**Q16610**	**1**	13	13	13	29.8	168.24
Q16769	**Q16769**	**1**	6	6	6	21.1	68.299
Q24JP5	**Q24JP5**	**1**	4	4	4	5.9	43.418
Q4KMG0	**Q4KMG0**	**1**	3	3	3	4.3	31.865
Q53EL9	**Q53EL9**	**1**	10	10	10	14.5	83.766
Q5VU97	**Q5VU97**	**1**	4	4	4	3.6	23.616
Q63HQ2	**Q63HQ2**	**1**	3	3	3	3.9	19.155
Q6EMK4	**Q6EMK4**	**1**	9	9	9	17.4	186.89
Q6MZW2	**Q6MZW2**	**1**	11	9	9	17.5	171.2
Q6UX71	**Q6UX71**	**1**	6	6	6	15.1	62.89
Q6UXB8	**Q6UXB8**	**1**	5	5	5	11.4	30.96
Q6UXD5	**Q6UXD5**	**1**	5	5	5	11	37.671
Q7Z3B1	**Q7Z3B1**	**1**	3	3	3	12.7	32.078
Q7Z7G0	**Q7Z7G0**	**1**	15	15	15	18.2	167.24
Q7Z7M0	**Q7Z7M0**	**1**	5	5	5	2.3	39.839
Q86SR1	**Q86SR1;Q49A17**	**2**	3	3	3	8	21.142
Q86UD1	**Q86UD1**	**1**	6	6	6	32.2	102.91
Q86UX2	**Q86UX2**	**1**	16	16	16	19.6	109.66
Q86VB7	**Q86VB7**	**1**	6	6	6	5.5	38.041
Q8IUK5	**Q8IUK5**	**1**	5	5	5	15.6	36.648
Q8IV08	**Q8IV08**	**1**	5	5	5	13.3	33.83
Q8IWV2	**Q8IWV2;Q9UQ52**	**2**	9	9	9	10.3	56.444
Q8IZJ3	**Q8IZJ3**	**1**	25	25	25	20	220.3

Q8N3J6	**Q8N3J6**	**1**	5	5	5	16.1	33.849
Q8N475	**Q8N475**	**1**	28	28	26	39.9	213.27
Q8N4T0	**Q8N4T0**	**1**	1	1	1	2.7	16.935
Q8NCC3	**Q8NCC3**	**1**	5	5	5	17.5	32.24
Q8NES3	**Q8NES3**	**1**	2	2	2	5.3	12.552
Q8NFZ8	**Q8NFZ8**	**1**	3	3	3	10.3	23.635
Q8NHP8	**Q8NHP8**	**1**	6	6	6	11.9	36.429
Q8TEU8	**Q8TEU8**	**1**	4	4	4	6.9	26.557
Q8WXD2	**Q8WXD2**	**1**	3	3	3	9	25.104
Q8WY21	**Q8WY21**	**1**	4	4	4	4.2	29.83
Q92484	**Q92484**	**1**	5	5	5	10.6	39.877
Q92520	**Q92520**	**1**	11	11	11	53.3	168.54
Q92563	**Q92563**	**1**	4	4	4	10.8	26.9
Q92743	**Q92743**	**1**	7	7	7	20.8	55.675
Q92752	**Q92752**	**1**	13	13	13	13.8	102.97
Q92765	**Q92765**	**1**	7	7	7	25.5	72.878
Q92820	**Q92820**	**1**	9	9	9	32.7	121.64
Q92823	**Q92823**	**1**	26	26	26	27.9	323.31
Q92859	**Q92859**	**1**	13	13	13	13.4	99.688
Q96FE7	**Q96FE7**	**1**	2	2	2	9.9	12.625
Q96GW7	**Q96GW7**	**1**	9	8	8	7.6	48.927
Q96IY4	**Q96IY4**	**1**	11	11	11	30.3	183.93
Q96JP9	**Q96JP9**	**1**	7	7	7	11.8	66.714
Q96KN2	**Q96KN2**	**1**	15	15	15	35.3	185.51
Q96KR1	**Q96KR1**	**1**	2	2	2	2.8	12.152
Q96PD5	**Q96PD5**	**1**	22	22	22	58.9	323.31
Q96S86	**Q96S86;Q86UW8**	**2**	11	11	11	36.9	68.837
Q96S96	**Q96S96**	**1**	8	8	8	51.1	184.07
Q99435	**Q99435**	**1**	4	4	4	4.8	24.124
Q99519	**Q99519**	**1**	5	5	5	11.3	40.607
Q99538	**Q99538**	**1**	4	4	4	13.2	23.446
Q99574	**Q99574**	**1**	14	14	14	39.3	175.57
Q99784	**Q99784**	**1**	3	3	3	7.6	19.147
Q99969	**Q99969**	**1**	6	6	6	55.8	60.145
Q99972	**Q99972**	**1**	17	17	17	35.9	227.83
Q9BQT9	**Q9BQT9**	**1**	5	5	5	6.6	40.122
Q9BRK5	**Q9BRK5**	**1**	7	7	7	20.2	46.417
Q9BSG5	**Q9BSG5**	**1**	2	2	2	12.2	46.199
Q9BTY2	**Q9BTY2**	**1**	5	5	5	12.2	29.111
Q9BU40	**Q9BU40**	**1**	4	4	4	11.3	39.109
Q9BXJ4	**Q9BXJ4**	**1**	4	4	4	16.3	32.871
Q9BXP8	**Q9BXP8**	**1**	12	12	12	8.8	133.3
Q9BY67	**Q9BY67**	**1**	7	7	7	25.8	150.38
Q9BYH1	**Q9BYH1**	**1**	3	3	3	2.7	18.941
Q9GZX9	**Q9GZX9**	**1**	1	1	1	6.7	15.954
Q9H3G5	**Q9H3G5**	**1**	6	6	6	13.4	40.653
Q9H4D0	**Q9H4D0**	**1**	4	4	4	4.8	22.147
Q9HAT2	**Q9HAT2**	**1**	7	7	7	17.2	72.464
Q9HCB6	**Q9HCB6**	**1**	23	23	23	34.4	323.31
Q9NPH3	**Q9NPH3**	**1**	3	3	3	5.3	17.759
Q9NPR2	**Q9NPR2**	**1**	10	10	10	14.8	67.866
Q9NQ79	**Q9NQ79**	**1**	21	21	21	38	323.31
Q9NR34	**Q9NR34**	**1**	4	4	4	6.3	24.324
Q9NS85	**Q9NS85**	**1**	2	2	2	9.8	17.04
Q9NZ08	**Q9NZ08**	**1**	5	5	5	6.7	32.907
Q9NZP8	**Q9NZP8**	**1**	6	5	5	15	96.637
Q9P0K1	**Q9P0K1**	**1**	2	2	2	2.4	12.094
Q9P121	**Q9P121;Q14982**	**2**	8	8	8	27.9	55.458
Q9P2S2	**Q9P2S2;P58401**	**2**	6	5	5	4.1	36.951
Q9P2V4	**Q9P2V4**	**1**	4	4	4	6.6	25.765
Q9UBM4	**Q9UBM4**	**1**	16	16	16	50.6	323.31
Q9UBP4	**Q9UBP4**	**1**	14	14	14	45.7	323.31
Q9UBR2	**Q9UBR2**	**1**	4	4	4	15.8	45.375
Q9UBX1	**Q9UBX1**	**1**	6	6	6	14.3	39.973
Q9UBX7	**Q9UBX7**	**1**	3	3	3	10.6	16.457
Q9UGM5	**Q9UGM5**	**1**	7	7	7	25.4	52.387
Q9UHG2	**Q9UHG2**	**1**	3	3	3	14.2	23.986
Q9UHI8	**Q9UHI8**	**1**	2	2	2	5.3	15.754
Q9UHL4	**Q9UHL4**	**1**	12	12	12	31.3	168.94

Q9UK55	**Q9UK55**	**1**	6	6	6	14.4	40.513
Q9ULX7	**Q9ULX7**	**1**	2	2	2	6.5	15.747
Q9UM22	**Q9UM22**	**1**	3	3	3	15.6	31.724
Q9UMR5	**Q9UMR5**	**1**	4	4	4	16.2	28.724
Q9UNW1	**Q9UNW1**	**1**	8	8	8	20.5	64.13
Q9Y287	**Q9Y287**	**1**	2	2	2	12.4	13.394
Q9Y2E5	**Q9Y2E5**	**1**	1	1	1	1.4	22.135
Q9Y4C0	**Q9Y4C0;Q9HDB5;Q9ULB1**	**3**	25	25	24	18.9	273.07
Q9Y4L1	**Q9Y4L1**	**1**	2	2	2	2	13.798
Q9Y5W5	**Q9Y5W5**	**1**	10	10	10	32.2	208.16
Q9Y5Y7	**Q9Y5Y7**	**1**	1	1	1	5.3	14.275
Q9Y646	**Q9Y646**	**1**	5	5	5	12.5	37.522
Q9Y6R7	**Q9Y6R7**	**1**	73	73	73	29.7	323.31
O95967	**O95967**	**1**	2	2	2	4.7	11.631
P13473	**P13473**	**1**	2	2	2	4.1	11.679
P15848	**P15848**	**1**	2	2	2	3.9	11.684
Q07954	**Q07954**	**1**	2	2	2	0.5	11.688
Q03167	**Q03167**	**1**	2	2	2	3.1	11.702
P00761	**P00761**	**1**	2	2	2	7.8	11.72
P21817	**P21817**	**1**	2	2	2	0.6	11.729
P17931	**P17931**	**1**	2	2	2	7.2	11.749
O00187	**O00187**	**1**	2	2	2	3.9	11.782
P62258	**P62258;P63104;P27348;Q04917;P31946; P61981;P31947**	**7**	2	2	2	7.5	11.815
Q8TD57	**Q8TD57**	**1**	2	2	2	0.7	11.953
O95390	**O95390**	**1**	2	2	2	7.1	11.962
Q17R60	**Q17R60**	**1**	2	2	2	2.9	12.02
Q02487	**Q02487**	**1**	2	2	2	2.7	11.298
P02788	**P02788**	**1**	1	1	1	1.8	11.337
P14151	**P14151**	**1**	2	2	2	7	11.527
P14780	**P14780**	**1**	1	1	1	2.3	7.118
Q8IUB2	**Q8IUB2**	**1**	1	1	1	3.9	7.1685
Q16706	**Q16706**	**1**	1	1	1	1.8	7.1721
P24593	**P24593**	**1**	1	1	1	5.1	7.2033
O95196	**O95196**	**1**	1	1	1	2.3	7.308
Q96FE5	**Q96FE5**	**1**	1	1	1	2.1	7.3426
Q9NT99	**Q9NT99**	**1**	1	1	1	2.2	7.5007
A2NJV5	**A2NJV5;A0A0A0MRZ7;A0A075B6S6; A0A075B6S2;A0A075B6P5;A0A087WW87; P06310;P01615;P01614**	**9**	1	1	1	10.8	7.532
Q8TAA9	**Q8TAA9**	**1**	1	1	1	2.3	7.6023
P15289	**P15289**	**1**	1	1	1	3.4	7.6072
O75815	**O75815**	**1**	1	1	1	2.4	7.614
P11362	**P11362**	**1**	1	1	1	1.6	7.8361
P61812	**P61812**	**1**	1	1	1	3.9	7.8453
Q9BZR6	**Q9BZR6**	**1**	1	1	1	2.5	7.8486
Q9UBF8	**Q9UBF8**	**1**	1	1	1	1.7	7.9582
P01861	**P01861**	**1**	7	1	1	30	8.0328
Q8WZA1	**Q8WZA1**	**1**	1	1	1	2.9	8.0635
P09211	**P09211**	**1**	1	1	1	9.5	8.164
P00505	**P00505**	**1**	1	1	1	3.3	8.3258
P17405	**P17405**	**1**	1	1	1	1.6	8.3747
P07093	**P07093**	**1**	1	1	1	3.5	8.7218
P20849	**P20849**	**1**	1	1	1	1.5	8.9629
O43405	**O43405**	**1**	1	1	1	2	9.3877
P47972	**P47972**	**1**	2	2	2	4.6	10.637
P15924	**P15924**	**1**	2	2	2	0.9	10.911
O94991	**O94991**	**1**	2	2	2	3.8	10.914
Q96DT5	**Q96DT5**	**1**	2	2	2	0.5	10.927
Q70CQ2	**Q70CQ2**	**1**	2	2	2	1	10.981
Q8NEK5	**Q8NEK5**	**1**	2	2	2	7.7	10.984
P55268	**P55268**	**1**	1	1	1	0.6	10.999
Q99453	**Q99453**	**1**	2	2	2	5.1	11.058
P0CAP1	**P0CAP1**	**1**	2	2	2	5.6	11.088
P07315	**P07315**	**1**	2	2	2	12.6	11.093
O75493	**O75493**	**1**	2	2	2	5.8	11.12
Q86Y38	**Q86Y38**	**1**	2	2	2	2.6	11.132
Q8N8K9	**Q8N8K9**	**1**	2	2	2	4.3	11.18
Q9H254	**Q9H254**	**1**	2	2	2	0.9	11.181
P49257	**P49257**	**1**	1	1	1	2.4	6.9305
Q9BXJ0	**Q9BXJ0**	**1**	1	1	1	6.2	6.9334

Q9UNN8	**Q9UNN8**	**1**	1	1	1	7.1	6.9596
Q5TFQ8	**Q5TFQ8;P78324**	**2**	1	1	1	3.5	6.9756
Q5KU26	**Q5KU26**	**1**	1	1	1	1.3	7.0039

Table S3.1 - Proteins found differentially expressed in PDR compared to ERM. Proteins highlighted in red and green represent. respectively. underexpressed and overexpressed proteins in PDR compared to ERM.

Main Protein	Protein names	log2 Fold change	-Log Student's T-test p-value	Student's T-test q-value	Student's T-test Difference	Student's T-test Test statistic
P19022	Cadherin-2	-5.34	3.09	0.00	-4.44	-5.44
Q15904	V-type proton ATPase subunit S1	-5.00	1.40	0.02	-3.62	-2.44
P17050	Alpha-N-acetylgalactosaminidase	-4.65	2.48	0.00	-3.52	-4.15
P10451	Osteopontin	-4.53	2.14	0.01	-3.69	-3.60
Q9P121	Neurotrimin	-4.30	1.62	0.01	-3.30	-2.75
Q96S96	Phosphatidylethanolamine-binding protein 4	-4.17	1.23	0.03	-3.46	-2.18
O75629	Protein CREG1	-4.15	3.61	0.00	-2.58	-5.94
P16035	Metalloproteinase inhibitor 2	-4.12	2.17	0.01	-3.95	-3.66
Q08380	Galectin-3-binding protein	-4.11	3.02	0.00	-4.30	-5.26
Q9HAT2	Sialate O-acetylesterase	-4.08	1.46	0.02	-2.43	-2.44
P01034	Cystatin-C	-4.08	3.17	0.00	-3.60	-5.44
O60888	Protein CutA	-3.94	1.99	0.01	-3.93	-3.38
Q92752	Tenascin-R	-3.88	2.19	0.01	-2.95	-3.58
P07686	Beta-hexosaminidase subunit beta	-3.80	1.19	0.03	-3.10	-2.10
O75787	Renin receptor	-3.73	1.91	0.01	-2.93	-3.16
P30086	Phosphatidylethanolamine-binding protein 1	-3.71	1.25	0.03	-2.05	-2.12
P20933	N(4)-(beta-N-acetylglucosaminyl)-L-asparaginase	-3.51	2.12	0.01	-3.36	-3.53
Q8N475	Follistatin-related protein 5	-3.34	1.65	0.01	-3.00	-2.77
P06865	Beta-hexosaminidase subunit alpha	-3.31	1.27	0.02	-3.98	-2.26
Q9Y4C0	Neurexin-3	-3.27	2.26	0.01	-4.14	-3.84
P39060	Collagen alpha-1(XVIII) chain	-3.27	2.01	0.01	-3.05	-3.32
Q99972	Myocilin	-3.20	1.72	0.01	-2.97	-2.87
Q92859	Neogenin	-3.02	1.66	0.01	-2.52	-2.74
Q96GW7	Brevican core protein	-2.96	1.98	0.01	-2.98	-3.27
Q7Z7G0	Target of Nesh-SH3	-2.92	2.78	0.00	-2.62	-4.48
P61769	Beta-2-microglobulin	-2.87	1.49	0.02	-2.60	-2.50
P15586	N-acetylglucosamine-6-sulfatase	-2.81	2.77	0.00	-2.68	-4.47
Q99519	Sialidase-1	-2.79	2.54	0.00	-2.34	-4.01
Q9BXJ4	Complement C1q tumor necrosis factor-related protein 3	-2.77	2.50	0.00	-2.77	-4.06
Q13510	Acid ceramidase	-2.77	1.64	0.01	-2.42	-2.69
Q92520	Protein FAM3C	-2.75	2.40	0.01	-2.49	-3.83
P48058	Glutamate receptor 4	-2.73	1.66	0.01	-2.16	-2.70
P61916	NPC intracellular cholesterol transporter 2	-2.61	2.00	0.01	-2.68	-3.26
P16870	Carboxypeptidase E	-2.59	2.61	0.00	-2.76	-4.23
P07602	Prosaposin	-2.50	2.06	0.01	-2.52	-3.33
Q99574	Neuroserpin	-2.49	2.50	0.00	-2.69	-4.04
P40189	Interleukin-6 receptor subunit beta	-2.49	1.33	0.02	-2.44	-2.27
O15537	Retinoschisin	-2.49	2.95	0.00	-2.30	-4.65
P22304	Iduronate 2-sulfatase	-2.49	2.22	0.01	-2.84	-3.62
P23471	Receptor-type tyrosine-protein phosphatase zeta	-2.47	1.33	0.02	-3.21	-2.31
Q8IV08	Phospholipase D3	-2.46	1.81	0.01	-2.48	-2.95
A8MV23	Serpin E3	-2.42	2.21	0.01	-2.42	-3.53
Q92823	Neuronal cell adhesion molecule	-2.40	2.11	0.01	-2.57	-3.41
P10645	Chromogranin-A	-2.29	2.04	0.01	-2.18	-3.23
Q9HCB6	Spondin-1	-2.27	3.18	0.00	-2.27	-5.02
P05067	Amyloid-beta precursor protein	-2.25	3.02	0.00	-2.17	-4.71
O14594	Neurocan core protein	-2.24	1.87	0.01	-2.55	-3.05
Q08629	Testican-1	-2.21	2.39	0.01	-2.42	-3.81
Q99435	Protein kinase C-binding protein NELL2	-2.19	1.10	0.05	-1.43	-1.84
Q9NQ79	Cartilage acidic protein 1	-2.18	2.95	0.00	-2.35	-4.67
O00391	Sulfhydryl oxidase 1	-2.17	1.70	0.01	-2.06	-2.72
P08294	Extracellular superoxide dismutase [Cu-Zn]	-2.17	2.62	0.00	-2.24	-4.11
Q9Y5W5	Wnt inhibitory factor 1	-2.12	1.39	0.02	-2.27	-2.33
P07711	Cathepsin L1	-2.12	1.27	0.03	-2.87	-2.20
Q06481	Amyloid-like protein 2	-2.10	2.62	0.00	-2.57	-4.20
Q9UHL4	Dipeptidyl peptidase 2	-2.09	1.77	0.01	-2.20	-2.84
Q12860	Contactin-1	-2.09	1.70	0.01	-2.22	-2.75
P14618	Pyruvate kinase PKM	-2.06	1.74	0.01	-2.00	-2.77
P19021	Peptidyl-glycine alpha-amidating monooxygenase	-2.01	1.73	0.01	-1.99	-2.76
O14773	Tripeptidyl-peptidase 1	-1.98	1.74	0.01	-1.99	-2.77
Q9UBR2	Cathepsin Z	-1.88	3.94	0.00	-1.86	-6.01
Q92820	Gamma-glutamyl hydrolase	-1.86	2.23	0.01	-2.38	-3.54
Q92765	Secreted frizzled-related protein 3	-1.86	2.66	0.00	-2.13	-4.12
Q13332	Receptor-type tyrosine-protein phosphatase S	-1.83	1.39	0.02	-2.13	-2.31
P60174	Triosephosphate isomerase	-1.80	1.91	0.01	-2.04	-3.01
P98164	Low-density lipoprotein receptor-related protein 2	-1.79	2.33	0.01	-2.11	-3.63
P43251	Biotinidase	-1.77	1.20	0.04	-1.95	-2.04
P13591	Neural cell adhesion molecule 1	-1.77	1.51	0.02	-2.31	-2.50
Q92743	Serine protease HTRA1	-1.76	1.28	0.03	-1.57	-2.09
Q9NPR2	Semaphorin-4B	-1.74	1.65	0.02	-1.90	-2.63
Q9Y646	Carboxypeptidase Q	-1.71	1.17	0.04	-2.32	-2.03
Q16769	Glutaminyl-peptide cyclotransferase	-1.71	2.17	0.01	-1.88	-3.34
P02458	Collagen alpha-1(II) chain	-1.65	1.27	0.03	-2.39	-2.18
P01033	Metalloproteinase inhibitor 1	-1.63	1.07	0.05	-2.35	-1.90
Q86UD1	Out at first protein homolog	-1.57	1.61	0.02	-1.73	-2.55
O94985	Calsyntenin-1	-1.53	2.11	0.01	-1.83	-3.24
P51693	Amyloid-like protein 1	-1.50	2.05	0.01	-1.63	-3.08
Q9UBM4	Opticin	-1.50	2.21	0.01	-1.39	-3.18

O75326	Semaphorin-7A	-1.31	2.12	0.01	-1.60	-3.17
Q9H3G5	Probable serine carboxypeptidase CPVL	-1.25	1.40	0.03	-1.26	-2.17
Q9BY67	Cell adhesion molecule 1	-1.25	1.36	0.03	-1.21	-2.10
Q14515	SPARC-like protein 1	-1.25	2.22	0.01	-1.49	-3.25
P23142	Fibulin-1	-1.25	1.35	0.03	-1.68	-2.20
Q16270	Insulin-like growth factor-binding protein 7	-1.19	1.36	0.03	-1.14	-2.08
P09871	Complement C1s subcomponent	-1.18	2.92	0.00	-1.26	-3.95
O43505	Beta-1.4-glucuronyltransferase 1	-1.16	3.01	0.00	-1.22	-4.02
P51888	Prolargin	-1.15	1.53	0.02	-1.51	-2.39
Q13822	Ectonucleotide pyrophosphatase/phosphodiesterase family ERMber 2	-1.14	2.30	0.01	-1.14	-3.13
Q9UBP4	Dickkopf-related protein 3	-1.10	1.56	0.02	-1.08	-2.28
P00746	Complement factor D	-1.07	1.17	0.05	-1.38	-1.91
P41222	Prostaglandin-H2 D-isomerase	-1.00	3.00	0.01	-1.05	-3.80
Q12805	EGF-containing fibulin-like extracellular matrix protein 1	-0.95	2.51	0.01	-1.01	-3.23
P05452	Tetranectin	-0.93	1.11	0.05	-1.44	-1.85
P07339	Cathepsin D	-0.87	1.83	0.02	-0.88	-2.45
P10745	Retinol-binding protein 3	-0.69	1.27	0.05	-0.81	-1.85
P36955	Pigment epithelium-derived factor	-0.63	2.13	0.02	-0.60	-2.39
P10909	Clusterin	-0.51	2.79	0.02	-0.50	-2.60
P00751	Complement factor B	0.57	1.44	0.05	0.64	1.89
P05543	Thyroxine-binding globulin	0.63	1.74	0.02	0.83	2.32
P08185	Corticosteroid-binding globulin	0.78	1.36	0.04	0.88	1.98
P01031	Complement C5	0.81	2.22	0.01	0.79	2.71
P06727	Apolipoprotein A-IV	0.88	2.04	0.01	0.94	2.70
Q14520	Hyaluronan-binding protein 2	0.94	1.37	0.04	0.82	1.95
P08697	Alpha-2-antiplasmin	0.96	2.99	0.01	0.84	3.48
P05546	Heparin cofactor 2	0.97	1.39	0.04	0.87	2.00
P18428	Lipopolysaccharide-binding protein	1.09	1.32	0.04	1.05	2.00
P06681	Complement C2	1.12	1.37	0.04	0.94	2.01
P00734	Prothrombin	1.24	1.65	0.02	0.99	2.34
P08603	Complement factor H	1.34	2.18	0.01	1.11	2.98
P07358	Complement component C8 beta chain	1.51	1.33	0.04	1.20	2.06
Q9UGM5	Fetuin-B	1.60	1.98	0.01	2.02	3.10
P35908	Keratin. type II cytoskeletal 2 epidermal	1.63	2.36	0.01	1.50	3.42
P02743	Serum amyloid P-component	1.75	2.58	0.01	1.50	3.71
P00740	Coagulation factor IX	3.74	1.58	0.01	2.29	2.59
P08253	72 kDa type IV collagenase	ND PDR	1.40	0.02	-3.43	-2.43
Q8NHP8	Putative phospholipase B-like 2	ND PDR	3.50	0.00	-3.36	-6.06
Q8TEU8	WAP. Kazal. immunoglobulin. Kunitz and NTR domain-containing protein 2	ND PDR	1.43	0.02	-1.58	-2.28
Q99969	Retinoic acid receptor responder protein 2	ND PDR	1.94	0.01	-3.35	-3.24

Table S3.2 - Proteins found differentially expressed in PDR compared to dry AMD. Proteins highlighted in red and green represent. respectively. underexpressed and overexpressed proteins in PDR compared to dry AMD.

Main Protein	Protein names	log2 Fold change	-Log Student's T-test p-value	Student's T-test q-value	Student's T-test Difference	Student's T-test Test statistic
P19022	Cadherin-2	-5.35	1.96	0.01	-3.82	-3.57
Q08380	Galectin-3-binding protein	-4.93	2.70	0.00	-4.97	-5.27
O75787	Renin receptor	-4.87	1.87	0.01	-3.39	-3.36
Q6MZW2	Follistatin-related protein 4	-4.79	1.47	0.03	-3.17	-2.65
P01034	Cystatin-C	-4.62	3.63	0.00	-4.29	-7.68
P61769	Beta-2-microglobulin	-4.54	2.71	0.00	-4.18	-5.19
P16035	Metalloproteinase inhibitor 2	-4.38	1.59	0.02	-3.82	-2.90
P10451	Osteopontin	-4.35	1.77	0.02	-3.71	-3.22
Q92752	Tenascin-R	-4.33	3.02	0.01	-3.33	-5.73
Q96S96	Phosphatidylethanolamine-binding protein 4	-4.26	1.60	0.02	-3.65	-2.91
Q9P121	Neurotrimin	-4.26	1.47	0.03	-3.33	-2.66
P07686	Beta-hexosaminidase subunit beta	-4.14	1.56	0.02	-4.00	-2.87
P48058	Glutamate receptor 4	-4.13	1.81	0.02	-3.05	-3.22
P30086	Phosphatidylethanolamine-binding protein 1	-3.96	1.60	0.03	-2.62	-2.83
Q15904	V-type proton ATPase subunit S1	-3.89	1.90	0.01	-3.06	-3.38
P06865	Beta-hexosaminidase subunit alpha	-3.88	1.32	0.03	-4.71	-2.46
P13611	Versican core protein	-3.70	1.40	0.03	-4.02	-2.57
Q9Y4C0	Neurexin-3	-3.47	1.32	0.03	-3.49	-2.42
P10645	Chromogranin-A	-3.42	2.51	0.01	-3.27	-4.59
O60888	Protein CutA	-3.39	1.65	0.02	-3.82	-3.01
Q9HAT2	Sialate O-acetylesterase	-3.37	1.33	0.04	-2.39	-2.36
Q92859	Neogenin	-3.21	1.54	0.03	-2.81	-2.74
Q8N475	Follistatin-related protein 5	-3.19	1.87	0.01	-3.76	-3.40
P20933	N(4)-(beta-N-acetylglucosaminyl)-L-asparaginase	-3.18	1.67	0.02	-3.11	-2.99
P40189	Interleukin-6 receptor subunit beta	-3.17	1.50	0.03	-3.06	-2.70
Q96GW7	Brevican core protein	-3.16	2.36	0.01	-3.82	-4.36
Q13510	Acid ceramidase	-3.15	2.38	0.01	-3.57	-4.37
Q99519	Sialidase-1	-3.12	1.23	0.04	-2.11	-2.18
P15586	N-acetylglucosamine-6-sulfatase	-2.99	2.85	0.01	-3.17	-5.30
O75503	Ceroid-lipofuscinosis neuronal protein 5	-2.84	2.27	0.01	-2.79	-4.02
A8MV23	Serpin E3	-2.82	1.32	0.03	-2.71	-2.37
Q8IV08	Phospholipase D3	-2.78	1.33	0.03	-2.61	-2.39
P05067	Amyloid-beta precursor protein	-2.76	2.74	0.00	-2.52	-4.87
Q9Y5W5	Wnt inhibitory factor 1	-2.75	1.74	0.02	-2.79	-3.08
Q9NQ79	Cartilage acidic protein 1	-2.73	2.87	0.00	-2.79	-5.23
O15537	Retinoschisin	-2.61	2.81	0.00	-2.84	-5.12
Q9UBR2	Cathepsin Z	-2.60	3.50	0.02	-2.49	-6.50
P61916	NPC intracellular cholesterol transporter 2	-2.58	2.70	0.01	-2.94	-4.90
Q99574	Neuroserpin	-2.57	2.09	0.01	-2.91	-3.71
Q92520	Protein FAM3C	-2.53	2.39	0.01	-2.18	-4.08
Q12860	Contactin-1	-2.52	2.01	0.01	-2.62	-3.51
P22304	Iduronate 2-sulfatase	-2.49	1.74	0.02	-2.62	-3.06
Q06481	Amyloid-like protein 2	-2.47	2.41	0.01	-2.81	-4.29
O14594	Neurocan core protein	-2.44	2.15	0.01	-2.78	-3.80
P51888	Prolargin	-2.40	1.80	0.02	-2.43	-3.13
P16870	Carboxypeptidase E	-2.39	2.21	0.01	-2.62	-3.86
O94985	Calsyntenin-1	-2.37	2.41	0.01	-2.34	-4.17
P23515	Oligodendrocyte-myelin glycoprotein	-2.34	1.66	0.02	-2.78	-2.93
Q08629	Testican-1	-2.32	2.44	0.01	-2.56	-4.28
Q9HCB6	Spondin-1	-2.30	3.31	0.01	-2.45	-6.04
P14618	Pyruvate kinase PKM	-2.27	2.19	0.01	-2.30	-3.76
O00391	Sulfhydryl oxidase 1	-2.22	1.72	0.02	-2.35	-2.98
P19021	Peptidyl-glycine alpha-amidating monooxygenase	-2.09	1.23	0.04	-2.03	-2.18
Q9BXJ4	Complement C1q tumor necrosis factor-related protein 3	-2.06	2.20	0.01	-2.33	-3.78
Q92823	Neuronal cell adhesion molecule	-2.05	1.31	0.04	-2.12	-2.31
Q9UHL4	Dipeptidyl peptidase 2	-2.02	1.19	0.05	-1.98	-2.12
O75326	Semaphorin-7A	-2.01	2.85	0.01	-2.14	-4.90
P0CAP1	Myocardial zonula adherens protein	-1.99	1.34	0.04	-1.53	-2.25
P98164	Low-density lipoprotein receptor-related protein 2	-1.96	1.42	0.03	-1.77	-2.41
Q16769	Glutaminyl-peptide cyclotransferase	-1.87	2.00	0.01	-2.10	-3.38
Q9BSG5	Retbindin	-1.86	1.76	0.02	-2.69	-3.10
O14773	Tripeptidyl-peptidase 1	-1.85	2.02	0.02	-2.23	-3.44
P13591	Neural cell adhesion molecule 1	-1.81	1.20	0.04	-2.26	-2.15
Q7Z7G0	Target of Nesh-SH3	-1.72	1.54	0.03	-1.91	-2.62
Q86UD1	Out at first protein homolog	-1.47	1.67	0.03	-1.80	-2.79
O43505	Beta-1.4-glucuronyltransferase 1	-1.41	2.81	0.01	-1.50	-4.41
P51693	Amyloid-like protein 1	-1.39	1.60	0.03	-1.42	-2.58
P07339	Cathepsin D	-1.36	2.65	0.01	-1.44	-4.11
P08294	Extracellular superoxide dismutase [Cu-Zn]	-1.35	1.60	0.03	-1.47	-2.59
Q9UBM4	Opticin	-1.33	1.80	0.02	-1.52	-2.90
Q9H3G5	Probable serine carboxypeptidase CPVL	-1.25	1.63	0.03	-1.60	-2.69
Q9UBP4	Dickkopf-related protein 3	-1.15	2.10	0.01	-1.43	-3.30
Q12805	EGF-containing fibulin-like extracellular matrix protein 1	-1.08	2.44	0.01	-1.13	-3.54
Q13822	Ectonucleotide pyrophosphatase/phosphodiesterase family member 2	-0.99	2.07	0.02	-1.05	-3.00
Q14515	SPARC-like protein 1	-0.82	1.39	0.04	-1.38	-2.28
P13473	Lysosome-associated membrane glycoprotein 2	-0.73	1.68	0.04	-0.69	-2.24
P10909	Clusterin	-0.66	2.16	0.03	-0.62	-2.58

P09871	Complement C1s subcomponent	-0.58	1.57	0.04	-0.98	-2.35
P36955	Pigment epithelium-derived factor	-0.54	1.86	0.03	-0.68	-2.39
P05156	Complement factor I	-0.44	2.14	0.04	-0.44	-2.19
P02774	Vitamin D-binding protein	0.62	2.18	0.03	0.63	2.62
P00748	Coagulation factor XII	0.67	1.98	0.03	0.76	2.61
P01031	Complement C5	0.71	1.74	0.03	0.74	2.35
P05546	Heparin cofactor 2	1.01	2.04	0.02	1.07	2.97
P06681	Complement C2	1.29	3.24	0.01	1.31	4.88
P08603	Complement factor H	1.45	1.94	0.02	1.27	2.98
P15169	Carboxypeptidase N catalytic chain	2.07	1.50	0.03	2.27	2.61
P13671	Complement component C6	2.10	1.91	0.02	1.62	3.10
P03952	Plasma kallikrein	2.15	1.94	0.02	1.75	3.18
P02743	Serum amyloid P-component	2.61	2.09	0.01	2.00	3.51
P08253	72 kDa type IV collagenase	ND PDR	1.74	0.01	-4.34	-3.20
P33908	Mannosyl-oligosaccharide 1.2-alpha-mannosidase IA	ND PDR	1.39	0.03	-2.62	-2.48
Q8NHP8	Putative phospholipase B-like 2	ND PDR	2.80	0.01	-4.09	-5.38
Q8TEU8	WAP. Kazal. immunoglobulin. Kunitz and NTR domain-containing protein 2	ND PDR	2.73	0.01	-2.70	-4.90
Q99969	Retinoic acid receptor responder protein 2	ND PDR	2.12	0.01	-3.54	-3.84

Table S4.1 - Results of DAVID bioinformatics analysis of differentially expressed proteins found in vitreous humor proteome of PDR patients compared with ERM control samples. Proteins are classified according to gene ontology (Go terms) for biological process. cellular component (orange). and molecular function (green). and GAD database (grey) with a FDR<10%.

Category	Term	Count	%	P-value	Pop Hits	Pop Total	Fold Enrichment	FDR
GOTERM_MF	GO:0004867~serine-type endopeptidase inhibitor activity	12	10.17	0.00	97	16881	18.48	5.22E-08
GOTERM_MF	GO:0004252~serine-type endopeptidase activity	12	10.17	0.00	255	16881	7.03	0.001
GOTERM_MF	GO:0005509~calcium ion binding	19	16.10	0.00	717	16881	3.96	0.001
GOTERM_MF	GO:0008191~metalloendopeptidase inhibitor activity	5	4.24	0.00	16	16881	46.68	0.004
GOTERM_MF	GO:0008201~heparin binding	9	7.63	0.00	160	16881	8.40	0.014
GOTERM_CC	GO:0005615~extracellular space	71	60.17	0.00	1347	18224	8.14	5.95E-46
GOTERM_CC	GO:0070062~extracellular exosome	87	73.73	0.00	2811	18224	4.78	7.77E-42
GOTERM_CC	GO:0005576~extracellular region	56	47.46	0.00	1610	18224	5.37	2.17E-24
GOTERM_CC	GO:0031012~extracellular matrix	21	17.80	0.00	296	18224	10.96	4.29E-12
GOTERM_CC	GO:0043202~lysosomal lumen	14	11.86	0.00	85	18224	25.44	9.64E-12
GOTERM_CC	GO:0005764~lysosome	18	15.25	0.00	226	18224	12.30	1.02E-10
GOTERM_CC	GO:0005578~proteinaceous extracellular matrix	18	15.25	0.00	268	18224	10.37	1.64E-09
GOTERM_CC	GO:0072562~blood microparticle	9	7.63	0.00	152	18224	9.14	0.007
GOTERM_CC	GO:0005604~basement membrane	7	5.93	0.00	79	18224	13.68	0.014
GOTERM_CC	GO:0031093~platelet alpha granule lumen	6	5.08	0.00	55	18224	16.85	0.03
GOTERM_BP	GO:0010951~negative regulation of endopeptidase activity	16	13.56	0.00	121	16792	19.48	4.55E-12
GOTERM_BP	GO:0002576~platelet degranulation	12	10.17	0.00	103	16792	17.16	1.41E-07
GOTERM_BP	GO:0007155~cell adhesion	20	16.95	0.00	459	16792	6.42	3.29E-07
GOTERM_BP	GO:0006508~proteolysis	18	15.25	0.00	500	16792	5.30	5.96E-05
GOTERM_BP	GO:0007417~central nervous system development	10	8.47	0.00	120	16792	12.27	1.75E-04
GOTERM_BP	GO:0006957~complement activation. alternative pathway	5	4.24	0.00	13	16792	56.65	0.002
GOTERM_BP	GO:0030207~chondroitin sulfate catabolic process	5	4.24	0.00	14	16792	52.61	0.002
GOTERM_BP	GO:0006956~complement activation	8	6.78	0.00	87	16792	13.54	0.003
GOTERM_BP	GO:0022617~extracellular matrix disassembly	7	5.93	0.00	76	16792	13.57	0.0184
GOTERM_BP	GO:0044267~cellular protein metabolic process	8	6.78	0.00	118	16792	9.99	0.0225
GOTERM_BP	GO:0030449~regulation of complement activation	5	4.24	0.00	30	16792	24.55	0.071
GOTERM_BP	GO:0030198~extracellular matrix organization	9	7.63	0.00	196	16792	6.76	0.082
GOTERM_BP	GO:0042340~keratan sulfate catabolic process	4	3.39	0.00	12	16792	49.10	0.095
GAD_DISEASE	Lymphoma. Non-Hodgkin	14	11.86	0.00	249	12971	6.95	1.44E-04
GAD_DISEASE	age-related macular degeneration	5	4.24	0.00	8	12971	77.21	4.19E-04
GAD_DISEASE	Type 2 Diabetes| edema | rosiglitazone	40	33.90	0.00	2198	12971	2.25	6.21E-04
GAD_DISEASE	Choroidal Neovascularization Macular Degeneration	6	5.08	0.00	22	12971	33.69	0.001
GAD_DISEASE	macular degeneration	12	10.17	0.00	254	12971	5.84	0.009
GAD_DISEASE	Choroid Diseases Macular Degeneration Peripheral Vascular Diseases	4	3.39	0.00	7	12971	70.59	0.027
GAD_DISEASE	Myopia	6	5.08	0.00	43	12971	17.24	0.0358
GAD_DISEASE	atherosclerosis	13	11.02	0.00	355	12971	4.52	0.042
GAD_DISEASE	Choroidal Neovascularization|Geographic Atrophy	4	3.39	0.00	9	12971	54.90	0.064

Table S4.2 - Results of DAVID bioinformatics analysis of differentially expressed proteins found in vitreous humor proteome of PDR patients compared with nAMD control samples. Proteins are classified according to gene ontology (Go terms) for biological process (blue). cellular component (orange) and molecular function (green). and GAD database (grey).

Category	Term	Count	%	P-Value	Pop Hits	Pop Total	Fold Enrichment	FDR
GOTERM_MF	GO:0004867~serine-type endopeptidase inhibitor activity	9	9.47	0.00	97	16881	17.60	4.82E-05
GOTERM_MF	GO:0005509~calcium ion binding	17	17.89	0.00	717	16881	4.50	9.73E-04
GOTERM_MF	GO:0008201~heparin binding	8	8.42	0.00	160	16881	9.48	0.025
GOTERM_MF	GO:0004185~serine-type carboxypeptidase activity	4	4.21	0.00	14	16881	54.19	0.059
GOTERM_CC	GO:0070062~extracellular exosome	65	68.42	0.00	2811	18224	4.44	1.69E-27
GOTERM_CC	GO:0005615~extracellular space	46	48.42	0.00	1347	18224	6.55	2.90E-23
GOTERM_CC	GO:0043202~lysosomal lumen	15	15.79	0.00	85	18224	33.85	1.14E-14
GOTERM_CC	GO:0005576~extracellular region	38	40.00	0.00	1610	18224	4.53	1.07E-12
GOTERM_CC	GO:0005764~lysosome	15	15.79	0.00	226	18224	12.73	1.18E-08
GOTERM_CC	GO:0031012~extracellular matrix	15	15.79	0.00	296	18224	9.72	4.26E-07
GOTERM_CC	GO:0005578~proteinaceous extracellular matrix	14	14.74	0.00	268	18224	10.02	1.40E-06
GOTERM_BP	GO:0007155~cell adhesion	18	18.95	0.00	459	16792	7.32	3.59E-07
GOTERM_BP	GO:0010951~negative regulation of endopeptidase activity	11	11.58	0.00	121	16792	16.96	1.19E-06
GOTERM_BP	GO:0030207~chondroitin sulfate catabolic process	6	6.32	0.00	14	16792	79.96	1.05E-05
GOTERM_BP	GO:0002576~platelet degranulation	8	8.42	0.00	103	16792	14.49	0.002
GOTERM_BP	GO:0007417~central nervous system development	8	8.42	0.00	120	16792	12.44	0.005
GOTERM_BP	GO:0030449~regulation of complement activation	5	5.26	0.00	30	16792	31.10	0.027
GOTERM_BP	GO:0042340~keratan sulfate catabolic process	4	4.21	0.00	12	16792	62.19	0.045
GAD_DISEASE	macular degeneration	10	10.53	0.00	254	12971	6.01	0.055

Table S5 - Final scheduled multiple reaction monitoring method with the list of precursors, peptides, and transitions monitored, as well as the dwell and retention times, declustering potential (DP), and collision energy CE for each transition.

Protein accession/Peptide/Transition	Q1 (m/z)	Q3 (m/z)	Dwell	DP	CE
sp|P06681|CO2_HUMAN.SSGQWQTPGATR.+2y8.light	638.307457	916.463541	24.6	80	30.3
sp|P06681|CO2_HUMAN.SSGQWQTPGATR.+2y7.light	638.307457	730.384228	24.6	80	30.3
sp|P06681|CO2_HUMAN.SSGQWQTPGATR.+2y6.light	638.307457	602.32565	24.6	80	30.3
sp|P06681|CO2_HUMAN.SSGQWQTPGATR.+2y5.light	638.307457	501.277972	24.6	80	30.3
sp|P06681|CO2_HUMAN.ESASLMVDR.+2y7.light	504.244949	791.408	19.53	80	23.7
sp|P06681|CO2_HUMAN.ESASLMVDR.+2y6.light	504.244949	720.370886	19.53	80	23.7
sp|P06681|CO2_HUMAN.ESASLMVDR.+2y5.light	504.244949	633.338857	19.53	80	23.7
sp|P06681|CO2_HUMAN.ESASLMVDR.+2y4.light	504.244949	520.254793	19.53	80	23.7
sp|P06681|CO2_HUMAN.GESGGAVFLER.+2y9.light	561.28292	935.494506	29.96	80	26.5
sp|P06681|CO2_HUMAN.GESGGAVFLER.+2y8.light	561.28292	848.462478	29.96	80	26.5
sp|P06681|CO2_HUMAN.GESGGAVFLER.+2y5.light	561.28292	663.382437	29.96	80	26.5
sp|P06681|CO2_HUMAN.GESGGAVFLER.+2y4.light	561.28292	564.314023	29.96	80	26.5
sp|P01024|CO3_HUMAN.IPIEDGSGEVVLSR.+2y11.light	735.893563	1147.558957	23.47	80	35.1
sp|P01024|CO3_HUMAN.IPIEDGSGEVVLSR.+2y10.light	735.893563	1018.516364	23.47	80	35.1
sp|P01024|CO3_HUMAN.IPIEDGSGEVVLSR.+2y9.light	735.893563	903.489421	23.47	80	35.1
sp|P01024|CO3_HUMAN.IPIEDGSGEVVLSR.+2y7.light	735.893563	759.435929	23.47	80	35.1
sp|P01024|CO3_HUMAN.LVAYYTLIGASGQR.+2y10.light	756.414465	1065.568734	26.65	80	36.1
sp|P01024|CO3_HUMAN.LVAYYTLIGASGQR.+2y9.light	756.414465	902.505406	26.65	80	36.1
sp|P01024|CO3_HUMAN.LVAYYTLIGASGQR.+2y7.light	756.414465	688.373663	26.65	80	36.1
sp|P01024|CO3_HUMAN.LVAYYTLIGASGQR.+2y6.light	756.414465	575.289599	26.65	80	36.1
sp|P01024|CO3_HUMAN.SNLDEDIIAEENIVSR.+2y9.light	908.949794	1030.55275	27.07	80	43.5
sp|P01024|CO3_HUMAN.SNLDEDIIAEENIVSR.+2y8.light	908.949794	917.468686	27.07	80	43.5
sp|P01024|CO3_HUMAN.SNLDEDIIAEENIVSR.+2y7.light	908.949794	846.431572	27.07	80	43.5
sp|P01031|CO5_HUMAN.TDAPDLPEENQAR.+2y9.light	728.339152	1071.506528	19.17	80	34.7
sp|P01031|CO5_HUMAN.TDAPDLPEENQAR.+2y8.light	728.339152	956.479585	19.17	80	34.7
sp|P01031|CO5_HUMAN.TDAPDLPEENQAR.+2y7.light	728.339152	843.395521	19.17	80	34.7
sp|P01031|CO5_HUMAN.TDAPDLPEENQAR.+2y5.light	728.339152	617.300164	19.17	80	34.7
sp|P01031|CO5_HUMAN.LQGTLPVEAR.+2y8.light	542.31148	842.473043	20.72	80	25.6
sp|P01031|CO5_HUMAN.LQGTLPVEAR.+2y7.light	542.31148	785.451579	20.72	80	25.6
sp|P01031|CO5_HUMAN.LQGTLPVEAR.+2y6.light	542.31148	684.403901	20.72	80	25.6
sp|P01031|CO5_HUMAN.LQGTLPVEAR.+2y5.light	542.31148	571.319837	20.72	80	25.6
sp|P01031|CO5_HUMAN.ATLLDIYK.+2y6.light	468.773668	764.455267	25.66	80	22
sp|P01031|CO5_HUMAN.ATLLDIYK.+2y5.light	468.773668	651.371203	25.66	80	22
sp|P01031|CO5_HUMAN.ATLLDIYK.+2y4.light	468.773668	538.287139	25.66	80	22
sp|P01031|CO5_HUMAN.ATLLDIYK.+2y3.light	468.773668	423.260196	25.66	80	22
sp|P13671|CO6_HUMAN.SEYGAALAWEK.+2y9.light	612.798403	1008.514908	23.54	80	29
sp|P13671|CO6_HUMAN.SEYGAALAWEK.+2y8.light	612.798403	845.451579	23.54	80	29
sp|P13671|CO6_HUMAN.SEYGAALAWEK.+2y7.light	612.798403	788.430115	23.54	80	29
sp|P13671|CO6_HUMAN.SEYGAALAWEK.+2y6.light	612.798403	717.393001	23.54	80	29
sp|P13671|CO6_HUMAN.GFVVAGPSR.+2y7.light	445.248152	685.399149	20.16	80	20.8
sp|P13671|CO6_HUMAN.GFVVAGPSR.+2y6.light	445.248152	586.330736	20.16	80	20.8
sp|P13671|CO6_HUMAN.GFVVAGPSR.+2y5.light	445.248152	487.262322	20.16	80	20.8
sp|P13671|CO6_HUMAN.GFVVAGPSR.+2y4.light	445.248152	416.225208	20.16	80	20.8
sp|P13671|CO6_HUMAN.QLEWGLER.+2y7.light	515.769448	902.473043	24.18	80	24.3

sp|P13671|CO6_HUMAN.QLEWGLER.+2y6.light	515.769448	789.388979	24.18	80	24.3
sp|P13671|CO6_HUMAN.QLEWGLER.+2y5.light	515.769448	660.346386	24.18	80	24.3
sp|P13671|CO6_HUMAN.QLEWGLER.+2y4.light	515.769448	474.267073	24.18	80	24.3
sp|P07358|CO8B_HUMAN.SGFSFGFK.+2y7.light	438.716153	789.393001	25.87	80	20.5
sp|P07358|CO8B_HUMAN.SGFSFGFK.+2y6.light	438.716153	732.371538	25.87	80	20.5
sp|P07358|CO8B_HUMAN.SGFSFGFK.+2y5.light	438.716153	585.303124	25.87	80	20.5
sp|P07358|CO8B_HUMAN.SGFSFGFK.+2y4.light	438.716153	498.271095	25.87	80	20.5
sp|P07358|CO8B_HUMAN.IPGIFELGISSQSDR.+2y10.light	809.925394	1091.532743	29.11	80	38.7
sp|P07358|CO8B_HUMAN.IPGIFELGISSQSDR.+2y9.light	809.925394	962.490149	29.11	80	38.7
sp|P07358|CO8B_HUMAN.IPGIFELGISSQSDR.+2y8.light	809.925394	849.406085	29.11	80	38.7
sp|P07358|CO8B_HUMAN.IPGIFELGISSQSDR.+2y6.light	809.925394	679.300558	29.11	80	38.7
sp|P07358|CO8B_HUMAN.LPLEYSYGEYR.+2y8.light	695.337892	1066.447616	24.11	80	33.1
sp|P07358|CO8B_HUMAN.LPLEYSYGEYR.+2y7.light	695.337892	937.405023	24.11	80	33.1
sp|P07358|CO8B_HUMAN.LPLEYSYGEYR.+2y6.light	695.337892	774.341694	24.11	80	33.1
sp|P07358|CO8B_HUMAN.LPLEYSYGEYR.+2y5.light	695.337892	687.309666	24.11	80	33.1
sp|P02748|CO9_HUMAN.VVEESELAR.+2y8.light	516.272021	932.468351	17.98	80	24.3
sp|P02748|CO9_HUMAN.VVEESELAR.+2y7.light	516.272021	833.399937	17.98	80	24.3
sp|P02748|CO9_HUMAN.VVEESELAR.+2y6.light	516.272021	704.357344	17.98	80	24.3
sp|P02748|CO9_HUMAN.VVEESELAR.+2y5.light	516.272021	575.314751	17.98	80	24.3
sp|P02748|CO9_HUMAN.AIEDYINEFSVR.+2y9.light	728.359356	1142.547664	28.13	80	34.7
sp|P02748|CO9_HUMAN.AIEDYINEFSVR.+2y8.light	728.359356	1027.520721	28.13	80	34.7
sp|P02748|CO9_HUMAN.AIEDYINEFSVR.+2y7.light	728.359356	864.457393	28.13	80	34.7
sp|P02748|CO9_HUMAN.AIEDYINEFSVR.+2y6.light	728.359356	751.373329	28.13	80	34.7
sp|P00740|FA9_HUMAN.SALVLQYLR.+2y7.light	531.818941	904.561464	27.07	80	25.1
sp|P00740|FA9_HUMAN.SALVLQYLR.+2y6.light	531.818941	791.4774	27.07	80	25.1
sp|P00740|FA9_HUMAN.SALVLQYLR.+2y5.light	531.818941	692.408986	27.07	80	25.1
sp|P00740|FA9_HUMAN.SALVLQYLR.+2y4.light	531.818941	579.324922	27.07	80	25.1
sp|P08603|CFAH_HUMAN.NTEILTGSWSDQTYPEGTQAIYK.+3y10.light	868.081769	1169.583716	30.1	80	39.7
sp|P08603|CFAH_HUMAN.NTEILTGSWSDQTYPEGTQAIYK.+3y9.light	868.081769	1006.520387	30.1	80	39.7
sp|P08603|CFAH_HUMAN.NTEILTGSWSDQTYPEGTQAIYK.+3y8.light	868.081769	909.467623	30.1	80	39.7
sp|P08603|CFAH_HUMAN.NTEILTGSWSDQTYPEGTQAIYK.+3y7.light	868.081769	780.42503	30.1	80	39.7
sp|P08603|CFAH_HUMAN.SPDVINGSPISQK.+2y9.light	671.354073	943.520721	20.58	80	31.9
sp|P08603|CFAH_HUMAN.SPDVINGSPISQK.+2y8.light	671.354073	830.436657	20.58	80	31.9
sp|P08603|CFAH_HUMAN.SPDVINGSPISQK.+2y7.light	671.354073	716.39373	20.58	80	31.9
sp|P08603|CFAH_HUMAN.SPDVINGSPISQK.+2y5.light	671.354073	572.340238	20.58	80	31.9
sp|P08603|CFAH_HUMAN.NGQWSEPPK.+2y8.light	521.751255	928.452307	17.06	80	24.6
sp|P08603|CFAH_HUMAN.NGQWSEPPK.+2y6.light	521.751255	743.372266	17.06	80	24.6
sp|P08603|CFAH_HUMAN.NGQWSEPPK.+2y5.light	521.751255	557.292953	17.06	80	24.6
sp|P08603|CFAH_HUMAN.NGQWSEPPK.+2y3.light	521.751255	341.218332	17.06	80	24.6
sp|P00734|THRB_HUMAN.TATSEYQTFFNPR.+2y8.light	781.367712	1072.521056	24.88	80	37.3
sp|P00734|THRB_HUMAN.TATSEYQTFFNPR.+2y7.light	781.367712	909.457727	24.88	80	37.3
sp|P00734|THRB_HUMAN.TATSEYQTFFNPR.+2y5.light	781.367712	680.351471	24.88	80	37.3
sp|P00734|THRB_HUMAN.TATSEYQTFFNPR.+2y4.light	781.367712	533.283057	24.88	80	37.3
sp|P00734|THRB_HUMAN.ELLESYIDGR.+2y8.light	597.803685	952.473437	25.24	80	28.3
sp|P00734|THRB_HUMAN.ELLESYIDGR.+2y7.light	597.803685	839.389373	25.24	80	28.3
sp|P00734|THRB_HUMAN.ELLESYIDGR.+2y6.light	597.803685	710.34678	25.24	80	28.3
sp|P00734|THRB_HUMAN.ELLESYIDGR.+2y5.light	597.803685	623.314751	25.24	80	28.3
sp|P00734|THRB_HUMAN.ETWTANVGK.+2y7.light	503.253631	775.409714	19.24	80	23.7
sp|P00734|THRB_HUMAN.ETWTANVGK.+2y6.light	503.253631	589.330401	19.24	80	23.7

sp|P00734|THRB_HUMAN.ETWTANVGK.+2y5.light	503.253631	488.282723	19.24	80	23.7
sp|P00734|THRB_HUMAN.ETWTANVGK.+2y4.light	503.253631	417.245609	19.24	80	23.7
sp|P01034|CYTC_HUMAN.ALDFAVGEYNK.+2y9.light	613.806228	1042.484001	24.18	80	29.1
sp|P01034|CYTC_HUMAN.ALDFAVGEYNK.+2y7.light	613.806228	780.388644	24.18	80	29.1
sp|P01034|CYTC_HUMAN.ALDFAVGEYNK.+2y6.light	613.806228	709.351531	24.18	80	29.1
sp|P01034|CYTC_HUMAN.ALDFAVGEYNK.+2y5.light	613.806228	610.283117	24.18	80	29.1
sp|P01034|CYTC_HUMAN.QIVAGVNYFLDVELGR.+3y8.light	598.324588	948.514908	32	80	26.7
sp|P01034|CYTC_HUMAN.QIVAGVNYFLDVELGR.+3y7.light	598.324588	801.446494	32	80	26.7
sp|P01034|CYTC_HUMAN.QIVAGVNYFLDVELGR.+3y6.light	598.324588	688.36243	32	80	26.7
sp|P01034|CYTC_HUMAN.QIVAGVNYFLDVELGR.+3y5.light	598.324588	573.335487	32	80	26.7
sp|P01034|CYTC_HUMAN.QIVAGVNYFLDVELGR.+3b7.light	598.324588	682.38825	32	80	26.7
sp|P05067|A4_HUMAN.THPHFVIPYR.+3y6.light	422.896251	794.455936	20.79	80	18.3
sp|P05067|A4_HUMAN.THPHFVIPYR.+3y4.light	422.896251	548.319108	20.79	80	18.3
sp|P05067|A4_HUMAN.THPHFVIPYR.+3y3.light	422.896251	435.235044	20.79	80	18.3
sp|P05067|A4_HUMAN.THPHFVIPYR.+3b6+2.light	422.896251	360.184823	20.79	80	18.3
sp|P05067|A4_HUMAN.VESLEQEAANER.+2y10.light	687.82842	1146.538556	19.24	80	32.7
sp|P05067|A4_HUMAN.VESLEQEAANER.+2y8.light	687.82842	946.422464	19.24	80	32.7
sp|P05067|A4_HUMAN.VESLEQEAANER.+2y7.light	687.82842	817.379871	19.24	80	32.7
sp|P05067|A4_HUMAN.VESLEQEAANER.+2y5.light	687.82842	560.2787	19.24	80	32.7
sp|Q06481|APLP2_HUMAN.WYFDLSK.+2y6.light	479.737085	772.387582	27.42	80	22.5
sp|Q06481|APLP2_HUMAN.WYFDLSK.+2y5.light	479.737085	609.324253	27.42	80	22.5
sp|Q06481|APLP2_HUMAN.WYFDLSK.+2y4.light	479.737085	462.255839	27.42	80	22.5
sp|Q06481|APLP2_HUMAN.WYFDLSK.+2y3.light	479.737085	347.228896	27.42	80	22.5
sp|Q06481|APLP2_HUMAN.GSGVGEQDGGLIGAEEK.+2y10.light	801.883923	988.494566	20.51	80	38.3
sp|Q06481|APLP2_HUMAN.GSGVGEQDGGLIGAEEK.+2y9.light	801.883923	873.467623	20.51	80	38.3
sp|Q06481|APLP2_HUMAN.GSGVGEQDGGLIGAEEK.+2y6.light	801.883923	646.340632	20.51	80	38.3
sp|Q06481|APLP2_HUMAN.GSGVGEQDGGLIGAEEK.+2y5.light	801.883923	533.256568	20.51	80	38.3
sp|O94985|CSTN1_HUMAN.ATEDVLVK.+2y7.light	437.74765	803.45091	18.54	80	20.4
sp|O94985|CSTN1_HUMAN.ATEDVLVK.+2y6.light	437.74765	702.403232	18.54	80	20.4
sp|O94985|CSTN1_HUMAN.ATEDVLVK.+2y5.light	437.74765	573.360639	18.54	80	20.4
sp|O94985|CSTN1_HUMAN.ATEDVLVK.+2y4.light	437.74765	458.333696	18.54	80	20.4
sp|O94985|CSTN1_HUMAN.EGLDLQVLEDSGR.+2y8.light	715.85972	903.453036	27.07	80	34.1
sp|O94985|CSTN1_HUMAN.EGLDLQVLEDSGR.+2y7.light	715.85972	775.394458	27.07	80	34.1
sp|O94985|CSTN1_HUMAN.EGLDLQVLEDSGR.+2y6.light	715.85972	676.326044	27.07	80	34.1
sp|O94985|CSTN1_HUMAN.EGLDLQVLEDSGR.+2y5.light	715.85972	563.24198	27.07	80	34.1
sp|O94985|CSTN1_HUMAN.AASEFESSEGVFLFPELR.+3y7.light	672.330067	921.519265	31.79	80	30.3
sp|O94985|CSTN1_HUMAN.AASEFESSEGVFLFPELR.+3y6.light	672.330067	774.450851	31.79	80	30.3
sp|O94985|CSTN1_HUMAN.AASEFESSEGVFLFPELR.+3y5.light	672.330067	661.366787	31.79	80	30.3
sp|O94985|CSTN1_HUMAN.AASEFESSEGVFLFPELR.+3y4.light	672.330067	514.298373	31.79	80	30.3
sp|P16870|CBPE_HUMAN.SNAQGIDLNR.+2precursor.light	544.278169	543.776797	18.47	80	25.7
sp|P16870|CBPE_HUMAN.SNAQGIDLNR.+2y8.light	544.278169	886.474105	18.47	80	25.7
sp|P16870|CBPE_HUMAN.SNAQGIDLNR.+2y7.light	544.278169	815.436992	18.47	80	25.7
sp|P16870|CBPE_HUMAN.SNAQGIDLNR.+2y6.light	544.278169	687.378414	18.47	80	25.7
sp|P16870|CBPE_HUMAN.SNAQGIDLNR.+2y4.light	544.278169	517.272886	18.47	80	25.7
sp|Q9UBM4|OPT_HUMAN.TAYLYAR.+2y6.light	429.229428	756.403901	19.46	80	20
sp|Q9UBM4|OPT_HUMAN.TAYLYAR.+2y5.light	429.229428	685.366787	19.46	80	20
sp|Q9UBM4|OPT_HUMAN.TAYLYAR.+2y4.light	429.229428	522.303458	19.46	80	20
sp|Q9UBM4|OPT_HUMAN.TAYLYAR.+2y3.light	429.229428	409.219394	19.46	80	20
sp|Q9UBM4|OPT_HUMAN.IDLSNNLISSIDNDAFR.+2y10.light	953.978886	1137.553478	30.66	80	45.7

sp|Q9UBM4|OPT_HUMAN.IDLSNNLISSIDNDAFR.+2y9.light	953.978886	1024.469414	30.66	80	45.7
sp|Q9UBM4|OPT_HUMAN.IDLSNNLISSIDNDAFR.+2y8.light	953.978886	937.437386	30.66	80	45.7
sp|Q9UBM4|OPT_HUMAN.IDLSNNLISSIDNDAFR.+2y5.light	953.978886	622.29435	30.66	80	45.7
sp|P10451|OSTP_HUMAN.YPDAVATWLNPDPSQK.+2y8.light	901.441408	898.462872	31.51	80	43.2
sp|P10451|OSTP_HUMAN.YPDAVATWLNPDPSQK.+2y7.light	901.441408	785.378808	31.51	80	43.2
sp|P10451|OSTP_HUMAN.YPDAVATWLNPDPSQK.+2y6.light	901.441408	671.335881	31.51	80	43.2
sp|P10451|OSTP_HUMAN.YPDAVATWLNPDPSQK.+2y4.light	901.441408	459.256174	31.51	80	43.2
sp|P10451|OSTP_HUMAN.ISHELDSASSEVN.+2b5.light	694.320427	580.308937	31.51	80	33
sp|P10451|OSTP_HUMAN.ISHELDSASSEVN.+2b7.light	694.320427	782.367909	31.51	80	33
sp|P10451|OSTP_HUMAN.ISHELDSASSEVN.+2b8.light	694.320427	853.405023	31.51	80	33
sp|P10451|OSTP_HUMAN.ISHELDSASSEVN.+2b9.light	694.320427	940.437051	31.51	80	33
sp|O15537|XLRS1_HUMAN.VISGILTQGR.+2y8.light	522.314023	831.468292	21.99	80	24.6
sp|O15537|XLRS1_HUMAN.VISGILTQGR.+2y7.light	522.314023	744.436263	21.99	80	24.6
sp|O15537|XLRS1_HUMAN.VISGILTQGR.+2y5.light	522.314023	574.330736	21.99	80	24.6
sp|O15537|XLRS1_HUMAN.VISGILTQGR.+2y4.light	522.314023	461.246672	21.99	80	24.6
sp|O15537|XLRS1_HUMAN.YSVQYR.+2y5.light	408.205952	652.3413	17.55	80	19
sp|O15537|XLRS1_HUMAN.YSVQYR.+2y4.light	408.205952	565.309272	17.55	80	19
sp|O15537|XLRS1_HUMAN.YSVQYR.+2y3.light	408.205952	466.240858	17.55	80	19
sp|O15537|XLRS1_HUMAN.LNWIYYK.+2y6.light	500.268553	886.445765	25.73	80	23.5
sp|O15537|XLRS1_HUMAN.LNWIYYK.+2y5.light	500.268553	772.402838	25.73	80	23.5
sp|O15537|XLRS1_HUMAN.LNWIYYK.+2y4.light	500.268553	586.323525	25.73	80	23.5
sp|O15537|XLRS1_HUMAN.LNWIYYK.+2y3.light	500.268553	473.239461	25.73	80	23.5
sp|Q92752|TENR_HUMAN.ITFTPSSGIASEVTVPK.+2y12.light	867.469634	1174.631394	20.23	80	41.5
sp|Q92752|TENR_HUMAN.ITFTPSSGIASEVTVPK.+2y11.light	867.469634	1087.599366	20.23	80	41.5
sp|Q92752|TENR_HUMAN.ITFTPSSGIASEVTVPK.+2y10.light	867.469634	1000.567337	20.23	80	41.5
sp|Q92752|TENR_HUMAN.ITFTPSSGIASEVTVPK.+2y8.light	867.469634	830.461809	20.23	80	41.5
sp|Q92752|TENR_HUMAN.DGQEAAFASYDR.+2y8.light	665.28893	900.421007	20.16	80	31.6
sp|Q92752|TENR_HUMAN.DGQEAAFASYDR.+2y7.light	665.28893	829.383893	20.16	80	31.6
sp|Q92752|TENR_HUMAN.DGQEAAFASYDR.+2y6.light	665.28893	758.34678	20.16	80	31.6
sp|Q92752|TENR_HUMAN.DGQEAAFASYDR.+2y5.light	665.28893	611.278366	20.16	80	31.6
sp|Q92752|TENR_HUMAN.DGQEAAFASYDR.+2y4.light	665.28893	540.241252	20.16	80	31.6
sp|P01011|AACT_HUMAN.DSLEFR.+2y4.light	383.690135	564.314023	20.44	80	17.8
sp|P01011|AACT_HUMAN.DSLEFR.+2y3.light	383.690135	451.229959	20.44	80	17.8
sp|P01011|AACT_HUMAN.DSLEFR.+2y2.light	383.690135	322.187366	20.44	80	17.8
sp|P01011|AACT_HUMAN.ADLSGITGAR.+2y8.light	480.75908	774.446828	20.23	80	22.6
sp|P01011|AACT_HUMAN.ADLSGITGAR.+2y7.light	480.75908	661.362764	20.23	80	22.6
sp|P01011|AACT_HUMAN.ADLSGITGAR.+2y6.light	480.75908	574.330736	20.23	80	22.6
sp|P01011|AACT_HUMAN.ADLSGITGAR.+2y4.light	480.75908	404.225208	20.23	80	22.6
sp|P01011|AACT_HUMAN.AVLDVFEEGTEASAATAVK.+2y12.light	954.48347	1134.563708	27.35	80	45.8
sp|P01011|AACT_HUMAN.AVLDVFEEGTEASAATAVK.+2y11.light	954.48347	1005.521115	27.35	80	45.8
sp|P01011|AACT_HUMAN.AVLDVFEEGTEASAATAVK.+2y7.light	954.48347	647.372266	27.35	80	45.8
sp|P01011|AACT_HUMAN.AVLDVFEEGTEASAATAVK.+2b4.light	954.48347	399.223811	27.35	80	45.8
sp|P36955|PEDF_HUMAN.LAAAVSNFGYDLYR.+2y9.light	780.396272	1134.52145	26.93	80	37.2
sp|P36955|PEDF_HUMAN.LAAAVSNFGYDLYR.+2y7.light	780.396272	933.446494	26.93	80	37.2
sp|P36955|PEDF_HUMAN.LAAAVSNFGYDLYR.+2y6.light	780.396272	786.37808	26.93	80	37.2
sp|P36955|PEDF_HUMAN.EIPDEISILLLGVAHFK.+3y9.light	632.02766	997.619313	35.74	80	28.3
sp|P36955|PEDF_HUMAN.EIPDEISILLLGVAHFK.+3y7.light	632.02766	771.451185	35.74	80	28.3
sp|P36955|PEDF_HUMAN.EIPDEISILLLGVAHFK.+3y6.light	632.02766	658.367121	35.74	80	28.3
sp|P36955|PEDF_HUMAN.DTDTGALLFIGK.+2y10.light	625.834985	1034.588073	28.2	80	29.7

sp|P36955|PEDF_HUMAN.DTDTGALLFIGK.+2y9.light	625.834985	919.56113	28.2	80	29.7
sp|P36955|PEDF_HUMAN.DTDTGALLFIGK.+2y8.light	625.834985	818.513451	28.2	80	29.7
sp|P36955|PEDF_HUMAN.DTDTGALLFIGK.+2y4.light	625.834985	464.286745	28.2	80	29.7
sp|Q9HCB6|SPON1_HUMAN.VTLSAAPPSYFR.+2y9.light	654.850969	995.494506	24.46	80	31.1
sp|Q9HCB6|SPON1_HUMAN.VTLSAAPPSYFR.+2y8.light	654.850969	908.462478	24.46	80	31.1
sp|Q9HCB6|SPON1_HUMAN.VTLSAAPPSYFR.+2y7.light	654.850969	837.425364	24.46	80	31.1
sp|Q9HCB6|SPON1_HUMAN.VTLSAAPPSYFR.+2y6.light	654.850969	766.38825	24.46	80	31.1
sp|Q9HCB6|SPON1_HUMAN.AAPSAEFSVDR.+2y9.light	575.280377	1007.47925	20.3	80	27.2
sp|Q9HCB6|SPON1_HUMAN.AAPSAEFSVDR.+2y8.light	575.280377	910.426487	20.3	80	27.2
sp|Q9HCB6|SPON1_HUMAN.AAPSAEFSVDR.+2y6.light	575.280377	752.357344	20.3	80	27.2
sp|Q9HCB6|SPON1_HUMAN.AAPSAEFSVDR.+2y5.light	575.280377	623.314751	20.3	80	27.2
sp|Q9Y4C0|NRX3A_HUMAN.SADYVNLALK.+2y8.light	547.298038	935.519659	30.73	80	25.8
sp|Q9Y4C0|NRX3A_HUMAN.SADYVNLALK.+2y7.light	547.298038	820.492716	30.73	80	25.8
sp|Q9Y4C0|NRX3A_HUMAN.SADYVNLALK.+2y6.light	547.298038	657.429387	30.73	80	25.8
sp|Q9Y4C0|NRX3A_HUMAN.SADYVNLALK.+2y5.light	547.298038	558.360973	30.73	80	25.8
sp|Q9Y4C0|NRX3A_HUMAN.GPETLYAGQK.+2y8.light	532.274563	909.467623	22.84	80	25.1
sp|Q9Y4C0|NRX3A_HUMAN.GPETLYAGQK.+2y7.light	532.274563	780.42503	22.84	80	25.1
sp|Q9Y4C0|NRX3A_HUMAN.GPETLYAGQK.+2y6.light	532.274563	679.377351	22.84	80	25.1
sp|Q9Y4C0|NRX3A_HUMAN.GPETLYAGQK.+2y5.light	532.274563	566.293287	22.84	80	25.1
sp|Q9Y4C0|NRX3A_HUMAN.GPETLYAGQK.+2y4.light	532.274563	403.229959	22.84	80	25.1
sp|Q9Y4C0|NRX3A_HUMAN.LAVGFSTTVK.+2y9.light	511.797674	909.504009	15.44	80	24.1
sp|Q9Y4C0|NRX3A_HUMAN.LAVGFSTTVK.+2y8.light	511.797674	838.466895	15.44	80	24.1
sp|Q9Y4C0|NRX3A_HUMAN.LAVGFSTTVK.+2y7.light	511.797674	739.398481	15.44	80	24.1
sp|Q9Y4C0|NRX3A_HUMAN.LAVGFSTTVK.+2y6.light	511.797674	682.377017	15.44	80	24.1
sp|Q08380|LG3BP_HUMAN.SDLAVPSELALLK.+2y9.light	678.392667	969.597909	28.69	80	32.2
sp|Q08380|LG3BP_HUMAN.SDLAVPSELALLK.+2y8.light	678.392667	870.529495	28.69	80	32.2
sp|Q08380|LG3BP_HUMAN.SDLAVPSELALLK.+2b3.light	678.392667	316.150312	28.69	80	32.2
sp|Q08380|LG3BP_HUMAN.SDLAVPSELALLK.+2b4.light	678.392667	387.187425	28.69	80	32.2
sp|Q08380|LG3BP_HUMAN.SQLVYQSR.+2y6.light	490.761623	765.425364	24.95	80	23
sp|Q08380|LG3BP_HUMAN.SQLVYQSR.+2y5.light	490.761623	652.3413	24.95	80	23
sp|Q08380|LG3BP_HUMAN.SQLVYQSR.+2y4.light	490.761623	553.272886	24.95	80	23
sp|Q08380|LG3BP_HUMAN.SQLVYQSR.+2b3.light	490.761623	329.181946	24.95	80	23
sp|Q08380|LG3BP_HUMAN.YSSDYFQAPSDYR.+2y8.light	799.841527	983.458121	22.98	80	38.2
sp|Q08380|LG3BP_HUMAN.YSSDYFQAPSDYR.+2y7.light	799.841527	836.389707	22.98	80	38.2
sp|Q08380|LG3BP_HUMAN.YSSDYFQAPSDYR.+2y6.light	799.841527	708.33113	22.98	80	38.2
sp|Q08380|LG3BP_HUMAN.YSSDYFQAPSDYR.+2y5.light	799.841527	637.294016	22.98	80	38.2
sp|Q92520|FAM3C_HUMAN.SALDTAAR.+2y6.light	402.714142	646.351865	18.33	80	18.7
sp|Q92520|FAM3C_HUMAN.SALDTAAR.+2y5.light	402.714142	533.267801	18.33	80	18.7
sp|Q92520|FAM3C_HUMAN.SALDTAAR.+2y4.light	402.714142	418.240858	18.33	80	18.7
sp|Q92520|FAM3C_HUMAN.SALDTAAR.+2b3.light	402.714142	272.160482	18.33	80	18.7
sp|Q92520|FAM3C_HUMAN.TGEVLDTK.+2y7.light	431.729457	761.40396	21.08	80	20.2
sp|Q92520|FAM3C_HUMAN.TGEVLDTK.+2y6.light	431.729457	704.382496	21.08	80	20.2
sp|Q92520|FAM3C_HUMAN.TGEVLDTK.+2y5.light	431.729457	575.339903	21.08	80	20.2
sp|Q92520|FAM3C_HUMAN.TGEVLDTK.+2y4.light	431.729457	476.271489	21.08	80	20.2
sp|Q92520|FAM3C_HUMAN.TGEVLDTK.+2y3.light	431.729457	363.187425	21.08	80	20.2
sp|P15586|GNS_HUMAN.AFQNVFAPR.+2y7.light	525.279983	831.447162	25	80	24.7
sp|P15586|GNS_HUMAN.AFQNVFAPR.+2y6.light	525.279983	703.388585	25	80	24.7
sp|P15586|GNS_HUMAN.AFQNVFAPR.+2y5.light	525.279983	589.345657	25	80	24.7
sp|P15586|GNS_HUMAN.AFQNVFAPR.+2y4.light	525.279983	490.277243	25	80	24.7

sp|P15586|GNS_HUMAN.TIDPELLGK.+2y7.light	493.281857	771.424696	25	80	23.2
sp|P15586|GNS_HUMAN.TIDPELLGK.+2y6.light	493.281857	656.397753	25	80	23.2
sp|P15586|GNS_HUMAN.TIDPELLGK.+2y4.light	493.281857	430.302396	25	80	23.2
sp|P15586|GNS_HUMAN.TIDPELLGK.+2b3.light	493.281857	330.165962	25	80	23.2
sp|Q9UBR2|CATZ_HUMAN.VGDYGSLSGR.+2y9.light	505.748713	911.421735	25	80	23.8
sp|Q9UBR2|CATZ_HUMAN.VGDYGSLSGR.+2y8.light	505.748713	854.400272	25	80	23.8
sp|Q9UBR2|CATZ_HUMAN.VGDYGSLSGR.+2y7.light	505.748713	739.373329	25	80	23.8
sp|Q9UBR2|CATZ_HUMAN.VGDYGSLSGR.+2y6.light	505.748713	576.31	25	80	23.8
sp|Q9UBR2|CATZ_HUMAN.NSWGEPWGER.+2y8.light	609.270344	1016.458455	25	80	28.9
sp|Q9UBR2|CATZ_HUMAN.NSWGEPWGER.+2y7.light	609.270344	830.379142	25	80	28.9
sp|Q9UBR2|CATZ_HUMAN.NSWGEPWGER.+2y5.light	609.270344	644.315085	25	80	28.9
sp|Q9UBR2|CATZ_HUMAN.NSWGEPWGER.+2y4.light	609.270344	547.262322	25	80	28.9
sp|P19022|CADH2_HUMAN.DVHEGQPLLNVK.+2y9.light	674.864608	997.567671	25	80	32.1
sp|P19022|CADH2_HUMAN.DVHEGQPLLNVK.+2y8.light	674.864608	868.525078	25	80	32.1
sp|P19022|CADH2_HUMAN.DVHEGQPLLNVK.+2y6.light	674.864608	683.445037	25	80	32.1
sp|P19022|CADH2_HUMAN.DVHEGQPLLNVK.+2b3.light	674.864608	352.161545	25	80	32.1
sp|P19022|CADH2_HUMAN.ESAEVEEIVFPR.+2y8.light	702.853906	988.546208	25	80	33.4
sp|P19022|CADH2_HUMAN.ESAEVEEIVFPR.+2y7.light	702.853906	889.477794	25	80	33.4
sp|P19022|CADH2_HUMAN.ESAEVEEIVFPR.+2y6.light	702.853906	760.435201	25	80	33.4
sp|P19022|CADH2_HUMAN.ESAEVEEIVFPR.+2y5.light	702.853906	631.392608	25	80	33.4
sp|P10645|CMGA_HUMAN.SGELEQEEER.+2y7.light	603.267664	932.431966	25	80	28.6
sp|P10645|CMGA_HUMAN.SGELEQEEER.+2y6.light	603.267664	819.347902	25	80	28.6
sp|P10645|CMGA_HUMAN.SGELEQEEER.+2y5.light	603.267664	690.305309	25	80	28.6
sp|P10645|CMGA_HUMAN.SGELEQEEER.+2y4.light	603.267664	562.246731	25	80	28.6
sp|P08294|SODE_HUMAN.VTGVVLFR.+2y7.light	445.776545	791.4774	25	80	20.8
sp|P08294|SODE_HUMAN.VTGVVLFR.+2y6.light	445.776545	690.429721	25	80	20.8
sp|P08294|SODE_HUMAN.VTGVVLFR.+2y5.light	445.776545	633.408258	25	80	20.8
sp|P08294|SODE_HUMAN.VTGVVLFR.+2y4.light	445.776545	534.339844	25	80	20.8
sp|P08294|SODE_HUMAN.VTGVVLFR.+2y3.light	445.776545	435.27143	25	80	20.8
sp|P08294|SODE_HUMAN.AVVVHAGEDDLGR.+2y10.light	669.34404	1068.506862	25	80	31.8
sp|P08294|SODE_HUMAN.AVVVHAGEDDLGR.+2y9.light	669.34404	969.438448	25	80	31.8
sp|P08294|SODE_HUMAN.AVVVHAGEDDLGR.+2y8.light	669.34404	832.379536	25	80	31.8
sp|P08294|SODE_HUMAN.AVVVHAGEDDLGR.+2b3.light	669.34404	270.181218	25	80	31.8
sp|Q99972|MYOC_HUMAN.ESPSGYLR.+2y6.light	454.727249	692.3726	25	80	21.3
sp|Q99972|MYOC_HUMAN.ESPSGYLR.+2y5.light	454.727249	595.319837	25	80	21.3
sp|Q99972|MYOC_HUMAN.ESPSGYLR.+2y4.light	454.727249	508.287808	25	80	21.3
sp|Q99972|MYOC_HUMAN.ESPSGYLR.+2y3.light	454.727249	451.266344	25	80	21.3
sp|Q99972|MYOC_HUMAN.IDTVGTDVR.+2y8.light	488.258913	862.426487	25	80	22.9
sp|Q99972|MYOC_HUMAN.IDTVGTDVR.+2y7.light	488.258913	747.399543	25	80	22.9
sp|Q99972|MYOC_HUMAN.IDTVGTDVR.+2y6.light	488.258913	646.351865	25	80	22.9
sp|Q99972|MYOC_HUMAN.IDTVGTDVR.+2y5.light	488.258913	547.283451	25	80	22.9
sp|P16035|TIMP2_HUMAN.EVDSGNDIYGNPIK.+2y12.light	760.865002	1292.611721	25	80	36.3
sp|P16035|TIMP2_HUMAN.EVDSGNDIYGNPIK.+2y6.light	760.865002	691.377351	25	80	36.3
sp|P16035|TIMP2_HUMAN.EVDSGNDIYGNPIK.+2y3.light	760.865002	357.249632	25	80	36.3
sp|Q02818|NUCB1_HUMAN.YLESLGEEQR.+2y8.light	612.298767	947.442865	25	80	29
sp|Q02818|NUCB1_HUMAN.YLESLGEEQR.+2y7.light	612.298767	818.400272	25	80	29
sp|Q02818|NUCB1_HUMAN.YLESLGEEQR.+2y6.light	612.298767	731.368243	25	80	29
sp|Q02818|NUCB1_HUMAN.YLESLGEEQR.+2y5.light	612.298767	618.284179	25	80	29
sp|Q02818|NUCB1_HUMAN.VNVPGSQAQLK.+2y9.light	570.822212	927.525807	25	80	27

sp|Q02818|NUCB1_HUMAN.VNVPGSQAQLK.+2y8.light	570.822212	828.457393	25	80	27
sp|Q02818|NUCB1_HUMAN.VNVPGSQAQLK.+2y7.light	570.822212	731.404629	25	80	27
sp|Q02818|NUCB1_HUMAN.VNVPGSQAQLK.+2b7.light	570.822212	682.351865	25	80	27
sp|Q02818|NUCB1_HUMAN.LPEVEVPQHL.+2y8.light	580.819138	950.494172	25	80	27.5
sp|Q02818|NUCB1_HUMAN.LPEVEVPQHL.+2y7.light	580.819138	821.451579	25	80	27.5
sp|Q02818|NUCB1_HUMAN.LPEVEVPQHL.+2y6.light	580.819138	722.383165	25	80	27.5
sp|Q02818|NUCB1_HUMAN.LPEVEVPQHL.+2y5.light	580.819138	593.340572	25	80	27.5
sp|Q02818|NUCB1_HUMAN.LPEVEVPQHL.+2y4.light	580.819138	494.272158	25	80	27.5
sp|Q02818|NUCB1_HUMAN.LPEVEVPQHL.+2y2.light	580.819138	269.160817	25	80	27.5
sp|Q99574|NEUS_HUMAN.EFSNMVTAK.+2y7.light	513.749867	750.381451	25	80	24.2
sp|Q99574|NEUS_HUMAN.EFSNMVTAK.+2y6.light	513.749867	663.349422	25	80	24.2
sp|Q99574|NEUS_HUMAN.EFSNMVTAK.+2y5.light	513.749867	549.306495	25	80	24.2
sp|Q99574|NEUS_HUMAN.EFSNMVTAK.+2y4.light	513.749867	418.26601	25	80	24.2
sp|Q99574|NEUS_HUMAN.AQLVEEWANSVK.+2y9.light	687.356616	1061.526201	25	80	32.7
sp|Q99574|NEUS_HUMAN.AQLVEEWANSVK.+2y8.light	687.356616	962.457787	25	80	32.7
sp|Q99574|NEUS_HUMAN.AQLVEEWANSVK.+2y7.light	687.356616	833.415194	25	80	32.7
sp|Q99574|NEUS_HUMAN.AQLVEEWANSVK.+2y6.light	687.356616	704.3726	25	80	32.7
sp|Q99574|NEUS_HUMAN.TGTILFMGR.+2y7.light	498.270769	837.465121	25	80	23.4
sp|Q99574|NEUS_HUMAN.TGTILFMGR.+2y6.light	498.270769	736.417442	25	80	23.4
sp|Q99574|NEUS_HUMAN.TGTILFMGR.+2y5.light	498.270769	623.333378	25	80	23.4
sp|Q99574|NEUS_HUMAN.TGTILFMGR.+2y4.light	498.270769	510.249314	25	80	23.4
sp|P01009|A1AT_HUMAN.ITPNLAEFAFSLYR.+2y9.light	821.435398	1103.552021	25	80	39.3
sp|P01009|A1AT_HUMAN.ITPNLAEFAFSLYR.+2y8.light	821.435398	1032.514908	25	80	39.3
sp|P01009|A1AT_HUMAN.ITPNLAEFAFSLYR.+2y7.light	821.435398	903.472314	25	80	39.3
sp|P01009|A1AT_HUMAN.ITPNLAEFAFSLYR.+2y6.light	821.435398	756.403901	25	80	39.3
sp|P01009|A1AT_HUMAN.LYHSEAFTVNFGDTEEAK.+3y9.light	686.65321	1010.442531	25	80	31
sp|P01009|A1AT_HUMAN.LYHSEAFTVNFGDTEEAK.+3y8.light	686.65321	896.399603	25	80	31
sp|P01009|A1AT_HUMAN.LYHSEAFTVNFGDTEEAK.+3y7.light	686.65321	749.331189	25	80	31
sp|P01009|A1AT_HUMAN.LYHSEAFTVNFGDTEEAK.+3b8.light	686.65321	949.441408	25	80	31
sp|P01009|A1AT_HUMAN.LSITGTYDLK.+2y9.light	555.805696	997.520053	25	80	26.2
sp|P01009|A1AT_HUMAN.LSITGTYDLK.+2y8.light	555.805696	910.488024	25	80	26.2
sp|P01009|A1AT_HUMAN.LSITGTYDLK.+2y7.light	555.805696	797.40396	25	80	26.2
sp|P01009|A1AT_HUMAN.LSITGTYDLK.+2y6.light	555.805696	696.356282	25	80	26.2
sp|P01009|A1AT_HUMAN.AVLTIDEK.+2y6.light	444.755475	718.398146	25	80	20.8
sp|P01009|A1AT_HUMAN.AVLTIDEK.+2y5.light	444.755475	605.314082	25	80	20.8
sp|P01009|A1AT_HUMAN.AVLTIDEK.+2y4.light	444.755475	504.266404	25	80	20.8
sp|P01009|A1AT_HUMAN.AVLTIDEK.+2y3.light	444.755475	391.18234	25	80	20.8
sp|P13591|NCAM1_HUMAN.VSSLTLK.+2y6.light	374.234179	648.392667	25	80	17.3
sp|P13591|NCAM1_HUMAN.VSSLTLK.+2y5.light	374.234179	561.360639	25	80	17.3
sp|P13591|NCAM1_HUMAN.VSSLTLK.+2y4.light	374.234179	474.32861	25	80	17.3
sp|P13591|NCAM1_HUMAN.VSSLTLK.+2y3.light	374.234179	361.244546	25	80	17.3

Supplementary Figure 1. MultiScatter plots comparing the correlation (Pearson) of all the vitreous samples analyzed in the label-free experiment before and after the removal of VH 219 from the statistical analysis.


0.875 0.902 0.861 0.923 0.878 0.896 0.788 0.831 0.785 0.781
0.875 0.897 0.857 0.919 0.905 0.895 0.794 0.804 0.784 0.829
0.902 0.897 0.839 0.908 0.896 0.895 0.813 0.808 0.784 0.808
0.861 0.857 0.839 0.859 0.863 0.857 0.824 0.861 0.824 0.835
0.923 0.919 0.908 0.859 0.905 0.908 0.784 0.826 0.759 0.778
0.878 0.905 0.896 0.863 0.905 0.913 0.822 0.834 0.827 0.851
0.896 0.895 0.895 0.857 0.908 0.913 0.791 0.817 0.776 0.804
0.788 0.794 0.813 0.824 0.784 0.822 0.791 0.864 0.91 0.886
0.831 0.804 0.808 0.861 0.826 0.834 0.817 0.864 0.856 0.86
0.785 0.784 0.784 0.824 0.759 0.827 0.776 0.91 0.856 0.888
0.781 0.829 0.808 0.835 0.778 0.851 0.804 0.886 0.86 0.888

Supplementary Figure 2. MRM results of the more significant candidate biomarkers. Statistical analysis (Kruskal-Wallis tests with an FDR<5%) and ROC curves were performed in GraphPad Prism Software to assess the ability of these proteins to distinguish between different disease groups, including (diabetic retinopathy/proliferative diabetic retinopathy group (DR/PDR), age-related macular degeneration (AMD), rhegmatogenous retinal detachment/proliferative vitreoretinopathy (RRD/PVR) and epiretinal membranes (ERM). Data are presented as mean ± SD with q-values of <0.05 (*) and q-value<0.01 (**).

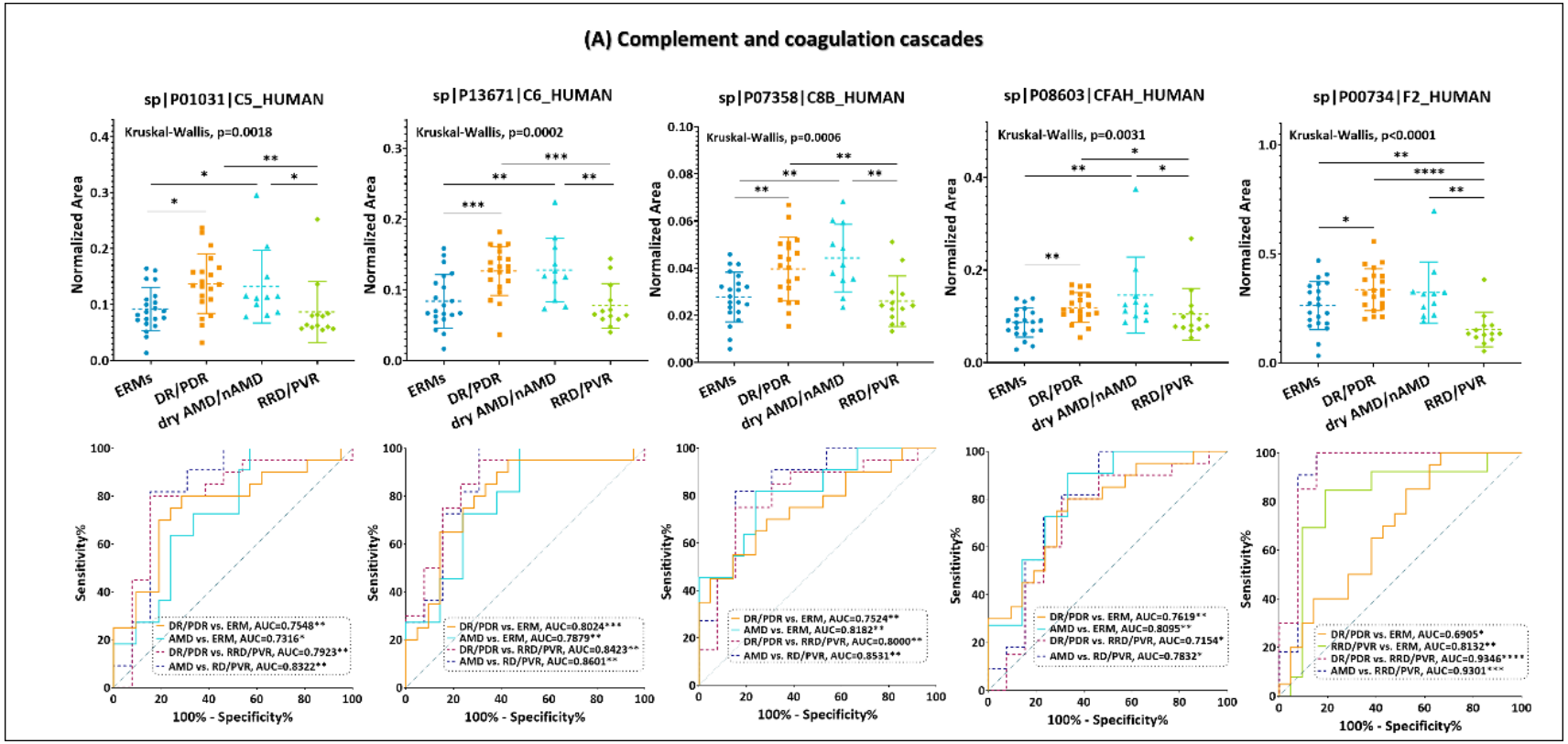

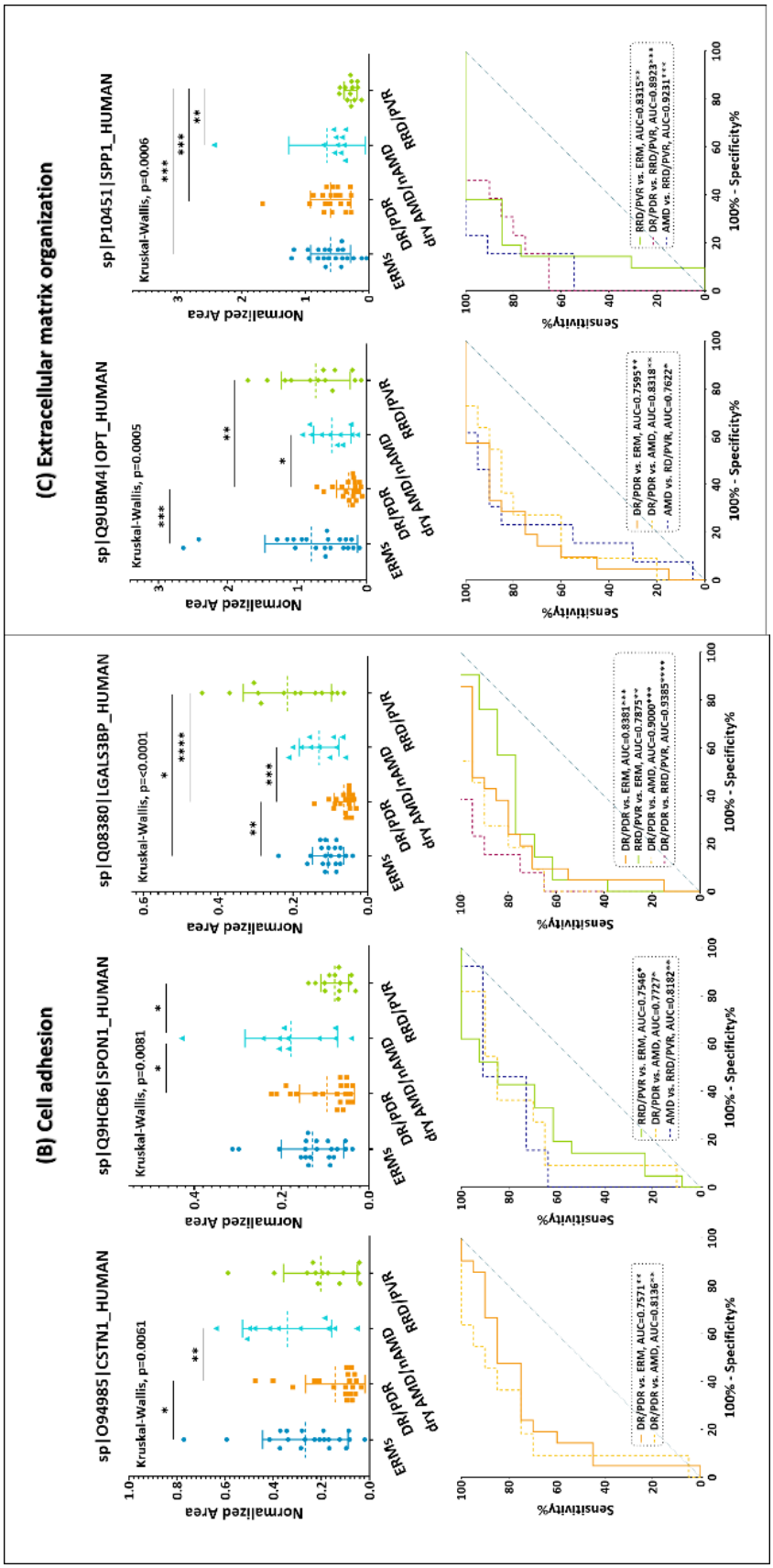
(B) Cell adhesion
(C) Extracellular matrix organization
sp|O94985|CSTN1_HUMAN
sp|Q9HCB6|SPON1_HUMAN
sp|Q08380|LGALS3BP_HUMAN
sp|Q9UBM4|OPT_HUMAN
sp|P10451|SPP1_HUMAN
Kruskal-Wallis, p=0.0061
Kruskal-Wallis, p=0.0081
Kruskal-Wallis, p=<0.0001
Kruskal-Wallis, p=0.0005
Kruskal-Wallis, p=0.0006
Normalized Area
ERMs
DR/PDR
AMD/rAMD
RRD/PVR
Sensitivity%
100% - Specificity%
DR/PDR vs. ERM, AUC=0.7571**
DR/PDR vs. AMD, AUC=0.8136**
RRD/PVR vs. ERM, AUC=0.7546*
DR/PDR vs. AMD, AUC=0.7727*
AMD vs. RRD/PVR, AUC=0.8182**
DR/PDR vs. ERM, AUC=0.8381***
RRD/PVR vs. ERM, AUC=0.7875**
DR/PDR vs. AMD, AUC=0.9000***
DR/PDR vs. RRD/PVR, AUC=0.9385****
DR/PDR vs. ERM, AUC=0.7595**
DR/PDR vs. AMD, AUC=0.8318**
AMD vs. RD/PVR, AUC=0.7622*
RRD/PVR vs. ERM, AUC=0.8315**
DR/PDR vs. RRD/PVR, AUC=0.8923***
AMD vs. RRD/PVR, AUC=0.9231***

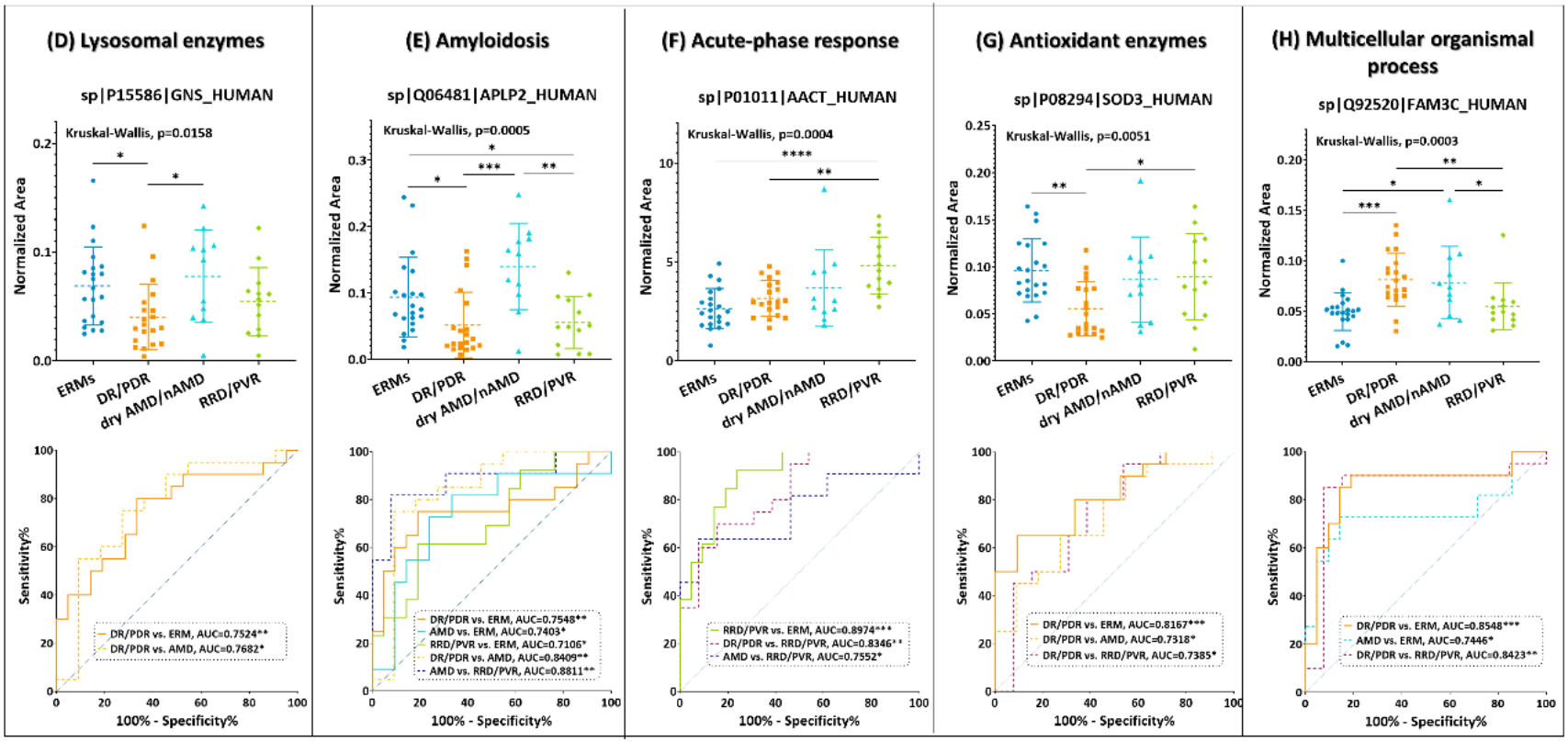
(D) Lysosomal enzymes
sp|P15586|GNS_HUMAN
Kruskal-Wallis, p=0.0158
Normalized Area
ERMs
DR/PDR
dry AMD/nAMD
RRD/PVR
Sensitivity%
100% - Specificity%
DR/PDR vs. ERM, AUC=0.7524**
DR/PDR vs. AMD, AUC=0.7682*
(E) Amyloidosis
sp|Q06481|APLP2_HUMAN
Kruskal-Wallis, p=0.0005
DR/PDR vs. ERM, AUC=0.7548**
AMD vs. ERM, AUC=0.7403*
RRD/PVR vs. ERM, AUC=0.7106*
DR/PDR vs. AMD, AUC=0.8409**
AMD vs. RRD/PVR, AUC=0.8811**
(F) Acute-phase response
sp|P01011|AACT_HUMAN
Kruskal-Wallis, p=0.0004
RRD/PVR vs. ERM, AUC=0.8974***
DR/PDR vs. RRD/PVR, AUC=0.8346**
AMD vs. RRD/PVR, AUC=0.7552*
(G) Antioxidant enzymes
sp|P08294|SOD3_HUMAN
Kruskal-Wallis, p=0.0051
DR/PDR vs. ERM, AUC=0.8167***
DR/PDR vs. AMD, AUC=0.7318*
DR/PDR vs. RRD/PVR, AUC=0.7385*
(H) Multicellular organismal process
sp|Q92520|FAM3C_HUMAN
Kruskal-Wallis, p=0.0003
DR/PDR vs. ERM, AUC=0.8548***
AMD vs. ERM, AUC=0.7446*
DR/PDR vs. RRD/PVR, AUC=0.8423**

Supplementary Figure 3. MRM results of less significant candidate biomarkers. Statistical analysis (Kruskal-Wallis tests with an FDR<5%) and ROC curves were performed in GraphPad Prism Software to assess the ability of these proteins to distinguish between different disease groups, as previously reported. Data are presented as mean ± SD with q-values of <0.05 (*) and q-value<0.01 (**).

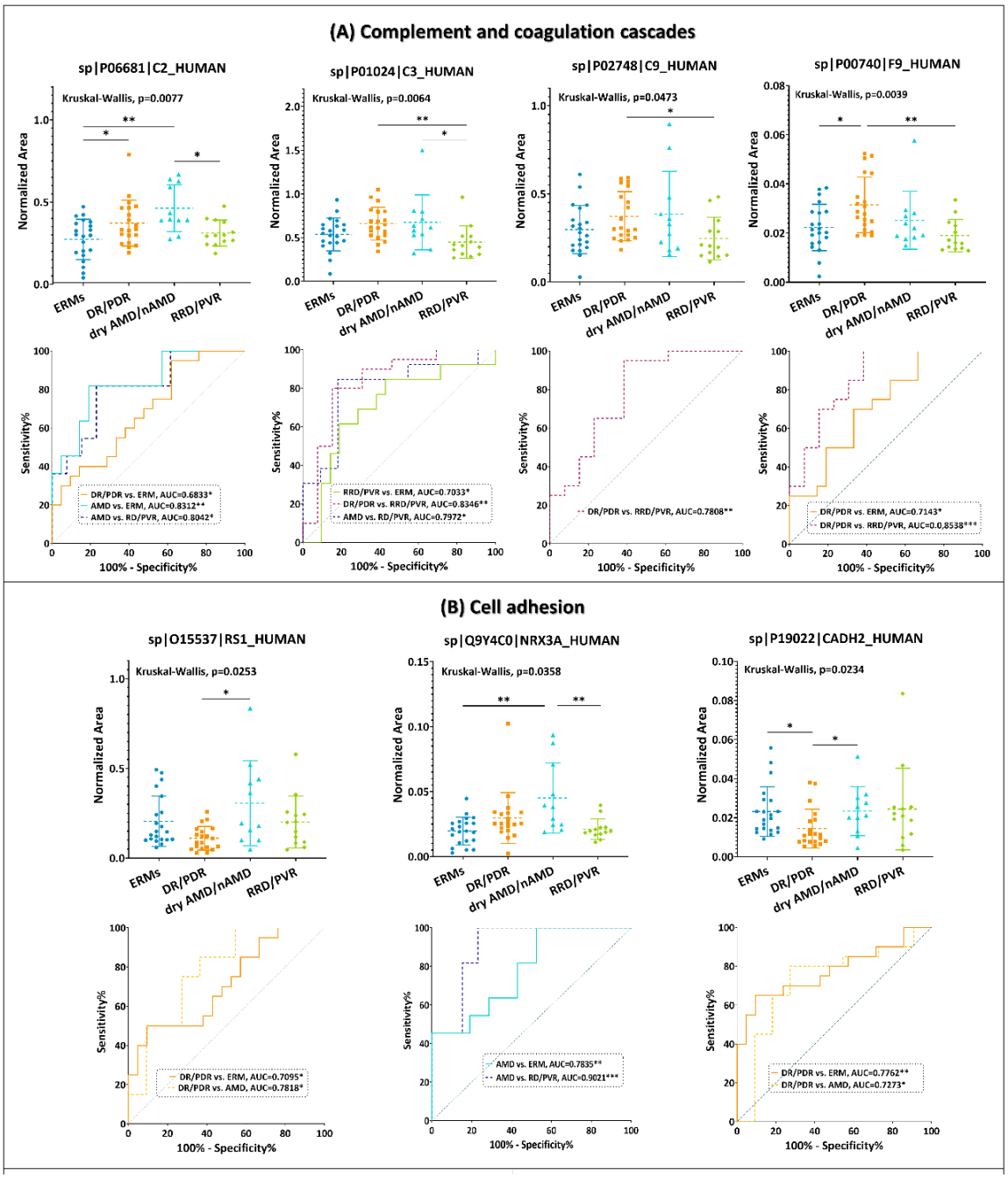

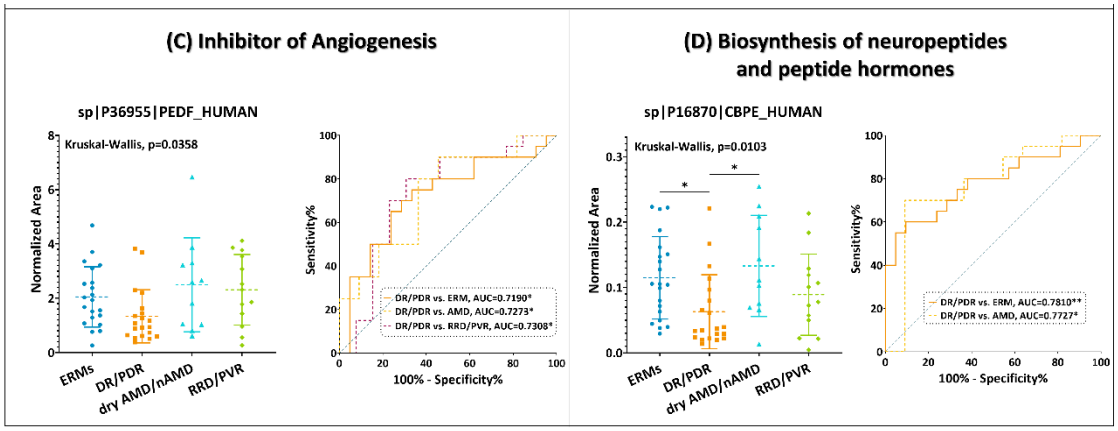

Supplementary Figure 4. MRM results of the non-differential candidate biomarkers. Statistical analysis (Kruskal-Wallis tests with an FDR<5%) and ROC curves were performed in GraphPad Prism Software to assess the ability of these proteins to distinguish between different disease groups, as previously reported. Data are presented as mean ± SD with q-values of <0.05 (*) and q-value<0.01 (**).

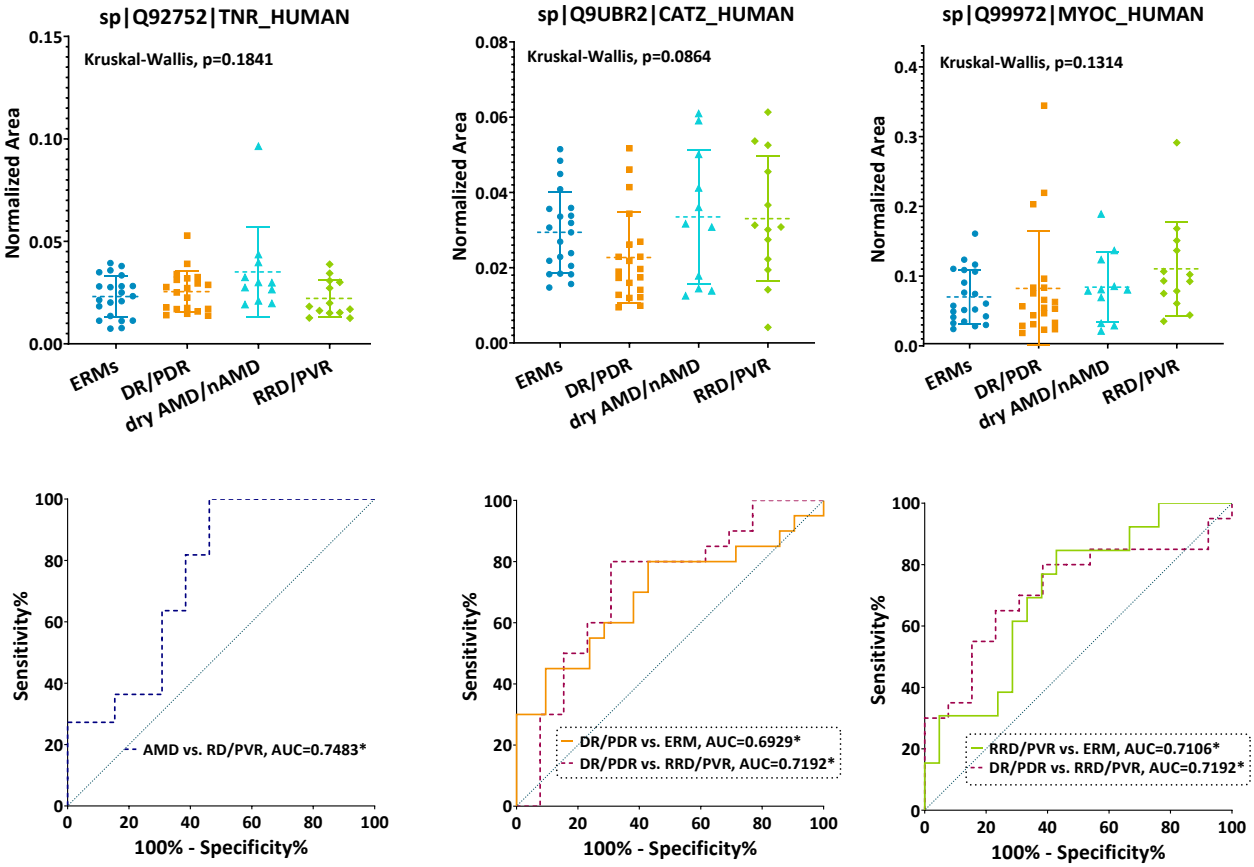

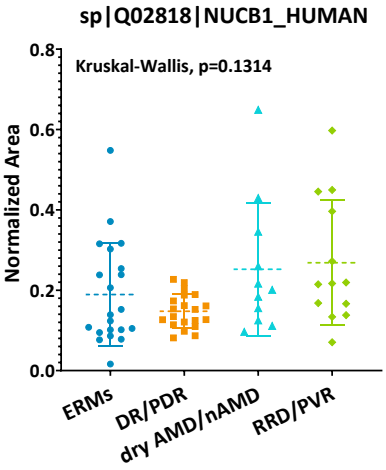
sp|Q02818|NUCB1_HUMAN
Kruskal-Wallis, p=0.1314
Normalized Area
0.0
0.2
0.4
0.6
0.8
ERMs
DR/PDR
dry AMD/nAMD
RRD/PVR

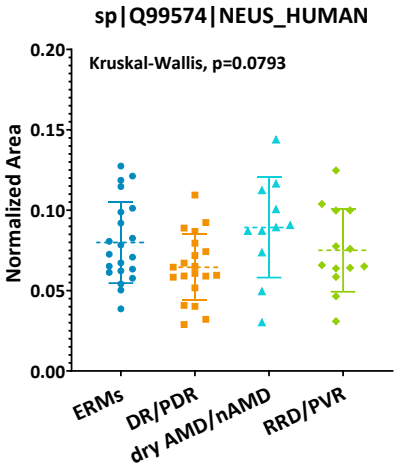
sp|Q99574|NEUS_HUMAN
Kruskal-Wallis, p=0.0793
Normalized Area
0.00
0.05
0.10
0.15
0.20
ERMs
DR/PDR
dry AMD/nAMD
RRD/PVR

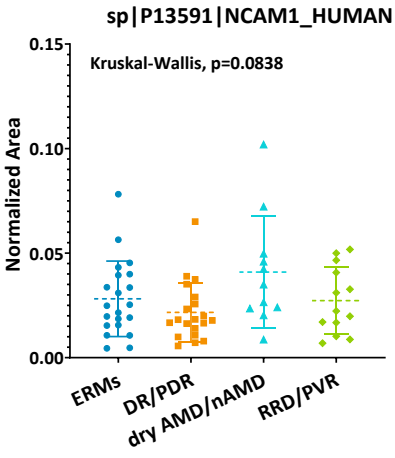
sp|P13591|NCAM1_HUMAN
Kruskal-Wallis, p=0.0838
Normalized Area
0.00
0.05
0.10
0.15
ERMs
DR/PDR
dry AMD/nAMD
RRD/PVR

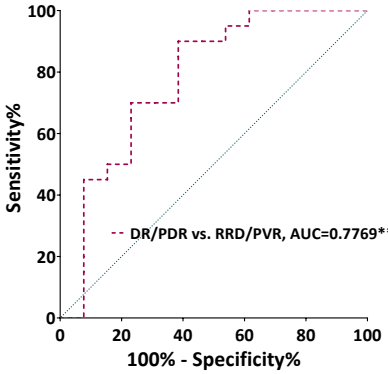
Sensitivity%
100% - Specificity%
DR/PDR vs. RRD/PVR, AUC=0.7769**
0
20
40
60
80
100

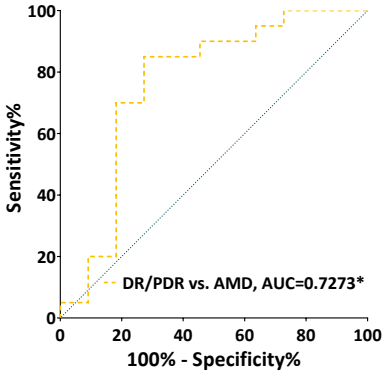
Sensitivity%
100% - Specificity%
DR/PDR vs. AMD, AUC=0.7273*
0
20
40
60
80
100

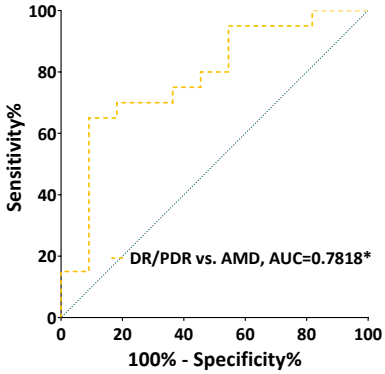
Sensitivity%
100% - Specificity%
DR/PDR vs. AMD, AUC=0.7818*
0
20
40
60
80
100

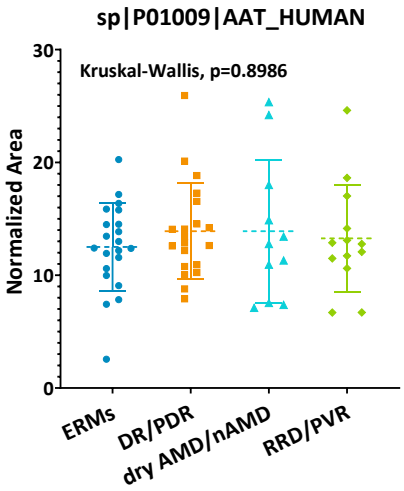
sp|P01009|AAT_HUMAN
Kruskal-Wallis, p=0.8986
Normalized Area
0
10
20
30
ERMs
DR/PDR
dry AMD/nAMD
RRD/PVR

Supplementary Figure 5. Comparison of normalized intensities from the label-free experiment with the results obtained in western blot analysis of (A) Chromogranin-A (CGMA) and (B) Metalloproteinase inhibitor 2 (TIMP2). Data are presented as mean ± SD with q-values of <0.05 (*) and q-value<0.01 (**).

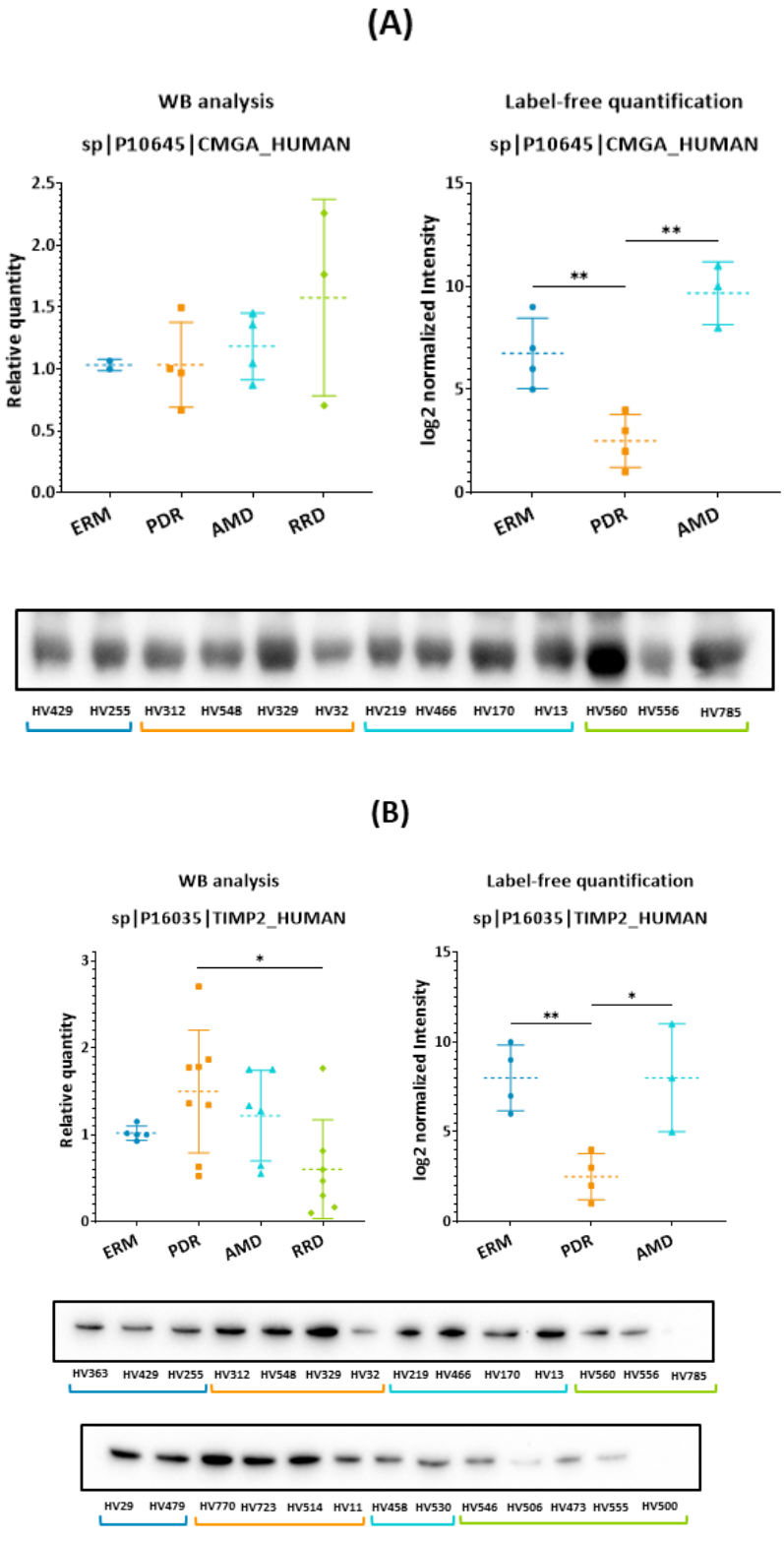

Supplementary Figure 6. Results obtained in the analysis of beta-amyloid (APP) by western blot.